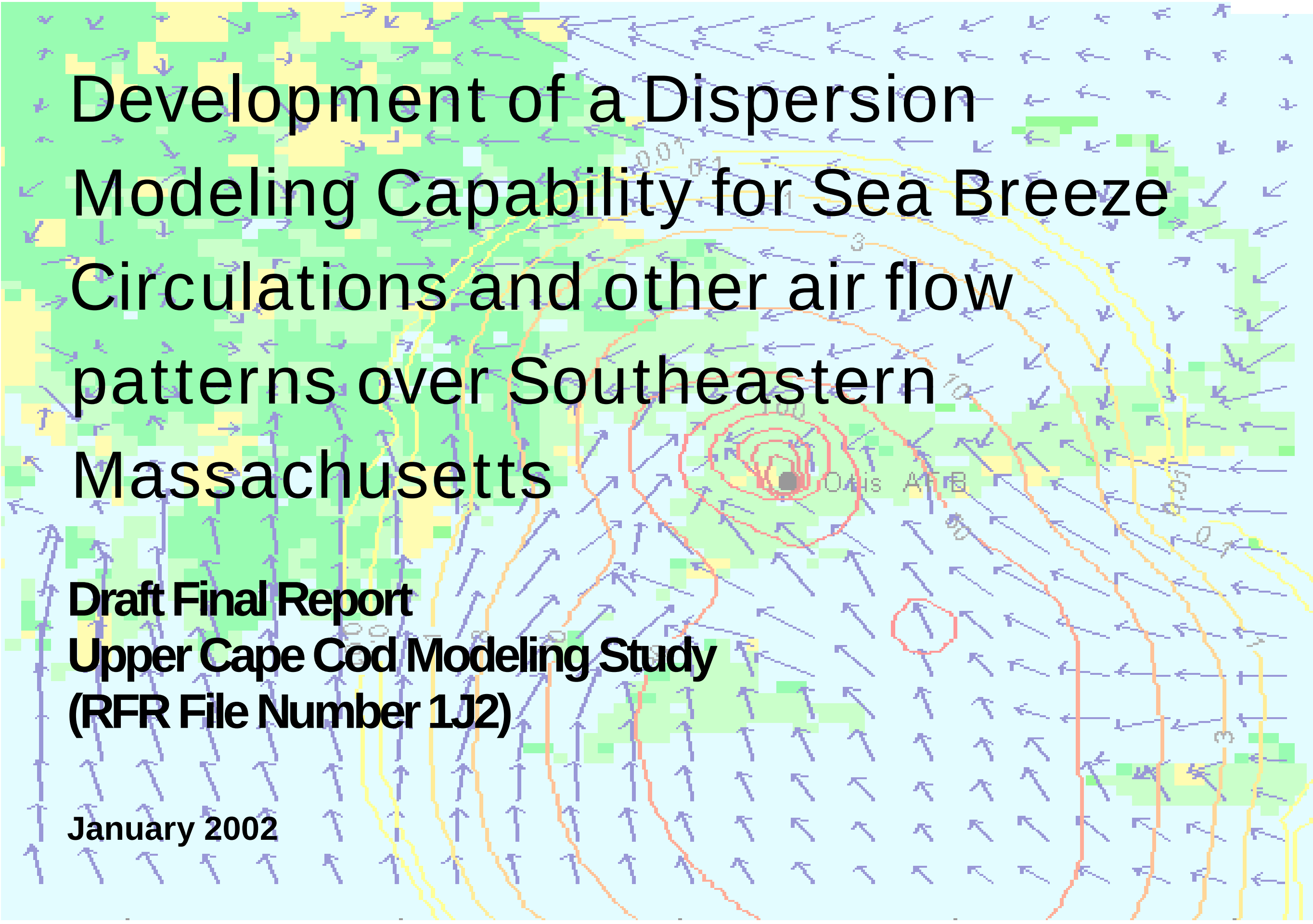

Development of a Dispersion Modeling Capability for Sea Breeze Circulations and other air flow patterns over Southeastern Massachusetts

Draft Final Report
Upper Cape Cod Modeling Study
(RFR File Number 1J2)

January 2002

Performed for

The Commonwealth of Massachusetts Department of Public Health
Bureau of Environmental Health Assessment
250 Washington Street
Boston, MA 02108

By

Egan Environmental Inc.
Beverly, MA 01915

In association with

Meteorology Consultants of Pennsylvania and **Integrals Unlimited**

State College, PA 16801 | **Portland, ME 04101**

Development of a Dispersion Modeling Capability for Sea Breeze Circulations and Other Air Flow Patterns over Southeastern Massachusetts

Draft Final Report

Upper Cape Cod Modeling Study (RFR File Number 1J2)

Performed for

The Commonwealth of Massachusetts Department of Public Health
Bureau of Environmental Health Assessment
250 Washington Street
Boston, MA 02108

By

Egan Environmental Inc.
75 Lothrop St.
Beverly, MA 01915
Tel: 978 524 7677
Fax: 978 927 8122
Email: bruce@Eganenvironmental.com

In association with

Meteorological Consultants of Pennsylvania
169 Creekside Drive
State College, PA 16801
Tel.: 814-863-1583
Fax: 814-865-3663
Email: seaman@ems.psu.edu

and

Integrals Unlimited
509 Chandler's Wharf
Portland, ME 04101
Tel:207-780-0594
Fax: 207-780-0594
Email: rjy@maine.rr.com

January 2002

Table of Contents

Acknowledgments

This project report is the result of a teaming effort of Principals from three groups: Dr. Bruce A. Egan, CCM, of Egan Environmental Inc., Dr. Nelson L. Seaman of Meteorological Consultants of Pennsylvania, and Dr. Robert J. Yamartino of Integrals Unlimited. We wish to acknowledge the important participation of Professor David R. Stauffer, Glenn K. Hunter, and Dr. Aijun Deng of the Meteorology Department of Pennsylvania State University in the analysis of meteorological events and computer operations. We also appreciate the modeling work performed by John Purdum, the programming support of Robert S. Egan and the editing support of Kristina J. Egan on behalf of Egan Environmental Inc. We also greatly appreciate the inspiration and unwavering support of Kevin Costas, M.P.H., of the Massachusetts Department of Public Health for our work on this project.

1 Executive Summary

This document reports on a model development effort performed for purposes of better quantifying the atmospheric dispersion of pollutants from various source types in the Upper Cape Cod region of Massachusetts. Because of the specific geography of Cape Cod which is basically surrounded by major water bodies, complex sea breeze fronts and circulations are important phenomena affecting air pollution in the area. Consideration of the detailed effects of such circulations is not commonly considered in air pollution dispersion analyses. The dynamics of such flows is well understood but the application of the meteorological principles to the scale of atmospheric flows affecting the Upper Cape has not been done and requires considerable modeling experience.

The modeling technology developed will be used by epidemiologists to better understand the role of sea and land breeze circulations in the dispersal of pollutants from important sources in the region. The adaptation of the MM5 mesoscale model to the Upper Cape is the key element of this project. The MM5 model has been successfully used as the basis for predicting meteorological fields applied in other air pollution studies. In this project, a fine grid scale(1.33 kilometer) version of the model was developed and customized to predict detailed three dimensional wind and temperature fields for three different two-day time periods when sea breeze circulations were expected in the summer of the year 2000. The case study events consist of periods of strong sea breeze circulations as well as occasions when land breeze effects are evident. This report includes a detailed description of the meteorology of the case study days, which those interested in the phenomena of sea and land breeze circulations for any number of reasons will find informative. Indeed this section of the report serves well as a tutorial for those with a wider interest in the subject.

The meteorological fields computed by this version of MM5 were used as input data to drive other models which include a trajectory model, TRAJEC, which shows where emissions are transported and a dispersion model, SCIPUFF, that is used to predict the resulting ground level pollutant concentrations from various sources within the region. MM5 is also used to drive another flow field model, CALMET, which interfaces with the dispersion model CALPUFF, also used to predict ground level concentration patterns. Calculations are compared to those from the EPA model ISCST3, a commonly used model in regulatory practice. The 3-D trajectories of sample hypothetical contaminated air parcels released from the different simulated sources illustrate the complexity of the sea breeze circulations. The dispersion models have varying capabilities to incorporate the complexities of the predicted flows. Four sources are simulated: two are large power plants, one is a ground level area source, and the fourth consists of two major highway segments near the Cape.

This report compares the results of these dispersion models for many of same case study events. The circulations cause very different air quality impacts from low-level pollutant releases compared to impacts from high level releases. Also the locations of the sources relative to the three nearby large water bodies is shown to be a very important factor for the models that better simulate the complex three dimensional aspects of the flows involved.

In addition to comparing predictions for the different models and source types, this report discusses the relative merits of using one model versus another for differing applications and differing meteorological flows.

The modeling capability is a deliverable product of the research and can be used directly by the Department of Public Health in future epidemiological studies. Future use and potential refinements to the technology also are discussed.

2 Introduction and Background

The Commonwealth of Massachusetts Department of Public Health Bureau of Environmental Health Assessment (BEHA) is performing an epidemiological care-control study of the incidence of lung cancer on Upper Cape Cod. Research performed to date has determined that the incidence of lung cancer is up to 30% higher in certain Upper Cape Cod towns than elsewhere in Massachusetts.

The incidence of lung cancer is expected to be in part associated with the atmospheric transport of carcinogenic materials from sources of pollutants to populated areas. The determination of how the atmospheric dispersion processes and pathways are affected by local meteorological factors is therefore an essential aspect in the determination of cause and effect relationships for epidemiological studies. This is especially true for an area such as southeastern Massachusetts and Cape Cod where meteorological conditions are strongly influenced by the presence of surrounding large bodies of water. Temperature differences between the land and water surfaces give rise to complex local circulations and in particular, sea and land breeze flows that strongly affect air flow patterns and air dispersion rates.

The nature of the sea breeze circulations on Cape Cod is well known by local pilots, especially those that fly small aircraft or gliders. Barnes (2000) by interviewing pilots and Charlton (2001) directly, describe that the complex flows observed include large vertical updrafts associated with sea breeze fronts that approach the middle of the Cape from either Cape Cod Bay or from Nantucket Sound. There are many occasions when both sea breezes occur resulting in converging flows over the middle of the Cape. Zanis (2001) has observed occasions when onshore, converging flows have simultaneously occurred along all three coasts including from the shores of Buzzards Bay. The converging flows result in updrafts which have been observed to carry pollutants from near ground-level sources upward, sometimes quite vigorously. Once aloft, these same pollutants have been observed to be carried by the return flow part in a "branch" of a sea breeze circulation that initially transports the higher elevation air back out to sea. This circulatory flow then results in a descent of pollutants back to the sea surface where they might again be carried at low levels over the land. The relatively low mixing depths common over the Cape have been observed by pilots on some occasions to trap emissions from the Canal Power Plant stacks below the inversion height and within the sea breeze circulation flow. On other occasions, the plumes have been seen to penetrate elevated inversions but later still descend toward the ground. These observations have obvious significance to the transport of pollutants over Upper Cape Cod. It is commonly held that the primary effects of daytime updrafts would increase the dilution of pollutants within such flows and therefore benefit nearby, local communities. In areas unaffected by marine influences, mixing depths would be deeper and updrafts would carry pollutants into a wind regime that normally would continuously dilute the pollutants and carry them far downwind. With the marine influence, the mixing depths tend to be lower and the pollutants may be partially recirculated rather than carried far away. This combination of factors has a negative impact on air quality.

Another mechanism that may also negatively affect air quality on the Upper Cape is the occurrence of land breeze circulations that take place at night and in the early morning. Land breezes are also thermally driven flows that result when the temperature of nearby water bodies is greater than that of the land. The air over the water then rises and the return flow aloft causes the descent of air over the land which then travels out to sea. The concern from an air pollution standpoint is that initially elevated plumes caught in the descending flow would be carried closer to the surface. Such flows at night would also have less turbulence so that emissions would be less diluted over time or transport distance.

Although atmospheric dispersion modeling has been a common tool for nearly four decades for assessing the impacts of sources of pollutant emissions on ambient air concentrations, the capabilities and reliability of the routinely used models is limited in complex situations. For example, the US EPA Industrial Source Model (ISC) that is recommended by EPA for most relatively flat terrain settings such as Cape Cod, and which was used in a health risk assessment of the burning of propellant bags in an earlier study (USACHPPM, 1999) is only capable of simulating dispersion along straight line trajectories. That is, emissions from a source for a given hour would be modeled as if the airflow went in a single direction from the source for all distances downwind. The model is incapable of tracking where the pollutants emitted during a given hour might go during subsequent hours when the winds would have changed direction and speed. The typical meteorological input data for ISC are hourly observations from an anemometer at a nearby airport. In ISC, the observed wind speed and direction is assumed to apply over the entire modeling domain for the hour being modeled. However, if the winds in an area are highly variable in space, the local anemometer measurement will clearly not be applicable to the larger region. To make matters worse, for Cape Cod studies using National Weather Service (NWS) data, one would have to rely upon data from Boston or Providence, RI. For example, in past applications of ISC on Cape Cod, NWS wind speed and direction data from Green Airport near Providence, RI have been used. These data would not be representative of what is occurring on the Cape for a large fraction of the time. However, even if data from a local meteorological tower were used, ISC cannot properly simulate the effects of rapidly changing meteorological conditions or the effects of recirculation of contaminants in complex airflows having substantial time and spatial variability. While ISC might be a reasonable model and Green Airport might provide reasonable meteorological input data for some applications and for some steady sets of meteorological conditions, proper simulation of the effects of complex meteorological flows on pollutant dispersion requires utilization of much more advanced modeling technologies that can simulate the meteorological flows directly.

A major objective of this project is to of develop an advanced dispersion modeling capability for the Upper Cape Cod region which would allow estimates of air pollution concentrations during complex meteorological flow conditions. To provide this capability, we have drawn upon state-of- the-art meteorological flow prediction models and customized these to the Upper Cape Cod location and land use.

The primary mesoscale circulations expected to be critical for meeting this objective are the *sea breeze* and the *land breeze*. These two types of wind circulations are driven by differential heating of land and water bodies. On a time scale of a day or two, sea-surface temperatures typically change only a fraction of a degree, while the diurnal range of surface temperatures over land may be as much as 15-20 C. This differential heating causes a strong temperature gradient to be established between the land and sea over distances as small as 10 kilometers (km) or less. The expansion of the warmer air over land during the daytime causes a drop in the surface air pressure, so that the resulting horizontal pressure gradient induces a shallow solenoidal wind circulation known as the sea breeze. The wind flow in the sea breeze is from sea to land. The wind speeds in the sea breeze are typically on the order of 2-8 meters per second ($ms^{-1)}$ and are controlled primarily by the strength of the land-sea temperature contrast, which is maximized under conditions having light synoptic-scale winds and clear skies.

The onshore advection of cool air from over the water by the sea breezes tends to compress the horizontal temperature gradient into a narrow zone known as the *sea-breeze front*. During favorable (nearly calm) large-scale wind conditions, this shallow sea-breeze front usually pushes inland during the afternoon as the land-sea temperature contrast approaches its maximum. The inland penetration of the sea breeze over the mainland may be as far as ~100 km inland in vigorous cases and where the land continues for such distances. At night, if temperatures over land fall significantly below the sea temperature, a reverse circulation known as the land breeze may develop. The depth of the onshore sea breeze is typically on the order of 100-1000 meters (m), while the land breeze is generally weaker in intensity and shallower.

3 Technical Approach

The project has four basic steps:

- The adaptation and customization of Penn State/NCAR MM5 model to the Upper Cape Cod region. This is described in Section 3.2, along with how the output of the model is used to drive other models.

- The selection of three different time periods during the summer of 2000, when local flow circulation /sea breeze phenomena of interest were expected to have occurred. The meteorological descriptions of the cases chosen and specifics of the manual analyses of the weather during those periods is described and illustrated in terms of weather maps in Section 4.1 of the report.

- The application of the MM5 model to the three different time periods. Detailed three-dimensional, fine-grid wind fields, temperatures, pressures and other meteorological parameters were predicted by MM5 on this fine grid for each grid point and time step in these simulations.

The verification of this model is performed on the basis of comparisons of the predicted meteorological fields to the objective manual analyses of the observed weather in the region for those same time periods. This is demonstrated by comparing weather maps of the predicted fields to the manual objective analyses based on reported information. This verification work is reported in detail in Section 4.2. Also included in these comparisons are statistical summaries of the predicted versus observed winds, pressures, temperatures, mixing ratios, and relative humidity for both the fine (1.33km) and coarser (4km) grid points.

The meteorological outputs of MM5 were then used as input data for the different dispersion and trajectory models. The traditional EPA regulatory model ISCST3 is also run; however, it is designed to use surface observations directly, and these were taken from the Hyannis-Barnstable Airport station. The results of these various model applications are presented in Sections 4.3 through 4.5. The reader will note some inconsistencies in the graphical representations of these results. Some of these inconsistencies are associated with the graphics packages themselves. For example, the SCIPUFF model is coupled directly to the MM5 outputs in longitude and latitude coordinates. The TRAJEC, CALMET and CALPUFF models use the MM5's alternative Lambert conformal coordinate system The ISCST3 model uses a Universal Transverse Mercator (UTM) coordinate system, consistent with USGS survey maps. . Time- is routinely reported by the MM5 system in terms of Greenwich Mean Time (often referred to as GMT, Z, or UTC) which is four hours later than Eastern Daylight Savings (EDT) time and five hours later than Eastern Standard Time (EST). Another difference in the graphic systems involves the display of isopleths of constant contaminant concentrations. The MM5/SCIPUFF model results are displayed in units of kilograms per cubic meter (kg/m3), consistent with the standard sub-set of units in the MKS (meters, kilogram, seconds) metric system. CALPUFF and ISC concentration results are displayed in units of micrograms per cubic meter (ug/m3), which are more conventionally used in air pollution applications. However, a user can simply, multiply kg/m^3 results by 10^9 to convert to units of ug/m3. The authors apologize the inconvenience of displaying results according to the different mapping systems and formats used in the native software of the models. Such inconsistencies can be eliminated in future applications.

The results of the model simulations are discussed relative to the capabilities of the individual models to predict air quality concentrations during specific meteorological conditions. The advantages and disadvantages of using one model versus another, or of using more than one model, are discussed in section 5.

The results of the model simulations are discussed in terms of the abilities of the individual models to predict air quality concentrations during specific meteorological conditions. The advantages and disadvantages of using one model versus another or of using more than one model are discussed in Section 5.

3.1 Numerical Simulation Flow Field Modeling

Conventional dispersion models have been driven by using historic meteorological data collected at nearby meteorological towers or from nearby airports. The limited amount of data available from such sources generally is reduced further to the values of wind speeds and directions and vertical temperature gradients at these locations. Such limited measurements clearly cannot capture the detail needed to describe complex airflows that vary spatially, as well as in time. Recent advances in computational fluid mechanics and meteorological modeling have resulted in the development of mathematical simulation models which attempt to predict the detailed flow fields from initial conditions and physical principles. In the MM5 model, for example, land and water surface attributes such as temperature, surface roughness, albedo and soil moisture content are assigned to each element of a fine grid representation of Cape Cod and its surroundings. An initial set of meteorological parameters interpolated from limited measurements is imposed to begin the model calculations. The simulation then utilizes the physical phenomena and relationships that occur in nature, represented by dynamical equations and parameterizations, to develop complex evolving meteorological predictions. As the sun rises, the land areas are heated more than the water areas. Resulting density differences cause parcels of the warmer air to expand and rise. This causes lower pressures to develop over the land which will tend to draw in air from nearby cooler (water) surfaces. All the meteorological factors that can be effectively parameterized are used. The predictive process continues forward in a series of short time steps, each based upon the results from the previous time step. As the simulation marches forward in time, it produces values of the parameters at each grid point or cell. The resulting fields of data can then be used to drive a dispersion model that tracks how an emitted pollutant travels with the wind and mixes with the ambient air.

The simulation models are described in greater detail in the sections that follow.

3.2 Model Descriptions

3.2.1 The Penn State/NCAR MM5 Meteorological Model

3.2.1.1 Features and Capabilities

The meteorological model used in this study is the fifth-generation non-hydrostatic Pennsylvania State University/National Center for Atmospheric Research (PSU/NCAR) mesoscale model, known as MM5. It is suitable for general meteorological applications at grid sizes ranging from 1 km to ~200 km. The MM5 is a three-dimensional (3-D) nested-grid, primitive-equation hydrodynamic model with a terrain-following σ (non-dimensionalized pressure) vertical coordinate, defined as

$$\sigma = \frac{p - p_t}{p_s - p_t} \qquad (1)$$

where, $p = p(x, y, \sigma, t)$ is the pressure, $p_s = p_s(x, y, t)$ is the surface pressure of the background field (described below), and p_t is the constant pressure at the top of the model. Here, *t* is time, and *x* and *y* are the horizontal directions on the model's Cartesian grid, with *x* being toward the east and *y* being toward the north at the center of the outermost domain. The pressure, $p = p_b(x, y, \sigma) + p'(x, y, \sigma, t)$, is defined using a time-invariant "background" pressure field, based on a standard atmospheric lapse rate, while a much smaller 3-D prognostic pressure perturbation field, p', represents the time-dependent departure from the background. This approach minimizes errors in the numerical calculations, especially over steep terrain.

Minimally, the MM5 contains 3-D predictive equations for *p*', the three wind components in the *x*, *y* and σ directions (*u*,*v*,*w*), temperature (*T*) and water-vapor mixing ratio (q_V), each of which are written in the mass-flux form. Options allow the user to select extra predictive equations needed to represent certain of the physical processes associated with turbulence and condensed water (see Section 3.2.1.2). The model uses a split semi-implicit temporal integration scheme to increase computational efficiency. The MM5 is flexible enough to be applied to a wide range of synoptic and mesoscale phenomena, including baroclinic storm development, tropical cyclones, sea breezes, mountain-induced circulations, and is suitable to investigate the role of various physical processes, such as convection and planetary boundary layer (PBL) influences. For a more complete description of the MM5 formalism, see Dudhia (1993) and Grell et al. (1994).

The horizontal grid system of the MM5 domains is based on the staggered Arakawa-B grid described by Arakawa and Lamb (1977). In this grid configuration, the wind components, *u* and *v*, are defined on the so-called "dot points" at the corners of each grid box, while all the other variables are defined at the "cross points" at the center of the boxes. The vertical structure of the model's grid is such that vertical motion, *w*, and the turbulent kinetic energy (*TKE)* are defined on the full sigma-layer boundaries. All other prognostic variables (*u*, *v*, *T*, and q_V) are defined on the half levels (i.e., the middle of the model layers) (see Grell et al. 1994 for details).

3.2.1.2 Customization to the Upper Cape Cod Region

In order to allow in-depth numerical studies of historical cases involving mesoscale wind circulations that could potentially affect air quality and human health in the vicinity of Upper Cape Cod, a customized version of the MM5 was developed. The primary mesoscale circulations expected to be important for meeting this objective are the *sea breeze* and the *land breeze*, which were described in Section 2.

The characteristics and physical origins of these mesoscale wind circulations dictate the approach used to customize the MM5 for the intended applications over Upper Cape Cod. Due to the relatively small area covered by the Cape and the limited horizontal scale of the sea breeze, the grid mesh used to represent the important wind circulations must be on the order of 1-5 km. At the same time, the vertical resolution in the lowest kilometer of the atmosphere must be rather fine in order to capture the vertical wind shear in these shallow sea and land breezes. Meanwhile, since these circulations are confined to the atmosphere's planetary boundary layer, where turbulence becomes an important physical process, it is important to use an advanced and accurate physics code to represent turbulent mixing. Finally, since true forecasts are not the immediate object of these experiments (i.e., historical cases are to be studied), it is possible to reduce the growth rate of errors in the model by assimilating the observed characteristics of the large-scale wind and mass fields as the model simulations proceed. This error-reduction method is known as four-dimensional data assimilation (FDDA). The following three sub-sections describe the details of the adaptations made to MM5 for the Upper Cape Cod Modeling Study.

3.2.1.2.1 Domains and Resolutions

For the simulation of sea breezes and land breezes over Cape Cod, the MM5 was configured with a set of four nested domains, as shown in Figure 1. The center of the outer domain is defined at latitude 40.0 N and longitude 75.0 W, with all nested domains defined relative to the parent grid. The domains are represented using the Lambert conformal map projection, true at 30 N and 60 N. The purpose of the large outer domain is to represent a region big enough that the synoptic-scale atmospheric systems responsible for the background wind field over the Northeast U.S. can be contained inside the MM5 domain. Next, the nesting capability of the MM5 is used to telescope down to the area of specific interest in southern New England. The successive domains have resolutions (mesh sizes) of 36 km, 12 km, 4 km and 1.33 km. The areas of the 4-km and 1.33-km domains are shown in greater detail in Figure 2, with 1^O X 1^O ticks added for reference (1 degree of latitude = 111 km).

The coarsest domain in this configuration (36-km grid) covers most of the eastern U.S. and southeastern Canada with a mesh of 61 X 73 points. The 12-km domain covers New England and the Middle Atlantic states with a mesh of 103 X 103 points. Next, the 4-km domain covers southeastern New England with a mesh of 151 X 151 points. Finally, the innermost 1.33-km domain over Cape Cod has 115 X 115 points.

Figure 1. Location of 36-km, 12-km, 4-km and 1.33-km nested domains for the MM5 configuration over Cape Cod.

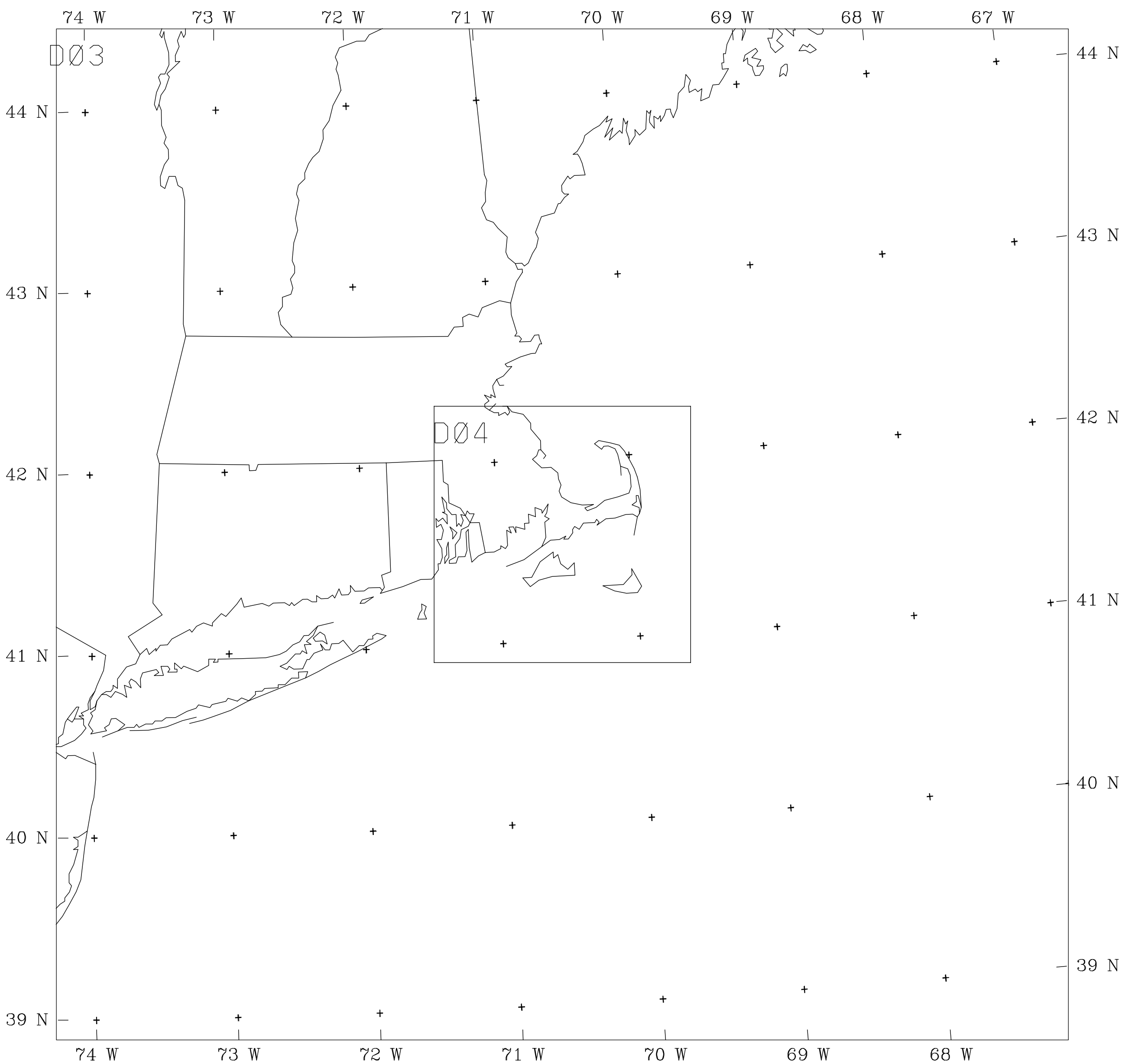

Figure 2. Location of 4-km and 1.33-km nested domains for the MM5 configuration over Cape Cod.

The terrain fields for the 4-km and 1.33 km domains are shown in Figures 3 and 4, respectively. Figure 3 indicates that the 4-km domain resolves the Berkshire Mts. in western MA, the Green Mts. in VT and the White Mts. in NH. Naturally, Figure 4 shows that there is very little topography in southeastern MA, with the highest terrain that can be resolved on Upper Cape Cod limited to less than 60 m MSL (mean sea level).

Next, a land-use array was generated for each of the four domains, based on a 25 category USGS land-use database. Physical parameters describing the characteristics of the lower boundary are assigned within the MM5 to each land-use category using a look-up table. These parameters are the albedo, soil moisture availability, emissivity, roughness length and thermal inertia, which are used in the model's calculations for the surface fluxes of heat, moisture and momentum (see Grell et al, 1994 for more details).

All four of the domains have 50 layers in the vertical direction (see Table 1). The calculations for winds, temperatures and moisture at the center of the lowest layer take place at ~12.5 m above ground level (AGL). Above the surface layer, the vertical resolution is 40-45 m though the atmosphere's first kilometer. Thereafter, the thickness of the layers increases gradually with height, so that there are 30 layers below 850 millibars (mb) (~1560 m above sea level). The top of the model was set at 50 mb for all domains.

3.2.1.2.2 Physics Selections

The grid configuration described in Section 3.2.1.2.1 encompasses four domains having horizontal resolutions of 36, 12, 4 and 1.33 km. On all of these domains, resolved-scale moist processes for clouds and rain were represented using explicit prognostic equations. Deep convection (thunderstorm) is handled separately through a sub-grid parameterization (Kain and Fritsch 1990). The Kain-Fritsch scheme generally is most accurate for grid sizes on the order of 10-40 km. It has a fully entraining/detraining cloud model and uses an energy-equilibrium closure. First, the potential for convective clouds is diagnosed by lifting low-level parcels to their saturation levels. Then, a convection-forming parcel is initiated from the saturated parcel below 700 mb having the highest θ_e (equivalent potential temperature). Rain is triggered when the cloud exceeds a critical depth (3-4 km). Once convection is initiated in a grid column, it continues until all convective available potential energy (CAPE) has been eliminated.

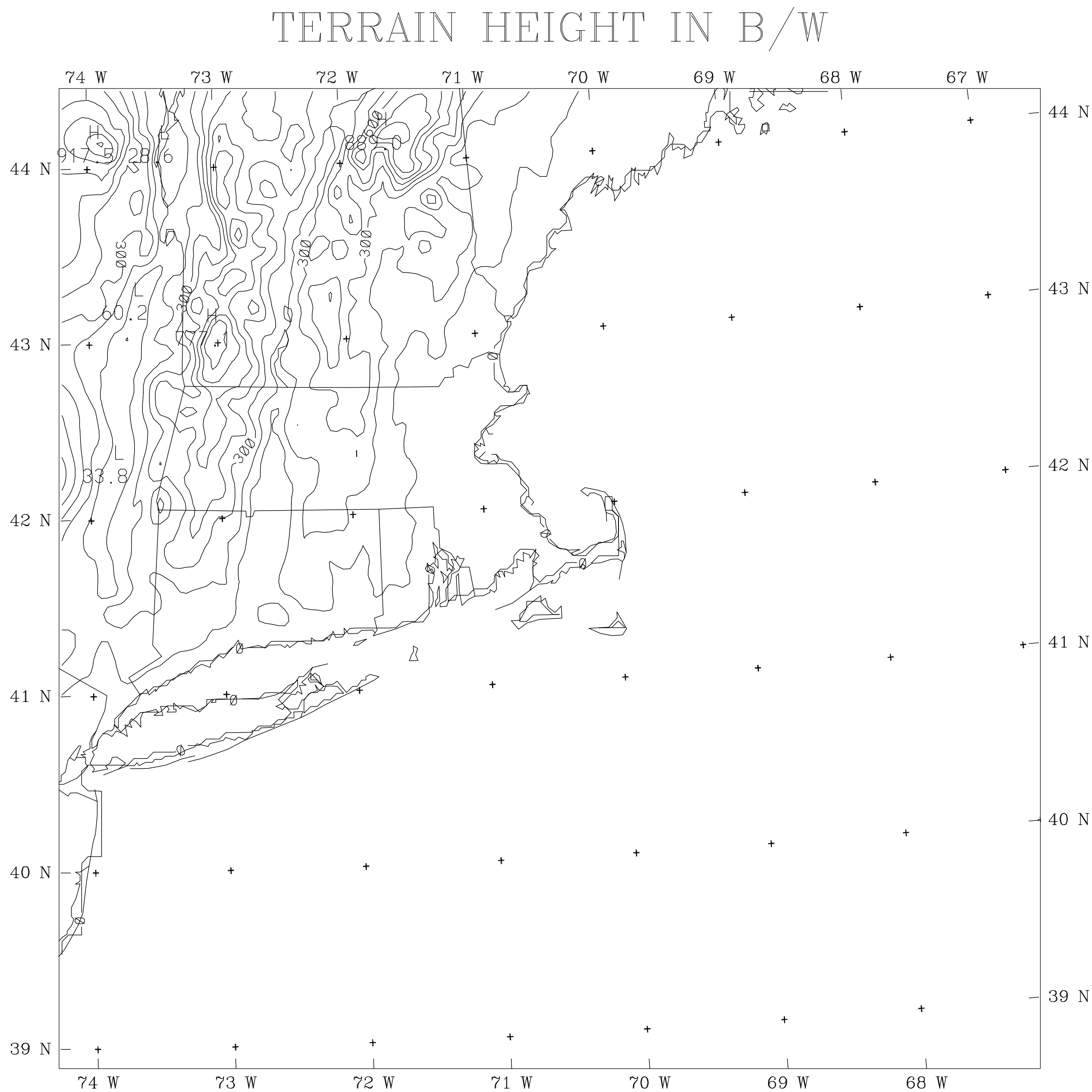

Figure 3. Terrain (m) for 4-km domain of the MM5 configuration over Cape Cod. Contour interval is 100 m.

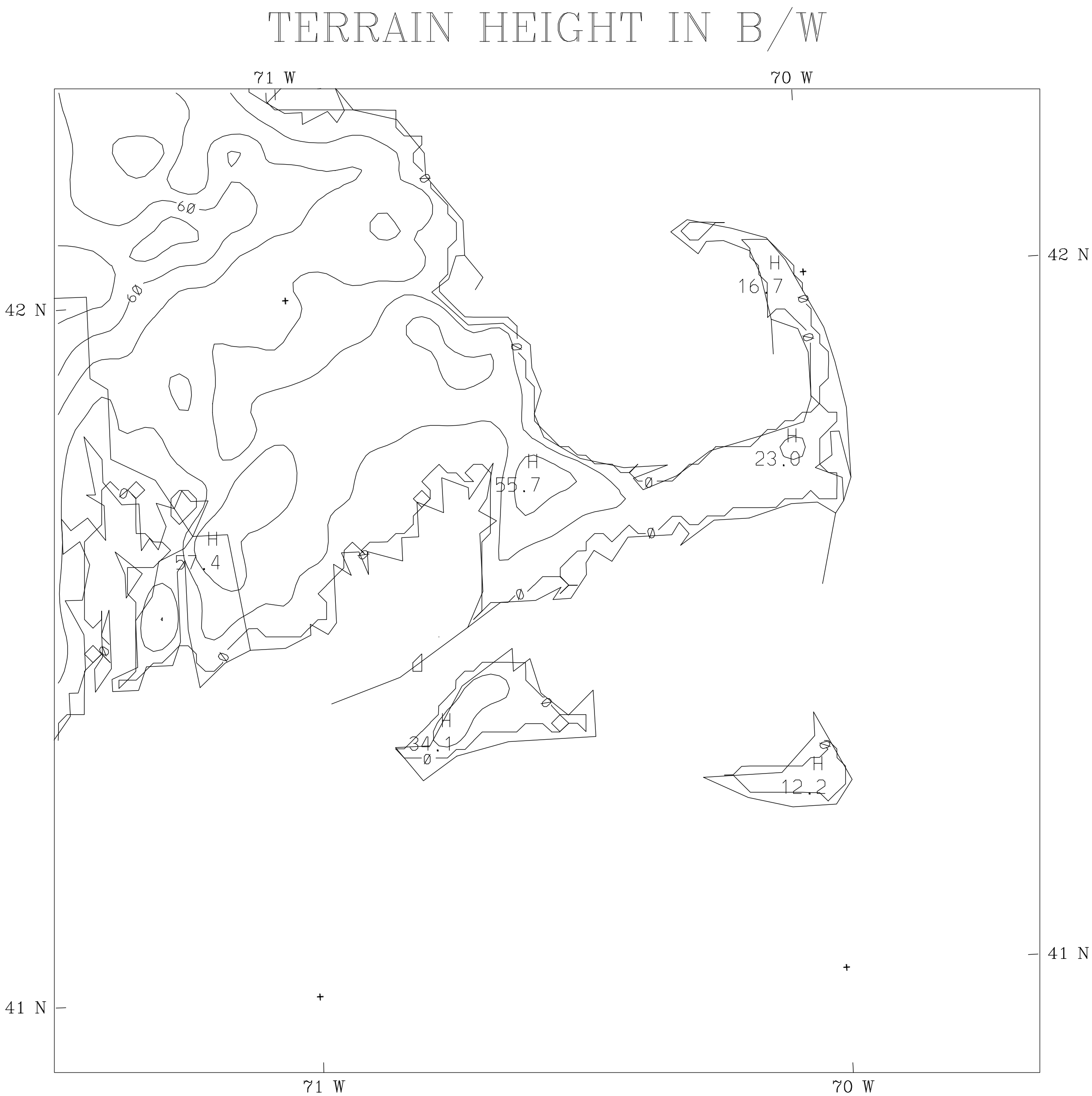

Figure 4. Terrain (m) for 1.33-km domain of the MM5 configuration over Cape Cod. Contour interval is 20 m.

Table 1. Vertical distribution of the 50 σ layers (layer boundaries are shown) and model-layer heights (m AGL). Calculations of u, v, T, and q are made at the center of layers.

Layer	**Error! Objects cannot be created from editing field codes.**	Height (m)	Layer	**Error! Objects cannot be created from editing field codes.**	Height (m)
51	1.000	0.0	25	0.868	1147.9
50	0.997	25.0	24	0.859	1229.9
49	0.992	66.9	23	0.849	1321.7
48	0.987	108.8	22	0.838	1423.5
47	0.982	150.9	21	0.823	1563.8
46	0.977	193.1	20	0.804	1744.3
45	0.972	235.4	19	0.780	1976.8
44	0.967	277.9	18	0.750	2275.1
43	0.962	320.5	17	0.716	2624.1
42	0.957	363.3	16	0.680	3007.5
41	0.952	406.1	15	0.641	3440.6
40	0.947	449.1	14	0.598	3941.9
39	0.942	492.3	13	0.552	4509.7
38	0.937	535.6	12	0.508	5087.9
37	0.932	579.0	11	0.464	5706.1
36	0.927	622.6	10	0.414	6457.6
35	0.922	666.3	9	0.366	7230.0
34	0.917	710.1	8	0.320	8028.4
33	0.912	754.1	7	0.276	8859.6
32	0.907	798.3	6	0.230	9823.5
31	0.902	842.6	5	0.184	10927.9
30	0.897	887.0	4	0.138	12249.6
29	0.892	931.6	3	0.092	13889.6
28	0.887	976.4	2	0.046	16135.1
27	0.882	1021.3	1	0.000	19865.2
26	0.876	1075.4			

No convective parameterization is needed on the 4-km and 1.33-km domains because they are assumed to be fine enough to resolve explicitly the main aspects of the convection (Weisman et al. 1997). This is equivalent to saying that the deep-convective updrafts are about the same size as the grid. However, this assumption may not be true universally on the 4-km domain, which can lead to some distortions in the propagation speed and vertical structure of the convective precipitation at that scale. When there is an external mechanism controlling the propagation of the convection, such as a frontal system, the explicit representation of all precipitation should be reasonably accurate, even on the 4-km domain. Under nearly all circumstances the 1.33-km domain is fine enough to resolve the primary structure of convective systems reasonably well.

The turbulence scheme used in the MM5 for this application is a 1.5-order closure approach developed by Gayno (1994) and described by Shafran et al. (2000). The Shafran et al. scheme has a 2^{nd}-order predictive equation for turbulent kinetic energy (TKE), while the eddy viscosity is a function of the predicted TKE and several stability-dependent mixing lengths. Turbulent fluxes of momentum, moisture and virtual potential temperature (θ_v) are parameterized using K-theory in which the turbulent transfer occurs down gradient. However, since basic K-theory fails under certain convective situations (Moeng and Wyngaard, 1989), counter gradient flux terms are included to correct the turbulent transport terms in the convective mixed layer (Gayno 1994). The TKE-predicting scheme has been designed to generate both shear-driven turbulence and in-cloud mixing associated with cloud-top radiative flux divergence (Stauffer and Seaman 1999). It has also been shown to predict better boundary-layer structure for convectively unstable conditions, compared to the Blackadar boundary-layer option in MM5 (Shafran et al. 2000). In addition, Stauffer et al. (1999) added the capability to account for the effects of saturation on the buoyancy production of TKE, which makes this 1.5-order scheme more accurate in cloudy or foggy conditions than the other turbulence parameterizations available in MM5.

In addition, the atmospheric and surface temperature tendencies due to short-wave and long-wave radiation flux divergences are calculated with a column radiation parameterization (Dudhia 1989). The Dudhia radiation scheme is based on a two-stream, single-band approach. It is fully interactive with dry air, water vapor and cloud liquid/ice.

3.2.1.2.3 Four-Dimensional Data Assimilation

Four-dimensional data assimilation (FDDA) is a process in which observations are used to correct for numerical errors in a model simulation, instead of using data only at the initial time. It has been shown to reduce the accumulation of errors during the assimilation period (e.g., Seaman et al. 1995, Michelson and Seaman 2000). The FDDA approach used in this application is based on a "nudging", or Newtonian relaxation, method developed by Stauffer and Seaman (1990, 1994). In this method, the model state is relaxed continuously at each time step toward the observed state by adding to the prognostic equations an artificial tendency term, which is based on the difference between the two states. The assimilation can be accomplished by nudging the model solutions towards gridded analyses based on observations (analysis nudging) or directly toward the individual observations (obs-nudging). In the present application, only analysis nudging is used, since there are very few (if any) special meteorological observations expected to be available routinely for support of ongoing applications over Upper Cape Cod.

The *analysis-nudging* term for a given variable is proportional to the difference between the model state and the observed analysis at each grid point. The general form of the FDDA term for the non-hydrostatic version of the MM5 predictive equations in flux form for any prognostic variable $\alpha(\tilde{x},t)$ is given by the last term in the following tendency equation:

$$\frac{\partial p^* \alpha}{\partial t} = F(\alpha, \tilde{x}, t) + G_\alpha \cdot W_\alpha(\tilde{x}, t) \cdot \varepsilon_\alpha \cdot p^* \cdot (\hat{\alpha_0} - \alpha) \qquad (2)$$

where p^* is defined as

$$p^* = p_s - p_t \qquad (3)$$

and where p_s is the surface pressure and p_t is the pressure at the top of the model's reference state. The function *F* represents the sum of all of the model's physical and dynamical forcing terms, such as advection, friction, pressure-gradient force and Coriolis force. The term G_α is the nudging factor and $W_\alpha(\tilde{x},t)$ is the four-dimensional weighting function that specifies the horizontal, vertical and temporal weighting applied to the analysis. Typical values for G_α are between 10^{-4} s^{-1} to 10^{-3} s^{-1} (Stauffer and Seaman 1990). The analysis confidence factor, ε_α, ranges between 0 and 1, and depends on both the quality of the observations and the spatial distribution of the observations that are used to create the analysis. The analyzed (observed) field at each grid point is represented by $\hat{\alpha_0}$.

The analysis-nudging approach of Stauffer and Seaman (1994) and Shafran et al. (2000) is used to assimilate gridded EDAS 3-D analyses generated by the National Center for Environmental Predictions (NCEP). These analyses are based on standard radiosondes taken by the National Weather Service (NWS), plus surface observations, data collected from commercial aircraft, radar wind profilers, etc. These analyses are available at 12-h intervals and are also used for the model's initial and lateral boundary conditions (described in Section 3.3.2). The 3-D analysis nudging is applied for wind, temperature and water vapor mixing ratio on the 36- and 12-km grids (summary given in Table 2). Table 2 also shows that the nudging coefficient, G, which determines the e-folding time (or rate) of the assimilation, is decreased on the 12-km domain, where mesobeta scale features become important in the model solutions.

Table 2. Summary of analysis-nudging parameters. Temperature is *T*, moisture is *q*, and *u* and *v* are the east-west and north-south horizontal wind components, respectively.

	3-D data	Nudging Factor, G
Source	108-km analyses based on NWS radiosondes	
Frequency	12 h	
Data types	u,v,T,q	108 and 36 km domains:
		G (U, v, T) = 3 X 10^{-4}
	(limited to region above 850 mb in Exps. 2D, 3A and 3B)	G(q) = 1 X 10^{-5}
		12 km domain:
		G (U, v, T) = 1 X 10^{-4} s^{-1})
		G(q) = 1 X 10^{-5} s^{-1}

As revealed in Table 2, the analysis-nudging approach described by Shafran et al. (2000) does not allow assimilation of the 3-D fields of wind, temperature and moisture below 850 mb. This strategy ensures that surface-based mesoscale features generated by the model (e.g., the sea-breeze and land-breeze) are not damped as a result of assimilating coarse-grid analyses that may not adequately resolve these mesoscale circulations.

No analysis nudging is applied on the 4-km and 1.33-km grids because the analyses, based on radiosonde data, cannot resolve the mesoscale features expected to develop on this domain. However, assimilation of the gridded analyses on the coarser grids still can have a positive impact on the 4-km and 1.33-km solutions by improving the accuracy of the lateral boundary conditions supplied from the 12-km domain.

3.2.1.3 Coupling to CALMET, A Meteorological Driver

One goal of the project is to demonstrate the use of the MM5 generated, meteorological fields to drive the EPA Guideline dispersion model, CALPUFF. Unfortunately, CALPUFF is not currently configured to read MM5 files directly, but is instead designed to read records generated by the CALMET meteorological model.

The CALMET Meteorological Model (Scire et al., 2000a) is a diagnostic meteorological modeling package capable of producing 3-D wind and temperature fields along with 2-D micro-meteorological fields (i.e., friction velocity, u*, convective velocity scale, w*, Monin-Obukhov length, L, and mixing height, H) that characterize the atmospheric boundary layer. CALMET was originally designed to be driven exclusively with standard NWS/NCDC (National Climate Data Center) weather data products, including surface, upper-air, and precipitation station data, but was subsequently modified to accept output from prognostic models, such as CSUMM and MM4/MM5 to enhance the realism of the diagnostic wind-field solver in data-sparse regions.

In this study, the primary role of CALMET is to serve as an intermediary between MM5 binary output and CALPUFF input. This role as a simple data re-formatter for MM4/5 was once considered by CALMET's developers, but later abandoned due to incompatibilities with MM4 coordinates and dissatisfaction with some of the original MM4 variable determinations, including mass divergence and mixing height. More recent upgrades to the turbulence physics by Shafran et al (2000) have alleviated many of the inconsistencies related to mixing-height calculations. Therefore, in this project, a brief attempt was made to resurrect this direct mode (called MM4ONLY), as its existence would greatly simplify and enhance the interface of the MM5 and CALMET models. However, the effort was halted when it was seen to require a major coding effort and would also create confusion as to whether the EPA-approved CALMET model was providing mass-consistent winds for CALPUFF or was merely serving as a conduit for MM5 data.

The only, currently-approved way to include the MM5 prognostic winds is to use CALMET's DAT.MM5 option by converting the MM5 output to pseudo-radiosonde soundings and include various radius-of-influence parameters in CALMET's control file, so that the user can dictate the relative weighting of real observations versus these pseudo-observational data. This mode of operation utilizes the prognostic horizontal wind components and temperatures, but ignores the micrometeorological boundary layer information generated by MM5.

Thus, generation of a meteorological data base, suitable for driving CALPUFF and based primarily on MM5 output fields, is somewhat more tedious to produce and involves the multiple steps, as described in detail in Sections 3.2.1.3.1 and 3.2.1.3.2.

3.2.1.3.1 MM5 Data Conversion to CALMET Input

The MM5 output files produced by Version 3 of the model are large, IEEE-standard, binary files. The large size of these files (about 690 MB per modeled day in this study) is dictated by the domain size (i.e., 115 by 115 grid points at 1.333 km horizontal resolution), the number of vertical levels (i.e., 50 levels from the surface to a pressure level of 50 mb or height of about 17 km) and the output frequency (1 hour intervals in this study).

Conversion of these MM5 output data to the more traditional pseudo-radiosonde input for CALMET is accomplished using the Earth Tech produced program, CALMM5. Unfortunately, the CALMM5 program has not yet been re-coded to read the MM5, Version 3 binary data, but requires the older, Version 2 binary format. Conversion of the rather new Version 3 binary file format to a comparable Version 2 output record structure is accomplished with the NCAR provided program V32V2. This older and somewhat bulkier structure (e.g., V3 header records are repeated in each V2 hourly output record) is then read by CALMM5. This program then takes the V2 data as input and creates vertical profiles of wind and temperature at each MM5 horizontal grid point. CALMM5 then writes these profiles to an ASCII file (with the file extension .MM5) that can be read directly by CALMET.

CALMET requires that these .MM5 records have header records that indicate the hour of the day as 00, 01 through 23. One problem we uncovered is that the V3 output records are frequently written a few seconds before the end of the hour, whereas the V2 outputs were always exactly on the hour. While not a conceptual problem, it can have serious consequences if the output record time of 01:59:59 is converted to hour 01 rather than rounded up to hour 02. We have modified the V32V2 conversion program to correct this minor problem and have altered the file “open” statements in V32V3, so that an IEEE V3 file produced by MM5 operating under LINUX may be read, while a Windows-compatible, COMPAQ compiler, standard binary V2 file is output.

The CALMM5 program was also compiled with the COMPAQ compiler, and .MM5 ASCII output files for subsequent input to CALMET were produced for:
i) test runs using the 12-km resolution MM5 data; and
ii) production runs using the 1.3333-km resolution MM5.

3.2.1.3.2 CALMET Input File Preparation

In addition to the above-mentioned .MM5 file, CALMET also requires:

- a geophysical input data file, GEO.DAT;
- a data file (e.g., UP.DAT) from at least one upper-air station;
- a data file (e.g., SURF.DAT) from at least one surface meteorological station; and
- a run control file, CALMET.INP.

The GEO.DAT file contains information on the land use category and terrain height for each horizontal cell in the simulation, and its preparation can be quite labor intensive. We have modified the CALMM5 program so that it simultaneously generates a GEO.DAT file for the MM5 domain (or sub-domain) selected in the CALMM5.INP control file. This is adequate provided that there is no intention to run CALMET on a scale finer than the fine MM5 scale of 1.3333 km, yet provides the user with the option to quickly produce CALMET runs on horizontal sub-domains of the full MM5 domain (i.e., of 115 by 115 gridpoints). As the outer-most boundary cells of MM5 simulations are generally not considered as reliable as interior portions of the grid, and in the interest of producing files of more manageable size, a 90 by 90 subdomain of the MM5 domain was chosen for all production runs of CALMET involving the 1.3333-km domain. This choice also means that only a 90 by 90 array of pseudo-radiosondes are output by CALMM5 to the MM5.DAT file.

The need for an upper-air, "UP.DAT"-style, file from at least one upper-air station would seem a bit unnecessary in applications involving use of MM5 data, as radiosonde soundings are taken only once every 12 hours, whereas MM5 "sounding" data is available every hour. To satisfy this CALMET requirement, we modified CALMM5 further, so that it outputs at least one profile (e.g., near Chatham) in the requisite UP.DAT format. This does represent a redundant use of the same data for both the .MM5 and UP.DAT file; however, this is not a problem and it enables CALMET to run in an “approved” mode. It should also be noted that CALMET runs are often made using “distant” radiosondes (i.e., located far from the modeling domain so as to exert little or no influence on meteorology within the domain) to circumvent the minimum one station requirement for the twice-daily radiosonde data that is much lower in space-time resolution than the MM5 profiles.

The SURF.DAT file containing surface data also seems a bit superfluous; however, it is minimally needed for the cloud cover observations taken at surface stations, as this is used in CALMET to compute stability class. The SURF.DAT file was constructed using data from the Hyannis Airport, as this data was thought to be much more relevant to the UCC domain than

NCDC data from T.F.Green Airport in Rhode Island. Unfortunately, the airport file format differs somewhat from the standard NCDC format, so a small conversion program was written to convert airport data to the SURF.DAT file structure.

CALMET run control files, CALMET.INP, were developed for each of the three chosen episodes. CALMET contains literally dozens of switches and options and the best way to understand these choices is to look at an existing CALMET.INP file with the help of the CALMET Graphical User Interface (GUI). For example, some of the more important option settings used in these runs are:

IRTYPE=1 to computes wind fields and micrometeorological variables
(u*, w*, L, zi, etc.)

LCALGRD = T computes added fields, such as 3-D fields of W velocities.

LLCONF = T rotates input winds from true north to map north
using a Lambert conformal projection.

NZ = 15 selects the number of vertical layers.

ZFACE=0.,20.,50.,100.,150.,200.,250.,300.,400.,500.,750.,1000.,1500.,
2500.,3500.,4500. gives the values of the NZ+1 cell face heights (m).

Given the space-time density of input MM5 wind data, additional CALMET.INP choices were guided by the intent to avoid any data extrapolations and minimize the role of supplementary surface and upper air data files. In fact, it was quickly discovered that inclusion of the Hyannis Airport surface winds created anomalous W fields in the CALMET output. These resulted from the fact that differences between MM5 and observed surface winds were compensated for with large W values. To avoid this problem, the coordinates of Hyannis Airport were shifted to the left-hand edge of the grid. Incidentally, another way to accommodate these differing airport winds would be to leave the airport coordinates unchanged and choose a very small "radius of influence" of surface stations.

3.2.1.4 Coupling to Trajectory and Dispersion Models

The MM5 model's meteorological fields are written out at 1-h intervals. These files are later ingested into the trajectory calculation program (Section 3.2.2.1) and the dispersion models (Sections 3.2.2.2, 3.2.2.3, and 3.2.2.4). For each of these trajectory and dispersion models, a simple interface code has been written to re-format the standard MM5 outputs into the form expected by the subsequent programs. The variable fields needed by these programs are the 3-D fields of p, u, v, w, T, and q. With the availability of the re-formatted fields, the trajectory and dispersion models operate independently, using the MM5 products as external meteorological drivers. That is, there is no feedback from the trajectory and dispersion models to the MM5.

3.2.2 Trajectory and Dispersion Models Employed

3.2.2.1 TRAJEC, a Trajectory Model

The Penn State TRAJEC program is designed to calculate the trajectories of one or more particles (or, parcels) based on a set of gridded 3-D wind data (u, v and w) distributed in space and time. TRAJEC operates with wind fields supplied by the MM5 mesoscale model (or analyses on a MM5-compatible grid) at uniform time intervals (1-h intervals in this case). Both forward and backward trajectories can be calculated. If vertical velocities are not available, TRAJEC can move parcels along constant-height-above-ground surfaces, or quasi-horizontally along constant-pressure or constant-potential temperature surfaces. In any case, the movement of particles is diagnosed through a series of small time steps using a two-step iterative process using a small time step of perhaps five minutes. The two-step iterative approach is designed to reduce transport error that can occur in curved flow when the wind at the beginning of a time step is assumed to apply throughout the interval. By using the iterative approach the trajectory calculations remain quite accurate, even without reducing the time step to very short intervals.

Parcels can be defined three ways: (a) individually, (b) as a series of particles released at specified time intervals from a given point (simulating a smoke stack), or (c) as a cloud of regularly spaced points over a specified sub-region of the domain. Particles are deactivated if they leave the domain through the lateral boundaries, but no deposition is allowed to the surface. TRAJEC includes a simple plotting package that shows the motion of the parcels in either the X-Y plane or the S-Z plane (where S is the horizontal distance downwind from the release point, following the flow).

TRAJEC provides a useful complement to a plume dispersion model, such as those discussed below, because it helps to isolate the role of transport while ignoring diffusion. Thus, by using both TRAJEC and a plume dispersion model, it is possible to investigate more thoroughly how important organized mesoscale circulations are to the dispersion of a plume over many hours. For example, in the case of the sea breeze, a plume may undergo shearing as it is advected in a solenoidal circulation that is modified by interaction with the large-scale wind field. In this case it can be difficult to isolate the role of the individual processes when using only a dispersion model because diffusion of the plume eventually broadens it so much that its response to a particular mesoscale feature can be indistinct. However, a particle trajectory based only on the

3-D resolved-scale wind field can be used to identify the role of local changes in the transport speed or direction that occur along specific boundaries in the atmosphere, such as the sea-breeze front. This aids in the interpretation of the overall dispersion represented in a plume model.

3.2.2.2 SCIPUFF

The SCIPUFF (Second-order Closure Integrated Puff) model is an advanced Gaussian-puff model developed at ARAP/Titan Corporation (Sykes et al. 1996, Sykes et al.1998). The dispersion model is based on a collection of 3-D Lagrangian "puffs" emitted from one or more sources, each having Gaussian concentrations that change over time as the puffs undergo transport and diffusion. SCIPUFF uses second-order closure turbulence techniques to relate measurable velocity statistics to the predicted dispersion rates. Together, these puffs describe the evolution of the three-dimensional concentration field over a range of spatial scales downwind of the source location. An important aspect of SCIPUFF is that the closure model provides a direct prediction of the statistical variance in the concentration field, so that the inherent uncertainty in the turbulent wind field can be used to estimate the uncertainty in the predicted plume dispersion.

SCIPUFF can make use of inhomogeneous velocity fields, such as produced through objective analysis or numerical predictions, by including a complete moment-tensor description for shear distortions and turbulent transport. The Lagrangian framework of SCIPUFF avoids the artificial diffusion problems that are associated with dispersion calculations performed on an Eulerian grid. The individual puffs increase in size due to shear distortions and turbulent dispersion and may grow in scale from a few meters to thousands of kilometers across. The puff method is very robust under coarse-resolution conditions (Sykes et al. 1998), but as a puff grows, local conditions at its centroid may no longer be representative of the entire puff. Therefore, SCIPUFF uses a splitting algorithm to divide the original puff into two smaller puffs whenever the puff size exceeds a critical value that depends on the resolution of the velocity field. By maintaining smaller puffs as the plume broadens with time, the dispersion model minimizes errors by avoiding highly inhomogeneous large puffs. On the other hand, in time the splitting algorithm could produce a very large number of puffs that would eventually cripple model efficiency. To prevent this, a merging algorithm combines overlapping puffs using a mass-conserving adaptive multi-grid approach. The efficiency of SCIPUFF also is aided by an adaptive time-stepping scheme that depends on the turbulence time scale, advection velocity, shear distortion rates and other physical processes. Each puff determines its own time step, that lengthens as the puff becomes larger and the relevant time scales grow.

While it is possible to uniquely describe the statistical mean value of concentrations in a turbulent environment (i.e., deterministic solutions for the means), the randomness within the turbulent fields produces uncertainty in the instantaneous solutions for dispersion problems. SCIPUFF also provides a quantitative value of the random variations in the concentrations due to the stochastic nature of the turbulent diffusion process (Sykes et al. 1998). The key aspect of the fluctuation variance prediction is the dissipation time-scale based on the internal fluctuation scale (Sykes et al. 1984, 1996). The variance prediction provides a quantitative probability distribution for the local concentration using the assumption of a clipped normal shape function (Lewellen and Sykes 1986). This probabilistic description of concentrations is the only meaningful way to describe and quantify the uncertainties in the field due to the randomness of the turbulence.

The mesoscale and synoptic-scale meteorological inputs to SCIPUFF (primarily winds and temperatures) can be specified as 3-D gridded fields, or the dispersion model can analyze these fields from a set of surface and upper-air data using an interpolation based on inverse-square distance weighting. The dispersion model also can accommodate irregular topography with a terrain-following vertical coordinate, similar to the MM5. Boundary-layer turbulence profiles can be specified directly, as from LES, but are usually diagnosed based on estimates of the surface heat flux and the shear stress, much like the turbulence source terms in the predictive equation for TKE used by Shafran et al. (2000). Source material can be introduced into the meteorological environment three ways: (a) as an instantaneous release, (b) as a steady plume over a specified time period, and (c) as a moving source. Thus, SCIPUFF can easily represent conditions encountered in a variety of cases, such as an explosion, a stack plume, or a moving ship plume.

3.2.2.3 ISCST3

The current EPA approved dispersion model for relatively level terrain areas is the Industrial Source Complex Model Short Term Version 3 (ISCST3) (EPA, 1995) is recommended in EPA's Guideline on Air Quality Modeling for applications to point sources (such as power plants), line sources (such as highways), and area sources (such as land fills or an area wide grouping of small sources). ISC3 is based upon the Gaussian –plume equation and assumes that contaminants flow in a straight line trajectory path from the emission point according to a single wind speed , direction and atmospheric stability condition.. It is typically used with a minimum of requirements for meteorological input data (e.g., nearest National Weather Service (NWS) wind speeds and directions, ceiling heights, cloud cover, and related determinations of the Pasquill-Gifford atmospheric stability classification for each hour). ISC3 is generally run with a sequence of hourly meteorological conditions to predict concentrations at receptors for averaging times of one hour up to a year. For any given hour, ISC3 assumes that dispersion conditions (i.e., wind, temperature, and turbulence fields) are the same at all spatial locations with the exception of close-in areas affected by building or structure downwash. The model is widely used for applications where the maximum concentrations are expected to be associated with downwash or conventional dispersion phenomena. The model is commonly used out to 50 km from a source, despite the fact that dispersion conditions are rarely uniform in space or constant in time for such distances. On the other hand, if the model is used to estimate concentrations at short distances from a source using local and representative meteorological data, the model can be expected to perform reasonably well. ISCST is the simplest model used in this study, and it is useful to compare the prediction from this model to those of the most complex models

3.2.2.4 CALPUFF

The CALPUFF model (Scire et al., 2000b) is a model that is seeing increasing use in regulatory applications. CALPUFF's integration with CALMET, a three-dimensional diagnostic meteorological data preprocessor, provides the ability to simulate realistic pollutant transport and dispersion over distances ranging from tens of meters to many hundreds of kilometers — a considerable advance over traditional, straight-line Gaussian plume models. Additionally, the CALPUFF system contains algorithms to simulate a wide variety of physicochemical phenomena including pollutant deposition and reaction/formation, building downwash, complex terrain flows, and land-water transitions. We now consider the workings of CALPUFF in greater detail and list other features along with their selection via CALPUFF's control file.

3.2.2.4.1 CALPUFF Modeling Fundamentals

Basically, the CALPUFF model simulates the impact of a source by creating puffs that correspond to source emissions released at intervals of a few minutes to one hour. The emission time represented by a single puff is determined internally based on several constraints, such as requiring this emission time, Δt_m, be less than the advective time scale, $\Delta t_a = \Delta x_m/u$, for the wind to move a puff across the cell size, Δx_m, of the meteorological input. In the case of using input winds having the high-spatial-resolution of 1.3333 km., a typical wind of several m/s would serve to limit Δt_m to a few hundred seconds. Thus, the emission from a single point source might demand ten or more puffs per hour. An interesting feature of the CALPUFF model that distinguishes it from its predecessor, MESOPUFF, is that it can also simulate emissions using "time-integrated slugs" as an alternative to puffs. These pollutant slugs yield receptor concentrations that are integrated over the source emission time and integrally-averaged over the receptor time, thus, eliminating the need for time-consuming, numerical integration to achieve desired accuracy. Another advantage of slugs is that under "steady-state" conditions (i.e., where the source strength is time-independent, the wind is constant in space and time, and Δx_m is quite large) and use of ISCST dispersion coefficients, one obtains a perfect match with the results of ISCST. This correspondence was seen as a very desirable reference point for a new regulatory model to gain acceptance and credibility. In practice, the teardrop shaped slugs also have some limitations. For example, slugs cannot exceed the cell size, Δx_m, as it cannot be assumed , in general, that the wind is the same in the adjacent cell. Also, older slugs being transported by changing winds, may travel across receptors at various oblique angles, and this condition requires a numerical integration over receptor time that can make this approach more computationally expensive than the case of using puffs. Hence, slugs are generally converted to equivalent puffs as soon as is reasonable (i.e., based on a number of constraints, such as the along-wind/cross-wind aspect ratio of the tear-drop shape relative to a circular puff).

One facet of the model that can be particularly important in coastal or mountainous environments is that CALPUFF transports slugs and puffs only using the horizontal wind and not the vertical component. This aspect results in a certain "robustness" (Chang, 2000) of its predictions relative to other puff and/or particle models that also allow Z-transport; however, it also means that certain phenomena involving significant updrafts and downdrafts, such as sea breezes and land breezes respectively, may not be simulated realistically. Recognizing this limitation, the developers recently added a provision that makes a puff grow in height in a convergence zone (i.e., a zone where there is significant updraft). In effect, this moves the center-of-mass of the puff upward and creates enhanced puff dilution without "lifting" ground-level puffs off the ground entirely. This is actually quite reasonable, because W velocities always must vanish at the impenetrable ground, so that updrafts are actually shear flows which stretch the puff in the vertical. Of course, elevated plumes would, in fact, be shifted upward by these updrafts, so not all aspects of updrafts are handled appropriately by the current treatment.

Presently, downdrafts are not treated in a comparable fashion -- or at all. This has important ramifications for the current study, where broad subsidences, involving downward W velocities of exceeding 5-10 cm/s can exist over much of the UCC region for hours at a time. This occurs particularly during nighttime hours, coinciding with one or more simultaneous land breeze situations and when vertical plume dispersion rates are already at low values of only a few cm/s. Such downward W velocities would cause elevated plumes to sink toward the ground and would cause ground level plumes to grow at reduced rates (or even contract) in the vertical while spreading out more rapidly in the horizontal. Such plume behaviors could cause ground-level exposures from elevated and surface releases to rise markedly in reality. Though such plume behavior is not considered in the EPA's ISCST model, it is not totally foreign to EPA models. For example, the CTDM+ model for dispersion in complex terrain allows for such effects in the transport of plumes over 3-D hills and 2-D ridges under stable conditions. In such cases, the flow speedup causes a compensatory vertical compression of streamlines, and thus shrinking plume σ_z. Modification of the CALPUFF model to include these effects of downward W is quite feasible and would be a desirable feature to have for future UCC modeling efforts.

3.2.2.4.2 CALPUFF Features and its Control File

As with the CALMET model, CALPUFF can be run in a variety of different modes, and these modal choices are set in the control file, CALPUFF.INP. For example, the control file enables the user to:

determine the start time and duration of the simulation;
declare the names (and directory paths) of all the relevant input and output files;
determine the position and coverage density of the gridded receptors plus input special receptor locations as desired;
choose from among several different types of dispersion coefficients;
choose between slug or puff mode;
choose to enable puff splitting: an option that allows greater modeling realism in shear flows, but at a greater computational cost;
set the number and types of sources to be modeled;
introduce source parameters, such as X-Y coordinates, release dimensions, release height, buoyancy and momentum fluxes, and time-independent source strengths (n.b., time-varying sources require supplemental data or files);
allow for the detailed treatment of sub-grid scale effects, such as small hills, terrain barriers, and coastline shapes for the purpose of invoking a lake/sea breeze module; and
specify the details of various depletion and transformation processes, such as dry deposition, wet removal, and linearized chemical transformations.

The present CALPUFF model can simulate a variety of source types. It's current treatment of buoyant and non-buoyant point and area sources includes all of the effects currently in other EPA Guideline dispersion models that are custom-made for such source types. CALPUFF can also model the limited subset of "line-sources" that correspond closely to the rooftop line-emissions from aluminum smelters. Thus, CALPUFF's treatment of line sources is not compatible with the objective of modeling of major highway line sources. Such highway line sources can be simulated using the area source (or more-precisely, an arbitrary polygon shaped area source) algorithm. Thus. one may input a highway segment as a rectangle that is the width of the roadway and as long as one desires. Unfortunately, this approach runs into difficulties if the roadway segment length exceeds the size of the meteorological grid dimension, Δx_m. As demonstrated later in this report, such a limitation was encountered in our efforts to model the Cape's Route 6. Dividing the Route 6 highway segment into 15-20 separate segments of a kilometer or so in length would have improved the realism of our modeling efforts dramatically, but such segmentation by manual means is highly error prone. It would be relatively easy to build such an automatic segmentation algorithm into CALPUFF were it to be used routinely for roadway impact studies.

3.3 Meteorological Flow Field Evaluations

In this section, we will discuss the meteorological data gathered for our analyses and the evaluations of the flow fields predicted by MM5 and of the flow fields computed by CALMET, on the basis of MM5 inputs.

3.3.1 Meteorological Data Collection

Three two-day duration meteorological event cases involving sea breeze and land breeze flow phenomena were chosen from data collected in the year 2000 for simulation with the numerical model. Our recommendations for these cases included three categories:
(1) a 48-hour period in the late spring or early summer when a strong sea breeze effect would be expected. This season is chosen on the basis of the relatively large contrast between temperatures of the land and water bodies(2) a 48-hour period that typifies an average summer day when sea breeze effects would be expected.
(3) a 48 hour period from late summer or early autumn when a relatively strong land breeze effect might be observed.

For all three categories, the specific dates are selected based on the synoptic-scale winds and the availability of meteorological observations. We used three different information sources for these purposes.

The first is an interactive internet site provided by The National Climate Data Center (NCDC). This site allows one to review the analysis of meteorological data for any specific location in 3-hour time steps for any day that data are available. The data are interpolated from archived analyses to a specified location. This data set is useful to search for the overall synoptic features that commonly are associated with sea and land breeze effects. Because of the coarse grid resolution of the archived analyses, local flow effects are not specifically seen in this data set. We used this data source to identify days and nights with clear skies, high pressure, light synoptic scale winds, large variations in solar radiation and large surface temperature differences between land and the ocean.

The second source of data is the meteorological data collected at airports on or near Cape Cod. We have obtained these data from the Northeast Regional Climate Center at Cornell University for nine stations. The data from these stations is limited to information of primary interest to aircraft operations, but includes on-the-hour observations of wind speed and direction. Some stations do not report at night when many airports close down operations. However, the data that are available allow us to compare spatial and temporal meteorological patterns on the regional scale.

The third data source is from a network of anemometers at five beaches on the Cape and in Duxbury established by a wind surfing group. These are located at Chapin Memorial Beach (near Barnstable on the north shore), West Falmouth (facing west southwest), Kalmus Park (near Hyannis, facing south). West Dennis (facing south) and Duxbury (facing east northeast). We obtained several months of this information for the summer of 2000. Because of the shoreline locations, these are excellent indicators of the presence of on or off shore flows. The data have been analyzed to see if convergence or divergence of the shoreline winds can be detected. Convergence of the flows would be expected when inland-directed airflows occur simultaneously from shorelines on opposite sides of the Upper Cape.

Based primarily upon the analysis of the beach-front data and the seasonal and synoptic-scale meteorology supportive of sea and land breeze phenomena, the 48-h periods of July 1 and 2, July 5and 6, and August 22 and 23, 2000, were selected for numerical studies. These dates were provided to the modelers at MCP. As discussed below, the MCP modelers used additional data resources to obtain more extensive publicly available meteorological data for these time periods for purposes of setting up the MM5 runs.

3.3.2 Input Data for MM5

Generation of initial and lateral boundary conditions for the outermost 36-km domain of the MM5 begins with acquisition of gridded analyses produced by the National Center for Environmental Predictions (NCEP). Specifically, analyses of the Eta Data Assimilation System (EDAS) are accessed from the Ready website of the National Oceanographic and Atmospheric Administration (NOAA). The Ready website address is:

http://www.arl.noaa.gov/ready.html

Once the user has reached the Ready home page, choose the link to "*Archived Meteorological Products*." On the Archived Meteorology page, the next link to choose is labeled "*Detailed information on model data archives at ARL*." This link places the user on a page that has a series of links to various NCEP models, including EDAS. Scrolling down to the EDAS section, there is a link to a *Read-Me* file providing information on the EDAS data sets. The data themselves can be accessed for all dates from 1997 to the present by choosing the link *"Eta Data Assimilation System (EDAS, 1997-)*."

Software has been written by the Meteorological Consultants of Pennsylvania that allows the user to merely define the desired date, in order to retrieve and process the EDAS fields into the formats needed for input to the MM5. It should also be mentioned that the NOAA Ready website has additional very useful links that can be easily used to access satellite pictures (both visible and infrared) and to make plotted charts of analyzed fields. These tools are easy to use and can be very helpful for finding cases that may be of particular interest.

The EDAS archive on the Ready site provides gridded meteorological analyses at 80-km horizontal resolution for temperature, horizontal wind components and relative humidity on constant-pressure levels. Also, the fields of sea-level pressure and surface temperature are needed and are available in the same data sets. The 3-D fields are accessed at the following mandatory and supplemental pressure levels: 1000, 975, 950, 925, 900, 875, 850, 825, 800, 750, 700, 650, 600, 550, 500, 400, 300, 250, 200, 150, 100, and 50 mb. Next, the EDAS fields are projected onto the outermost MM5 domain through bi-linear interpolation. (Ground temperature is defined as surface temperature over land, and sea-surface temperature over water.) Finally, the pressure-level analyses are interpolated vertically onto the model's σ levels (also see Table 1) to be used as the initial conditions. The 36-km analyses also are interpolated to the successive nested domains (i.e., 12-km fields from the 36-km domain, 4-km fields from the 12-km domain and 1.33-km fields from the 4-km domain).

The lateral boundary conditions of the MM5's 36-km domain are defined at 12-h intervals from analyses generated exactly as those used for the initial conditions. Each of the inner domains receive their lateral boundary conditions directly from the next outer domain (parent domain) at one-hour intervals. This is known as a one-way lateral boundary condition, since there is no feedback from the fine grids to their parent domains.

3.3.3 Beachfront Wind Data

In addition to airport and NOAA meteorological data available on Cape Cod, we found a local network of anemometers established and operated by a meteorological group (Iwindsurf.com) and located at various Massachusetts beaches. The data provides information on the wind speeds and directions on the shorelines where one would expect to see evidence of on or off shore flows. Because the information is not a standard set to be used in the MM5 model, our use was primarily to identify time periods when converging or diverging flows associated with thermally driven circulations would be expected. Appendix A discusses this data and the analyses performed with it.

3.3.4 Local Airport Data

Meteorological data was obtained from the Northeast Regional Climate Center at Cornell University at the following nine stations for the year 2000:

Chatham Municipal Airport
Hyannis Barnstable Municipal Airport
Vineyard Haven Martha's Vineyard Municipal Airport
Nantucket Memorial Airport
New Bedford Municipal Airport
Plymouth Municipal Airport
Taunton Municipal Airport
Provincetown Airport
Providence T.F. Green State Airport.

The data from these stations is limited in detail. Some stations do not operate at night when the airports close down. However, the information is assimilated into the coarse grid data used to initiate MM5. In this study, we have used data from the Hyannis –Barnstable Airport to run the ISCST3. Appendix B shows a typical set of data for Hyannis-Barnstable Municipal Airport. The time period covered is for July 1 through July 2, 2000.

3.4 Graphics Modeling Capabilities Utilized

3.4.1 NCAR Graphics

The output fields from MM5 can be viewed using the NCAR Graphics software. This package is readily available as freeware from NCAR and is loaded onto the PC computer used for MM5 applications. The MM5 data are processed onto convenient plots (surface and constant-pressure levels) using the PSU/NCAR MM5 post-processor, called Graph. NCAR provides an online documentation to guide the novice user. The Graph representations of MM5 fields can be viewed on the computer screen (monitor) or sent to a printer to make a hard copy.

3.4.2 CalDESK

CALMET and CALPUFF output generally consists of binary records of hour-by-hour fields of meteorological variables or concentrations. Processing of these data further to extract longer-term averages or to extract data subsets for output to ASCII files that are conveniently input to commercial graphical packages, was performed by the post-processing program CALPOST. CALPOST is an extremely useful package, especially for repetitive processing of a great many CALMET/CALPUFF output file in "batch" jobs; however, it is not the easiest to use if one wishes to peruse CALMET files along with the corresponding CALPUFF output files. For this function, the third-party software package, CalDESK, is extremely convenient.

Developed by Dr. Luis Matamala and Francisco Matamala of Enviromodelling Ltda. of Santiago, Chile, CalDESK 2.52 is a visual analysis tool for the CALMET/CALPUFF/CALGRID models. It allows the user to dynamically visualize output data in a number of different ways, making analysis fast and easy. CalDESK has a user-friendly visual interface that permits a wide range of functions to be performed with a few mouse clicks. For example, one can display computerized base maps or CALMET's land-use data to serve as a surrogate base map. One can then display wind vectors or flow streamlines from a particular CALMET run, and then superpose CALPUFF concentration isolines for the corresponding period. In addition to these surface XY views, CalDESK can also consider vertical cuts in XZ or YZ that are linked to the basic XY plot. Once the desired variables are selected for display, the user can easily scroll forward or backward in time through the linked CALMET/CALPUFF records, run animations, or output any desired frames to graphics files (e.g., JPEG format) or to "clipboard" entries that can be "pasted" into most Windows-compatible, word processor files.

CalDESK also has two advanced modules for data analysis: a basic statistics package and trajectory analysis. The trajectory module was recently upgraded to permit generation of 3-D trajectories (i.e., trajectories sensitive to the W winds) as well as the traditional trajectories sensitive only to the U and V wind components.

Because of the unique enhanced value it provides to the output of CALMET and CALPUFF, this software was purchased for this project and for delivery to the BEHA computer.

3.4.3 SURFER

The ISCST3 results in this study have been plotted using a proprietary software package, SURFER. This software interfaces easily with ISC and is readily available through retail software dealers or directly from Golden Software Inc. (www.goldensoftware.com) of Golden, CO. This software is not included in the deliverables for this project.

4 Model Demonstrations

4.1 Description of the Meteorological Event Test Cases

4.1.1 Case 1: Sea Breeze 1

Case 1 is defined as the period from 0000 UTC, 1 July - 0000 UTC, 3 July 2000. 0000 UTC corresponds to midnight Greenwich standard time, also referred to as 00:00 Z in the text. Midnight at Greenwich is 4 hours later than Eastern Daylight Time (EDT) applicable to the study period on Cape Cod. Thus 0000 UTC corresponds to 8:00PM (or 20:00 in military units) of the previous day. Case 1 was chosen to be a representative episode of sea-breeze development over upper Cape Cod. To understand the meteorological environment in which this sea breeze occurred, we examined both objective and manual mesoscale analyses at various scales. First, Figure 5 shows the EDAS objective analysis of winds and sea-level pressures produced by NCEP on its 80-km display mesh at 0000 UTC (2000, EDT). At the beginning of the Case 1, a weak cold front extends from Quebec, Canada, to southern NJ and is passing over Cape Cod into the Atlantic Ocean. Behind this front, winds over NY and New England are mostly from the west-northwest, while winds ahead of the front are from the southwest. A second slowly moving cold front with a weak 1011 mb low lies several hundred kilometers to the east, but it does not affect the Cape Cod region in this case. Figure 6 shows the manual mesoscale analysis of sea-level pressure at this time over the same area covered by the MM5's 4-km domain. The mesoscale analyses are useful because they can be used to resolve local features missed by the synoptic-scale EDAS automated analyses. The frontal pressure trough and the accompanying wind shift are clearly visible over southern New England in Figure 6. Wind speeds behind the front over land are about 5-8 knots (kts), with somewhat stronger winds of 10-15 kts over the ocean to the east of the front.

By the next morning, at 1200 UTC, 1 July, the cold front had moved about 200 km east of the New England coast and was beginning to dissipate (Figure 7). The pressure gradient over New England had weakened during the previous night, thereby reducing the large-scale geostrophic forcing of the winds and setting the stage for near-stagnant background conditions that are ideal for a sea breeze to develop. Winds over land were light and variable at this time. The manual analysis for 1800 UTC (1400 EDT) that afternoon (Figure 8) shows that the pressure gradient had continued to weaken and the cold front had dissipated. Winds over most of New England and eastern NY were from the northwest at 4-8 kts, but along coastal areas of RI and Cape Cod, they had shifted to become southwesterly (onshore). In Massachusetts Bay, a few observations indicate winds from southeast to northeast (onshore directions). This wind pattern indicates a coastal sea breeze has developed over RI and southeastern MA. Similar onshore winds are evident northward along the coast from MA to ME.

REAL-TIME ENVIRONMENTAL APPLICATIONS AND DISPLAY SYSTEM
http://www.arl.noaa.gov/ready.html

Click here for any error messages.

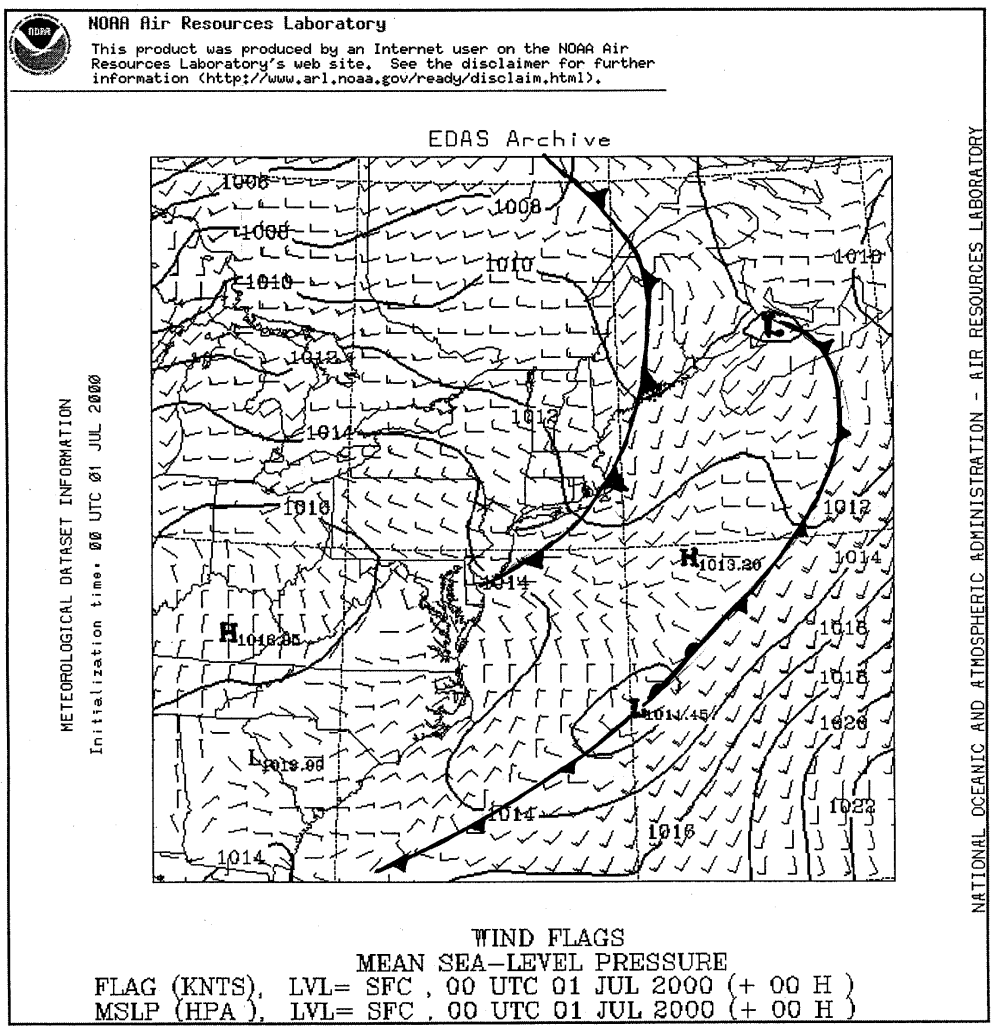

Figure 5. EDAS objective analysis of sea-level pressure (mb) over the Northeast U.S. for Case 1 at 0000 UTC, 1 July 2000. Isobar interval is 2 mb. Wind speeds (kts) are shown at 80 km resolution. Full barb = 10 kts, half barb = 5 kts. Fronts are analyzed manually based on winds and pressures.

Observed Data From 00UTC 01JUL2000

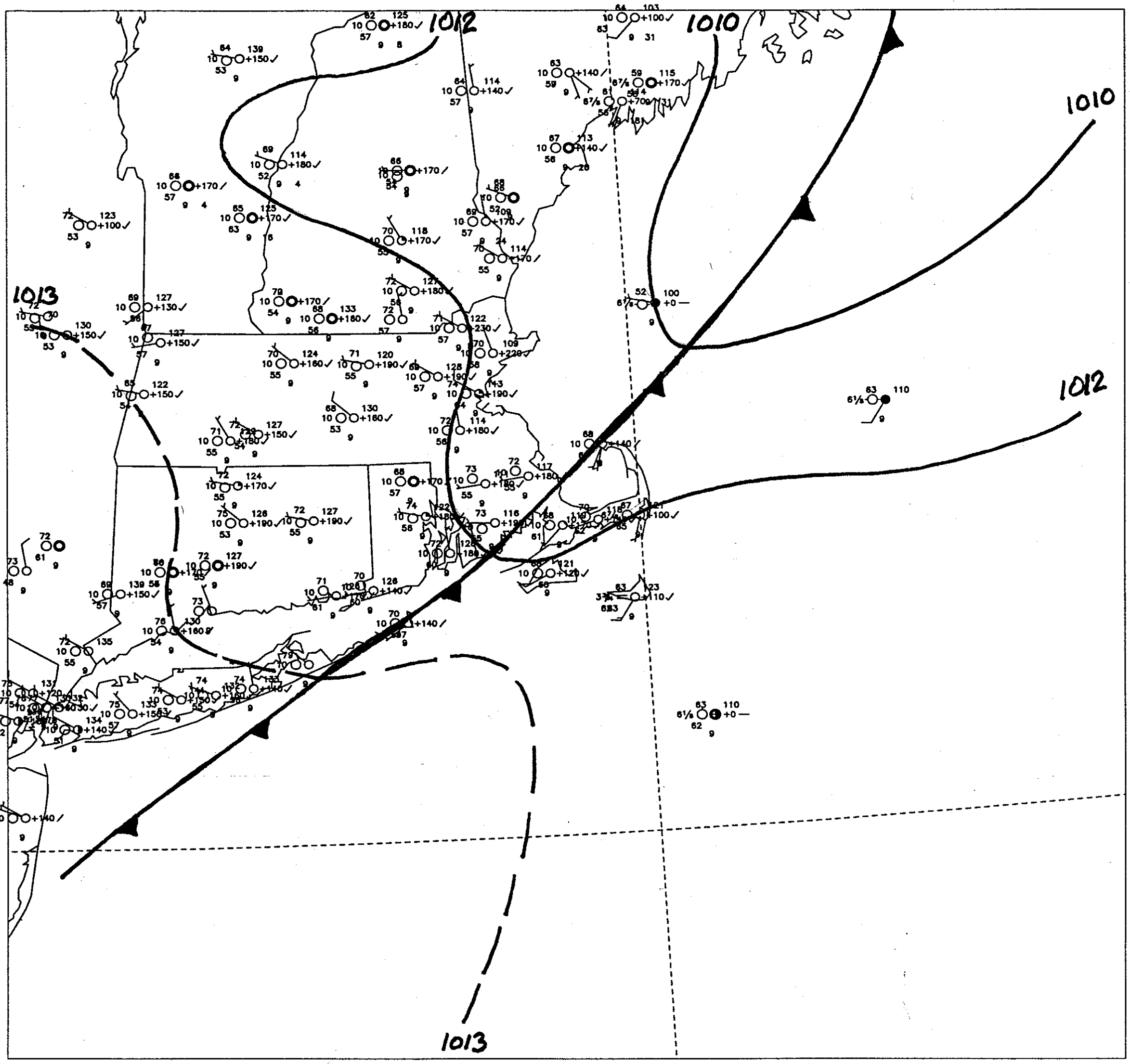

Figure 6. Manual analysis of sea-level pressure (mb) over the area of the 4-km MM5 domain for Case 1 at 0000 UTC, 1 July 2000. Standard isobar interval is 2 mb, with intermediate isobars shown as dashed lines.

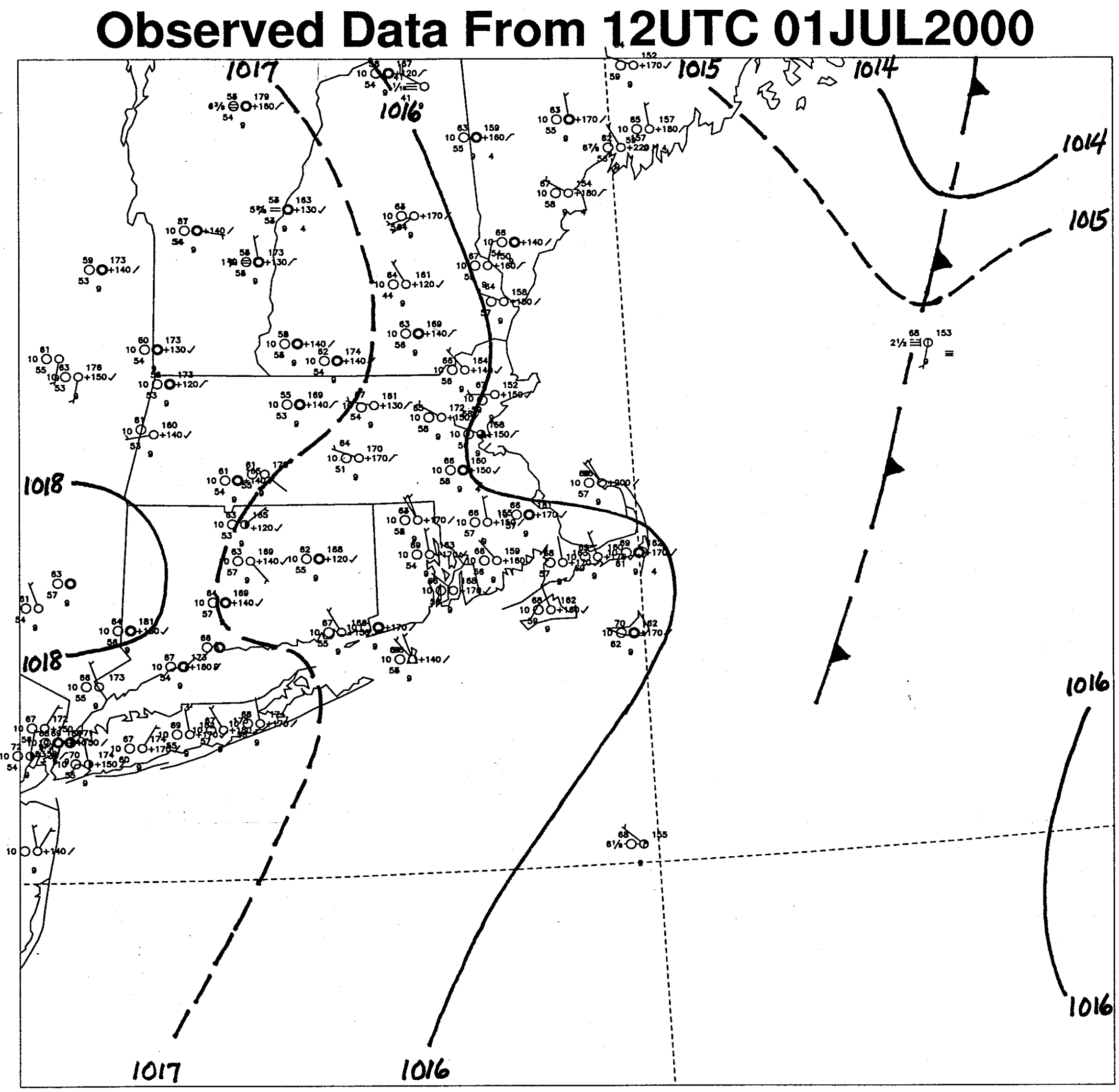

Figure 7. Manual analysis of sea-level pressure (mb) over the area of the 4-km MM5 domain for Case 1 at 1200 UTC, 1 July 2000. Standard isobar interval is 2 mb, with intermediate isobars shown as dashed lines.

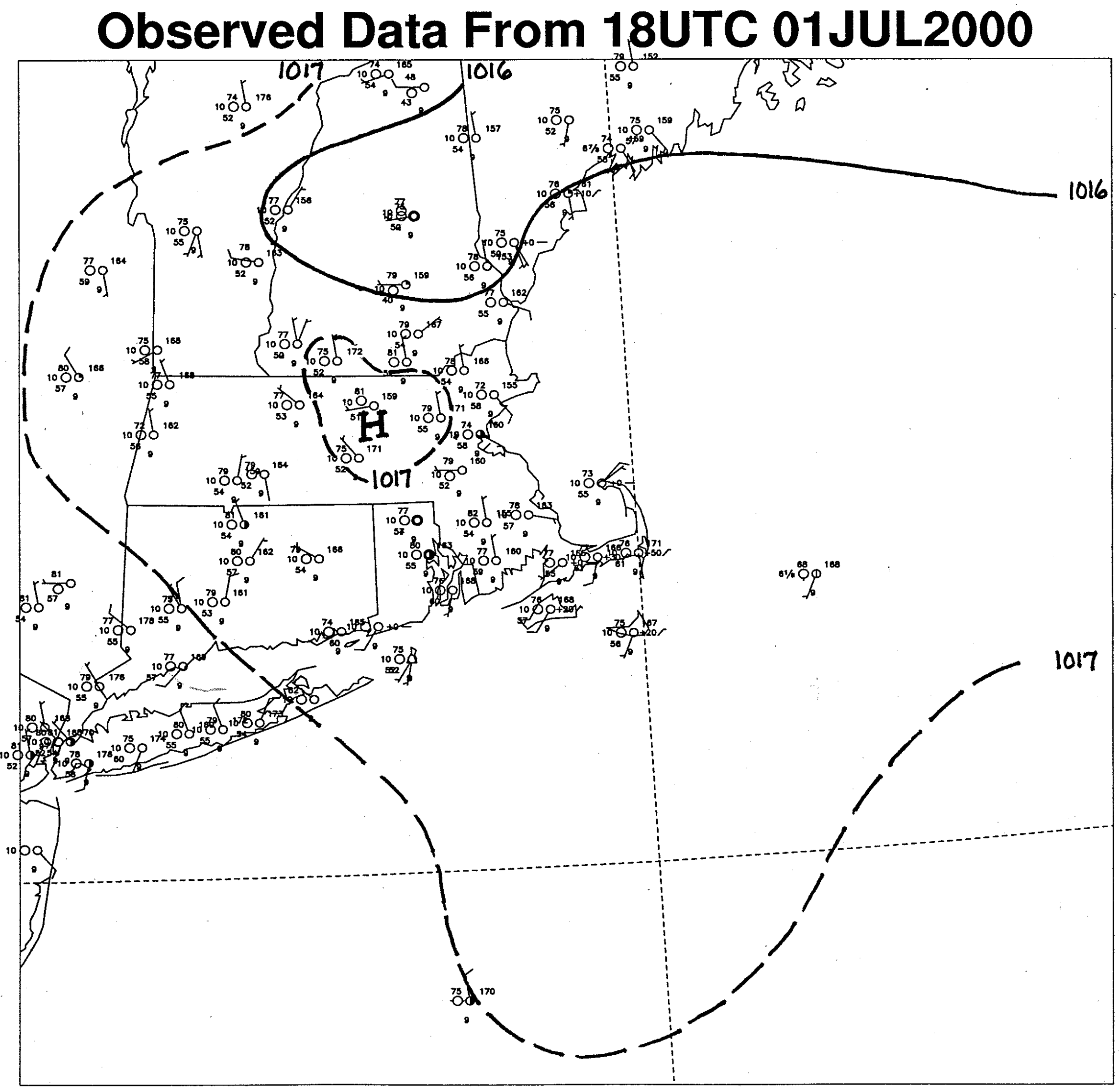

Figure 8. Manual analysis of sea-level pressure (mb) over the area of the 4-km MM5 domain for Case 1 at 1800 UTC, 1 July 2000. Standard isobar interval is 2 mb, with intermediate isobars shown as dashed lines.

By early evening, 0000 UTC, 2 July, two weak low-pressure centers had developed over southern New England (Figure 9). The regional scale background pressure gradient remained extremely weak at this time, so it seems likely that these low-pressure centers are the result of the diurnal heating of the land mass, relative to the ocean to the south and east. These thermally induced lows are so weak that they do not force cyclonic winds to develop, except in very localized areas. Winds along the coast continue to have onshore components from RI to ME. However, notice that the prevailing regional wind direction from NY through New England has shifted southwesterly by this time, so that it is less apparent whether the coastal winds still represent a strong sea breeze circulation. The general southwesterly flow continued and intensified somewhat through the night, so that the manual analysis on the following afternoon, 1800 UTC, 2 July, shows stronger pressure gradients than during the previous afternoon (Figure 10). Consequently, the sea-breeze pattern over Cape Cod is less obvious on 2 July because (on the south coast) it is in the same general southwesterly direction as the prevailing regional flow. Speeds in this area are about 8-13 kts at 1800 UTC. From Boston northward, southerly and southeasterly winds along the New England coast indicate clearly indicate a moderate sea breeze in that area that is distinct from the regional flow.

Returning to 1 July, the observations in Figures 11-13 show the influence of the sea breeze in 3-h intervals from 1800 to 0000 UTC. The approximate position of the sea-breeze front is shown in these manual analyses (dashed line with wedges showing the direction of movement of the marine air), within the accuracy that is possible from the spacing of these observations. Figure 11 indicates that, by 1800 UTC, 1 July, the sea breeze had already penetrated inland approximately 10-20 km. The thermally induced low over southeastern MA shown in Figure 11 was not obvious on the larger domain shown in Figure 8, but it is evident that it is the same pressure center found in this area a few hours later in Figure 9. Notice that the local winds that lie to the south and east of the sea-breeze front in southeastern MA are mostly directed toward the low, while those farther east on Cape Cod are mostly from the southwest in the direction of the prevailing synoptic-scale flow. This pattern seems consistent with a mature sea-breeze circulation, given the land-sea distribution of this domain. Next, at 2100 UTC (1700 EDT), when the sea breeze should normally have reached or passed its peak intensity, Figure 12 shows mostly the same wind pattern. However, the sea-breeze front has penetrated somewhat farther inland (~15-25 km) in the direction of the thermal low. The wind observations over Cape Cod in Figures 11 and 12 suggest that the southwesterly sea-breeze flow may extend across the entire upper peninsula, with very little if any reversal to give an onshore flow (from the north) on the north shore of the upper Cape. Given these observations, if such a reverse sea-breeze does exist on the north shore, it is likely to be fairly weak and should not penetrate more than 1-2 km inland.

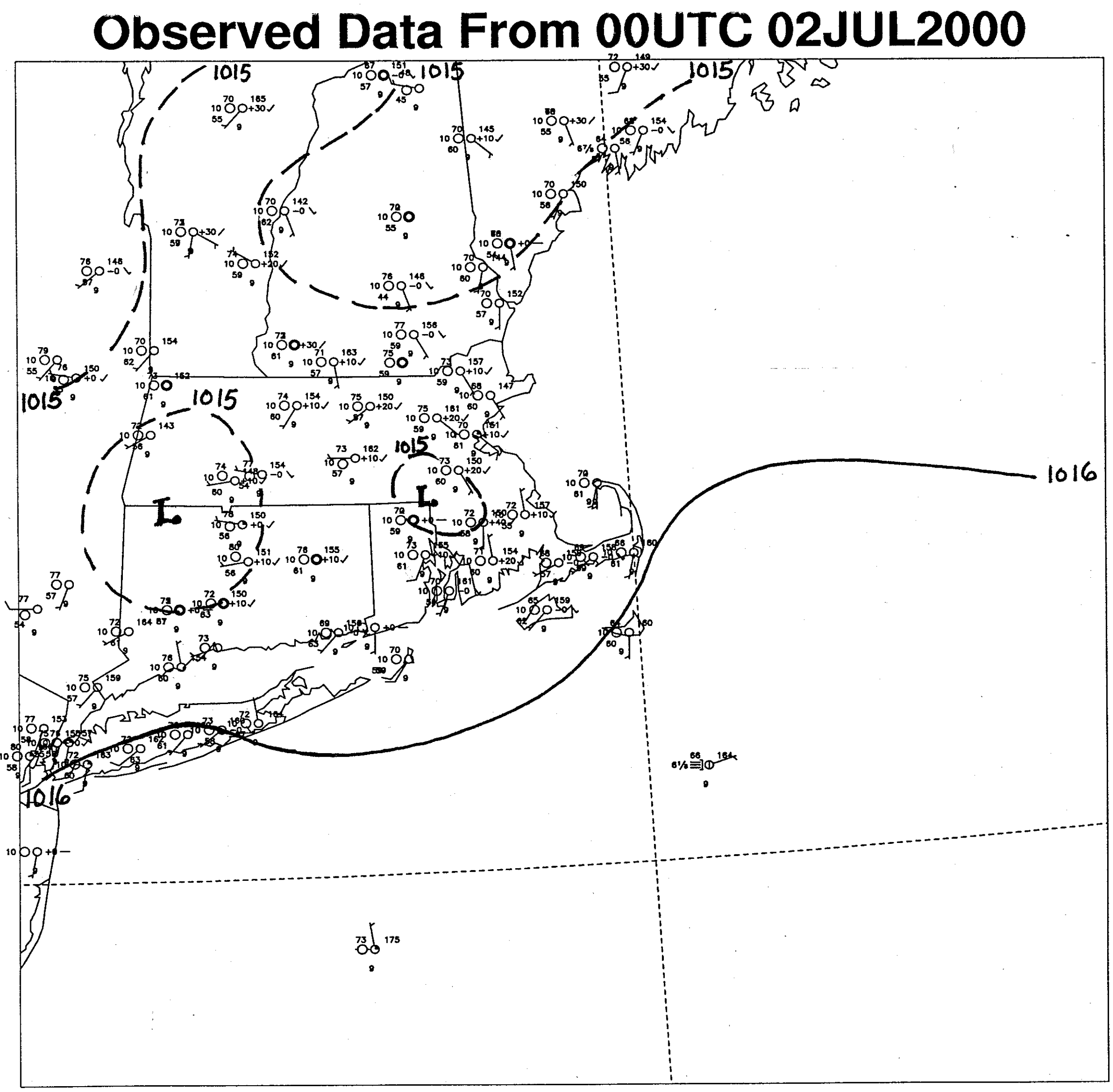

Figure 9. Manual analysis of sea-level pressure (mb) over the area of the 4-km MM5 domain for Case 1 at 0000 UTC, 2 July 2000. Standard isobar interval is 2 mb, with intermediate isobars shown as dashed lines.

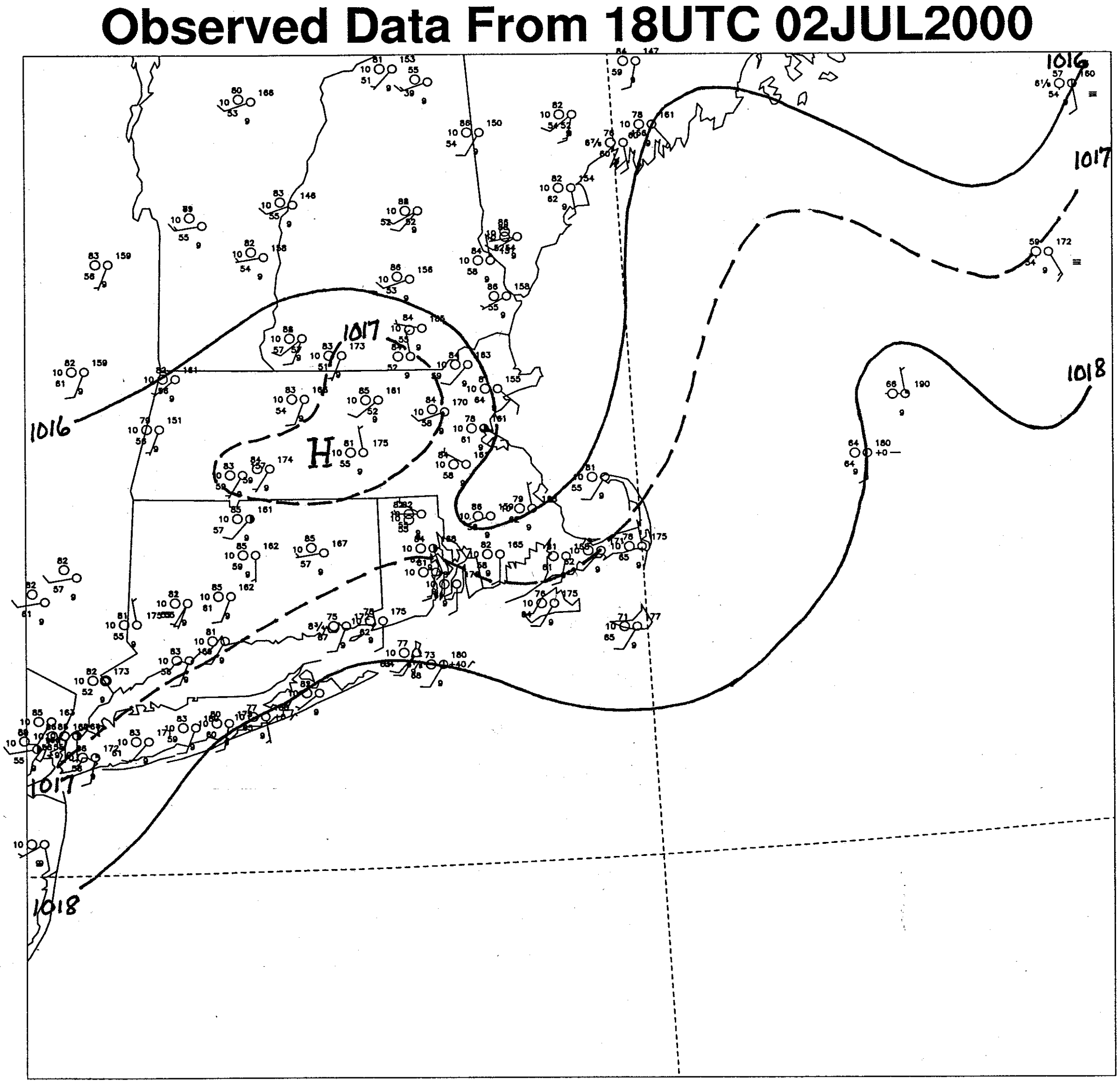

Figure 10. Manual analysis of sea-level pressure (mb) over the area of the 4-km MM5 domain for Case 1 at 1800 UTC, 2 July 2000. Standard isobar interval is 2 mb, with intermediate isobars shown as dashed lines.

Observed Data From 18UTC 01JUL2000

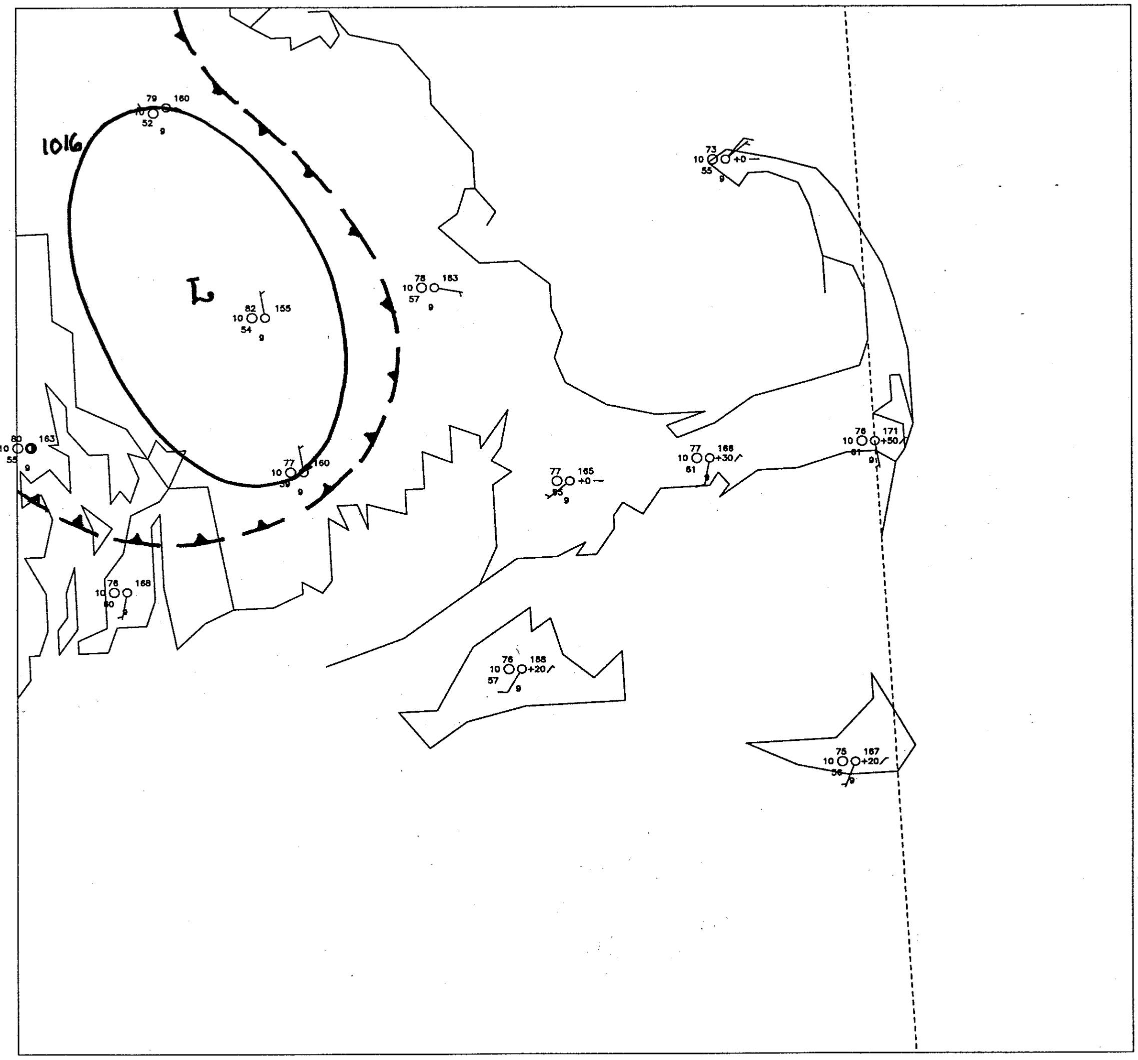

Figure 11 Manual analysis of sea-level pressure (mb) over the area of the 1.33-km MM5 domain for Case 1 at 1800 UTC, 1 July 2000. Standard isobar interval is 1 mb.

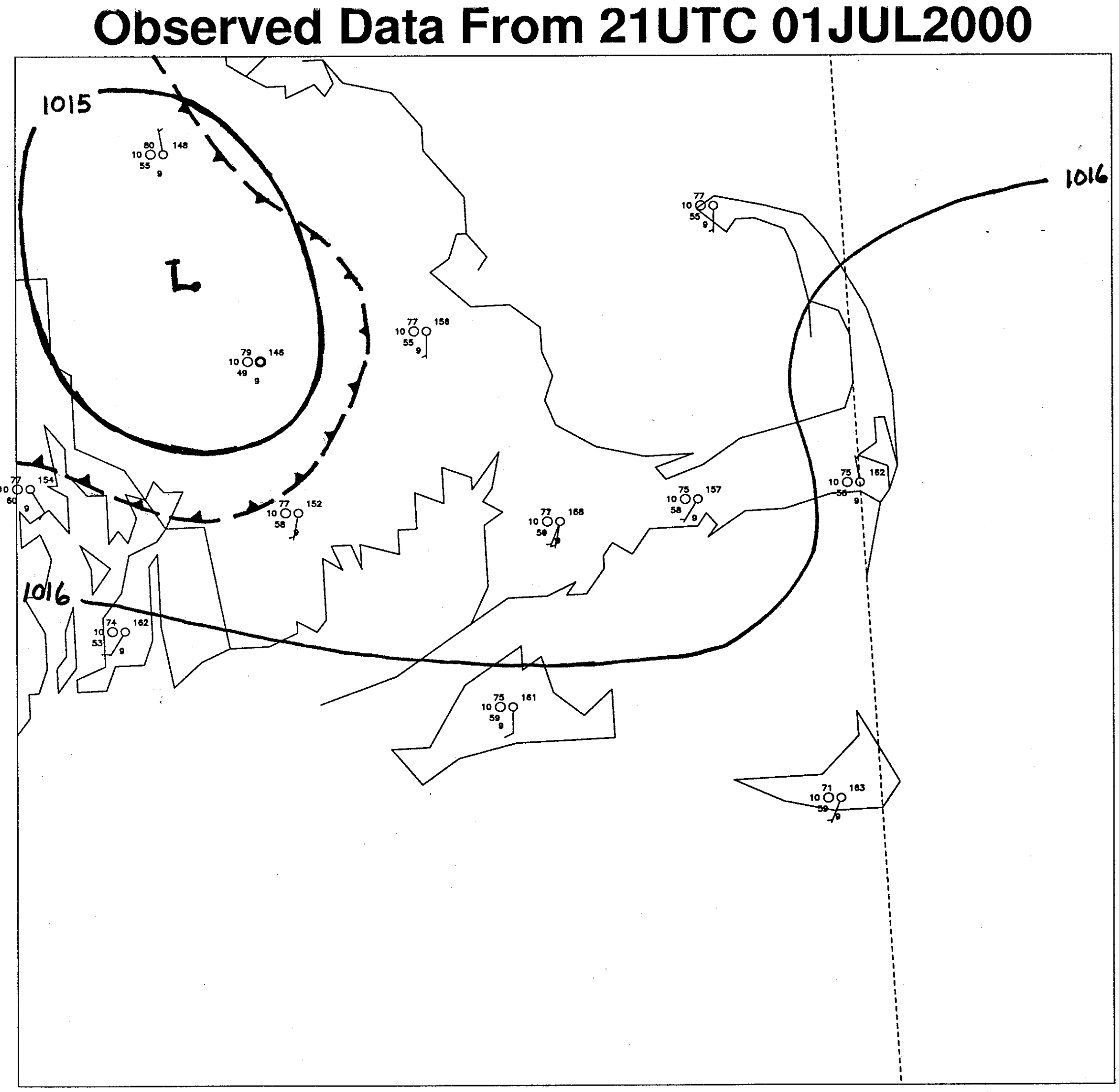

Figure 12 Manual analysis of sea-level pressure (mb) over the area of the 1.33-km MM5 domain for Case 1 at 2100 UTC, 1 July 2000. Standard isobar interval is 1 mb.

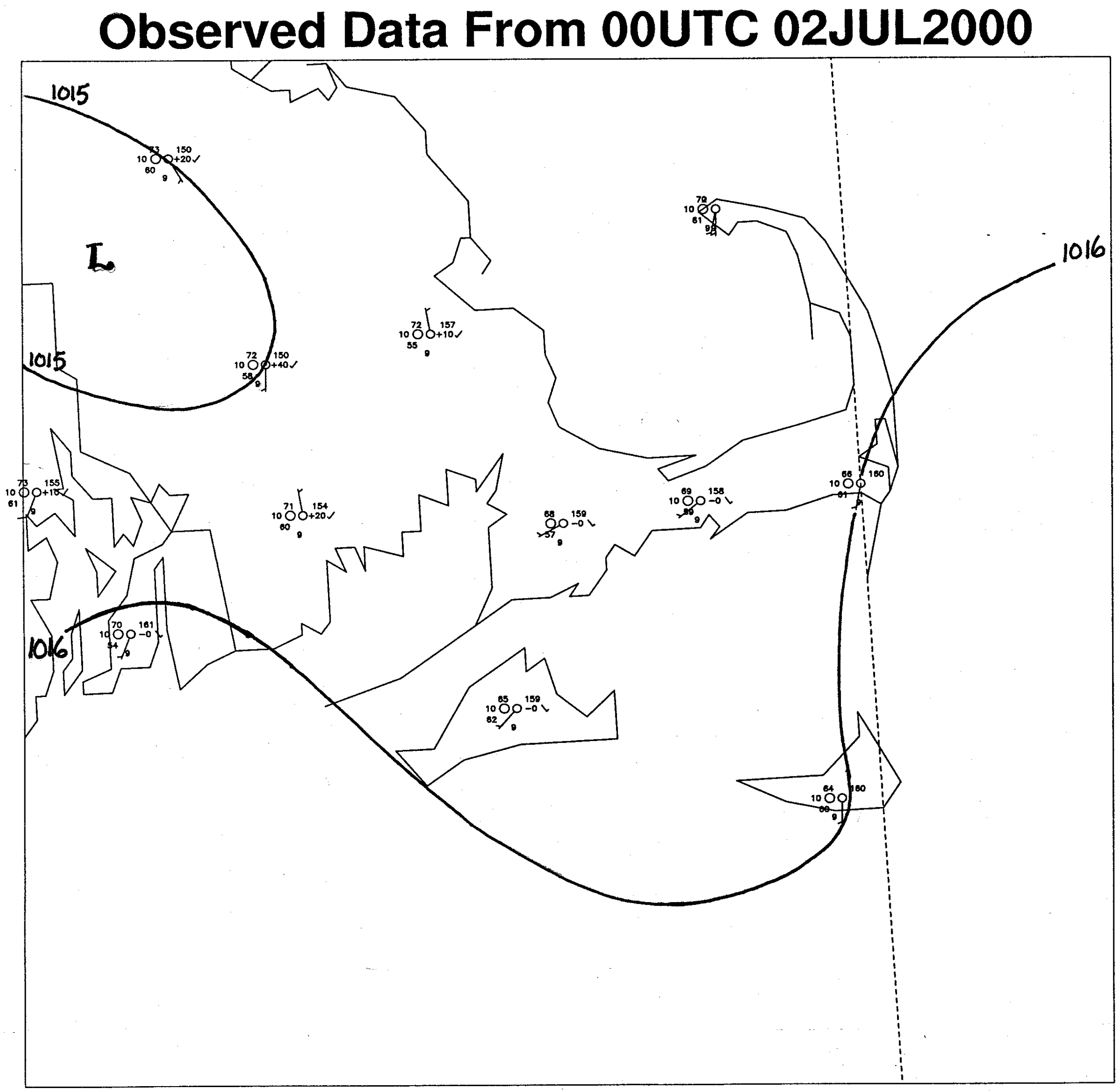

Figure 13 Manual analysis of sea-level pressure (mb) over the area of the 1.33-km MM5 domain for Case 1 at 0000 UTC, 2 July 2000. Standard isobar interval is 1 mb.

Finally, Figure 13 shows the local winds over the area at 0000 UTC, 2 July. The thermally induced low is a bit farther inland at this time, possibly because of the penetration of cool marine air into southeastern MA during the afternoon. Notice that some winds in southeast MA have become northerly at this time. Although the land already has cooled substantially from the daytime maximums, it remains warmer than the ocean, so this is not evidence of a land breeze. So, it appears that the marine air is being modified over land and the sea breeze is rapidly collapsing (no front is diagnosed at this time).

4.1.2 Case 2: Sea Breeze 2

Case 2 begins at 0000 UTC, 5 July, and ends at 0000 UTC, 7 July 2000. Figure 14 shows the synoptic-scale EDAS sea-level pressure analysis at the initial time of Case 2 for the Northeast U.S. In many respects, this case has many similar characteristics to the synoptic pattern of Case 1 (compare to Figure 5), with a cold front passing over eastern New England followed by west-northwesterly winds. However, on 5 July, there is a stronger low-pressure center over the St. Lawrence Valley in southeastern Canada, which intensifies to 990 mb over the next 24 h as it moves northeastward. Therefore, in this situation, the dynamical forcing around the synoptic-scale cyclonic system leads to stronger pressure gradients and low-level winds than were found in Case 1, where the cold front dissipated early in the episode. Figure 15 shows a manual analysis at the same time (0000 UTC, 5 July) over southern New England, which indicates that the frontal position is a bit west of the position indicated by the coarser EDAS analysis in Figure 14.

By the next morning at 1200 UTC, 5 July, the front had moved well to the southeast of New England as the Canadian low deepened rapidly (Figure 16). Notice that the surface winds are fairly brisk for early on a summer morning (4-10 kts), whereas the winds on the first morning in Case 1 were light and variable (Figure7). Later, in the early afternoon at 1800 UTC (2000 Eastern Daylight Time, EDT), Figure 17 indicates that the winds over New England remain northwesterly at about 8-14 kts in Case 2, while the cold front has continued to move slowly offshore. A trailing trough following the front has sagged southward to the coast of CT, RI and southern MA at 1800 UTC. Winds immediately ahead of the trough are west-southwesterly.

REAL-TIME ENVIRONMENTAL APPLICATIONS AND DISPLAY SYSTEM
http://www.arl.noaa.gov/ready.html

Click here for any error messages.

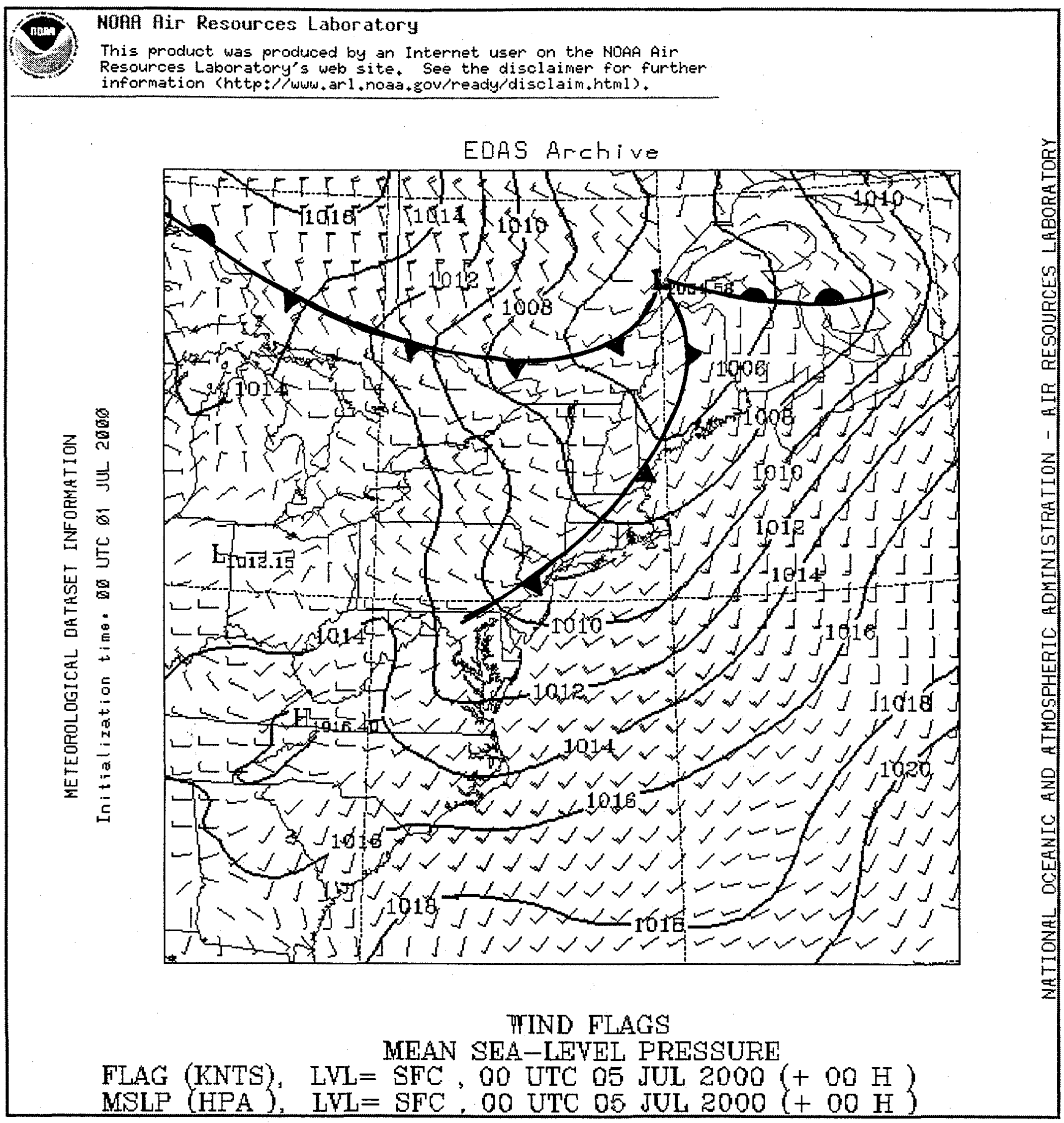

Figure 14. EDAS objective analysis of sea-level pressure (mb) over the Northeast U.S. for Case 2 at 0000 UTC, 5 July 2000. Isobar interval is 2 mb. Wind speeds (kts) are shown at 80-km resolution. Full barb = 10 kts, half barb = 5 kts. Fronts are analyzed manually based on winds and pressures.

Observed Data From 00UTC 05JUL2000

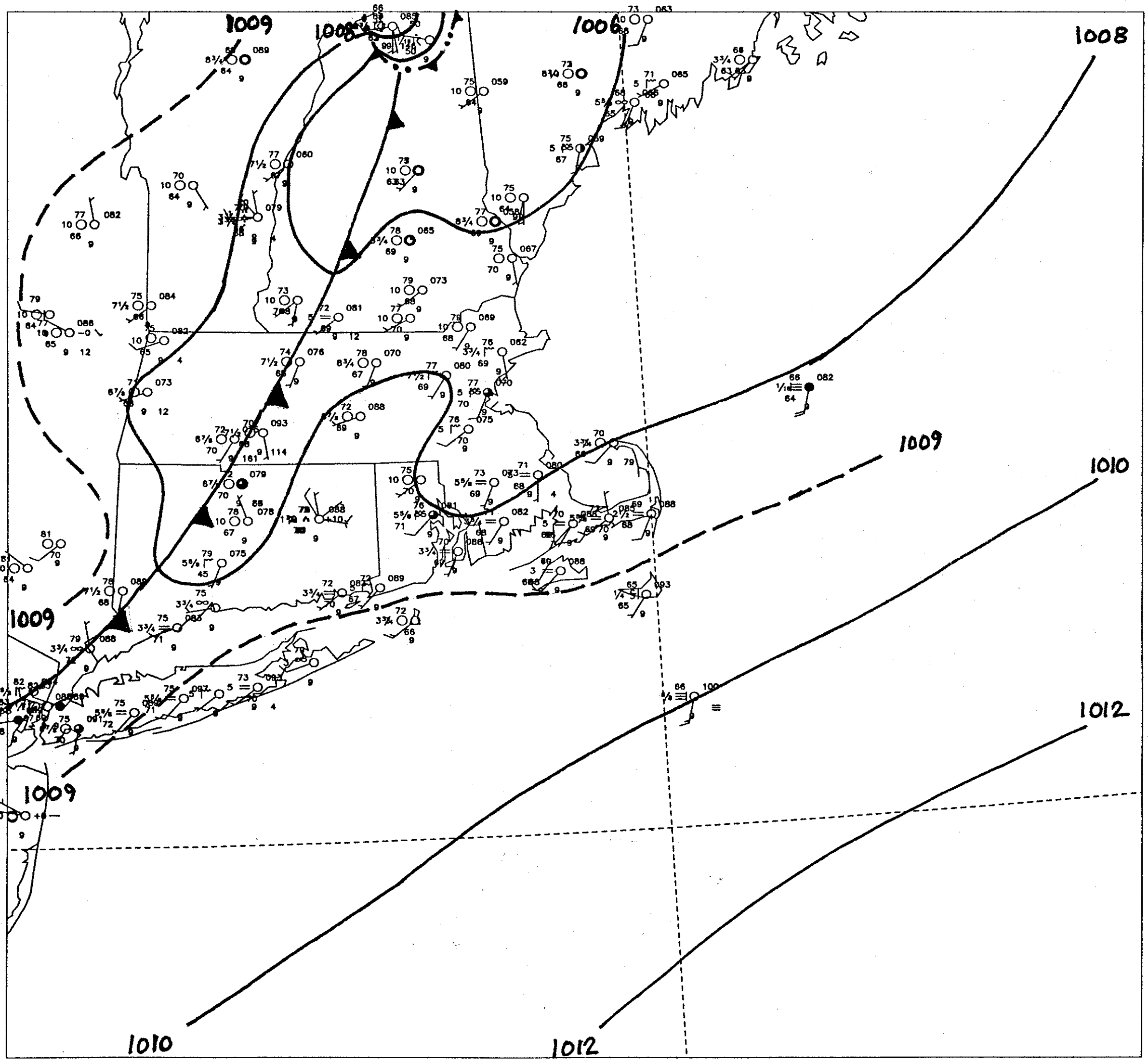

Figure 15. Manual analysis of sea-level pressure (mb) over the area of the 4-km MM5 domain for Case 2 at 0000 UTC, 5 July 2000. Standard isobar interval is 2 mb, with intermediate isobars shown as dashed lines. Dashed-dotted line with wedges represents a cold outflow boundary from a thunderstorm.

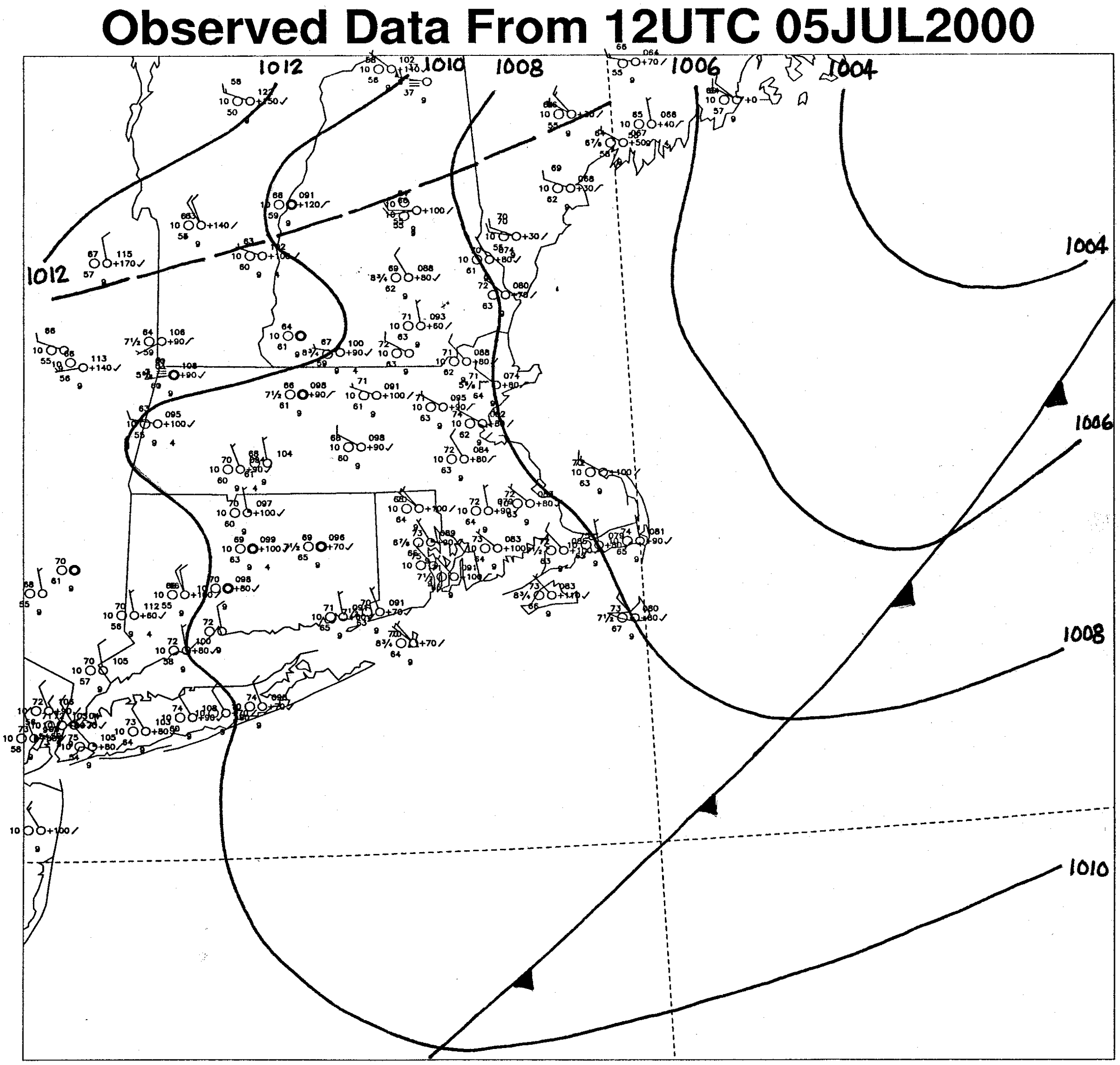

Figure 16. Manual analysis of sea-level pressure (mb) over the area of the 4-km MM5 domain for Case 2 at 1200 UTC, 5 July 2000. Standard isobar interval is 2 mb. Long dashed line indicates a surface trough.

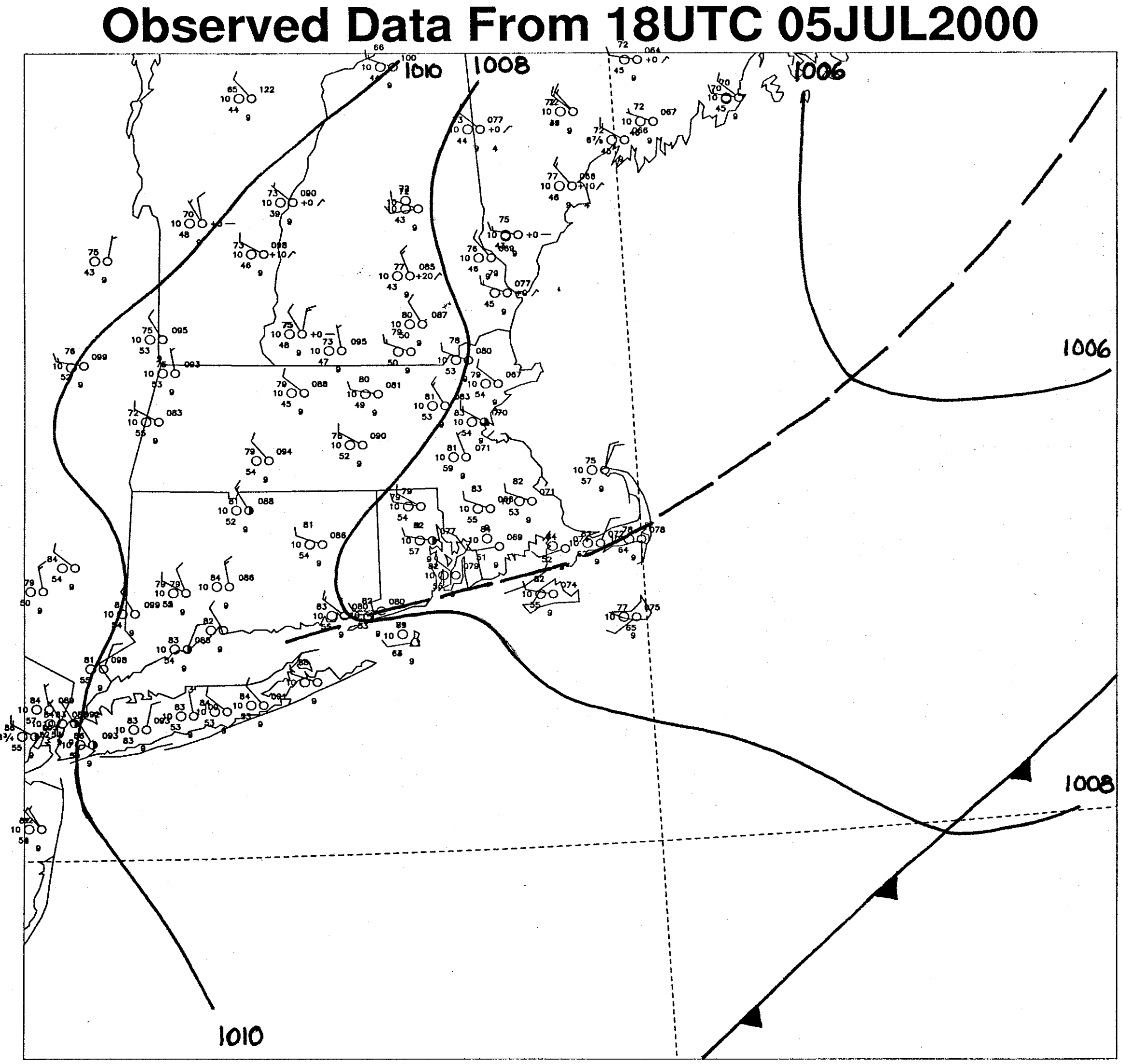

Figure 17. Manual analysis of sea-level pressure (mb) over the area of the 4-km MM5 domain for Case 2 at 1800 UTC, 5 July 2000. Standard isobar interval is 2 mb. Long dashed line indicates a surface trough.

Examination of the winds at coastal stations from ME to Boston show no sign of a sea breeze on this afternoon because of the strong northwesterly (offshore) flow behind the trough. This is consistent with the influence of the storm over Canada, which is approaching its peak intensity (not shown) and is still affecting southern New England on this day. Therefore, even the west-southwesterly winds ahead (south) of the trough do not represent a true sea breeze, but are caused by the baroclinic trough associated with the distant storm. Another indication of the strength of the synoptic-scale system and its ability to control the winds along the coast is found by examining the surface temperatures in Figure 17. The mid-afternoon temperatures over southern New England and Long Island are in the low to mid-80s F, but decrease steadily to the north. In northern VT and NH, the afternoon temperatures are in the mid-60s F under clear skies. This is very cool for early July and indicates strong cold advection over the entire area.

The final surface analysis for this day (0000 UTC, 6 July) is shown in Figure 18, which continues to show northwesterly flow over New England, including RI and Long Island. A small thermally induced low has formed over southeastern MA near the western end of the synoptic trough, but it has little effect on the winds at this time. Also, notice that the front over the Atlantic Ocean has become quasi-stationary, while the Canadian low has moved far enough northeastward (not shown) that the pressure gradient is beginning to weaken a bit.

As the Canadian storm moved further northeastward on the second day, 6 July, the pressure gradient in southern New England continued to weaken, although the surface low-pressure trough remained over the Gulf of Maine at 1800 UTC (Figure 19). Meanwhile, a new storm had developed during the night about 200 km east of Cape Hatteras, NC (not shown). As this low gradually strengthened during the day over the warm waters of the Gulf Stream, the sea-level pressures fell south of 40 N. In between the low-pressure trough to the north and the newly formed low to the south, a weak high-pressure ridge developed just south of New England and Long Island approximately along 41 N (Figure 19). This weak ridge set the stage for light winds over Cape Cod on the afternoon of 6 July.

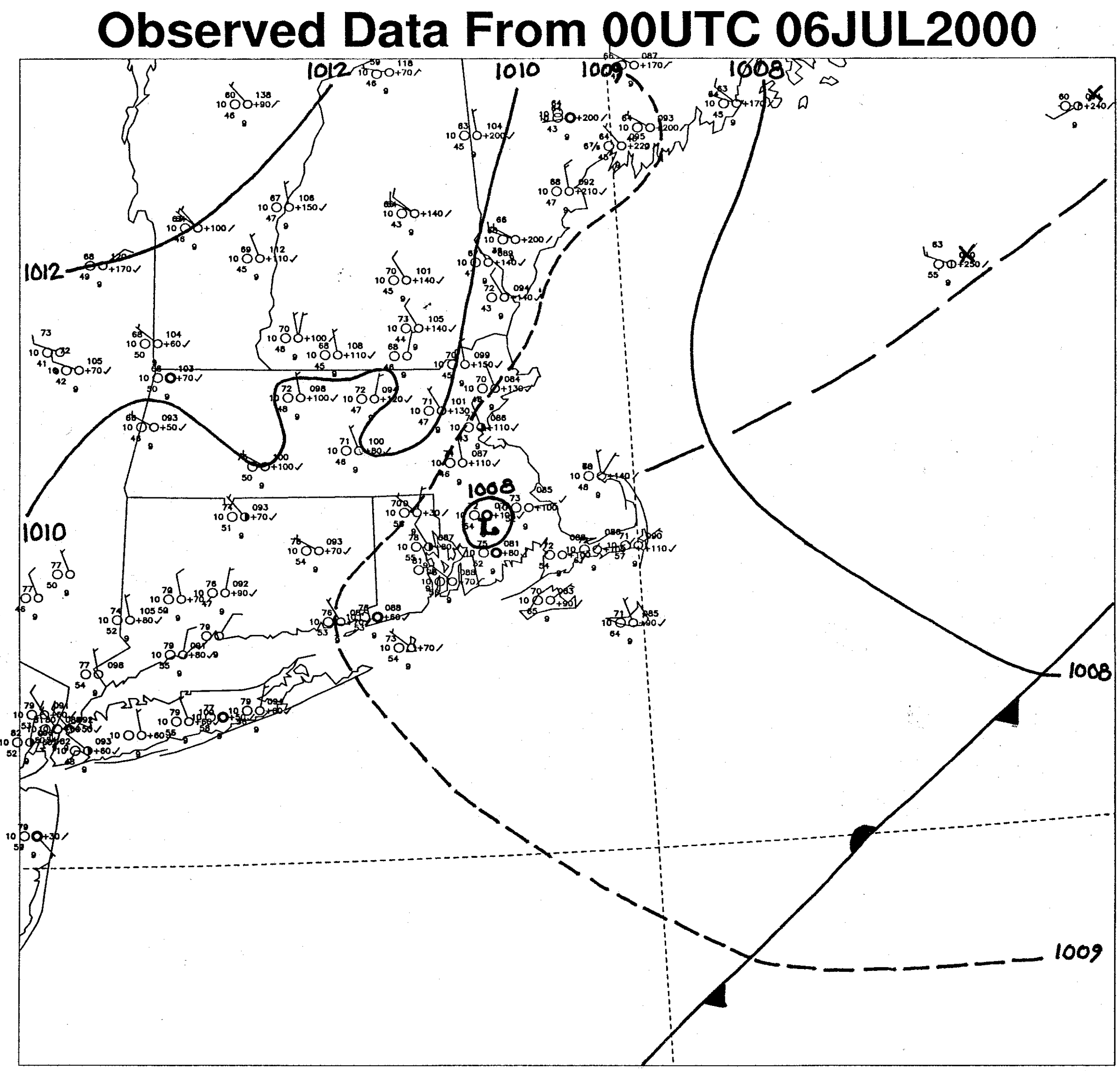

Figure 18. Manual analysis of sea-level pressure (mb) over the area of the 4-km MM5 domain for Case 2 at 0000 UTC, 6 July 2000. Standard isobar interval is 2 mb, with intermediate isobars shown as dashed lines. Long dashed line indicates a surface trough.

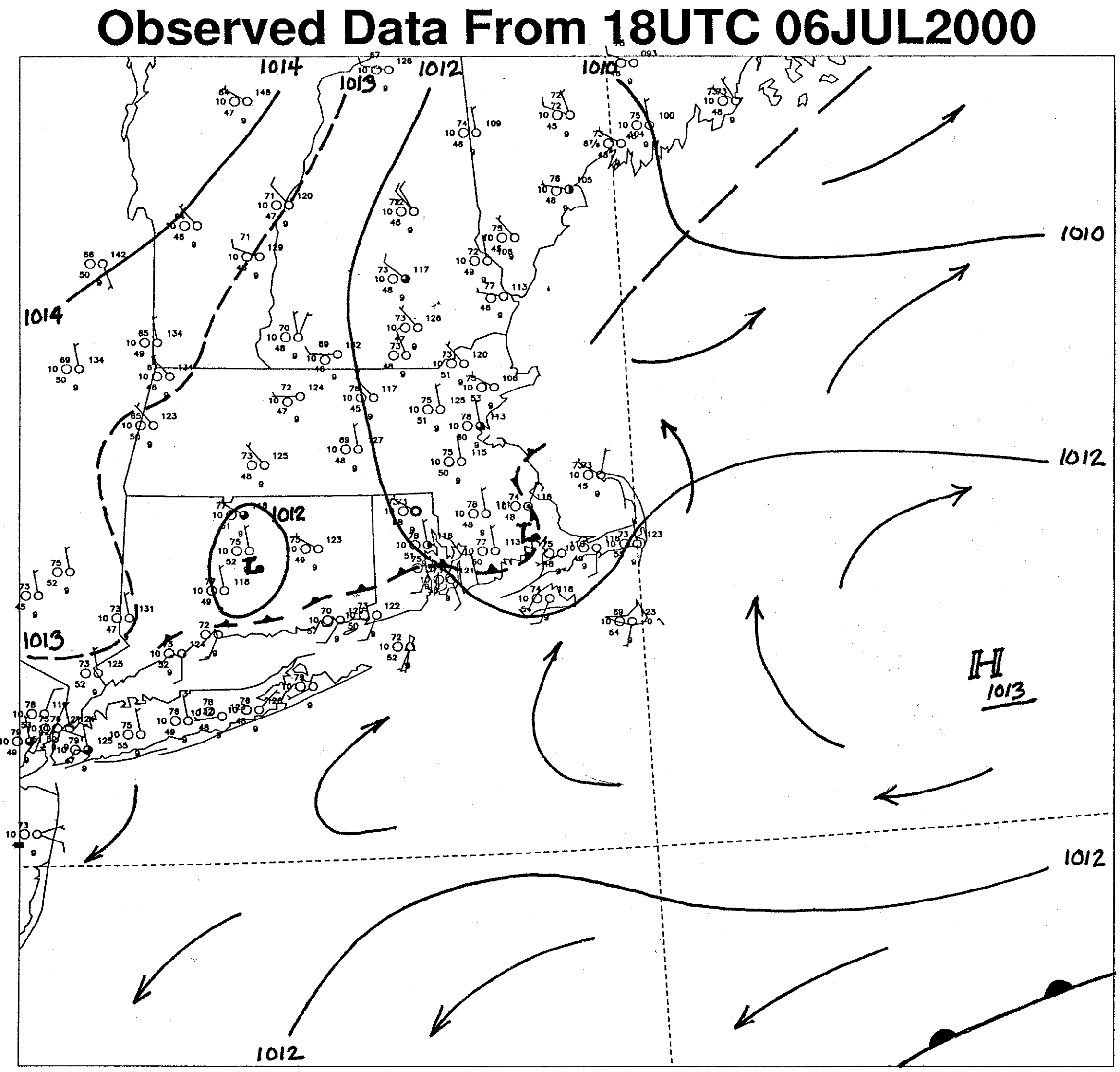

Figure 19. Manual analysis of sea-level pressure (mb) over the area of the 4-km MM5 domain for Case 2 at 1800 UTC, 6 July 2000. Standard isobar interval is 2 mb, with intermediate isobars shown as dashed lines. Long dashed line indicates a surface trough. Broken line with wedges represents the sea-breeze front. Arrows over the ocean indicate approximate streamline flow, based on EDAS analysis.

The weaker pressure gradient in the vicinity of the ridge at 1800 UTC allowed two thermally induced lows to form over CT and southeastern MA (Figure 19). These lows are very similar in location, strength and cause of origin to the thermal lows analyzed in Case 1 on the afternoon of the first day (see Figures 9, and 11-13). Here in Case 2, there is still no evidence of a coastal sea breeze from Boston to ME (north of the old trough) on 6 July. However, in southern New England, a sea breeze can be analyzed south and east of the thermal lows and north of the weak ridge. Also, notice that temperatures over southern New England are 5-10 F cooler on 6 July, compared to 5 July (compare Figures 17 and 19) as a consequence of the cold advection during the previous 24 h associated with the old Canadian storm. Thus, given a weaker than normal land-sea thermal contrast for this time of year, the sea breeze is expected to be somewhat less intense as well.

Figures 20 and 21 show the local manual analyses over southeastern MA and Cape Cod later on the same afternoon. At 2100 UTC (1700 EDT), Figure 20 shows the late-afternoon thermal low at its maximum intensity. The sea breeze has made its greatest inland penetration by this time and has reached almost the same position as found in Case 1 (see Figure 12). However, the temperature contrast between land and sea clearly is not as strong here on 6 July, compared to the previous day or Case 1.

This apparent incongruity can be explained by first noting that the position of the thermal low over southeastern MA is virtually the same in Cases 1 and 2. Thus, the sea-breeze front in this area is responding to the position of the thermal low, not simply the land-sea temperature contrast. This is an important conclusion, since it implies that the low and the inland penetration of the sea breeze are perhaps more common in summer than might otherwise be expected. The favored location for this thermal low over southeastern MA can be explained by its position between Narragansett Bay and Massachusetts Bay. Located between two water bodies, which remain relatively cool during daytime in the summer, this region experiences temperature excesses over a larger land mass than is available on Cape Cod. Therefore, it becomes the favored location for the thermal low, rather than the Cape. Figure 21 shows that, even when the thermal low and the sea-breeze front begin dissipating during the evening at 0000 UTC, 7 July (2000 EDT) as the land-sea temperature contrast begins to disappear, the winds over upper Cape Cod and southeastern MA continue to respond to the weakening low.

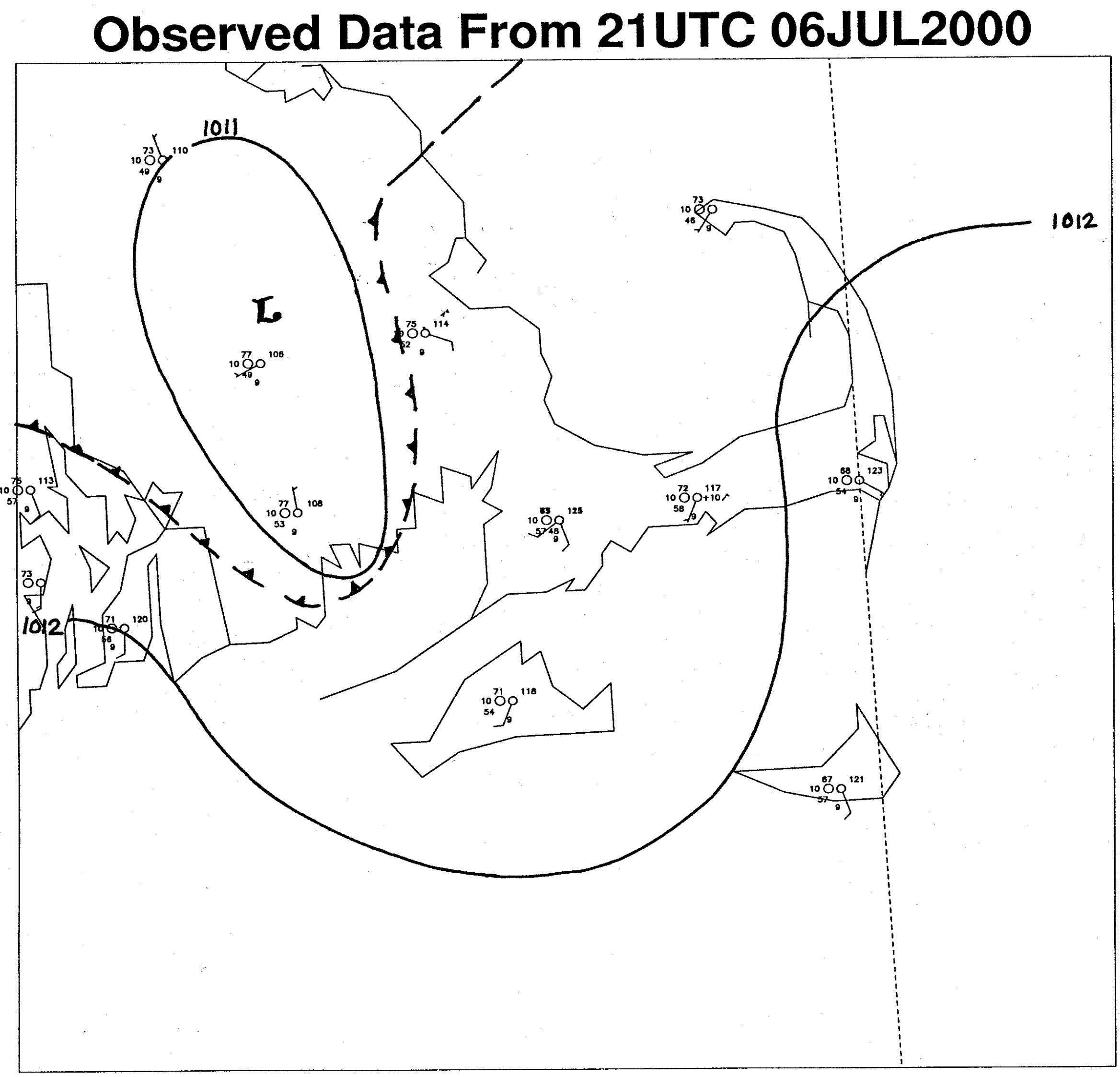

Figure 20 Manual analysis of sea-level pressure (mb) over the area of the 1.33-km MM5 domain for Case 2 at 2100 UTC, 6 July 2000. Standard isobar interval is 1 mb. Broken line with wedges represents the sea-breeze front.

Observed Data From 00UTC 07JUL2000

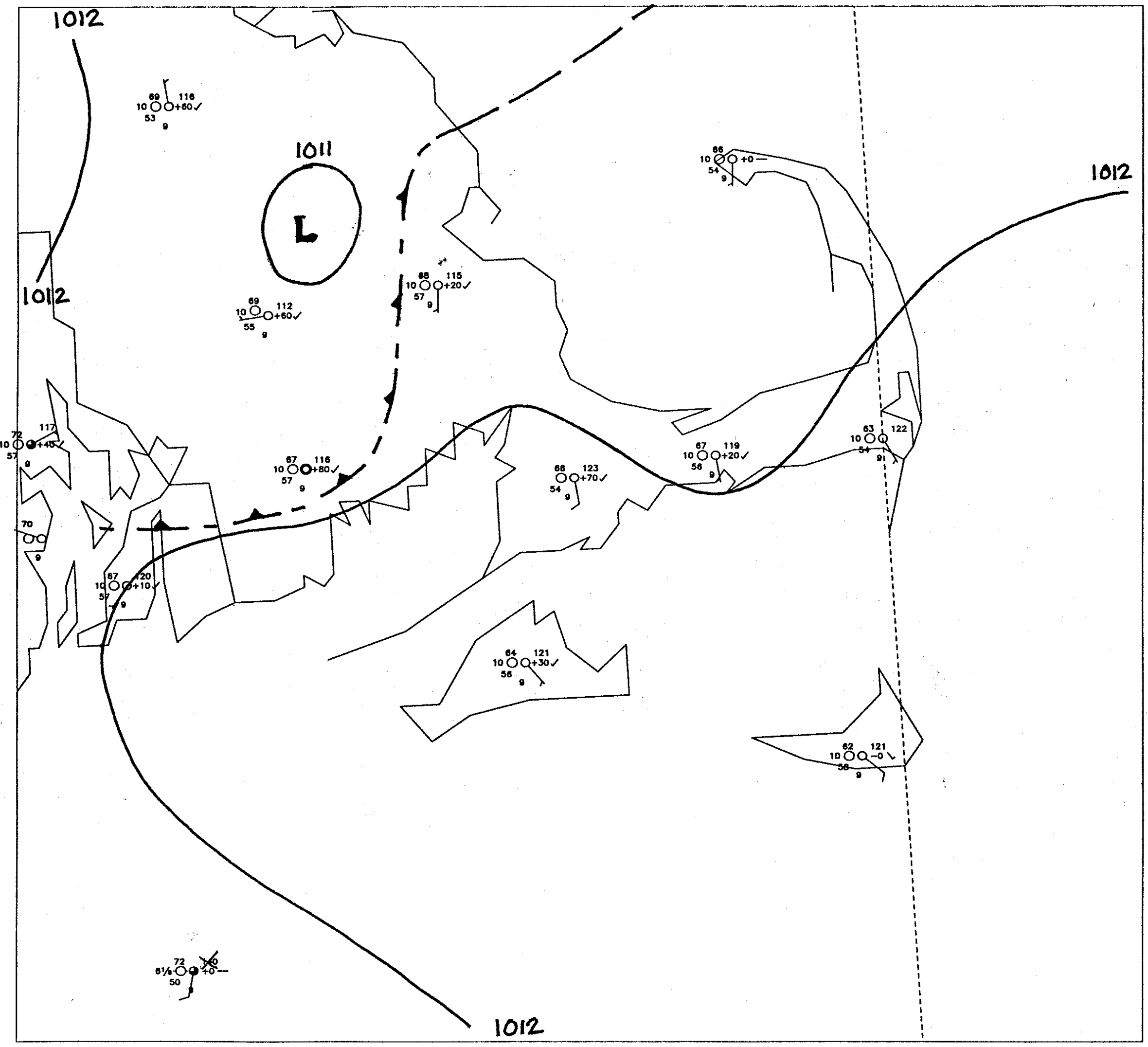

Figure 21 Manual analysis of sea-level pressure (mb) over the area of the 1.33-km MM5 domain for Case 2 at 0000 UTC, 7 July 2000. Standard isobar interval is 1 mb. Broken line with wedges and short dashes represents the dissipating sea-breeze front.

This condition is certainly not universal during the summer, because not all days have similar background synoptic conditions. However, weak pressure gradients and very gentle southwesterly large-scale flow are quite common during the warm season in this region. Thus, it is reasonable to expect that conditions often may be favorable for the formation of this thermal low. The implication of the thermal low is that the near-surface winds over upper Cape Cod can often turn counterclockwise to become southerly or even southeasterly when the background large-scale flow is weak and southwesterly. (A strong southwesterly wind would overpower the weak local pressure gradients and prevent significant rotation of the wind over land.) It should be noted, however, that there are no routine upper-air measurements over southeastern MA and upper Cape Cod, so it is unclear from these surface observations what the depth of the perturbed flow may be.

4.1.3 Case 3: Land Breeze

Case 3 spans the period from 0000 UTC, 21 August to 0000 UTC, 23 August 2000. This case is significantly different from the other two cases described above, in which abundant solar radiation caused the diurnal maximum temperatures over land to become considerably higher than the nearby ocean temperatures. Figure 22 shows the synoptic-scale EDAS sea-level pressure analysis over the eastern U.S. at 0000 UTC, 21 August, which is the initial time the Case 3. A large 1027-mb high is located over Lake Huron at this time, bringing cool northerly and northwesterly winds to the Mid-Atlantic region and western New England. Subsequent EDAS analyses show that this high pushed southeastward into the Mid-Atlantic region during the first 24 h and then continued southeast and off the Atlantic coast by the end of the episode (not shown). Especially during the first day, this high brought fairly strong cold advection to New England. Consequently, although skies were mostly clear, the land remained relatively cool during the day, suppressing the sea breeze. Meanwhile, with the nights becoming longer in late August and humidities becoming very low with the arrival of dry Canadian air (dew points were in the 40s F), nocturnal long-wave cooling dropped temperatures into the high 40s F in southeastern MA. Meanwhile, a short distance south of Nantucket, water temperatures were in the mid-60s F. This combination of cold land and warm water is a prime ingredient necessary to induce a land breeze.

The manual analyses generated over the area covered by the MM5's 4-km domain again reveal features not evident in the automated synoptic-scale EDAS analyses. Figure 23 shows the pressure field and the observations over southern New England during the first night at 0600 UTC, 21 August (0200 EDT). An old dissipating cold front lies over the Gulf of Maine at this time, but it is moving away from the region of interest. Examination of the wind observations in Figure 23 indicates that most inland stations are reporting calm winds, while most stations within 50 km of the coast are reporting northerly to westerly wind directions (that is, almost directly offshore). While the 15-kt northwesterly winds at Provincetown, MA clearly are caused by the geostrophic forcing and low friction over Massachusetts Bay, many of the other winds at coastal sites may be due to the land breeze (at least in part). It is not possible to attribute these coastal winds entirely to the land breeze because the dynamic forcing by pressure gradient (i.e., the geostrophic wind) is more or less in agreement with the observed winds at these stations. Thus, at best, we can say that there may be a land-breeze component at many of the coastal sites that acts to reinforce the geostrophic forcing and leads to a light offshore flow, while at many of the inland stations the winds remain calm.

The following afternoon, at 1800 UTC on 21 August, Figure 24 shows that the pressures are gradually rising across the region, although the pressure pattern and the intensity of the pressure gradients are mostly the same (despite a weaker pressure gradient in NH). Temperatures on this afternoon remain in the high 60s to low 70s F across New England. This is not high enough to generate a sea breeze, especially since water temperatures during the late summer are approaching their annual maximum. A very weak thermal low barely can be detected over southeastern MA, but it has no significant effect on the winds. From NY to ME, coastal winds are generally in the offshore direction from the north-northwest. By early evening, at 0000 UTC on 22 August, Figure 25 indicates that the thermal low remains barely visible, but is certainly too weak to have any important influence on the flow. However, the synoptic pressure gradient has weakened, especially in the southern half of the region.

REAL-TIME ENVIRONMENTAL APPLICATIONS AND DISPLAY SYSTEM
http://www.arl.noaa.gov/ready.html

Error messages.

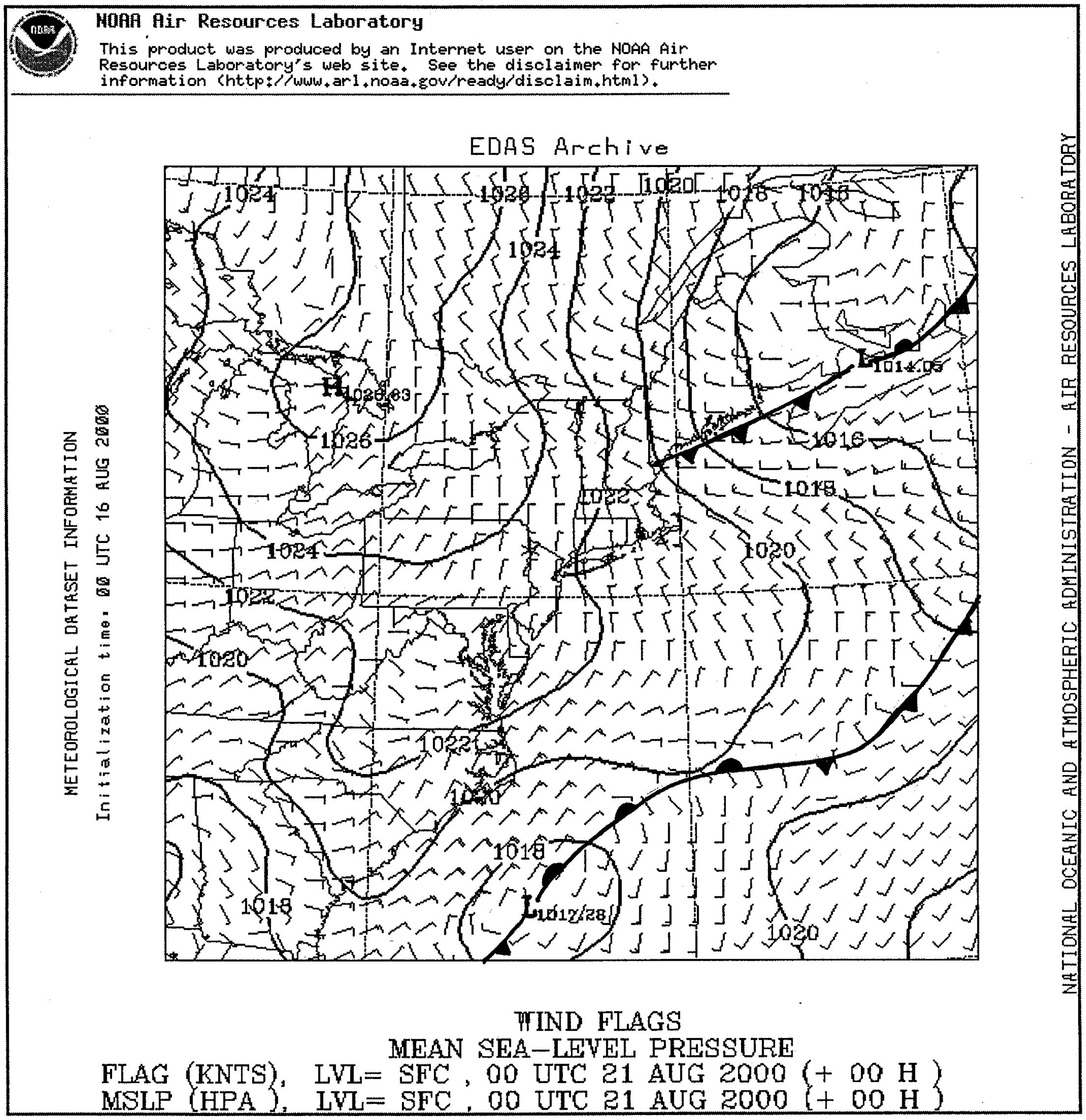

Figure 22. EDAS objective analysis of sea-level pressure (mb) over the Northeast U.S. for Case 3 at 0000 UTC, 21 August 2000. Isobar interval is 2 mb. Wind speeds (kts) are shown at 80-km resolution. Full barb = 10 kts, half barb = 5 kts. Fronts are analyzed manually based on winds and pressures.

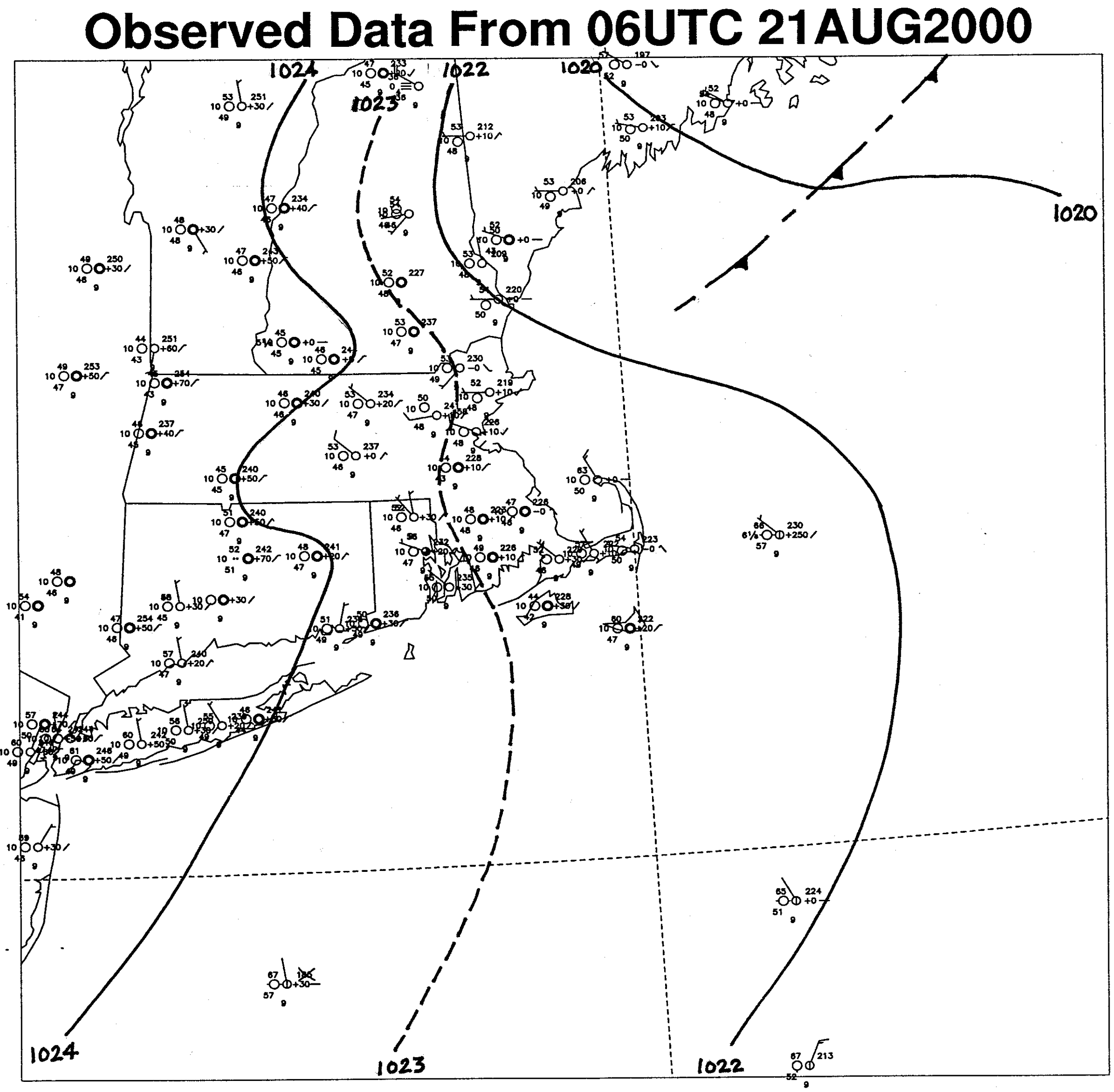

Figure 23. Manual analysis of sea-level pressure (mb) over the area of the 4-km MM5 domain for Case 3 at 0600 UTC, 21 August 2000. Standard isobar interval is 2 mb, with intermediate isobars shown as dashed lines. Dashed line with wedges represents dissipating cold front.

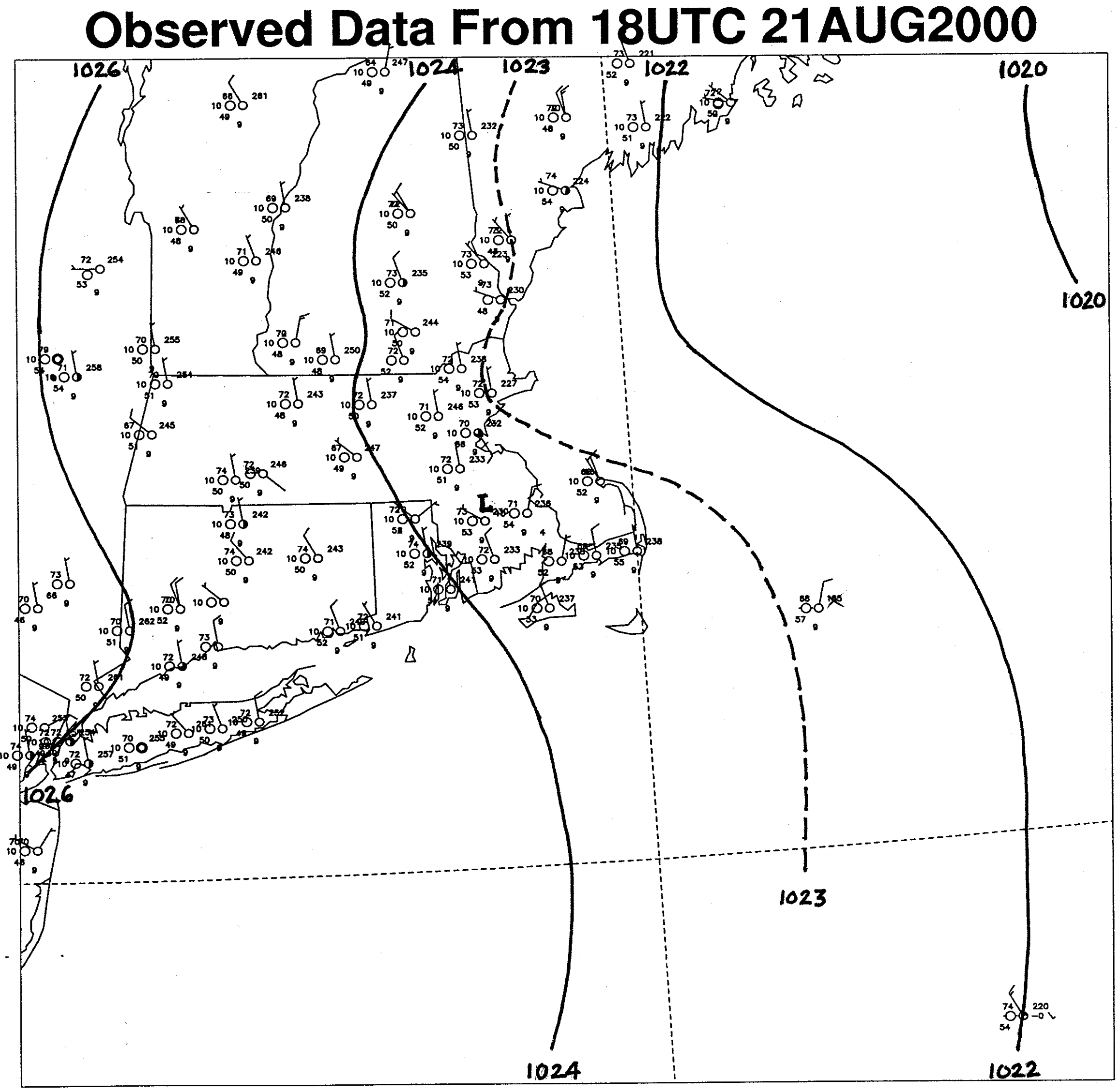

Figure 24. Manual analysis of sea-level pressure (mb) over the area of the 4-km MM5 domain for Case 3 at 1800 UTC, 21 August 2000. Standard isobar interval is 2 mb, with intermediate isobars shown as dashed line.

Observed Data From 00UTC 22AUG2000

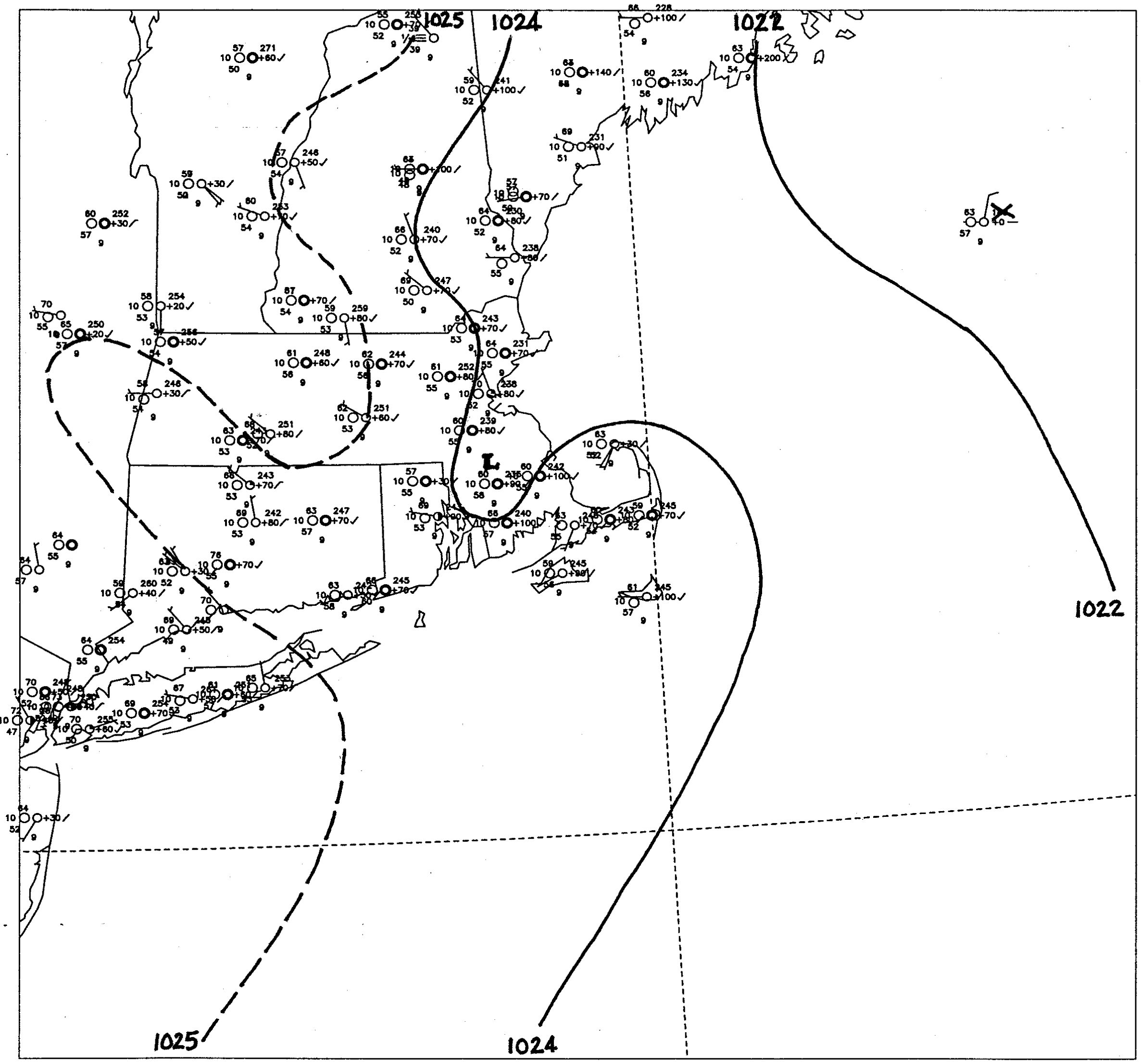

Figure 25. Manual analysis of sea-level pressure (mb) over the area of the 4-km MM5 domain for Case 3 at 0000 UTC, 22 August 2000. Standard isobar interval is 2 mb, with intermediate isobars shown as dashed line.

Figure 26 shows the manual analysis during the second night at 0900 UTC, 22 August. The pressure gradient by this time has become very weak and most inland stations report calm winds with temperatures in the high 40s F. Meanwhile, most coastal stations from ME to CT are reporting offshore flow at ~3-6 kts. Although the basic geostrophic forcing is mainly from the north, it is weak because of the anemic pressure gradient. Particularly near the shore from Boston to ME, the coastal winds are almost directly offshore from the west to west-northwest directions that are clearly at a large angle to the geostrophic forcing. At the few inland sites where non-zero winds are reported, most have directions between north-northwest and the northeast, or approximately parallel to the geostrophic forcing. Thus, on this night, it appears that the coastal winds in many areas do have a definite component that is forced by the land breeze.

Figure 27 reveals that the pressure gradient remains weak on the final afternoon, so that many stations from Long Island to Cape Cod have a wind direction that suggests a sea-breeze contribution to the flow. However, the movement of the synoptic high center off the Mid-Atlantic coast at this time (not shown) also is forcing the winds in this region to shift to the southwest direction. Finally, notice that sea-level pressures over southeastern MA are anomalously low, even though a distinct low-pressure center cannot be discerned.

The last two figures revisit the nocturnal periods of this case, but focus on the local region of southeastern MA. In Figure 28 (0600 UTC, 21 August, as in Figure 23), the sea level pressure reports over Cape Cod and southeastern MA indicate almost no gradients and all inland stations (plus the offshore islands) report calm winds. Stations around Narragansett Bay and Cape Cod report light northwesterly winds (except for Provincetown, where a 15-kt wind is blowing from the sea). The stations near the coast are also generally warmer than inland sites by 10-15 F. This thermal contrast and the offshore winds are consistent with a land breeze, but the northwesterly direction is also consistent with the geostrophic forcing, as discussed above. Therefore, for this region, the observed nocturnal winds on this first night are most likely the result of a combination of the two mechanisms, one acting at the synoptic scale and the other at the mesoscale.

In Figure 29, we see the local observations over Cape Cod and Southeastern MA on the early morning, as in Figure 26. As pointed out above, the pressure gradient over this area is extremely weak at 0900 UTC, 22 August, so geostrophic forcing is not likely to be important. Even Provincetown, with its marine exposure, is reporting only a 5-kt wind. Thus, there is stronger evidence on this night that the winds at the coastal stations could be due to a land breeze. The observations are not conclusive, however.

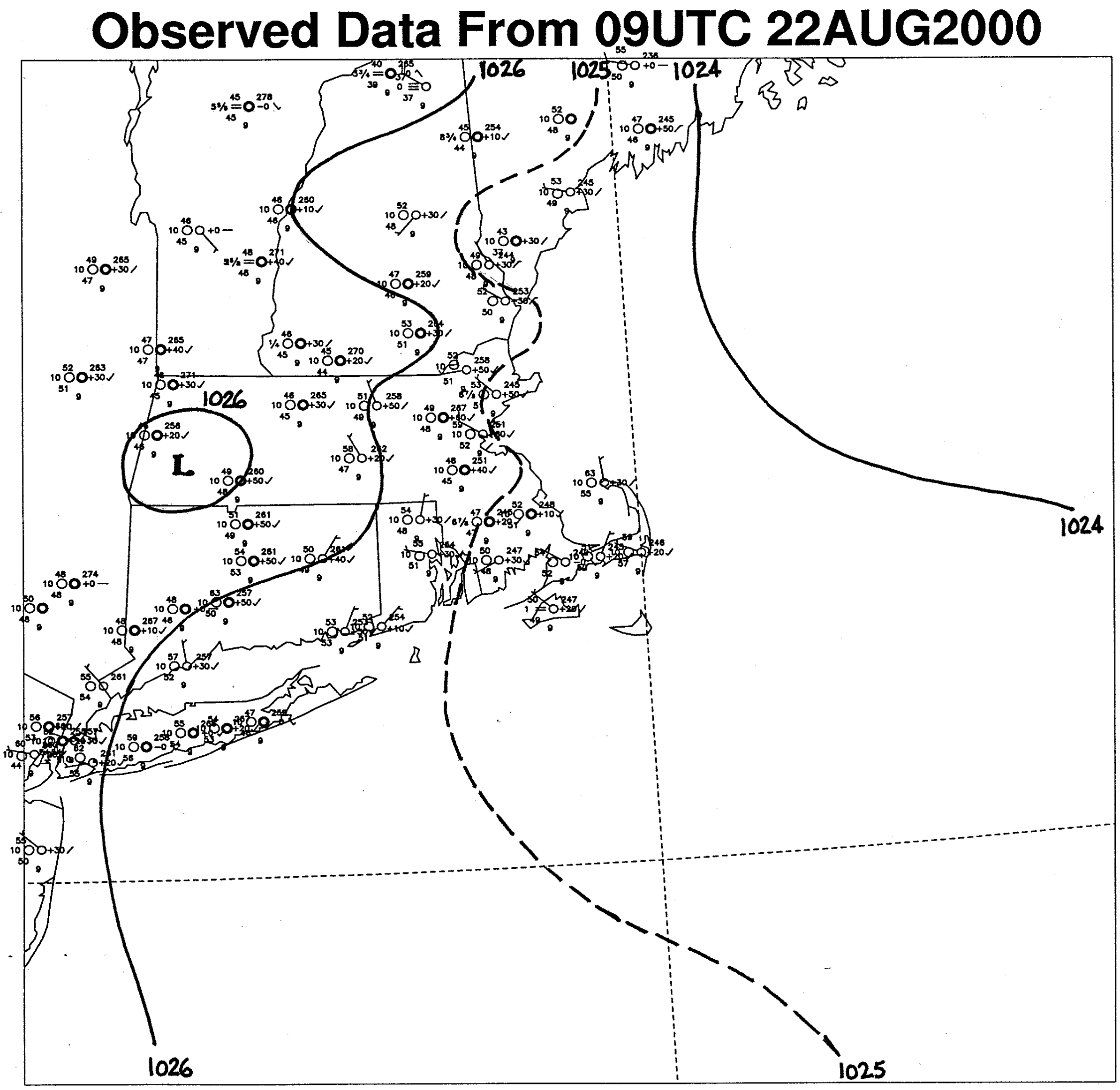

Figure 26. Manual analysis of sea-level pressure (mb) over the area of the 4-km MM5 domain for Case 3 at 0900 UTC, 22 August 2000. Standard isobar interval is 2 mb, with intermediate isobars shown as dashed lines.

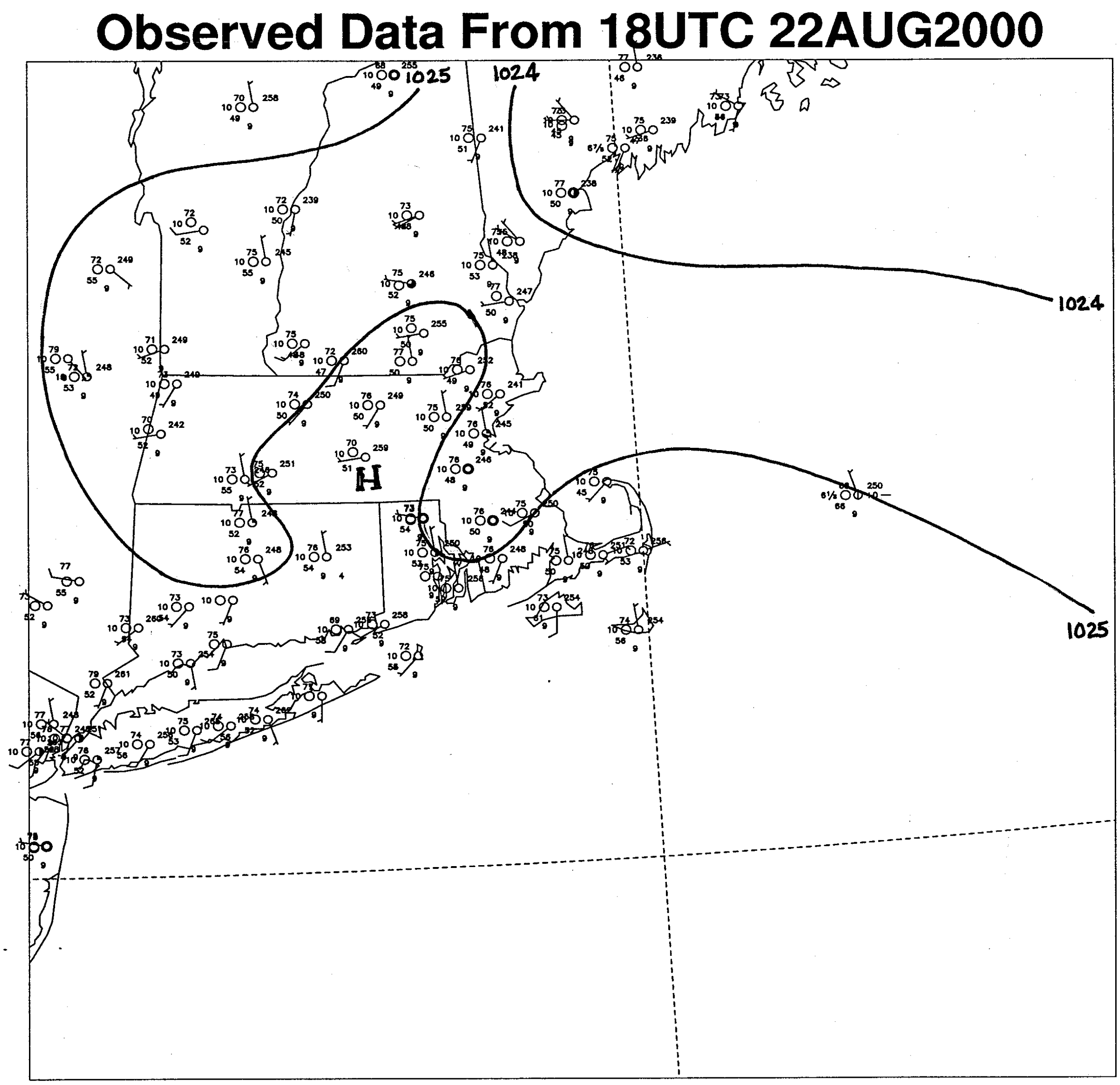

Figure 27. Manual analysis of sea-level pressure (mb) over the area of the 4-km MM5 domain for Case 3 at 1800 UTC, 22 August 2000. Standard Isobar interval is 1 mb.

Observed Data From 06UTC 21AUG2000

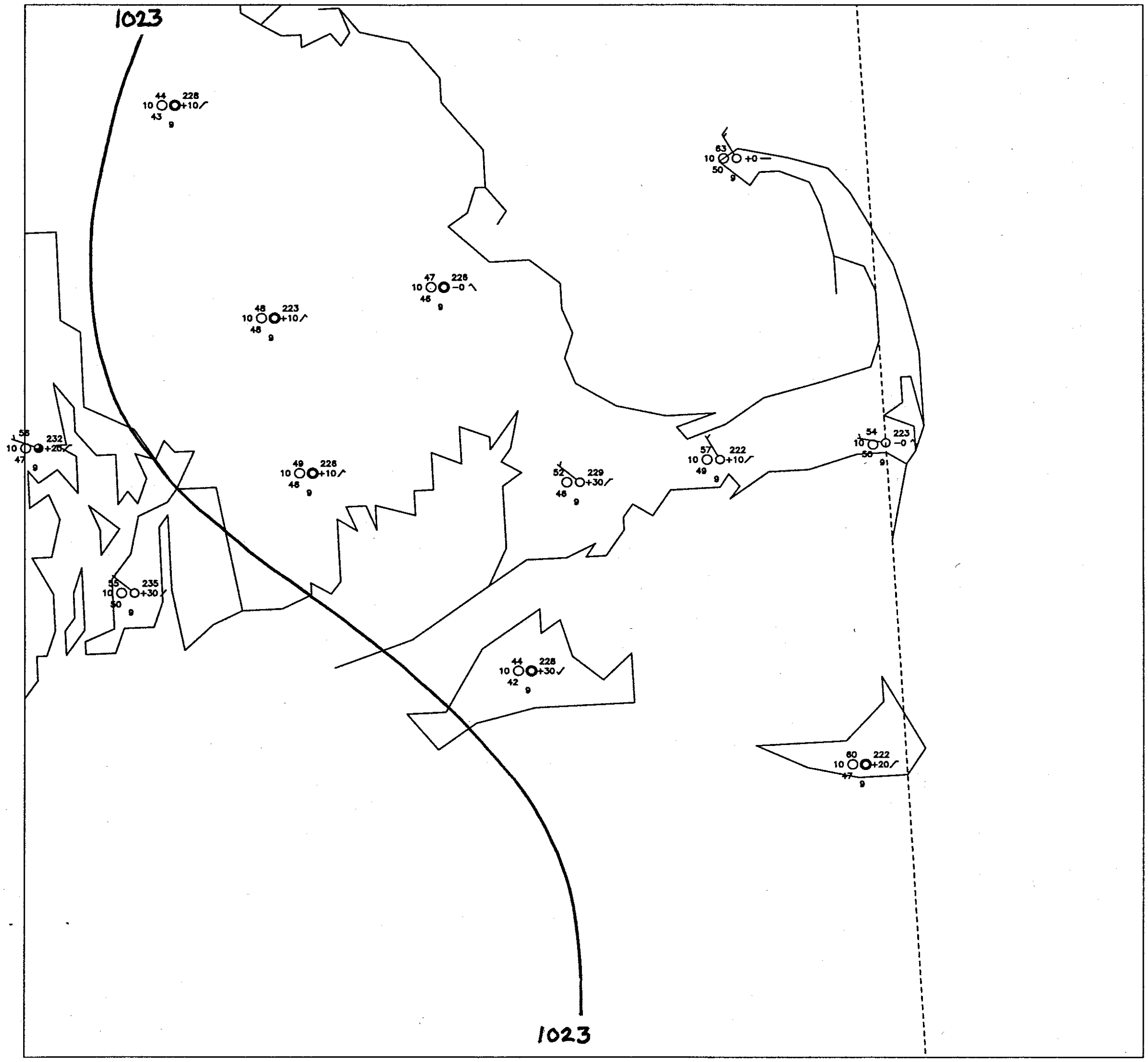

Figure 28 Manual analysis of sea-level pressure (mb) over the area of the 1.33-km MM5 domain for Case 3 at 0600 UTC, 21 August 2000. Standard isobar interval is 1 mb.

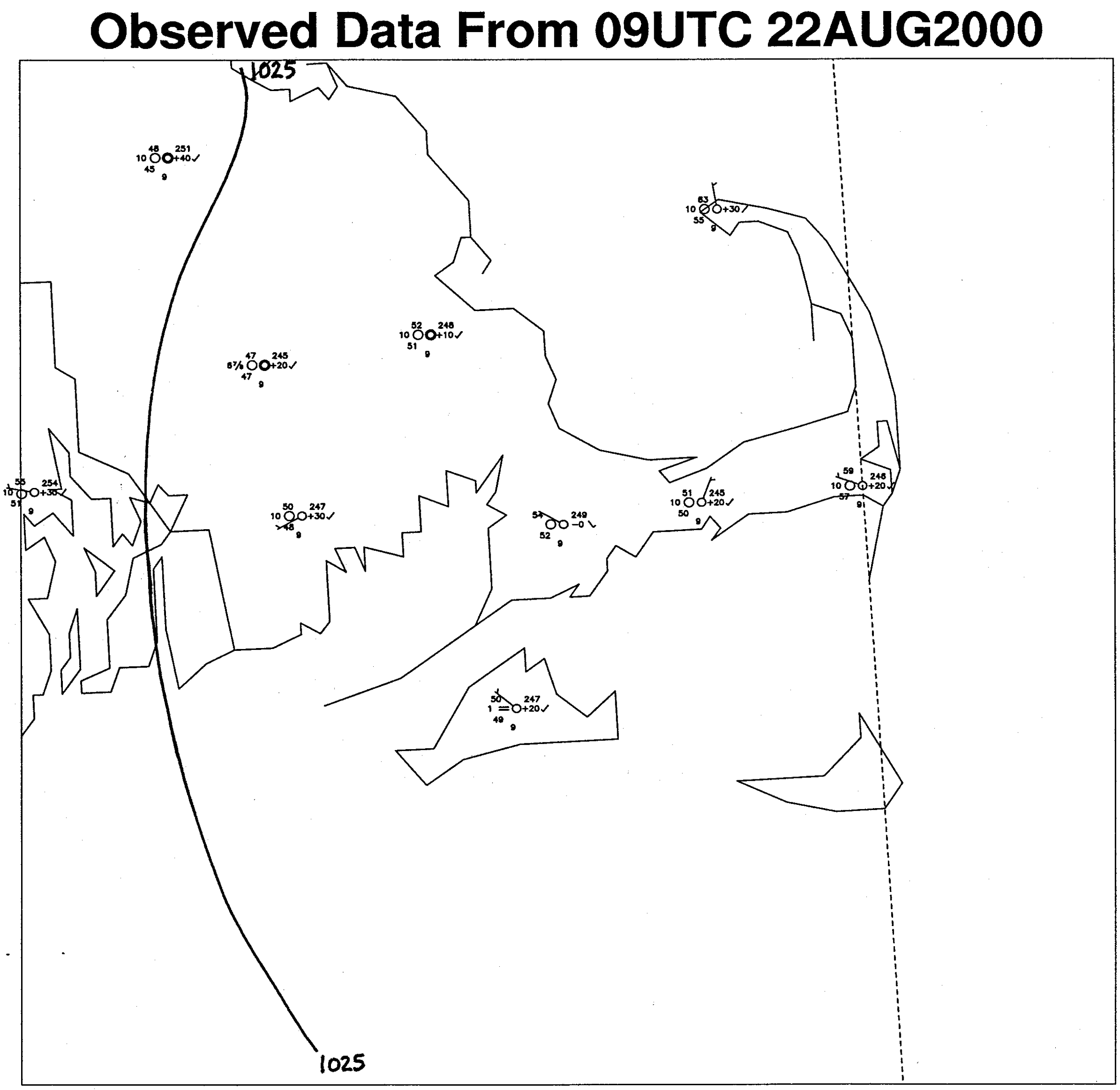

Figure 29 Manual analysis of sea-level pressure (mb) over the area of the 1.33-km MM5 domain for Case 3 at 0900 UTC, 22 August 2000. Standard isobar interval is 1 mb.

4.2

The MM5 model was used in this study to generate 48-h numerical solutions for each case and on all four domains, with grid resolutions of 36, 12, 4, and 1.33 km. We will focus on the model's 1.33-km solutions, which are designed to resolve the fine-scale details for the wind flow over Cape Cod and southeastern MA. For each case, examples of the important model fields will be presented to understand the basic flow and the structure of mesoscale features resolved by the model. Comparison of these model fields with the local mesoscale analyses discussed in Section 4.1 will be followed by an analysis of the statistic performance of the model in each case. As discussed in Section 3.2.1.3, CALMET fields are derived by reprocessing the meteorological fields generated by the MM5 model.

4.2.1 Case 1: Sea Breeze 1

Examination of the MM5 model fields generated in Case 1 begins with the winds in the surface layer (~12.5 m AGL) at 1200 UTC, 1 July 2000 (+12 h into the model run) (Figure 30). At this time, shortly after dawn on the first day of the episode, the wind flow in the model is very light and mostly from the northwest. Over land, the winds are ~1-3 kts (0.5-1.5 ms^{-1}). Over Massachusetts Bay, the speeds increase to 4-5 kts (2.0-2.5 ms^{-1}). These winds are mostly consistent with the observations for this time shown in Figure 7.

Next, at 1800 UTC that afternoon (+18 h, or 1400 EDT), Figure 31 shows that the surface-layer winds in the model have reversed direction to the south and southeast over most of the domain, and have accelerated to 2-6 ms^{-1}. The fastest winds, quite reasonably, are over the ocean, with weaker winds over land. These simulated winds can be compared to the observed reports in Figures 8 and 11. A comparison between Figures 11 and 31 indicates that the major mesoscale features shown in the manual analysis have been reproduced reasonably well in the MM5 solution. The most important feature common to both the observed and simulated winds is the penetration of marine air over southeastern MA behind the sea-breeze front. North and west of the sea-breeze front, winds over inland areas are very light and variable in direction.

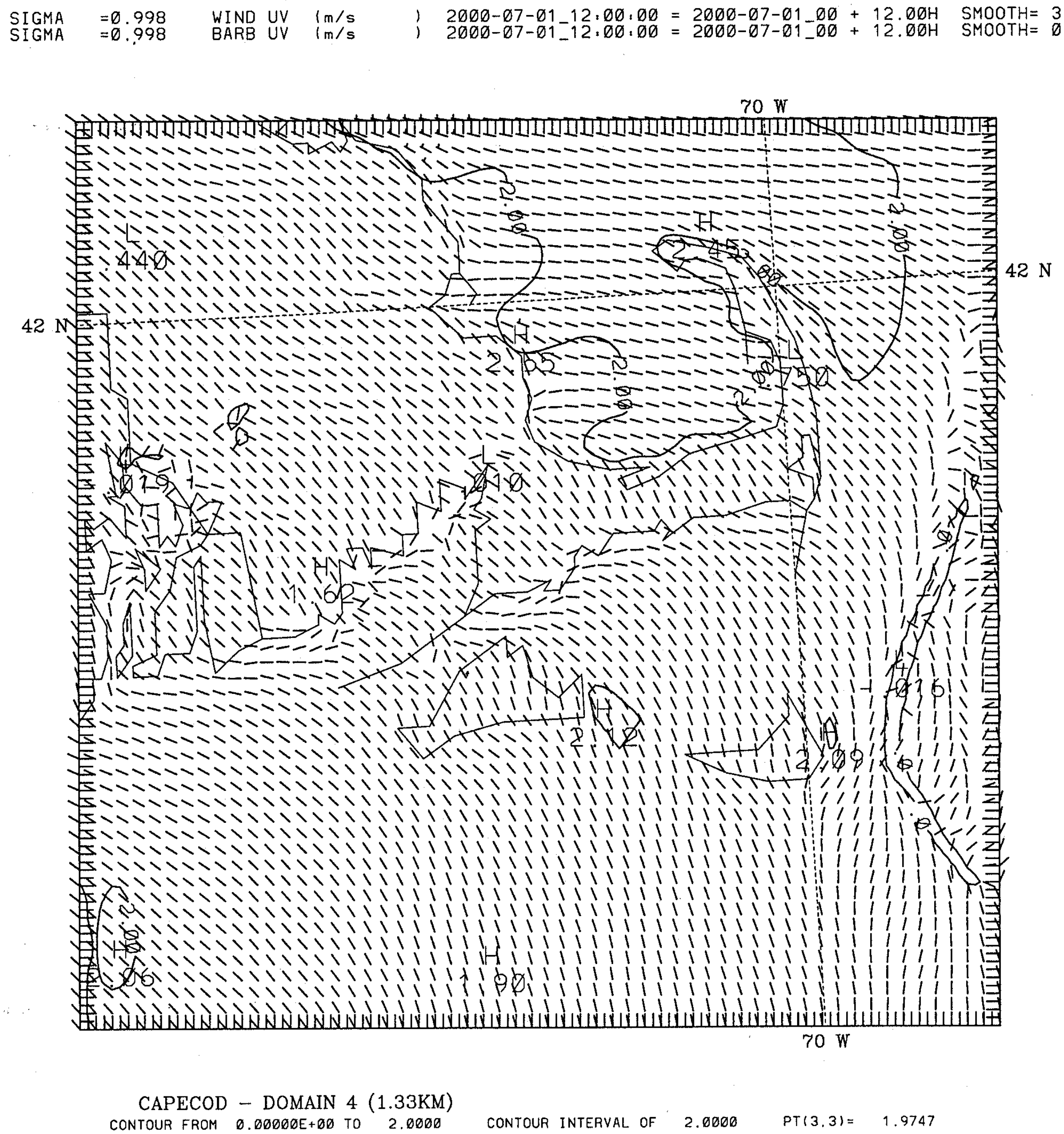

Figure 30. MM5 surface-layer wind (ms^{-1}) simulated on the 1.33-km domain in Case 1 valid at 1200 UTC, 1 July 2000 (+12 h). Full barb is 10 ms^{-1}. Contour interval is 2 ms^{-1}.

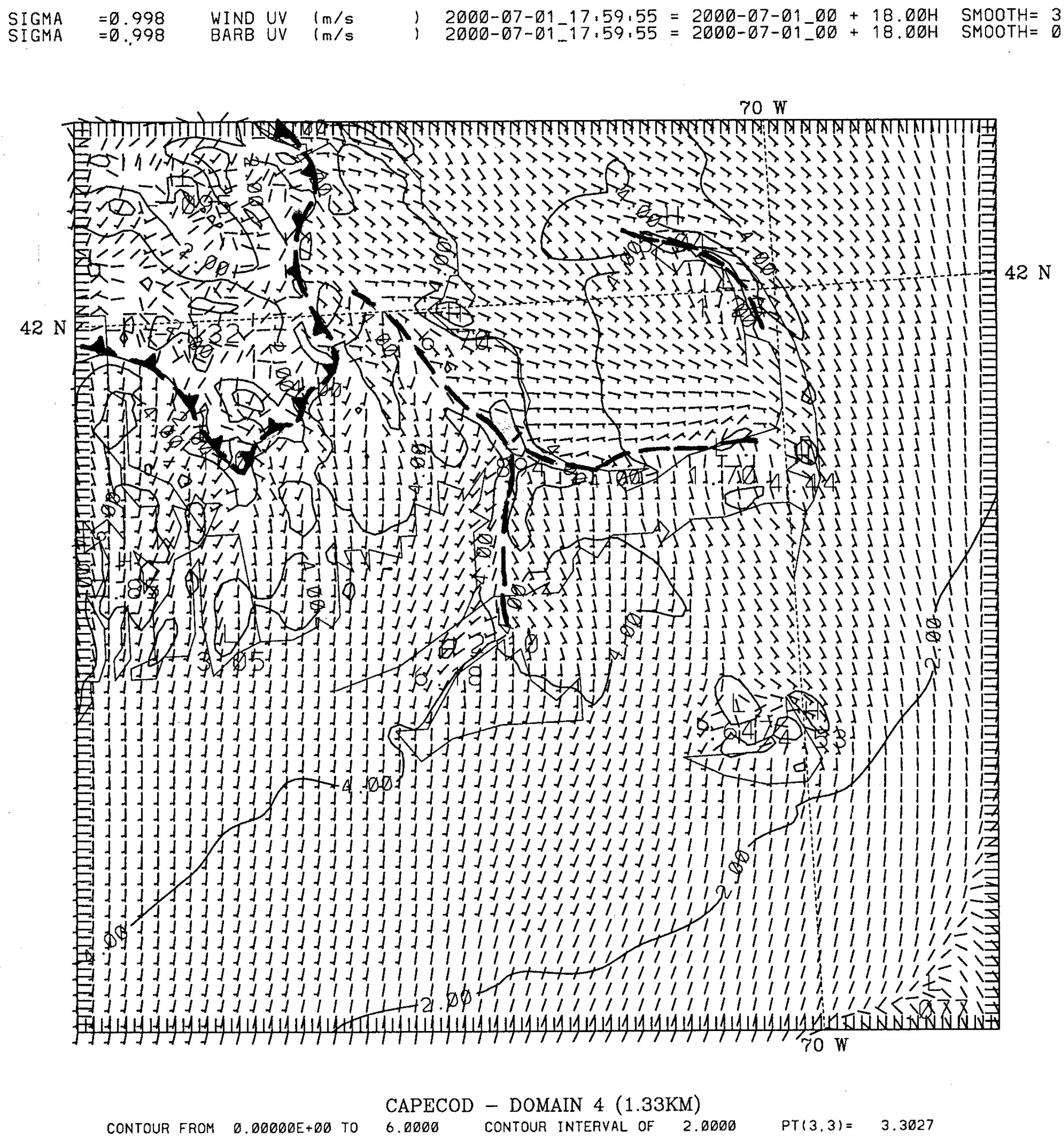

Figure 31. MM5 surface-layer wind (ms^{-1}) simulated on the 1.33-km domain in Case 1 valid at 1800 UTC, 1 July 2000 (+18 h). Full barb is 10 ms^{-1}. Contour interval is 2 ms^{-1}. Heavy dashed line with barbs represents the sea-breeze front. Dashed lines without wedges indicate convergence zones.

Also, notice that the predominantly southerly winds observed along the southern shore of Cape Cod, and on Martha's Vineyard and Nantucket Island in Figure 11 have a small westerly component, which changes to a slight easterly component on the southeastern elbow of the Cape. This pattern is captured quite well by the model, although the MM5 also shows important local distortions of the winds in the lee of the two islands and in the lee of Cape Cod over Massachusetts Bay. Although there are no observations in the lee of the two islands to confirm this otherwise reasonable pattern, the model's winds in eastern MA from Outer Cape Cod to the inland coastal areas south of Boston are from the east-southeast as observed. Moreover, Figure 31 shows distinct convergence zones over Upper Cape Cod and southeastern MA (southeast of the sea-breeze front) where different branches of the sea-breeze flow converge. There are even a few spots along the northern shore of Upper Cape Cod where the local winds have a northerly component in the otherwise easterly flow over Massachusetts Bay (just to the north of the convergence zone along this shore). The generally good model solution for the surface winds at this time is not perfect, however. The sea-breeze front has penetrated somewhat too far inland and the northeast wind observed at Provincetown erroneously was simulated in the model to be easterly (just north of another convergence zone over the tip of the Outer Cape).

It should be pointed out that there are many areas, especially close to the convergence zones, where the winds change direction drastically over a distance of only 1-3 km. This phenomenon is especially likely to occur on a day with gentle winds and weak large-scale forcing, as is true of 1 July. Thus, even a minor error in the simulated position of the sea-breeze front or a convergence zone can lead to very large errors, compared to the local observed wind directions. In such a case, statistics for the wind directions sometimes can appear to be quite poor, even though a careful inspection of the mesoscale structure of the flow reveals generally good agreement between the model and the observations. It should also be noted that minor position errors, such as found here, do not necessarily affect plume transport in a significant way, since that transport results from the integrated winds found downwind of an emissions source. The example shown in Figures 11 and 31 demonstrates that model evaluation should be done carefully using a variety of methods, rather than relying on a single approach.

Some additional information about the sea breeze on 1 July can be gained by examining the thermal and pressure fields. Figure 32 shows the strong contrast that developed between the surface-layer air temperatures over land and sea by 1800 UTC. Over the ocean south of Cape Cod, the air temperatures average about 16 C (61 F), while over southeastern MA, the temperatures north and west of the sea-breeze front are ~27-29 C (81-84 F). The large land-sea thermal contrast is responsible for the strong sea breeze in this case. Further inspection of Figure 32 reveals that the largest temperature gradients remain in the immediate vicinity of the shoreline, because the surface-layer air is modified very rapidly as it passes over the hot soil on land. Most of the thermal modification in the surface layer occurs in the first 1-3 km of onshore flow, so that the model predicts temperatures or 22-25 C (72-77 F) over Cape Cod and the two islands to its south. This rapid adjustment is confirmed by the observed temperatures for these

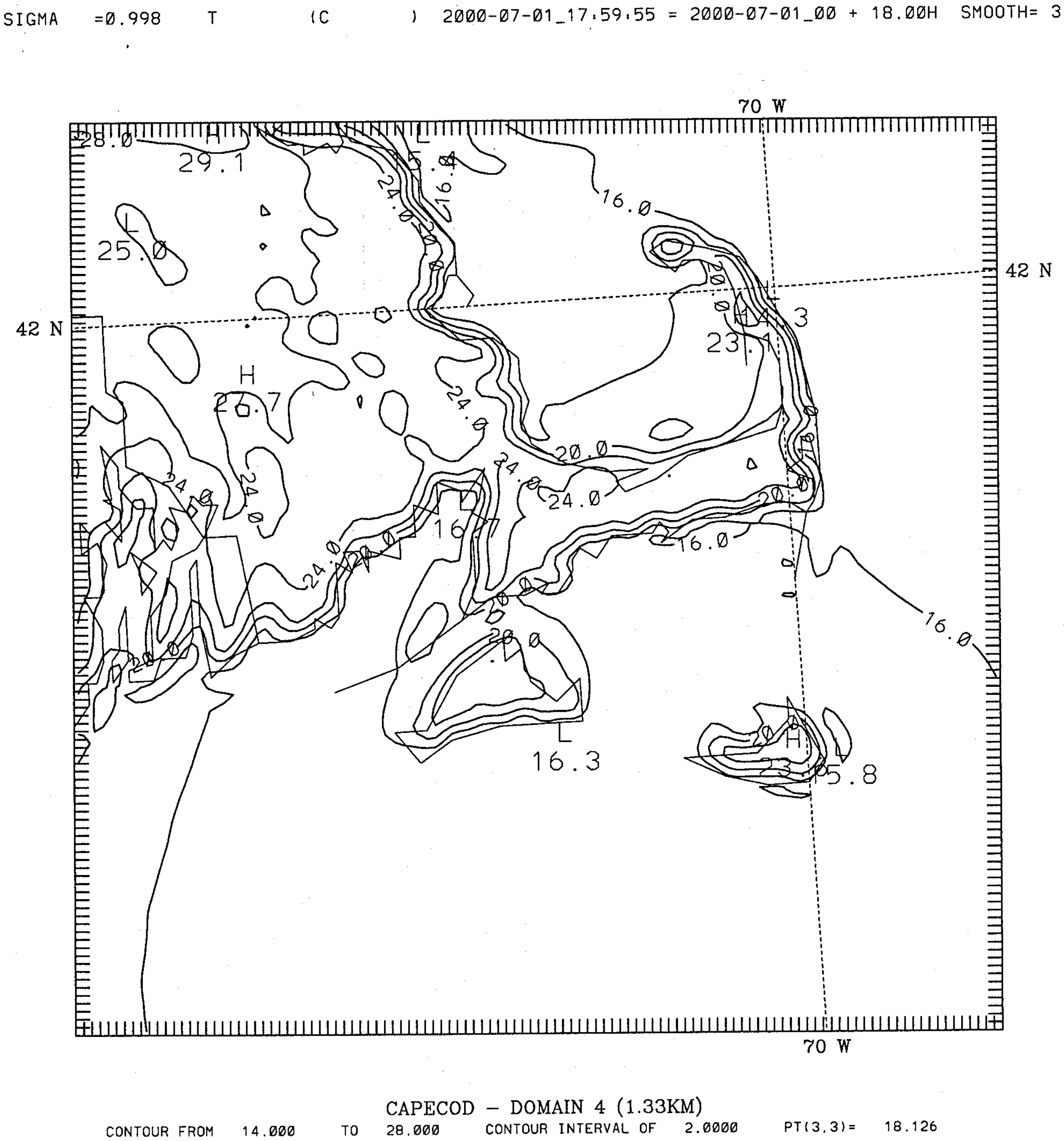

Figure 32. MM5 surface-layer temperatures (C) simulated on the 1.33-km domain in Case 1 valid at 1800 UTC, 1 July 2000 (+18 h). Contour interval is 2 C.

areas in Figure 11. Lastly at this time, the MM5-simulated sea-level pressure field on the 4-km domain over southern New England (not shown) indicated that the model has captured the main aspects of the analysis shown in Figure 8. For example, the generally weak synoptic pressure gradient, with comparatively higher pressures over the Atlantic Ocean and lower pressures over NH and ME were represented. However, in the model, the pressure was somewhat too low in southern NH, which strengthened the pressure gradient between that area and Cape Cod. This, in turn, led to a weak southwesterly geostrophic wind over southeastern MA, which may have allowed the sea breeze to penetrate inland more rapidly in the model than was observed (as discussed above).

By 2100 UTC, 1 July, (+21 h, or 1700 EDT) the simulated sea breeze had penetrated even farther inland, almost to the northwest corner of the 1.33-km domain, so that southerly winds covered almost the entire area (Figure 33). Also, the convergence zones have been modified and extended into three more-or-less parallel lines that originate in the lee of an island or a peninsula. The two eastern convergence lines bend downwind to follow the shorelines of eastern MA (south of Boston) and Outer Cape Cod.

The depth of the PBL at 2100 UTC is shown in Figure 34. The boundary layer is deepest (1600-2600 m) in the northwest corner of the domain, ahead of the sea-breeze front, while it is much lower (~50 - 300 m) in most regions where the cool marine air has become established. At this late-afternoon time, the solar heating of the soil is not as intense and the sea breeze is a bit stronger over land than at 1800 UTC. Therefore, the inland surface-temperature maximum is a bit cooler and the land-sea contrast at the shorelines has weakened a bit (not shown). However, comparison of Figures 33 and 34 shows that the PBL in the modified marine air mass is considerably deeper than average along the convergence zones than in other areas under marine influence. These zones, therefore, can act as potentially important "virtual chimneys" that can carry low-level pollutants to much higher levels (nearly 1000 m over Upper Cape Cod and 1400 m over southeastern MA). The lifting mechanism is through a combination of the eddy transport supplied by turbulence in the boundary layer and the mean upward motion caused by horizontal convergence of the low-level winds (as analyzed from the beachfront observations). Once lofted to the top of the locally deeper PBL, horizontal advection by the mid-level winds will tend to carry the pollutants downwind, where lower PBL heights exist away from the surface convergence zones. For example, Figure 35 shows the wind field at 925 mb, or about 900 m above sea level. After being removed from the influence of the surface-based turbulent mixing, the pollutants in these elevated plumes can remain aloft, thereby reducing the concentrations at the surface over considerable distances.

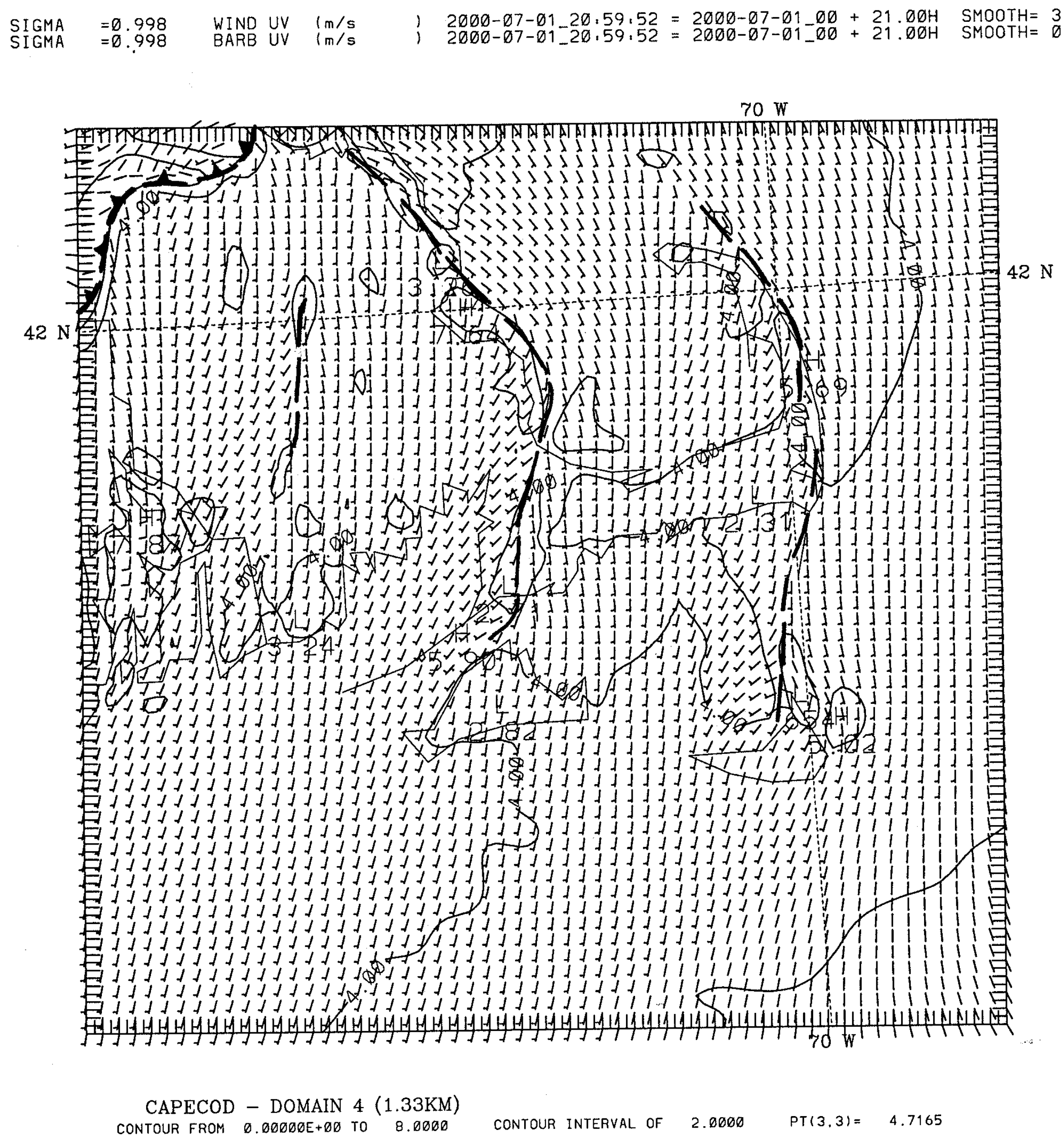

Figure 33. MM5 surface-layer wind (ms^{-1}) simulated on the 1.33-km domain in Case 1 valid at 2100 UTC, 1 July 2000 (+21 h). Full barb is 10 ms^{-1}. Contour interval is 2 ms^{-1}. Heavy dashed line with barbs represents the sea-breeze front. Dashed lines without wedges indicate convergence zones.

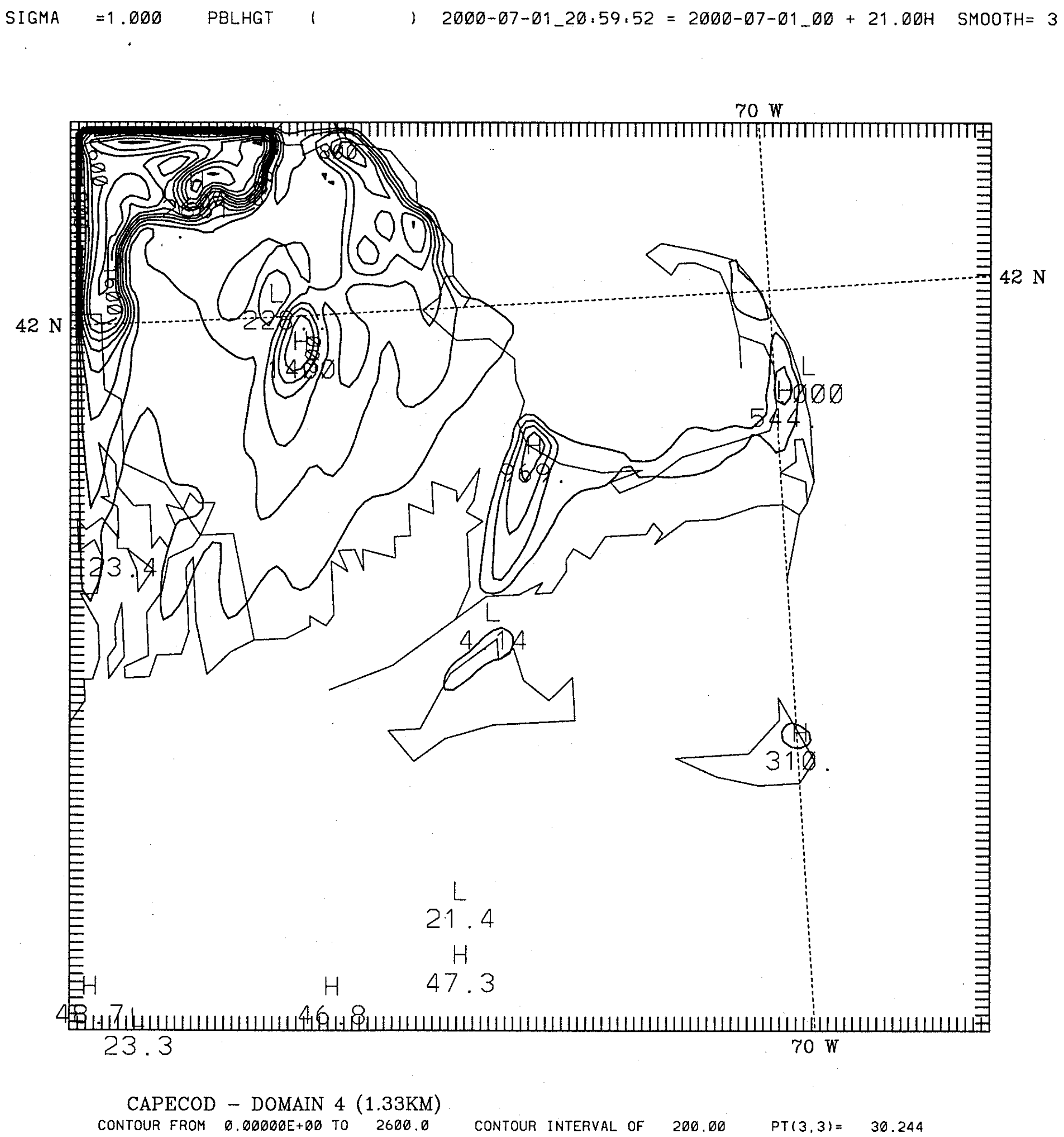

Figure 34. MM5 boundary-layer depths (m) simulated on the 1.33-km domain in Case 1 valid at 2100 UTC, 1 July 2000 (+21 h). Contour interval is 200 m.

This scenario of lofting plumes was recognized by Seaman and Michelson (2000) as a mechanism that could inject ozone and other species above the PBL along the Appalachian Lee Trough (APLT) in eastern PA and NJ during an air-pollution episode in July 1995. As a potential mechanism acting in the area of southeastern MA and Upper Cape Cod, it could be important on days when the sea breeze is active. For example, the deep PBL over Upper Cape Cod on 1 July suggests that emissions from some of the primary local emissions sources in that area may be rapidly evacuated from the lower layers and detrained aloft at a level where they can be transported over large distances for many hours before having another opportunity to affect the surface. It should be noted, however, that just as the convergence zones associated with different branches of the sea breeze undergo considerable evolution during the day, so may the location and depth of the PBL maximums along the convergence zones. More study, including dispersion modeling, is necessary to understand the likely fate of local emissions in such a complex case.

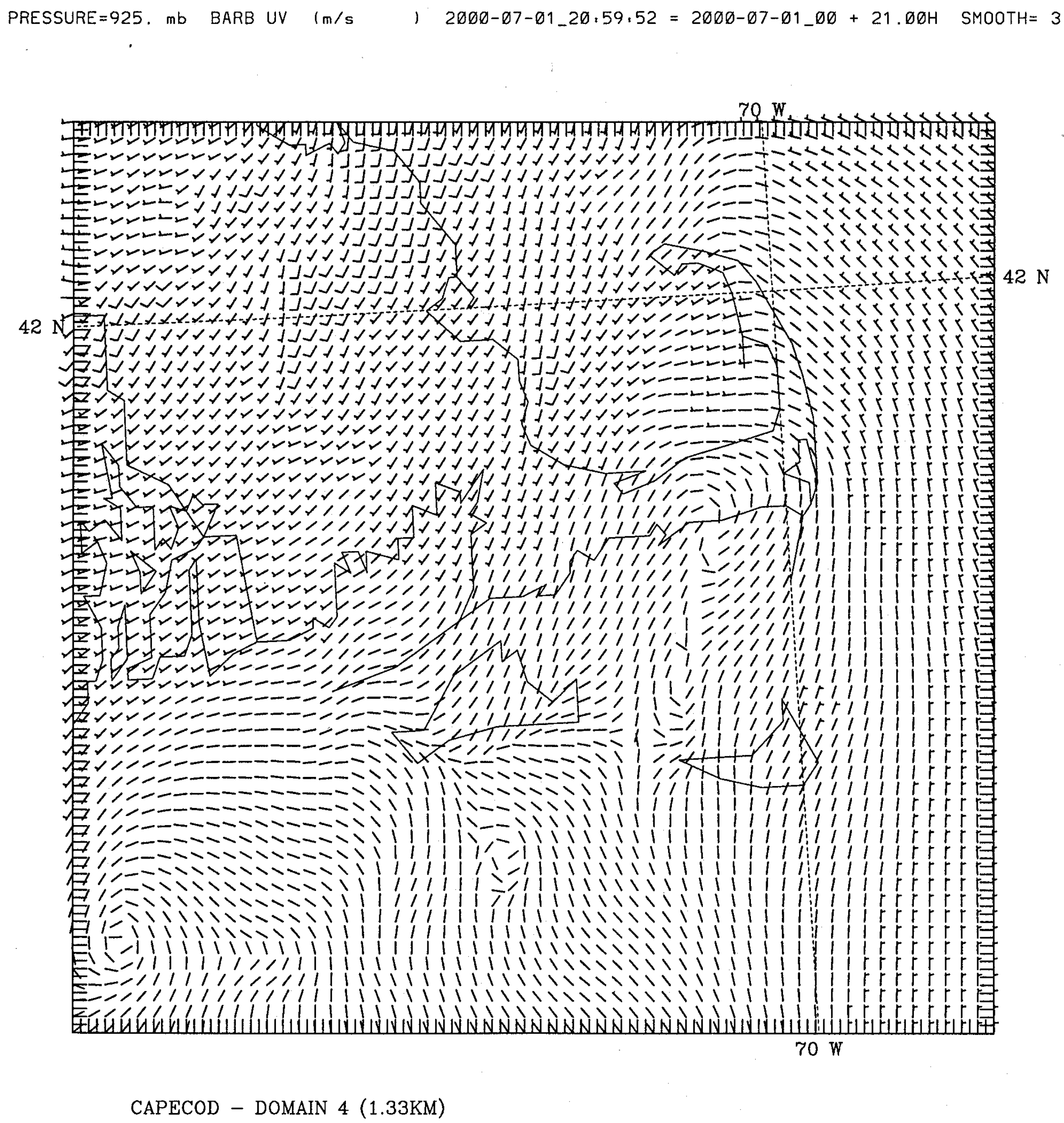

Figure 35. MM5 wind (ms^{-1}) simulated at 925 mb on the 1.33-km domain in Case 1 valid at 2100 UTC, 1 July 2000 (+21 h). Full barb is 10 ms^{-1}.

As a final examination of the MM5 fields produced by the MM5 model for Case 1, we present the surface-layer winds and PBL depths on the second afternoon, at 1800 UTC, 2 July (+42 h) in Figures 36 and 37. The model-simulated winds in Figure 36 compare rather well to the observed winds at the same time at most sites (see Figure 10). As on the previous day, the model has simulated a fairly robust sea breeze front that has penetrated well inland by early afternoon, plus several convergence zones over Cape Cod and in the lee of Martha's Vineyard. The positions of these features are generally similar to those found at 1800 UTC on 1 July (Figure 31), but with minor differences. Figure 37 shows that the PBL depth is quite low in the coastal areas of southeastern MA as the sea-breeze front penetrates steadily inland. The locally deeper PBL depths over UCC are re-emerging on this second day along the convergence zones over land within the regions dominated by cool marine air. These results indicate that, at least for cases in which the synoptic-scale forcing produces light southwesterly flow, the features found on 1 July are mostly repeated. However, one can expect subtle changes due to differences in the land-sea thermal contrast and the mean background wind direction and speed.

Next, Tables 3-8 show the results of the statistical evaluation of the MM5 for Case 1. Tables 3-5 present the statistics for the 1.33-km domain, while Tables 6-8 are for the 4-km domain. All statistics are calculated at 3-h intervals by interpolating the model solutions to the location of NWS observation sites. The tables give the root mean square error, the mean absolute error, the mean error, and the percent of model-predicted values that verify within an arbitrary threshold (Stauffer and Seaman 1990). The root mean square error (RMS error) gives a large weight to the greatest individual errors, so that it gives the user a sense of the typical magnitude of the largest errors. The mean absolute error gives the magnitude of the most common error. The mean error gives the size of the model's bias. The percent of points within the threshold gives a sense of the frequency of small errors in the model solutions, where "small" in this situation has been defined according to the size of errors generally thought to have little impact on air-chemistry calculations.

The tables present the statistics separately for the initial conditions and for the rest of the simulation period (3-48 h) for three different layers, or zones: (1) the surface layer, (2) the zone containing the boundary layer (45-1000 m) and (3) the lower troposphere above most PBL influences (1000-5000 m). Note that there is only one upper-air station in the 1.33-km domain (Chatham, MA), so that the statistics for the two zones above the surface in Table 3 may not be representative of the full domain. In addition to Chatham, the 4-km domain also includes the NWS upper-air stations at Portland, ME, Albany, NY, and Brookhaven, NY. All of these stations launch their radiosonde balloons twice per day (at 0000 and 1200 UTC). However, at the surface there are 10-15 reporting sites (depending on the time of day) in the 1.33-km domain and 90-100 in the 4-km domain. For the surface sites, the comparisons are made every 3 h, or eight times per day. Thus, it is much easier to get meaningful statistical results for the surface layer than for the upper levels.

Examination of the statistics for Case 1 shows some interesting trends. First, note that the model's simulated wind speeds during the 3-48 h period tend to be as accurate, or even more accurate, than the speeds contained in the EDAS objective analyses used at the initial time (see Tables 3 and 6). This is quite remarkable and suggests that the model is responding well to local mesoscale surface influences. The largest wind-speed errors during the simulation period occur in the 45-1000 m layer containing the PBL, where the model tends to over-predict the wind speeds by 1-2 ms^{-1}. This error is thought to be due to an underestimation of the MM5's downward momentum flux in the PBL, which can be corrected in future studies. The speed errors decrease significantly above the PBL in the 1000-5000 m layer, where they become only moderately larger than the analysis errors.

The wind direction errors during the 3-48 h model simulations are only moderately greater than the direction errors in the analyses. Mean errors (biases) for the wind direction are generally less than 10 degrees in the model solutions, except in the PBL (45-1000 m) where the directions are known to change rapidly with height. Some notes about the wind direction errors are worthwhile. First, the analyzed surface wind directions have fairly large RMS errors (35-45 degrees) and low biases (less than 15 degrees) because local effects such as buildings, hills, and other obstacles can easily distort the wind measurements near the ground. These effects rapidly disappear with height. Furthermore, on these two fine-grid domains, where coastal influences are very important, small errors in the timing of sea-breeze development or in the position of a convergence zone can easily cause very large direction errors at specific times and locations. However, this does not mean that the model has failed in any major way, because it is virtually impossible to reproduce the exact positions of such intense local features. Thus, it is encouraging that the model produces rather low biases for the simulated wind directions, even though the RMS errors and mean absolute errors indicate that there are apparently many individual sites with large departures from the observations. This is confirmed by the percentage of wind directions that verify within the 20-degree threshold, which shows scores below 50% at the surface. The statistical performance of the MM5 for wind speed and direction in this case is quite similar to published values of performance typically found for mesoscale models applied in air-quality episodes.

Overall the other statistics for temperature, moisture (relative humidity and mixing ratio) and sea-level pressure are also quite acceptable, especially in the sense that the model's biases are low. However, note that although the bias for the surface temperature is small on both domains, the RMS error and mean absolute error is considerably larger. The low biases result from the nature of the mean error, which allows positive and negative errors to cancel each other. However, the other two statistics do not allow for such cancellations, so that their errors appear large. Physically, the cause of this condition is that the MM5, like many models, tends to overestimate the surface temperature during the night (when minimum temperatures are observed) and underestimate the temperatures during the afternoon (when maximum temperatures are observed). This type of error can at least be minimized in future studies by using an alternative long-wave radiation scheme and by the assimilation of surface temperature data through the MM5's FDDA scheme.

Lastly, note that the statistics for the 1.33-km and 4-km domains are mostly consistent with one another. The wind and humidity fields are slightly more accurate on the 1.33-km domain, while the temperatures appear slightly more accurate on the 4-km domain.

Table 3. Statistical summary of MM5 performance for wind speed and direction in Case 1 (1-2 July 2000) on the 1.33-km domain.

Wind Speed (ms^{-1})	RMS Error	Mean Abs. Error	Mean Error	% Within 2.0 ms^{-1}
0 h (Initial Cond's.)				
Surface (~12 m AGL)	1.83	1.38	0.35	70.6
45-1000 m AGL	0.85	0.85	-0.84	100.0
1000-5000 m AGL	0.80	0.80	-0.78	86.7
3 -48 h Simulation				
Surface (~12 m AGL)	1.46	1.23	0.09	81.6
45-1000 m AGL	2.07	2.07	1.69	60.0
1000-5000 m AGL	1.03	1.03	0.53	91.4
Wind Direction (deg.)	**RMS Error**	**Mean Abs. Error**	**Mean Error**	**% Within 20 deg.**
0 h (Initial Cond's.)				
Surface (~12 m AGL)	34.5	24.3	-2.6	52.9
45-1000 m AGL	13.7	13.7	13.7	87.0
1000-5000 m AGL	2.7	2.7	-1.0	100.0
3 -48 h Simulation				
Surface (~12 m AGL)	54.3	40.5	-9.1	42.5
45-1000 m AGL	21.6	21.6	-20.0	62.2
1000-5000 m AGL	29.7	29.7	7.1	70.7

Table 4. Statistical summary of MM5 performance for temperature and sea-level pressure in Case 1 (1-2 July 2000) on the 1.33-km domain.

Temperature (C)	RMS Error	Mean Abs. Error	Mean Error	% Within 2.0 C
0 h (Initial Cond's.)				
Surface (~12 m AGL)	1.42	1.09	0.96	82.4
45-1000 m AGL	0.89	0.89	0.75	91.3
1000-5000 m AGL	0.45	0.45	0.30	100.0
3 -48 h Simulation				
Surface (~12 m AGL)	2.69	2.20	-0.08	56.7
45-1000 m AGL	1.52	1.52	-1.51	85.9
1000-5000 m AGL	0.52	0.52	0.08	100.0

Sea-Level Pres. (mb)	RMS Error	Mean Abs. Error	Mean Error	% Within 2.5 mb
0 h (Initial Cond's.)	0.75	0.68	-0.66	100.0
3 -48 h Simulation	0.71	0.63	0.31	100.0

Table 5. Statistical summary of MM5 performance for mixing ratio and relative humidity in Case 1 (1-2 July 2000) on the 1.33-km domain.

Mixing Ratio (g kg^{-1})	RMS Error	Mean Abs. Error	Mean Error	% Within 1 g kg^{-1}
0 h (Initial Cond's.)				
Surface (~12 m AGL)	0.60	0.60	-0.60	100.0
45-1000 m AGL	0.22	0.22	-0.18	100.0
1000-5000 m AGL	0.19	0.19	0.09	100.0
3 -48 h Simulation				
Surface (~12 m AGL)	3.00	3.00	-1.83	50.0
45-1000 m AGL	0.97	0.97	-0.17	70.7
1000-5000 m AGL	0.72	0.72	0.46	68.3
Rel. Humidity (percent)	**RMS Error**	**Mean Abs. Error**	**Mean Error**	**% Within 10 percent**
0 h (Initial Cond's.)				
Surface (~12 m AGL)	6.51	5.45	-3.00	82.4
45-1000 m AGL	6.02	6.02	-5.05	82.6
1000-5000 m AGL	3.27	3.27	-0.04	100.0
3 -48 h Simulation				
Surface (~12 m AGL)	10.60	8.59	-1.38	64.7
45-1000 m AGL	8.58	8.58	5.38	71.4
1000-5000 m AGL	9.17	9.17	6.01	53.3

Table 6. Statistical summary of MM5 performance for wind speed and direction in Case 1 (1-2 July 2000) on the 4-km domain.

Wind Speed (ms^{-1})	RMS Error	Mean Abs. Error	Mean Error	% Within 2.0 ms^{-1}
0 h (Initial Cond's.)				
Surface (~12 m AGL)	1.73	1.44	0.38	67.5
45-1000 m AGL	1.43	1.25	-0.84	85.6
1000-5000 m AGL	1.26	1.06	-0.72	81.7
3 -48 h Simulation				
Surface (~12 m AGL)	1.71	1.42	-0.40	72.8
45-1000 m AGL	2.85	2.41	0.39	48.4
1000-5000 m AGL	1.83	1.61	0.45	65.4
Wind Direction (deg.)	**RMS Error**	**Mean Abs. Error**	**Mean Error**	**% Within 20 deg.**
0 h (Initial Cond's.)				
Surface (~12 m AGL)	43.0	32.0	-11.2	44.6
45-1000 m AGL	22.4	16.3	-3.5	74.4
1000-5000 m AGL	5.5	4.6	-2.7	100.0
3 -48 h Simulation				
Surface (~12 m AGL)	60.6	44.7	-6.5	39.8
45-1000 m AGL	39.3	31.5	-12.7	47.0
1000-5000 m AGL	22.7	22.2	-5.8	70.0

Table 7 Statistical summary of MM5 performance for temperature and sea-level pressure in Case 1 (1-2 July 2000) on the 4-km domain.

Temperature (C)	RMS Error	Mean Abs. Error	Mean Error	% Within 2.0 C
0 h (Initial Cond's.)				
Surface (~12 m AGL)	1.63	1.26	0.17	80.0
45-1000 m AGL	0.57	0.45	0.30	97.8
1000-5000 m AGL	0.62	0.47	0.32	100.0
3 -48 h Simulation				
Surface (~12 m AGL)	2.55	2.06	0.55	59.9
45-1000 m AGL	1.10	0.94	-0.46	92.1
1000-5000 m AGL	0.73	0.60	0.25	99.2
Sea-Level Pres. (mb)	**RMS Error**	**Mean Abs. Error**	**Mean Error**	**% Within 2.5 mb**
0 h (Initial Cond's.)	0.83	0.69	-0.60	100.0
3 -48 h Simulation	0.83	0.68	0.14	100.0

Table 8. Statistical summary of MM5 performance for mixing ratio and relative humidity in Case 1 (1-2 July 2000) on the 4-km domain.

Mixing Ratio (g kg^{-1})	RMS Error	Mean Abs. Error	Mean Error	% Within 1 g kg^{-1}
0 h (Initial Cond's.)				
Surface (~12 m AGL)	0.80	0.70	0.41	75.0
45-1000 m AGL	0.53	0.45	0.19	88.0
1000-5000 m AGL	0.21	0.17	0.04	100.0
3 -48 h Simulation				
Surface (~12 m AGL)	2.46	1.93	-0.16	37.5
45-1000 m AGL	1.69	1.38	-0.20	53.3
1000-5000 m AGL	1.06	0.87	0.24	57.1

Rel. Humidity (percent)	RMS Error	Mean Abs. Error	Mean Error	% Within 10 percent
0 h (Initial Cond's.)				
Surface (~12 m AGL)	10.11	8.20	2.13	68.2
45-1000 m AGL	5.14	4.61	0.01	95.7
1000-5000 m AGL	4.03	3.09	-1.04	98.3
3 -48 h Simulation				
Surface (~12 m AGL)	12.80	10.24	-4.63	57.8
45-1000 m AGL	11.18	9.62	5.38	71.4
1000-5000 m AGL	9.17	9.17	1.42	63.0

4.2.2 Case 2: Sea Breeze 2

The second case, as described in Section 4.1.2, was characterized by the passage of a moderate-strength cold front through New England early on 5 July 2000. The northwesterly winds that dominated behind the front on 5 July gradually weakened to allow the formation of a localized sea breeze over Cape Cod and southeastern MA near the end of the episode on the afternoon of 6 July. Although the front did not produce widespread rain over New England, a few showers were reported, including a thunderstorm in northern NH at 0000 UTC, 5 July (Figure 15). Figure 38 shows that the MM5 generated a few isolated light showers over MA during the first 12 h of the simulation period, with some heavier rains predicted over the ocean south of RI and Cape Cod. A GOES-8 infrared satellite image from 0000 UTC (not shown) indicates that middle clouds existed in this area and Figure 15 shows fog over southeastern MA, Long Island, and coastal areas of CT and RI at that time. Since widespread fog is not common at 0000 UTC (2000 EDT) over this area in early July (about a half hour before sunset), it seems quite possible that offshore rain showers did occur, even though we have no direct verification for the model's prediction over the water. In any case, the predicted rain ended that evening as the front swept off the coast and no more precipitation occurred in the model for the rest of the episode, as observed.

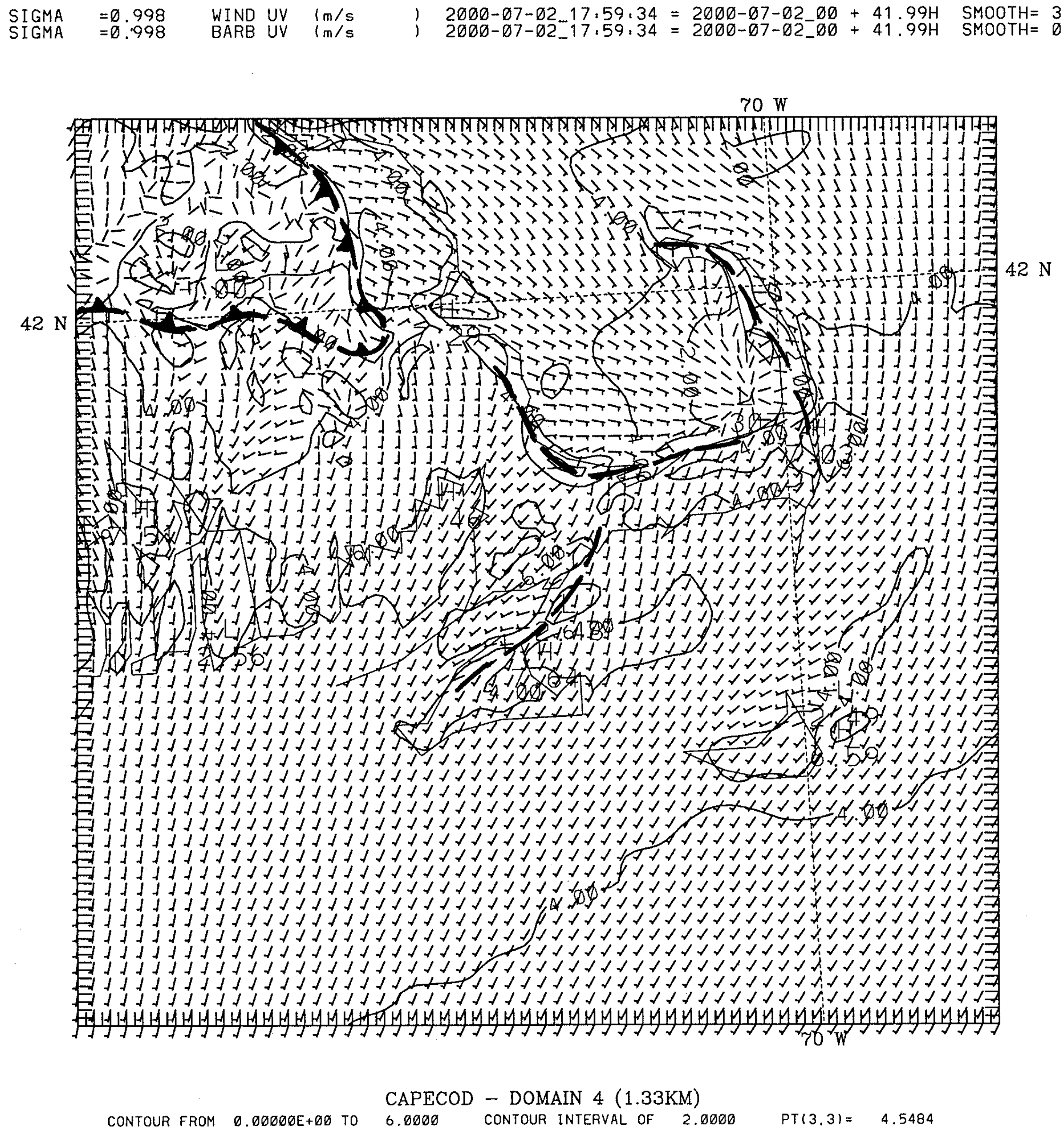

Figure 36. MM5 surface-layer wind (ms^{-1}) simulated on the 1.33-km domain in Case 1 valid at 1800 UTC, 2 July 2000 (+42 h). Full barb is 10 ms^{-1}. Contour interval is 2 ms^{-1}. Heavy dashed line with barbs represents the sea-breeze front. Dashed lines without wedges indicate convergence zones.

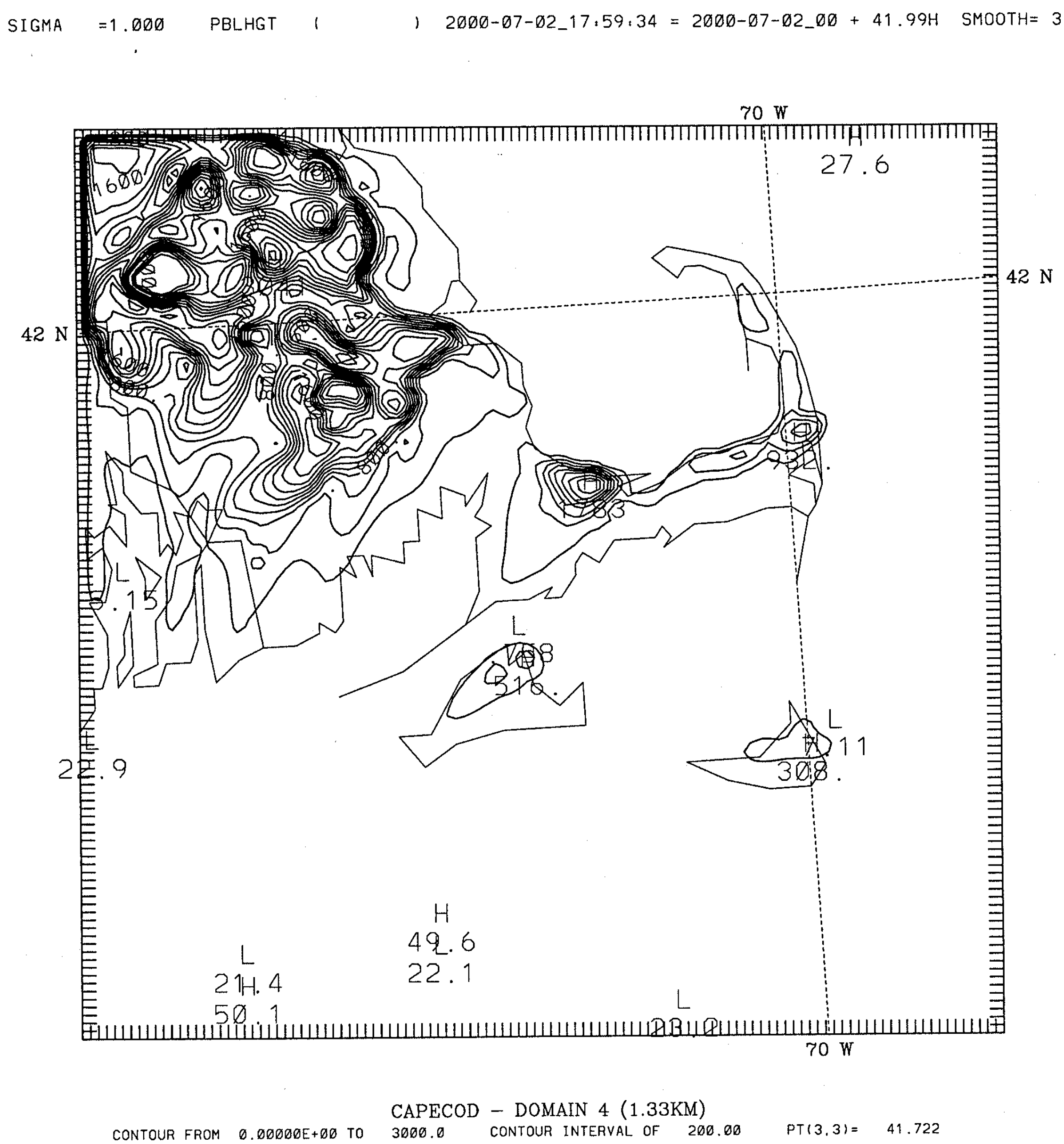

Figure 37. MM5 boundary-layer depths (m) simulated on the 1.33-km domain in Case 1 valid at 1800 UTC, 2 July 2000 (+42 h). Contour interval is 200 m.

By the first morning, at 1200 UTC, northwesterly surface winds of 6-12 kts (3-6 ms^{-1}) had become established over the entire 1.33-km domain (Figure 39). On average, the winds tended to be a bit faster over water, where frictional deceleration was reduced, but overall the flow was fairly uniform. This simulated wind pattern is confirmed by Figure 16.
As the day progressed, however, the winds over the region were influenced by the passage of a post-frontal trough at about 1800 UTC, 5 July (shown in the analysis of Figure 17). Observations show that this trough disrupted the widespread northwesterly flow, bringing southwesterlies to Martha's Vineyard, Nantucket and southwestern Cape Cod and northeasterly winds at Provincetown and on central Cape Cod (Figure 17). The MM5-simulated surface-layer winds at the same time are shown in Figure 40. The most obvious characteristic of the model's wind field at this time is its chaotic patterns, due to the rapidly weakening pressure gradient. However, upon closer inspection, the MM5's winds reveal some remarkable details that are consistent with the observations. First, over southeastern MA and eastern RI, the winds are mostly from the northwest at speeds that average ~ 8-12 kts (4-6 ms^{-1}). The winds in this part of the domain are organized into bands, with alternating convergence and divergence lines oriented roughly with the wind direction. This kind of pattern is common in sheared boundary-layer flows and the observations over the same area in Figure 17 show similar individual reports with winds varying between west and north-northwesterly. In Figure 40, the main convergence zone lies along the south shore of Upper Cape Cod, the innermost (northwest) shore of Buzzard's Bay, and the cost of RI. South of this convergence zone, winds are mostly from the south to southwest, which is in general agreement with the winds south of the trough in Figure 17. Thus, the model appears to have simulated the position of the trough fairly well on this local domain, while it is revealed at this very fine scale to be sinuous in shape, rather than linear. This is also consistent with the weakening background pressure gradient. Furthermore, notice that the winds over Upper and Outer Cape Cod are mostly from the north to northeast directions, with easterlies over parts of Massachusetts Bay. This surprising exception to the general northwesterly flow found north of the trough appears related to the local patterns of heating and cooling of air flowing over land and sea in the vicinity of the Cape and the Bay (not shown), combined with the separate influence of the nearby synoptic pressure trough.

Aloft, at 925 mb (~900 m above sea level), the winds are much more uniform in direction at 1800 UTC, 5 July, with northwesterlies dominating the entire 1.33-km domain (Figure 41). However, the speeds are notably faster to the north of the trough position, at ~16-26 kts (8-13 ms^{-1}), while they decelerate to 10-18 kts (5-9 ms^{-1}) to its south. Thus, there is a great deal of shear in the low-level winds at this time. The depth of the PBL on the first afternoon is about 1200-2300 m over southeastern MA and westernmost Cape Cod (near Buzzard's Bay), but is only 200-700 m over the rest of the Cape (not shown) and less than 200 m over the sea.

SIGMA =1.000 TEND RNT (mm) 2000-07-05_12:00:00 = 2000-07-05_00 + 12.00H SMOOTH= 3

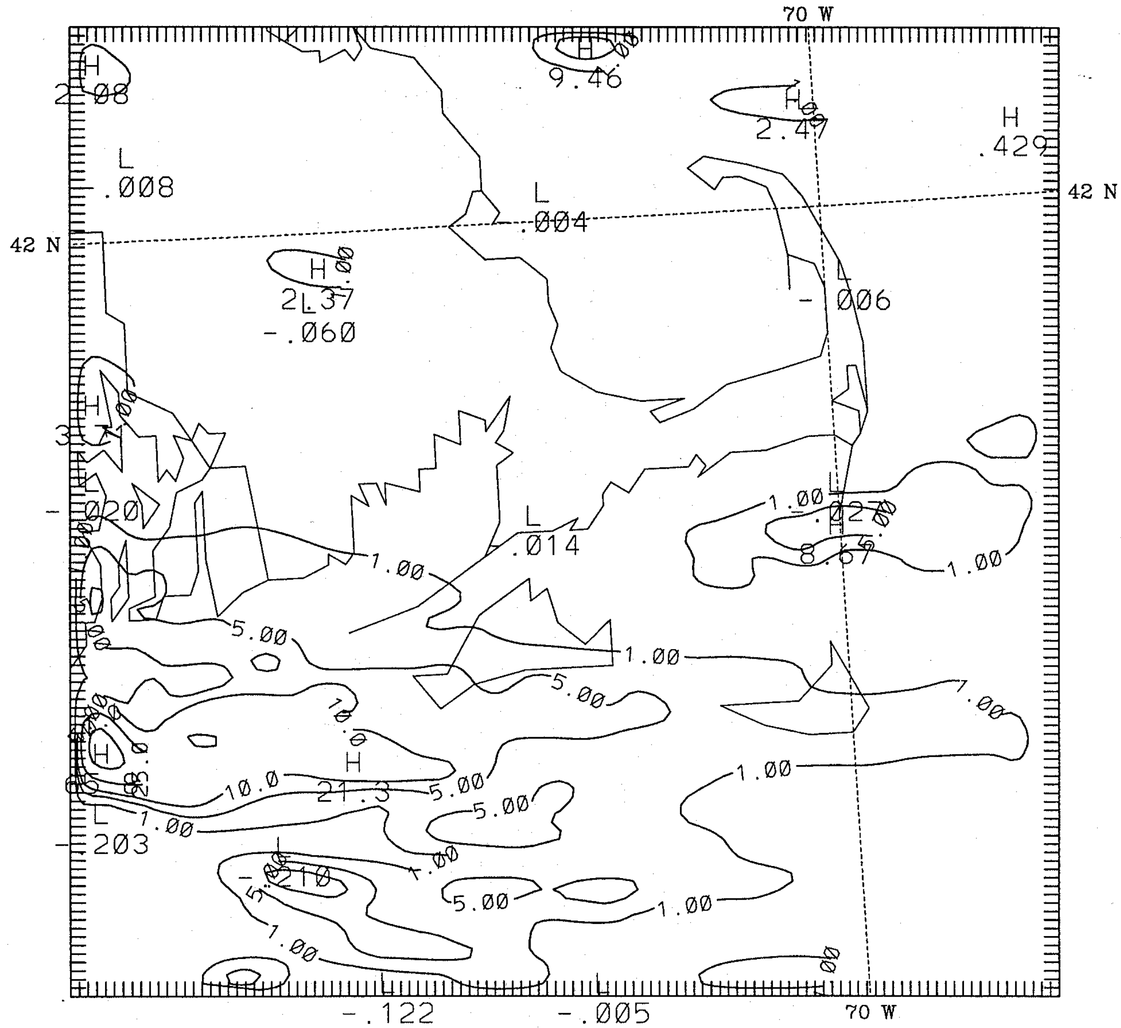

CAPECOD CASE 2 – DOMAIN 4 (1.33KM)
CONTOUR FROM 000000 TO 000000 CONTOUR INTERVAL OF 5.0000 PT(3,3)= 0.66713E-01

Figure 38. MM5 total rainfall (mm) simulated on the 1.33-km domain in Case 2 valid at 1200 UTC, 5 July 2000 (+12 h). Contours are at 1, 5, 10 and 25 mm.

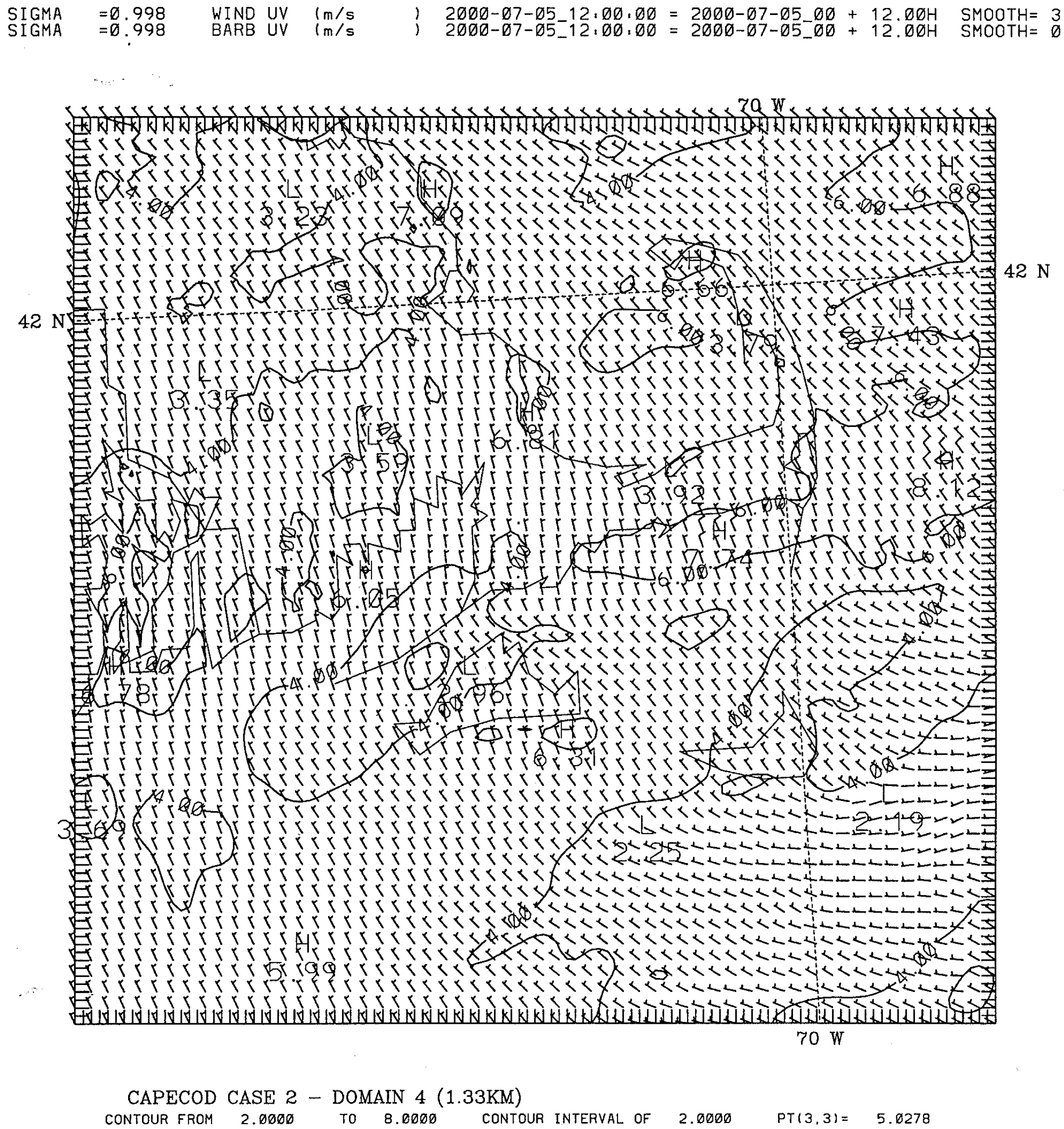

Figure 39. MM5 surface-layer wind (ms^{-1}) simulated on the 1.33-km domain in Case 2 valid at 1200 UTC, 5 July 2000 (+12 h). Full barb is 10 ms^{-1}. Contour interval is 2 ms^{-1}.

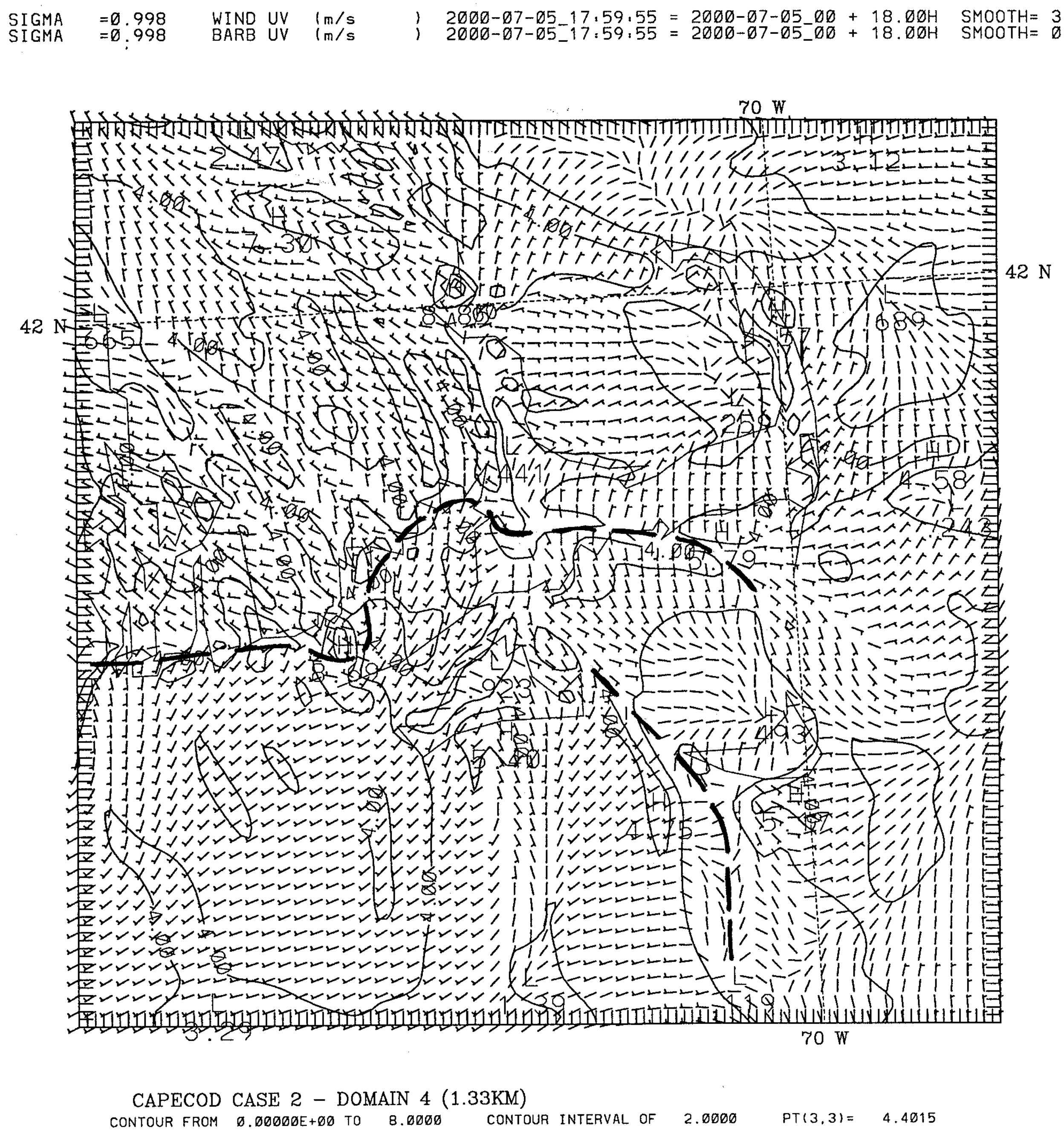

Figure 40. MM5 surface-layer wind (ms^{-1}) simulated on the 1.33-km domain in Case 2 valid at 1800 UTC, 5 July 2000 (+18 h). Full barb is 10 ms^{-1}. Contour interval is 2 ms^{-1}. Dashed lines indicate convergence zones.

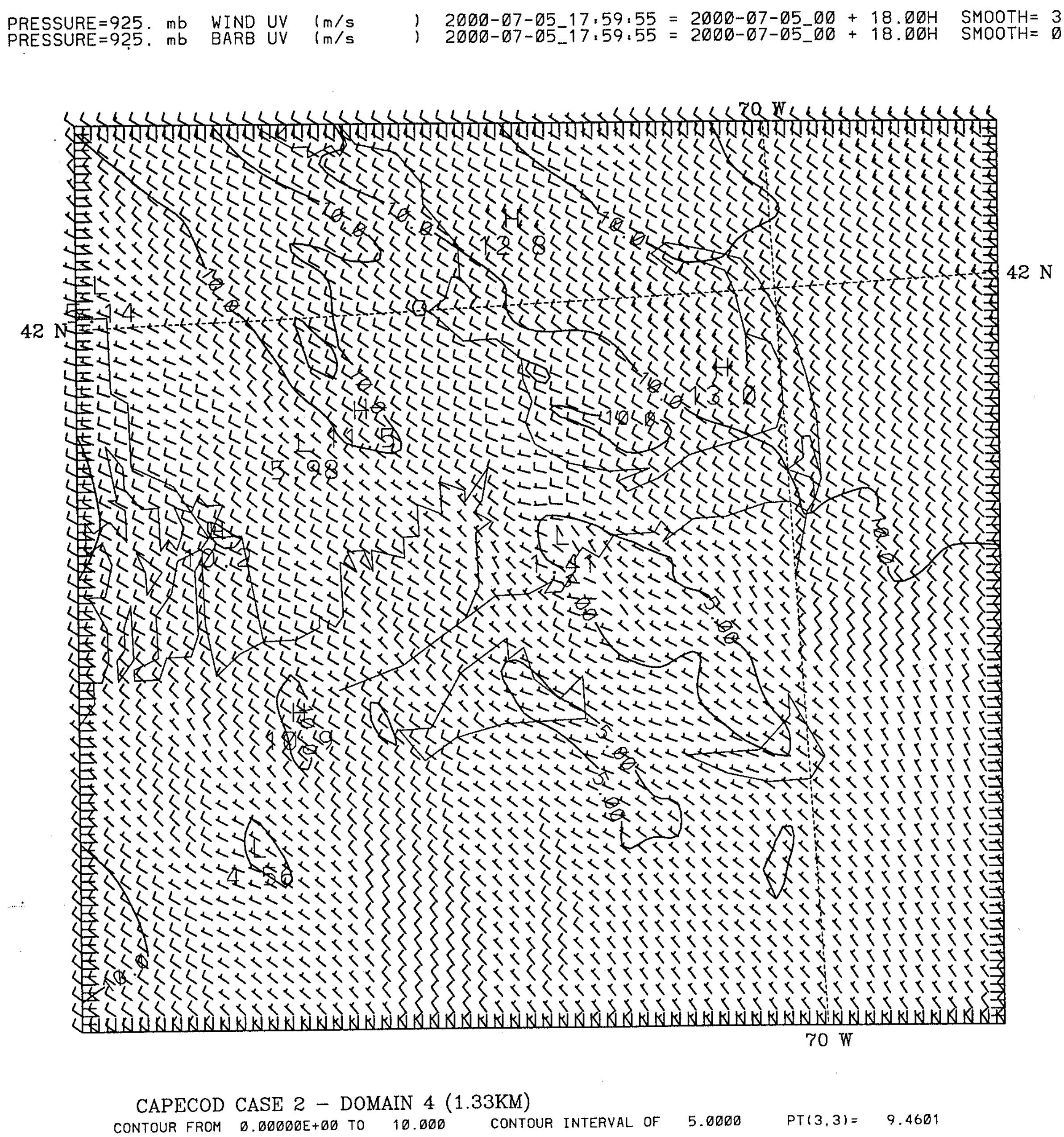

Figure 41. MM5 wind (ms^{-1}) simulated at 925 mb on the 1.33-km domain in Case 2 valid at 1800 UTC, 5 July 2000 (+18 h). Full barb is 10 ms^{-1}.

By the next afternoon at 1800 UTC, 6 July, the northwesterly winds had weakened over New England, as shown by the observations in Figure 19. Solar heating caused temperatures in the model to rise to 24-25 C (75-78 F) over southeastern MA on this afternoon, with 20-23 C (68-73 F) over Cape Cod (Figure 42), which agrees well with the data. These temperatures are a bit lower than in Case 1, so the coastal temperature gradients were less extreme on this day (compare to Figure 32). In response to the heating, the MM5 generated a thermally induced 1011-mb low pressure center south of Boston at 42.0 N at 1800 UTC (not shown), which is in good agreement with the thermal low analyzed in Figure 19.

Next, Figure 43 shows the surface-layer wind field generated by the model at 1800 UTC, 6 July. Similar to Case 1, the sea-breeze front has pushed inland over southeastern MA and is in about the correct position at this time (compare to Figure 19). North and west of the sea-breeze front, the winds in the thermal low are weak and chaotic. Over Cape Cod and downwind of Nantucket and Martha's Vineyard, different local sea breezes generated by the particular land-sea distribution collide in the convergence zones shown in Figure 43. Of particular interest in this case are the northerly and northeasterly winds along the north shore of Upper Cape Cod and on the seaward (eastern) shore of Outer Cape Cod. There is even a light northerly component on the tip of the Cape at Provincetown. Meanwhile, strong southwesterly winds penetrate into the western end of the Cape through Buzzard's Bay. The winds in the center of the two islands, however, are south to southeasterly, rather than southwesterly as observed. Nevertheless, despite some local errors, the overall wind pattern appears to be very realistic for this day and is consistent with most of the observations.

We complete the evaluation of the model's wind patterns at 1800 UTC, 6 July, by examining the PBL depth and the mid-level winds (Figures 44 and 45). The PBL depth at this time is quite deep over all land areas (800- 2300 m), except where the sea breeze has penetrated inland over southeastern MA (Figure 44). Although there is no way to verify this pattern, due to the absence of relevant upper-air data over the region, this pattern is consistent with the intense solar heating and very light winds. Figure 45 shows that, even at 925 mb, the winds are quite weak at this time, except over the northeast part of the 1.33-km domain, where the remnant northwesterly flow remains at ~10-15 kts (5-7 ms^{-1}). Consequently, at least at this time, emissions originating from Upper Cape Cod and southeastern MA should be mixed through fairly deep layers, but will not be subject to rapid horizontal advection.

Finally, the continued evolution of the sea breeze in the MM5 on the afternoon of 6 July can be seen by examining the surface-layer winds and the PBL depth at 2100 UTC. Figure 46 shows that the sea-breeze front had penetrated into the northwest corner of the 1.33-km domain over southeastern MA. By comparison, Figure 20 indicates that although the thermal low was well developed at this time, the observed sea-breeze front did not make such rapid progress inland. Meanwhile, as in Case 1, the late afternoon PBL depth becomes quite shallow over Cape Cod (well behind the sea-breeze front), with regions of deeper PBLs organized along the shifting convergence zones (Figure 47). This pattern is so consistent in the model simulations of sea-breeze Cases 1 and 2 that we can be reasonably confident that they are quite real. Moreover, we can infer that these pockets of low-level convergence and deeper PBL depths provide regions where pollutants are likely to be lofted during the afternoon, even though the general depth of the PBL is much less over Upper Cape Cod.

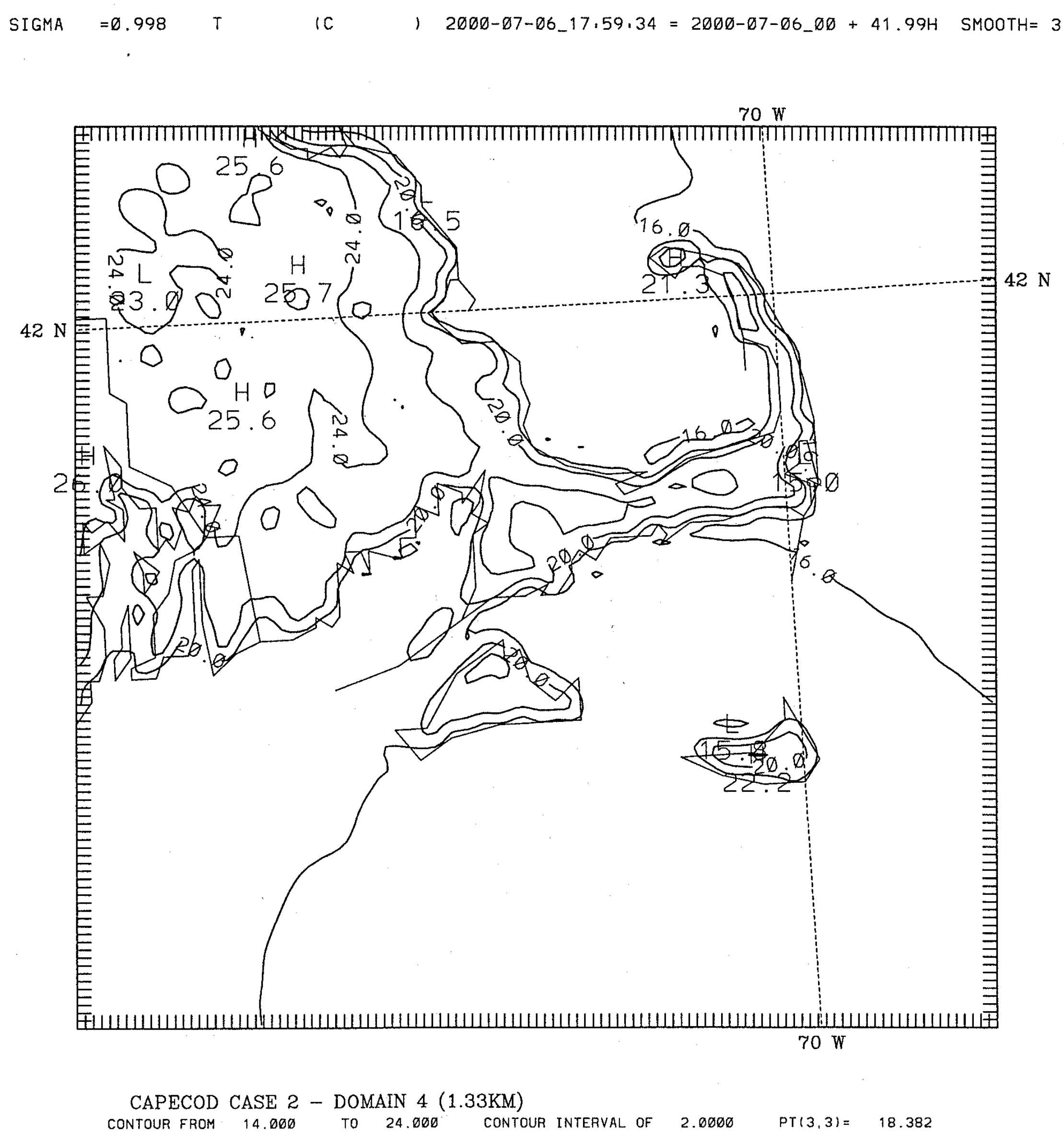

Figure 42. MM5 surface-layer temperatures (C) simulated on the 1.33-km domain in Case 2 valid at 1800 UTC, 6 July 2000 (+42 h). Contour interval is 2 C.

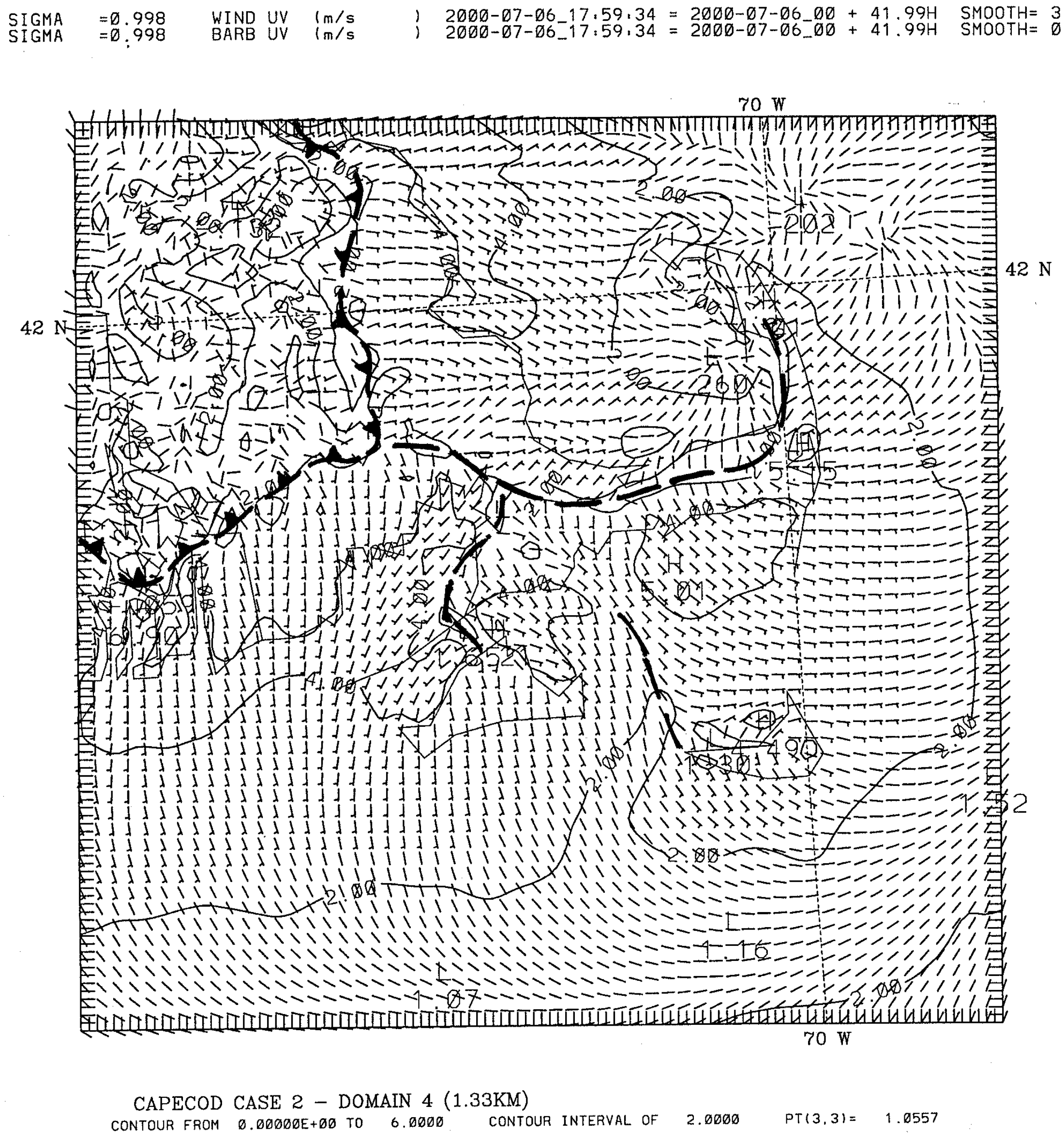

Figure 43. MM5 surface-layer wind (ms^{-1}) simulated on the 1.33-km domain in Case 2 valid at 1800 UTC, 6 July 2000 (+42 h). Full barb is 10 ms^{-1}. Contour interval is 2 ms^{-1}. Heavy dashed line with barbs represents the sea-breeze front. Dashed lines without wedges indicate convergence zones.

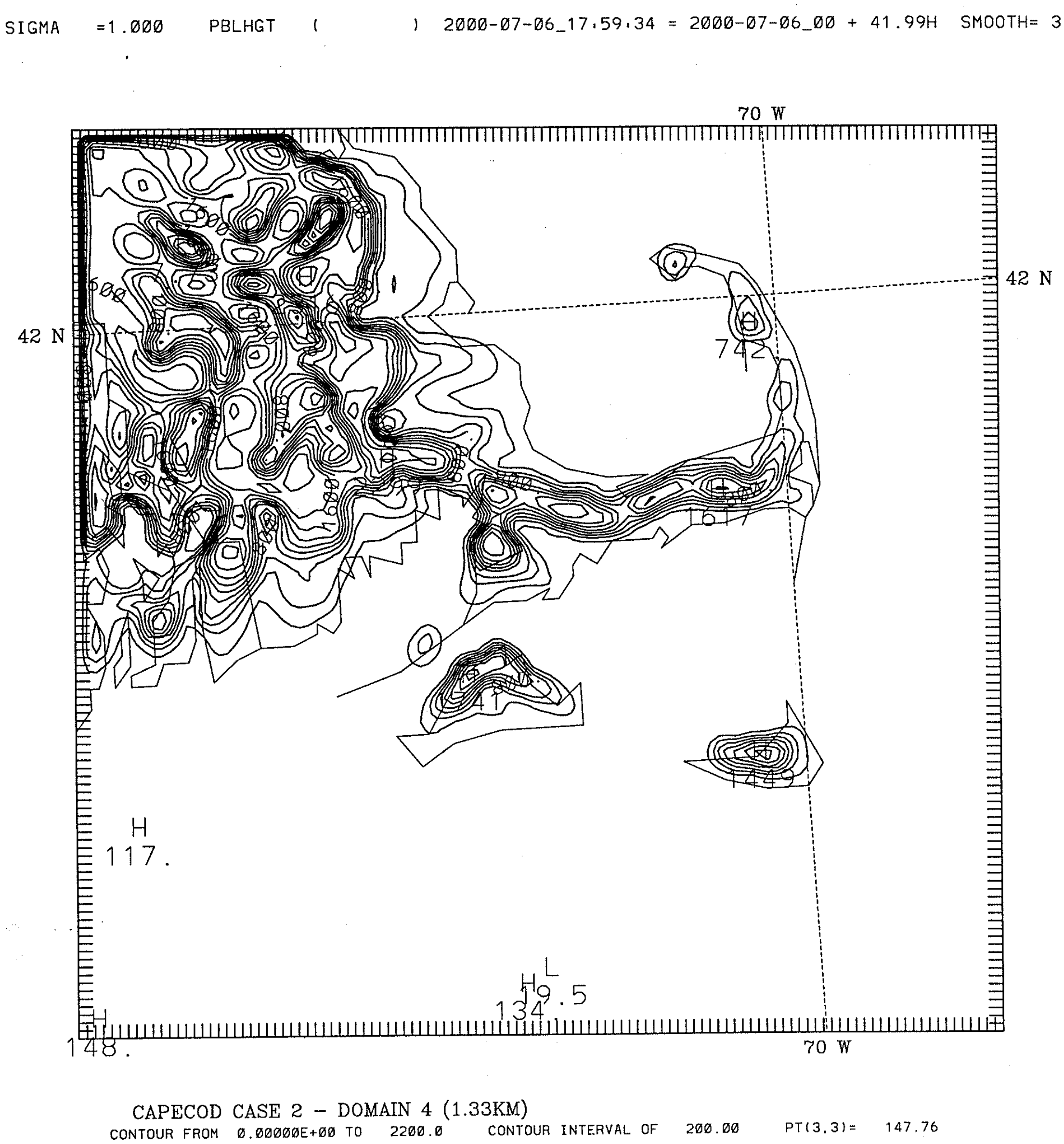

Figure 44. MM5 boundary-layer depths (m) simulated on the 1.33-km domain in Case 2 valid at 1800 UTC, 6 July 2000 (+42 h). Contour interval is 200 m.

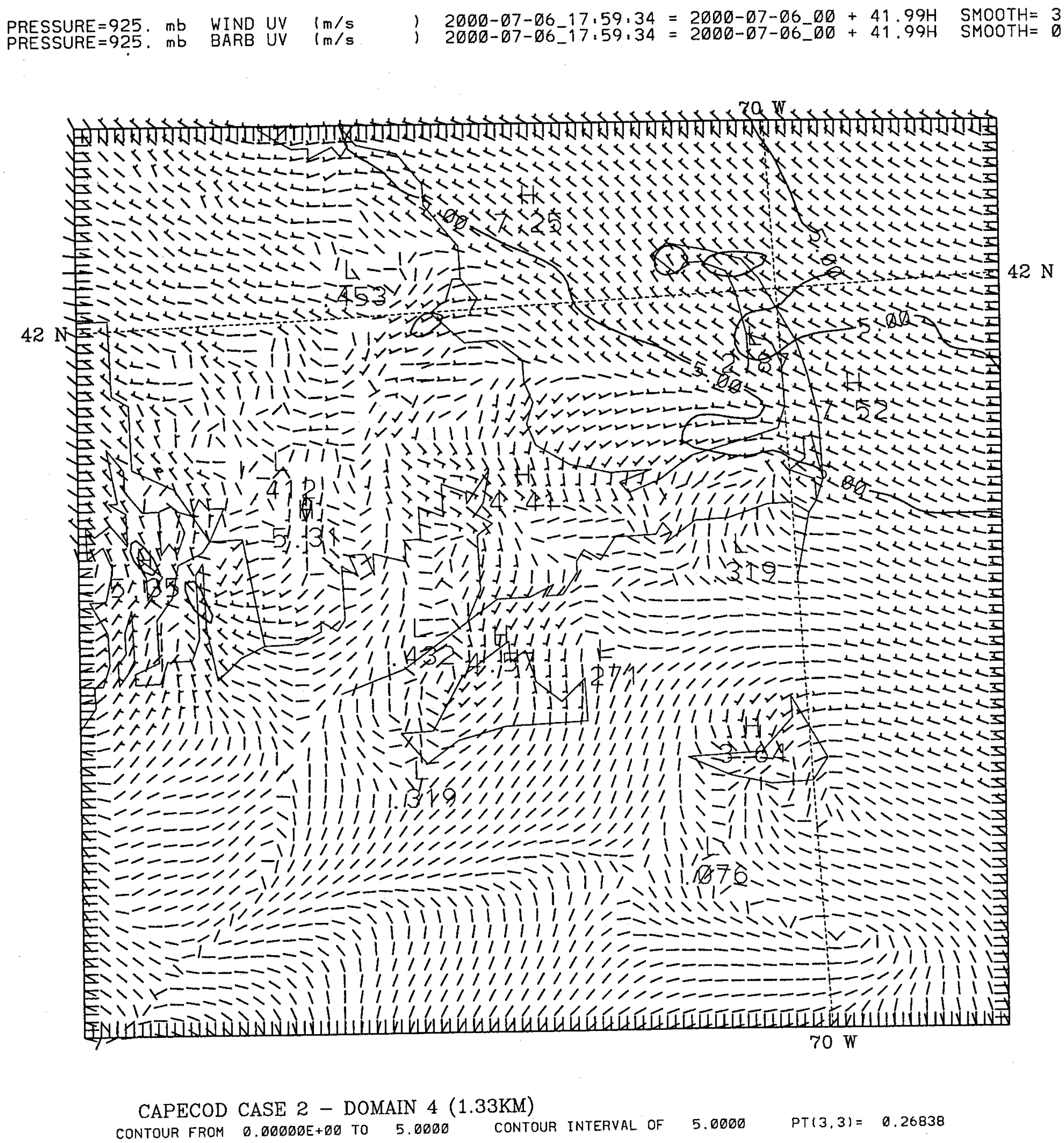

Figure 45. MM5 wind (ms^{-1}) simulated at 925 mb on the 1.33-km domain in Case 2 valid at 1800 UTC, 6 July 2000 (+42 h). Full barb is 10 ms^{-1}.

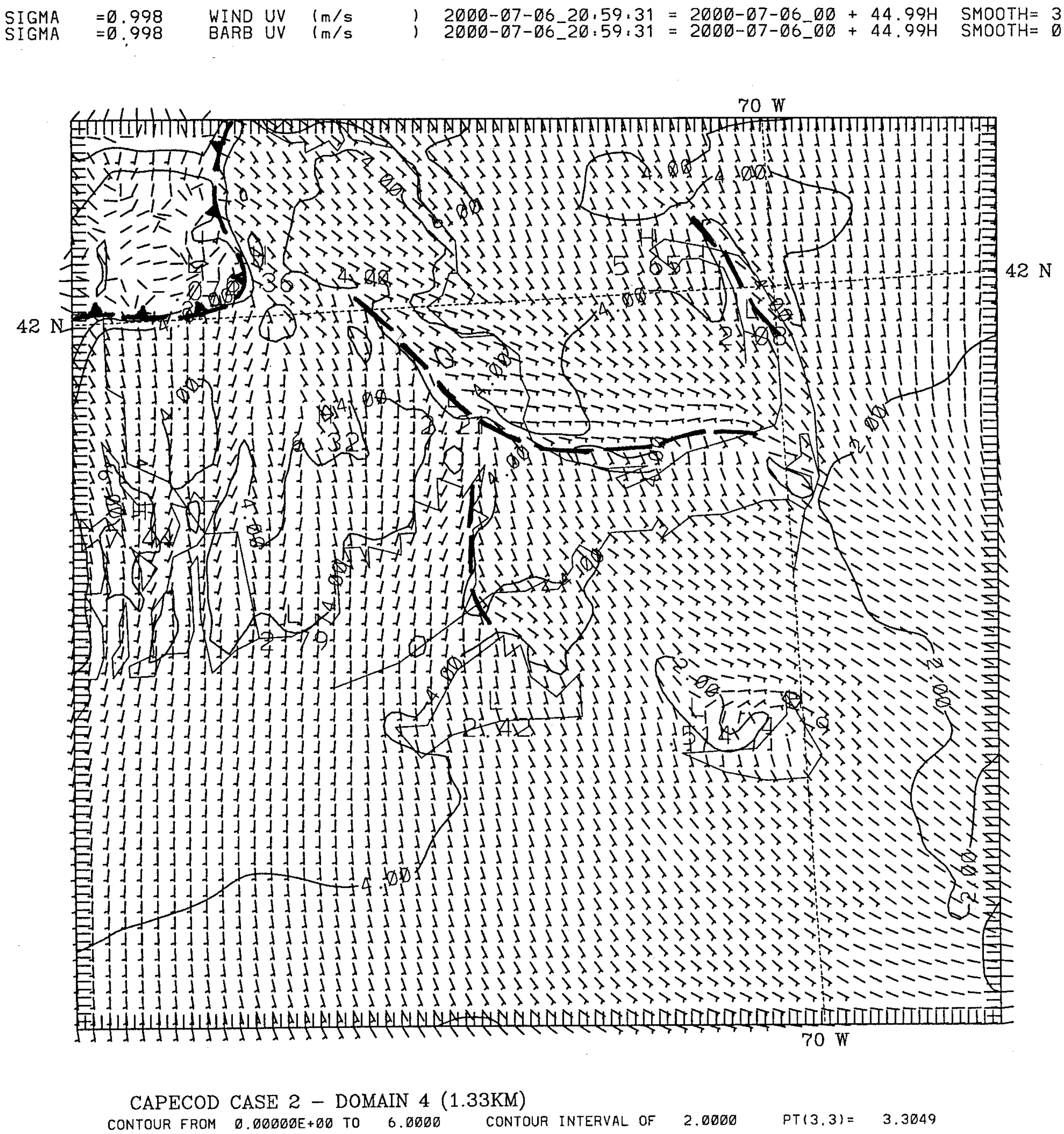

Figure 46. MM5 surface-layer wind (ms^{-1}) simulated on the 1.33-km domain in Case 2 valid at 2100 UTC, 6 July 2000 (+45 h). Full barb is 10 ms^{-1}. Contour interval is 2 ms^{-1}. Heavy dashed line with barbs represents the sea-breeze front. Dashed lines without wedges indicate convergence zones.

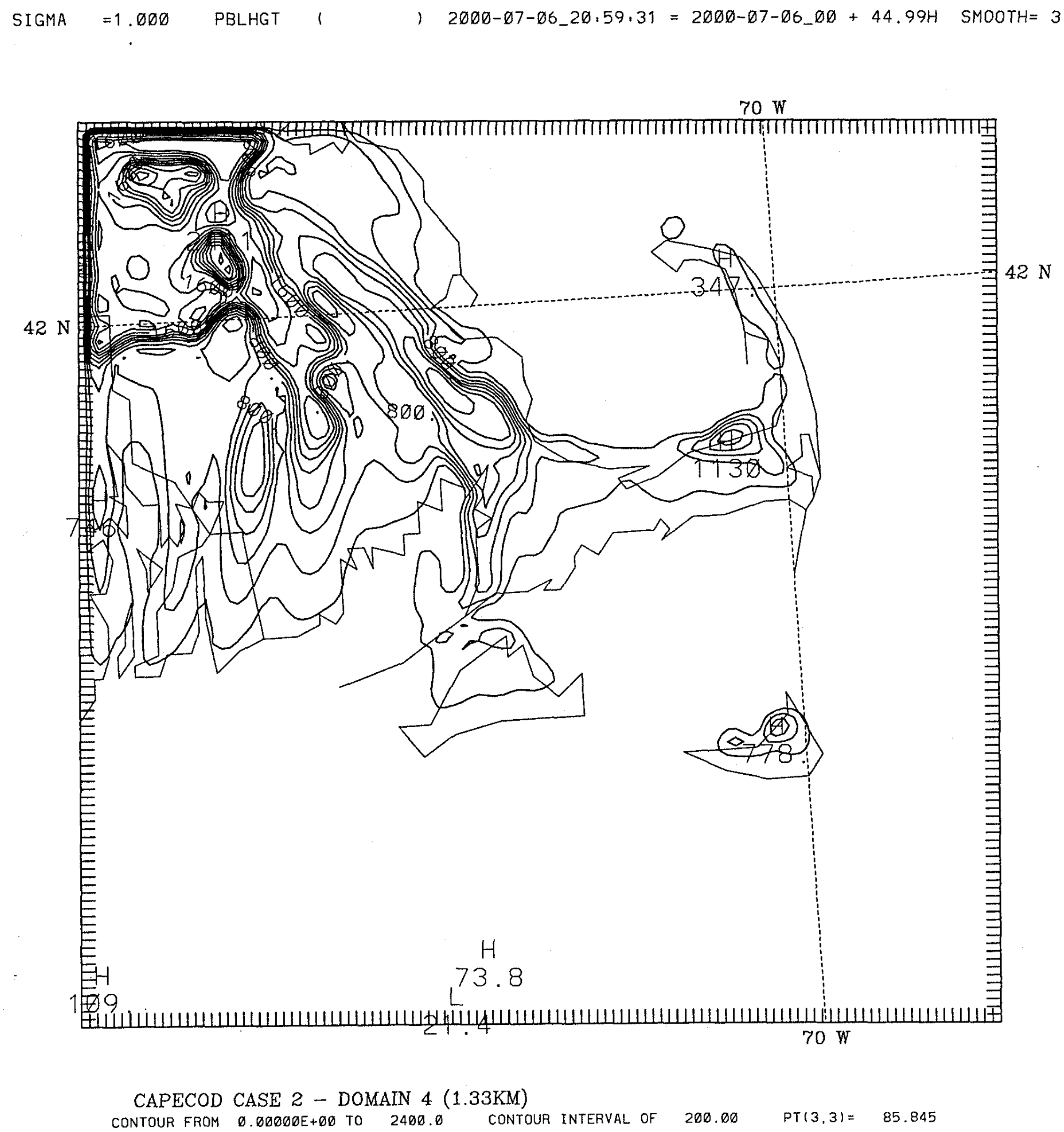

Figure 47. MM5 boundary-layer depths (m) simulated on the 1.33-km domain in Case 2 valid at 2100 UTC, 6 July 2000 (+45 h). Contour interval is 200 m.

The statistical summaries for Case 2 are presented in Tables 9-14. Overall, the trends in the statistics for Case 2 (5-6 July) are quite similar to those of Case 1 shown in Tables 3-8. This is an expected result because the same model and experiment design are used and both cases are dominated by sea breezes that develop in a post-frontal environment.

Despite the general similarities of the statistics for these two sea-breeze cases, a few comments are appropriate to highlight the more significant results that appear upon closer examination. First, inspection of the wind-speed statistics in Table 9 shows that the mean errors (the biases) of the 1.33-km simulation are very small, indicating that the transport speeds should be reliable. The RMS errors and mean absolute errors for wind speed are significantly greater in the lower troposphere (1000-5000 m, above the PBL) in Case 2, compared to Case 1, which may be related to the stronger dynamics of the cold-frontal trough in this case. Maximum wind speeds over New England in this case are ~28 ms^{-1} near 5000 m, versus only 20 ms^{-1} in Case 1, which accounts for the larger RMS error and mean absolute error for wind speed in the uppermost zone.

The Case 2 wind-direction statistics on the 1.33-km domain are mostly similar to those of Case 1. Despite rather large errors at individual points (reflected in the large RMS errors and mean absolute errors), the mean error for wind direction remains very small at all levels. As in Case 1, it appears that the local directional errors are related mostly to minor errors in the timing and placement of convergence zones associated with the mesoscale sea-breeze circulations, since the comparisons of analyzed and model-predicted patterns shown above in the figures reveal generally good agreement. Moreover, it should be noted that the errors for the surface-layer wind directions found in the analyses (initial conditions) also are quite large due to local factors unresolved in the analyses. Similar effects due to surface obstacles contribute to the errors in the model-simulated wind directions.

The error statistics calculated for the temperature field on the 1.33-km domain (Table 10) indicate that the MM5 had smaller biases in the 3-48 h simulations for Case 2 than did the analyses used to initialize the model. Thus, the model has done well in developing the local gradients of temperature that had been heavily smoothed in the EDAS analyses. Furthermore, the MM5-simulated temperature errors found in the surface layer and PBL are considerably less than those in Case 1. This result appears to be due to a more accurate depiction of the daily maximum and minimum temperature extremes in this case.

The model's sea-level pressure errors and moisture errors for Case 2 (Tables 10 and 11) are quite low and are similar in most respects to those found in Case 1, except that the RMS errors and mean absolute errors for relative-humidity tend to be somewhat greater in Case 2. The statistical patterns for Case 2 are quite similar on the 4-km domain (Tables 12-14) and the 1.33-km domain (Tables 9-11). Thus, as with Case 1, the results of the meteorological model simulations for Case 2 appear to have suitable accuracy for use in air-quality investigations.

Table 9. Statistical summary of MM5 performance for wind speed and direction in Case 2 (5-6 July 2000) on the 1.33-km domain.

Wind Speed (ms^{-1})	RMS Error	Mean Abs. Error	Mean Error	% Within 2.0 ms^{-1}
0 h (Initial Cond's.)				
Surface (~12 m AGL)	1.67	1.33	0.77	73.3
45-1000 m AGL	0.37	0.37	-0.23	100.0
1000-5000 m AGL	0.59	0.59	0.20	100.0
3 -48 h Simulation				
Surface (~12 m AGL)	1.58	1.31	-0.32	76.7
45-1000 m AGL	1.76	1.76	1.17	66.3
1000-5000 m AGL	3.17	3.17	-0.28	50.0

Wind Direction (deg.)	RMS Error	Mean Abs. Error	Mean Error	% Within 20 deg.
0 h (Initial Cond's.)				
Surface (~12 m AGL)	42.0	22.7	-10.0	66.7
45-1000 m AGL	5.8	5.8	-2.1	91.3
1000-5000 m AGL	3.4	3.4	-1.4	100.0
3 -48 h Simulation				
Surface (~12 m AGL)	58.6	44.1	-4.0	39.5
45-1000 m AGL	36.0	36.0	7.2	54.3
1000-5000 m AGL	15.2	15.2	-0.2	43.3

Table 10. Statistical summary of MM5 performance for temperature and sea-level pressure in Case 2 (5-6 July 2000) on the 1.33-km domain.

Temperature (C)	RMS Error	Mean Abs. Error	Mean Error	% Within 2.0 C
0 h (Initial Cond's.)				
Surface (~12 m AGL)	1.31	1.08	0.62	80.0
45-1000 m AGL	1.71	1.71	1.71	56.5
1000-5000 m AGL	0.58	0.58	0.32	100.0
3 -48 h Simulation				
Surface (~12 m AGL)	2.15	1.75	-0.18	63.8
45-1000 m AGL	1.14	1.14	-1.13	85.9
1000-5000 m AGL	0.98	0.98	-0.14	83.3
Sea-Level Pres. (mb)	**RMS Error**	**Mean Abs. Error**	**Mean Error**	**% Within 2.5 mb**
0 h (Initial Cond's.)	0.40	0.32	-0.14	100.0
3 -48 h Simulation	0.73	0.66	0.52	100.0

Table 11. Statistical summary of MM5 performance for mixing ratio and relative humidity in Case 2 (5-6 July 2000) on the 1.33-km domain.

Mixing Ratio (g kg^{-1})	RMS Error	Mean Abs. Error	Mean Error	% Within 1 g kg^{-1}
0 h (Initial Cond's.)				
Surface (~12 m AGL)	0.24	0.24	-0.24	100.0
45-1000 m AGL	0.20	0.20	0.07	100.0
1000-5000 m AGL	0.46	0.46	-0.44	86.7
3 -48 h Simulation				
Surface (~12 m AGL)	2.27	2.27	0.45	25.0
45-1000 m AGL	1.36	1.36	-0.44	35.9
1000-5000 m AGL	0.97	0.97	-0.52	48.3

Rel. Humidity (percent)	RMS Error	Mean Abs. Error	Mean Error	% Within 10 percent
0 h (Initial Cond's.)				
Surface (~12 m AGL)	3.34	2.59	-1.93	100.0
45-1000 m AGL	9.04	9.04	-9.04	47.8
1000-5000 m AGL	8.00	8.00	-7.87	80.0
3 -48 h Simulation				
Surface (~12 m AGL)	12.44	9.94	-2.13	59.5
45-1000 m AGL	10.02	10.02	0.25	47.8
1000-5000 m AGL	14.64	14.64	-8.80	51.7

Table 12. Statistical summary of MM5 performance for wind speed and direction in Case 2 (5-6 July 2000) on the 4-km domain.

Wind Speed (ms^{-1})	RMS Error	Mean Abs. Error	Mean Error	% Within 2.0 ms^{-1}
0 h (Initial Cond's.)				
Surface (~12 m AGL)	1.68	1.34	0.11	83.0
45-1000 m AGL	1.14	0.94	-0.35	94.5
1000-5000 m AGL	1.04	0.89	-0.23	91.7
3 -48 h Simulation				
Surface (~12 m AGL)	1.76	1.45	-0.34	73.1
45-1000 m AGL	2.72	2.25	0.53	52.3
1000-5000 m AGL	3.13	2.73	0.31	51.7

Wind Direction (deg.)	RMS Error	Mean Abs. Error	Mean Error	% Within 20 deg.
0 h (Initial Cond's.)				
Surface (~12 m AGL)	46.1	31.4	-5.5	50.0
45-1000 m AGL	8.0	6.4	-4.1	94.5
1000-5000 m AGL	5.5	4.5	-1.7	90.0
3 -48 h Simulation				
Surface (~12 m AGL)	53.3	39.3	-3.5	40.7
45-1000 m AGL	39.7	30.2	-1.8	53.1
1000-5000 m AGL	18.5	15.1	-2.4	85.0

Table 13. Statistical summary of MM5 performance for temperature and sea-level pressure in Case 2 (5-6 July 2000) on the 4-km domain.

Temperature (C)	RMS Error	Mean Abs. Error	Mean Error	% Within 2.0 C
0 h (Initial Cond's.)				
Surface (~12 m AGL)	1.95	1.60	0.85	65.3
45-1000 m AGL	0.96	0.67	0.57	89.1
1000-5000 m AGL	0.57	0.48	0.32	100.0
3 -48 h Simulation				
Surface (~12 m AGL)	1.96	1.59	0.29	69.2
45-1000 m AGL	1.25	1.10	-0.32	86.4
1000-5000 m AGL	1.35	1.11	-0.03	85.3
Sea-Level Pres. (mb)	**RMS Error**	**Mean Abs. Error**	**Mean Error**	**% Within 2.5 mb**
0 h (Initial Cond's.)	0.66	0.53	-0.17	100.0
3 -48 h Simulation	0.89	0.73	0.31	99.2

Table 14. Statistical summary of MM5 performance for mixing ratio and relative humidity in Case 2 (5-6 July 2000) on the 4-km domain.

Mixing Ratio (g kg^{-1})	RMS Error	Mean Abs. Error	Mean Error	% Within 1 g kg^{-1}
0 h (Initial Cond's.)				
Surface (~12 m AGL)	1.01	0.83	-0.15	75.0
45-1000 m AGL	0.45	0.36	0.14	94.6
1000-5000 m AGL	0.52	0.43	0.08	91.7
3 -48 h Simulation				
Surface (~12 m AGL)	1.49	1.20	0.29	43.8
45-1000 m AGL	1.34	1.16	-0.39	48.4
1000-5000 m AGL	1.05	0.89	-0.33	57.7

Rel. Humidity (percent)	RMS Error	Mean Abs. Error	Mean Error	% Within 10 percent
0 h (Initial Cond's.)				
Surface (~12 m AGL)	10.99	8.43	-0.47	65.9
45-1000 m AGL	5.75	4.44	-1.95	85.9
1000-5000 m AGL	7.14	5.76	-1.47	90.0
3 -48 h Simulation				
Surface (~12 m AGL)	10.89	8.50	-3.00	67.0
45-1000 m AGL	11.32	9.63	-1.74	59.0
1000-5000 m AGL	17.11	14.25	-6.03	50.8

4.2.3 Case 3: Land Breeze

Generally, there are two primary requirements needed to develop a discernable land breeze. First, the land must become cooler than the nearby water body to produce the local pressure gradient that generates the land breeze. Second, the background synoptic-scale winds must be very weak. Otherwise, the local pressure gradient will be overwhelmed by the synoptic pressure gradient. Unlike the sea breeze, which often is accompanied by a fairly deep convective boundary layer (perhaps 1.0-1.5 km in depth) ahead of the sea-breeze front, the convective boundary layer formed over water that accompanies a land breeze may be only a few hundred meters deep. Thus, land breezes tend to be rather shallow and the resulting pressure gradient tends to be weaker than that found in a well-developed sea breeze. Wind speeds in the land breeze tend to be only on the order of 1-3 ms^{-1}, so even a weak synoptic-scale wind can mask its presence. Consequently, the land breeze is generally a somewhat fragile phenomenon. Any significant turbulence that develops over land, such as may occur due to a nocturnal wind shear, can lead to downward momentum transport into the lowest levels, which can disrupt the land breeze. Given the land-sea configuration of Cape Cod and southeastern MA, a land breeze for a completely calm synoptic situation is likely to exhibit divergent surface winds over land, with mostly westerly directions over the coast near Massachusetts Bay and mostly northerly directions from RI to Upper Cape Cod.

In the analysis of Case 3, the land breeze was difficult to detect on the nights of 21 and 22 August 2000 due to a weak but persistent northwesterly synoptic-scale flow (see Section 4.1.3). However, in the MM5, the land breeze was heavily masked by a stronger than observed northwesterly flow over the 1.33-km domain. The root cause of the model's failure to show a clear land breeze in this case appears related to a stronger-than-observed sea-level pressure gradient that provided geostrophic forcing over the region (not shown). The pressure errors themselves were small (see statistical summary below), but there was a tendency in the model to build the high-pressure ridge from the Great Lakes toward New England too rapidly, which kept the pressure gradient from relaxing sufficiently to allow the winds to die. Consequently, Figure 48 shows the MM5-simulated surface-layer winds at 0600 UTC (0200 EDT, +6h), 21 August, from the northwest at 5-7 kts (2.5-3.5 ms^{-1}) over land and 8-15 kts (4-8 ms^{-1}) over the sea. The wind directions in the model are fairly uniform in all parts of the 1.33-km domain, with coastal directions of ~305 degrees over Massachusetts Bay and ~320 degrees from RI to Upper Cape Cod (weak directional divergence). Figures 23 and 28 confirm that the wind from the sea at Provincetown on the tip of Cape Cod was 15 kts from the northwest at this time, but in particular, the winds over most of the interior of southeastern MA were observed to be calm. This stronger-than-observed northwesterly surface wind over land persisted in the model through the rest of the night and into the first hours after sunrise (not shown). Thus, the first requirement for detecting a land breeze was not met by the model on the first night.

Figure 49 shows the model's surface-layer temperature at 0600 UTC, 21 August. Notice that the temperature over the ocean from Nantucket southward is greater than 18 C (64.5 F), while temperatures over land have fallen to ~13 C (55 F). The cooling over land in this case is considerably weaker than observed, since Figure 28 shows temperatures over southeastern MA on the order of ~7-9 C (44-49 F) at this time. Thus, the land-sea temperature gradient, although directed seaward as expected, is too weak by about 50%. This error is most likely due primarily to insufficient nocturnal longwave radiation flux divergence in the model's lower layers. However, some vertical mixing due to shear-generated turbulence (the winds ~900 m above sea

level were 9-10 ms^{-1}, or 18-20 kts) may have contributed to prevent or weaken the pooling of cold air near the ground (not shown).
Consistent with land-breeze theory, Figure 50 indicates that the boundary layer is very shallow over land and deepens gradually to ~500 m over the warmer waters south of Nantucket. However, this thermal contrast is insufficient to develop an obvious land-breeze circulation in this case. The acceleration of the surface winds over the ocean is mostly due to much lower surface roughness and friction, compared to the land. Over the next 3 h, the surface temperatures over land fell by only ~1 C (2 F) in the MM5, so the error in the thermal contrast found at 0600 UTC was not corrected sufficiently to develop a noticeable land breeze later on the first night (not shown).

On the second night, 22 August, the model produced mostly similar thermal and wind characteristics as on the first night, which argues against a strong land-breeze mechanism in the numerical solutions. However, by this time, the background synoptic pressure gradient had weakened somewhat and the winds at 925 mb (~900 m above sea level) had dropped to ~10 kts (5 ms^{-1}) (not shown). Thus, Figure 51 shows slightly weaker surface-layer winds at 0900 UTC (0500 EDT, or +33 h), 22 August, with speeds of 3-6 kts (~1.5-3.0 ms^{-1}) over land and 7- 10 kts (~3.5-5.0 ms^{-1}) over the ocean. The observed and simulated wind speeds at the coastal stations from Provincetown, MA to Providence, RI, are in fairly good agreement. However, comparison of Figures 29 and 51 shows that the model again failed to simulate the mostly calm winds observed over southeastern MA. As on the previous night, wind directions produced by the MM5 are mostly from the northwest, with only modest directional divergence along the coasts. Thus, the model's winds do not exhibit a significant land-breeze signature on this night.

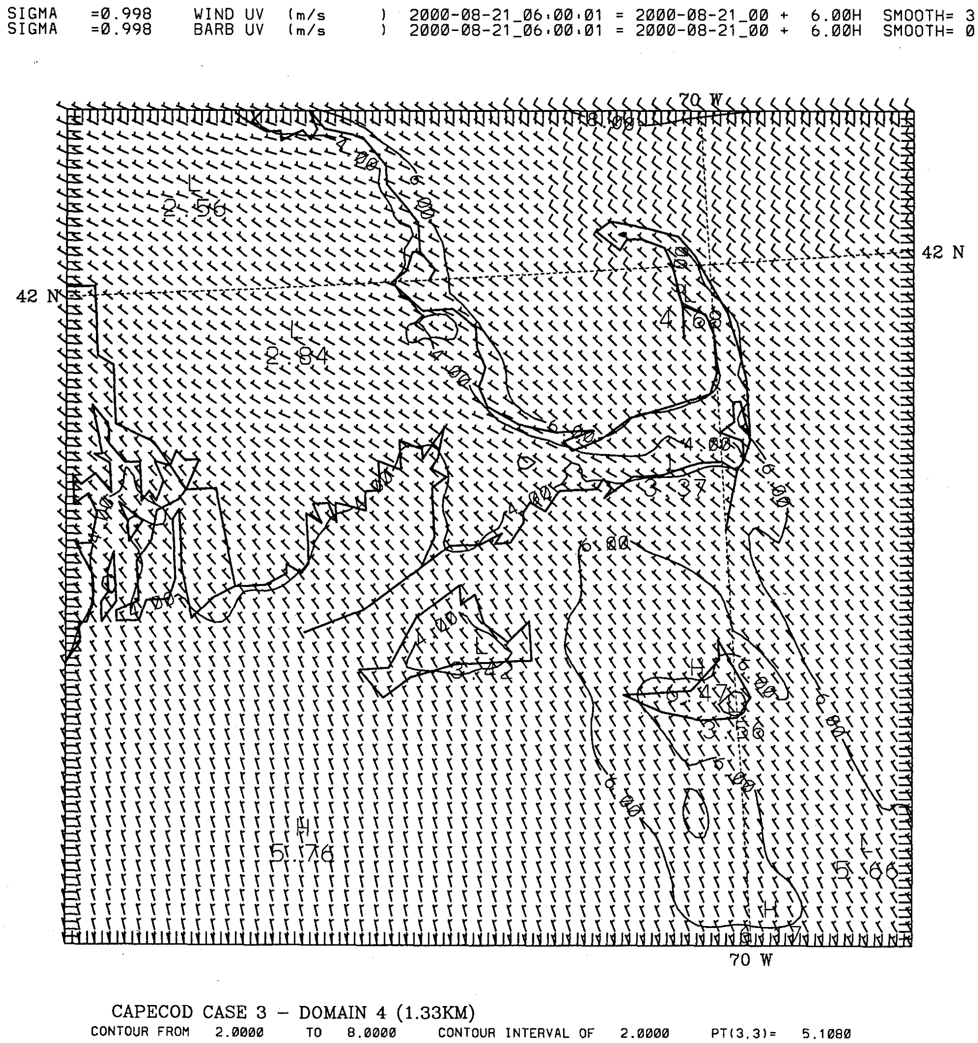

Figure 48. MM5 surface-layer wind (ms^{-1}) simulated on the 1.33-km domain in Case 3 valid at 0600 UTC, 21 August 2000 (+6 h). Contour interval is 2 ms^{-1}. Full barb is 10 ms^{-1}.

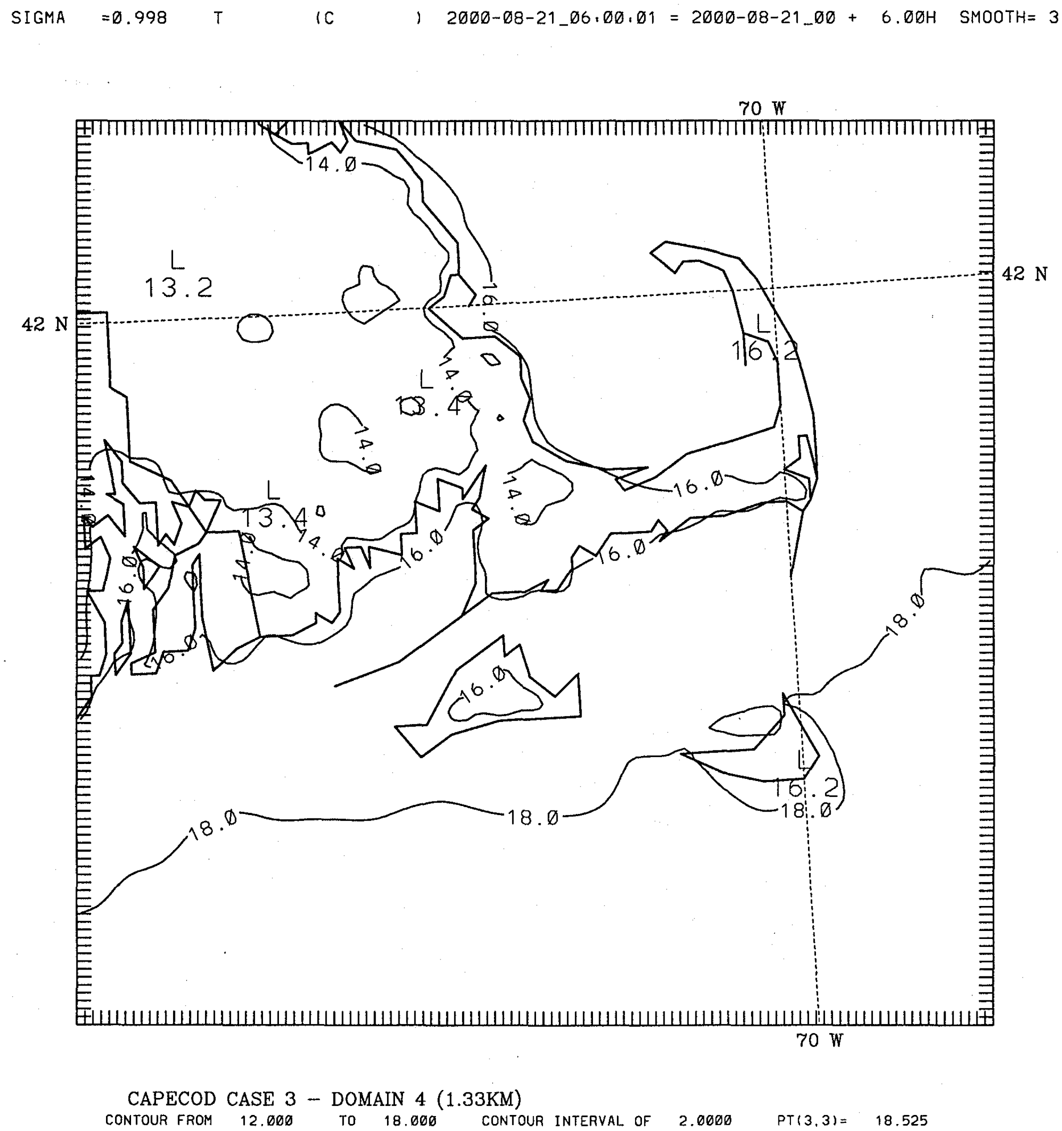

Figure 49. MM5 surface-layer temperatures (C) simulated on the 1.33-km domain in Case 3 valid at 0600 UTC, 21 August 2000 (+6 h). Contour interval is 2 C.

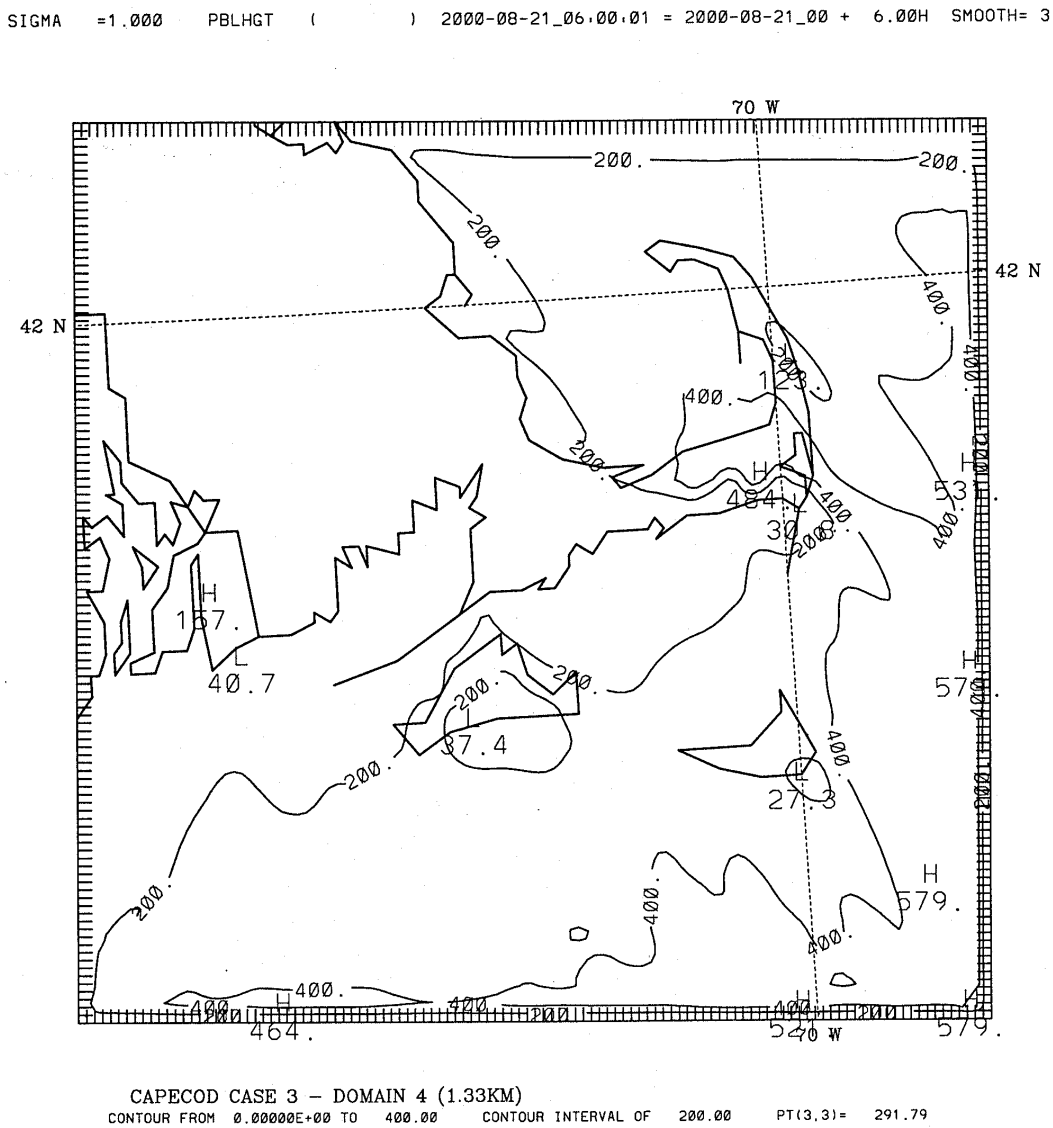

Figure 50. MM5 boundary-layer depth (m) simulated on the 1.33-km domain in Case 3 valid at 0600 UTC, 21 August 2000 (+6 h). Contour interval is 200 m.

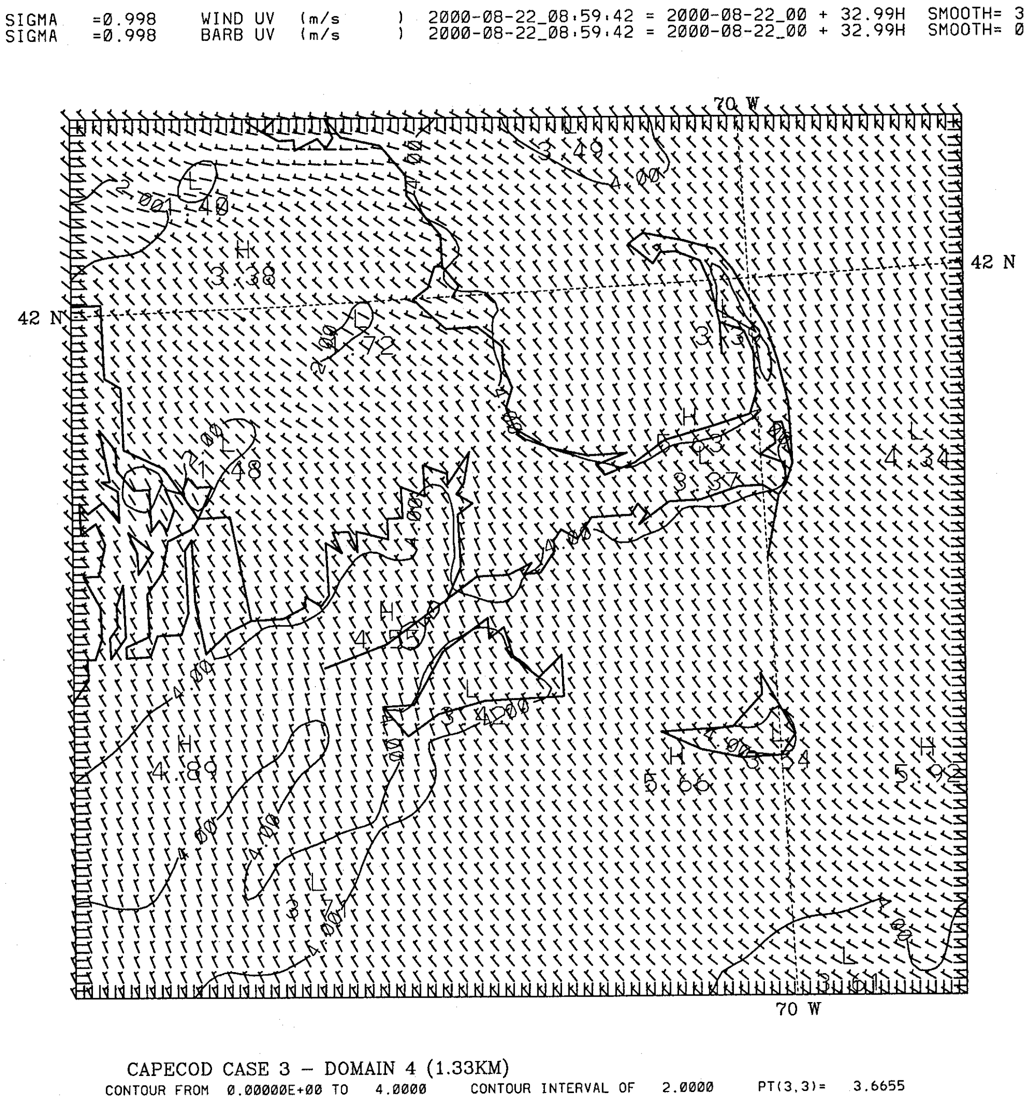

Figure 51. MM5 surface-layer wind (ms^{-1}) simulated on the 1.33-km domain in Case 3 valid at 0900 UTC, 22 August 2000 (+33 h). Contour interval is 2 ms^{-1}. Full barb is 10 ms^{-1}.

In Figure 52, the temperature field at 0900 UTC, 22 August, is very similar to that shown in Figure 49 for 21 August, although the 18 C isotherm is closer to the coast and the maximum temperatures over the ocean are nearly 20 C (68 F). Thus, the land-sea thermal contrast is only slightly greater than during the night before. Comparison of Figures 28 and 29 shows that in general the observed surface temperatures over southeastern MA on 22 August were warmer by several degrees than on 21 August, so the actual thermal forcing for a possible land breeze was indeed weaker. Consistent with the slower surface wind speeds simulated on 22 August, which would tend to reduce the model's surface sensible heat flux, the predicted boundary-layer growth rate in the air advected over the ocean was reduced by about half (not shown).

In summary, for both nights of Case 3 the nocturnal winds produced in the MM5 are dominated by a modest northwesterly synoptic-scale flow, rather than the land-breeze mechanism. Over land the model's nocturnal winds in the surface layer are consistently too fast. However, the model did capture the correct trend toward weaker pressure gradients and slower winds on the second night. There is a discernable difference in the simulated wind directions along the eastern and southern shores of southeastern MA, with a modest divergence that suggests at least a weak land-breeze component in the low-level winds. Wind speeds developed by the MM5 along the coast are also in fairly good agreement with those observed (especially on 22 August). Nevertheless, even though the model did weaken the low-level winds on 22 August so that a weak land breeze component is likely to be present, it appears that the MM5's solutions are still dominated by the weak synoptic-scale northwesterly wind flow.

SIGMA =0.998 T (C) 2000-08-22_08:59:42 = 2000-08-22_00 + 32.99H SMOOTH= 3

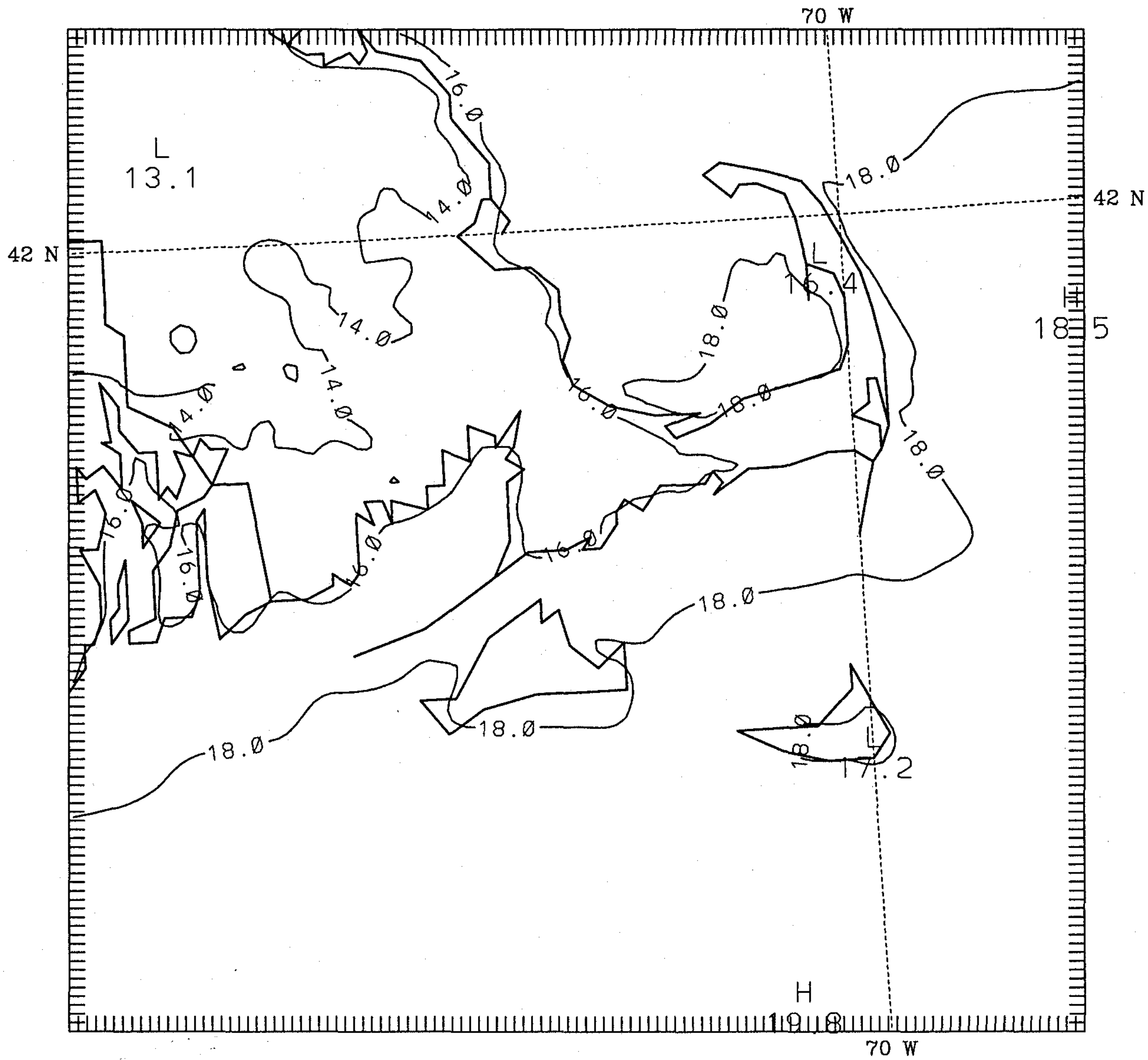

CAPECOD CASE 3 - DOMAIN 4 (1.33KM)
CONTOUR FROM 12.000 TO 18.000 CONTOUR INTERVAL OF 2.0000 PT(3,3)= 19.284

Figure 52. MM5 surface-layer temperatures (C) simulated on the 1.33-km domain in Case 3 valid at 0900 UTC, 22 August 2000 (+33 h). Contour interval is 2 C.

Finally, the statistical analysis of Case 3, in which a weak land breeze was detected, is documented in Tables 15-20. Again, the statistics for this case show a great deal of similarity to those recorded for Cases 1 and 2. This indicates consistent accuracy in the model solutions, which is very desirable for air-quality applications.

One of the most notable features of the statistics for the wind speed on the 1.33-km domain is that there are fairly large errors in the EDAS analyzed winds used for the initial conditions (Table 15). For example, in the surface layer the initial RMS error is 2.35 ms^{-1} and the initial mean error indicates a positive speed bias of 1.90 ms^{-1}. During the 3 - 48 h simulation period for Case 3, the MM5's wind-speed errors decrease significantly from those in the analyses.

However, as in Case 1, the layer between 45-1000 m has a strong positive bias in the MM5 simulation of Case 3 (2.22 ms^{-1}). This raises an interesting problem concerning the interpretation of the statistics. Recall that there is only one upper-air radiosonde site (Chatham, MA) in the 1.33-km domain, with 23 model levels in this zone. Chatham is located near the "elbow" of Cape Cod facing the Atlantic Ocean. In this area, the Cape is relatively narrow and one would expect the sounding to reflect predominantly marine influences, rather than land influences. In this marine environment, therefore, the PBL should remain quite shallow through most of these episodes, so that near Chatham, most of the zone between 45-1000 m should be above the top of the PBL (day and night). Thus, the winds in this zone should not be decelerated significantly by surface friction. Apparently, the model solutions in this area are responding according to this concept, but the actual winds in that zone are decelerated considerably. At present, the reason for the slower observed winds at Chatham in the 45-1000 m zone is not clear. Confirmation that phenomenon is a local effect that is not representative of the rest of New England is found in Table 18, where the speed bias for this same layer is only 0.53 ms^{-1}. Further investigation is needed to understand this unusual response in the observed mid-level winds over this section of Cape Cod.

By contrast, the wind-direction statistics for the 1.33-km domain in Case 3 are, overall, the best for the three cases simulated in this study. The mean direction errors (bias) for Case 3, shown in Table 15, are consistently small for both the initial analysis and the model simulation. As expected, the RMS errors in the surface layer are large, reflecting the influence of surface obstacles and small position and timing errors for the model's sea-breeze circulations. However, above the surface, the RMS errors and mean absolute errors for the model simulation are significantly smaller than in Cases 1 and 2. Thus, overall, the winds are simulated with considerable accuracy in this case.

The statistics for the model-simulated temperatures on the 1.33-km domain in Case 3 (summarized in Table 16) reveal that the MM5 produced an accuracy that is consistent with that found in Cases 1 and 2. The most notable result for this variable is that the model has overcome a very large warm bias (+2.35 C) in the initial surface-temperature field supplied to the MM5 from the EDAS. The MM5's surface temperature errors are consistently smaller than in the initial conditions. Further comparison of the temperature errors for the three cases shows that there is a consistent bias toward cool temperatures on the order of -1.1 to -1.5 C in the MM5's simulations on the 1.33-km domain for the zone between 45-1000 m. This cool bias above the surface is reduced by at least a factor of 3 on the 4-km domain, which is less dominated by the marine environment. While it is not large enough to cause a serious problem, this cool bias above the surface does suggest that a consistent error exists which may be reduced by further study and correction of the PBL physics.

The statistics presented in Tables 16 and 17 show that the MM5 has performed quite well on the 1.33-km domain for the moisture and sea-level pressure fields. However, the model's relative humidity errors in the zone between 45-1000 m have a moist bias of ~12.5 %. If this were a general result, it might indicate a problem, but on the fine-mesh domain, it represents data from only one radiosonde site. The same mean error, or bias, calculated on the 4-km domain is only -1.74% (slight dry bias), which indicates excellent agreement with the data. Thus, it is likely that the statistic based on the single site on the 1.33-km domain is not representative of the overall model performance in Case 3.

In summary, the MM5 statistical evaluations for the three cases indicate solutions which are in generally good agreement with the observations. That is, the error statistics are generally similar to those found in many previous cases in which air quality issues were paramount. Since episodes with poor air quality tend to have weak synoptic-scale forcing and are dominated by mesoscale circulations driven by local surface features, they tend to represent significant challenges for numerical models. In particular, the model physics is of great importance for simulating these mesoscale features. Thus, the overall positive results verified by the statistical evaluations of the MM5 solutions in Cases 1 and 2 indicates that the model can represent the most important aspects of the Cape Cod sea breeze. The model also performed with similar statistical skill for Case 3, but a detailed examination of the wind patterns described earlier suggests that low-level speeds were somewhat too high, which adversely affected the model's ability to simulate the moderate surface-layer divergence of the observed land breeze.

Table 15. Statistical summary of MM5 performance for wind speed and direction in Case 3 (21-22 August 2000) on the 1.33-km domain.

Wind Speed (ms^{-1})	RMS Error	Mean Abs. Error	Mean Error	% Within 2.0 ms^{-1}
0 h (Initial Cond's.)				
Surface (~12 m AGL)	2.35	2.11	1.90	40.0
45-1000 m AGL	0.65	0.65	0.61	91.3
1000-5000 m AGL	1.22	1.22	-1.09	93.3
3 -48 h Simulation				
Surface (~12 m AGL)	1.60	1.35	0.13	78.5
45-1000 m AGL	2.24	2.24	2.22	42.4
1000-5000 m AGL	1.52	1.52	1.02	65.0
Wind Direction (deg.)	**RMS Error**	**Mean Abs. Error**	**Mean Error**	**% Within 20 deg.**
0 h (Initial Cond's.)				
Surface (~12 m AGL)	30.5	19.1	7.3	80.0
45-1000 m AGL	4.7	4.7	3.8	95.7
1000-5000 m AGL	2.1	2.1	0.7	100.0
3 -48 h Simulation				
Surface (~12 m AGL)	51.6	40.9	-3.6	41.8
45-1000 m AGL	18.1	18.1	5.4	65.2
1000-5000 m AGL	9.4	9.4	2.3	61.7

Table 16. Statistical summary of MM5 performance for temperature and sea-level pressure in Case 3 (21-22 August 2000) on the 1.33-km domain.

Temperature (C)	RMS Error	Mean Abs. Error	Mean Error	% Within 2.0 C
0 h (Initial Cond's.)				
Surface (~12 m AGL)	2.93	2.42	2.35	46.7
45-1000 m AGL	0.21	0.21	-0.01	100.0
1000-5000 m AGL	0.56	0.56	-0.14	100.0
3 -48 h Simulation				
Surface (~12 m AGL)	2.39	1.97	0.74	63.2
45-1000 m AGL	1.45	1.45	-1.40	60.9
1000-5000 m AGL	0.73	0.73	0.03	95.0
Sea-Level Pres. (mb)	**RMS Error**	**Mean Abs. Error**	**Mean Error**	**% Within 2.5 mb**
0 h (Initial Cond's.)	0.43	0.36	-0.26	100.0
3 -48 h Simulation	0.63	0.57	0.33	100.0

Table 17. Statistical summary of MM5 performance for mixing ratio and relative humidity in Case 3 (21-22 August 2000) on the 1.33-km domain.

Mixing Ratio (g kg^{-1})	RMS Error	Mean Abs. Error	Mean Error	% Within 1 g kg^{-1}
0 h (Initial Cond's.)				
Surface (~12 m AGL)	1.17	1.17	1.17	0.0
45-1000 m AGL	0.21	0.21	0.21	100.0
1000-5000 m AGL	0.30	0.30	0.07	93.3
3 -48 h Simulation				
Surface (~12 m AGL)	2.12	2.12	2.12	25.0
45-1000 m AGL	1.10	1.10	0.74	57.6
1000-5000 m AGL	0.55	0.55	-0.09	81.7
Rel. Humidity (percent)	**RMS Error**	**Mean Abs. Error**	**Mean Error**	**% Within 10 percent**
0 h (Initial Cond's.)				
Surface (~12 m AGL)	16.64	13.15	-9.81	53.3
45-1000 m AGL	1.90	1.90	1.88	100.0
1000-5000 m AGL	5.43	5.43	-2.59	86.7
3 -48 h Simulation				
Surface (~12 m AGL)	12.47	10.30	-3.59	58.8
45-1000 m AGL	13.01	13.01	12.48	39.13
1000-5000 m AGL	9.46	9.46	-1.97	60.0

Table 18. Statistical summary of MM5 performance for wind speed and direction in Case 3 (21-22 August 2000) on the 4-km domain.

Wind Speed (ms^{-1})	RMS Error	Mean Abs. Error	Mean Error	% Within 2.0 ms^{-1}
0 h (Initial Cond's.)				
Surface (~12 m AGL)	1.68	1.34	0.11	83.0
45-1000 m AGL	1.14	0.94	-0.35	94.5
1000-5000 m AGL	1.04	0.89	-0.23	91.7
3 -48 h Simulation				
Surface (~12 m AGL)	1.76	1.45	-0.34	73.1
45-1000 m AGL	2.72	2.25	0.53	52.3
1000-5000 m AGL	3.13	2.73	0.31	51.7

Wind Direction (deg.)	RMS Error	Mean Abs. Error	Mean Error	% Within 20 deg.
0 h (Initial Cond's.)				
Surface (~12 m AGL)	46.1	31.4	-5.5	50.0
45-1000 m AGL	8.0	6.4	-4.1	94.5
1000-5000 m AGL	5.5	4.5	-1.7	90.0
3 -48 h Simulation				
Surface (~12 m AGL)	53.3	39.3	-3.5	40.7
45-1000 m AGL	39.7	30.2	-1.8	53.1
1000-5000 m AGL	18.5	15.1	-2.4	85.0

Table 19. Statistical summary of MM5 performance for temperature and sea-level pressure in Case 3 (21-22 August 2000) on the 4-km domain.

Temperature (C)	RMS Error	Mean Abs. Error	Mean Error	% Within 2.0 C
0 h (Initial Cond's.)				
Surface (~12 m AGL)	1.95	1.60	0.85	65.3
45-1000 m AGL	0.96	0.67	0.57	89.1
1000-5000 m AGL	0.57	0.48	0.32	100.0
3 -48 h Simulation				
Surface (~12 m AGL)	1.96	1.59	0.29	69.2
45-1000 m AGL	1.25	1.10	-0.32	86.4
1000-5000 m AGL	1.35	1.11	-0.03	85.3

Sea-Level Pres. (mb)	RMS Error	Mean Abs. Error	Mean Error	% Within 2.5 mb
0 h (Initial Cond's.)	0.66	0.53	-0.17	100.0
3 -48 h Simulation	0.89	0.73	0.31	99.2

Table 20. Statistical summary of MM5 performance for mixing ratio and relative humidity in Case 3 (21-22 August 2000) on the 4-km domain.

Mixing Ratio (g kg^{-1})	RMS Error	Mean Abs. Error	Mean Error	% Within 1 g kg^{-1}
0 h (Initial Cond's.)				
Surface (~12 m AGL)	1.01	0.83	-0.15	75.0
45-1000 m AGL	0.45	0.36	0.14	94.6
1000-5000 m AGL	0.52	0.43	0.08	91.7
3 -48 h Simulation				
Surface (~12 m AGL)	1.49	1.20	0.29	43.8
45-1000 m AGL	1.34	1.16	-0.39	48.4
1000-5000 m AGL	1.05	0.89	-0.33	57.7
Rel. Humidity (percent)	**RMS Error**	**Mean Abs. Error**	**Mean Error**	**% Within 10 percent**
0 h (Initial Cond's.)				
Surface (~12 m AGL)	10.99	8.43	-0.47	65.9
45-1000 m AGL	5.75	4.44	-1.95	85.9
1000-5000 m AGL	7.14	5.76	-1.47	90.0
3 -48 h Simulation				
Surface (~12 m AGL)	10.89	8.50	-3.00	67.0
45-1000 m AGL	11.32	9.63	-1.74	59.0
1000-5000 m AGL	17.11	14.25	-6.03	50.8

4.3 Dispersion Model Results for SCIPUFF

4.3.1 Input Information

This section provides dispersion modeling comparisons for the different models and for different types of sources. Because there are no suitable air quality data available to compare to the model predictions, the section focuses on the capabilities of the models in simulating the patterns of pollution that would be expected in the complex meteorological flows. Continuous releases from two power plants, a ground level area source and two line source segments, representing emissions from highway traffic are simulated. The total emission rates , on a gram per second basis (g/s) for each of the sources and for each of the model runs are the same. Also, all of the dispersion models used here are mass-conserving. Therefore, we will be primarily discussing differences in the distribution of pollutants for the different meteorological events as predicted by the different models.
The specific sources simulated and the nominal emission rates and parameters for these sources are listed in Table 21.

The Brayton Point and Canal power plants are large power plants with relatively tall stacks and buoyant plumes. The exhaust parameters were obtained from the Massachusetts Department of Environmental Protection. They are full load values and constant for all the simulated hours. In reality, the exit temperatures and exit velocities and emission rates would be expected to vary with load. The emission rate from each plant was given a value of 100g/s. The emissions from these facilities are initially released well above the ground surface. Their interaction with sea breeze circulations depends critically upon the time of release and the depth of the sea breeze flow.

Table 21. Source Locations and Emission Rates and Exit Parameters.

Emissions related Input data	Units					
Source		Canal Plant	Brayton Point	Otis AFB	Route 3 Section	Route 6 Section
Location		Sandwich, MA	Somerset, MA			
Type of Source		Point	Point	Area	Line	Line
Longitude	Degrees, Decimal minutes	70, 30.632	71, 11.6	70, 31.305		
Latitude(N)	Degrees, Decimal minutes	41, 46.208	41, 42.6	41, 39.464		
UTM Easting	m	374437	317507	373301	See Below	See Below
UTM Northing	m	4625358	4619905	4612912	See Below	See Below
Base elevation	m	3.70	4.60	33.83	30.47	30.47
Release height above surface	m	152.37	152.40	1.00	2.00	2.00
Stack diameter	m	5.49	5.64			
Stack exit velocity	m/s	29.02	33.47			
Exhaust gas flow rate	m3/s	686.96	836.19			
Stack exit temperature	K	400.93	469.00			
Nominal emission rate	g/s	100	100	100		
Area Source area	m2			1.00E+04		
Area source emission rate	g/m2/s			1.00E-02		
Line source start UTM Easting	m				371586	371677
Line source start UTM Northing	m				4628769	4625118
Line source end UTM Easting	m				371677	386739
Line source end UTM Northing	m				4625118	4615674
Line Source Length	km				3.65	17.78
Line source emission rate	g/m/s				0.0047	0.0047
Total emissions for highway segment	g/s				17.0	83.0

Two highway segments consisting of a 3.65 km stretch of Route 3 north of the Cape Cod Canal and a 17.78 km stretch of Route 6 to the east of the canal were simulated as two line-type sources. The total emissions for the two segments are 100g/s. This would correspond to an emission rate of 20 grams per vehicle mile and a traffic rate of about 1350 vehicles per hour on both segments. The release height of these emissions is assumed to be 2 meters above the surface. The area-type source hypothesized at Otis Air Force Base is 100 by 100 meters square and emissions are assumed to be released 1 meter above the surface. The emission rate for the entire area simulated is again100 g/s

4.3.2 Dispersion Results from SCIPUFF

For the SCIPUFF experiments, four runs were made for each of the three meteorological cases, with each run containing one emissions source. This experiment design isolated the spread and evolution of the individual emission sources. The two power plants and the area source were simulated readily by SCIPUFF as it already has the capability to model these types of sources. : The 22-km stretch of highway along MA highways 3 and 6 was represented in SCIPUFF as a string of surface point sources at 1-km spacing because the public version of SCIPUFF utilized in this study does not support line sources at this time. The 100 g s^{-1} total emission rate was divided equally among the 22 point sources, each representing a 1-km segment of the highway.

In the figures representing the SCIPUFF surface concentrations, each source point is always represented as an inverted equilateral triangle. Since the emission rates are set arbitrarily in these experiments, we are interested only in the direction and spread of the plumes and their relative concentrations. The SCIPUFF results are presented as a series of figures showing plume surface concentrations associated with each source on a case-by-case basis. It should be noted that the SCIPUFF model had to be restarted at intervals of about 10-12 h during the 48-h cases to prevent the number of puffs from becoming so large that the model ran very slowly. However, this does not affect the accuracy of the plume calculations.

4.3.2.1 Case 1 SCIPUFF Results

For Case 1, the history of the plume surface concentrations from the Brayton Point plant is summarized in Figures 53-57. Early on the first morning (0900 UTC (5 AM EDT), 1 July), Figure 53 shows that the plume is blowing offshore on mostly northwesterly winds. Maximum surface concentrations at this time are ~8.6 $X 10^{-10}$ kg/m^3 south of Martha's Vineyard, or about 70 km downwind of Brayton Point. The very low surface concentrations and the downwind location of the maximum produced by SCIPUFF are consistent with the stable nocturnal boundary layer over the cool land and the cool near-coast waters. As the plume is advected farther southward, where the sea-surface temperatures are warmer, the marine boundary layer gradually becomes deeper and turbulence begins to mix the plume downward to the ocean surface (this process is called fumigation). This accounts for the southern position of the maximum surface concentrations in Figure 53. Note that the figures show the maximum values occurring at ground level on the right boundary of the map outline. Note also that the colors assigned to concentration value ranges are determined for each figure by the maximum concentrations encountered and therefore may differ from one figure to another. The range of values illustrated for these SCIPUFF results covers seven orders of magnitude from the highest to lowest. Most air pollution regulatory applications would not be concerned with concentrations that are less than three or four orders of magnitude below the maximum values.

By afternoon, at 1800 UTC, 1 July, the onset of the southwesterly sea-breeze flow in the Brayton Point area has turned the plume's direction toward the northeast, so that it takes a mostly overland trajectory (Figure 54). Notice that the shifting wind directions in the sea-breeze flow and the strong vertical and horizontal mixing in the convectively unstable boundary layer have caused the plume to spread horizontally as an enormous blob, rather than having the narrow-plume pattern found during the previous night. Also, the maximum surface concentration has increased by an order of magnitude to 9.15 X 10^{-9} kg/m^3 and is located only several kilometers downwind of Brayton Point. The higher maximum concentration close to the plant is due to strong fumigation caused by the intense turbulence in the convectively unstable boundary layer that rapidly mixes the plume to the surface.

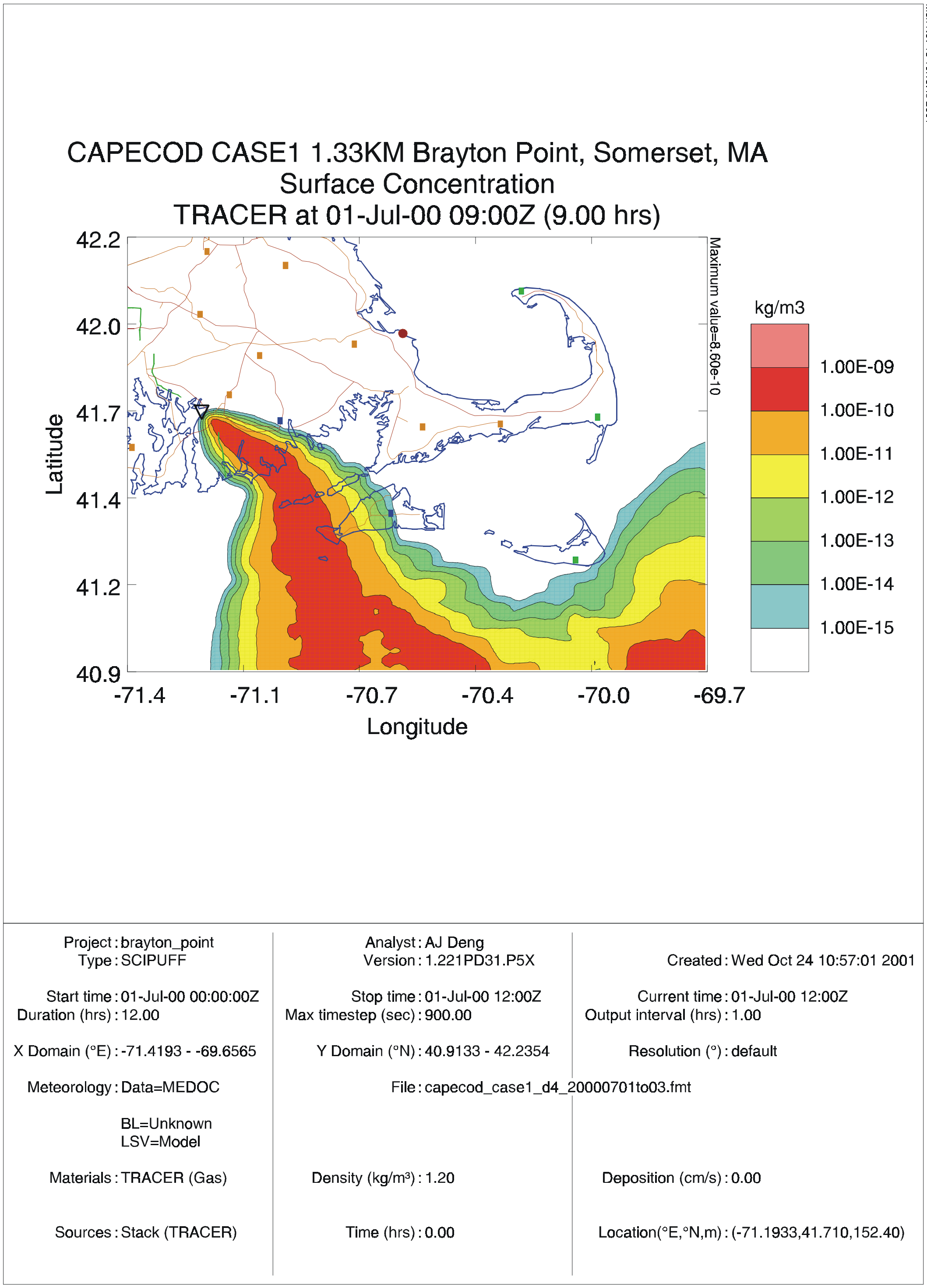

Figure 53. SCIPUFF surface concentrations of inert tracer (kg/m^3) released from the Brayton Point plant at Somerset, MA, as a continuous plume. Concentrations shown on the 1.33-km domain in Case 1 are valid at 0900 UTC, 1 July 2000 (+9 h). Maximum concentration is shown at the upper right of the panel. (The number of hours that SCIPUFF has been running is shown in parentheses at the top of the figure.)

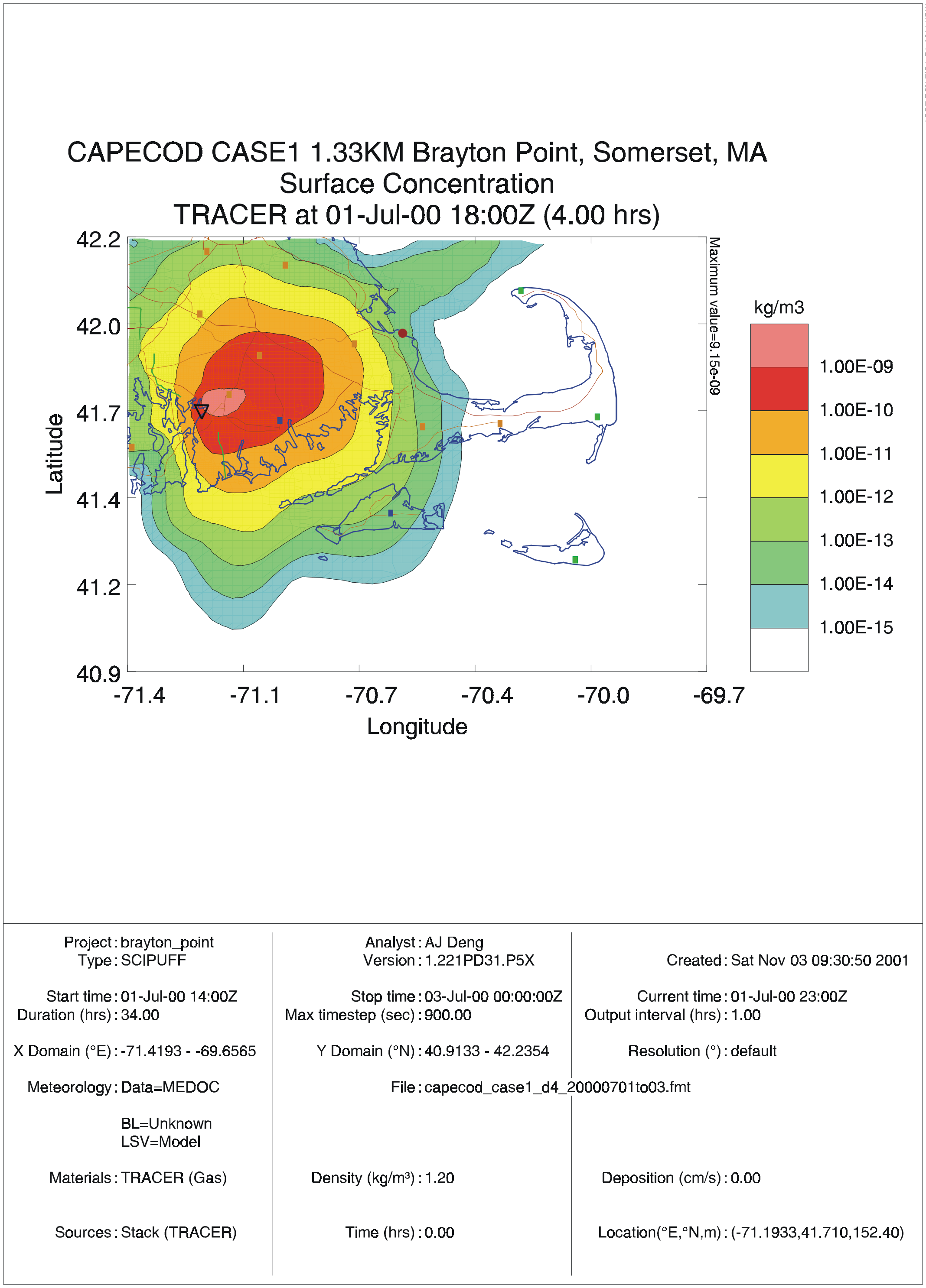

Figure 54. SCIPUFF surface concentrations of inert tracer (kg/m^3) released from the Brayton Point plant at Somerset, MA, as a continuous plume. Concentrations shown on the 1.33-km domain in Case 1 are valid at 1800 UTC, 1 July 2000 (+18 h). Maximum concentration is shown at the upper right of the panel. (The number of hours that SCIPUFF has been running is shown in parentheses at the top of the figure.)

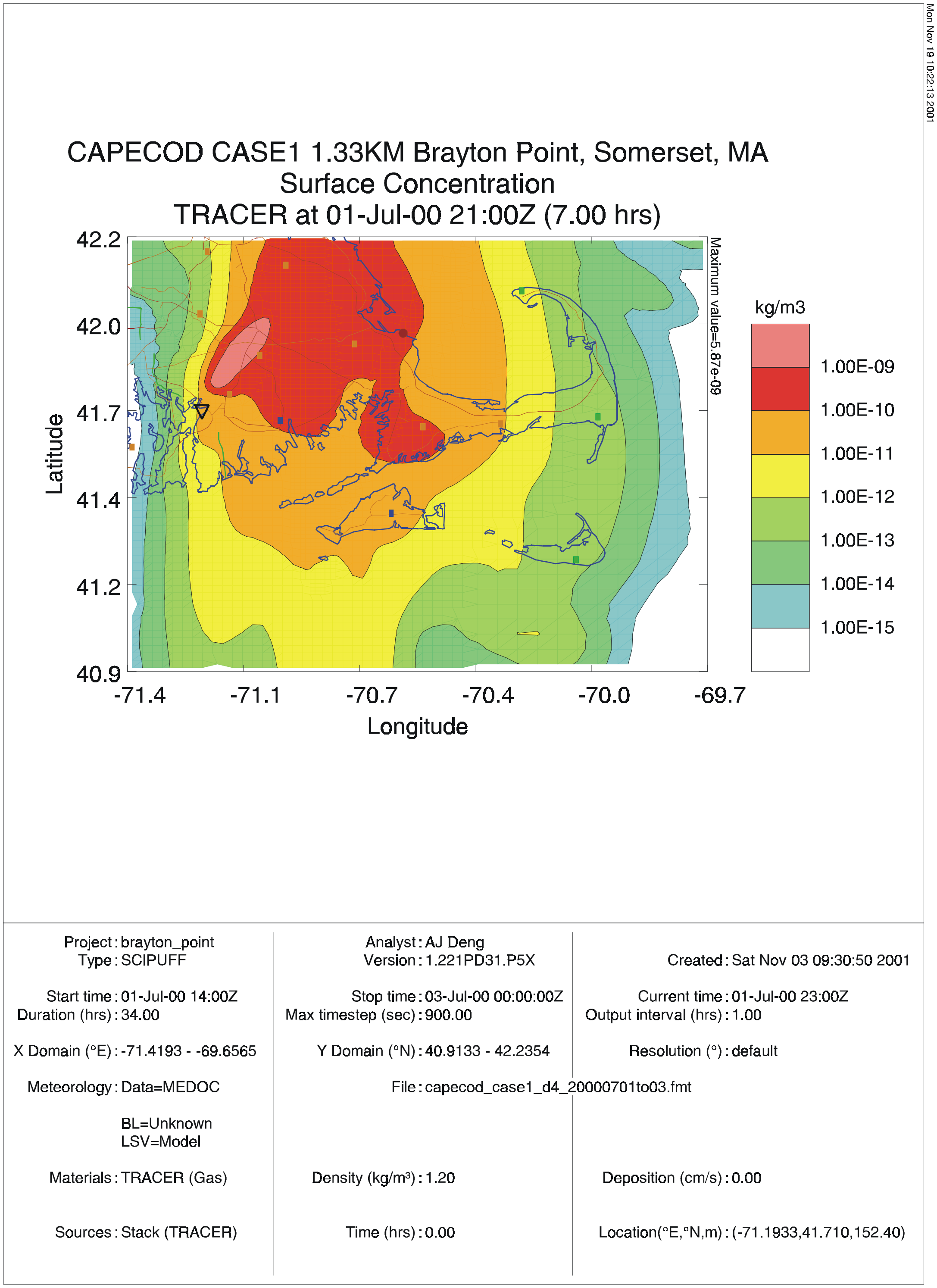

Figure 55. SCIPUFF surface concentrations of inert tracer (kg/m^3) released from the Brayton Point plant at Somerset, MA, as a continuous plume. Concentrations shown on the 1.33-km domain in Case 1 are valid at 2100 UTC, 1 July 2000 (+21 h). Maximum concentration is shown at the upper right of the panel. (The number of hours that SCIPUFF has been running is shown in parentheses at the top of the figure.)

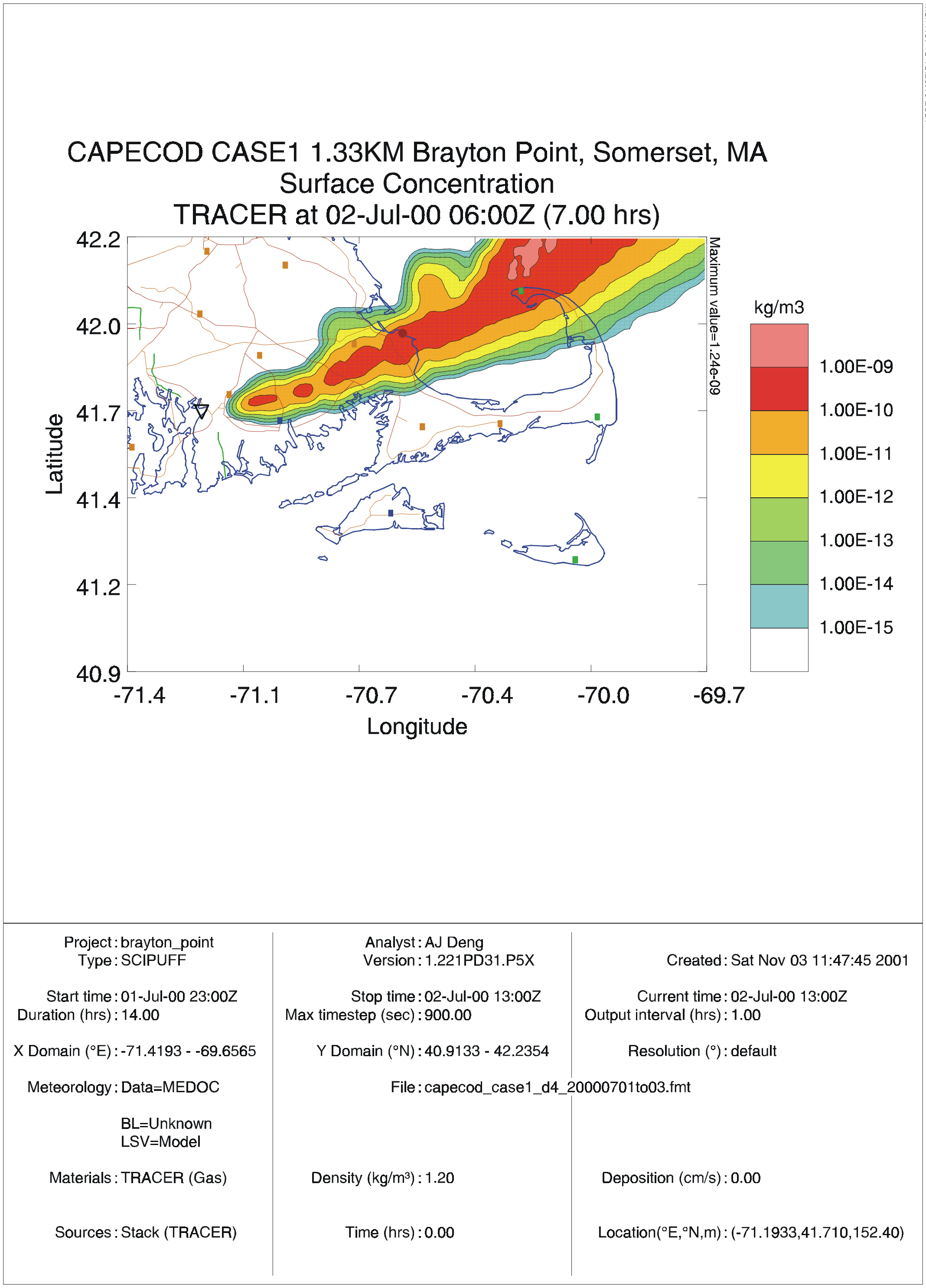

Figure 56. SCIPUFF surface concentrations of inert tracer (kg/m^3) released from the Brayton Point plant at Somerset, MA, as a continuous plume. Concentrations shown on the 1.33-km domain in Case 1 are valid at 0600 UTC, 2 July 2000 (+30 h). Maximum concentration is shown at the upper right of the panel. (The number of hours that SCIPUFF has been running is shown in parentheses at the top of the figure.

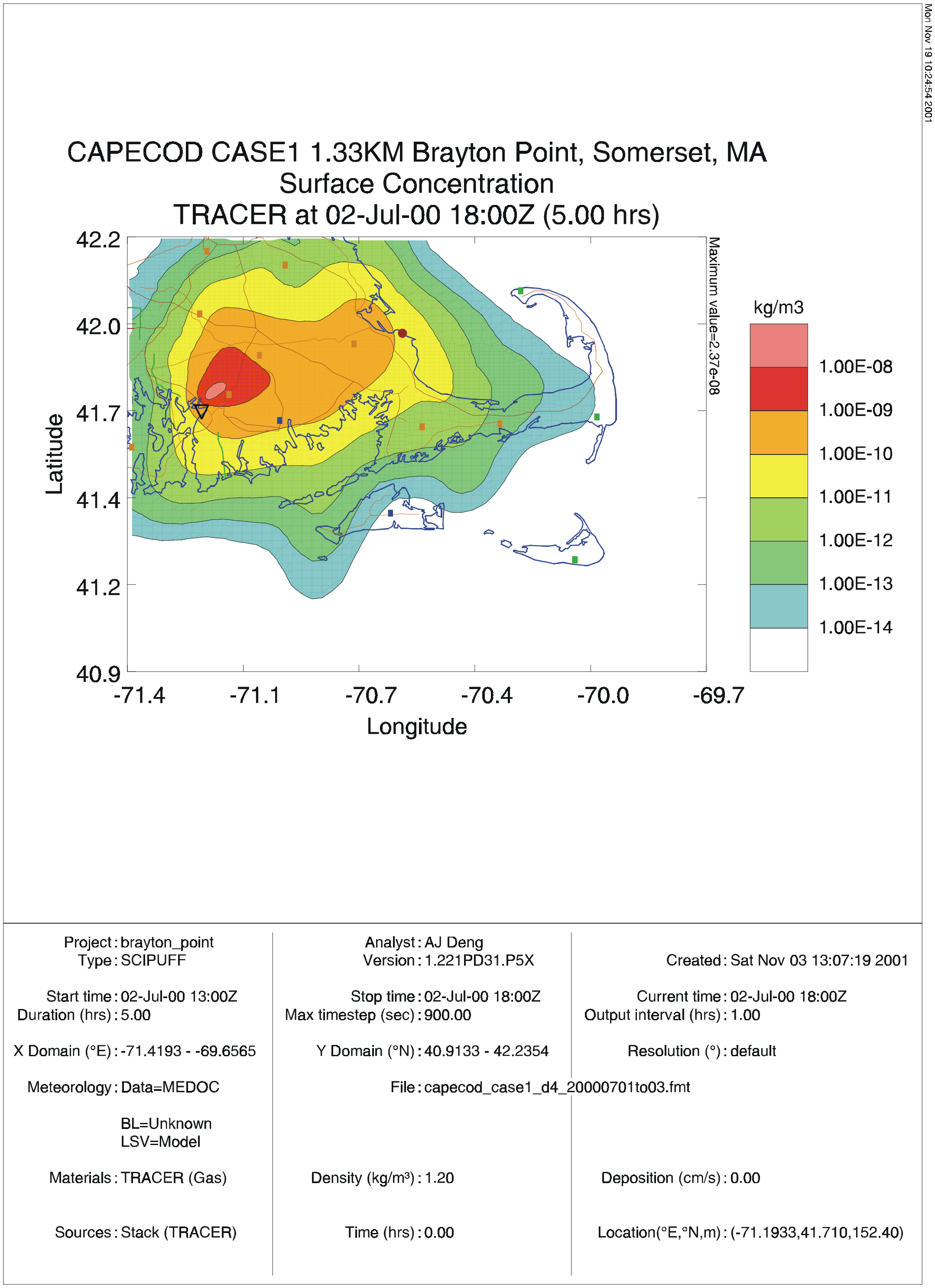

Figure 57. SCIPUFF surface concentrations of inert tracer (kg/m^3) released from the Brayton Point plant at Somerset, MA, as a continuous plume. Concentrations shown on the 1.33-km domain in Case 1 are valid at 1800 UTC, 2 July 2000 (+42 h). Maximum concentration is shown at the upper right of the panel. (The number of hours that SCIPUFF has been running is shown in parentheses at the top of the figure.)

As the sea-breeze front continues moving inland through the afternoon of 1 July, the Brayton Point plume continues to spread northward, until it covers all of southeastern MA by 2100 UTC (Figure 55). At this time, as sunset approaches, the intensity of the turbulence is beginning to weaken, so that the maximum surface concentrations shift downwind about 15 km from the plant and are reduced to ~6 X 10^{-9} kg/m^3. By that evening, at 0600 UTC, 2 July (+ 30 h, second day of Case 1), the synoptic-scale flow has shifted to southwesterly, as is evident from the path of the stable nocturnal plume (Figure 56). As on the first night, maximum nocturnal concentrations are small and over the ocean at about 90 km downwind of Brayton Point.

Finally, Figure 57 shows that on the second afternoon, at 1800 UTC (+42 h), the renewed sea breeze has again begun to spread the plume northward from the direction dictated by the background southwesterly winds. The maximum surface concentrations in the plume again have risen by early afternoon ~24 X 10^{-9} kg/m^3 about 5 km from Brayton Point. Hence, because the mesoscale sea-breeze winds change the local directions quite drastically, they appear capable of spreading the surface plume from Brayton Point across most or all of southeastern MA and Cape Cod whenever the synoptic-scale winds are weak and from the southwest to northwest directions. These synoptic conditions are quite common over New England during the warm season. Furthermore, comparison of the relative concentration maximums at the different times shown in Figures 52-57 indicates that the highest surface concentrations often occur near 1800 UTC, when the growing boundary layer can cause the plume to be mixed downward to the surface at distances only a few kilometers downwind of the Brayton Point plant. If the boundary layer continues to grow deeper during the afternoon, maximum surface concentrations can actually decline.

Next, Figures 58-61 show SCIPUFF results for the Canal plant at Sandwich, MA, in Case 1. Although there are many similarities to the results shown above for the Brayton Point plant, there are significant differences, as well. For example, at 0900 UTC, 1 July (+9 h), Figure 58 shows that, instead of a single gradually spreading plume, the nocturnal surface plume from the Canal plant is irregular and spread over a broad area southeast of Cape Cod. (The prevailing northwesterly winds become very weak and variable in this area, as shown at 1200 UTC in Figure 30). Surface concentrations are very low (~8 X 10^{-11} kg/m^3), indicating that the plume remains trapped aloft by quite stable air close to the surface. The small amount of the tracer that does impact the surface has maximums in several areas, including both near-source and far-downwind locations. By late on the first afternoon, at 2100 UTC, 1 July (+21 h), the southeasterly sea-breeze winds over Massachusetts Bay have turned the Canal plume northwestward in the direction of Boston (Figure 59). This direction is consistent with the MM5's simulated surface winds at this time (Figure 33). Most of the plume lies to the east of the convergence zone that separates the two main branches of the regional sea breezes in southeastern MA at this time. As is typical for this area, daytime turbulence causes the afternoon maximum surface concentration (~5.7 X 10^{-9} kg/m^3) to be located just downwind of the Canal plant (close to the shore of the Bay). A weaker secondary maximum is found about 40 km downwind close to Boston as the plume returns to the coast.

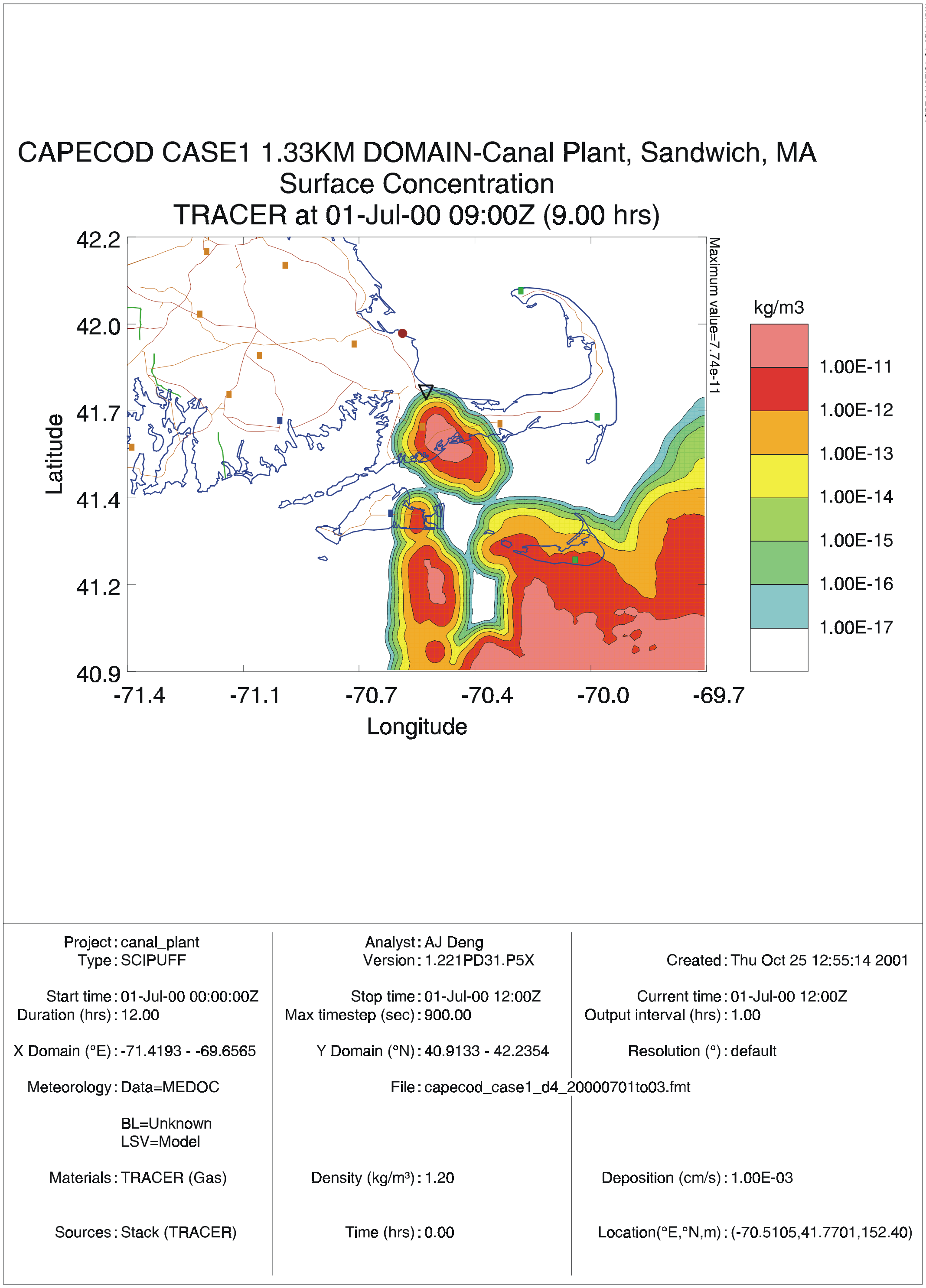

Figure 58. SCIPUFF surface concentrations of inert tracer (kg/m^3) released from the Canal plant at Sandwich, MA, as a continuous plume. Concentrations shown on the 1.33-km domain in Case 1 are valid at 0900 UTC, 1 July 2000 (+9 h). Maximum concentration is shown at the upper right of the panel. (The number of hours that SCIPUFF has been running is shown in parentheses at the top of the figure.)

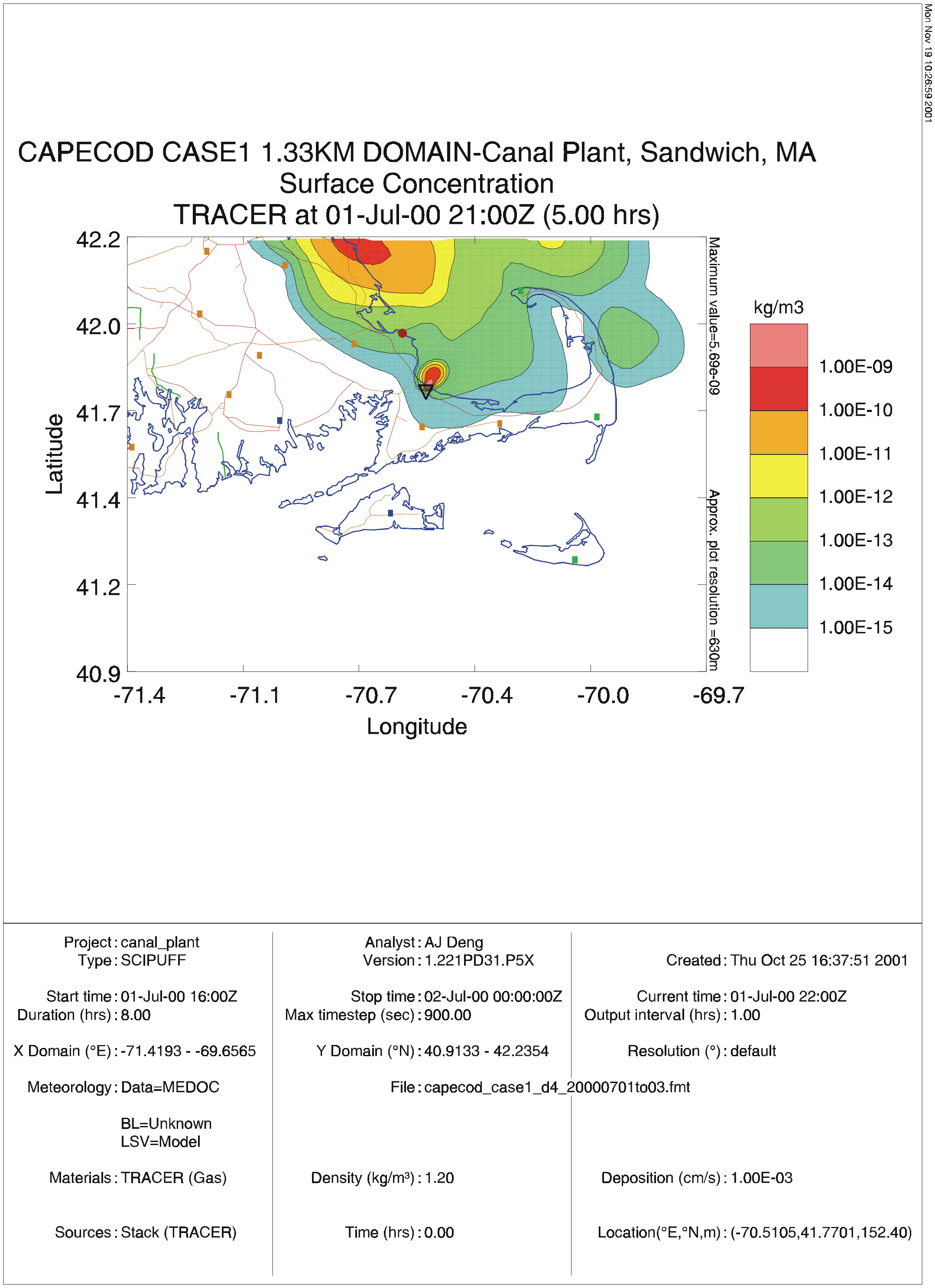

Figure 59. SCIPUFF surface concentrations of inert tracer (kg/m^3) released from the Canal plant at Sandwich, MA, as a continuous plume. Concentrations shown on the 1.33-km domain in Case 1 are valid at 2100 UTC, 1 July 2000 (+21 h). Maximum concentration is shown at the upper right of the panel. (The number of hours that SCIPUFF has been running is shown in parentheses at the top of the figure.)

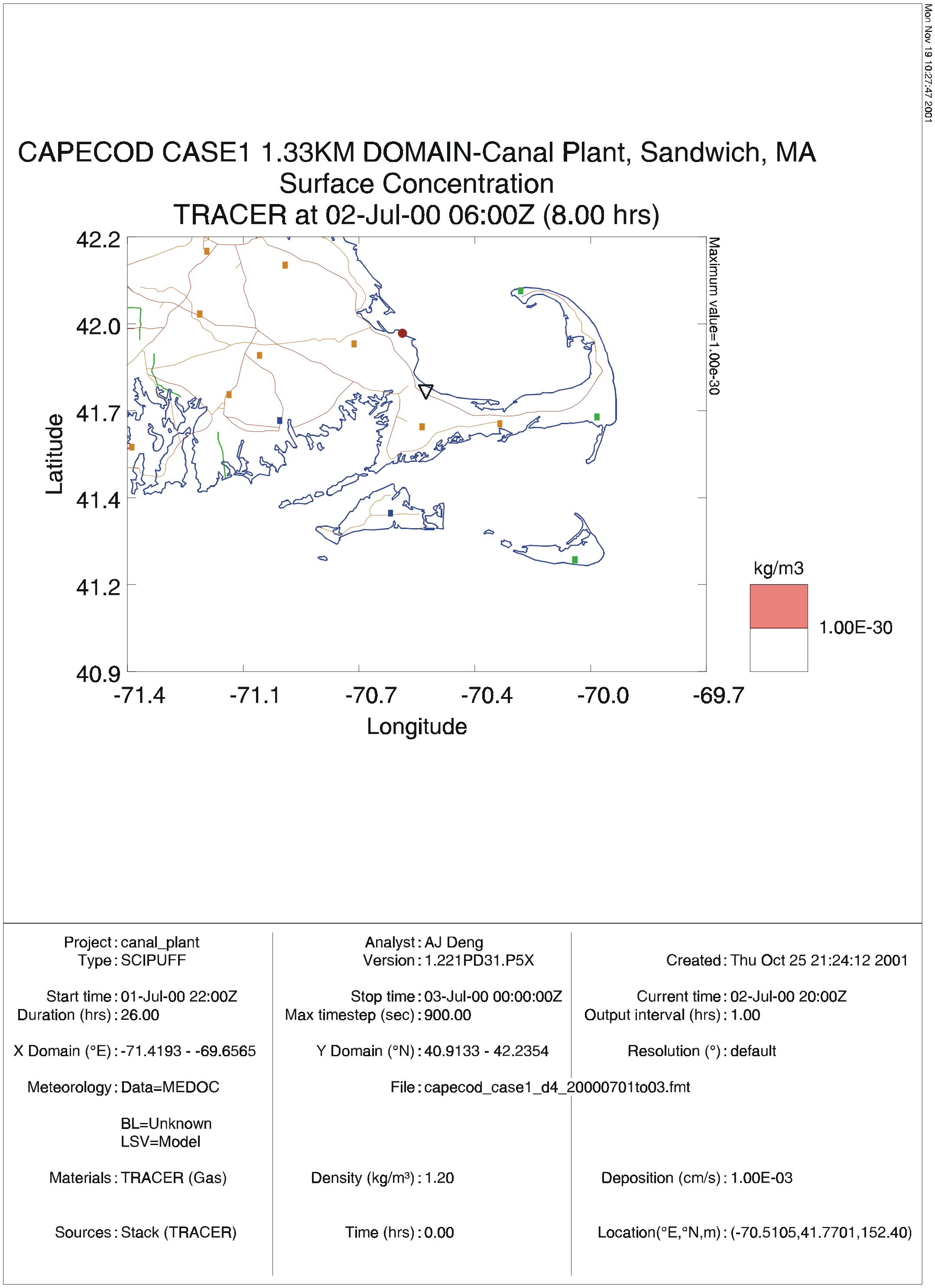

Figure 60. SCIPUFF surface concentrations of inert tracer (kg/m^3) released from the Canal plant at Sandwich, MA, as a continuous plume. Concentrations shown on the 1.33-km domain in Case 1 are valid at 0600 UTC, 2 July 2000 (+30 h). Maximum concentration is shown at the upper right of the panel. (The number of hours that SCIPUFF has been running is shown in parentheses at the top of the figure.)

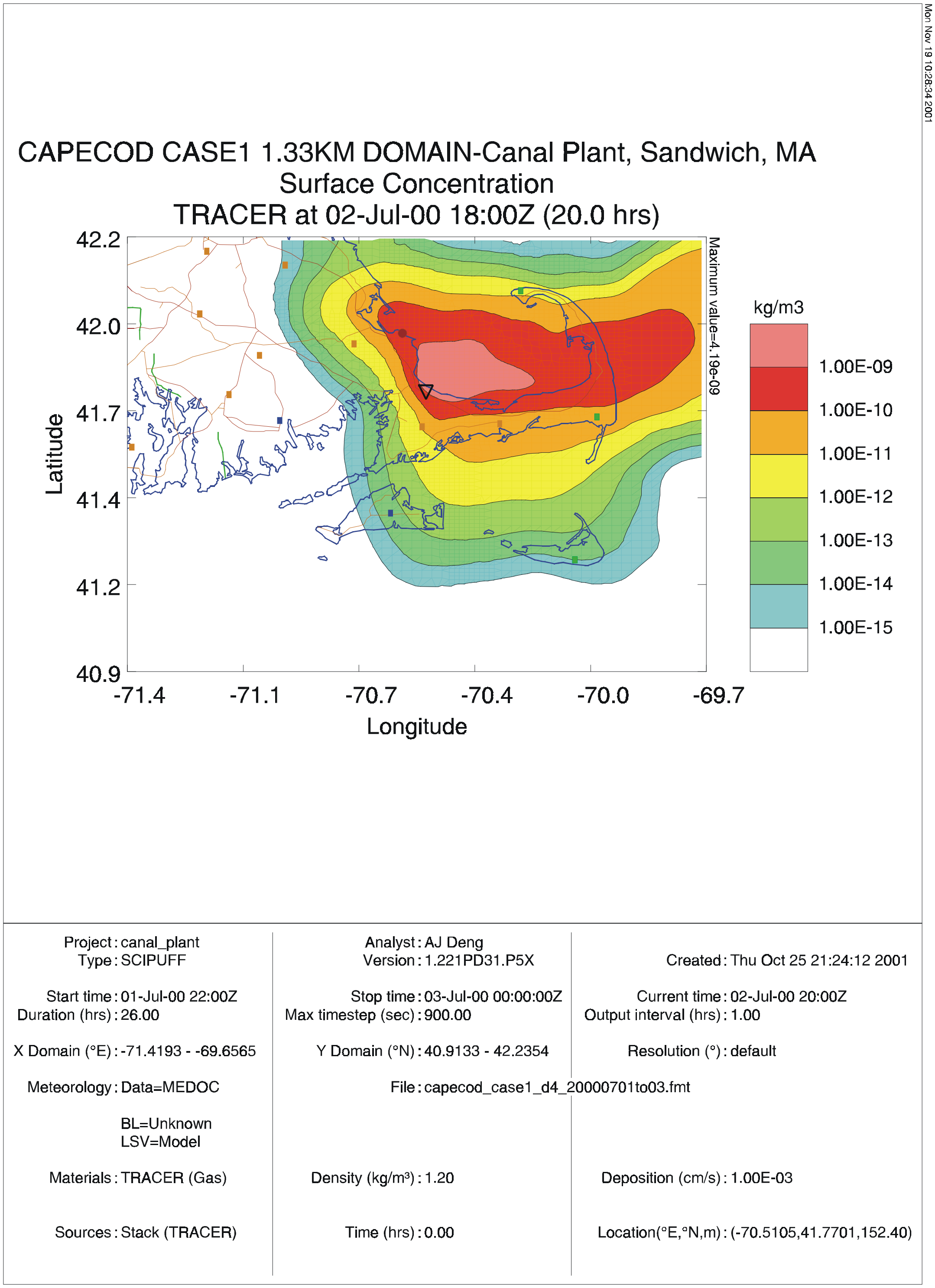

Figure 61. SCIPUFF surface concentrations of inert tracer (kg/m^3) released from the Canal plant at Sandwich, MA, as a continuous plume. Concentrations shown on the 1.33-km domain in Case 1 are valid at 1800 UTC, 2 July 2000 (+42 h). Maximum concentration is shown at the upper right of the panel. (The number of hours that SCIPUFF has been running is shown in parentheses at the top of the figure.)

On the second night (2 July), when the synoptic flow has become southwesterly over the region, the lower atmosphere becomes very stable over the cool waters of Massachusetts Bay. Thus, the plume from the Canal plant at 0600 UTC (+30 h), 2 July, essentially is prevented from reaching the surface at all (Figure 60). However, once the solar heating regenerates the sea breeze on the final afternoon, at 1800 UTC (+42 h), 2 July, Figure 61 shows the Canal plant plume again becomes fairly widespread at the surface. Maximum surface concentrations are somewhat lower on this day (~4 X 10^{-9} kg/m^3), perhaps because the shifting position of the sea-breeze convergence zone has caused the plume to split, with part headed eastward and part headed northwestward toward Boston. The movement of the plume can be compared to the sharply discontinuous surface winds at this time (see Figure 36).

The behavior of the SCIPUFF plume released from the highway line source for Case 1 is shown in Figures 62-66. During the first night, at 0900 UTC (+9 h), 1 July, Figure 62 shows that the plume from the surface line source is advected southeastward on the light northwesterly winds. Maximum concentrations at this time are much higher (~1.2 X 10^{-5} kg/m^3), compared to concentrations from the power plants, because the source is at the surface and the wind direction is aligned approximately parallel to the highway. In the afternoon at 1800 UTC (+18 h), 1 July, the maximum surface concentrations are about the same (~1.4 X 10^{-5} kg/m^3), but with the plume heading northwest in response to the sea breeze blowing from Massachusetts Bay (Figure 63). A bit later, at 2100 UTC (+21 h), Figure 64 shows that the highway plume is drifting northward over the Bay, but maximum surface concentrations remain almost the same along the highway.

During the second night, at 0600 UTC (+30 h), 2 July, the stable southwesterly synoptic flow carries the highway plume over Massachusetts Bay and Outer Cape Cod (Figure 65).

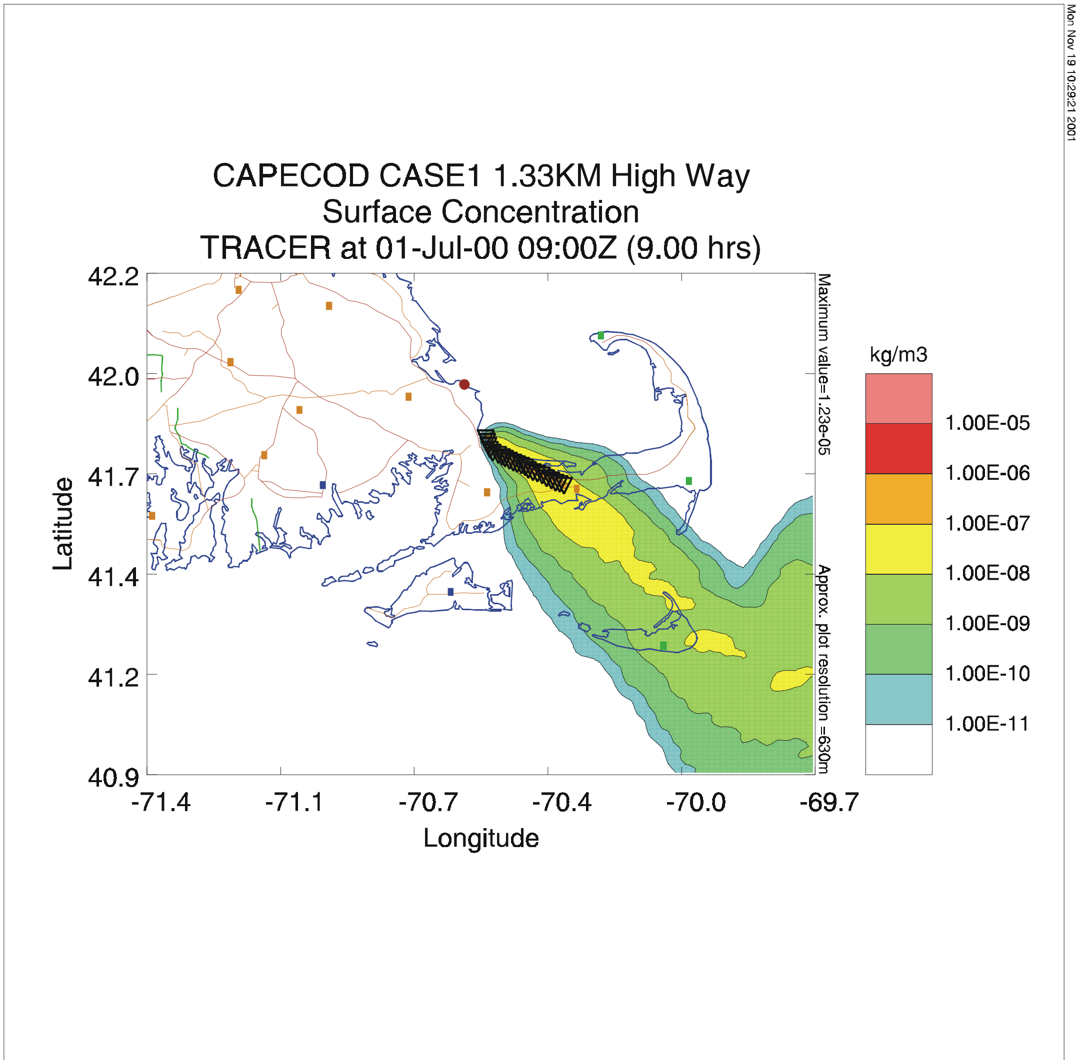

Project : high_way Type : SCIPUFF	Analyst : AJ Deng Version : 1.221PD31.P5X	Created : Sat Nov 17 15:16:39 2001
Start time : 01-Jul-00 00:00:00Z Duration (hrs) : 15.00	Stop time : 01-Jul-00 15:00Z Max timestep (sec) : 900.00	Current time : 01-Jul-00 15:00Z Output interval (hrs) : 1.00
X Domain (°E) : -71.4193 - -69.6565	Y Domain (°N) : 40.9133 - 42.2354	Resolution (°) : default
Meteorology : Data=MEDOC BL=Unknown LSV=Model	File : capecod_case1_d4_20000701to03.fmt	
Materials : TRACER (Gas)	Density (kg/m³) : 1.20	Deposition (cm/s) : 1.00E-03
Sources (22) : Stack (TRACER) Stack (TRACER) Stack (TRACER)	Time (hrs) : 0.00 0.00 0.00	Location(°E,°N,m) : (-70.5258,41.8068,2.00) (-70.5214,41.7979,2.00) (-70.5189,41.7879,2.00)

Figure 62. SCIPUFF surface concentrations of inert tracer (kg/m^3) released as a continuous plume along MA Routes 3 and 6. Concentrations shown on the 1.33-km domain in Case 1 are valid at 0900 UTC, 1 July 2000 (+9 h). Maximum concentration is shown at the upper right of the panel. (The number of hours that SCIPUFF has been running is shown in parentheses at the top of the figure.)

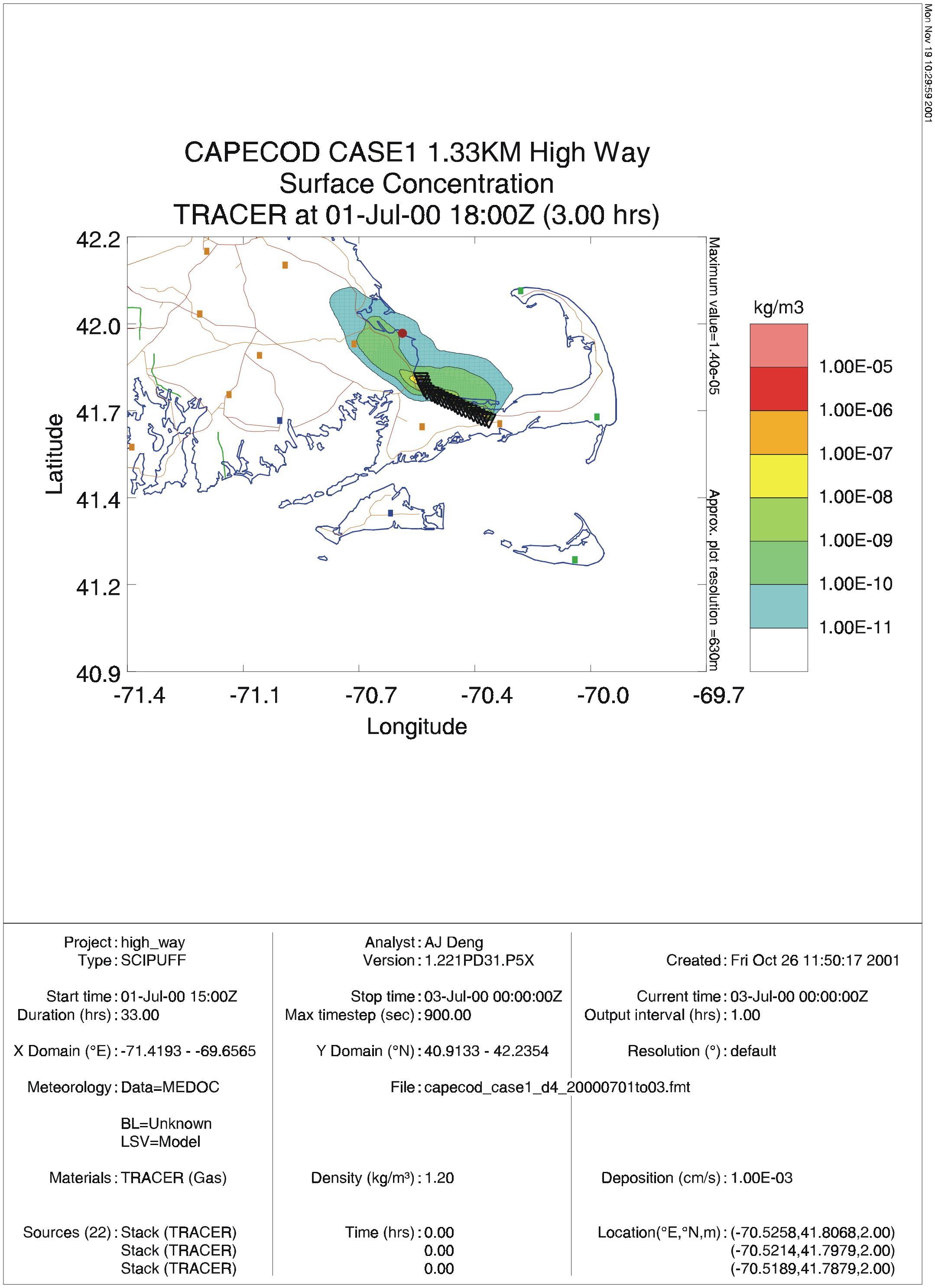

Figure 63. SCIPUFF surface concentrations of inert tracer (kg/m^3) released as a continuous plume along MA Routes 3 and 6. Concentrations shown on the 1.33-km domain in Case 1 are valid at 1800 UTC, 1 July 2000 (+18 h). Maximum concentration is shown at the upper right of the panel. (The number of hours that SCIPUFF has been running is shown in parentheses at the top of the figure.)

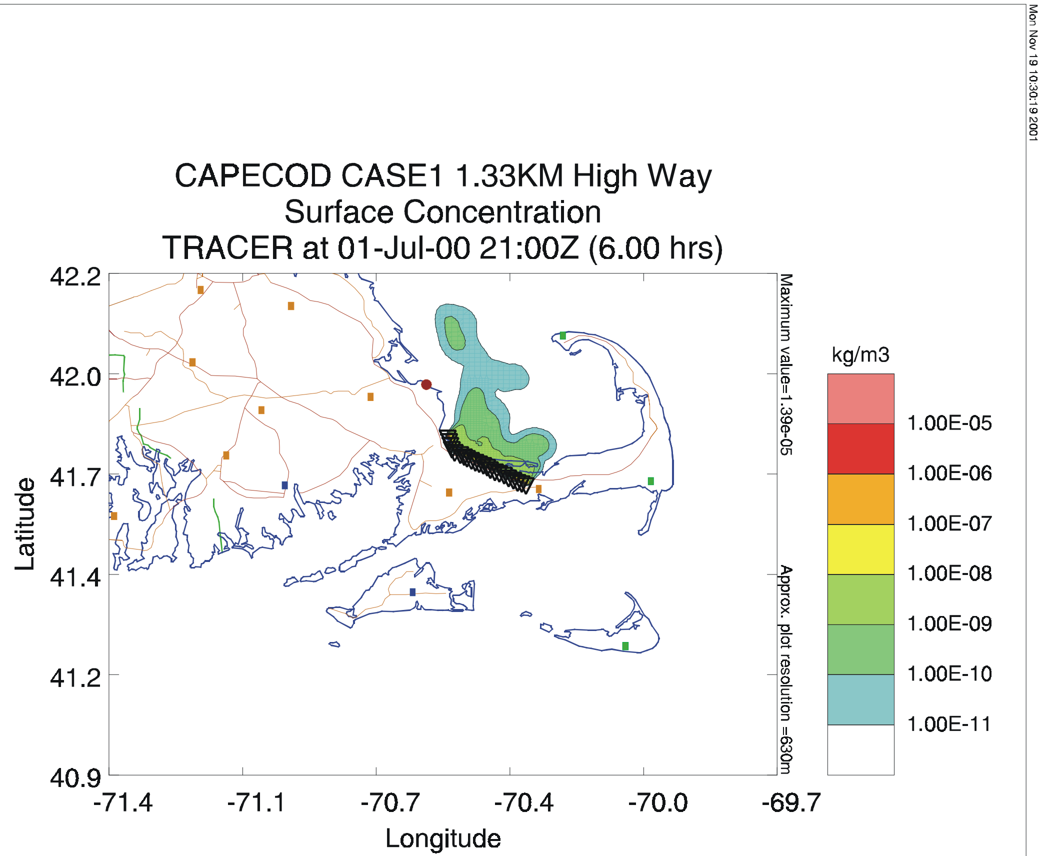

Project : high_way Type : SCIPUFF	Analyst : AJ Deng Version : 1.221PD31.P5X	Created : Fri Oct 26 11:50:17 2001
Start time : 01-Jul-00 15:00Z Duration (hrs) : 33.00	Stop time : 03-Jul-00 00:00:00Z Max timestep (sec) : 900.00	Current time : 03-Jul-00 00:00:00Z Output interval (hrs) : 1.00
X Domain (°E) : -71.4193 - -69.6565	Y Domain (°N) : 40.9133 - 42.2354	Resolution (°) : default
Meteorology : Data=MEDOC	File : capecod_case1_d4_20000701to03.fmt	
BL=Unknown LSV=Model		
Materials : TRACER (Gas)	Density (kg/m³) : 1.20	Deposition (cm/s) : 1.00E-03
Sources (22) : Stack (TRACER) Stack (TRACER) Stack (TRACER)	Time (hrs) : 0.00 0.00 0.00	Location(°E,°N,m) : (-70.5258,41.8068,2.00) (-70.5214,41.7979,2.00) (-70.5189,41.7879,2.00)

Figure 64. SCIPUFF surface concentrations of inert tracer (kg/m^3) released as a continuous plume along MA Routes 3 and 6. Concentrations shown on the 1.33-km domain in Case 1 are valid at 2100 UTC, 1 July 2000 (+21 h). Maximum concentration is shown at the upper right of the panel. (The number of hours that SCIPUFF has been running is shown in parentheses at the top of the figure.)

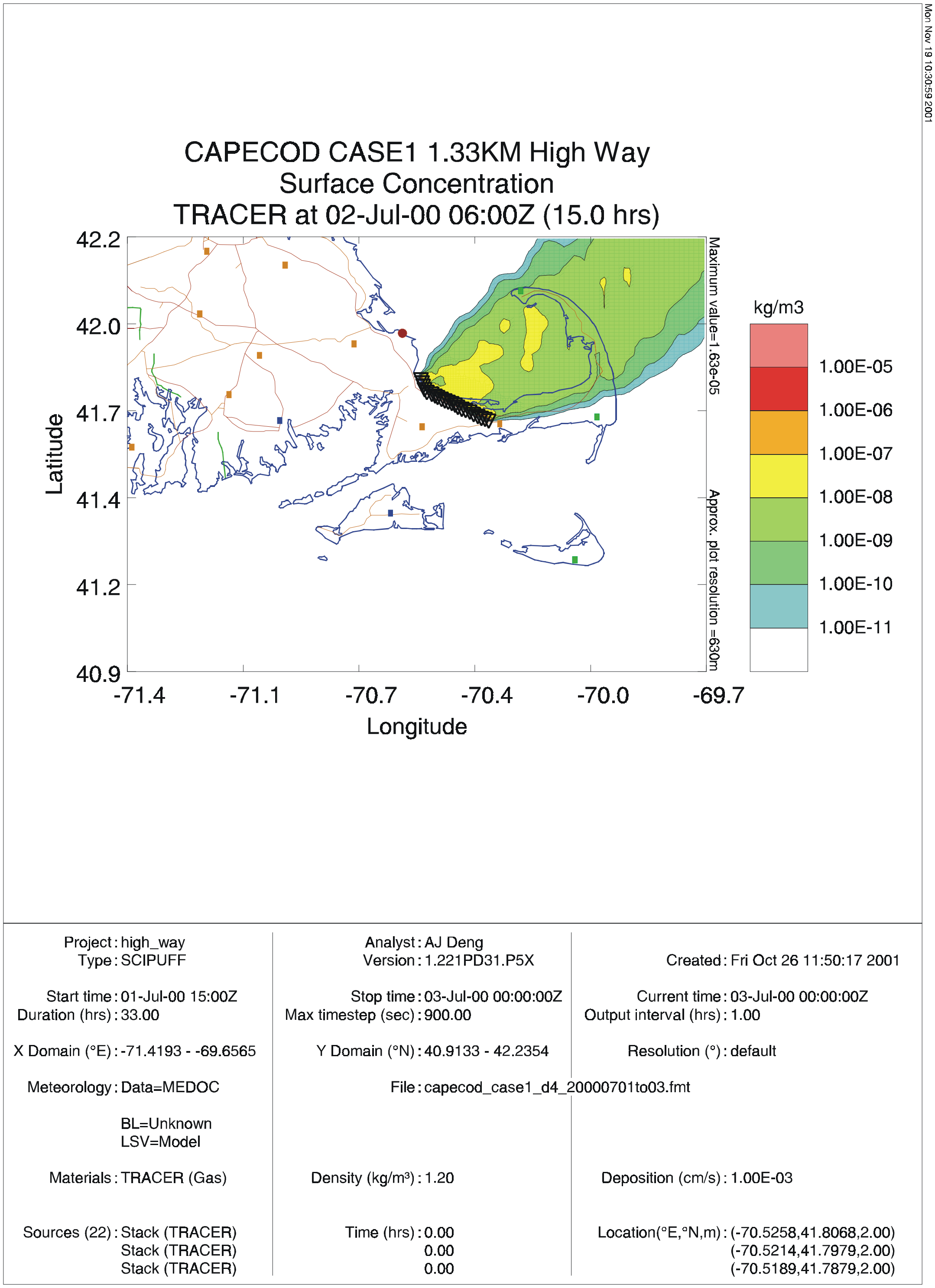

Figure 65. SCIPUFF surface concentrations of inert tracer (kg/m^3) released as a continuous plume along MA Routes 3 and 6. Concentrations shown on the 1.33-km domain in Case 1 are valid at 0600 UTC, 2 July 2000 (+30 h). Maximum concentration is shown at the upper right of the panel. (The number of hours that SCIPUFF has been running is shown in parentheses at the top of the figure.)

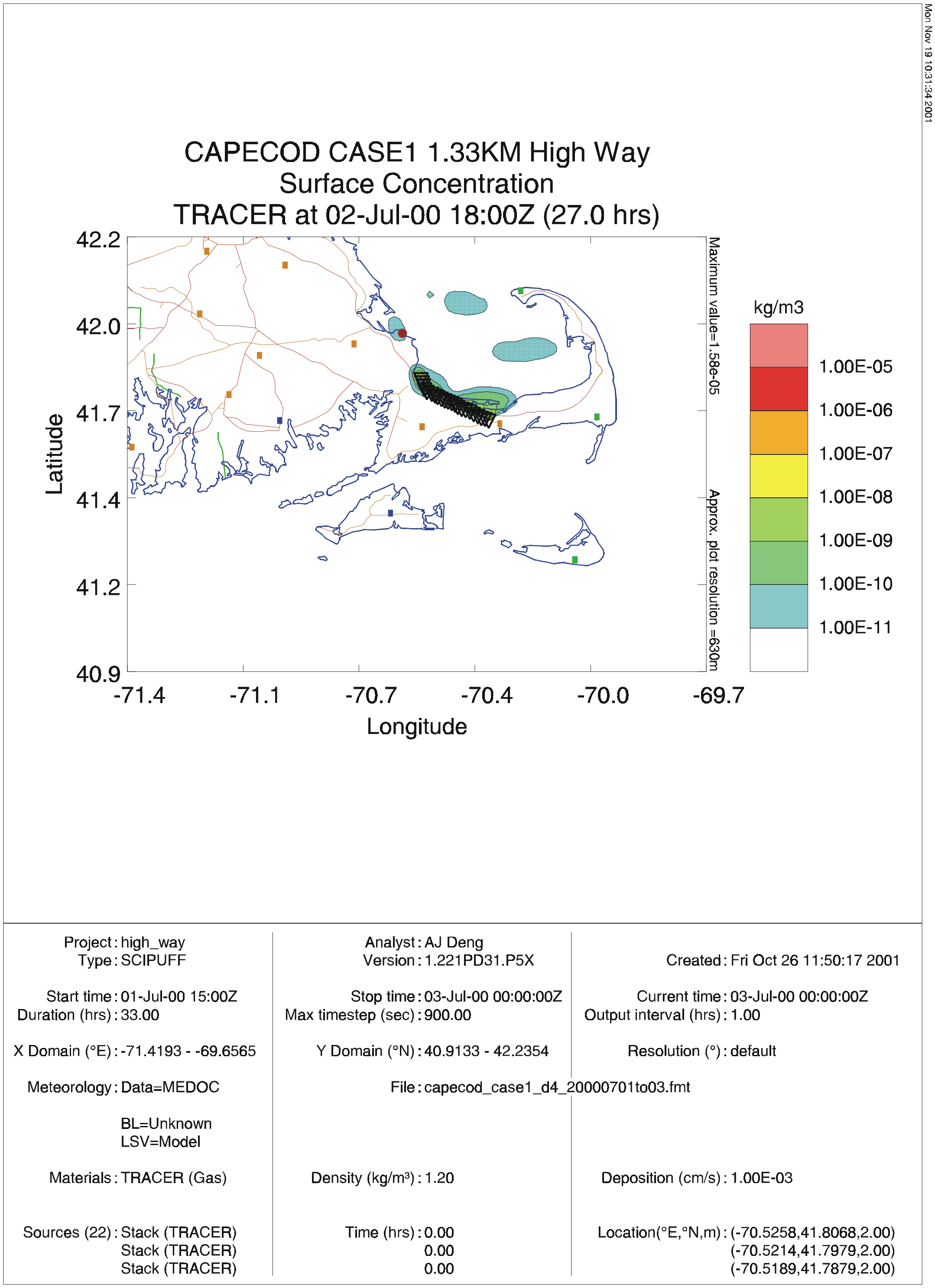

Figure 66. SCIPUFF surface concentrations of inert tracer (kg/m^3) released as a continuous plume along MA Routes 3 and 6. Concentrations shown on the 1.33-km domain in Case 1 are valid at 1800 UTC, 2 July 2000 (+42 h). Maximum concentration is shown at the upper right of the panel. (The number of hours that SCIPUFF has been running is shown in parentheses at the top of the figure.)

Maximum concentrations are a bit higher at this time (~1.6 X 10^{-5} kg/m^3), possibly because of a combination of light winds and high stability over land near the roadway. Finally, at 1800 UTC (+42 h) on the second afternoon, Figure 66 shows that the concentrations remain high near the highway, but are quickly dissipated by the mixing in the sea breeze.

The fourth emission source used in this study of Case 1 is an area source located at Otis Air Force Base (AFB), which has a release height of 1 m above ground level (AGL). Since the tracer is released in SCIPUFF close to the ground, surface concentrations tend to be rather high until turbulence can transport the tracer upward. Figure 67 shows the surface tracer concentrations at 0900 UTC (+9h), 1 July 2000. As noted for the other sources described above, the nocturnal advection on this first night carries the emission plume southeastward on northwesterly winds. The nocturnal boundary layer over land is stable in this case. Maximum concentrations of ~7.7 X 10^{-6} kg/m^3, occur very close to Otis AFB, but gradually decrease in the downwind direction beyond Nantucket Island as the marine boundary layer becomes unstable and begins to deepen over warmer water. This pattern is opposite to that shown earlier for the nocturnal behavior of the plumes emitted by the power plants (e.g., Figure 53), which had their largest concentrations far downwind in the same region where the marine boundary layer deepens at the southern boundary of the 1.33-km domain. In the case of the elevated power-plant plumes, the deepening marine layer finally allowed turbulence to mix the plume downward to the surface. However, in the case of the plume from Otis AFB, the same deeper turbulent marine layer dilutes the plume that had been hugging the surface. In both cases, the turbulence vertically transports the pollutants "down-gradient" toward the region of lower initial concentrations.

Figure 68 indicates that, by early afternoon at 1800 UTC (+18 h), 1 July, the sea breeze was carrying the surface plume from Otis AFB northwestward over southeastern MA.

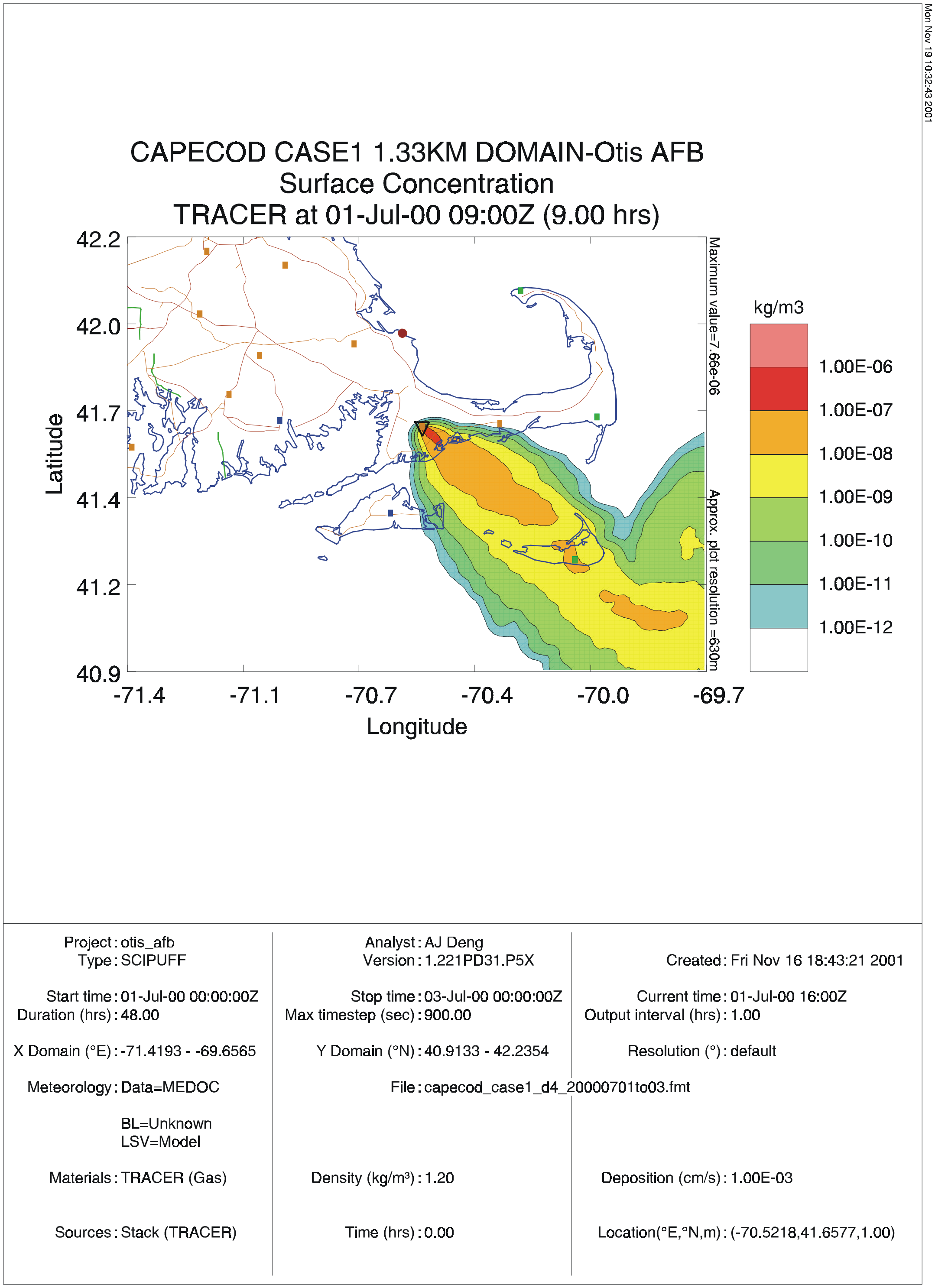

Figure 67. SCIPUFF surface concentrations of inert tracer (kg/m^3) released from Otis AFB as a continuous plume. Concentrations shown on the 1.33-km domain in Case 1 are valid at 0900 UTC, 1 July 2000 (+9 h). Maximum concentration is shown at the upper right of the panel. (The number of hours that SCIPUFF has been running is shown in parentheses at the top of the figure.)

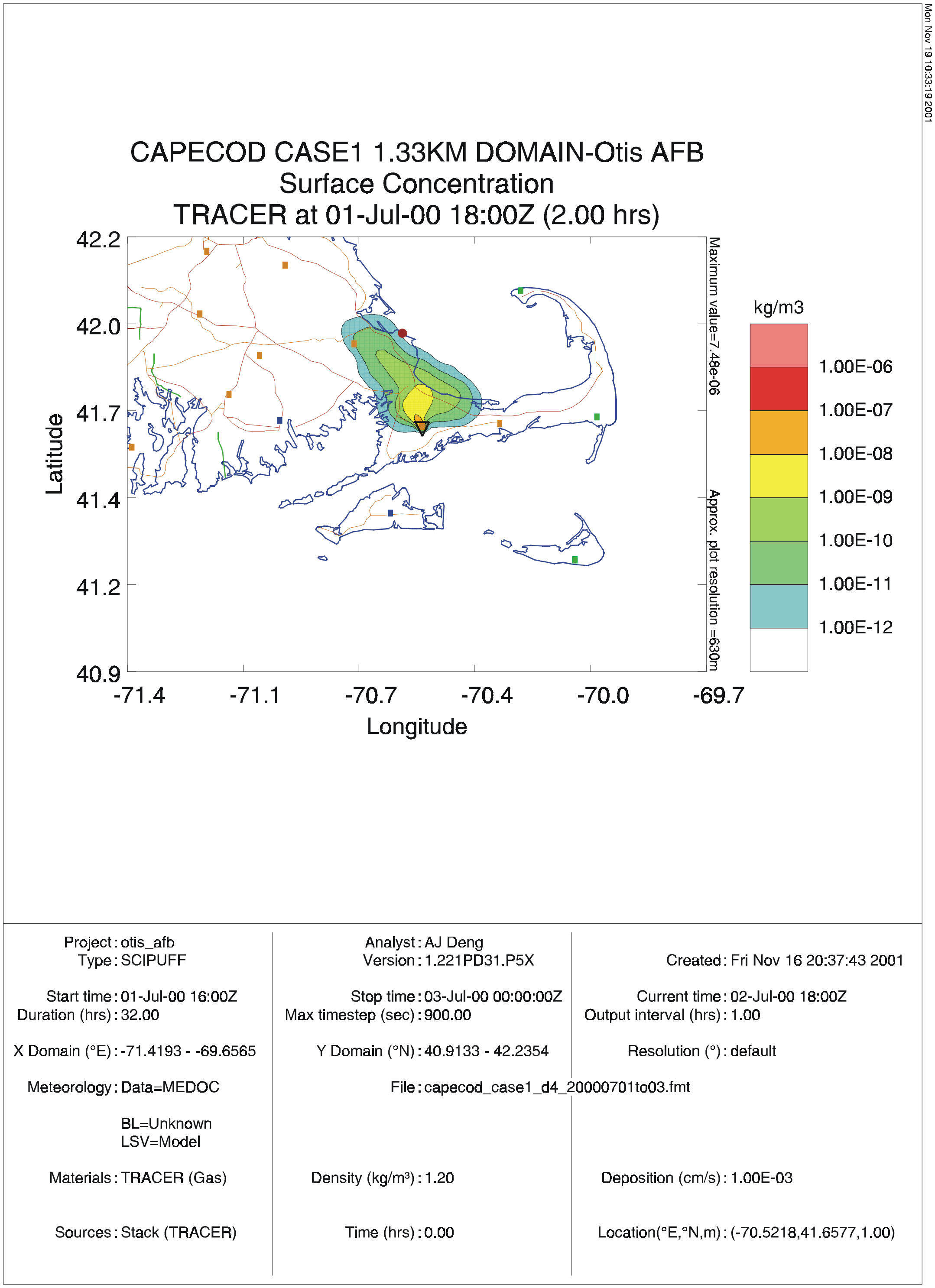

Figure 68. SCIPUFF surface concentrations of inert tracer (kg/m^3) released from Otis AFB as a continuous plume. Concentrations shown on the 1.33-km domain in Case 1 are valid at 1800 UTC, 1 July 2000 (+18 h). Maximum concentration is shown at the upper right of the panel. (The number of hours that SCIPUFF has been running is shown in parentheses at the top of the figure.)

Maximum surface concentrations are larger close to the immediate site of the emissions (~7.5 X 10^{-6} kg/m^3), but they decrease rapidly in the downwind direction due to mixing in the convectively unstable daytime boundary layer over Upper Cape Cod. Three hours later at 2100 UTC (+21 h), Figure 69 shows that the shifting sea breeze winds have advected the Otis plume north-northeastward to Massachusetts Bay, where it then turns toward the northwest in the direction of Boston. Maximum concentrations have increased slightly to ~8.2 X 10^{-6} kg/m^3. The direction and spread of the plume from Otis AFB at 2100 UTC, 1 July, is very similar to that described above for the plume from the Canal power plant (compare to Figure 59).

On the second night, at 0600 UTC (+30 h), 2 July, the boundary layer over land has again become stable so that the Otis AFB plume becomes more narrow and is advected northeastward with the prevailing synoptic-scale wind flow (Figure 70). Maximum concentrations are again close to the AFB (~1 X 10^{-5} kg/m^3). Finally, on the second day, Figures 71 and 72 show the same plume at 1800 UTC (+42 h) and 2100 UTC (+45 h), 2 July. By 1800 UTC, the plume has broadened considerably, compared to the nocturnal pattern of Figure 70, but the southwesterly winds over Cape Cod continue to advect it east-northeastward. By 2100 UTC, however, the maturing sea-breeze circulation over Massachusetts Bay has turned the downwind portion of the plume to the north of Provincetown. At the same time, the boundary-layer turbulence is weakening over land as the sun begins to set, so that the part of the plume closest to the AFB is already beginning to become narrow again as it changes into its nocturnal (stable) mode. Maximum concentrations on this second afternoon are located close to the AFB (~7.5-8.5 X 10^{-6} kg/m^3).

In summary, the behavior of the four plumes studied in Case 1, using SCIPUFF with MM5 model-generated winds and temperatures, all show the influence of the sea breeze during the daytime and the background synoptic-scale winds at night. Between them, practically all of Cape Cod and southeastern MA is exposed to one or more of the plumes in these simulations. It should be recalled that the emissions rates were set arbitrarily for this demonstration, so the relative concentrations between the plumes must not, by themselves, be considered meaningful. However, the shifting position and relative concentrations shown at different times for individual plumes do contain useful information about plume behavior in the region as a function of the synoptic-scale wind, local sea-breeze forcing, boundary-layer depth and turbulence intensity. The Brayton Point plume appears to have the widest distribution over land because it can become trapped in the southeastern-MA inland sea breeze for much of the day. However, this same plume may undergo the most vigorous turbulent mixing in the deep convectively unstable boundary layer over land, so that it can be diluted most easily.

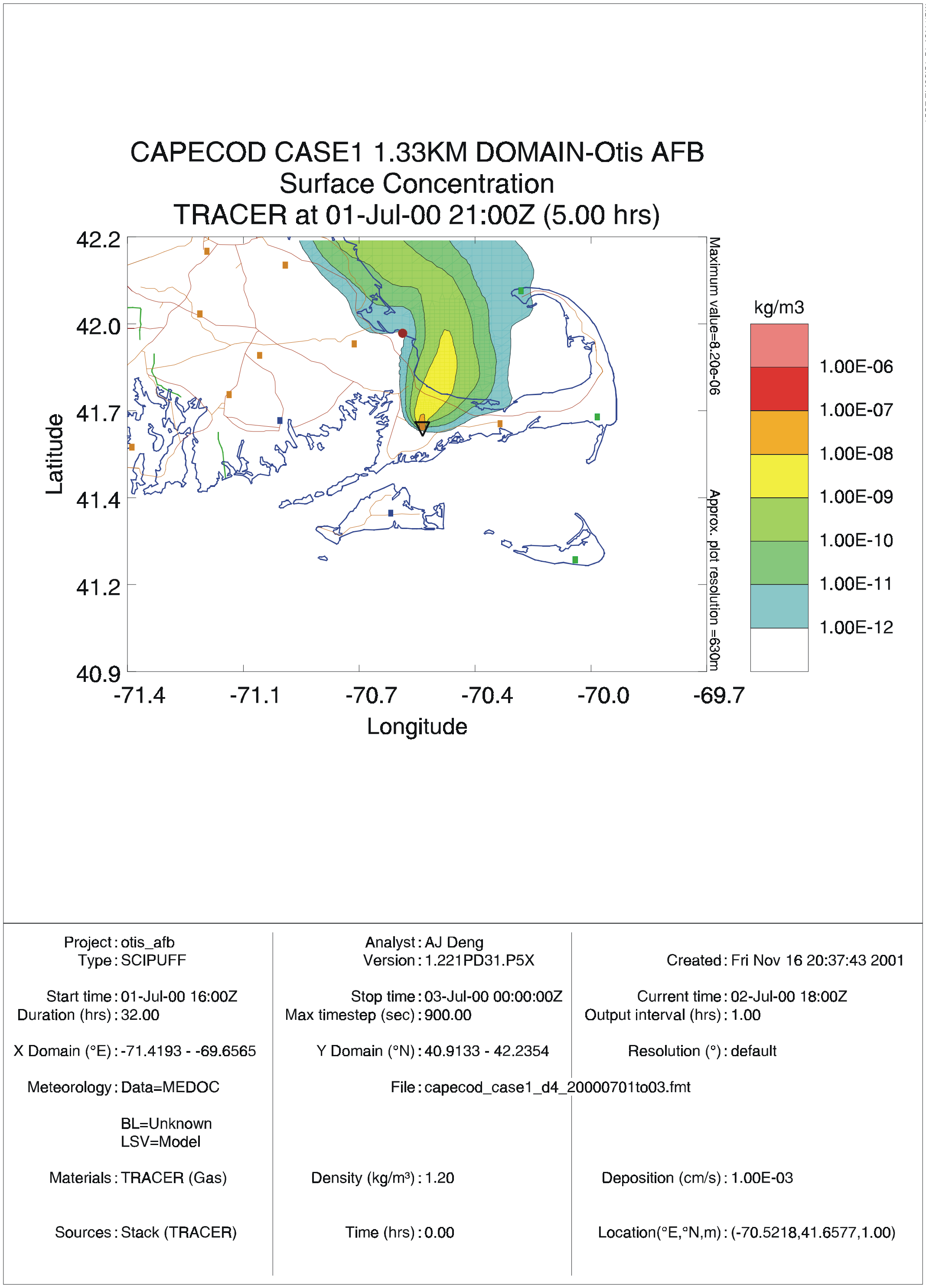

Figure 69. SCIPUFF surface concentrations of inert tracer (kg/m^3) released from Otis AFB as a continuous plume. Concentrations shown on the 1.33-km domain in Case 1 are valid at 2100 UTC, 1 July 2000 (+21 h). Maximum concentration is shown at the upper right of the panel. (The number of hours that SCIPUFF has been running is shown in parentheses at the top of the figure.)

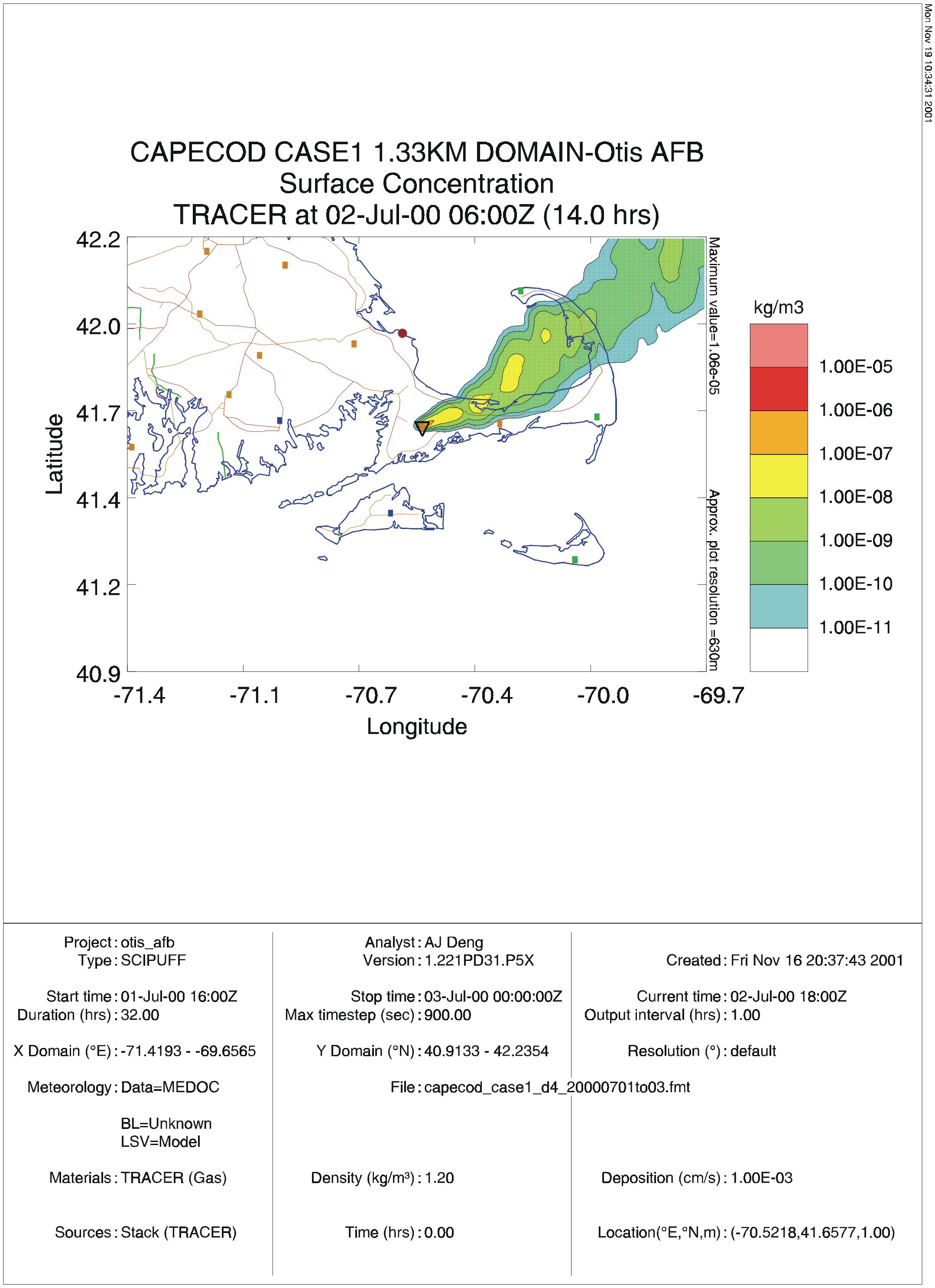

Figure 70. SCIPUFF surface concentrations of inert tracer (kg/m^3) released from Otis AFB as a continuous plume. Concentrations shown on the 1.33-km domain in Case 1 are valid at 0600 UTC, 2 July 2000 (+30 h). Maximum concentration is shown at the upper right of the panel. (The number of hours that SCIPUFF has been running is shown in parentheses at the top of the figure.)

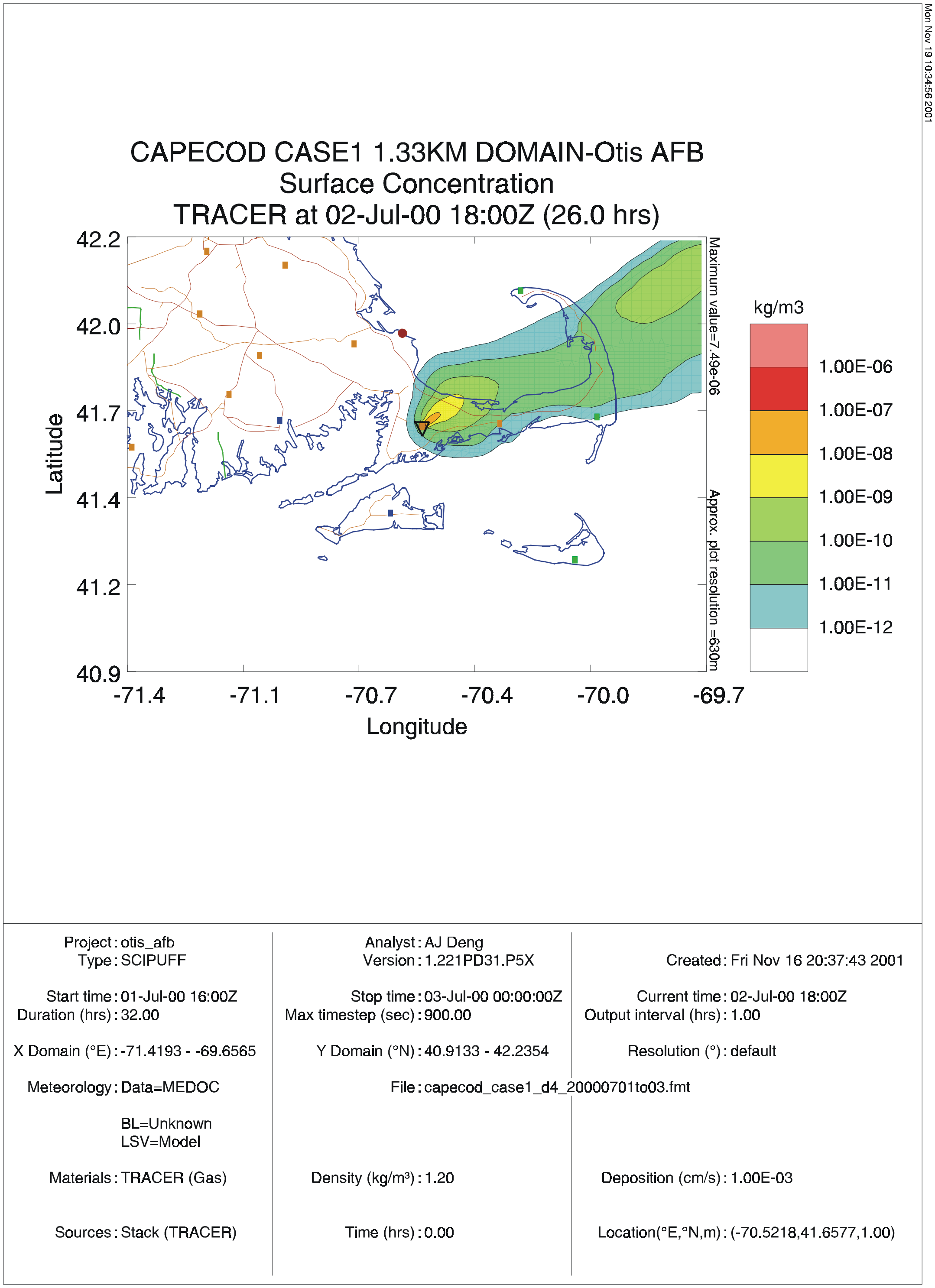

Figure 71. SCIPUFF surface concentrations of inert tracer (kg/m^3) released from Otis AFB as a continuous plume. Concentrations shown on the 1.33-km domain in Case 1 are valid at 1800 UTC, 2 July 2000 (+42 h). Maximum concentration is shown at the upper right of the panel. (The number of hours that SCIPUFF has been running is shown in parentheses at the top of the figure.)

Mon Nov 19 10:35:26 2001

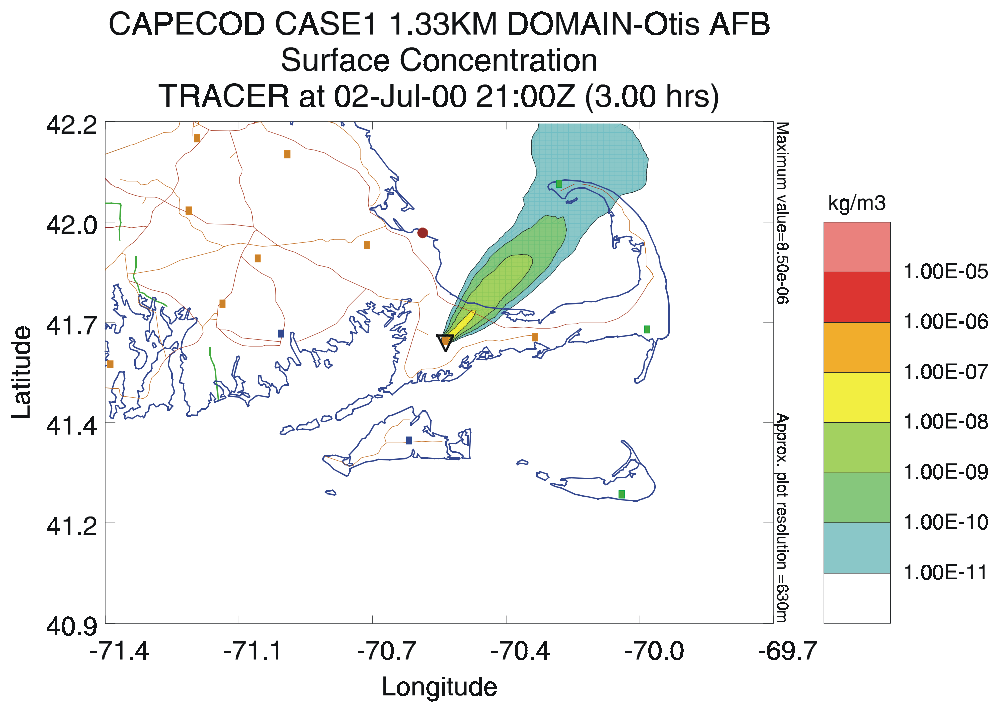

Project : otis_afb Type : SCIPUFF	Analyst : AJ Deng Version : 1.221PD31.P5X	Created : Sat Nov 17 12:39:40 2001
Start time : 02-Jul-00 18:00Z Duration (hrs) : 6.00	Stop time : 03-Jul-00 00:00:00Z Max timestep (sec) : 900.00	Current time : 03-Jul-00 00:00:00Z Output interval (hrs) : 1.00
X Domain (°E) : -71.4193 - -69.6565	Y Domain (°N) : 40.9133 - 42.2354	Resolution (°) : default
Meteorology : Data=MEDOC BL=Unknown LSV=Model	File : capecod_case1_d4_20000701to03.fmt	
Materials : TRACER (Gas)	Density (kg/m³) : 1.20	Deposition (cm/s) : 1.00E-03
Sources : Stack (TRACER)	Time (hrs) : 0.00	Location(°E,°N,m) : (-70.5218,41.6577,1.00)

Figure 72. SCIPUFF surface concentrations of inert tracer (kg/m^3) released from Otis AFB as a continuous plume. Concentrations shown on the 1.33-km domain in Case 1 are valid at 2100 UTC, 2 July 2000 (+45 h). Maximum concentration is shown at the upper right of the panel. (The number of hours that SCIPUFF has been running is shown in parentheses at the top of the figure.)

4.3.2.2

Case 2 SCIPUFF Results

As demonstrated by the analyses discussed in Section 4.1.2, Case 2 began with the passage of a cold front through southeastern MA around 0900 UTC, 5 July 2000 (see Figures 14-16). The effect of this frontal passage can be easily seen in the SCIPUFF simulations of the Brayton Point plume at 0600 UTC (+6 h) and 1200 UTC (+12 h), 5 July (Figures 73 and 74, respectively), based on the MM5 winds and temperatures. Figure 73 shows that, in the pre-frontal environment, the plume is being advected toward the east-northeast, with maximum surface concentrations during the stable nocturnal period of ~2 X 10^{-9} kg/m^3. As was shown in the SCIPUFF results from Case 1 (Section 4.3.1.1), the nocturnal maximum from a power plant tends to be several tens of kilometers downwind of the source because the elevated plume from a tall stack is initially prevented from reaching the surface due to the stable thermal structure. The same conditions apply for the Brayton Point plume at this time. By 1200 UTC, 5 July, the cold front has passed through southeastern MA and is about 75 km southeast Nantucket Island. The frontal passage has brought northwesterly winds to southern New England, so the Brayton Point plume is now directed toward the south-southeast. Note that the broad area of low tracer concentrations south of Cape Cod (over Martha's Vineyard and Nantucket Islands) is due to the north-northwesterly post-frontal winds acting on the old plume shown in Figure 73. In addition to the distinct change in the advection, Figure 74 shows that the maximum surface concentration at 1200 UTC has increased by an order of magnitude to ~2 X 10^{-8} kg/m^3, and the position of the maximum is now close to Brayton Point. The cause for these changes in maximum concentration and position of the maximum is related to turbulence generated by the MM5's post-frontal wind shear, since solar heating is insufficient to develop a deep convectively driven boundary layer so early in the morning.

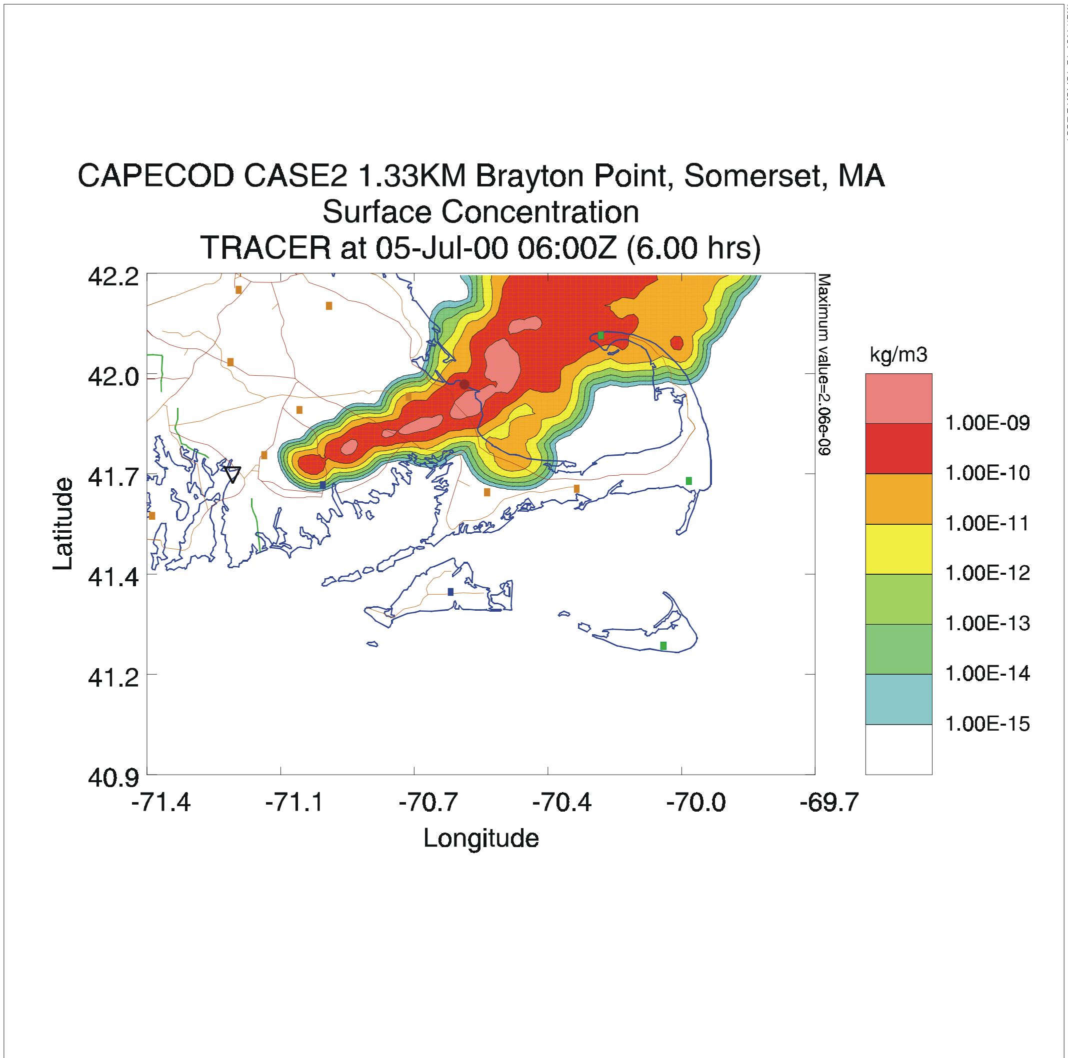

Project : brayton_point
Type : SCIPUFF

Analyst : AJ Deng
Version : 1.221PD31.P5X

Created : Mon Oct 29 10:31:21 2001

Start time : 05-Jul-00 00:00:00Z
Duration (hrs) : 16.00

Stop time : 05-Jul-00 16:00Z
Max timestep (sec) : 900.00

Current time : 05-Jul-00 16:00Z
Output interval (hrs) : 1.00

X Domain (°E) : -71.4193 - -69.6565

Y Domain (°N) : 40.9133 - 42.2354

Resolution (°) : default

Meteorology : Data=MEDOC

File : capecod_case2_d4_20000705to07.fmt

BL=Unknown
LSV=Model

Materials : TRACER (Gas)

Density (kg/m³) : 1.20

Deposition (cm/s) : 0.00

Sources : Stack (TRACER)

Time (hrs) : 0.00

Location(°E,°N,m) : (-71.1933,41.710,152.40)

Figure 73. SCIPUFF surface concentrations of inert tracer (kg/m^3) released from the Brayton Point plant at Somerset, MA, as a continuous plume. Concentrations shown on the 1.33-km domain in Case 2 are valid at 0600 UTC, 5 July 2000 (+6 h). Maximum concentration is shown at the upper right of the panel. (The number of hours that SCIPUFF has been running is shown in parentheses at the top of the figure.)

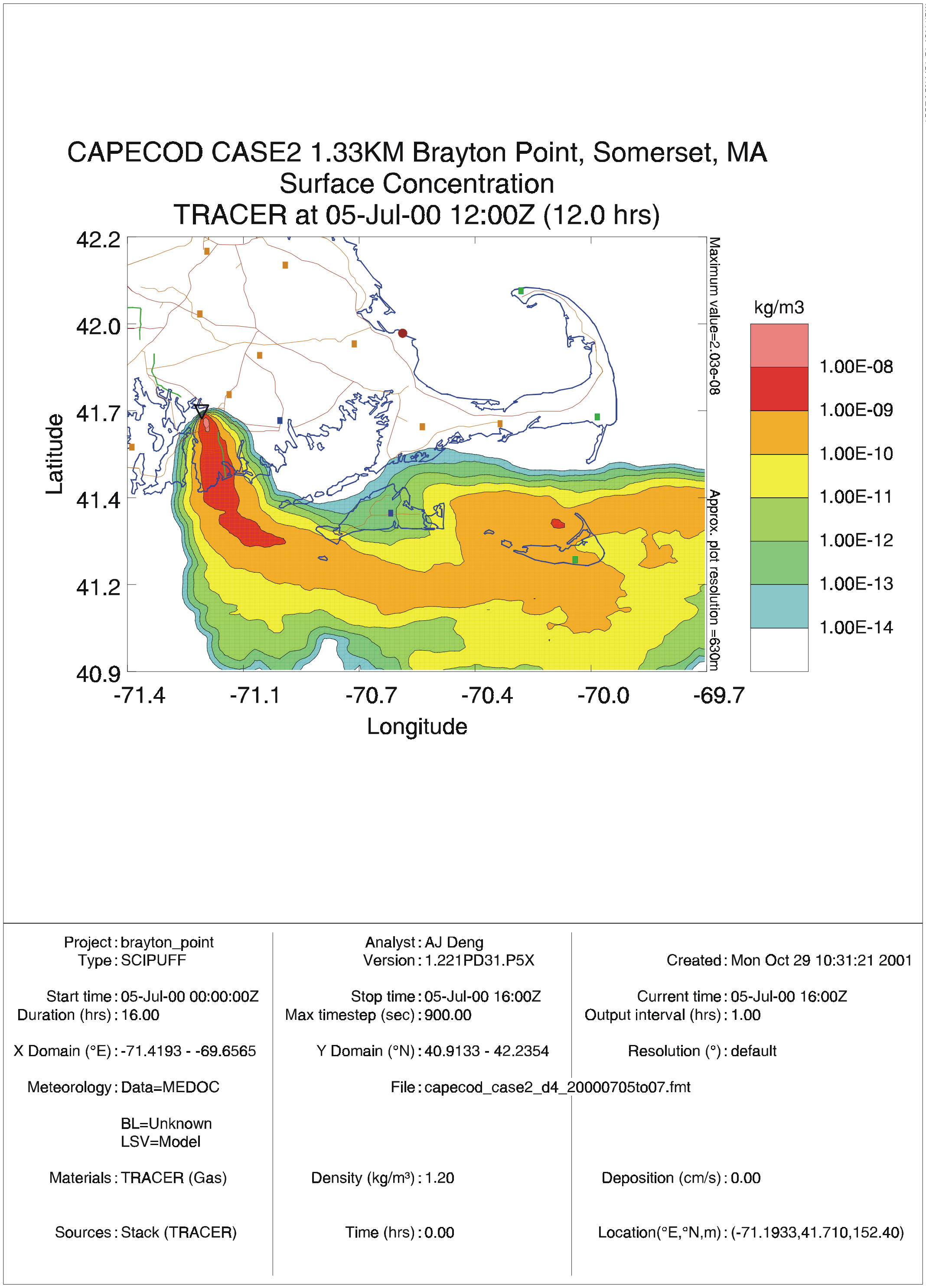

Figure 74. SCIPUFF surface concentrations of inert tracer (kg/m^3) released from the Brayton Point plant at Somerset, MA, as a continuous plume. Concentrations shown on the 1.33-km domain in Case 2 are valid at 1200 UTC, 5 July 2000 (+12 h). Maximum concentration is shown at the upper right of the panel. (The number of hours that SCIPUFF has been running is shown in parentheses at the top of the figure.)

Figure 75 indicates that, by 1800 UTC (+18 h), 5 July, the Brayton Point plume has shifted to the area around Buzzard's Bay. This change is in response to the weakening synoptic flow and the growth of the afternoon sea breeze (also see Figure 40). The intensified vertical mixing in the afternoon has caused the maximum surface concentration at 1800 UTC to decrease somewhat to ~1 X 10^{-8} kg/m^3. However, during the second night at 0600 UTC, 6 July (+30 h), Figure 76 shows that the increasing stability of the lower atmosphere again traps most of the plume above the surface until it has been advected downwind (toward the southwest on this evening) away from Brayton Point. Maximum concentrations at this time are reduced to ~2 X 10^{-9}kg/m^3 south of RI.

For Case 2, the background synoptic-scale flow weakened on the second day, so that a well-developed sea-breeze was produced in MM5, as was observed. The SCIPUFF simulation of the Brayton Point plume on the second day reflects this change. Figure 77 shows that the plume was widely dispersed over southeastern MA by the sea-breeze at 1800 UTC, 6 July (+42 h). This globular pattern, with a maximum surface concentration of ~1.3 X 10^{-8} kg/m^3 is very similar to the pattern found on the afternoon of 1 July (Figure 54). Over the next three hours, the mature sea breeze carries the heaviest concentrations north-northeastward from Brayton Point, while lower concentrations spread far to the east over Cape Cod (Figure 78). Again, this is very similar to the evolution of the plume dispersion found in Case 1 (see Figure 55).

Next, Figures 79-83 show briefly the evolution of the plume from the Canal plant as simulated by SCIPUFF for Case 2. First, Figure 79 shows the response of the plume to the passage of the cold front early in the episode. At 1200 UTC (+12 h), 5 July, the wind has recently shifted from west-southwesterly to north-northwesterly, which is reflected in the plume pattern at this time. The maximum surface concentration is very close to the Canal plant (~3.5 X 10^{-8} kg/m^3,) due to the post-frontal turbulence which has mixed the plume rapidly to the surface. By 1800 UTC (+18 h), 5 July, Figure 80 shows that the highest concentrations are located along the east-west convergence zone between two opposing branches of the sea breeze over Upper Cape Cod (compare to Figure 40), but the maximum concentration has decreased as the boundary layer has grown (~6.8 X 10^{-9} kg/m^3). The stretching (deformation) of the plume maximum in the east-west direction is similar to the known behavior near the synoptic-scale fronts that accompany baroclinic storms, but it occurs in this case on a much more localized scale.

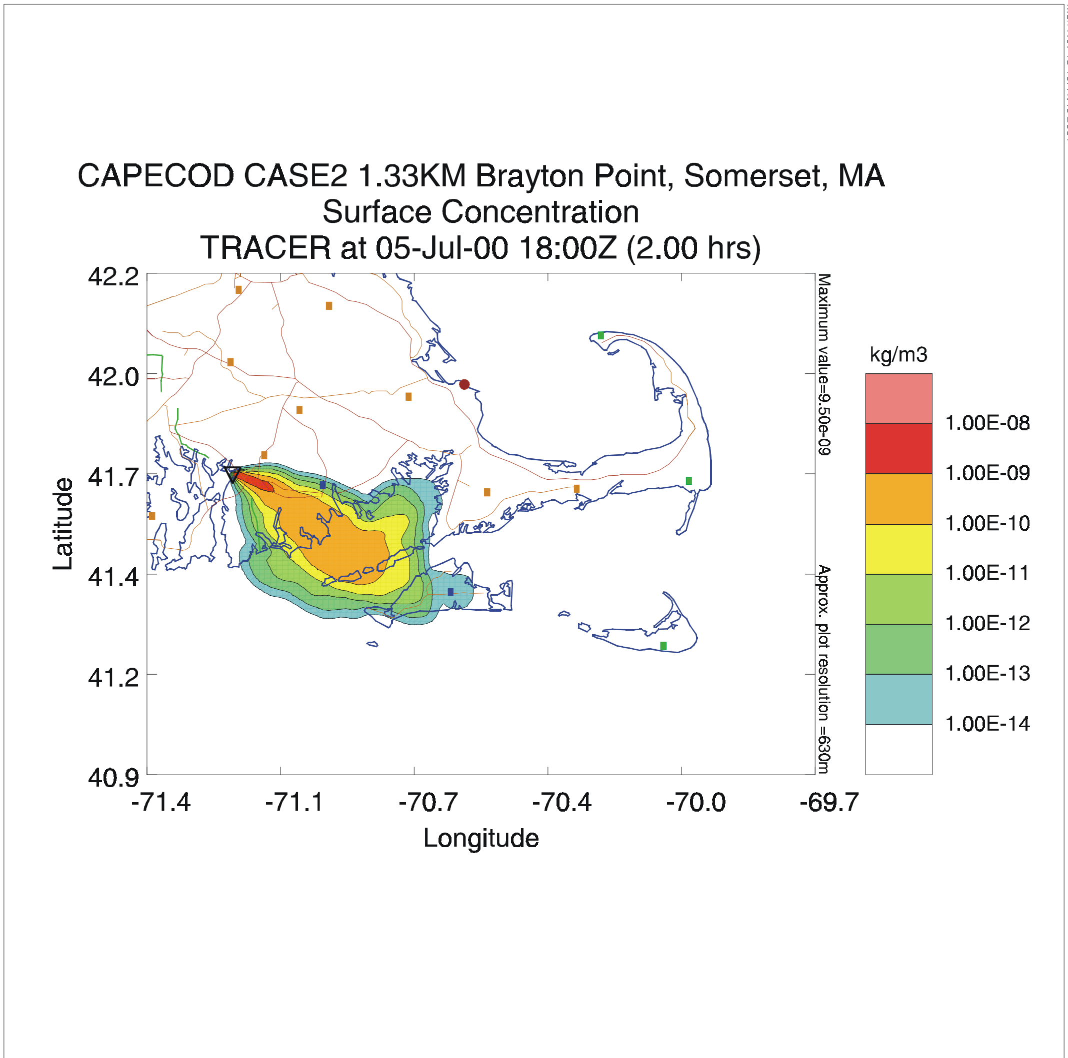

Project : brayton_point Type : SCIPUFF	Analyst : AJ Deng Version : 1.221PD31.P5X	Created : Mon Oct 29 11:56:16 2001
Start time : 05-Jul-00 16:00Z Duration (hrs) : 4.00	Stop time : 05-Jul-00 20:00Z Max timestep (sec) : 900.00	Current time : 05-Jul-00 20:00Z Output interval (hrs) : 1.00
X Domain (°E) : -71.4193 - -69.6565	Y Domain (°N) : 40.9133 - 42.2354	Resolution (°) : default
Meteorology : Data=MEDOC	File : capecod_case2_d4_20000705to07.fmt	
BL=Unknown LSV=Model		
Materials : TRACER (Gas)	Density (kg/m³) : 1.20	Deposition (cm/s) : 0.00
Sources : Stack (TRACER)	Time (hrs) : 0.00	Location(°E,°N,m) : (-71.1933,41.710,152.40)

Figure 75. SCIPUFF surface concentrations of inert tracer (kg/m^3) released from the Brayton Point plant at Somerset, MA, as a continuous plume. Concentrations shown on the 1.33-km domain in Case 2 are valid at 1800 UTC, 5 July 2000 (+18 h). Maximum concentration is shown at the upper right of the panel. (The number of hours that SCIPUFF has been running is shown in parentheses at the top of the figure.)

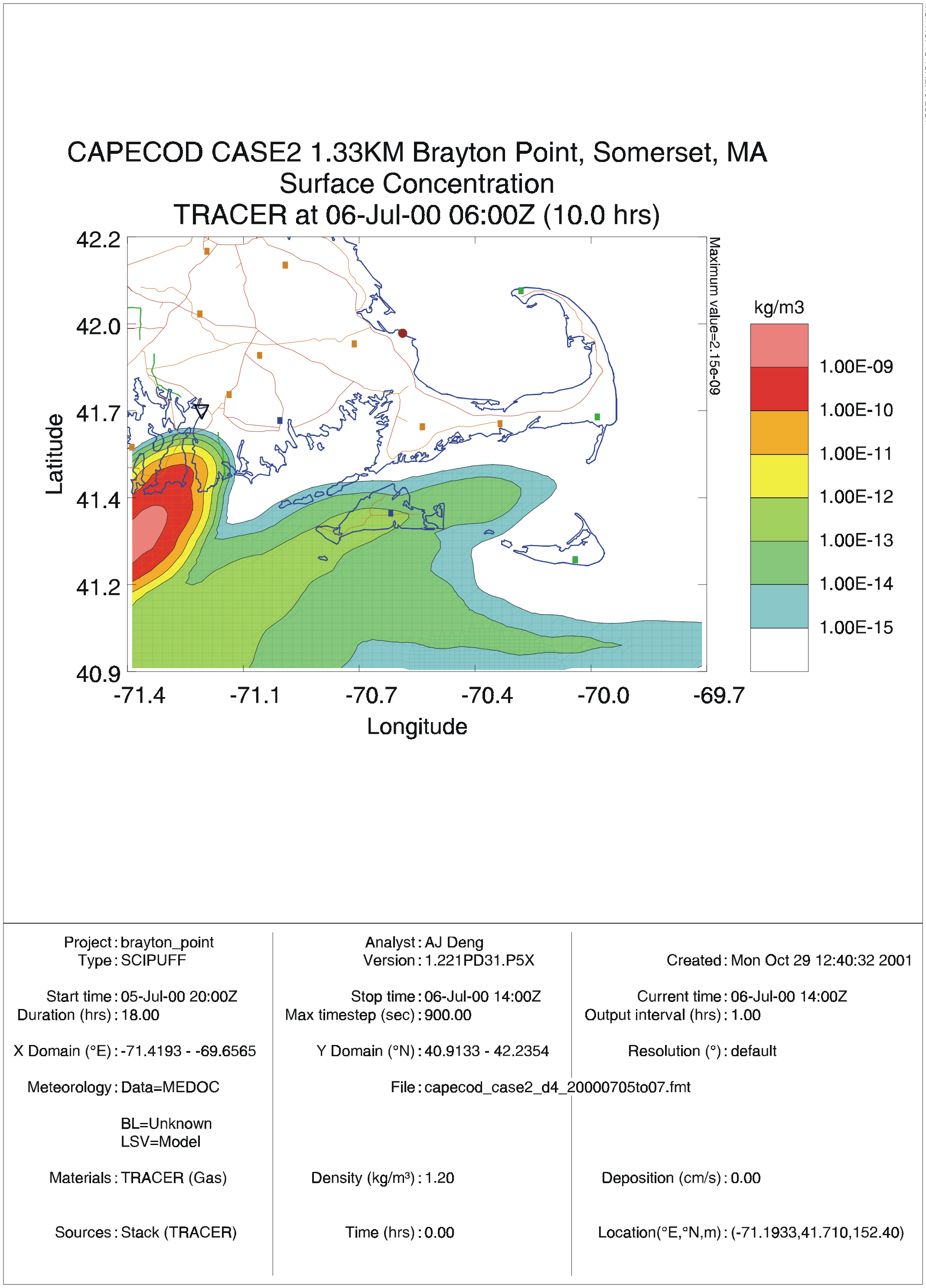

Figure 76. SCIPUFF surface concentrations of inert tracer (kg/m^3) released from the Brayton Point plant at Somerset, MA, as a continuous plume. Concentrations shown on the 1.33-km domain in Case 2 are valid at 0600 UTC, 6 July 2000 (+30 h). Maximum concentration is shown at the upper right of the panel. (The number of hours that SCIPUFF has been running is shown in parentheses at the top of the figure.)

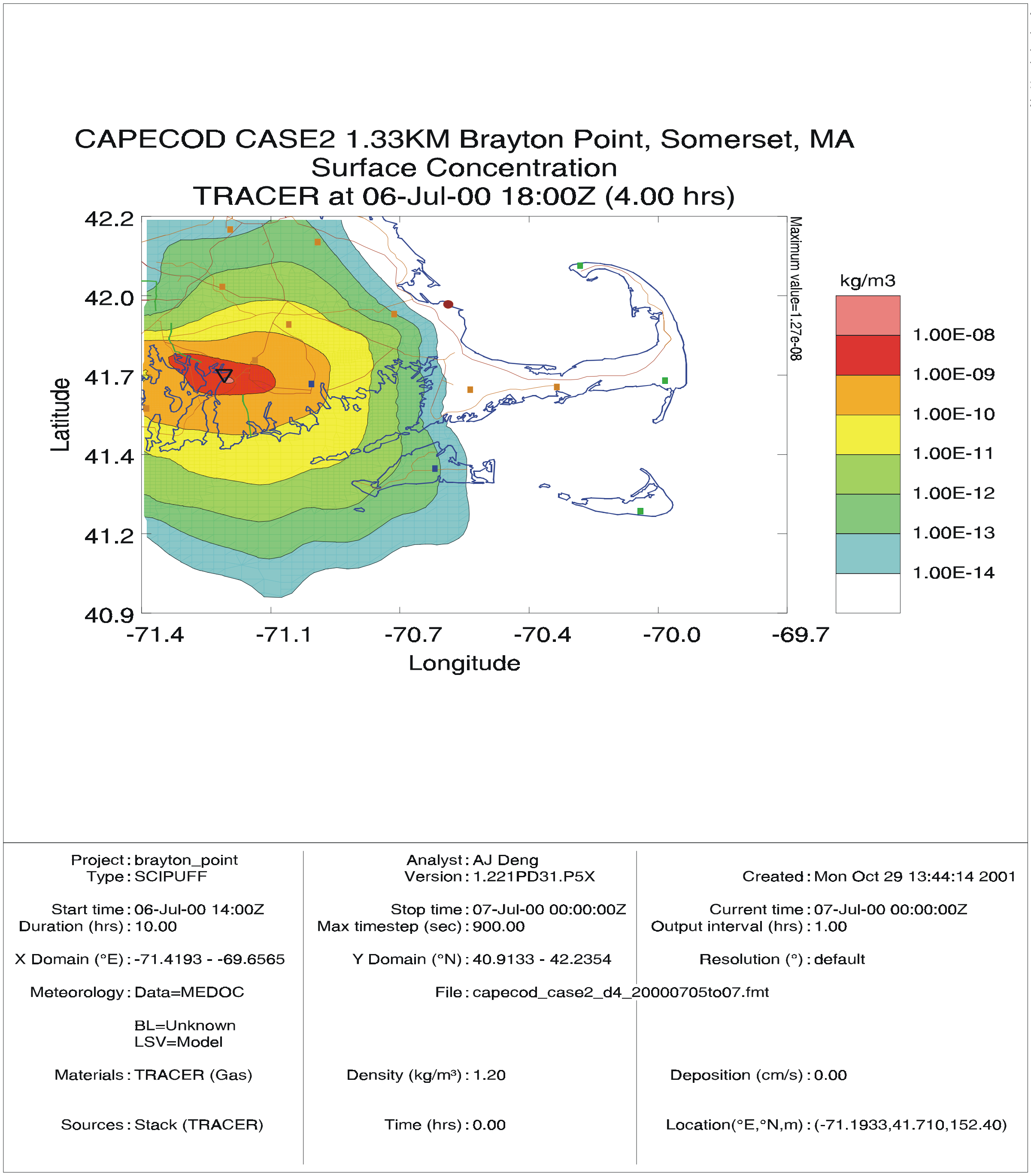

Figure 77. SCIPUFF surface concentrations of inert tracer (kg/m^3) released from the Brayton Point plant at Somerset, MA, as a continuous plume. Concentrations shown on the 1.33-km domain in Case 2 are valid at 1800 UTC, 6 July 2000 (+42 h). Maximum concentration is shown at the upper right of the panel. (The number of hours that SCIPUFF has been running is shown in parentheses at the top of the figure.)

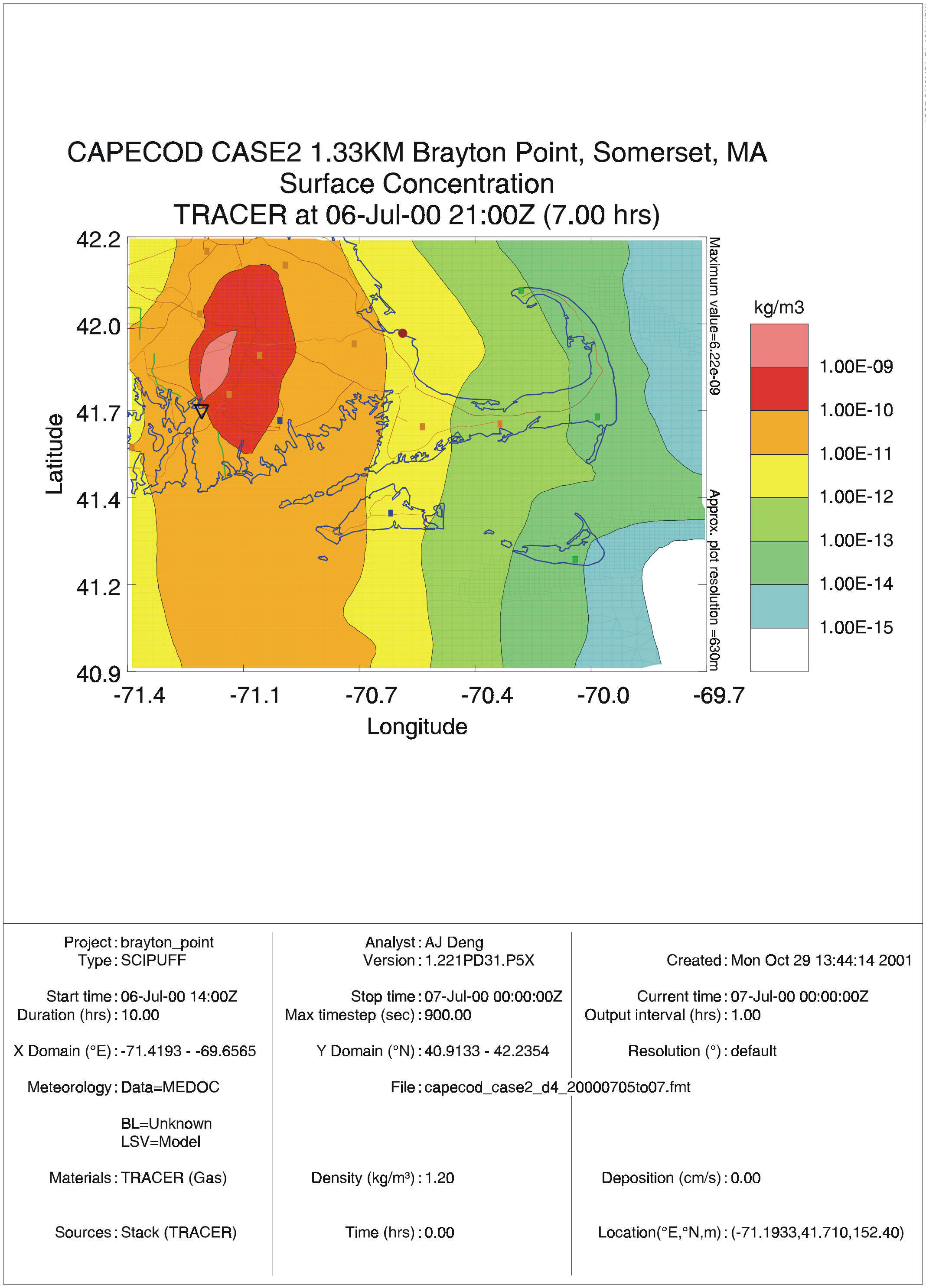

Figure 78. SCIPUFF surface concentrations of inert tracer (kg/m^3) released from the Brayton Point plant at Somerset, MA, as a continuous plume. Concentrations shown on the 1.33-km domain in Case 2 are valid at 2100 UTC, 6 July 2000 (+45 h). Maximum concentration is shown at the upper right of the panel. (The number of hours that SCIPUFF has been running is shown in parentheses at the top of the figure.)

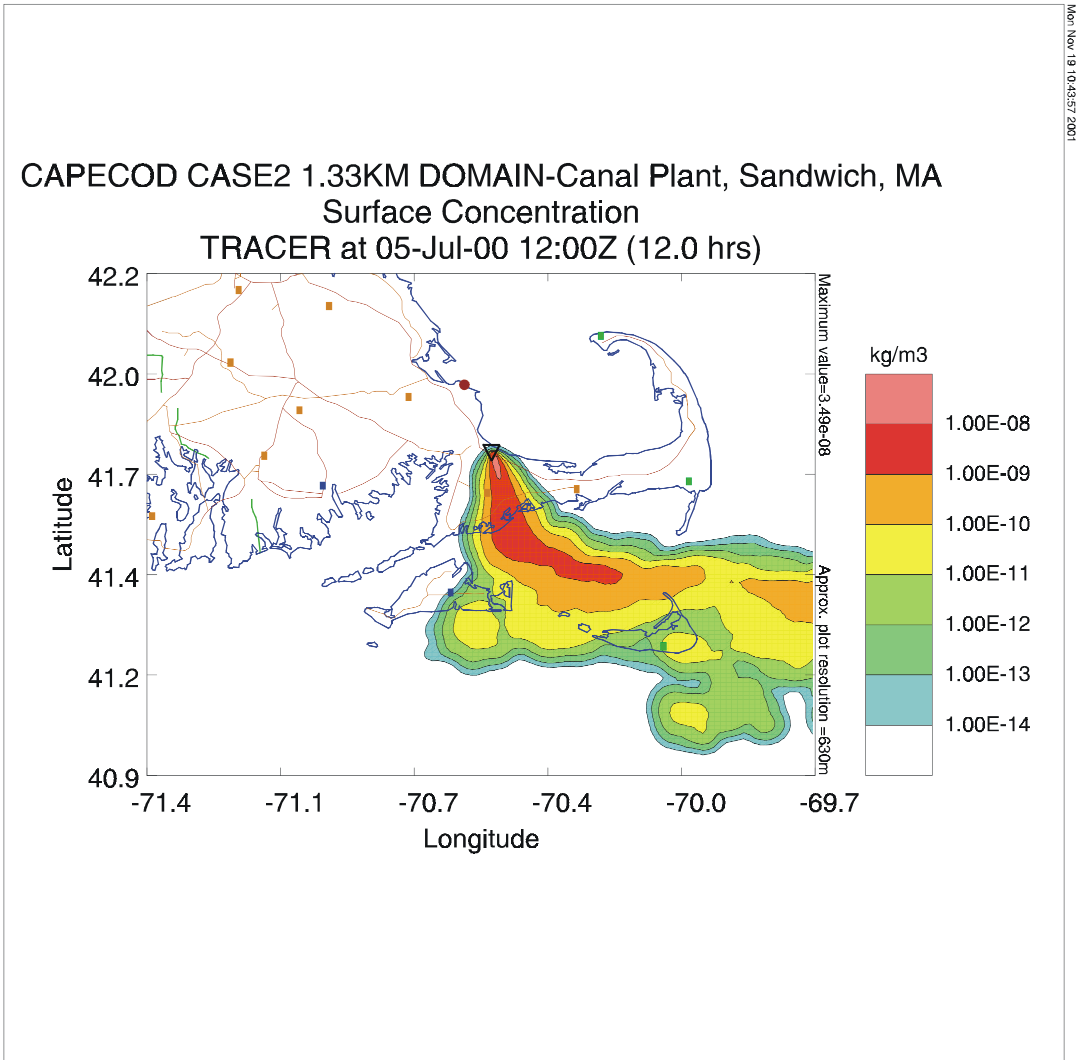

Project : canal_plant Type : SCIPUFF	Analyst : AJ Deng Version : 1.221PD31.P5X	Created : Mon Oct 29 15:09:03 2001
Start time : 05-Jul-00 00:00:00Z Duration (hrs) : 20.00	Stop time : 05-Jul-00 20:00Z Max timestep (sec) : 900.00	Current time : 05-Jul-00 20:00Z Output interval (hrs) : 1.00
X Domain (°E) : -71.4193 - -69.6565	Y Domain (°N) : 40.9133 - 42.2354	Resolution (°) : default
Meteorology : Data=MEDOC BL=Unknown LSV=Model	File : capecod_case2_d4_20000705to07.fmt	
Materials : TRACER (Gas)	Density (kg/m³) : 1.20	Deposition (cm/s) : 1.00E-03
Sources : Stack (TRACER)	Time (hrs) : 0.00	Location(°E,°N,m) : (-70.5105,41.7701,152.40)

Figure 79. SCIPUFF surface concentrations of inert tracer (kg/m^3) released from the Canal plant at Sandwich, MA, as a continuous plume. Concentrations shown on the 1.33-km domain in Case 2 are valid at 1200 UTC, 5 July 2000 (+12 h). Maximum concentration is shown at the upper right of the panel. (The number of hours that SCIPUFF has been running is shown in parentheses at the top of the figure.)

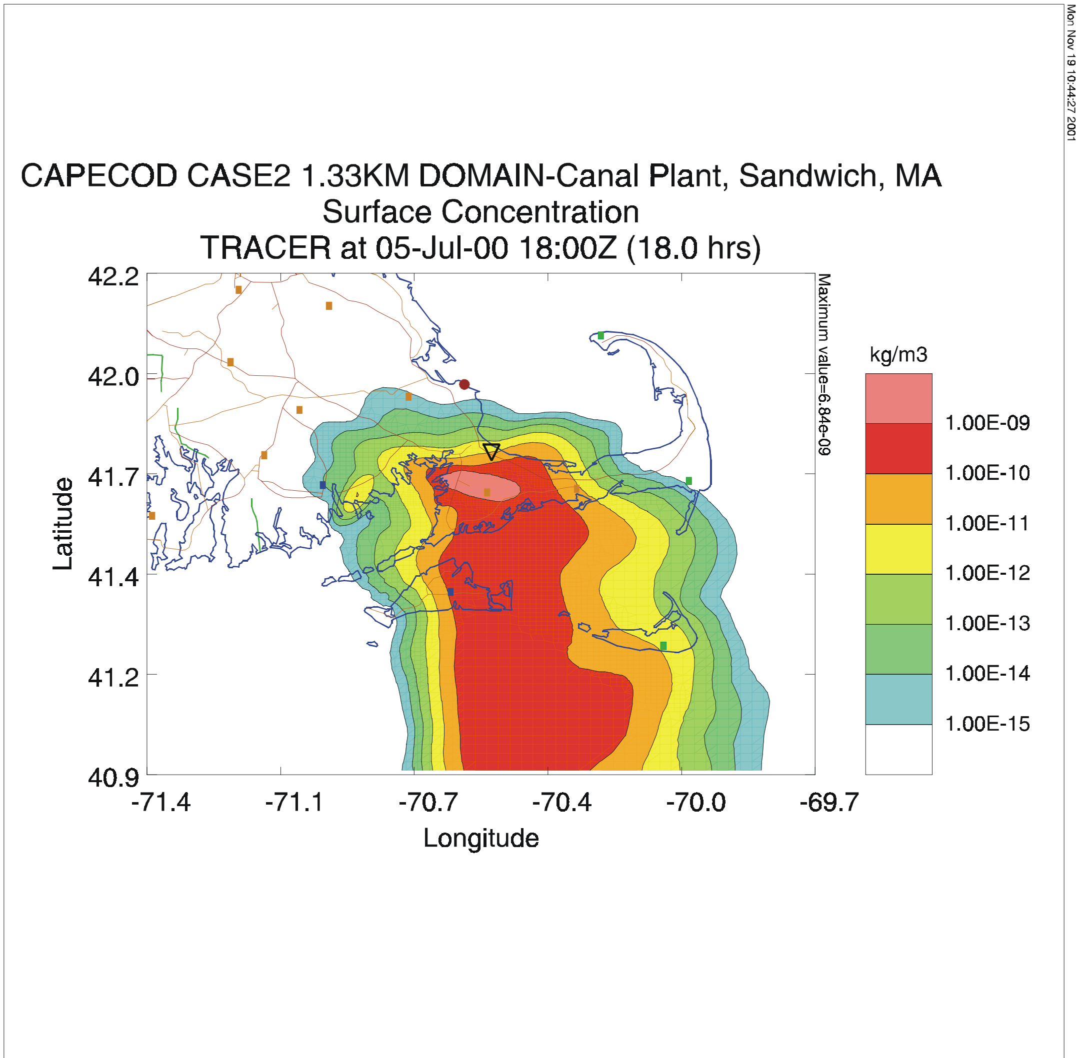

Project : canal_plant Type : SCIPUFF	Analyst : AJ Deng Version : 1.221PD31.P5X	Created : Mon Oct 29 15:09:03 2001
Start time : 05-Jul-00 00:00:00Z Duration (hrs) : 20.00	Stop time : 05-Jul-00 20:00Z Max timestep (sec) : 900.00	Current time : 05-Jul-00 20:00Z Output interval (hrs) : 1.00
X Domain (°E) : -71.4193 - -69.6565	Y Domain (°N) : 40.9133 - 42.2354	Resolution (°) : default
Meteorology : Data=MEDOC BL=Unknown LSV=Model	File : capecod_case2_d4_20000705to07.fmt	
Materials : TRACER (Gas)	Density (kg/m³) : 1.20	Deposition (cm/s) : 1.00E-03
Sources : Stack (TRACER)	Time (hrs) : 0.00	Location(°E,°N,m) : (-70.5105,41.7701,152.40)

Figure 80. SCIPUFF surface concentrations of inert tracer (kg/m^3) released from the Canal plant at Sandwich, MA, as a continuous plume. Concentrations shown on the 1.33-km domain in Case 2 are valid at 1800 UTC, 5 July 2000 (+18 h). Maximum concentration is shown at the upper right of the panel. (The number of hours that SCIPUFF has been running is shown in parentheses at the top of the figure.)

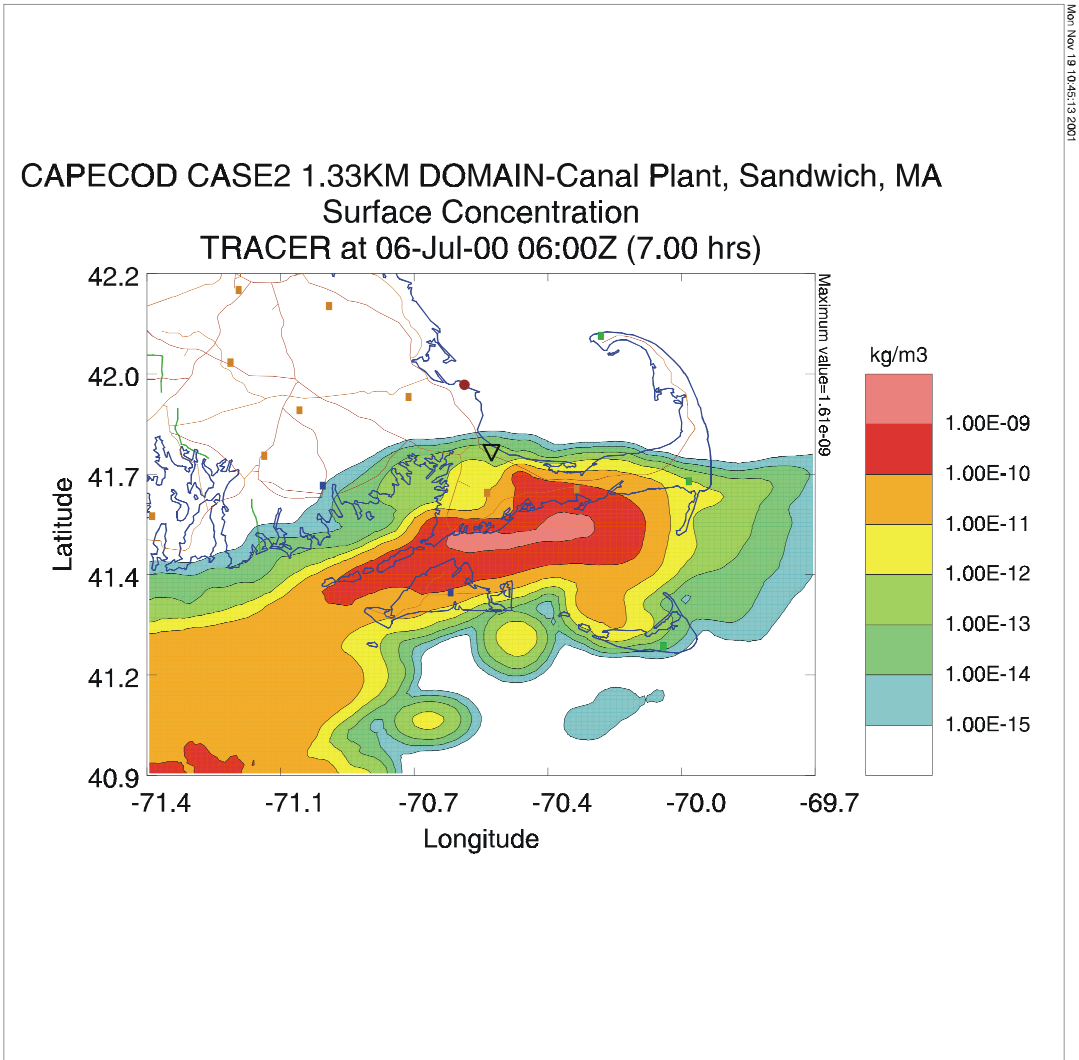

Project : canal_plant Type : SCIPUFF	Analyst : AJ Deng Version : 1.221PD31.P5X	Created : Mon Oct 29 21:23:20 2001
Start time : 05-Jul-00 23:00Z Duration (hrs) : 25.00	Stop time : 07-Jul-00 00:00:00Z Max timestep (sec) : 900.00	Current time : 06-Jul-00 09:00Z Output interval (hrs) : 1.00
X Domain (°E) : -71.4193 - -69.6565	Y Domain (°N) : 40.9133 - 42.2354	Resolution (°) : default
Meteorology : Data=MEDOC BL=Unknown LSV=Model	File : capecod_case2_d4_20000705to07.fmt	
Materials : TRACER (Gas)	Density (kg/m³) : 1.20	Deposition (cm/s) : 1.00E-03
Sources : Stack (TRACER)	Time (hrs) : 0.00	Location(°E,°N,m) : (-70.5105,41.7701,152.40)

Figure 81. SCIPUFF surface concentrations of inert tracer (kg/m^3) released from the Canal plant at Sandwich, MA, as a continuous plume. Concentrations shown on the 1.33-km domain in Case 2 are valid at 0600 UTC, 6 July 2000 (+30 h). Maximum concentration is shown at the upper right of the panel. (The number of hours that SCIPUFF has been running is shown in parentheses at the top of the figure.)

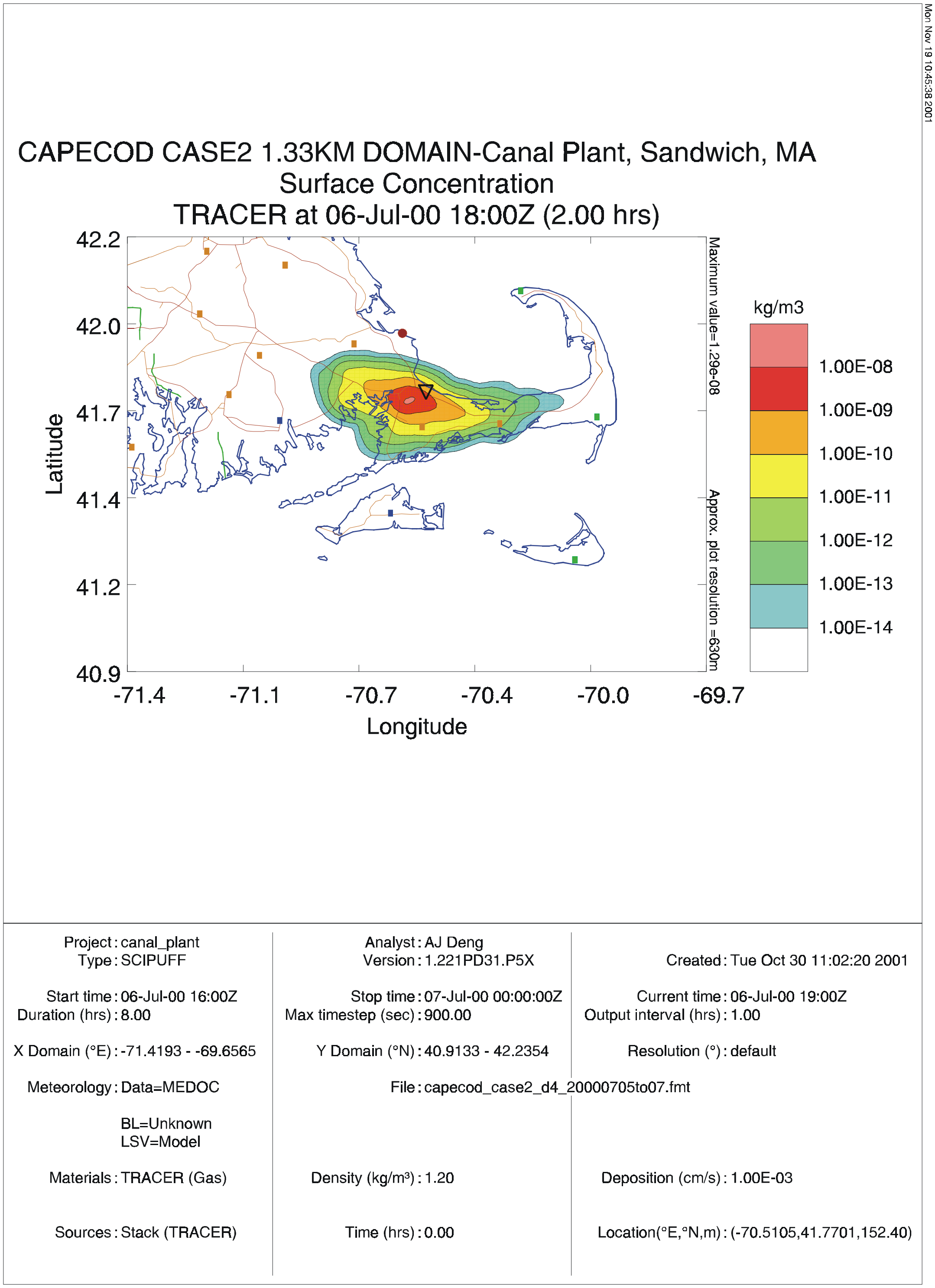

Figure 82. SCIPUFF surface concentrations of inert tracer (kg/m^3) released from the Canal plant at Sandwich, MA, as a continuous plume. Concentrations shown on the 1.33-km domain in Case 2 are valid at 1800 UTC, 6 July 2000 (+42 h). Maximum concentration is shown at the upper right of the panel. (The number of hours that SCIPUFF has been running is shown in parentheses at the top of the figure.)

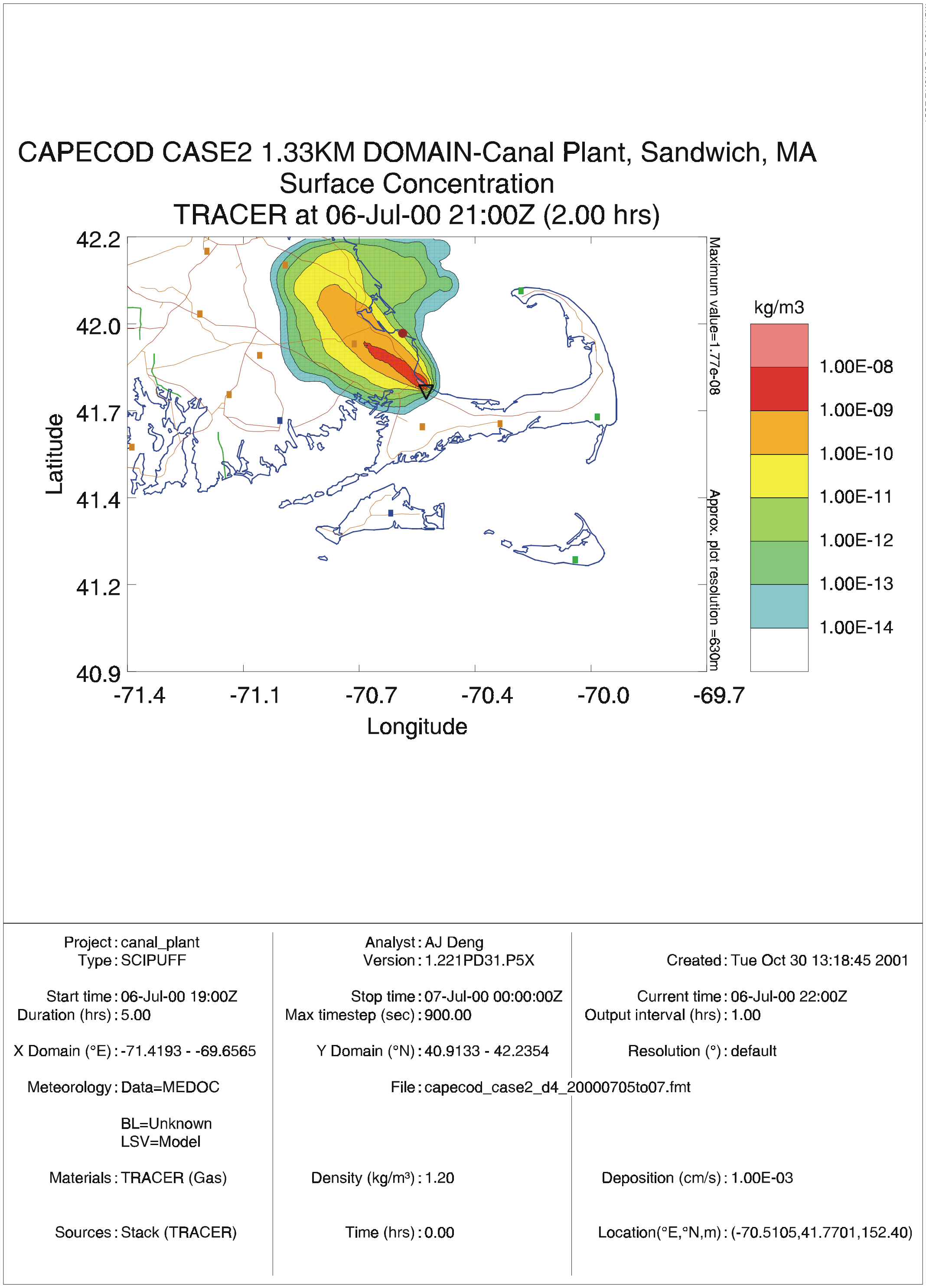

Figure 83 SCIPUFF surface concentrations of inert tracer (kg/m^3) released from the Canal plant at Sandwich, MA, as a continuous plume. Concentrations shown on the 1.33-km domain in Case 2 are valid at 2100 UTC, 6 July 2000 (+45 h). Maximum concentration is shown at the upper right of the panel. (The number of hours that SCIPUFF has been running is shown in parentheses at the top of the figure.)

On the second night of Case 2, at 0600 UTC (+30 h), 6 July, Figure 81 indicates that most of the plume lies along the south shore of Upper Cape Cod, with an orientation that is mostly in the east-west direction. Concentrations are lower at this time (~1.6 X 10^{-9} kg/m^3). Also, recall that in other stable nocturnal periods in this region, most of the plume transport was driven by the synoptic-scale winds. However, in this case, note that the dominant background wind direction at this time is west-southwesterly while the highest concentrations are about 25 km south of the Canal plant. Since there are no northerly surface winds in the area, the synoptic-scale flow cannot explain the position of the plume's surface maximum on this night.

Further examination of the MM5 model results at 0000 UTC, 6 July (+24 h), suggests that pollutants were lofted in the sea-breeze convergence zone during the late afternoon and then were advected southward by the winds at 500-1200 m (e.g., see Figure 41). This mid-level return branch is roughly opposite to the low-level wind direction in the sea breeze. Once this elevated plume is over the ocean south of Cape Cod, it sinks to the surface between Upper Cape Cod and Martha's Vineyard in the return branch of the sea-breeze circulation. This sinking motion should naturally occur in a band roughly parallel to the shore, which is consistent with the orientation of the plume in shown Figure 81. Once back near the surface over the cool coastal waters, the re-circulated plume travels east-northeastward with the observed synoptic-scale surface winds as the sea breeze decays near sunset on the night of 6 July (not shown). . Thus, the simulated circulations leading to the plume pattern shown in Figure 81 are very complex, but they are consistent with the wind observations and with know behavior of the evolving and decaying sea breeze.

Finally, the behavior of the Canal plant plume on the afternoon of 6 July is shown for 1800 UTC (+42 h) and 2100 UTC (+45 h) in Figures 82 and 83, respectively. On this afternoon, the sea breeze is quite vigorous, with a strong convergence zone over Upper Cape Cod. The highest concentrations at 1800 UTC (Figure 82) are a few kilometers west of the Canal plant (~1.3 X 10^{-8} kg/m^3). As the sea breeze continues to evolve later that afternoon, Figure 83 shows that the plume heads northwestward with the sea-breeze toward southeastern MA, producing somewhat higher surface concentrations (~1.8 X 10^{-8} kg/m^3) than at 1800 UTC.

There are few surprises in the SCIPUFF results of Case 2 for the plume associated with the highway line source in Upper Cape Cod (Figures 84-87). As in Case 1, the surface concentrations are very high because the emissions occur close to the surface (2 m). The plume follows the surface winds reasonably well. At 1800 UTC on both afternoons (+18 and +42 h), Figures 85 and 87 show that most of the plume remains over Upper Cape Cod, since it is entrained into the convergence zone that forms in this case between the two branches of the sea breeze initiated along the north and south shores of the Cape.

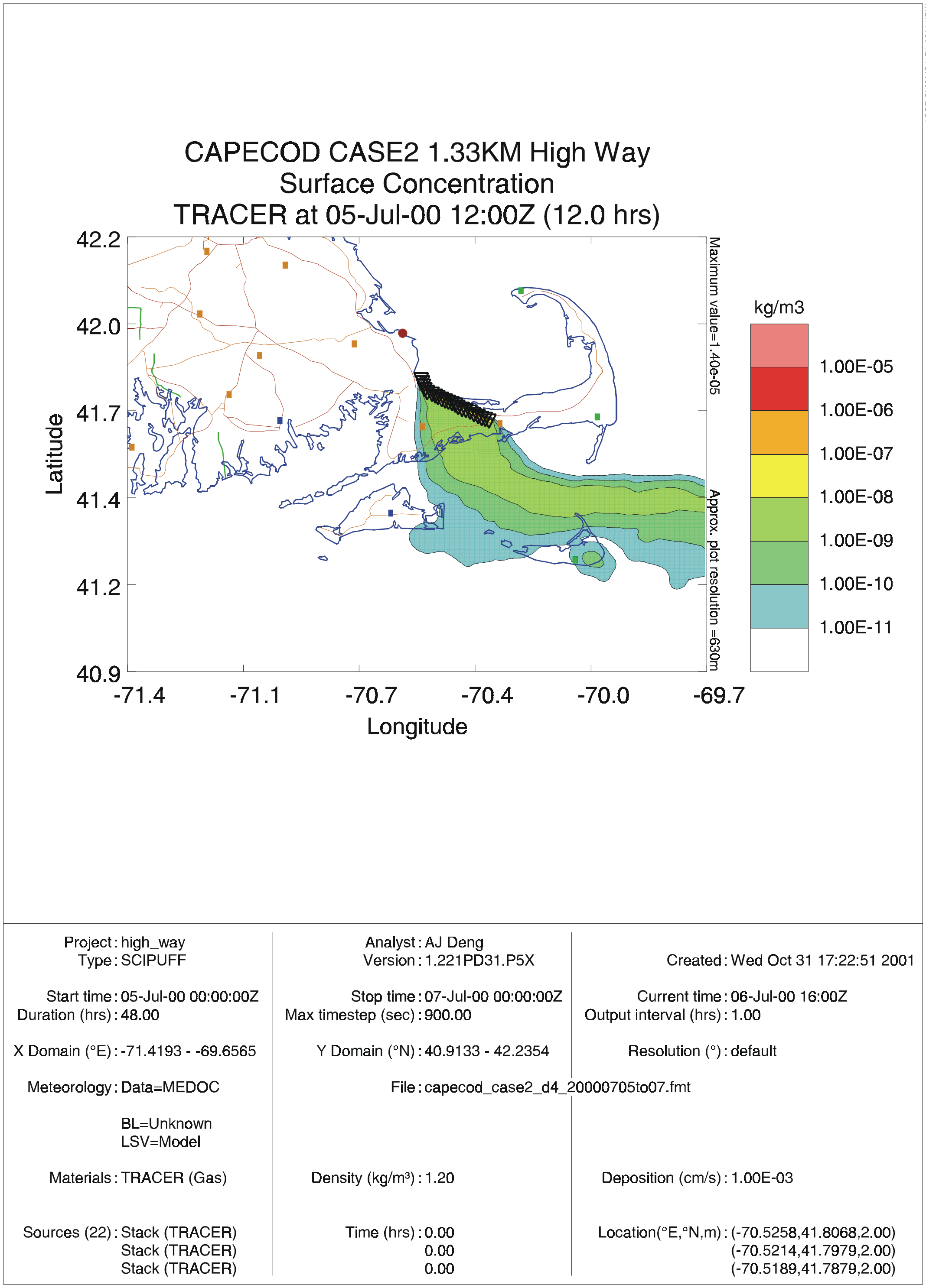

Figure 84. SCIPUFF surface concentrations of inert tracer (kg/m^3) released as a continuous plume along MA Routes 3 and 6. Concentrations shown on the 1.33-km domain in Case 2 are valid at 1200 UTC, 5 July 2000 (+12 h). Maximum concentration is shown at the upper right of the panel. (The number of hours that SCIPUFF has been running is shown in parentheses at the top of the figure.)

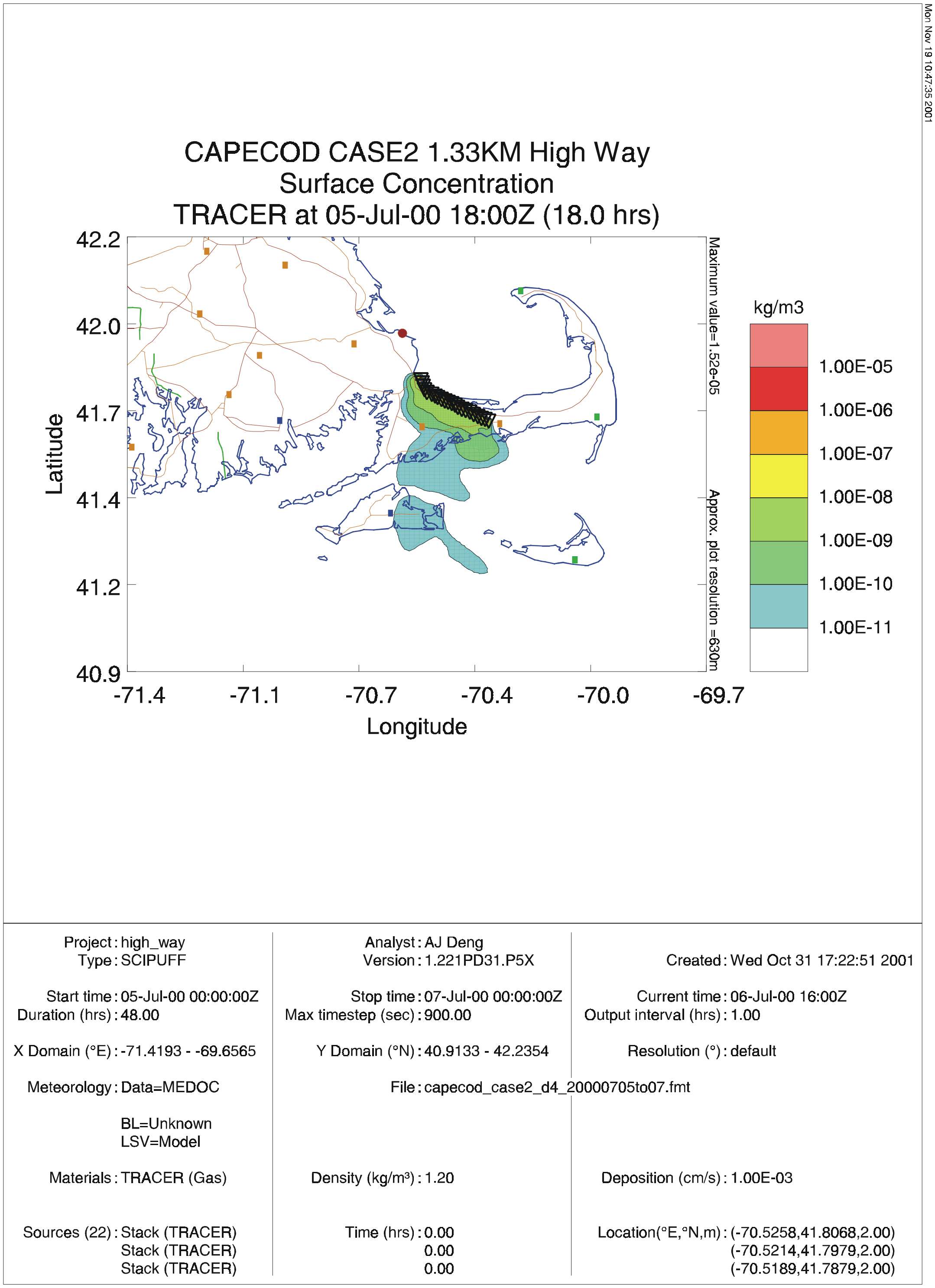

Figure 85. SCIPUFF surface concentrations of inert tracer (kg/m^3) released as a continuous plume along MA Routes 3 and 6. Concentrations shown on the 1.33-km domain in Case 2 are valid at 1800 UTC, 5 July 2000 (+18 h). Maximum concentration is shown at the upper right of the panel. (The number of hours that SCIPUFF has been running is shown in parentheses at the top of the figure.)

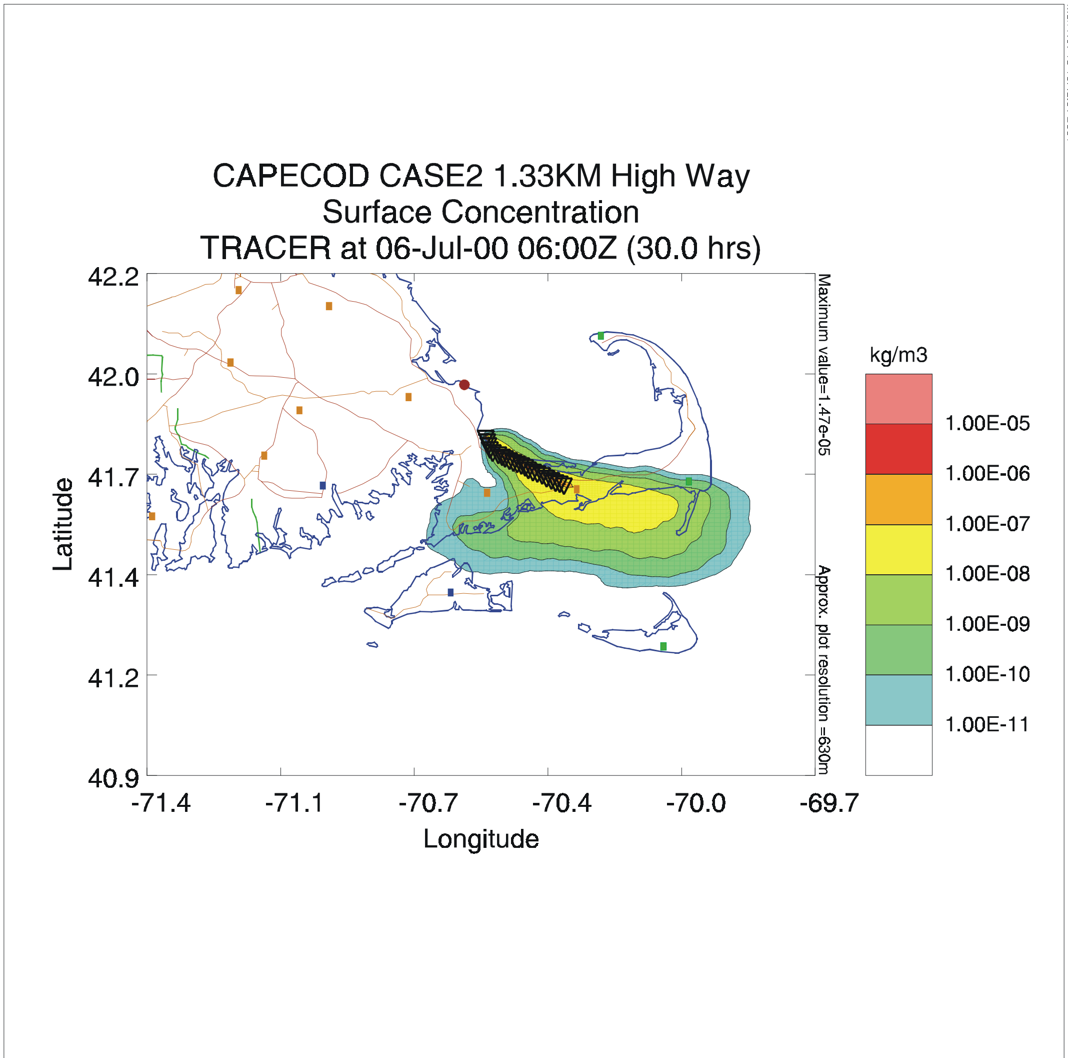

Project : high_way Type : SCIPUFF	Analyst : AJ Deng Version : 1.221PD31.P5X	Created : Wed Oct 31 17:22:51 2001
Start time : 05-Jul-00 00:00:00Z Duration (hrs) : 48.00	Stop time : 07-Jul-00 00:00:00Z Max timestep (sec) : 900.00	Current time : 06-Jul-00 16:00Z Output interval (hrs) : 1.00
X Domain (°E) : -71.4193 - -69.6565	Y Domain (°N) : 40.9133 - 42.2354	Resolution (°) : default
Meteorology : Data=MEDOC	File : capecod_case2_d4_20000705to07.fmt	
BL=Unknown LSV=Model		
Materials : TRACER (Gas)	Density (kg/m³) : 1.20	Deposition (cm/s) : 1.00E-03
Sources (22) : Stack (TRACER) Stack (TRACER) Stack (TRACER)	Time (hrs) : 0.00 0.00 0.00	Location(°E,°N,m) : (-70.5258,41.8068,2.00) (-70.5214,41.7979,2.00) (-70.5189,41.7879,2.00)

Figure 86. SCIPUFF surface concentrations of inert tracer (kg/m^3) released as a continuous plume along MA Routes 3 and 6. Concentrations shown on the 1.33-km domain in Case 2 are valid at 0600 UTC, 6 July 2000 (+30 h). Maximum concentration is shown at the upper right of the panel. (The number of hours that SCIPUFF has been running is shown in parentheses at the top of the figure.)

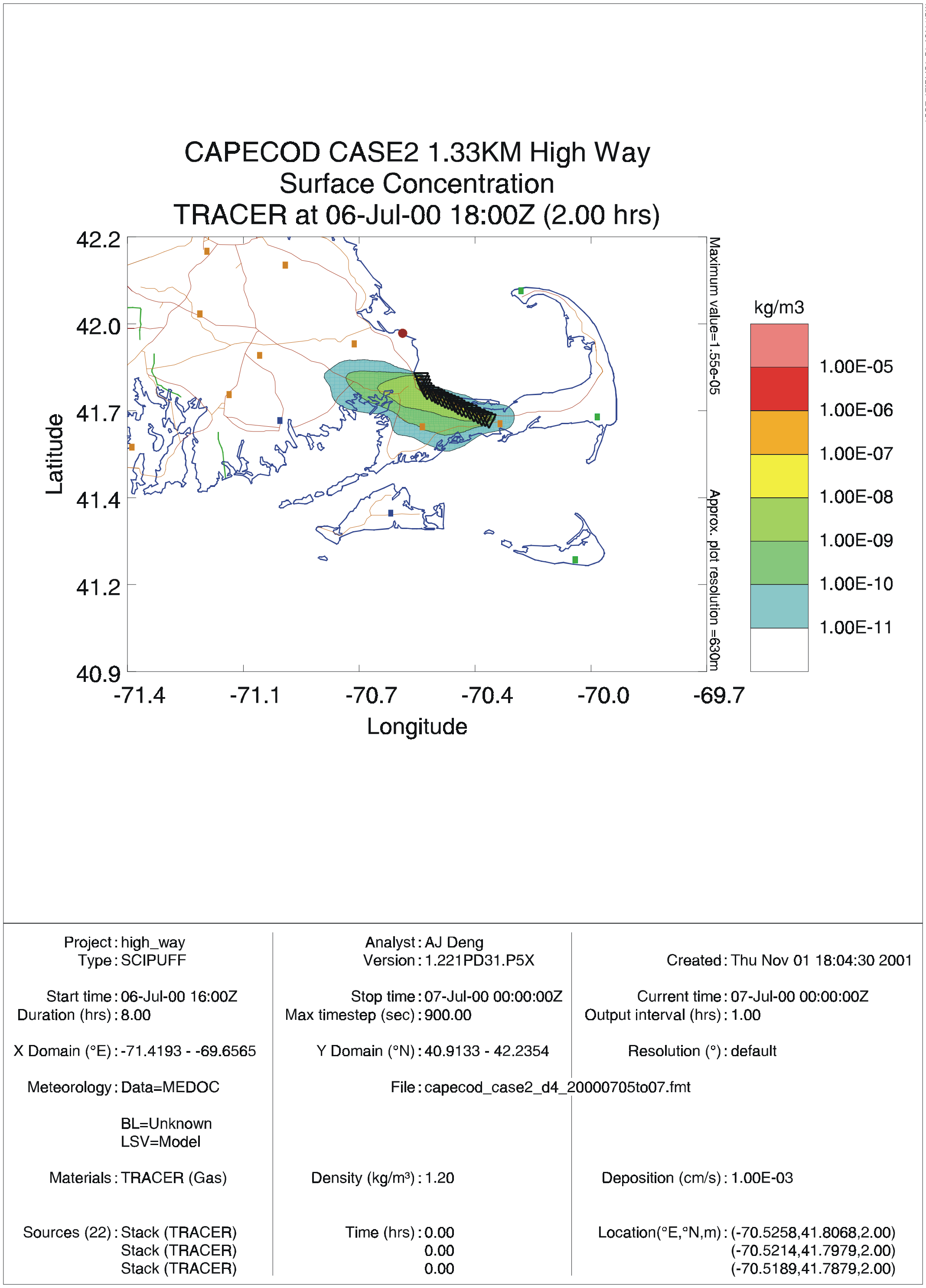

Figure 87. SCIPUFF surface concentrations of inert tracer (kg/m^3) released as a continuous plume along MA Routes 3 and 6. Concentrations shown on the 1.33-km domain in Case 2 are valid at 1800 UTC, 6 July 2000 (+42 h). Maximum concentration is shown at the upper right of the panel. (The number of hours that SCIPUFF has been running is shown in parentheses at the top of the figure.)

The fourth emission site, Otis AFB, is also a surface source over Upper Cape Cod. Figure 88 shows this plume at 0600 UTC (+6 h) on 5 July, shortly before the cold front passes over the Cape. As expected, the plume is traveling toward the east-northeast at this time. Once the front passes, at about 0900 UTC, the plume begins moving in the direction of Nantucket Island (not shown).

At 1800 UTC (+18 h), 5 July, the surface plume from Otis AFB (Figure 89) at first appears to be inconsistent with the MM5's development of the sea breeze circulation shown in Figure 40. That is, the plume in Figure 89 lies toward the south of the AFB, while Figure 40 shows the sea-breeze winds everywhere south of Upper Cape Cod are opposite in direction to the apparent motion of the plume. This apparent contradiction is explained by recalling that the actual circulations take place in three dimensions and evolve with time. Specifically, recall that the prevailing low-level wind on the previous night had become northerly (e.g. Figure 39) following the passage of a cold front through southeastern MA early in case 2. Thus, the surface plume from Otis AFB was carried southward of Nantucket Island on the morning of July 5 before the sea breeze developed. Once the sea breeze became established around noon, the southerly winds in this mesoscale circulation merely acted to gradually move the remnant surface plume back slowly toward the southern shore of UCC. Near 1800 UTC, when the sea breezes moving inland from the northern and southern shores of UCC had converged over Otis, fresh surface emissions were lofted in the vertical winds of the convergence zone. As they reached the zone near 800-1000 m, above the sea breeze, they became entrained into the northwesterly mid–level synoptic-scale flow (see Figure 41). Thus, despite the southerly sea breeze winds south of Otis, there is no mechanism at this time to carry the emissions northward, either at the surface or aloft., Later at 0600 UTC, 6 July (+30 h), once the sea breeze has decayed, Figure 90 shows that the Otis plume (still over the ocean south of Upper Cape Cod) is being advected toward the northeast by the synoptic-scale winds. Finally, Figure 91 shows that during the next afternoon at 1800 UTC (+42 h), the Otis plume reverses direction and heads northwestward, once the sea breeze has been re-established.

As shown earlier for the MM5 solutions, the SCIPUFF results for Cases 1 and 2 show many similarities. The sea breeze becomes dominant for both cases, accounting for the plume motion, especially during the daytime. Moreover, the sea breeze is responsible for complex three-dimensional transport of the plumes, especially on 6 July during Case 2. Meteorological observations alone, most of which are available only at the surface, are completely inadequate for understanding these complex wind patterns.

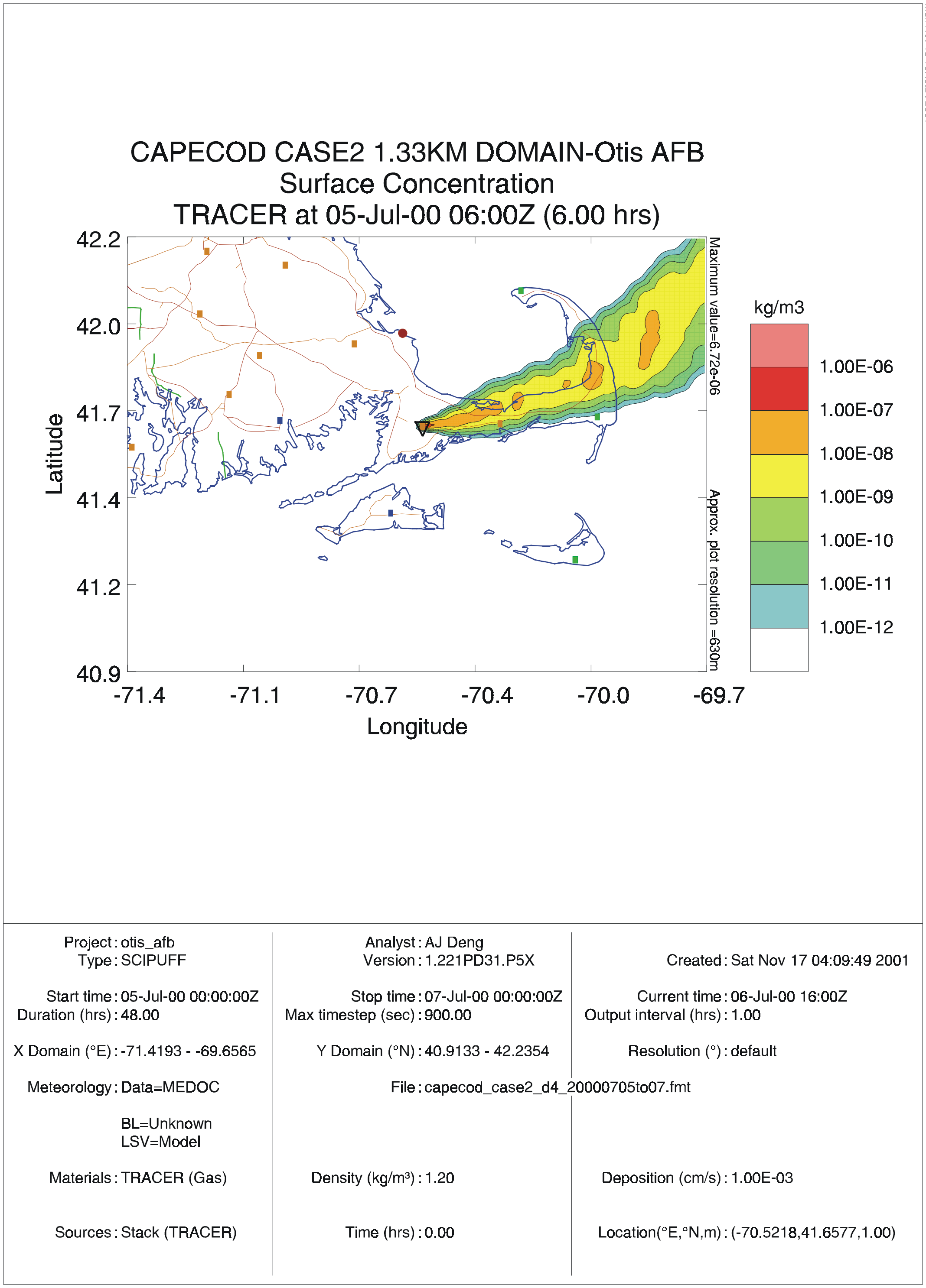

Figure 88. SCIPUFF surface concentrations of inert tracer (kg/m^3) released from Otis AFB as a continuous plume. Concentrations shown on the 1.33-km domain in Case 2 are valid at 0600 UTC, 5 July 2000 (+6 h). Maximum concentration is shown at the upper right of the panel. (The number of hours that SCIPUFF has been running is shown in parentheses at the top of the figure.)

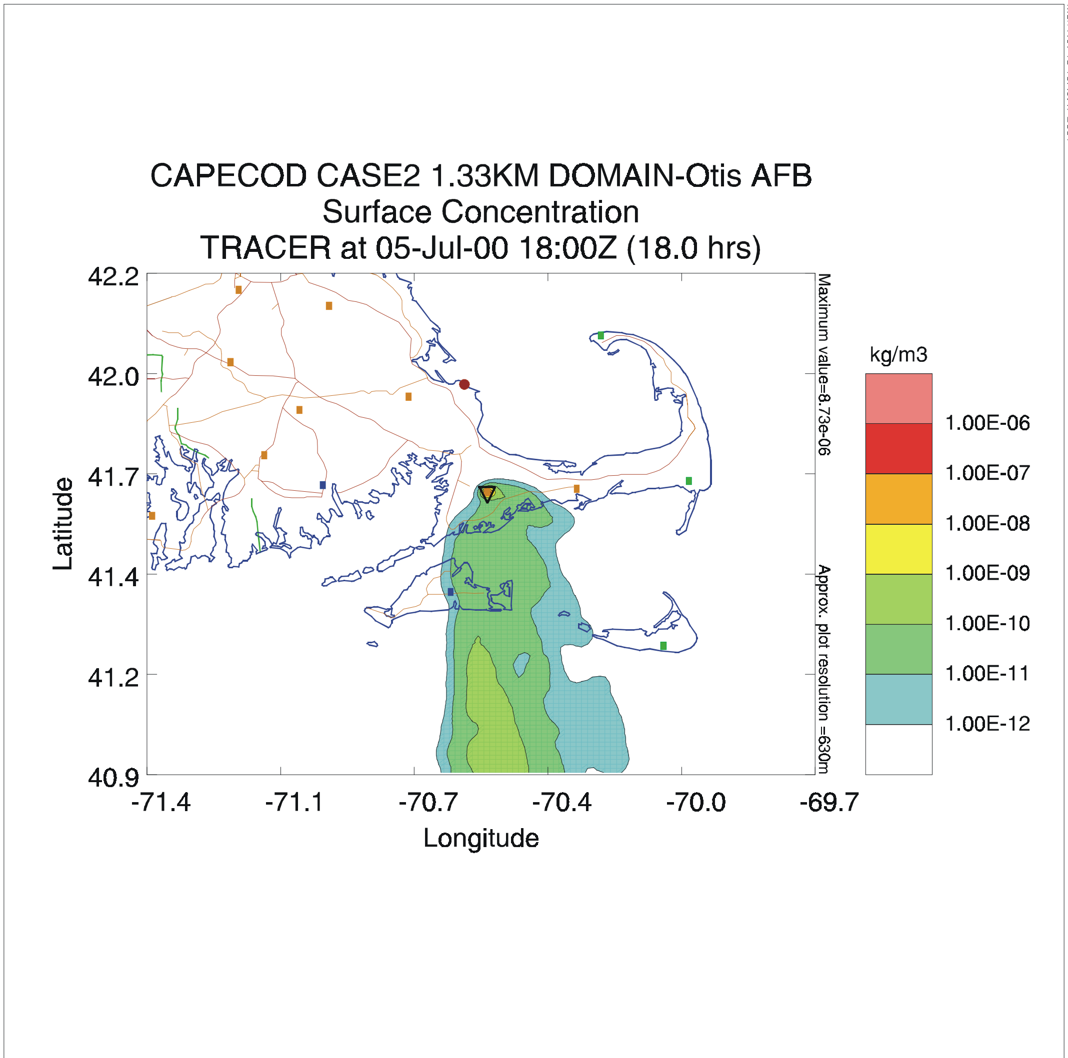

Project : otis_afb Type : SCIPUFF	Analyst : AJ Deng Version : 1.221PD31.P5X	Created : Sat Nov 17 04:09:49 2001
Start time : 05-Jul-00 00:00:00Z Duration (hrs) : 48.00	Stop time : 07-Jul-00 00:00:00Z Max timestep (sec) : 900.00	Current time : 06-Jul-00 16:00Z Output interval (hrs) : 1.00
X Domain (°E) : -71.4193 - -69.6565	Y Domain (°N) : 40.9133 - 42.2354	Resolution (°) : default
Meteorology : Data=MEDOC BL=Unknown LSV=Model	File : capecod_case2_d4_20000705to07.fmt	
Materials : TRACER (Gas)	Density (kg/m³) : 1.20	Deposition (cm/s) : 1.00E-03
Sources : Stack (TRACER)	Time (hrs) : 0.00	Location(°E,°N,m) : (-70.5218,41.6577,1.00)

Figure 89. SCIPUFF surface concentrations of inert tracer (kg/m^3) released from Otis AFB as a continuous plume. Concentrations shown on the 1.33-km domain in Case 2 are valid at 1800 UTC, 5 July 2000 (+18 h). Maximum concentration is shown at the upper right of the panel. (The number of hours that SCIPUFF has been running is shown in parentheses at the top of the figure.)

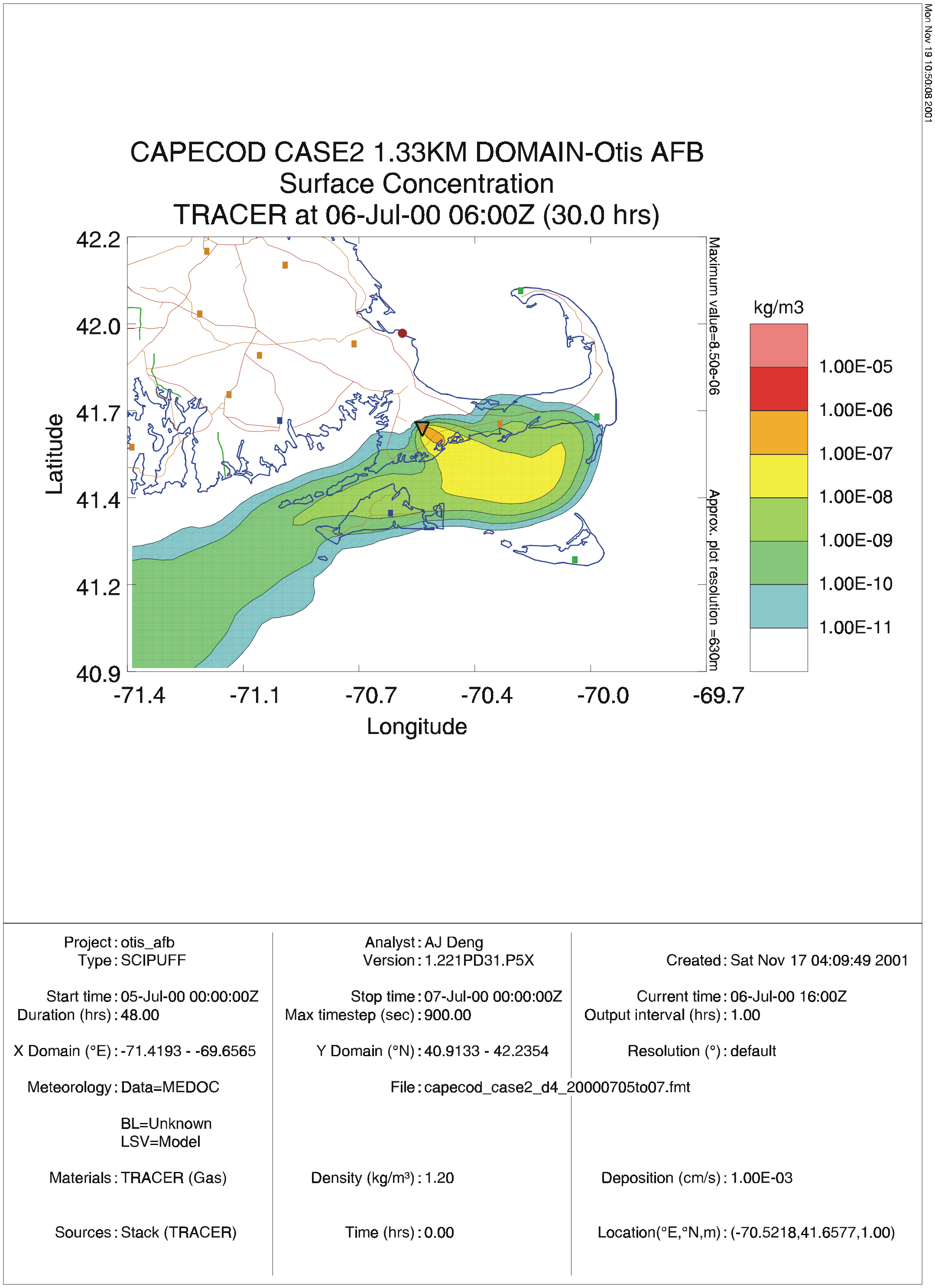

Figure 90. SCIPUFF surface concentrations of inert tracer (kg/m^3) released from Otis AFB as a continuous plume. Concentrations shown on the 1.33-km domain in Case 2 are valid at 0600 UTC, 6 July 2000 (+30 h). Maximum concentration is shown at the upper right of the panel. (The number of hours that SCIPUFF has been running is shown in parentheses at the top of the figure.)

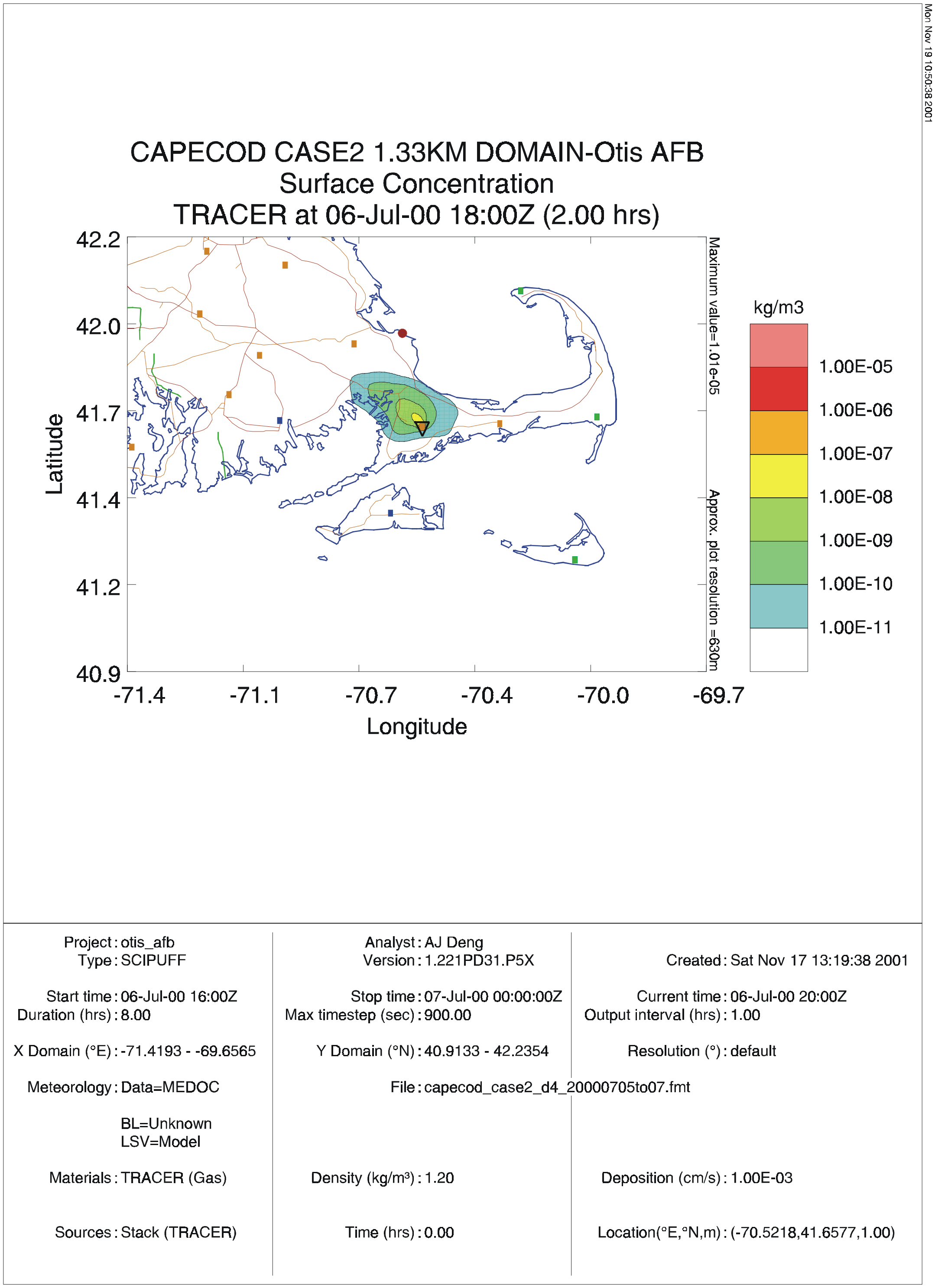

Figure 91. SCIPUFF surface concentrations of inert tracer (kg/m^3) released from Otis AFB as a continuous plume. Concentrations shown on the 1.33-km domain in Case 2 are valid at 1800 UTC, 6 July 2000 (+42h). Maximum concentration is shown at the upper right of the panel. (The number of hours that SCIPUFF has been running is shown in parentheses at the top of the figure.)

4.3.2.3 Case 3 SCIPUFF Results

In this section we present the results from SCIPUFF for Case 3, in which evidence is sought for a land breeze over southeastern MA and Upper Cape Cod. The evolution of the plume from the Brayton Point plant is summarized briefly in Figures 92-98. On the first evening, the flow is mostly from the northwest over the entire 1.33-km domain, so at 0600 UTC (+6 h), 21 August, the Brayton Point plume travels south southeastward and out to sea (Figure 92). Maximum surface concentrations are ~1.4 X 10^{-9} kg/m^3 at the southern border of the domain, about 70 km downwind of the power plant. The basic northwesterly flow continued through the night and the following morning, so that at 1800 UTC (+18 h), 21 July, Figure 93 shows a pattern similar to Figure 92, except that the maximum concentration now is close to Brayton Point and higher in value (~1.4 X 10^{-8} kg/m^3) due to more vigorous mixing in the convectively unstable afternoon boundary layer. However, the sea breeze eventually grows strong enough late in the afternoon to turn the winds over southeastern MA and Upper Cape Cod into the south and southwesterly directions (not shown). The result at 0000 UTC (+24 h), 22 August, is a reversal of the advective direction for the Brayton Point plume, as shown in Figure 94. Although the plume now covers much of southeastern MA, the maximum concentration (~2 X 10^{-9} kg/m^3) has decreased by an order of magnitude due to further vertical mixing of the plume.

By the middle of the second night, at 0600 UTC (+30 h), 22 August, the Brayton Point surface plume is shown in Figure 95 stretching east northeastward from the power plant to Massachusetts Bay and Lower Cape Cod. This presents an interesting issue for interpretation

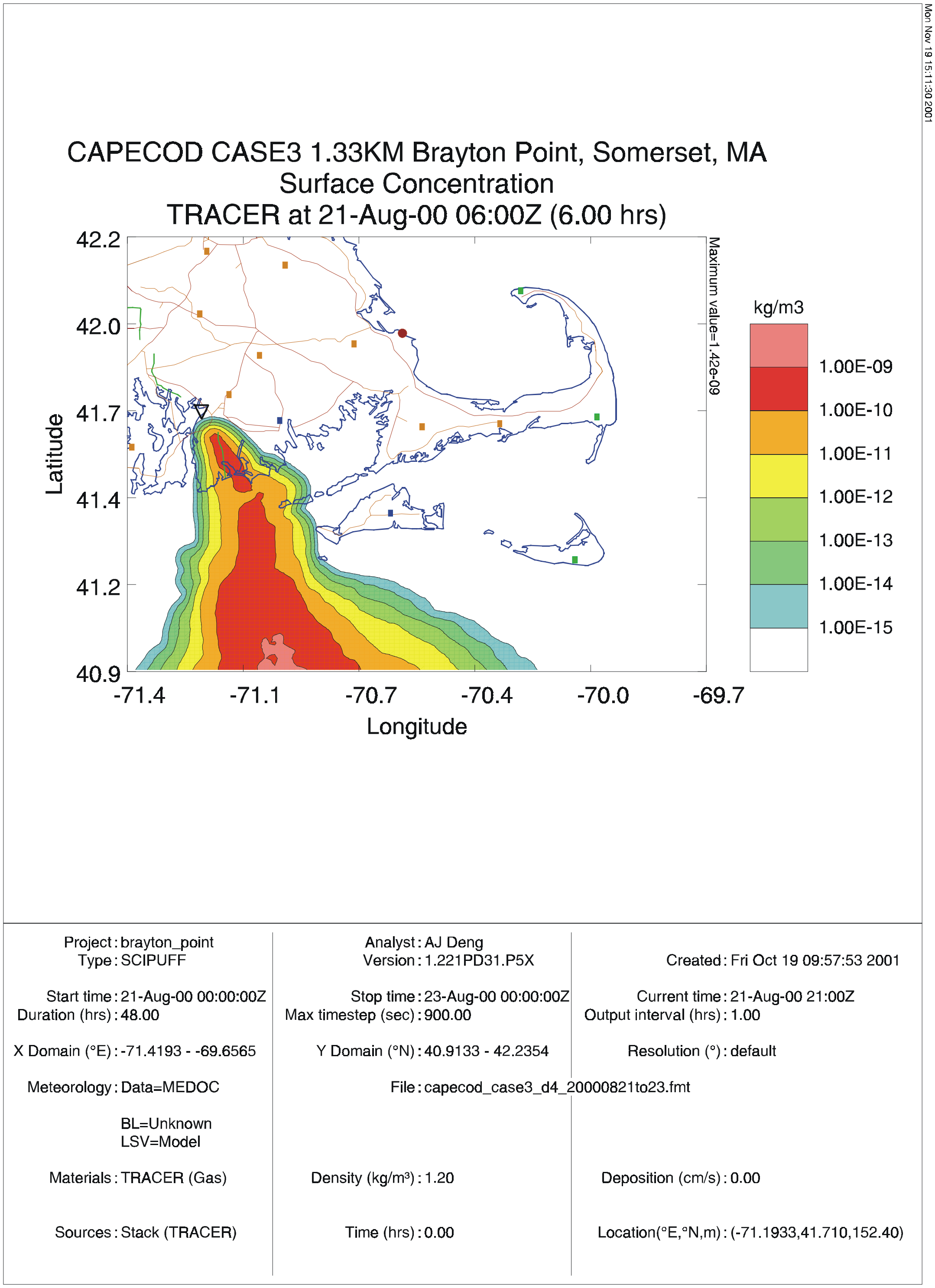

Figure 92. SCIPUFF surface concentrations of inert tracer (kg/m^3) released from the Brayton Point plant at Somerset, MA, as a continuous plume. Concentrations shown on the 1.33-km domain in Case 3 are valid at 0600 UTC, 21 August 2000 (+6 h). Maximum concentration is shown at the upper right of the panel. (The number of hours that SCIPUFF has been running is shown in parentheses at the top of the figure.)

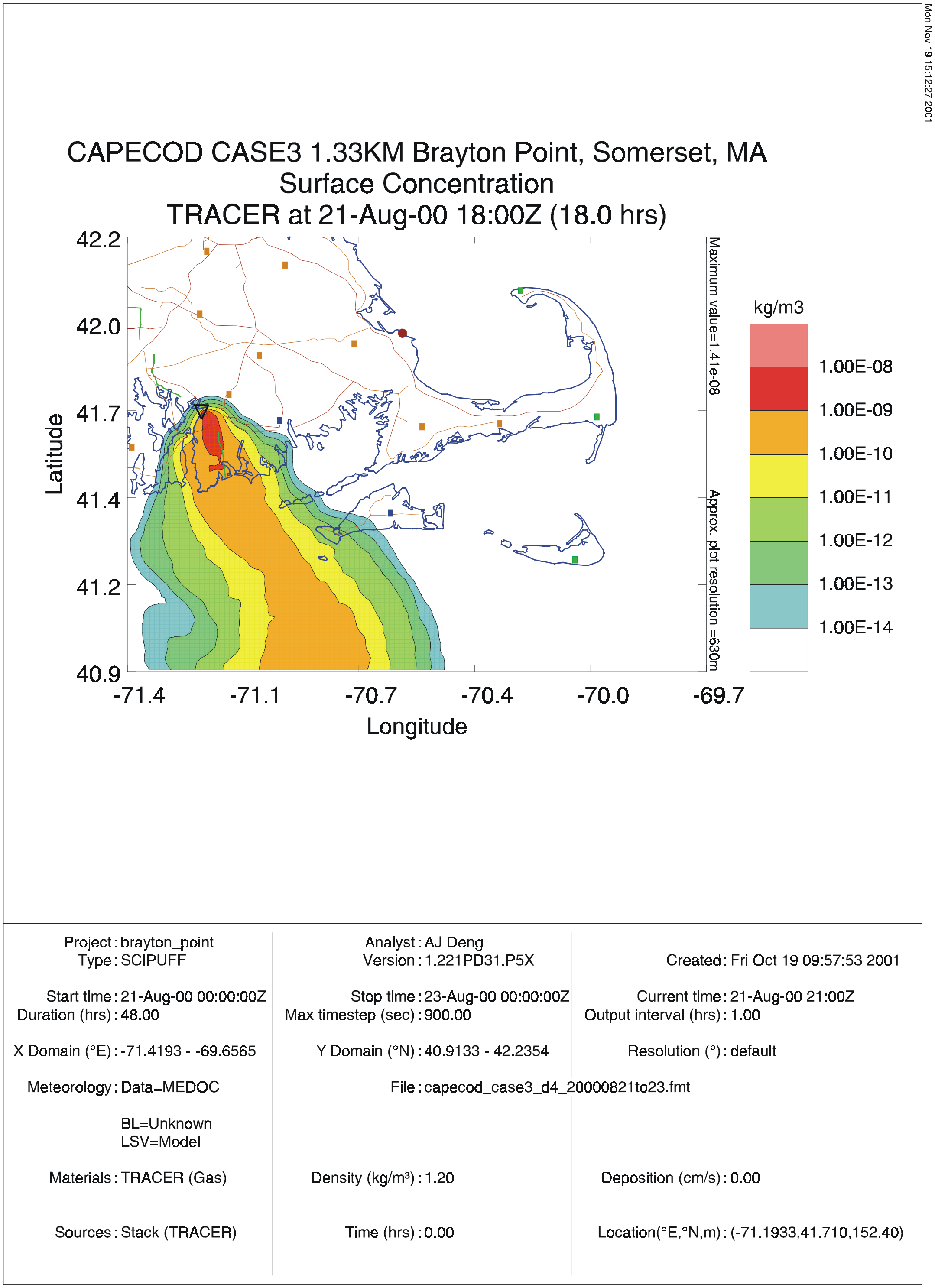

Figure 93. SCIPUFF surface concentrations of inert tracer (kg/m^3) released from the Brayton Point plant at Somerset, MA, as a continuous plume. Concentrations shown on the 1.33-km domain in Case 3 are valid at 1800 UTC, 21 August 2000 (+18 h). Maximum concentration is shown at the upper right of the panel. (The number of hours that SCIPUFF has been running is shown in parentheses at the top of the figure.)

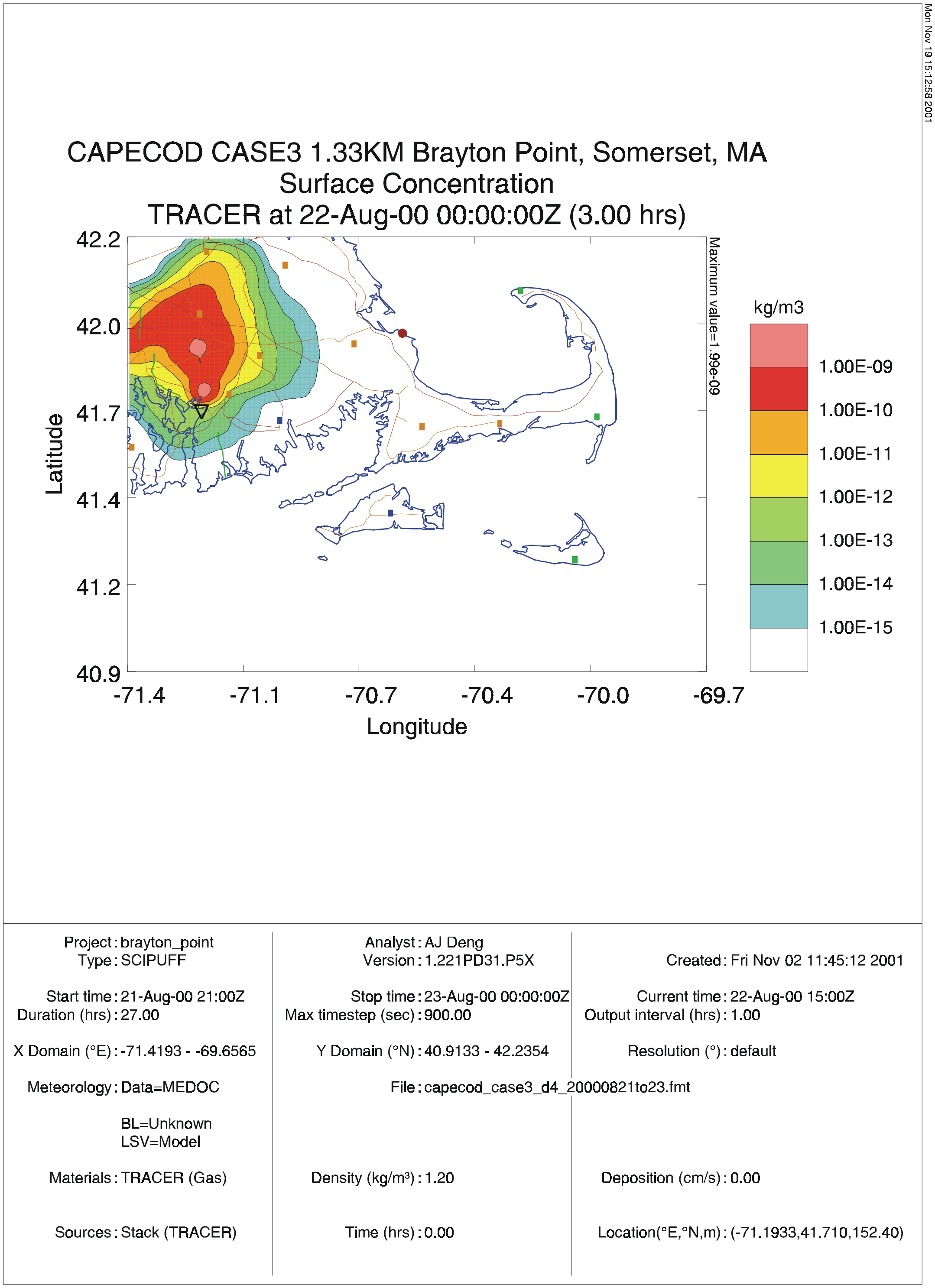

Figure 94. SCIPUFF surface concentrations of inert tracer (kg/m^3) released from the Brayton Point plant at Somerset, MA, as a continuous plume. Concentrations shown on the 1.33-km domain in Case 3 are valid at 0000 UTC, 22 August 2000 (+24 h). Maximum concentration is shown at the upper right of the panel. (The number of hours that SCIPUFF has been running is shown in parentheses at the top of the figure.)

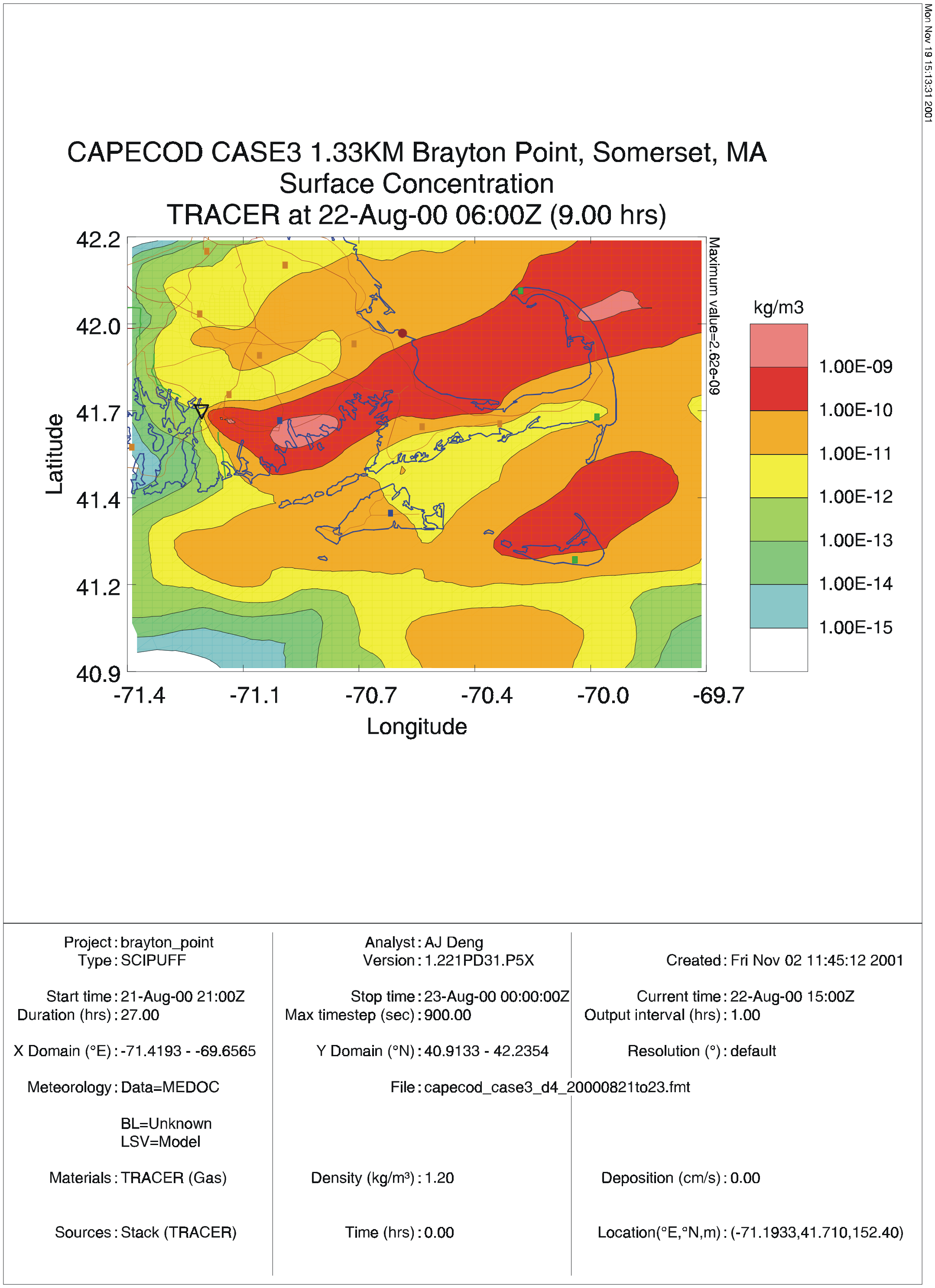

Figure 95. SCIPUFF surface concentrations of inert tracer (kg/m^3) released from the Brayton Point plant at Somerset, MA, as a continuous plume. Concentrations shown on the 1.33-km domain in Case 3 are valid at 0600 UTC, 22 August 2000 (+30 h). Maximum concentration is shown at the upper right of the panel. (The number of hours that SCIPUFF has been running is shown in parentheses at the top of the figure.)

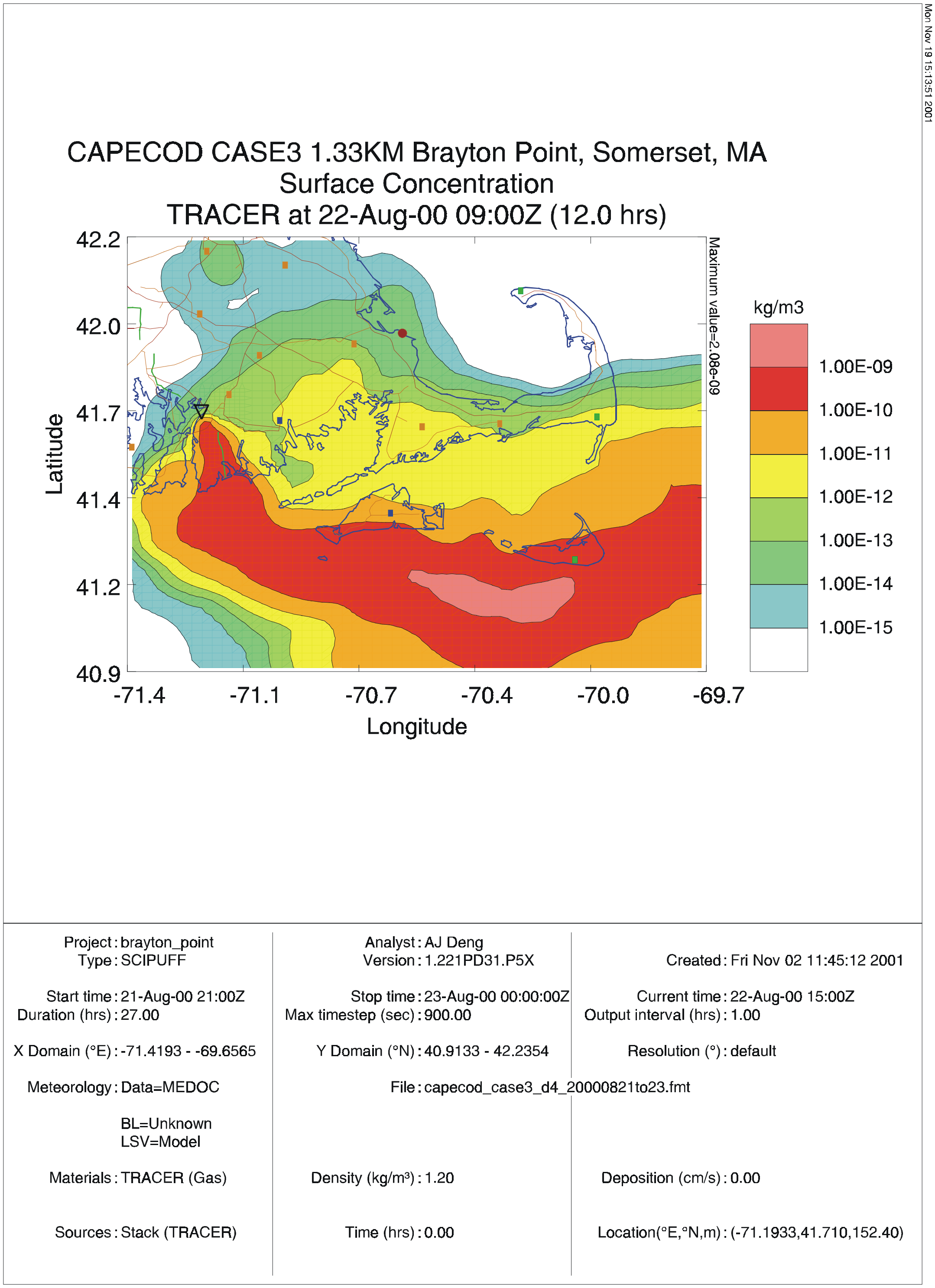

Figure 96. SCIPUFF surface concentrations of inert tracer (kg/m^3) released from the Brayton Point plant at Somerset, MA, as a continuous plume. Concentrations shown on the 1.33-km domain in Case 3 are valid at 0900 UTC, 22 August 2000 (+33 h). Maximum concentration is shown at the upper right of the panel. (The number of hours that SCIPUFF has been running is shown in parentheses at the top of the figure.)

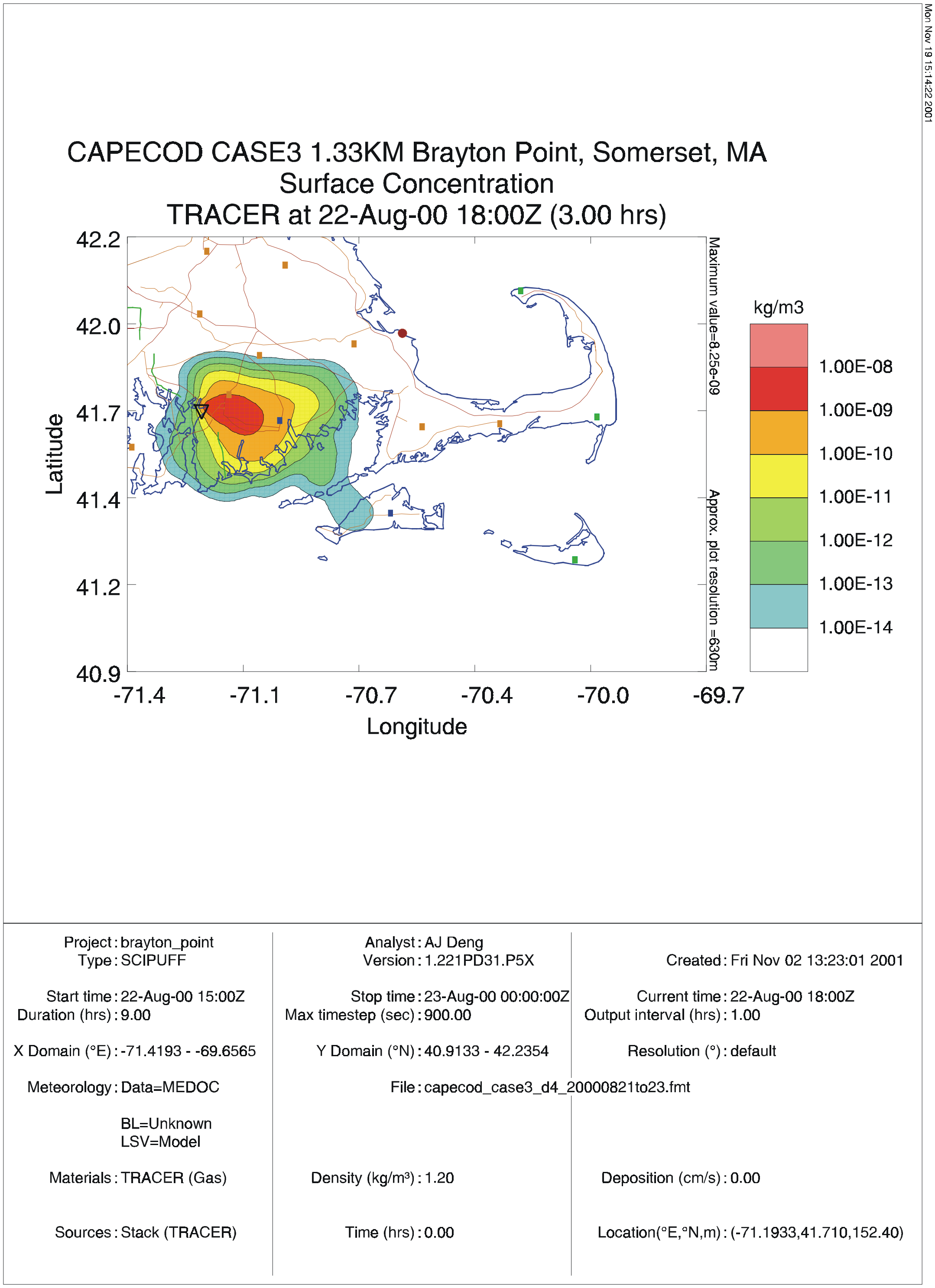

Figure 97. SCIPUFF surface concentrations of inert tracer (kg/m^3) released from the Brayton Point plant at Somerset, MA, as a continuous plume. Concentrations shown on the 1.33-km domain in Case 3 are valid at 1800 UTC, 22 August 2000 (+42 h). Maximum concentration is shown at the upper right of the panel. (The number of hours that SCIPUFF has been running is shown in parentheses at the top of the figure.)

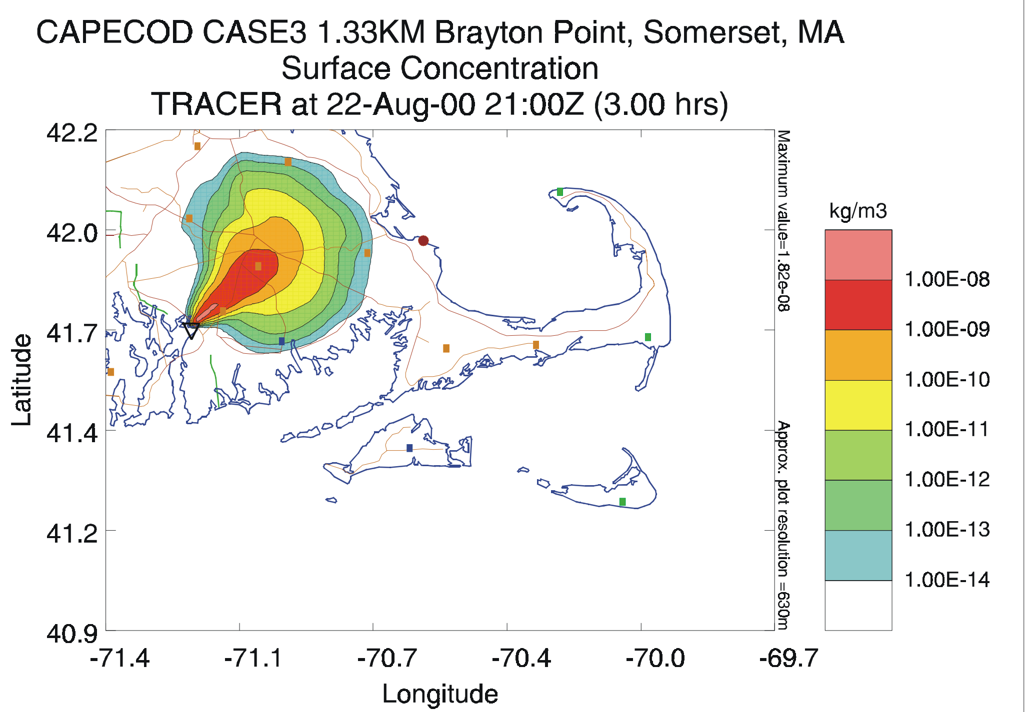

Project : brayton_point Type : SCIPUFF	Analyst : AJ Deng Version : 1.221PD31.P5X	Created : Fri Nov 02 14:49:01 2001
Start time : 22-Aug-00 18:00Z Duration (hrs) : 6.00	Stop time : 23-Aug-00 00:00:00Z Max timestep (sec) : 900.00	Current time : 23-Aug-00 00:00:00Z Output interval (hrs) : 1.00
X Domain (°E) : -71.4193 - -69.6565	Y Domain (°N) : 40.9133 - 42.2354	Resolution (°) : default
Meteorology : Data=MEDOC BL=Unknown LSV=Model	File : capecod_case3_d4_20000821to23.fmt	
Materials : TRACER (Gas)	Density (kg/m³) : 1.20	Deposition (cm/s) : 0.00
Sources : Stack (TRACER)	Time (hrs) : 0.00	Location(°E,°N,m) : (-71.1933,41.710,152.40)

Figure 98. SCIPUFF surface concentrations of inert tracer (kg/m^3) released from the Brayton Point plant at Somerset, MA, as a continuous plume. Concentrations shown on the 1.33-km domain in Case 3 are valid at 2100 UTC, 22 August 2000 (+45 h). Maximum concentration is shown at the upper right of the panel. (The number of hours that SCIPUFF has been running is shown in parentheses at the top of the figure.)

because the surface winds on the second night are mostly from the northwest by 0900 UTC (+33 h), as shown in Figure 51. The answer lies in the transition from the southerly sea-breeze circulation at 0000 UTC, 22 August (not shown), to the northwesterly nocturnal flow at 0900 UTC, 22 August. During the intervening hours the low-level flow over southeastern MA and Cape Cod has rotated clockwise, so that between 0300 UTC and 0600 UTC, west-southwesterlies dominate the area, producing the plume shown in Figure 95.

Furthermore, the maximum surface concentration in the plume at 0600 UTC is located in southeastern MA just west of Buzzard's Bay (~2.6 X 10^{-9} kg/m^3). This represents an increase in the surface concentrations during the night, compared to 0000 UTC, which is a very different behavior than was found in other stable nocturnal periods investigated in Cases 1 and 2. Since there is no evidence that the plume has been mixed downward by turbulence on 22 August, subsidence (downward motion) related to the divergence of low-level winds in the nocturnal land breeze is the only viable explanation. Even though the land breeze was partially masked by the northwesterly synoptic flow, apparently it is strong enough to bring the plume to the ground and raise the surface concentrations far above their typical nocturnal values. Later on the second night, by 0900 UTC, 22 August (+33 h), the northwesterlies were re-established over southeastern MA, so that Figure 96 shows the Brayton Point plume is being advected southeastward past Martha's Vineyard and Nantucket Islands. Maximum surface concentrations at this time are still high for the nocturnal period (~2 X 10^{-9} kg/m^3), but the maximum is south of these islands, rather than over the mainland.

On the second day of Case 3, at 1800 UTC (+42 h), 22 August, the sea breeze over southeastern MA was better developed than on the first day. Figure 97 shows the Brayton Point plume drifting slowly eastward as the sea breeze takes hold in the area. Maximum surface concentrations, which had been unusually high during the stable conditions of the previous night due to subsidence in the land breeze, now rose to ~8.3 X 10^{-9} kg/m^3 just east of Brayton Point. As the episode comes to a close, the plume at 2100 UTC (+45 h) continues to respond to the maturing sea breeze by heading northeastward into the interior of southeastern MA with a maximum surface concentration of ~1.8 X 10^{-8} kg/m^3 (Figure 98).

Shifting attention to the Canal plant, Figure 99 reveals the plume drifting southeastward on the first night at 0600 UTC (+ 6 h), 21 August. As is common during the stable nocturnal periods, the maximum surface concentration at this time is south of Nantucket Island (~2 X 10^{-9} kg/m^3) with no detectable surface plume over Cape Cod. At the end of the first afternoon, the surface plume at 0000 UTC (+24 h), 22 August, shows the effect of the sea breeze. Part of the plume has drifted southeastward from the Canal plant, while another lobe has been advected northwestward toward southeastern MA (Figure 100) in the sea breeze.

On the second night, the Canal plume responded to the rotation of the low-level winds in much the same way as found for the Brayton Point plume. Figure 101 shows the Canal plume at 0600 UTC (+30 h), when the winds are blowing primarily from the west. The plume is "skipping" up and down at this time. It hits the ground along the north shore of Upper Cape Cod and again downwind east of Lower Cape Cod. Maximum surface concentrations are very small during this period of high stability (~1 X 10^{-10} kg/m^3). Later the same night, at 0900 UTC (+33 h), the winds have rotated further and are blowing from the northwest over the Canal Plant (see Figure 51). Figure 102 shows that the Canal plume continues to skip up and down, across Upper Cape Cod and over the sea just north of Nantucket, while concentrations remain less than 1 X 10^{-9} kg/m3. Finally, on the second afternoon at 1800 UTC (+42 h), 22 August, Figure 103 indicates that the plume from the Canal plant is heading westward toward southeast MA as the

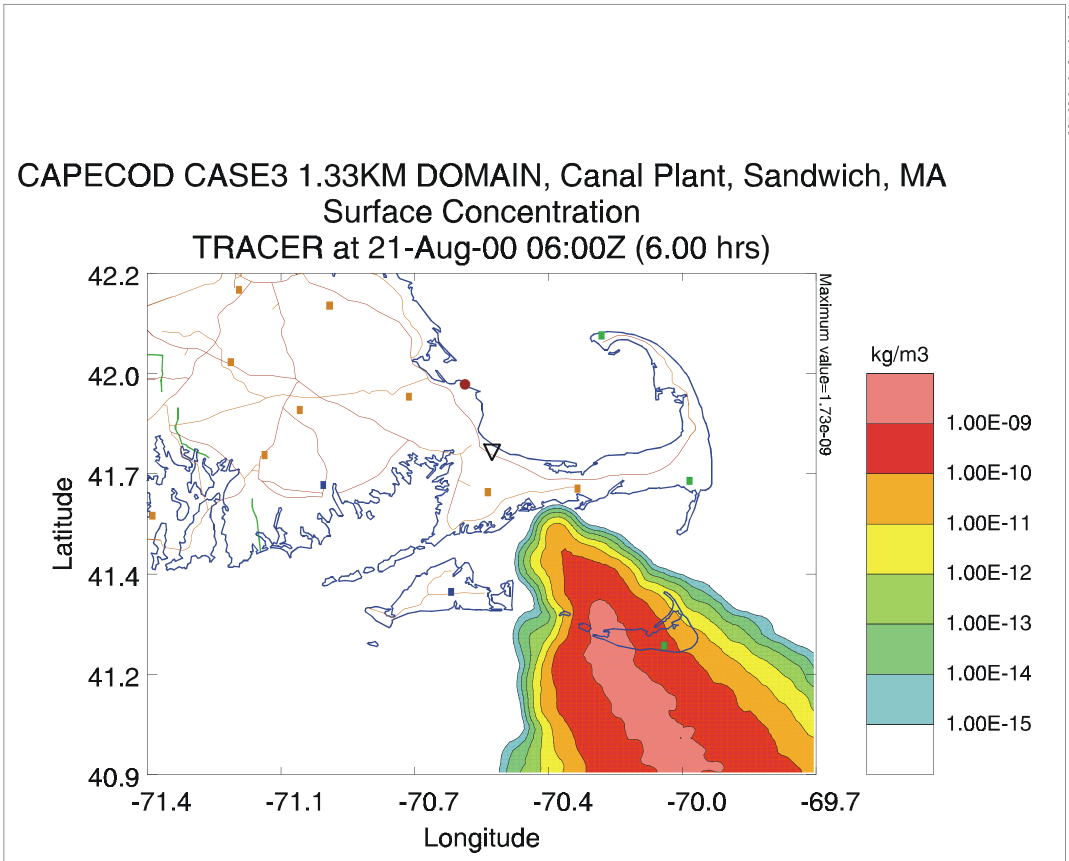

Project : canal_plant Type : SCIPUFF	Analyst : AJ Deng Version : 1.221PD31.P5X	Created : Sun Nov 04 11:18:34 2001
Start time : 21-Aug-00 00:00:00Z Duration (hrs) : 21.00	Stop time : 21-Aug-00 21:00Z Max timestep (sec) : 900.00	Current time : 21-Aug-00 21:00Z Output interval (hrs) : 1.00
X Domain (°E) : -71.4193 - -69.6565	Y Domain (°N) : 40.9133 - 42.2354	Resolution (°) : default
Meteorology : Data=MEDOC BL=Unknown LSV=Model	File : capecod_case3_d4_20000821to23.fmt	
Materials : TRACER (Gas)	Density (kg/m³) : 1.20	Deposition (cm/s) : 1.00E-03
Sources : Stack (TRACER)	Time (hrs) : 0.00	Location(°E,°N,m) : (-70.5105,41.7701,152.40)

Figure 99. SCIPUFF surface concentrations of inert tracer (kg/m^3) released from the Canal plant at Sandwich, MA, as a continuous plume. Concentrations shown on the 1.33-km domain in Case 3 are valid at 0600 UTC, 21 August 2000 (+6 h). Maximum concentration is shown at the upper right of the panel. (The number of hours that SCIPUFF has been running is shown in parentheses at the top of the figure.)

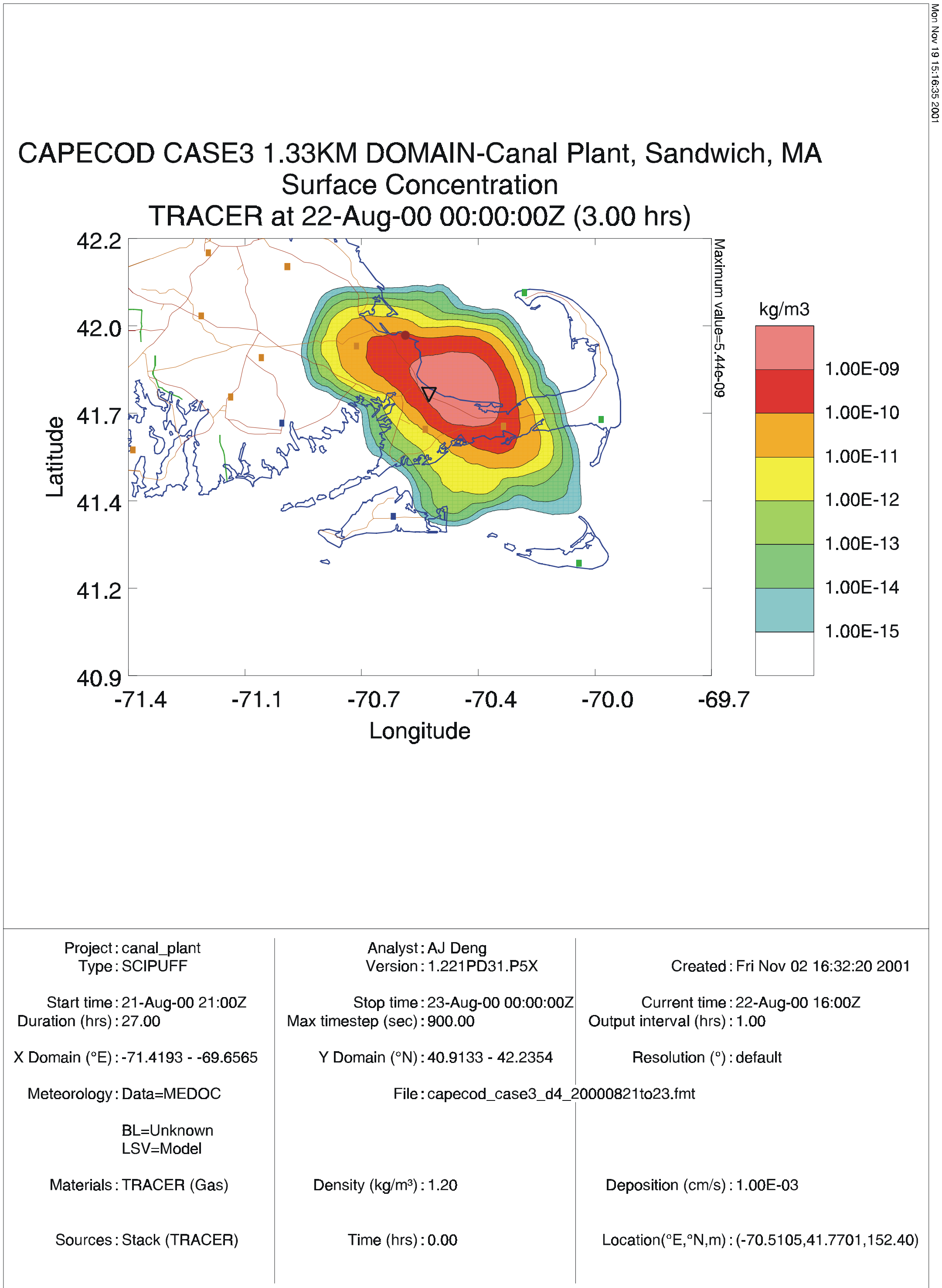

Figure 100. SCIPUFF surface concentrations of inert tracer (kg/m^3) released from the Canal plant at Sandwich, MA, as a continuous plume. Concentrations shown on the 1.33-km domain in Case 3 are valid at 0000 UTC, 22 August 2000 (+24 h). Maximum concentration is shown at the upper right of the panel. (The number of hours that SCIPUFF has been running is shown in parentheses at the top of the figure.)

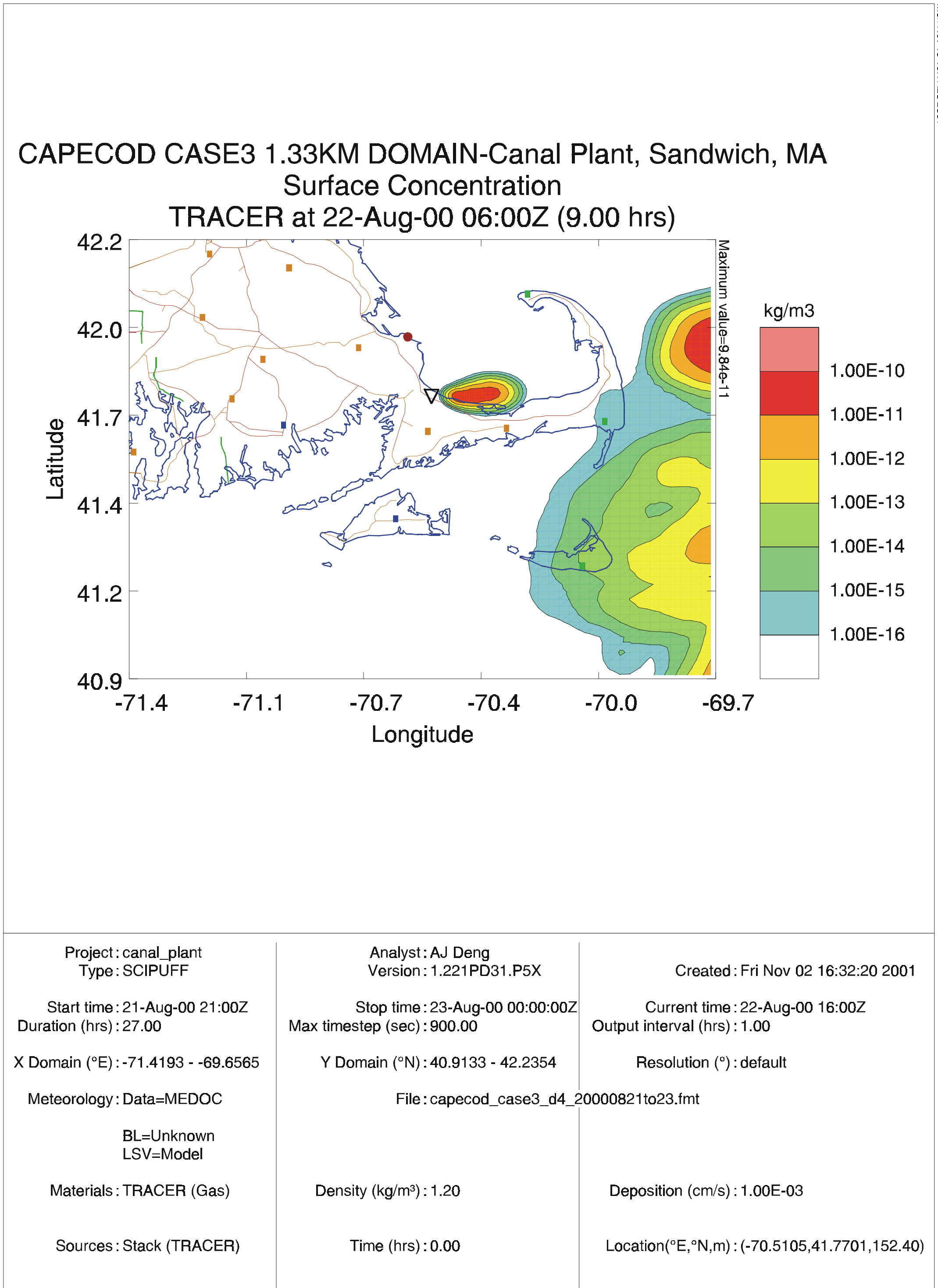

Figure 101. SCIPUFF surface concentrations of inert tracer (kg/m^3) released from the Canal plant at Sandwich, MA, as a continuous plume. Concentrations shown on the 1.33-km domain in Case 3 are valid at 0600 UTC, 22 August 2000 (+30 h). Maximum concentration is shown at the upper right of the panel. (The number of hours that SCIPUFF has been running is shown in parentheses at the top of the figure.)

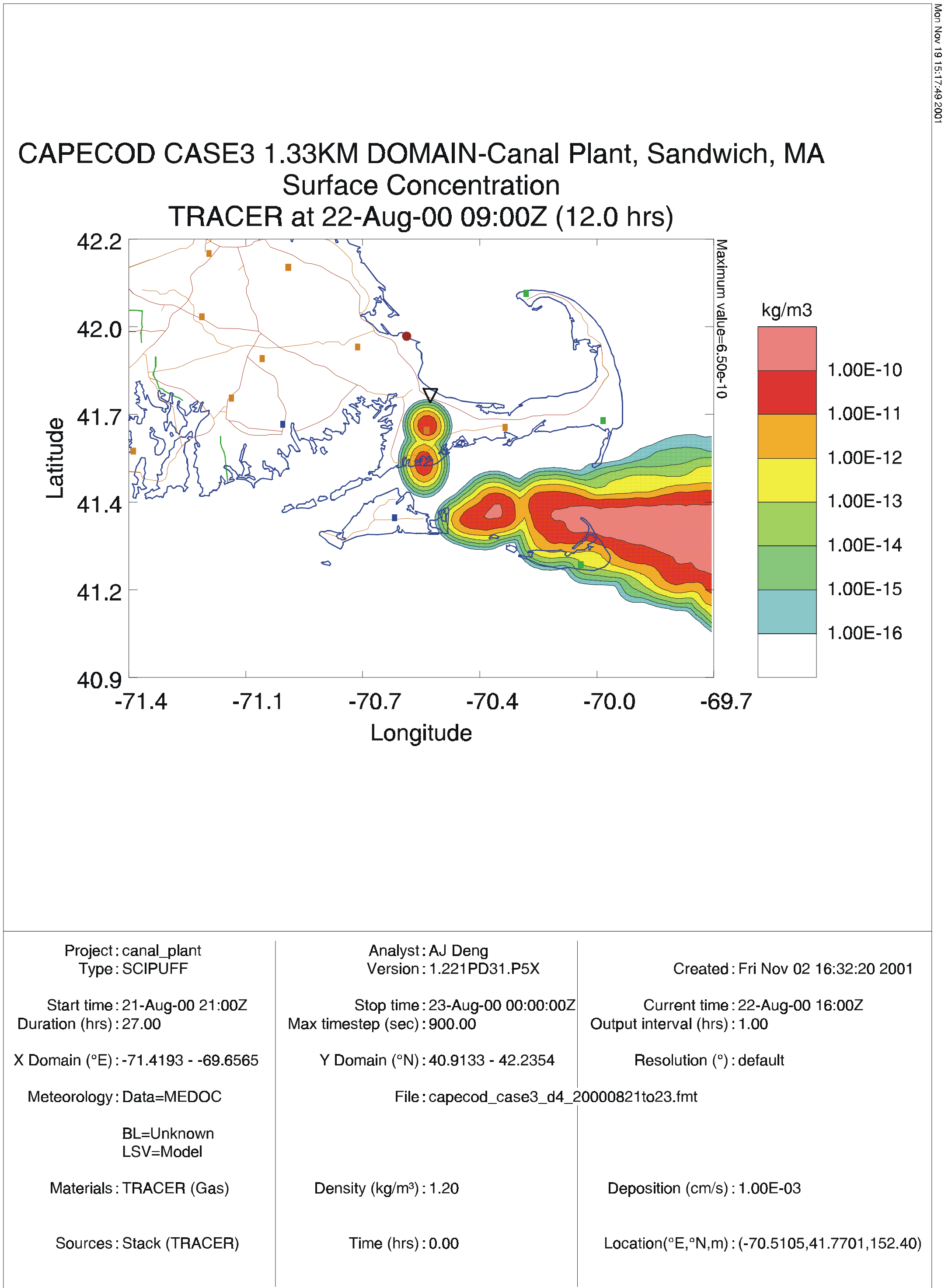

Figure 102. SCIPUFF surface concentrations of inert tracer (kg/m^3) released from the Canal plant at Sandwich, MA, as a continuous plume. Concentrations shown on the 1.33-km domain in Case 3 are valid at 0900 UTC, 22 August 2000 (+33 h). Maximum concentration is shown at the upper right of the panel. (The number of hours that SCIPUFF has been running is shown in parentheses at the top of the figure.)

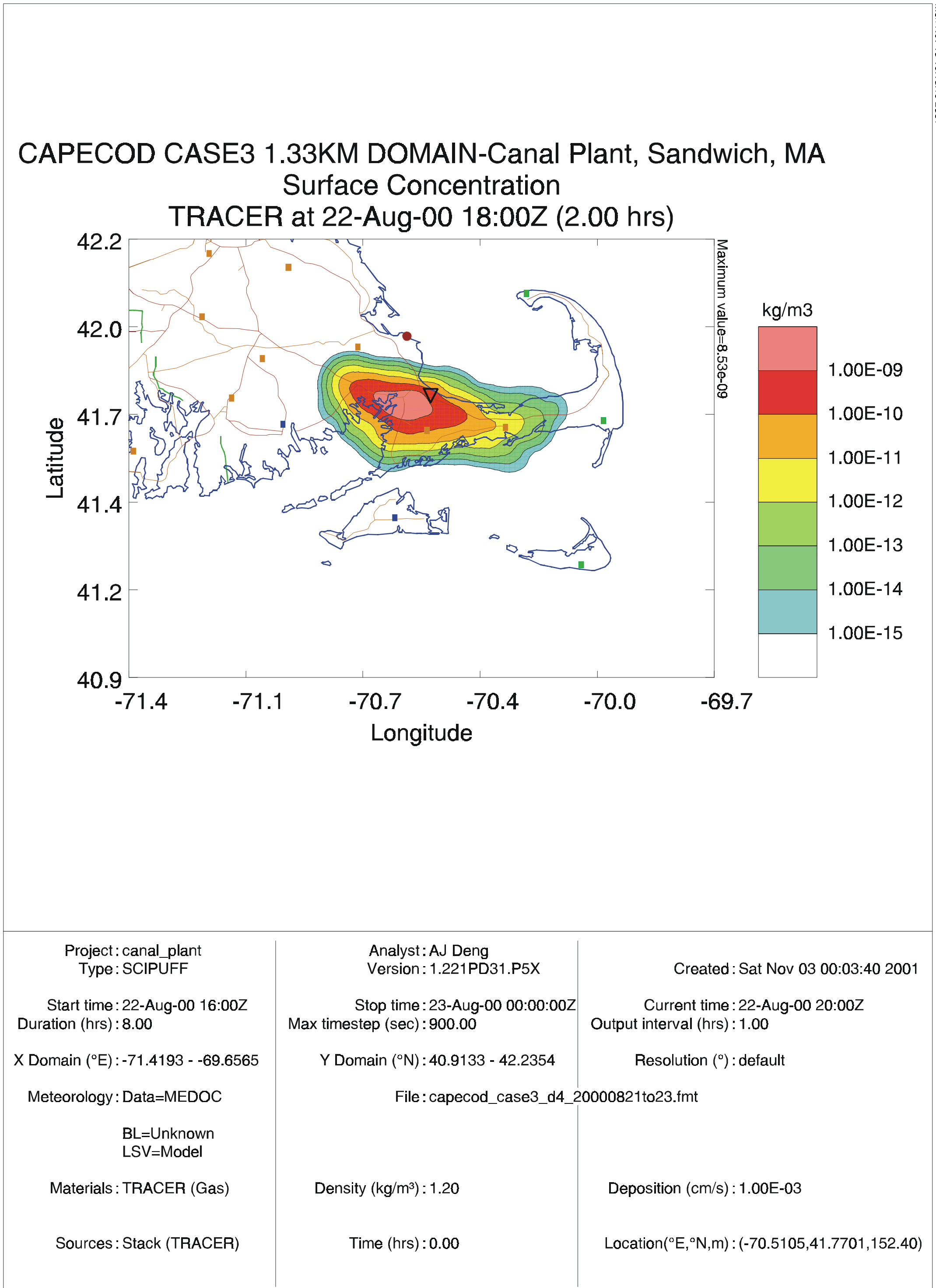

Figure 103. SCIPUFF surface concentrations of inert tracer (kg/m^3) released from the Canal plant at Sandwich, MA, as a continuous plume. Concentrations shown on the 1.33-km domain in Case 3 are valid at 1800 UTC, 22 August 2000 (+42 h). Maximum concentration is shown at the upper right of the panel. (The number of hours that SCIPUFF has been running is shown in parentheses at the top of the figure.)

sea breeze intensifies. As is common during the daytime, the deepening of the turbulent boundary layer leads to higher afternoon surface concentrations than during the night (~8.5 X 10^{-9} kg/m^3) through the fumigation mechanism.

The surface plume emitted along the highway running through Upper Cape Cod is shown in Figures 104-107. As in the other two cases, the highway plume in Case 3 responds most strongly to the surface wind directions, while maintaining roughly a constant maximum concentration of ~1.35-1.95 X 10^{-5} kg/m^3. The greatest difference between the daytime and nocturnal highway plumes is how far downwind they are able to maintain large concentrations close to the surface. The higher intensity of the turbulence and the deeper boundary-layer depths during the day consistently loft the tracer plumes away from the surface within a few kilometers downwind of the highway. By contrast, the nocturnal highway plumes have surprisingly high surface concentrations for many kilometers downwind.

Finally, Figures 108-112 show the SCIPUFF results for the plume emitted from Otis AFB in Case 3. The behavior of this surface plume is very predictable, following the same general pattern as noted for the Canal plant. However, because the emissions are close to the surface, the nocturnal maximum surface concentrations tend to be close to the source, rather than far downwind. No other unusual behavior was noted for the plume in this case.

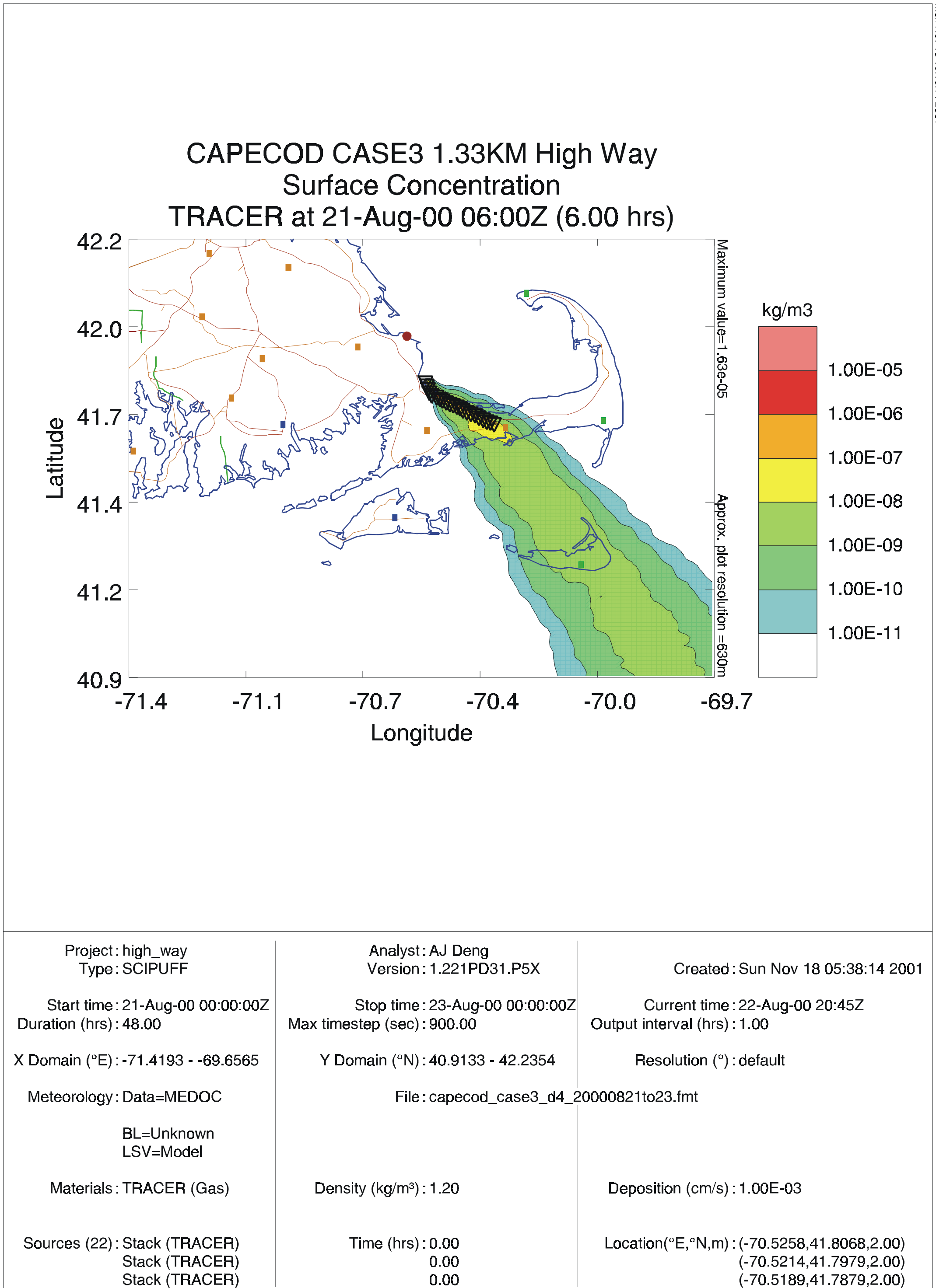

Figure 104. SCIPUFF surface concentrations of inert tracer (kg/m^3) released as a continuous plume along MA Routes 3 and 6. Concentrations shown on the 1.33-km domain in Case 3 are valid at 0600 UTC, 21 August 2000 (+6 h). Maximum concentration is shown at the upper right of the panel. (The number of hours that SCIPUFF has been running is shown in parentheses at the top of the figure.)

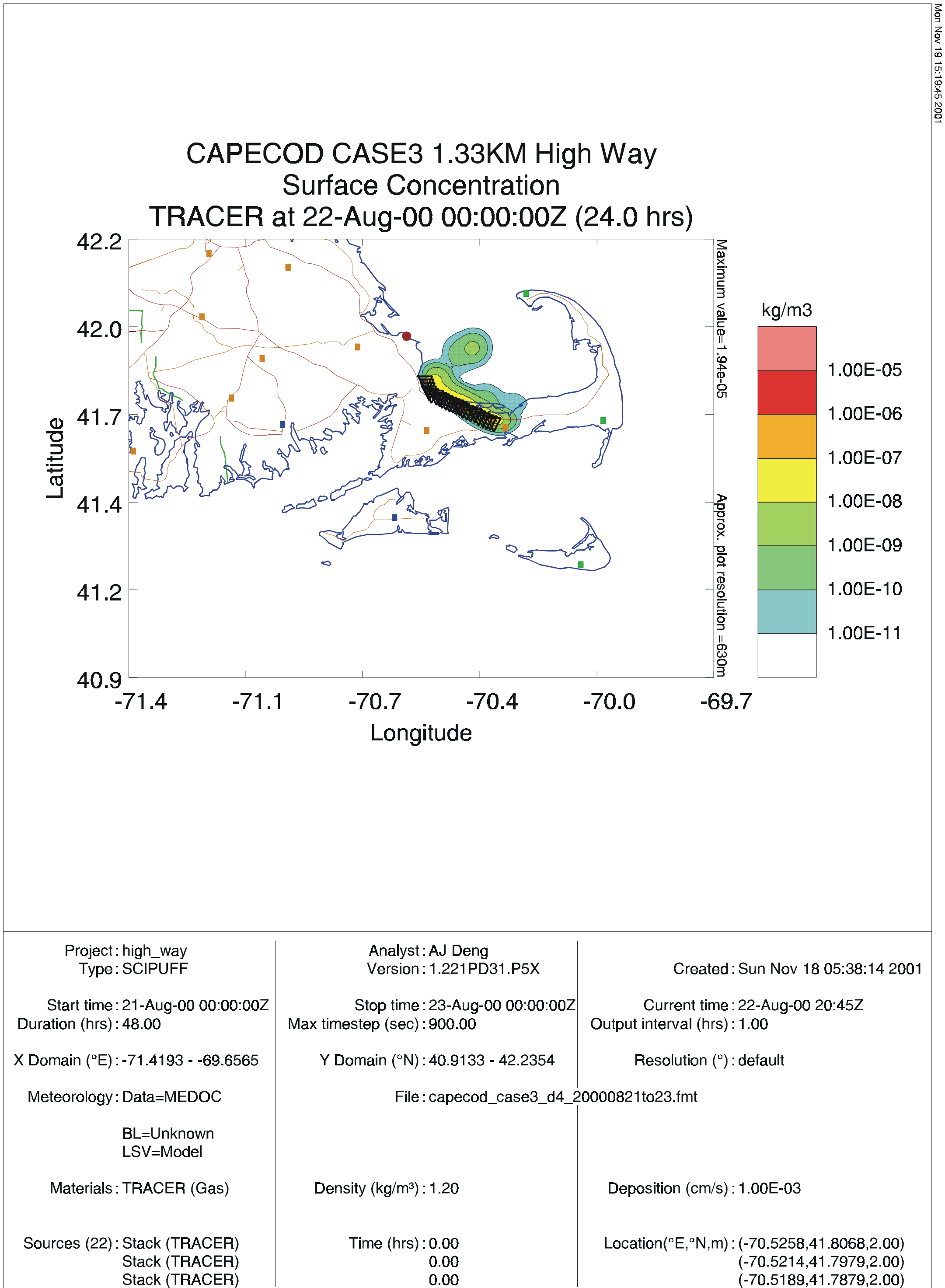

Figure 105. SCIPUFF surface concentrations of inert tracer (kg/m^3) released as a continuous plume along MA Routes 3 and 6. Concentrations shown on the 1.33-km domain in Case 3 are valid at 0000 UTC, 22 August 2000 (+24 h). Maximum concentration is shown at the upper right of the panel. (The number of hours that SCIPUFF has been running is shown in parentheses at the top of the figure.)

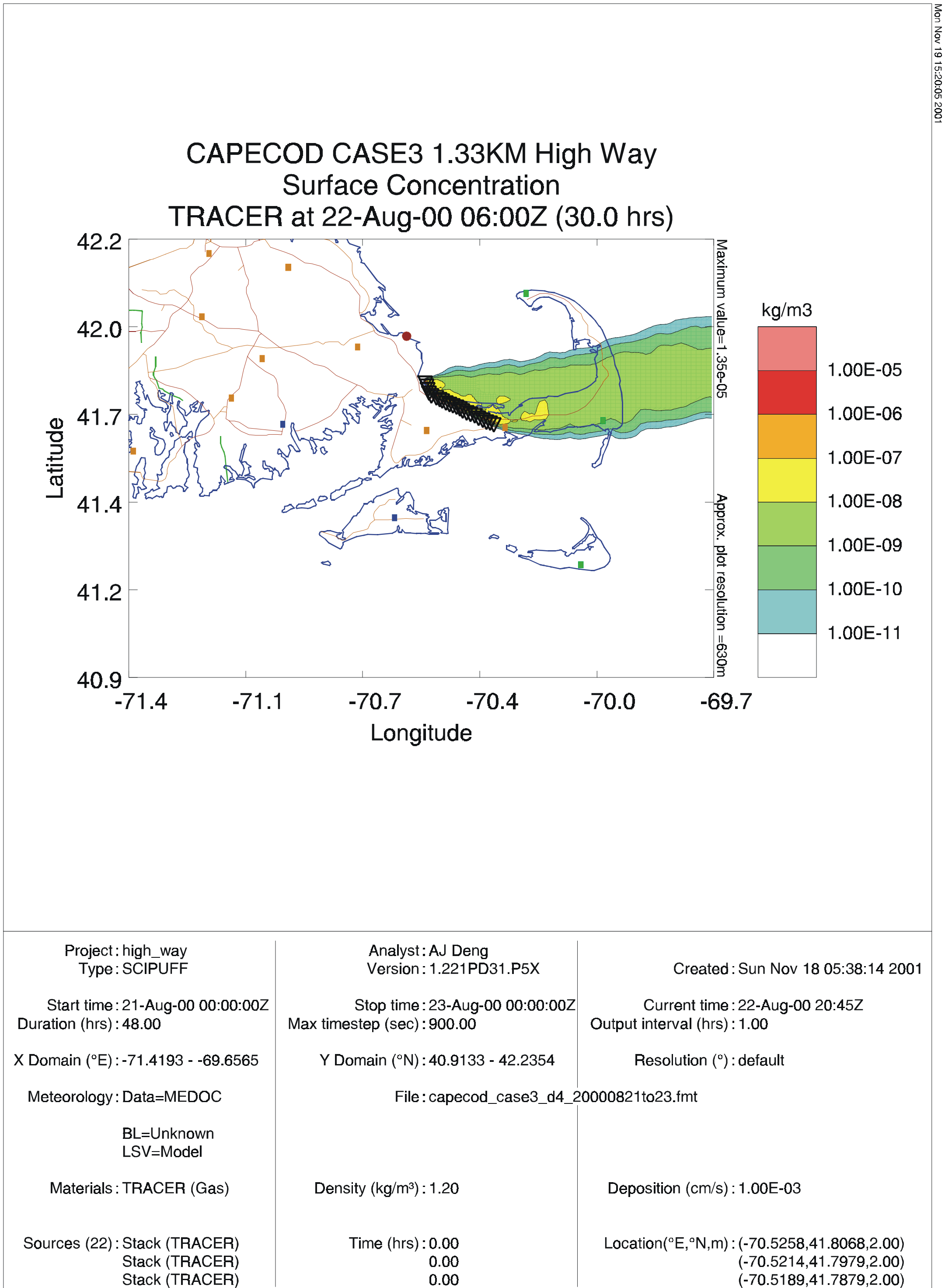

Figure 106. SCIPUFF surface concentrations of inert tracer (kg/m^3) released as a continuous plume along MA Routes 3 and 6. Concentrations shown on the 1.33-km domain in Case 3 are valid at 0600 UTC, 22 August 2000 (+30 h). Maximum concentration is shown at the upper right of the panel. (The number of hours that SCIPUFF has been running is shown in parentheses at the top of the figure.)

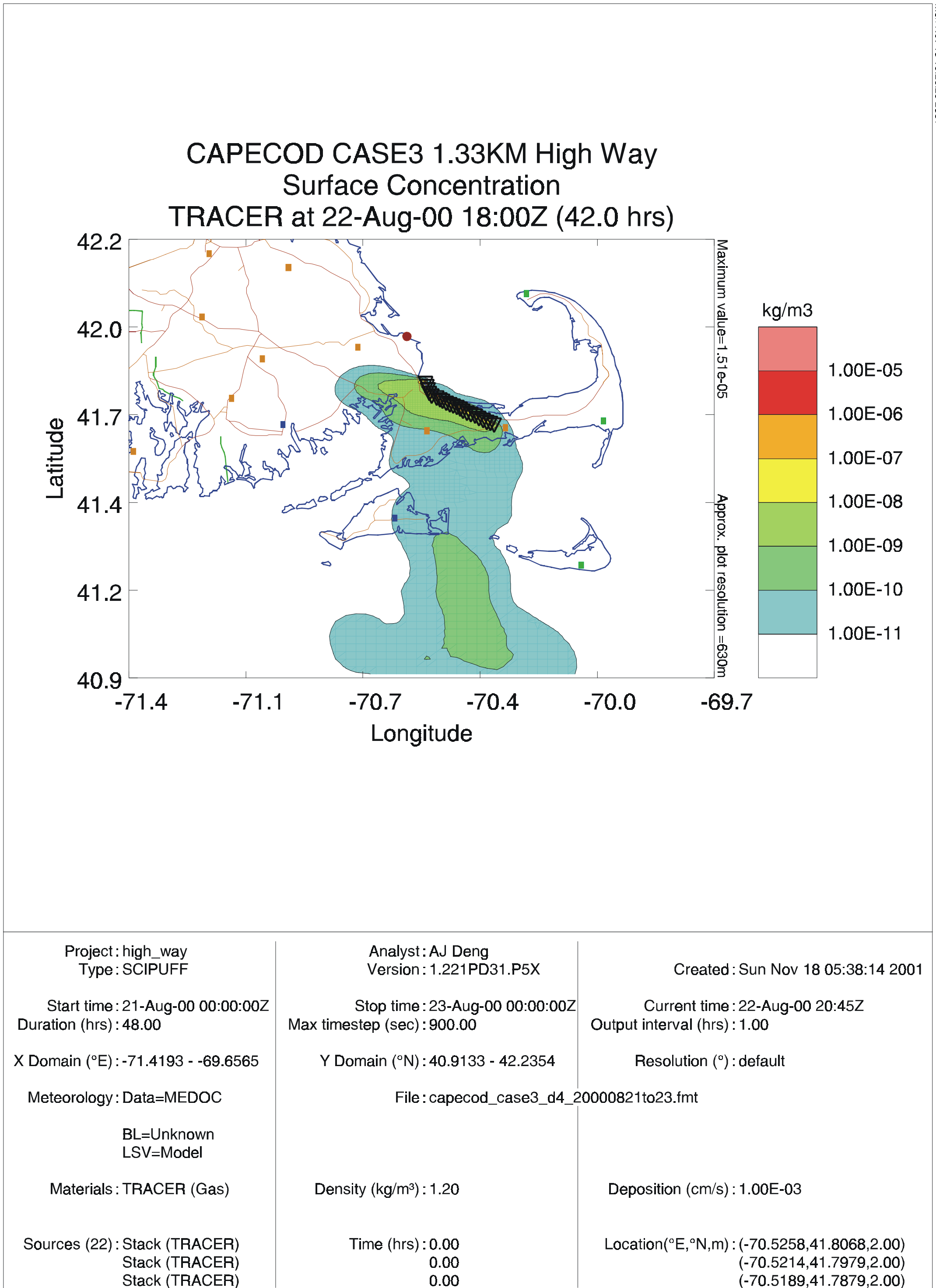

Figure 107. SCIPUFF surface concentrations of inert tracer (kg/m^3) released as a continuous plume along MA Routes 3 and 6. Concentrations shown on the 1.33-km domain in Case 3 are valid at 1800 UTC, 22 August 2000 (+42 h). Maximum concentration is shown at the upper right of the panel. (The number of hours that SCIPUFF has been running is shown in parentheses at the top of the figure.)

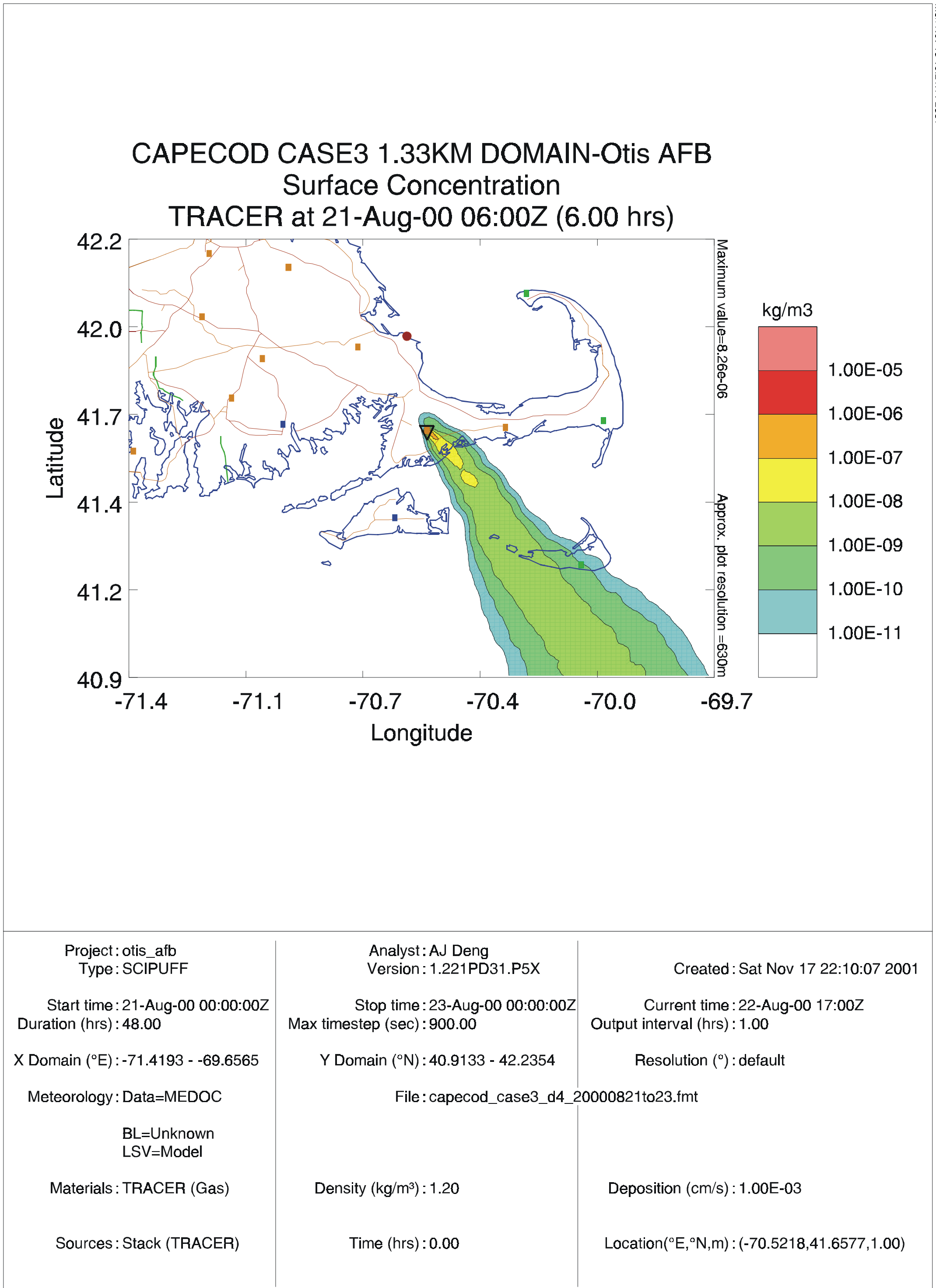

Figure 108. SCIPUFF surface concentrations of inert tracer (kg/m^3) released from Otis AFB as a continuous plume. Concentrations shown on the 1.33-km domain in Case 3 are valid at 0600 UTC, 21 August 2000 (+6 h). Maximum concentration is shown at the upper right of the panel. (The number of hours that SCIPUFF has been running is shown in parentheses at the top of the figure.)

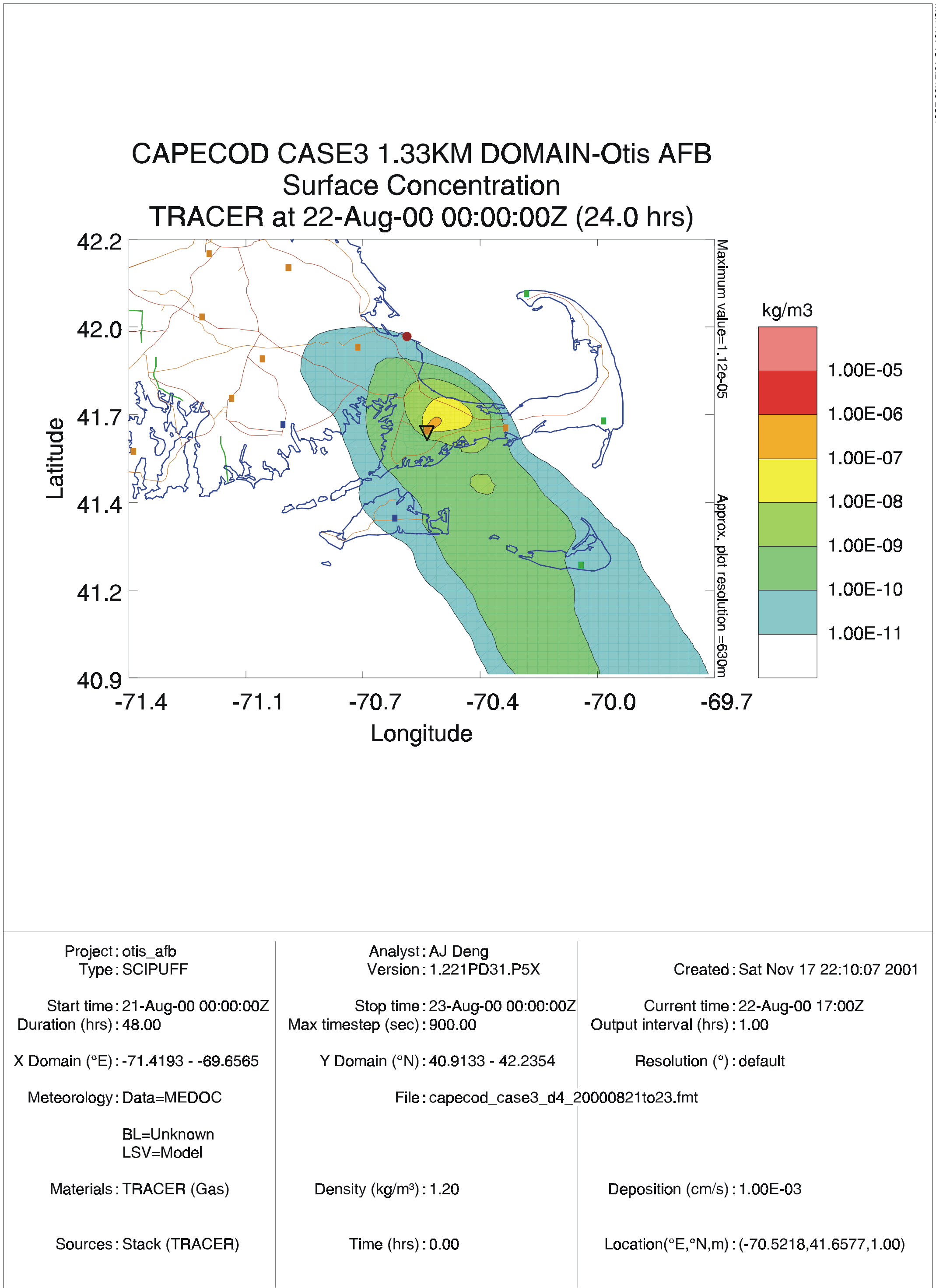

Figure 109. SCIPUFF surface concentrations of inert tracer (kg/m^3) released from Otis AFB as a continuous plume. Concentrations shown on the 1.33-km domain in Case 3 are valid at 0000 UTC, 22 August 2000 (+24 h). Maximum concentration is shown at the upper right of the panel. (The number of hours that SCIPUFF has been running is shown in parentheses at the top of the figure.)

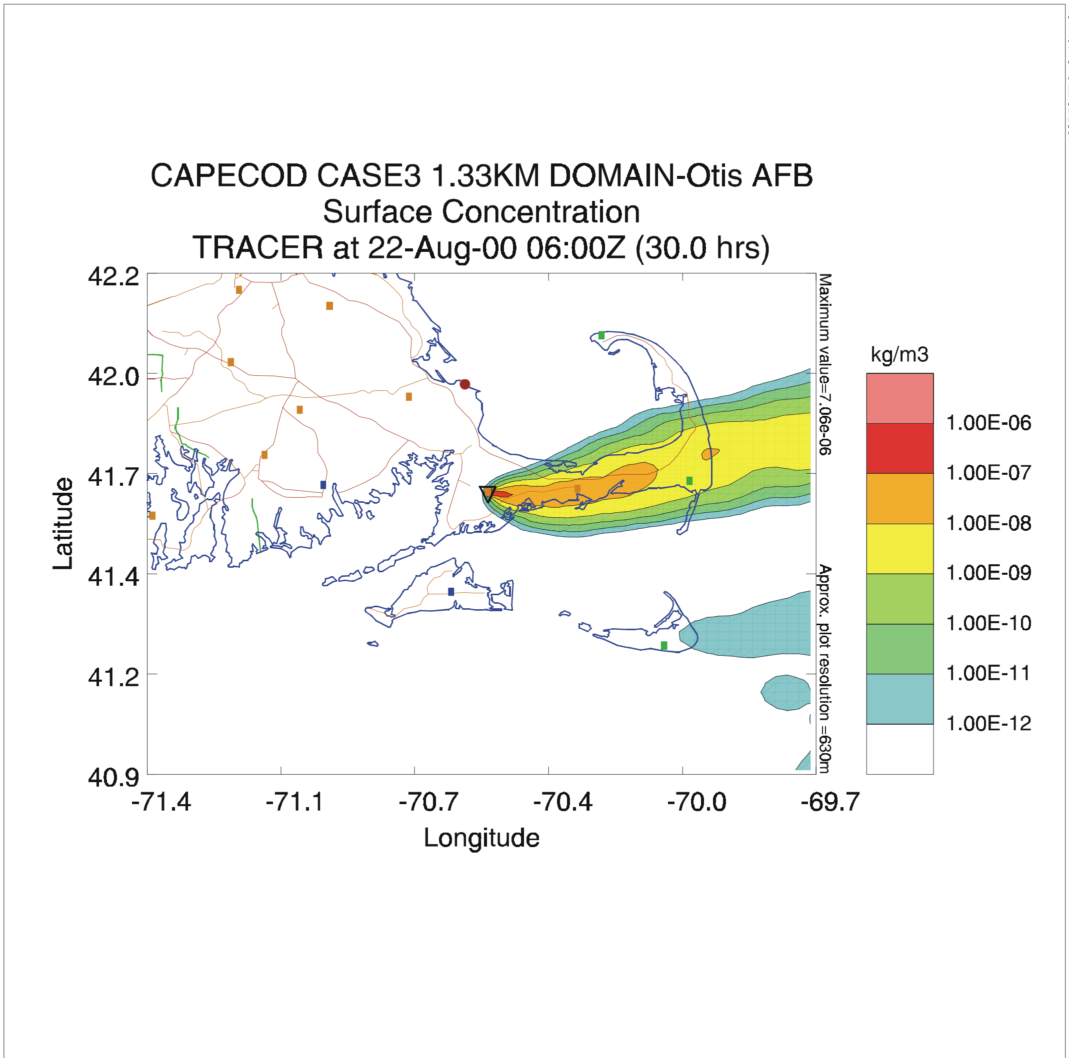

Project : otis_afb Type : SCIPUFF	Analyst : AJ Deng Version : 1.221PD31.P5X	Created : Sat Nov 17 22:10:07 2001
Start time : 21-Aug-00 00:00:00Z Duration (hrs) : 48.00	Stop time : 23-Aug-00 00:00:00Z Max timestep (sec) : 900.00	Current time : 22-Aug-00 17:00Z Output interval (hrs) : 1.00
X Domain (°E) : -71.4193 - -69.6565	Y Domain (°N) : 40.9133 - 42.2354	Resolution (°) : default
Meteorology : Data=MEDOC BL=Unknown LSV=Model	File : capecod_case3_d4_20000821to23.fmt	
Materials : TRACER (Gas)	Density (kg/m³) : 1.20	Deposition (cm/s) : 1.00E-03
Sources : Stack (TRACER)	Time (hrs) : 0.00	Location(°E,°N,m) : (-70.5218,41.6577,1.00)

Figure 110. SCIPUFF surface concentrations of inert tracer (kg/m^3) released from Otis AFB as a continuous plume. Concentrations shown on the 1.33-km domain in Case 3 are valid at 0600 UTC, 22 August 2000 (+30 h). Maximum concentration is shown at the upper right of the panel. (The number of hours that SCIPUFF has been running is shown in parentheses at the top of the figure.)

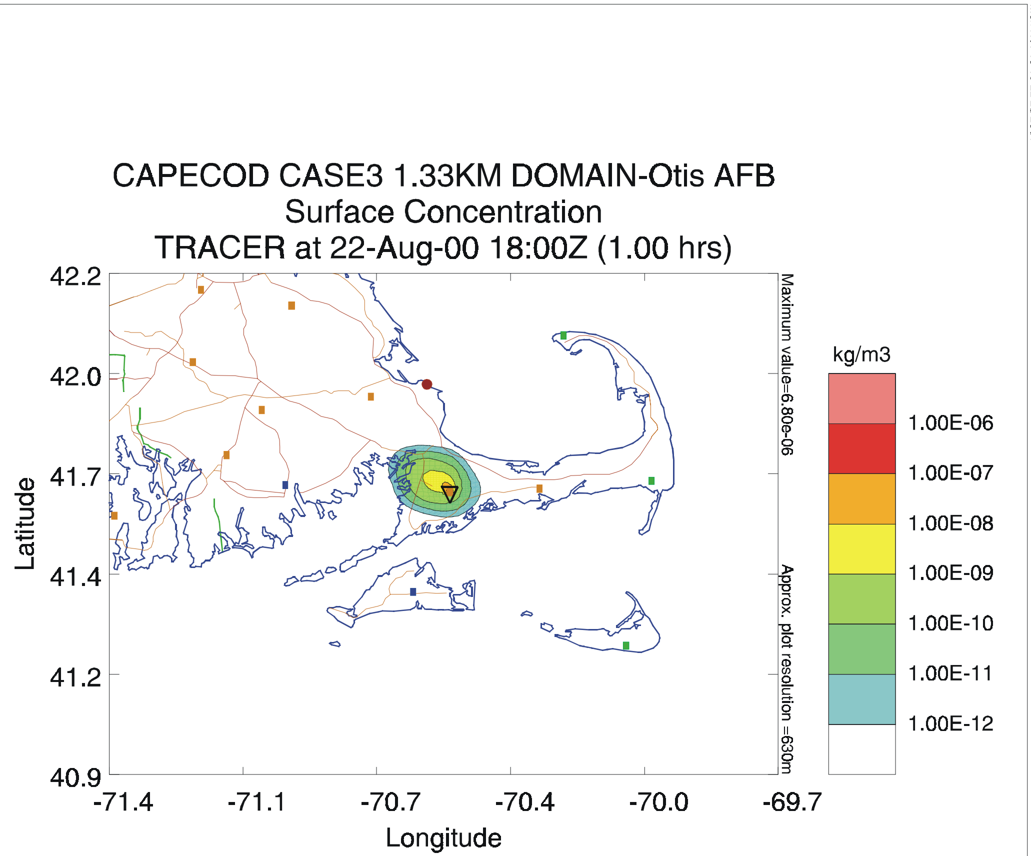

Project : otis_afb Type : SCIPUFF	Analyst : AJ Deng Version : 1.221PD31.P5X	Created : Sun Nov 18 04:35:09 2001
Start time : 22-Aug-00 17:00Z Duration (hrs) : 7.00	Stop time : 23-Aug-00 00:00:00Z Max timestep (sec) : 900.00	Current time : 22-Aug-00 21:00Z Output interval (hrs) : 1.00
X Domain (°E) : -71.4193 - -69.6565	Y Domain (°N) : 40.9133 - 42.2354	Resolution (°) : default
Meteorology : Data=MEDOC BL=Unknown LSV=Model	File : capecod_case3_d4_20000821to23.fmt	
Materials : TRACER (Gas)	Density (kg/m³) : 1.20	Deposition (cm/s) : 1.00E-03
Sources : Stack (TRACER)	Time (hrs) : 0.00	Location(°E,°N,m) : (-70.5218,41.6577,1.00)

Figure 111. SCIPUFF surface concentrations of inert tracer (kg/m^3) released from Otis AFB as a continuous plume. Concentrations shown on the 1.33-km domain in Case 3 are valid at 1800 UTC, 22 August 2000 (+42 h). Maximum concentration is shown at the upper right of the panel. (The number of hours that SCIPUFF has been running is shown in parentheses at the top of the figure.)

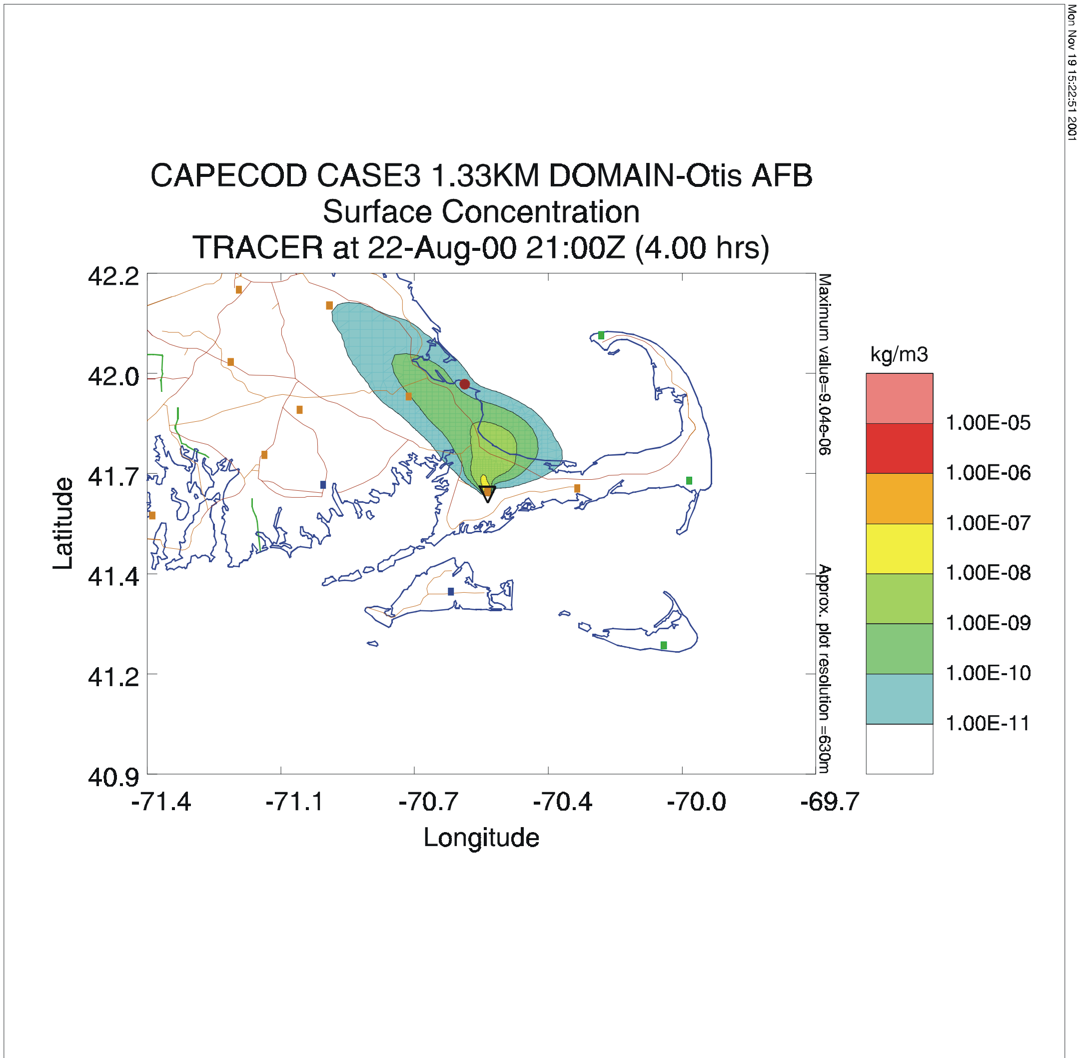

Project : otis_afb Type : SCIPUFF	Analyst : AJ Deng Version : 1.221PD31.P5X	Created : Sun Nov 18 04:35:09 2001
Start time : 22-Aug-00 17:00Z Duration (hrs) : 7.00	Stop time : 23-Aug-00 00:00:00Z Max timestep (sec) : 900.00	Current time : 22-Aug-00 21:00Z Output interval (hrs) : 1.00
X Domain (°E) : -71.4193 - -69.6565	Y Domain (°N) : 40.9133 - 42.2354	Resolution (°) : default
Meteorology : Data=MEDOC BL=Unknown LSV=Model	File : capecod_case3_d4_20000821to23.fmt	
Materials : TRACER (Gas)	Density (kg/m³) : 1.20	Deposition (cm/s) : 1.00E-03
Sources : Stack (TRACER)	Time (hrs) : 0.00	Location(°E,°N,m) : (-70.5218,41.6577,1.00)

Figure 112. SCIPUFF surface concentrations of inert tracer (kg/m^3) released from Otis AFB as a continuous plume. Concentrations shown on the 1.33-km domain in Case 3 are valid at 2100 UTC, 22 August 2000 (+45 h). Maximum concentration is shown at the upper right of the panel. (The number of hours that SCIPUFF has been running is shown in parentheses at the top of the figure.)

4.4

4.4.1 Demonstrations

In this section, results from forward trajectory calculations are presented, based on the TRAJEC program applied to the MM5 3-D wind fields. Parcels are released from each of the four emission sites at 6-h intervals through the 48-h period covered by the three episodes. The horizontal releasing locations for the four points, in terms of latitude, longitude and height above mean sea level (MSL), are given in Table 22. The table also defines the heights at which the plumes are released, which requires some explanation. Here, the release heights for the highway parcels and the parcels from Otis AFB are assigned to the middle of the MM5's surface layer (12.5 m). For the two power plants at Somerset (Brayton Point plant) and Sandwich (Canal plant), the hot gases emitted from the stacks cause the plumes to rise several hundred meters above the height of the stacks before they become neutrally buoyant. Plume rise is dependent on the temperature of the stack exhaust, the stability of the atmosphere and the winds.

In the dispersion models (SCIPUFF and CALPUFF), the plume rise is calculated based on the stack exhaust temperature, and on the winds and local stability (determined by the MM5 thermal field) , as they evolve over time. However, for simplicity, we assume here for the purpose of the trajectory calculations that the atmosphere is stable during the nighttime from 0000 UTC to 1200 UTC, and is unstable during the daytime from 1200 UTC to 0000 UTC. During each 12-h stable period a single plume height rise is assumed, even though the actual stability may change gradually. This simplified approach makes it easier to interpret the path taken by the center of each plume, as calculated by TRAJEC using the MM5 3-D wind fields. The difference in the final plume release heights for Brayton Point and the Canal plant is mainly due to the differences in their exhaust temperatures, while the stacks both have the same height.

Table 22. Location and final release height of the plumes emitted from four sources in the vicinity of Upper Cape Cod.

Source	Brayton Point Somerset, MA	Canal Plant Sandwich, MA	MA Routes 3 and 6	Otis AFB
Latitude (deg., decimal min.)	41^o 42.6'	41^o 46.2'	41^o 44.4'	41^o 39.5'
Longitude (deg., decimal min.)	71^o 11.6'	70^o 30.6'	70^o 27.8'	70^o 31.3'
Plume release ht. (m) Under unstable Conditions	555.1	699.7	12.5	12.5
Plume release ht. (m) Under stable Conditions	265.9	387.3	12.5	12.5

In the figures describing the 6-h trajectories, each release is treated as a material parcel, similar to a neutrally buoyant balloon. The figures are presented on horizontal maps of the 1.33-km domain. Two parallel lines are plotted for each parcel, where the separation of the lines is used to represent the height above the ground. When the parcels are at the surface (~1000 mb), the lines overlap (i.e., they appear as one line), while the lines gradually separate at higher altitudes.

For reference, each figure displays a wedge-shaped key at the lower right that gives the separation of the two lines from 1000 mb (~ 0 m MSL) to 800 mb (~2000 m MSL). Thus, referring to Table 22, a parcel released from the Brayton Point plant during the day is initialized at 699.7 m, or about 930 mb. In this case, the initial separation of the two lines for this parcel will be approximately 0.33 times the maximum separation for 800 mb shown in the key. If the parcel subsequently rises as it is advected downwind, the lines will gradually become farther apart. If it sinks, the lines will appear to converge.

Before viewing the results of the parcel trajectory calculations, a word of caution is appropriate. The SCIPUFF plume-dispersion fields and the TRAJEC trajectories must, of course, be consistent with one another because they are based on the same MM5 fields. However, interpretation of their respective results is not always straightforward because they depict very different information. SCIPUFF plots show the surface "footprint" concentrations of a dispersed 3-D plume. The horizontal location of the maximum surface concentration may be very different from the location of the maximum at some level above the ground. This possibility is quite likely to occur in situations having strong vertical wind shear, such as occurs in sea breeze and land breeze cases. These thermally driven mesoscale circulations tend to be quite shallow, so that the surface wind directions can be very different than those found several hundred meters aloft, where the synoptic-scale flow prevails. TRAJEC, on the other hand, calculates the path taken by a neutrally buoyant parcel as it is advected from its release point by the 3-D wind field. It may be considered, in a loose sense, to reveal the approximate path of a puff's center of mass. If most of that mass is advected vertically several hundred meters above the surface, we can expect that the trajectory (for any of the cases investigated here) will appear to be quite different from that implied by the surface footprint of the dispersed plume calculated by SCIPUFF. Therefore, keeping in mind that TRAJEC depicts the path of the approximate center of mass (without consideration of dispersion), while SCIPUFF depicts the dispersed surface plume concentrations, the two displays together can give great insight into the 3-D processes that affect the plume. In both cases, occasional reference back to the analyzed and model-simulated wind fields shown above is apt to be quite helpful.

4.4.1.1 Case 1 Trajectories

For Case 1 (1-2 July 2000), the trajectories are summarized in Figures 113-120. The path of each set of four parcels, released at 6-h intervals, reveals much information that confirms and supplements the information contained in the SCIPUFF plots developed from the MM5 fields generated for this case (Section 4.3.1.1). In Figure 113, the parcels initially move toward the east, while the cold front is still in the area of Cape Cod, but they soon rotate anticyclonically (clockwise) as the northwesterly winds behind the cold front become better established over the area several hours later. The separation of the parallel lines for Parcels 1 and 2, released from the Brayton Point and Canal plants respectively, indicates that these parcels are emitted at and remain several hundred meters above the surface near 970 mb (also see Table 22). Later on the first night, from 0600 to 1200 UTC, 1 July, Figure 114 shows that the parcels released from the power plants (Parcels 1 and 2) are transported rapidly southward by winds aloft that are almost due northerly, while the parcels released close to the surface from the highway and Otis AFB (Parcels 3 and 4, respectively) are advected by more gentle northwesterly winds (compare to Figure 30).

Figure 115 shows the path taken by the parcels in Case 1 during the morning and early afternoon of 1 July (1200 - 1800 UTC), when the sea breeze begins to grow and the convergence zones become established over Cape Cod and southeastern MA (compare to Figure 31). For this transition period, Parcel 1 from the Brayton Point plant begins at 387 m MSL and travels southward on northerly winds for about an hour and 15 minutes (0915 EDT). This places the parcel close to the coastline in southeastern RI just as the sea breeze begins to develop. Since the depth of the sea breeze over land usually is at least 400-500 m deep, Parcel 1 turns cyclonically (counter-clockwise) over the next three hours. After +3.5 h (1130 EDT), the parcel is heading inland over southeastern MA at about its original height behind the fast-moving sea-breeze front. Between +4-5 h (1200 - 1300 EDT), the parcel accelerates northward as the sea breeze intensifies. However, during this time, the sea-breeze front was not moving inland as rapidly as the winds carrying Parcel 1. Consequently, just after +5 h (1315 EDT), Parcel 1 encounters the sea-breeze front then in southeastern MA (see Figure 31), which causes the parcel to be lofted rapidly to around 880 mb (~1200 m MSL) by the vertical winds in the frontal zone. At this height, Parcel 1 encounters the west-northwesterly synoptic-scale winds that persist aloft and which cause it to turn sharply toward the east in the final half hour of this 6-h segment in Case 1. Thus, careful examination and intercomparison of the wind and trajectory figures yields much insight into the fate of the emissions from the Brayton Point plant on this day. This sort of detail in the transport mechanism often is masked by the diffusion processes acting on the plume, which are included in the SCIPUFF calculations (also see Figure 54).

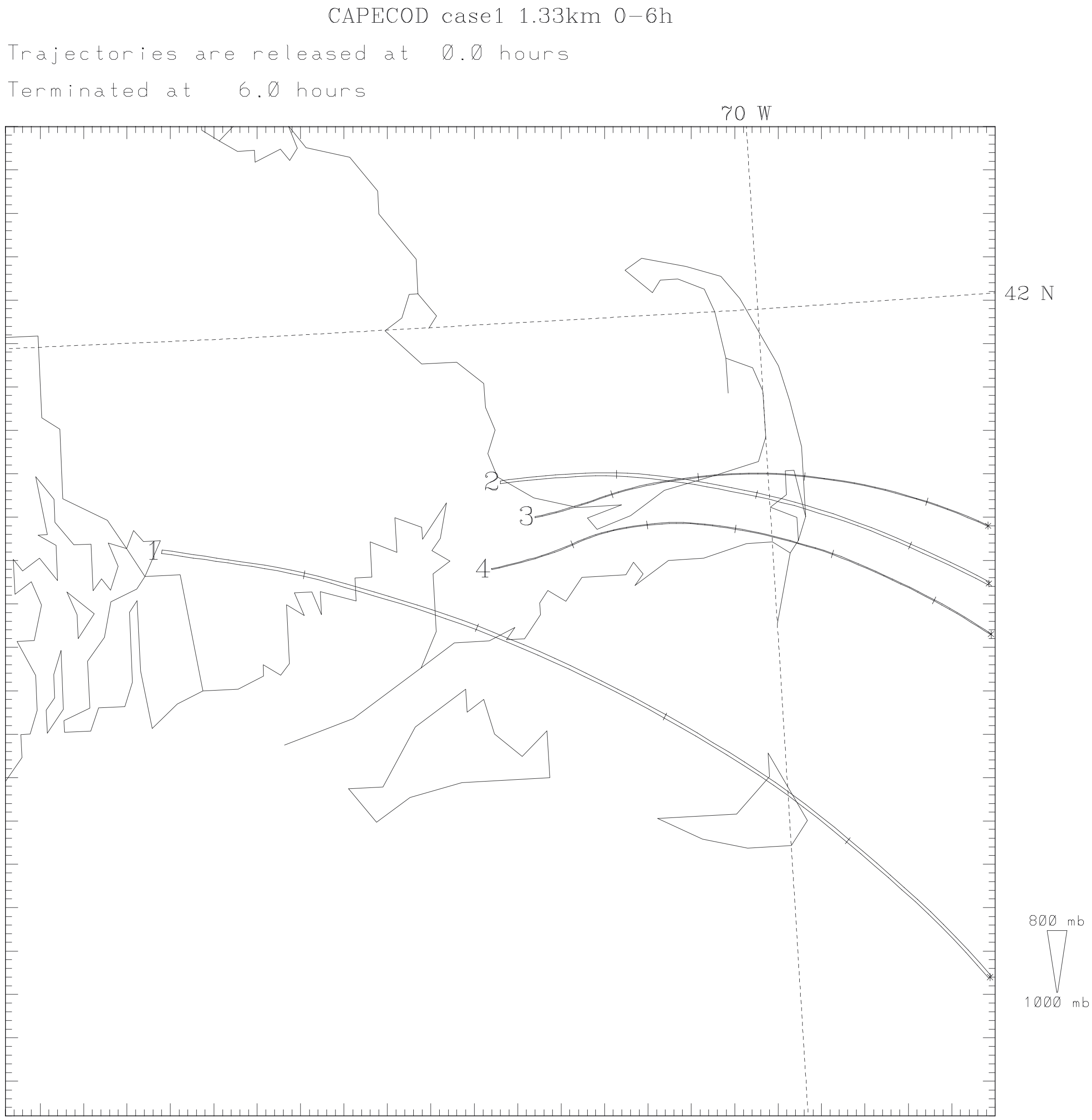

Figure 113. Six-hour TRAJEC forward trajectories based on MM5-simulated winds in Case 1. Release time is 0000 UTC, 1 July 2000 (+0 - 6 h). Parcel 1 is Brayton Point plant. Parcel 2 is Canal plant. Parcel 3 is middle of highway segment. Parcel 4 is Otis AFB. Tick marks shown on trajectories give positions at 1-h intervals, or until the parcels exit the domain.

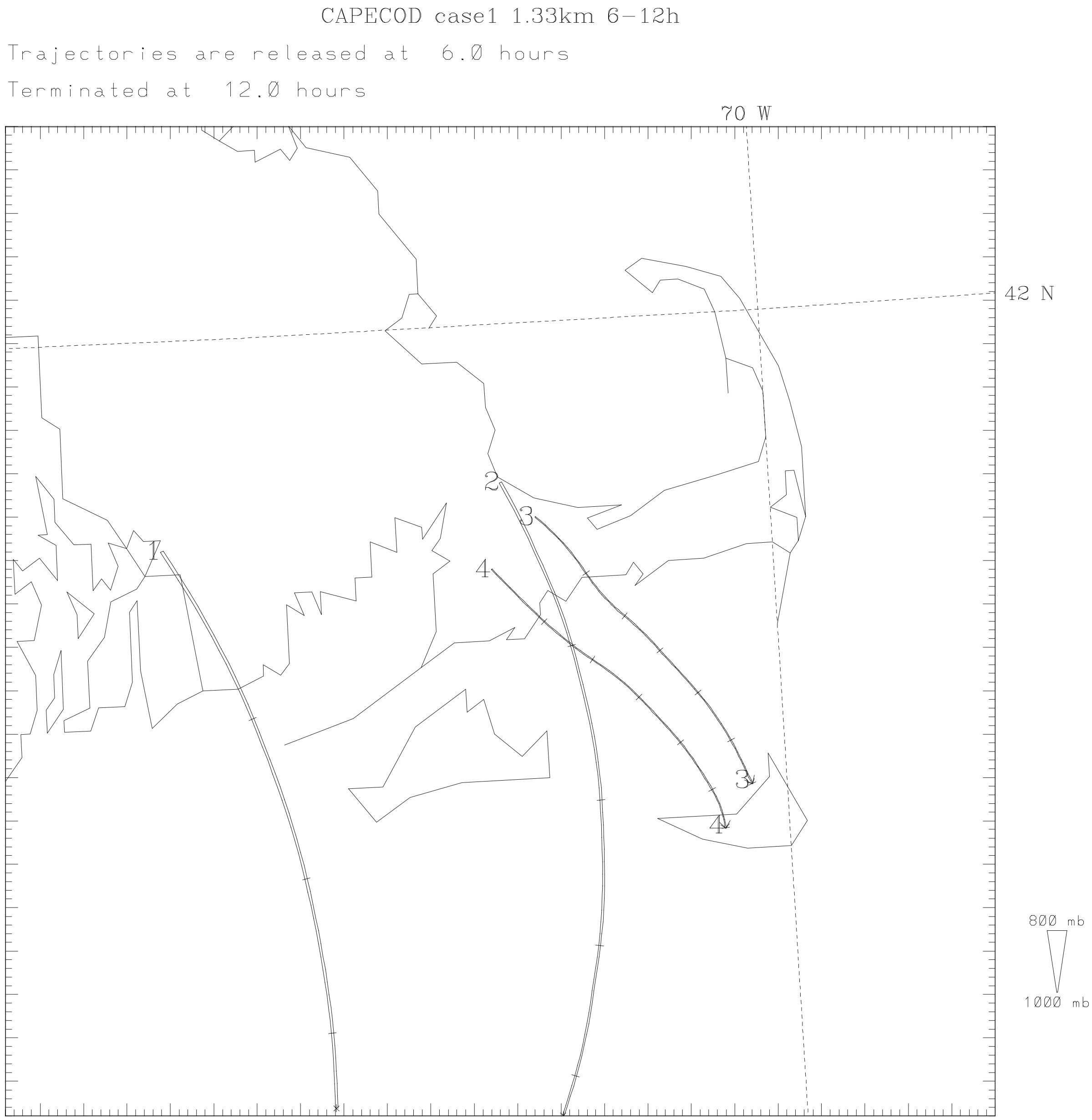

Figure 114. Six-hour TRAJEC forward trajectories based on MM5-simulated winds in Case 1. Release time is 0600 UTC, 1 July 2000 (+6 - 12 h). Parcel 1 is Brayton Point plant. Parcel 2 is Canal plant. Parcel 3 is middle of highway segment. Parcel 4 is Otis AFB. Tick marks shown on trajectories give positions at 1-h intervals, or until the parcels exit the domain.

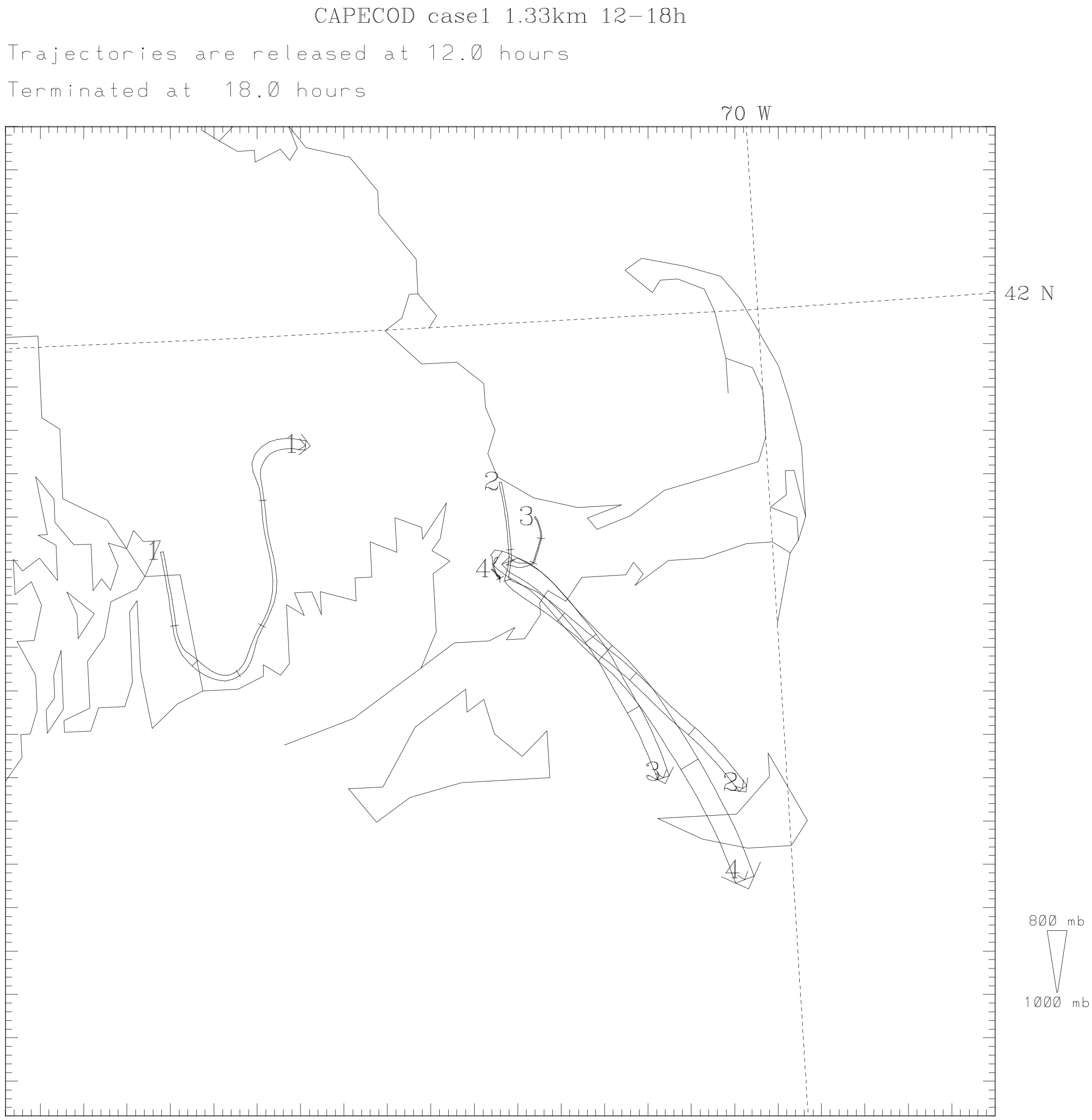

Figure 115. Six-hour TRAJEC forward trajectories based on MM5-simulated winds in Case 1. Release time is 1200 UTC, 1 July 2000 (+12 - 18 h). Parcel 1 is Brayton Point plant. Parcel 2 is Canal plant. Parcel 3 is middle of highway segment. Parcel 4 is Otis AFB. Tick marks shown on trajectories give positions at 1-h intervals, or until the parcels exit the domain.

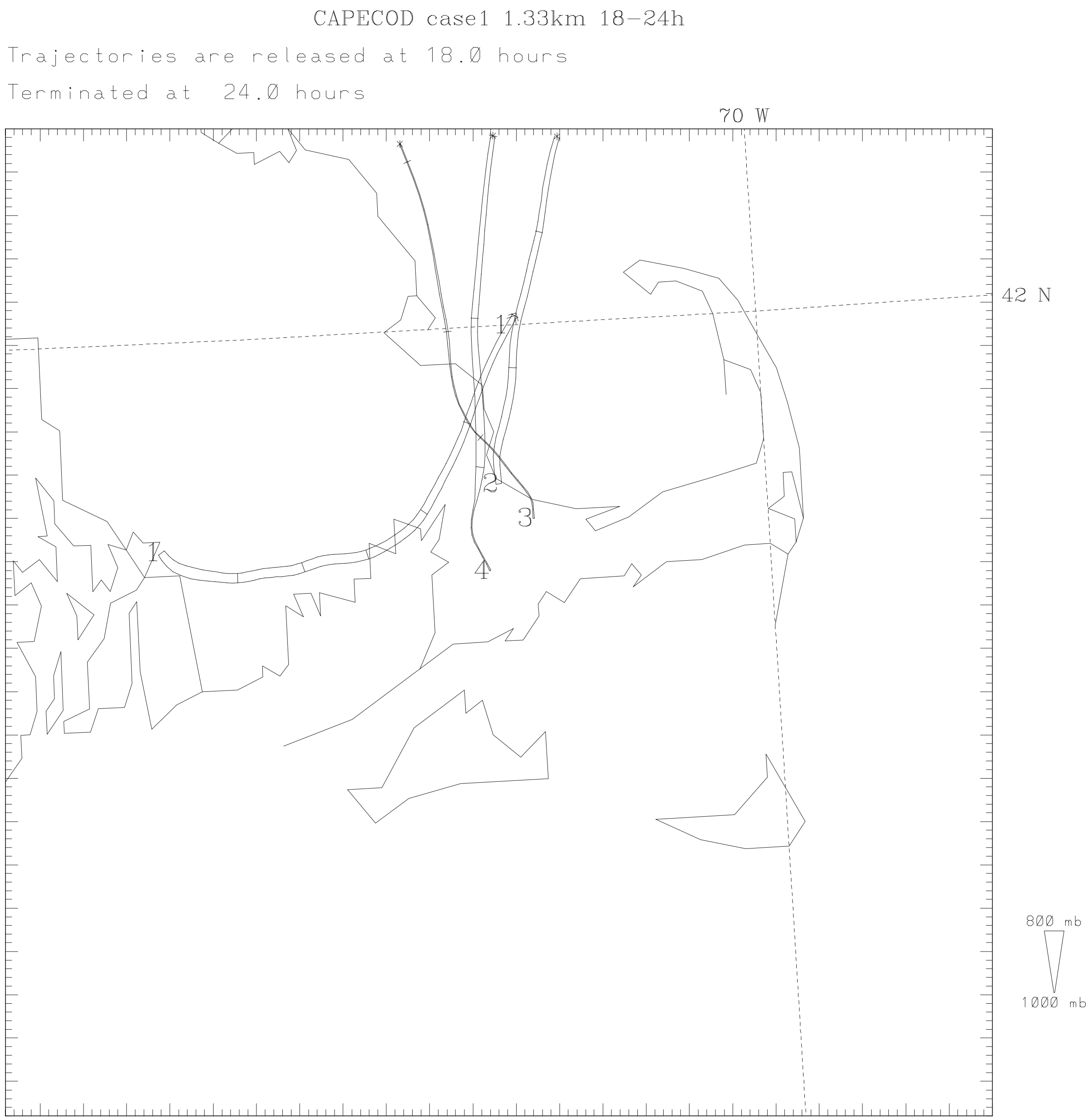

Figure 116. Six-hour TRAJEC forward trajectories based on MM5-simulated winds in Case 1. Release time is 1800 UTC, 1 July 2000 (+18 - 24 h). Parcel 1 is Brayton Point plant. Parcel 2 is Canal plant. Parcel 3 is middle of highway segment. Parcel 4 is Otis AFB. Tick marks shown on trajectories give positions at 1-h intervals, or until the parcels exit the domain.

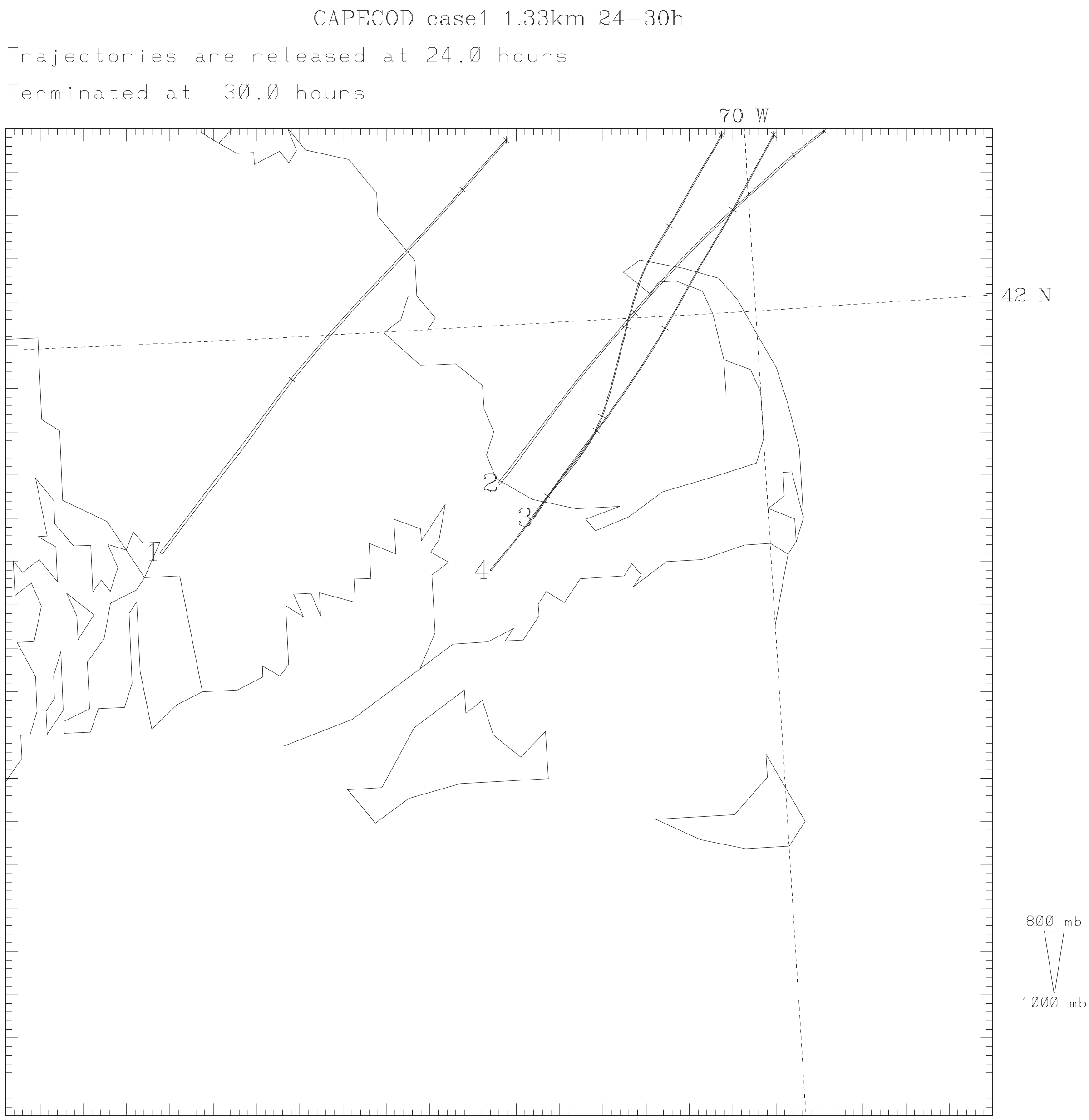

Figure 117. Six-hour TRAJEC forward trajectories based on MM5-simulated winds in Case 1. Release time is 0000 UTC, 2 July 2000 (+24 - 30 h). Parcel 1 is Brayton Point plant. Parcel 2 is Canal plant. Parcel 3 is middle of highway segment. Parcel 4 is Otis AFB. Tick marks shown on trajectories give positions at 1-h intervals, or until the parcels exit the domain.

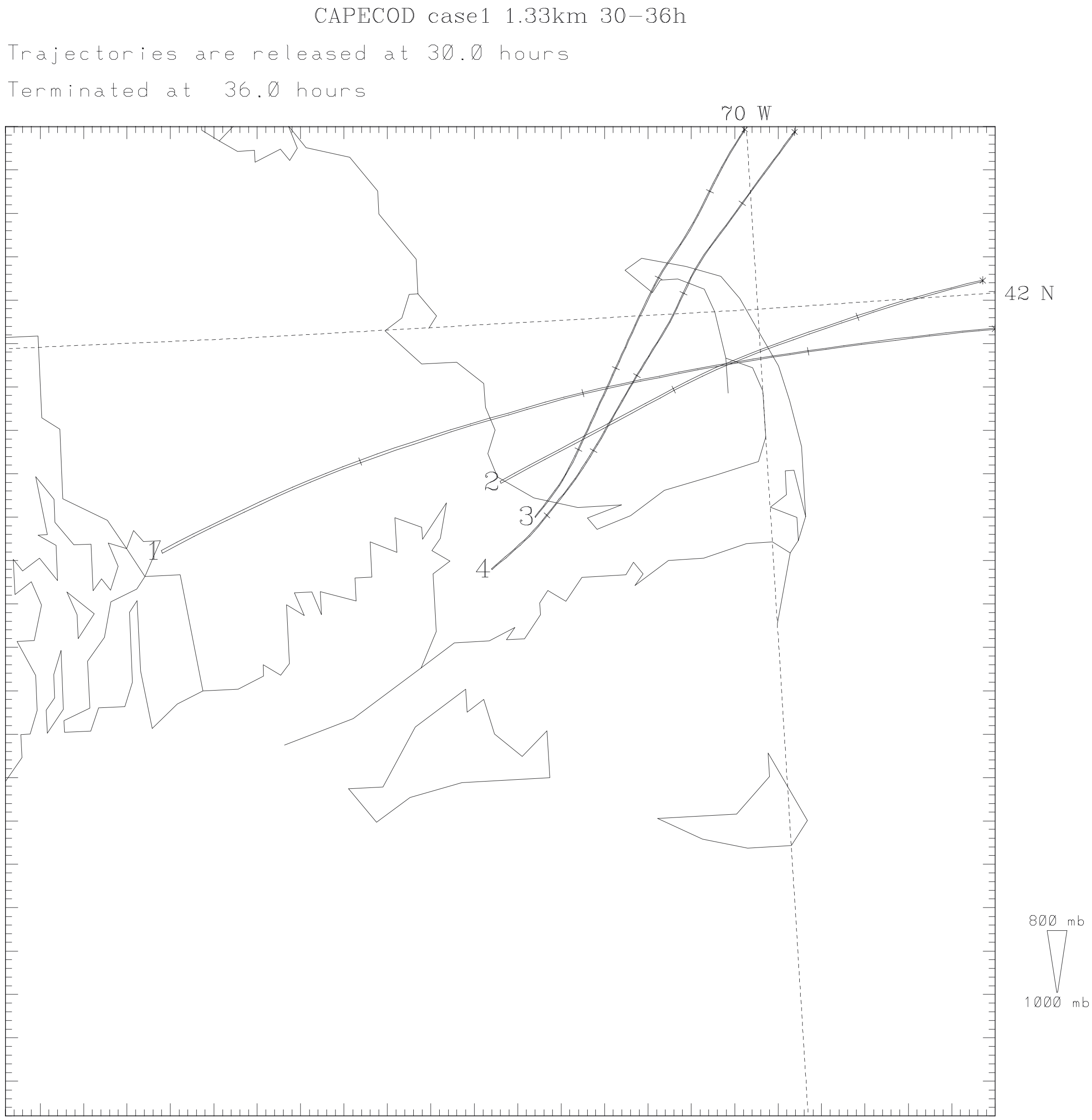

Figure 118. Six-hour TRAJEC forward trajectories based on MM5-simulated winds in Case 1. Release time is 0600 UTC, 2 July 2000 (+30 - 36 h). Parcel 1 is Brayton Point plant. Parcel 2 is Canal plant. Parcel 3 is middle of highway segment. Parcel 4 is Otis AFB. Tick marks shown on trajectories give positions at 1-h intervals, or until the parcels exit the domain.

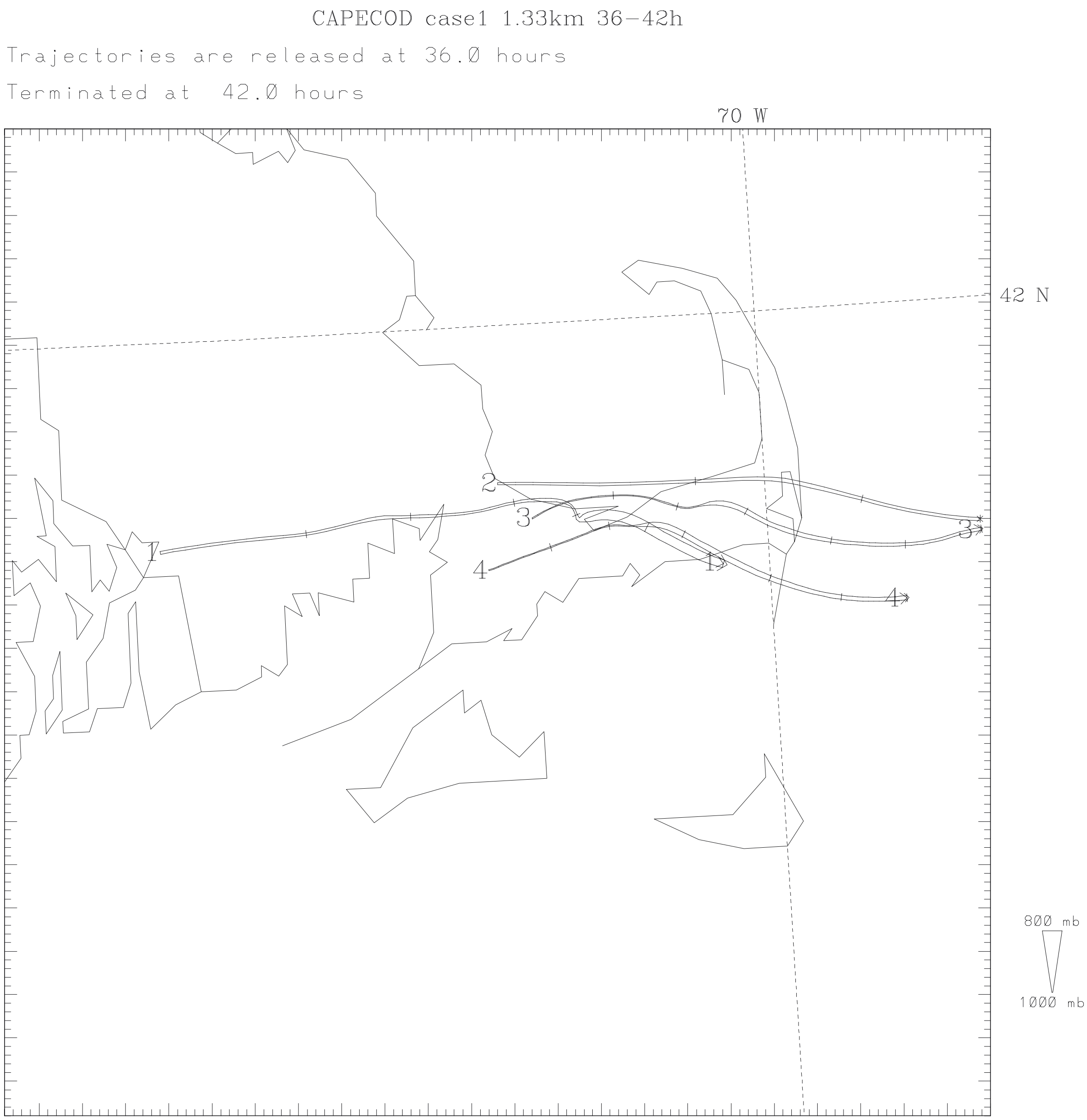

Figure 119. Six-hour TRAJEC forward trajectories based on MM5-simulated winds in Case 1. Release time is 1200 UTC, 2 July 2000 (+36 - 42 h). Parcel 1 is Brayton Point plant. Parcel 2 is Canal plant. Parcel 3 is middle of highway segment. Parcel 4 is Otis AFB. Tick marks shown on trajectories give positions at 1-h intervals, or until the parcels exit the domain.

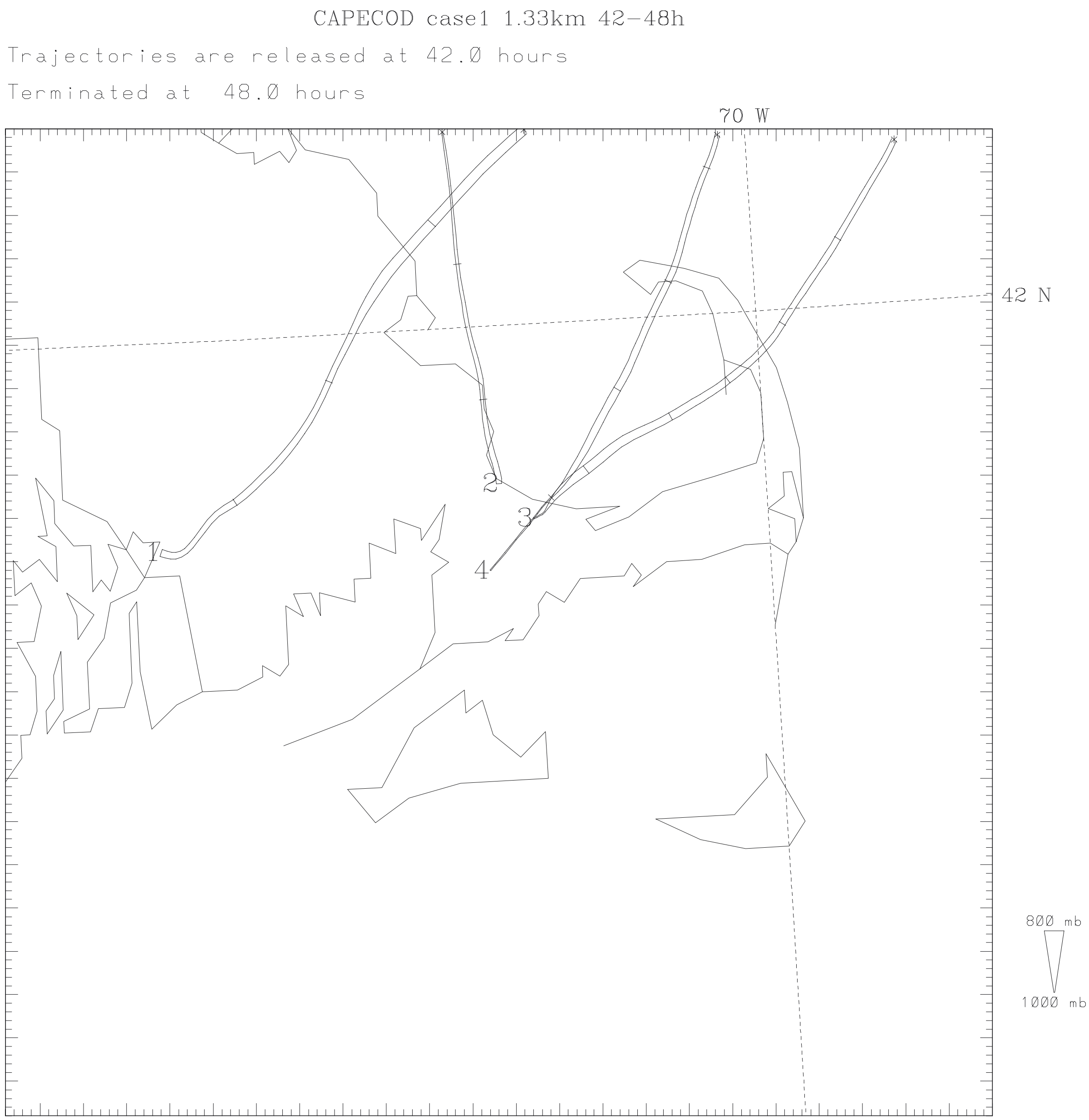

Figure 120. Six-hour TRAJEC forward trajectories based on MM5-simulated winds in Case 1. Release time is 1800 UTC, 2 July 2000 (+42 - 48 h). Parcel 1 is Brayton Point plant. Parcel 2 is Canal plant. Parcel 3 is middle of highway segment. Parcel 4 is Otis AFB. Tick marks shown on trajectories give positions at 1-h intervals, or until the parcels exit the domain.

For the same time segment, the other three parcels released on Upper Cape Cod (Parcels 2-4) become entrained into the rising plume that forms at the convergence point of three separate sea-breeze fronts during the late morning (about +3 h, or 1100 EDT) near Otis AFB (Figure 115). The result is that all three parcels are lofted rapidly to 900-800 mb (1000-2000 m MSL), after which they travel southeastward on the synoptic-scale mid-level winds. This result confirms the hypothesis that the convergence zone between two sea breezes (or, three sea breezes in this case) can be an effective region for removing surface-based emissions from the boundary layer. Once at this altitude, the horizontal winds carry the parcels seaward over regions where the PBL is much more shallow, and where they can remain in a zone that is no longer in contact (through turbulent mixing) with the surface. It should be noted, however, that since the sea breeze convergence zones are constantly evolving and moving (compare Figures 31 and 33), the effect of these zones on the emitted plumes can change considerably over time.

Next, during the late afternoon on 1 July, Figure 116 shows the parcels from the four emission sites traveling north or northeast on the matured sea-breeze winds (compare with Figure 33). The most notable feature at this time can be seen by examining the trajectory of Parcel 4 between +18 - 24 h. Emitted near the surface from Otis AFB, Parcel 4 travels northward over land for 1.5 h (until 1530 EDT). After remaining close to the surface for the first 45 minutes, it encounters a convergence zone located at that time near the Canal plant, where it rises to ~900 mb (~1000 m). Since the southerly winds have become quite deep by this time, Parcel 4 continues northward over Massachusetts Bay. However, over the Bay, Parcel 4 begins gradually sinking again, because the return branch of the sea breeze over the water must subside to compensate for the low-level advection of air mass that is directed onshore. By about +21 h (1700 EDT), the Parcel 4 has subsided to ~950 mb (~500 m MSL) after which it leaves the 1.33-km domain. This behavior is thoroughly consistent with the expected circulations in a complex sea-breeze environment.

Figures 117 and 118 show the parcel trajectories on the second night of Case 1. The parcels travel with the southwesterly winds in the stable nocturnal regime. It should be pointed out, however, that the plumes from the power plants (Parcels 1 and 2) experience gradual subsidence, especially over the water. This is consistent with the SCIPUFF results during the nocturnal periods, which showed that the highest surface concentrations were located well downwind of the source points for these plants.

On the second day, Figures 119 and 120 show the trajectories as the sea breeze re-developed. However, since the synoptic-scale winds had become southwesterly by this time, the sharp changes in parcel directions are not as evident on this day. Note that Figure 120 shows the plume from the Canal plant (Parcel 2) moving northward close to the west shore of Massachusetts Bay in response to the mature sea breeze in that area (also see Figure 36), while the other parcels travel toward the northeast. Again, this reveals the complexity of the 3-D flow in such cases and the strong directional shear at different levels. As on 1 July, Parcel 2 experiences significant sinking motions in the return branch of the east Massachusetts sea breeze, while the other parcels farther from land experience negligible sinking.

4.4.1.2 Case 2 Trajectories

Next, Figures 121-128 present the TRAJEC results for Case 2 (5-6 July 2000). In this second sea-breeze case, Figures 121 and 122 show all parcels traveling toward the northeast or east on the pre-frontal southwesterly flow that prevailed in this region early in the period (see also

Figure 15). It should be noted that, because of the strong winds ahead of the front, these parcels do not remain inside the 1.33-km domain for the full 6-h segments. Figure 121 indicates that, between +0 - 6 h, the parcels leave the domain after about 4 h. Later that night, as the front is approaching Cape Cod, Figure 122 shows that the parcels leave the eastern side of the domain only ~3 h after their release (+9 h, or 0900 UTC). The next morning, the time segment shown in Figure 123 for +12 - 18 h shows the impact of the winds in the post-frontal environment. As expected, the parcels now head directly southward and out to sea within a couple of hours on the brisk northerly winds behind the front. By the time the sea breeze develops over Upper Cape Cod and southeastern MA later in the morning, these parcels are well to the south and away from its influence.

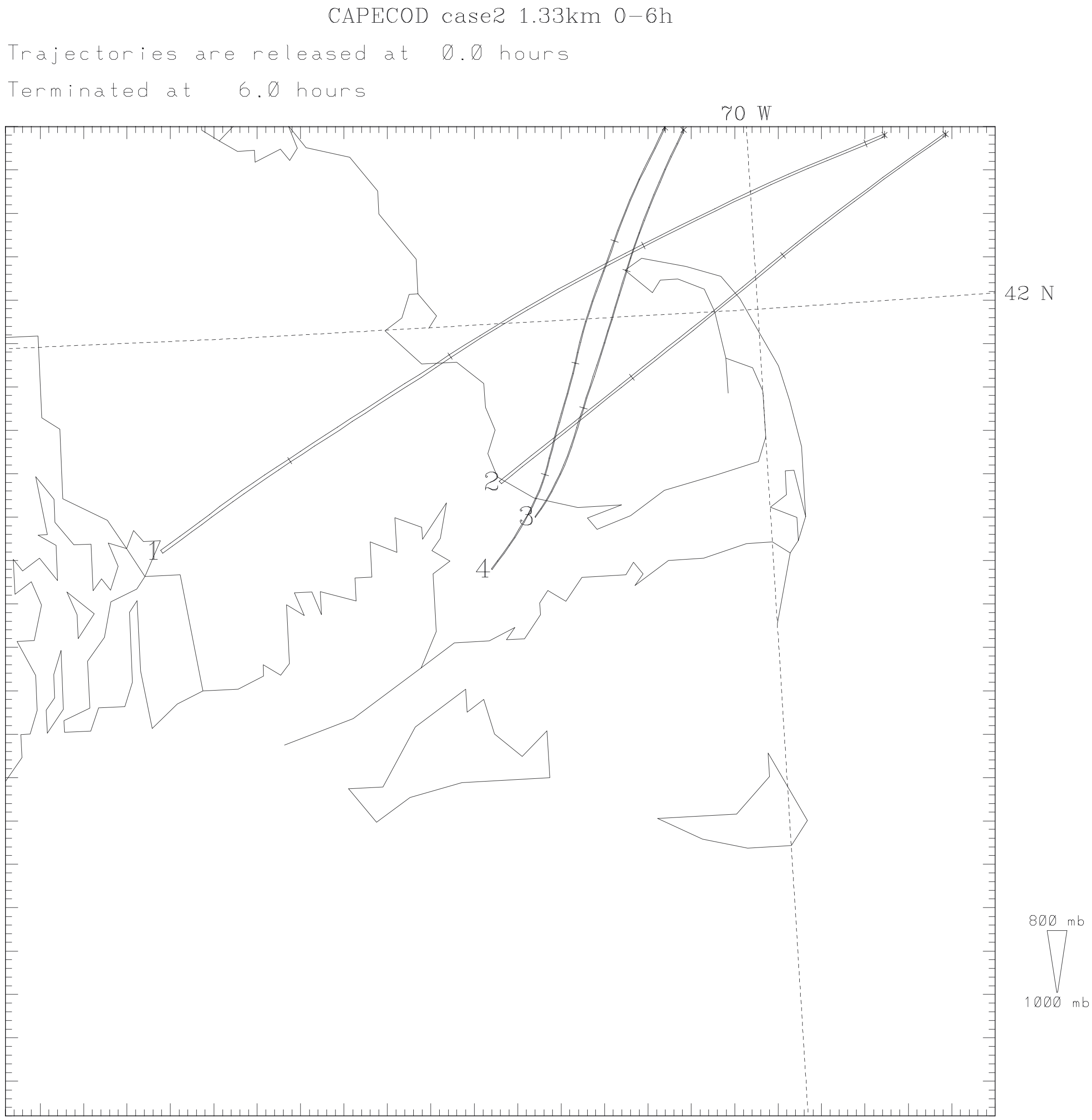

Figure 121. Six-hour TRAJEC forward trajectories based on MM5-simulated winds in Case 2. Release time is 0000 UTC, 5 July 2000 (+0 - 6 h). Parcel 1 is Brayton Point plant. Parcel 2 is Canal plant. Parcel 3 is middle of highway segment. Parcel 4 is Otis AFB. Tick marks shown on trajectories give positions at 1-h intervals, or until the parcels exit the domain.

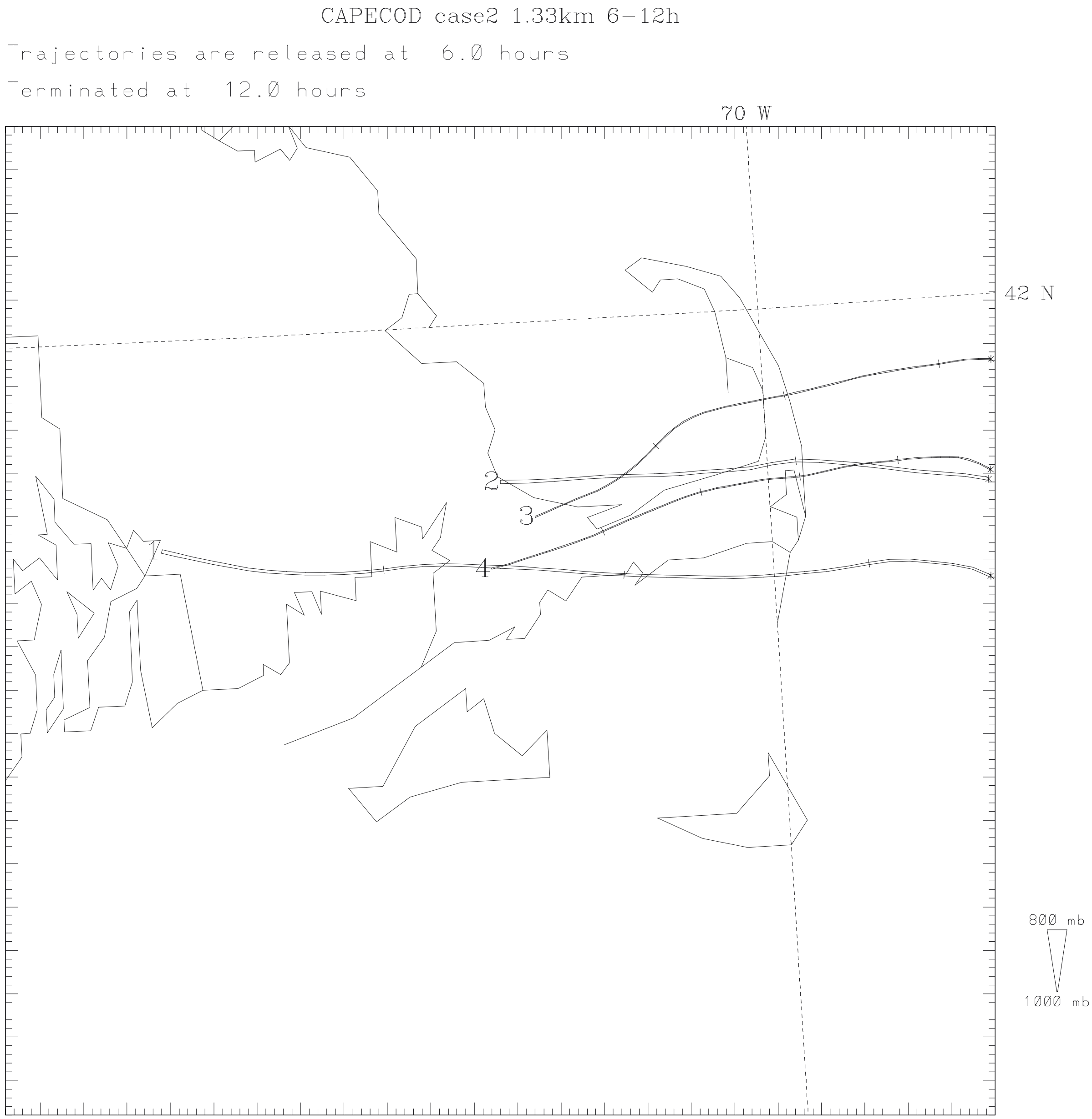

Figure 122. Six-hour TRAJEC forward trajectories based on MM5-simulated winds in Case 2. Release time is 0600 UTC, 5 July 2000 (+6 - 12 h). Parcel 1 is Brayton Point plant. Parcel 2 is Canal plant. Parcel 3 is middle of highway segment. Parcel 4 is Otis AFB. Tick marks shown on trajectories give positions at 1-h intervals, or until the parcels exit the domain.

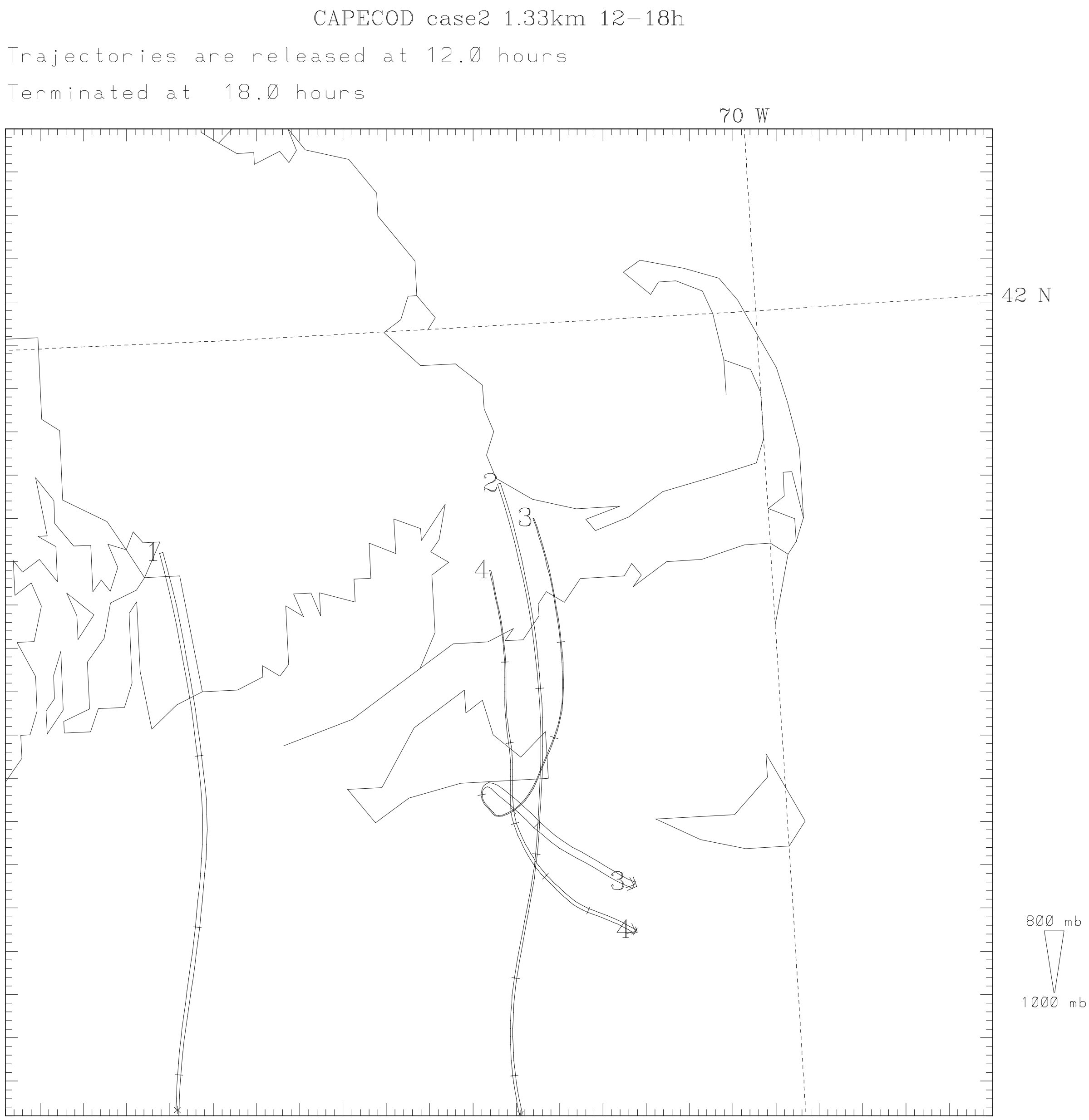

Figure 123. Six-hour TRAJEC forward trajectories based on MM5-simulated winds in Case 2. Release time is 1200 UTC, 5 July 2000 (+12 - 18 h). Parcel 1 is Brayton Point plant. Parcel 2 is Canal plant. Parcel 3 is middle of highway segment. Parcel 4 is Otis AFB. Tick marks shown on trajectories give positions at 1-h intervals, or until the parcels exit the domain.

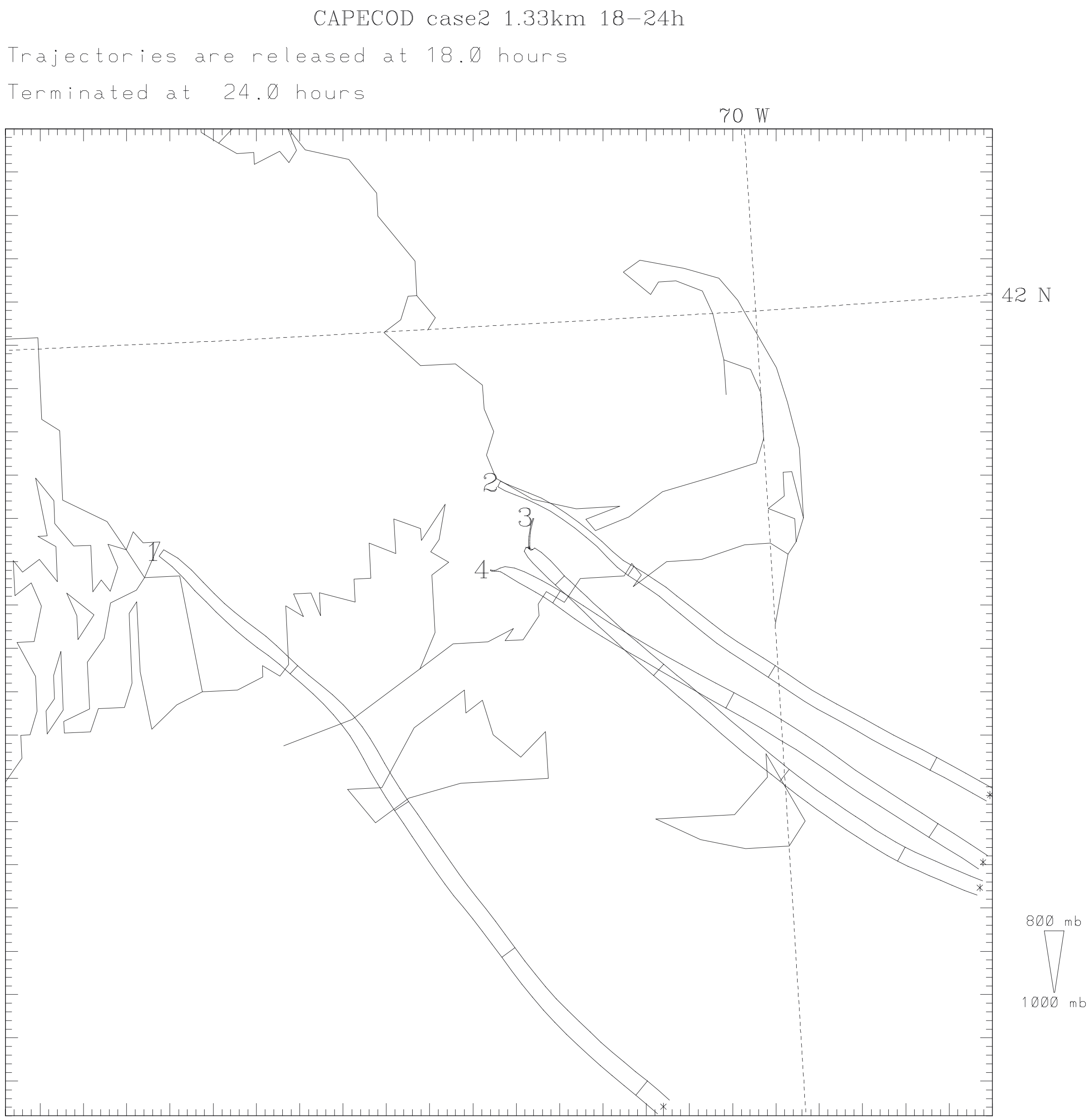

Figure 124. Six-hour TRAJEC forward trajectories based on MM5-simulated winds in Case 2. Release time is 1800 UTC, 5 July 2000 (+18 - 24 h). Parcel 1 is Brayton Point plant. Parcel 2 is Canal plant. Parcel 3 is middle of highway segment. Parcel 4 is Otis AFB. Tick marks shown on trajectories give positions at 1-h intervals, or until the parcels exit the domain.

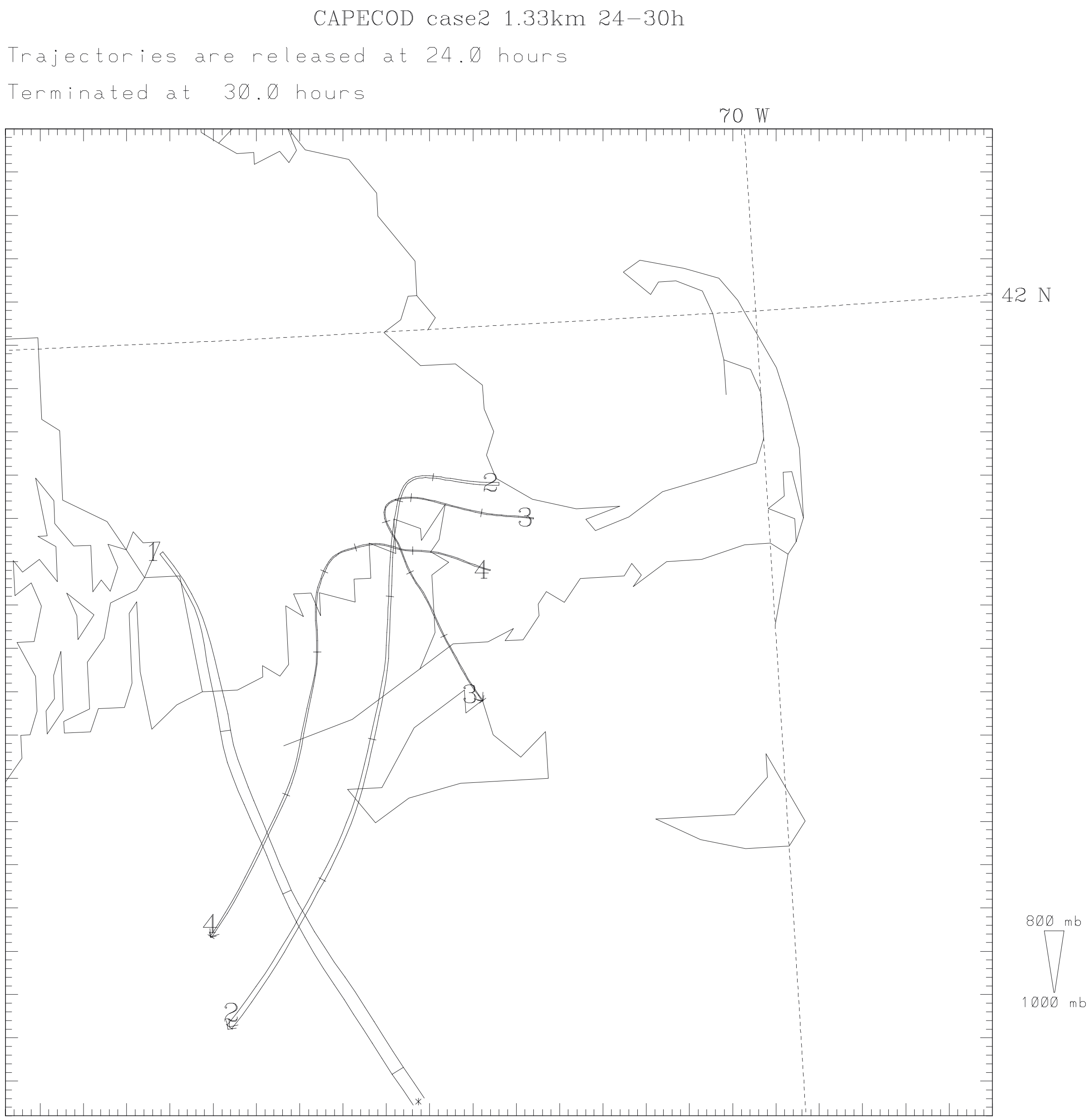

Figure 125. Six-hour TRAJEC forward trajectories based on MM5-simulated winds in Case 2. Release time is 0000 UTC, 6 July 2000 (+24 - 30 h). Parcel 1 is Brayton Point plant. Parcel 2 is Canal plant. Parcel 3 is middle of highway segment. Parcel 4 is Otis AFB. Tick marks shown on trajectories give positions at 1-h intervals, or until the parcels exit the domain.

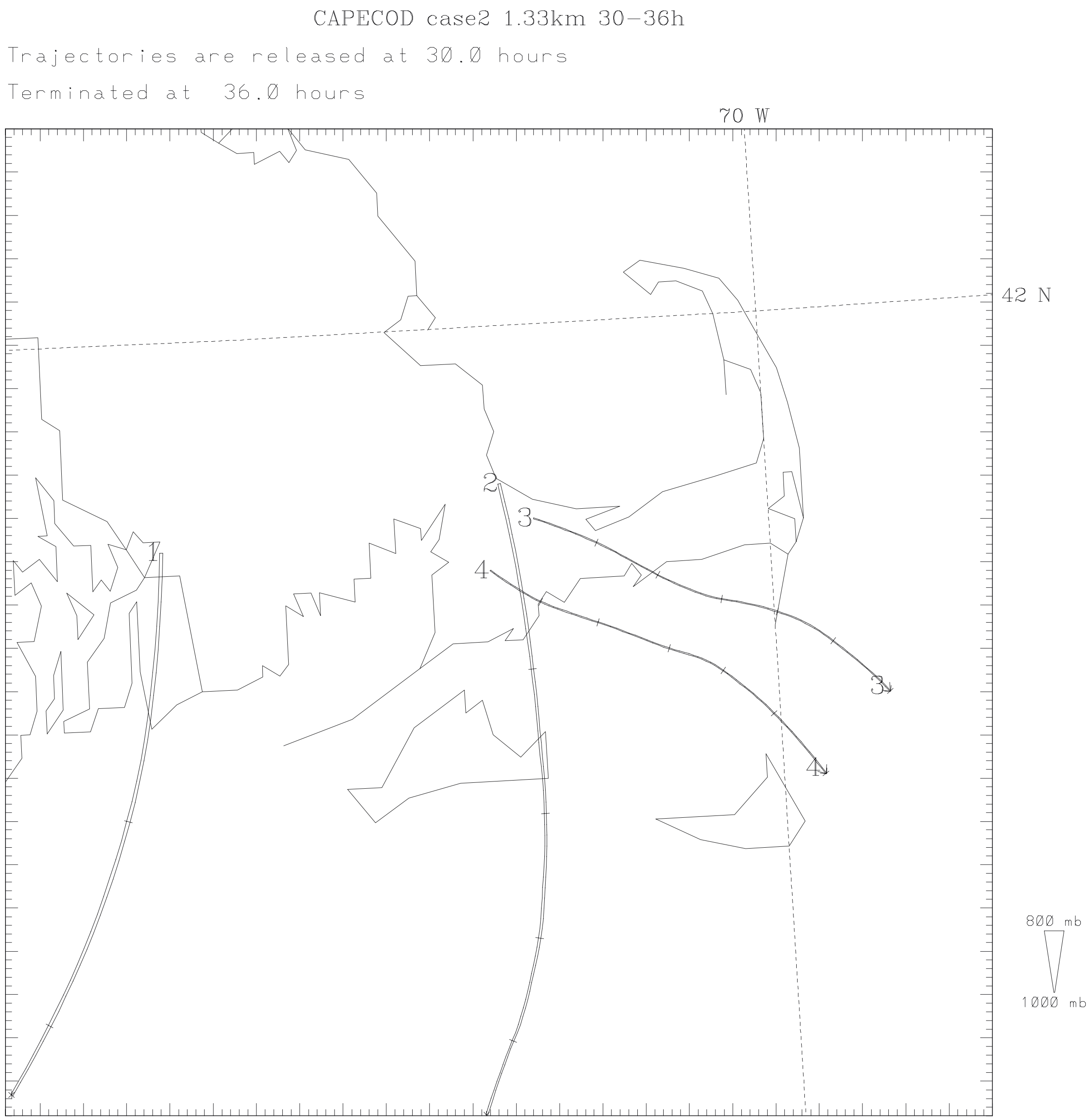

Figure 126. Six-hour TRAJEC forward trajectories based on MM5-simulated winds in Case 2. Release time is 0600 UTC, 6 July 2000 (+30 - 36 h). Parcel 1 is Brayton Point plant. Parcel 2 is Canal plant. Parcel 3 is middle of highway segment. Parcel 4 is Otis AFB. Tick marks shown on trajectories give positions at 1-h intervals, or until the parcels exit the domain.

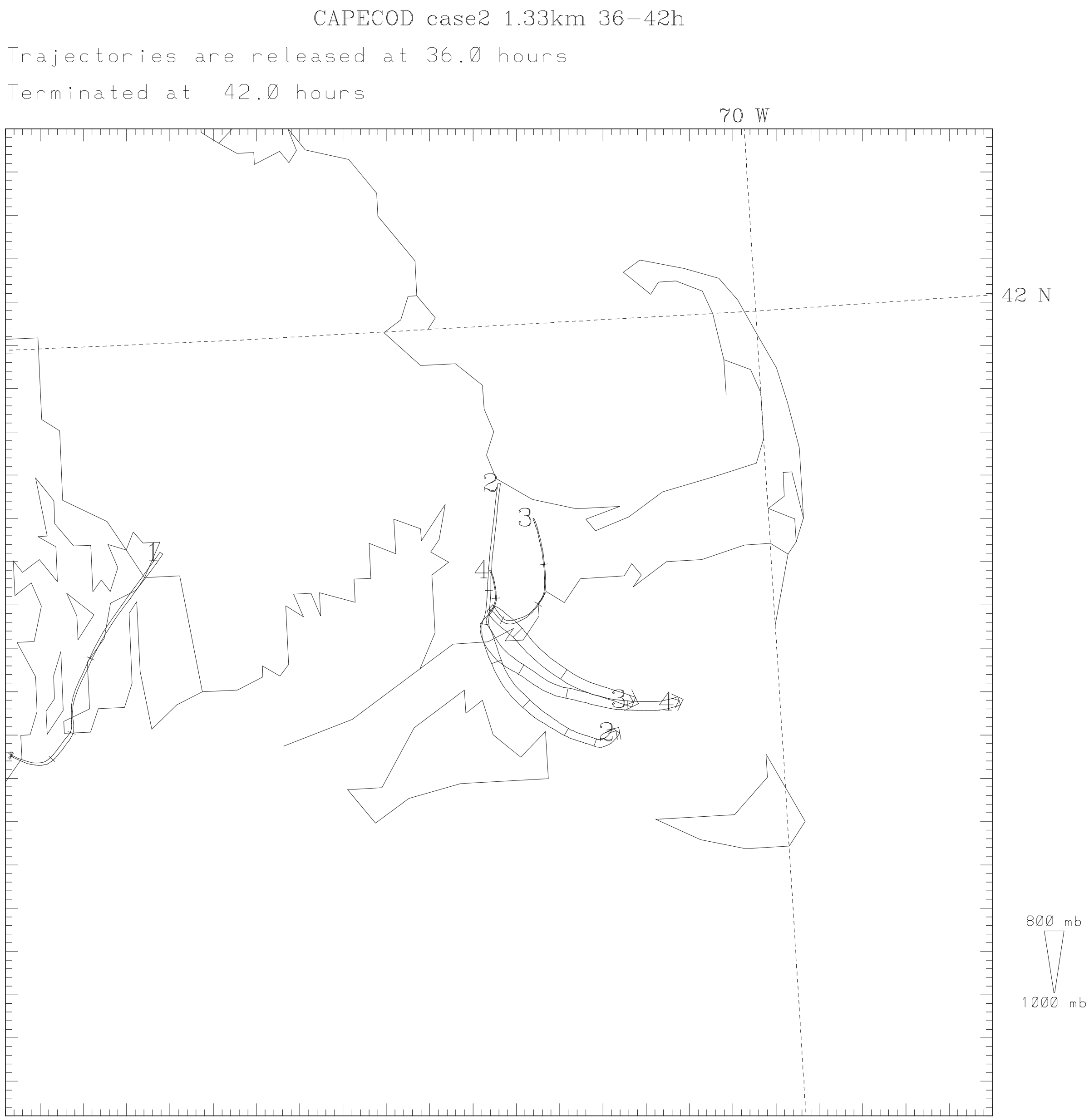

Figure 127. Six-hour TRAJEC forward trajectories based on MM5-simulated winds in Case 2. Release time is 1200 UTC, 6 July 2000 (+36 - 42 h). Parcel 1 is Brayton Point plant. Parcel 2 is Canal plant. Parcel 3 is middle of highway segment. Parcel 4 is Otis AFB. Tick marks shown on trajectories give positions at 1-h intervals, or until the parcels exit the domain.

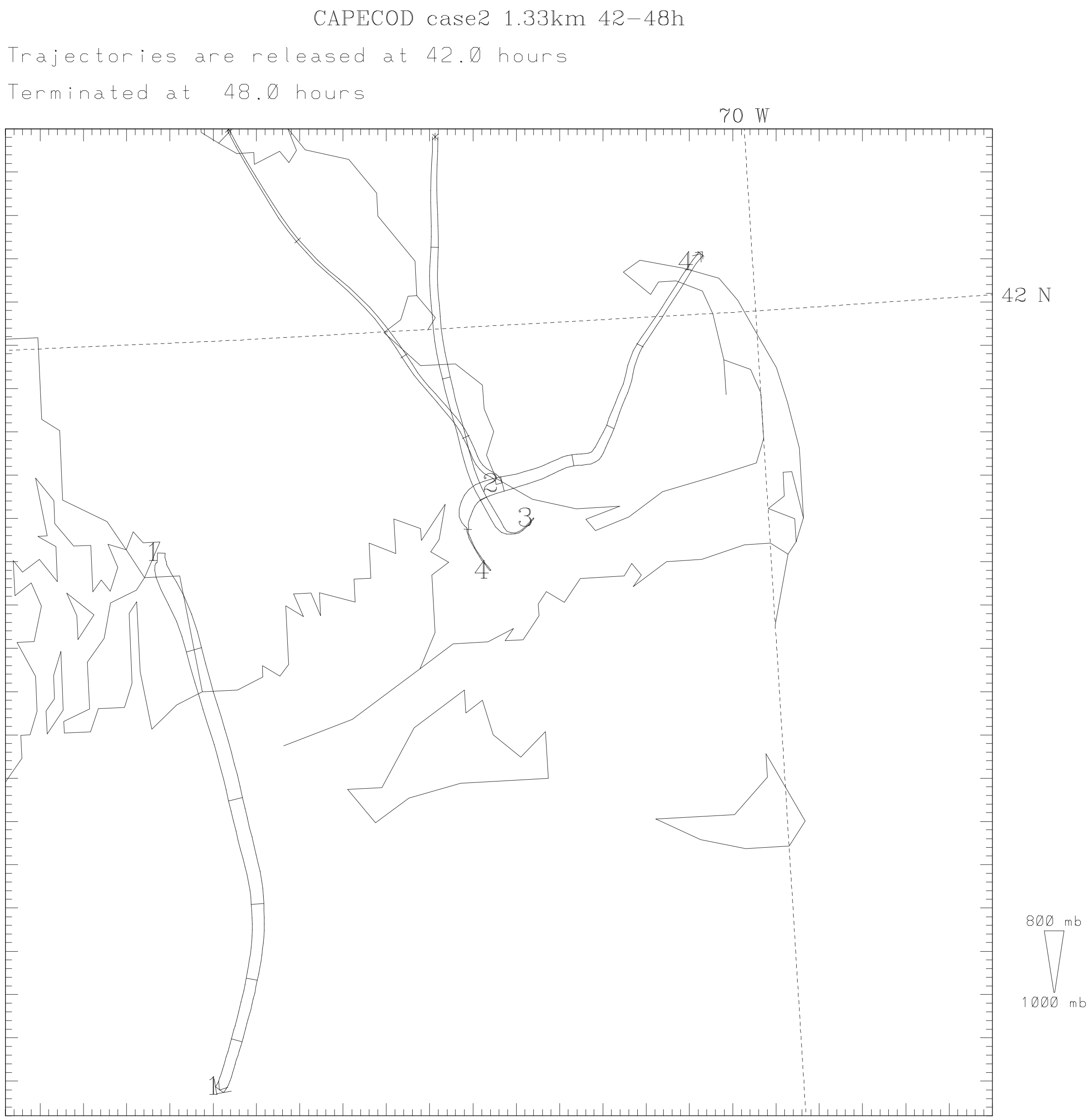

Figure 128. Six-hour TRAJEC forward trajectories based on MM5-simulated winds in Case 2. Release time is 1800 UTC, 6 July 2000 (+42 - 48 h). Parcel 1 is Brayton Point plant. Parcel 2 is Canal plant. Parcel 3 is middle of highway segment. Parcel 4 is Otis AFB. Tick marks shown on trajectories give positions at 1-h intervals, or until the parcels exit the domain.

The lone exception to this pattern in Figure 123 can be seen in the trajectory for Parcel 3, which was emitted along the highway (MA Routes 3 and 6). This parcel initially remains close to the surface as it travels southward across Upper Cape Cod and just to the east of Martha's Vineyard. Once it reaches the southeast end of the island about + 14.5 h (1030 EDT), it becomes entrained into a newly formed island breeze that forms in the lee (south) of Martha's Vineyard. The island breeze first causes deceleration and then a reversal of the direction of the parcel, so that it begins heading slowly northward around +16 h (1200 EDT). As Parcel 4 approaches the south shore of the island, it encounters a local convergence zone that rapidly lifts it to about ~600 m MSL. At this height, it is above the island breeze, so that it again heads southward and out to sea. A remnant of this island-breeze convergence zone can be seen several hours later at 1800 UTC (1400 EDT) in Figure 40.

On the afternoon of 5 July in Case 2, Figure 124 shows that the parcels released from all four sites travel toward the southeast at 1.5-2.0 km MSL. Emitted near +18 h (1400 EDT), even Parcels 3 and 4 rise rapidly from the surface to high levels due to the strong convergence zones over Upper Cape Cod (see Figure 40). Once aloft, they follow the synoptic wind directions, as shown in Figure 41. By the second evening, Figure 125 reveals a curious trajectory pattern for the four parcels that originate at 0000 UTC, 6 July (+24 h). Parcels 1 and 3 turn toward the southeast over the Atlantic Ocean, even though Parcel 1 rises to over 1000 m MSL before leaving the coast, while Parcel 3 remains very close to the surface. Meanwhile, Parcels 2 and 4 are advected toward the southwest, even though their points of origin approximately bracket that of Parcel 3. These trajectories illustrate how subtle difference in height and speed of parcels, relative to the changing wind pattern, can lead to unusual advection patterns.

Later on the night of 6 July, between + 30 - 36 h, the pattern shown in Figure 126 is much easier to interpret. The two low-level trajectories for Parcels 3 and 4 travel toward the southeast. Meanwhile, the winds aloft are more northerly, so Parcels 1 and 2 head toward the south. Also note that the winds aloft are considerably faster than at the surface due to the virtual absence of the influence of surface friction. Thus, Parcels 1 and 2 leave the 1.33-km domain in 3 - 5 h, while parcels 3 and 4 remain well inside the domain after 6 h.

On the second day of Case 2, Figure 127 shows the influence of the reinvigorated sea breeze. Parcels 2-4 initially travel southward over Upper Cape Cod and then encounter the sea-breeze front during its early stage of development just north of the south shore around +39 h (1100 EDT). When they encounter the front, the parcels rise rapidly to around 1000 m, after which they are advected east-southeastward in the upper level wind above the sea breeze. Once this return branch of the sea breeze carries the parcels over the ocean, they begin to gradually subside east of Martha's Vineyard (especially noticeable in the trajectory of Parcel 2). Finally, during the late afternoon o 6 July (+42 - 48 h), Figure 128 shows a very complex set of trajectories, with each parcel heading in a different direction. This pattern is related to a weak and highly variable synoptic wind pattern over the 1.33-km domain at this time, especially in the higher levels (see Figure 45).

4.4.1.3 Case 3 Trajectories

The final set of trajectories, calculated from the MM5 solutions for Case 3 (21-22 August 2000), are presented in Figures 129-136. Recall that in Case 3, the land breeze was the primary focus of the experiment, although daytime sea breezes developed as well. First, Figures 129 and 130 present the trajectories of Parcels 1-4 on the first night, from +0 - 6 h and +6 - 12 h, respectively. For both 6-h time segments the parcels travel southeastward at moderate speed and most of them leave the domain before the periods are completed (also see Figure 48). In Figure 129, Parcel 1 from the Brayton Point plant does not appear to change altitude significantly, although in Figure 130 (+6 - 12 h), it appears to sink very slowly once it leaves land. For the other elevated plume, Parcel 2 from the Canal plant sinks toward the surface during the first 6-h segment (Figure 129), but the sinking motion is less evident later in Figure 130. In Figure 130, some modest directional shear is evident between the surface layer (where Parcels 3 and 4 are released) and the layers several hundred meters above MSL (where Parcel 2 is released). Otherwise, the parcel trajectories give no evidence of significant wind divergence during the first night.

During the morning hours, Figure 131 shows that the parcels emitted at 1200 UTC, 21 August, are still under the influence of north-northwesterly winds, so that all four parcels are quickly advected south of Nantucket and Martha's Vineyard before mid-morning. Thus, by the time that the sea breeze develops in the late morning, the parcels are much too far south over the ocean to respond to the sea breeze. However, by the time that the next set of parcels is released at 1800 UTC (1400 EDT), 21 August, Figure 132 shows that they encounter a fairly well developed sea-breeze circulation. There is still a fairly strong background northerly wind component on this afternoon (Figure 24), so all the parcels initially move toward the south shore. Parcel 1, released at nearly 700 m MSL in the unstable afternoon PBL (see Table 22), soon rises farther to around 1200 m MSL as it encounters the sea-breeze front over the eastern border of RI. Once it rises to this level, it proceeds rapidly south southeastward on brisk winds. Meanwhile, Figure 132 shows that Parcels 3-4 encounter a sea-breeze frontal zones very close to the south shore of Upper Cape Cod. The moderate background winds from the north prevented the sea breeze from penetrating very far inland on 21 August, so these two parcels are able to rise from the surface layer to 800-1000 m MSL only when they are within 4 km of the coast. Once they rise above the sea-breeze circulation in the vertical winds of this convergence zone, they are accelerated south southeastward in the same mid-level flow that affects Parcel 1.

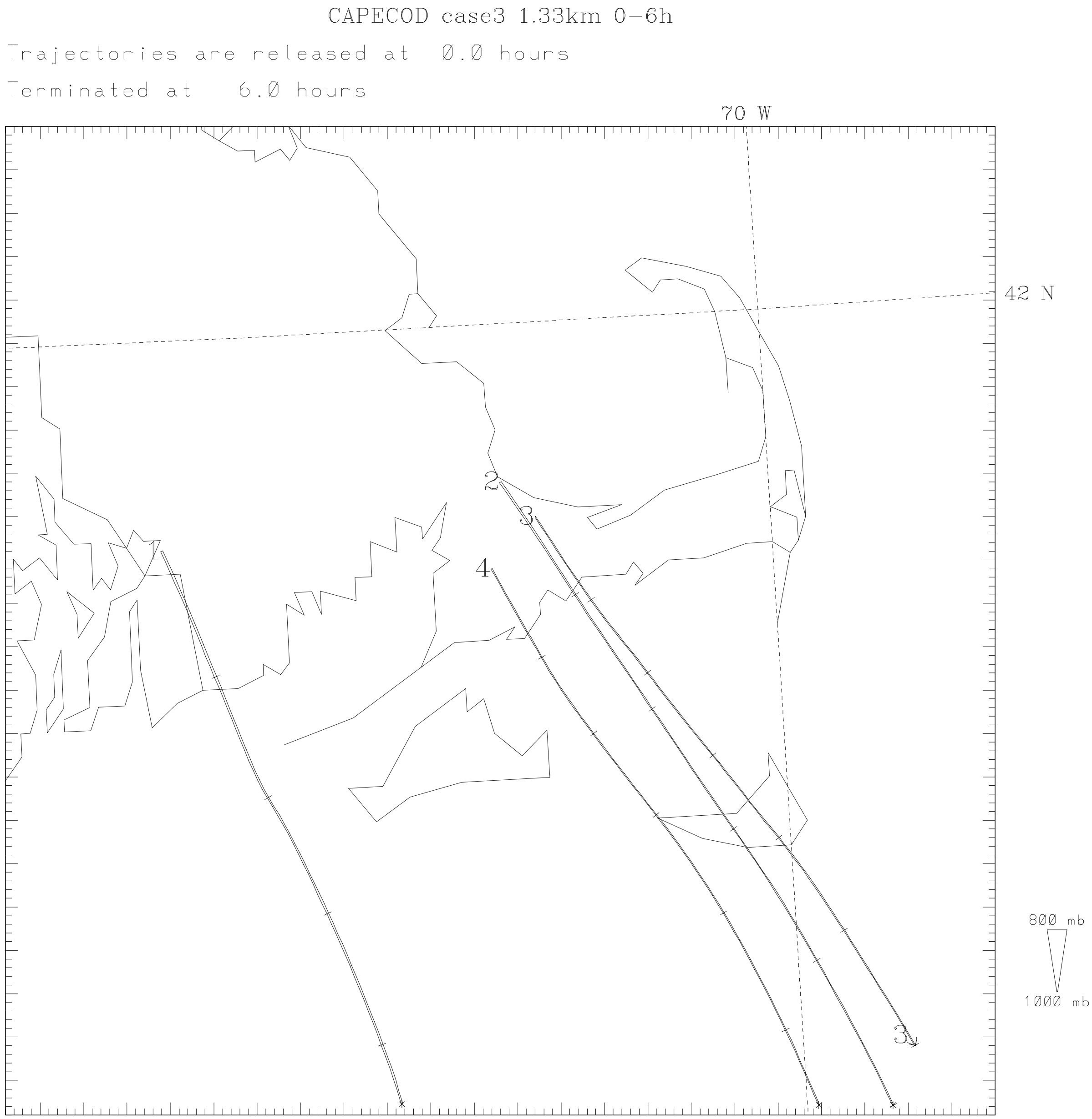

Figure 129. Six-hour TRAJEC forward trajectories based on MM5-simulated winds in Case 3. Release time is 0000 UTC, 21 August 2000 (+0 - 6 h). Parcel 1 is Brayton Point plant. Parcel 2 is Canal plant. Parcel 3 is middle of highway segment. Parcel 4 is Otis AFB. Tick marks shown on trajectories give positions at 1-h intervals, or until the parcels exit the domain.

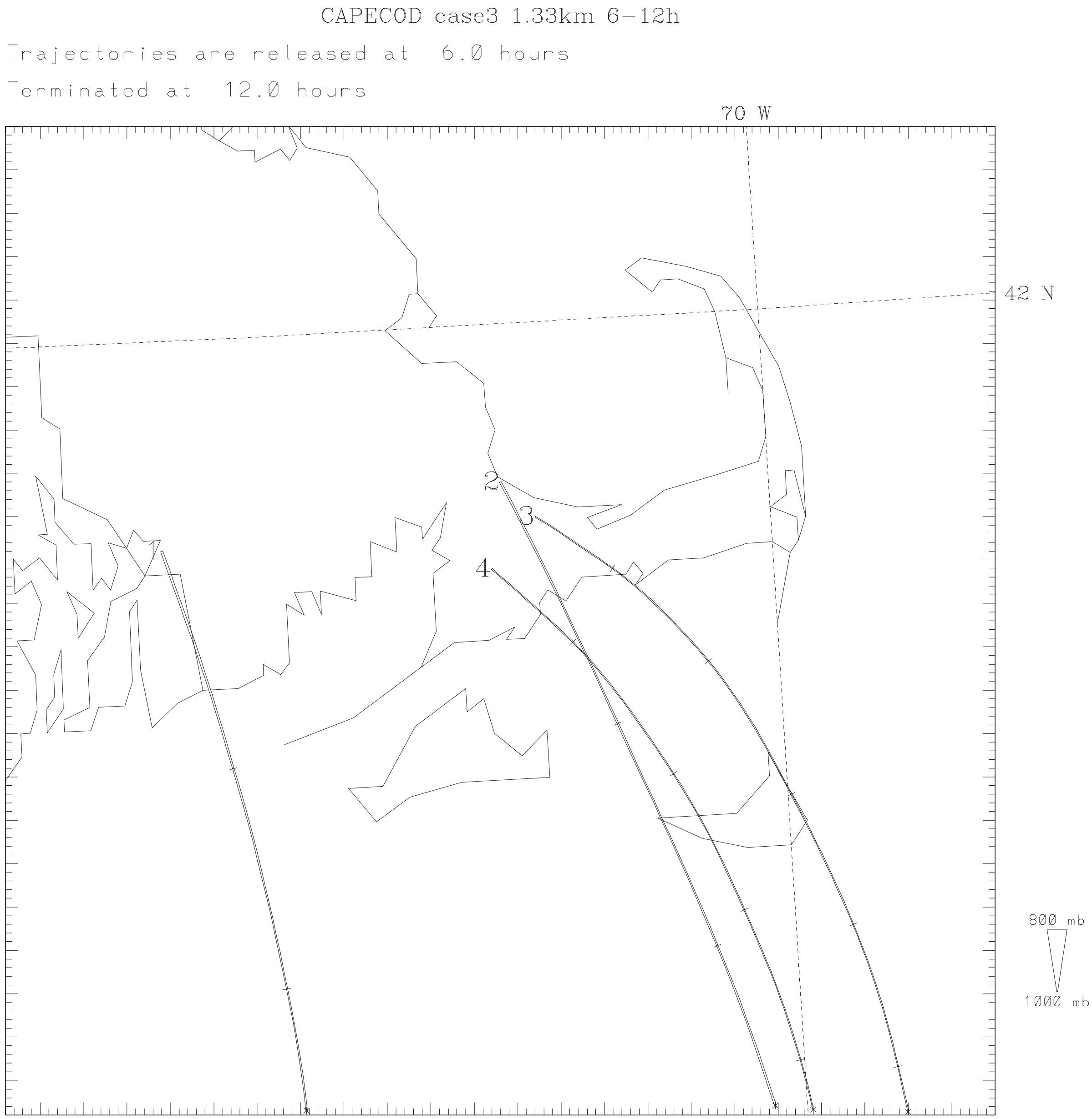

Figure 130. Six-hour TRAJEC forward trajectories based on MM5-simulated winds in Case 3. Release time is 0600 UTC, 21 August 2000 (+6 - 12 h). Parcel 1 is Brayton Point plant. Parcel 2 is Canal plant. Parcel 3 is middle of highway segment. Parcel 4 is Otis AFB. Tick marks shown on trajectories give positions at 1-h intervals, or until the parcels exit the domain.

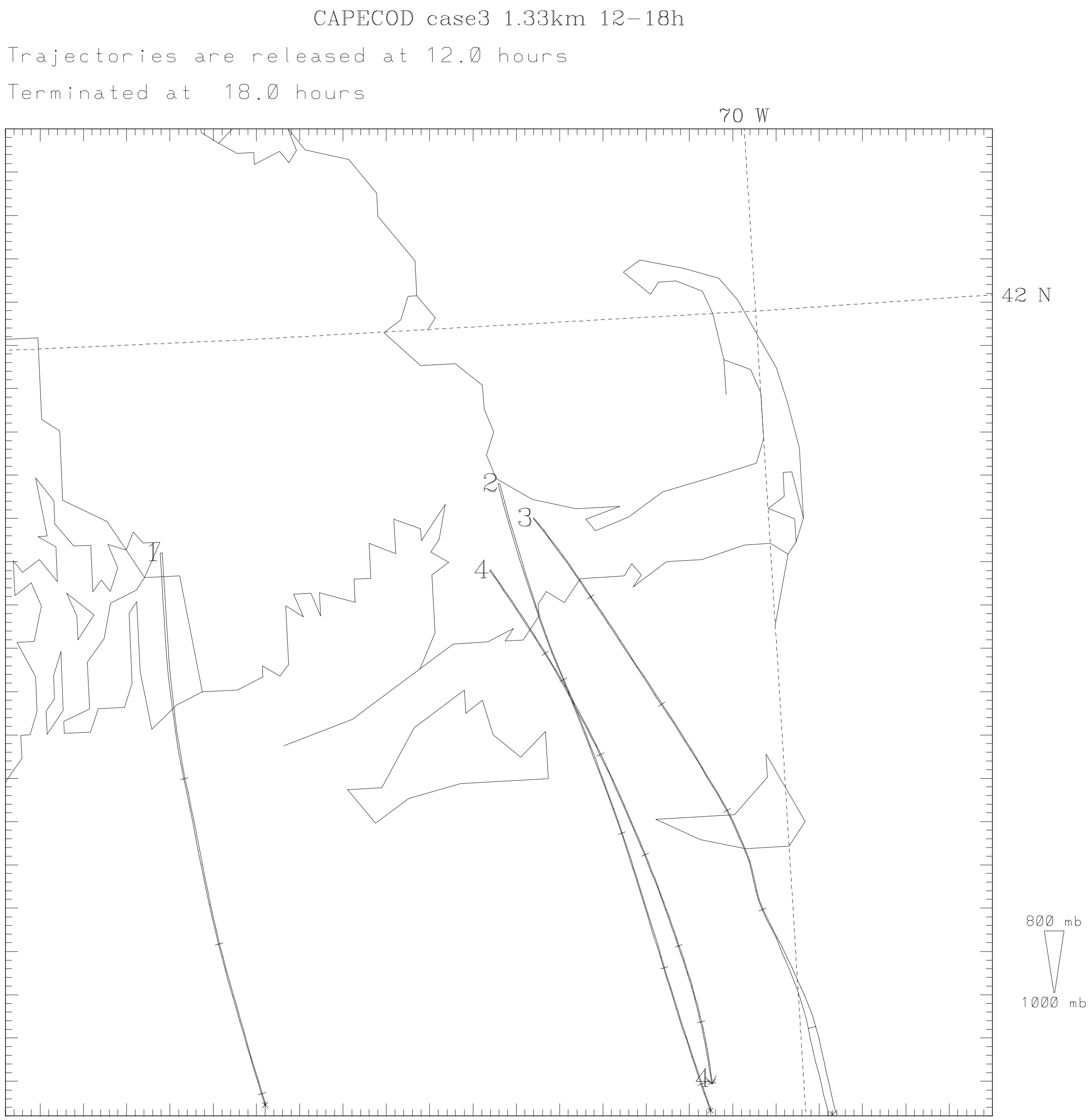

Figure 131. Six-hour TRAJEC forward trajectories based on MM5-simulated winds in Case 3. Release time is 1200 UTC, 21 August 2000 (+12 - 18 h). Parcel 1 is Brayton Point plant. Parcel 2 is Canal plant. Parcel 3 is middle of highway segment. Parcel 4 is Otis AFB. Tick marks shown on trajectories give positions at 1-h intervals, or until the parcels exit the domain.

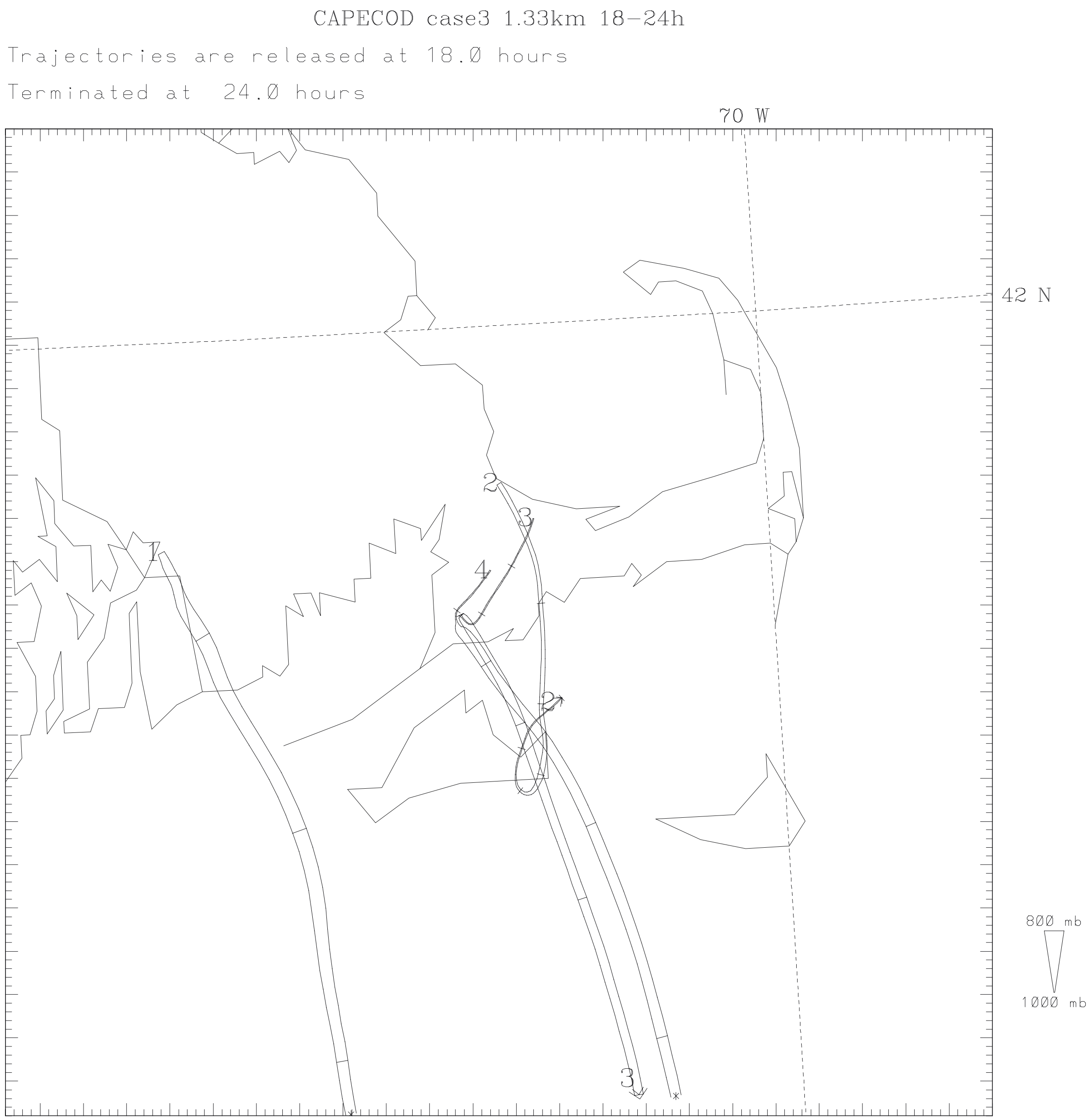

Figure 132. Six-hour TRAJEC forward trajectories based on MM5-simulated winds in Case 3. Release time is 1800 UTC, 21 August 2000 (+18 - 24 h). Parcel 1 is Brayton Point plant. Parcel 2 is Canal plant. Parcel 3 is middle of highway segment. Parcel 4 is Otis AFB. Tick marks shown on trajectories give positions at 1-h intervals, or until the parcels exit the domain.

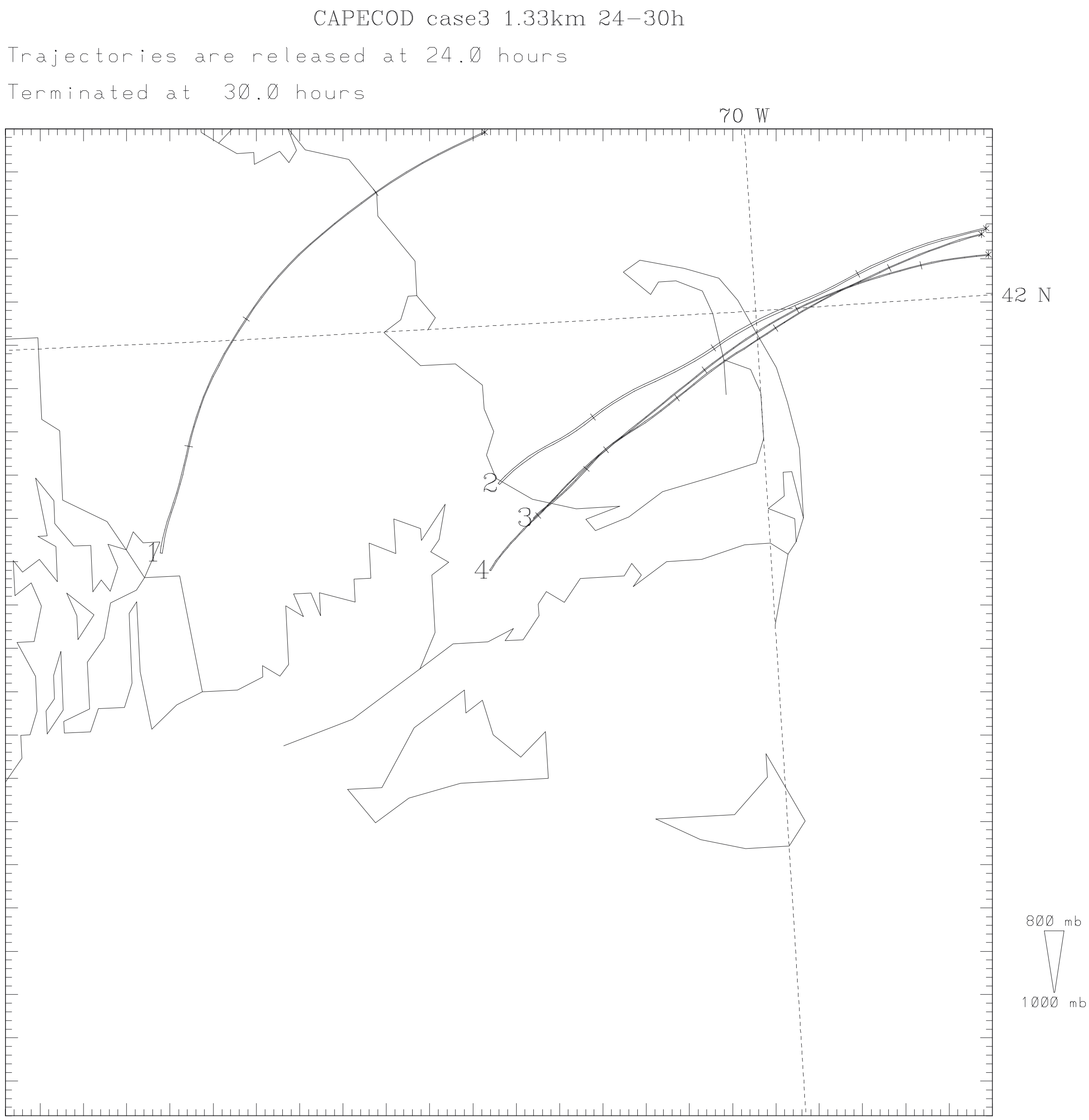

Figure 133. Six-hour TRAJEC forward trajectories based on MM5-simulated winds in Case 3. Release time is 0000 UTC, 22 August 2000 (+24 - 30 h). Parcel 1 is Brayton Point plant. Parcel 2 is Canal plant. Parcel 3 is middle of highway segment. Parcel 4 is Otis AFB. Tick marks shown on trajectories give positions at 1-h intervals, or until the parcels exit the domain.

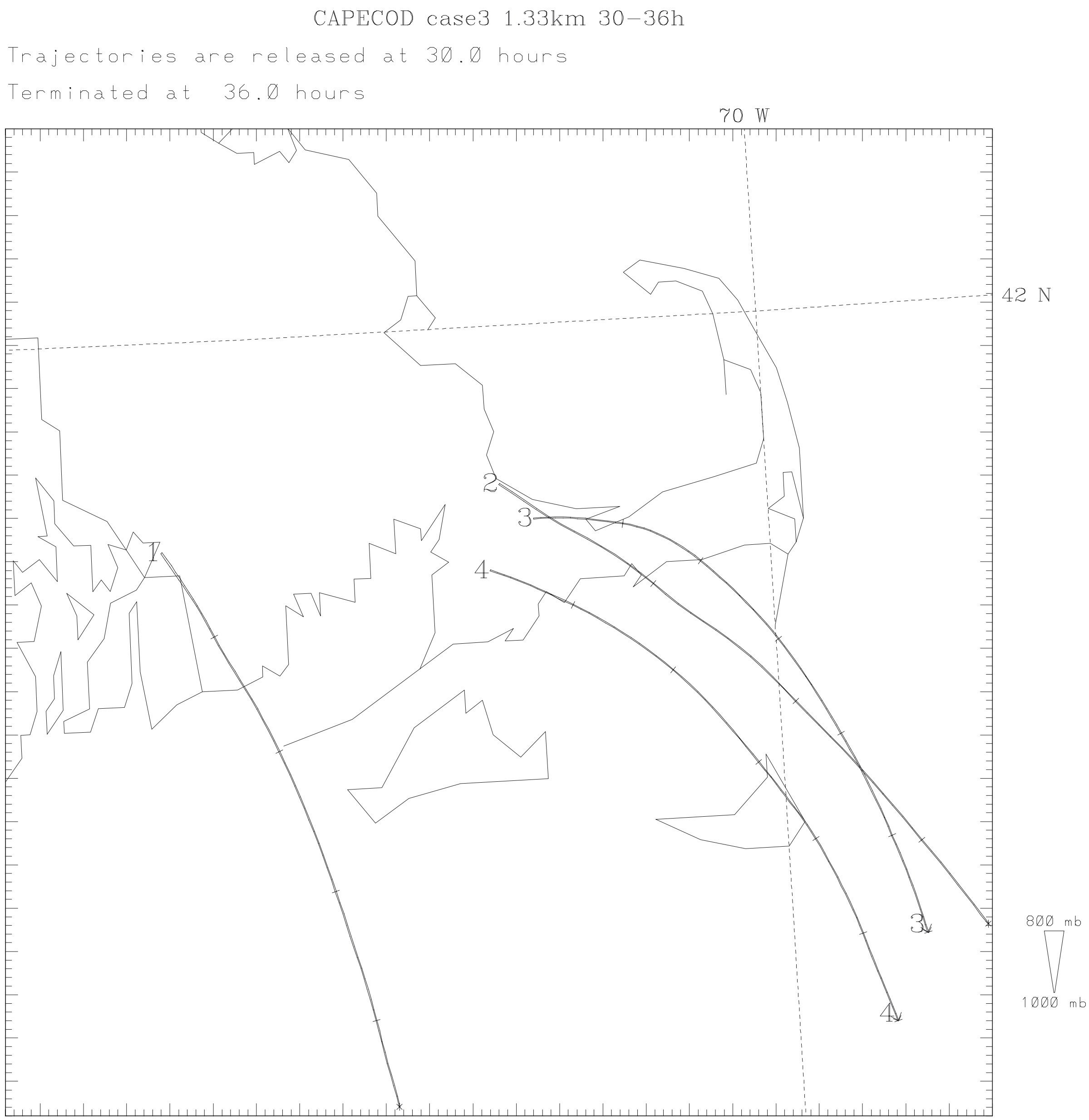

Figure 134. Six-hour TRAJEC forward trajectories based on MM5-simulated winds in Case 3. Release time is 0600 UTC, 22 August 2000 (+30 - 36 h). Parcel 1 is Brayton Point plant. Parcel 2 is Canal plant. Parcel 3 is middle of highway segment. Parcel 4 is Otis AFB. Tick marks shown on trajectories give positions at 1-h intervals, or until the parcels exit the domain.

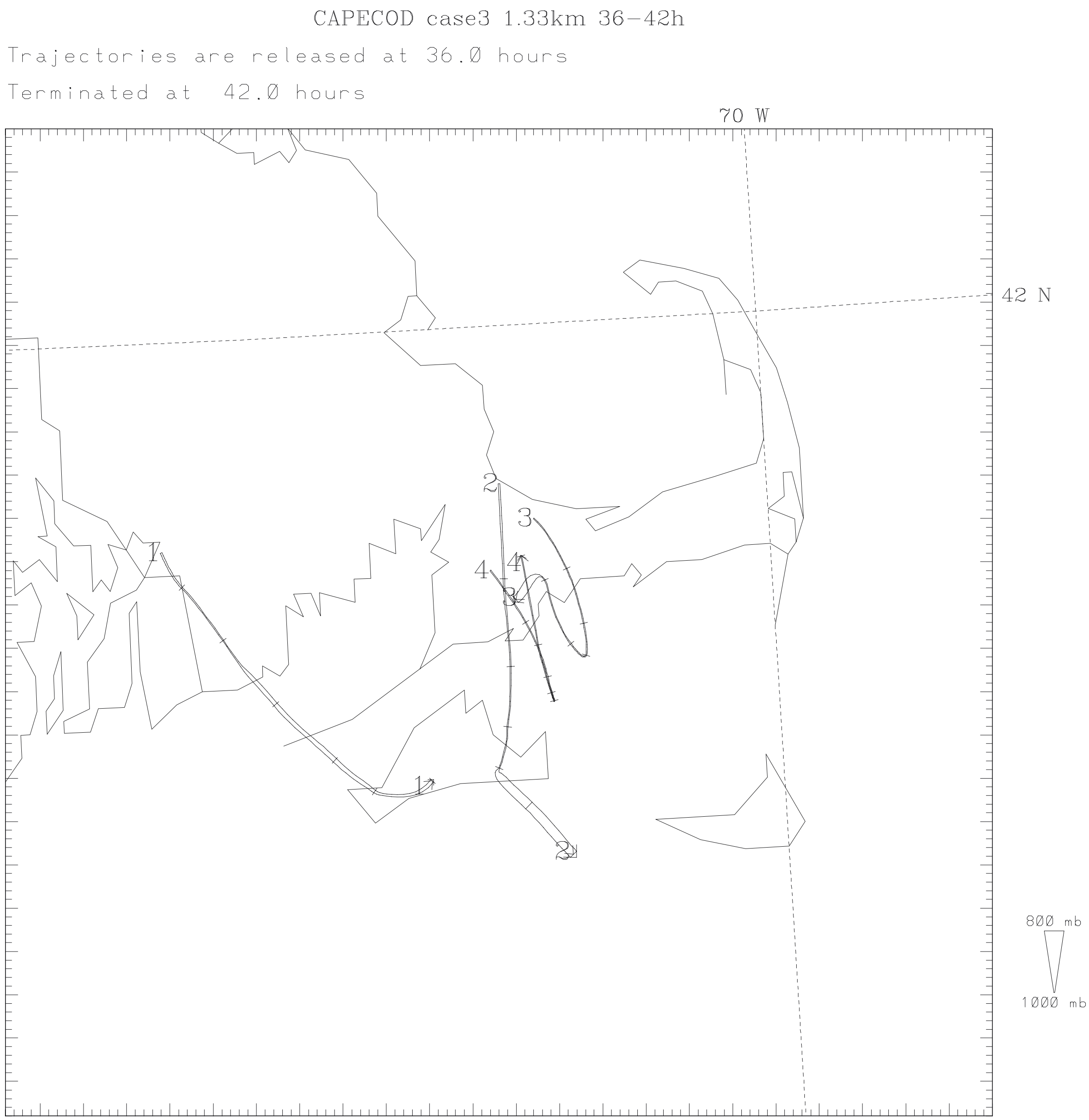

Figure 135. Six-hour TRAJEC forward trajectories based on MM5-simulated winds in Case 3. Release time is 1200 UTC, 22 August 2000 (+36 - 42 h). Parcel 1 is Brayton Point plant. Parcel 2 is Canal plant. Parcel 3 is middle of highway segment. Parcel 4 is Otis AFB. Tick marks shown on trajectories give positions at 1-h intervals, or until the parcels exit the domain.

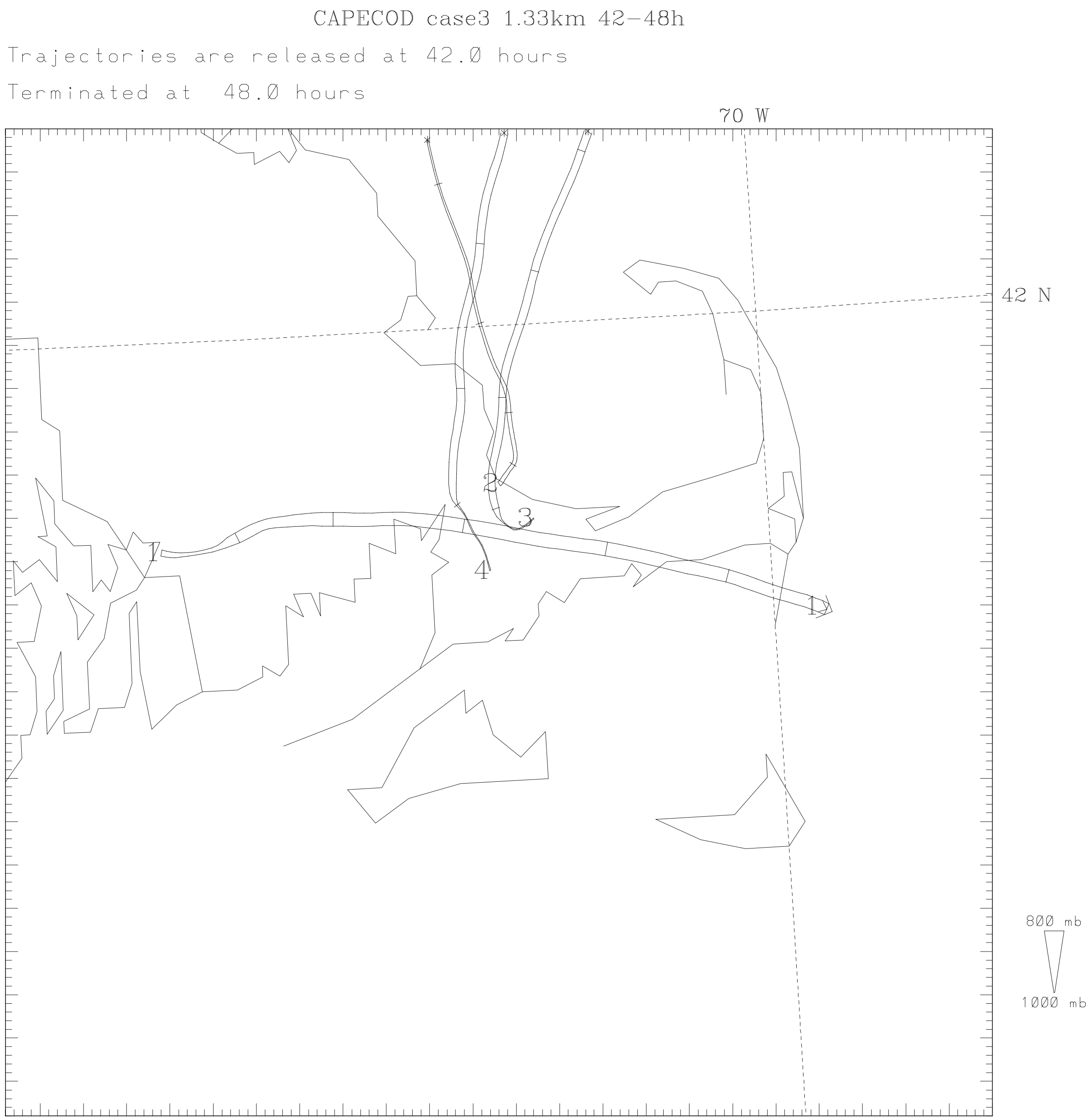

Figure 136. Six-hour TRAJEC forward trajectories based on MM5-simulated winds in Case 3. Release time is 1800 UTC, 22 August 2000 (+42 - 48 h). Parcel 1 is Brayton Point plant. Parcel 2 is Canal plant. Parcel 3 is middle of highway segment. Parcel 4 is Otis AFB. Tick marks shown on trajectories give positions at 1-h intervals, or until the parcels exit the domain.

Meanwhile, Parcel 2 from the Canal plant exhibits a much different trajectory on the afternoon of 21 August 2000. This parcel is released at 555 m MSL in the unstable afternoon PBL at the northeast end of the Cape Cod Canal, so it passes over the top of the sea-breeze front near the south shore of the Cape without any apparent influence due to the coastal circulation. Since it remains close to 500 m MSL, it approaches the east end of Martha's Vineyard hundreds of meters below the paths taken by Parcels 3 and 4, where an island breeze developed by late afternoon (see Figure 25). As Parcel 2 passes just seaward from the south shore of the island, it decelerates and rapidly sinks in the return branch of the island breeze. Once this parcel descends to the surface layer, it become entrained into the northward-moving island breeze over Martha's Vineyard and continues northeastward as it is entrained into the expanded mainland sea-breeze circulation near the end of the 6-h segment (0000 UTC, 22 August).

Reviewing the trajectories in Figure 132, there are three reasons that the island breeze was able to affect Parcel 2 over Martha's Vineyard around 2100 UTC, while the sea breeze did not affect it significantly when it passed the coast of Cape Cod at 1900 UTC. First, the extra two hours from 1900 to 2100 UTC allowed more time for the sea-breeze and island-breeze circulations to intensify toward their daily maximum strength (normally around 2000-2200 UTC, or 1600-1800 EDT). Second, the development of the sea breeze over the south shore of Upper Cape Cod acted in this case to provide a crucial buffer that shielded Martha's Vineyard from the prevailing north-northwesterly synoptic-scale flow. Thus, the island-breeze circulation was able to develop more vigorously than it would have without this effect. Third, by 0000 UTC, 22 August, the surface-layer winds over the region were beginning to shift and create a southwesterly synoptic flow (see Figure 25). The deceleration of Parcel 2 due to the island-breeze circulation allowed it to remain in this vicinity until the background wind-shift occurred, rather than quickly exiting from the domain like the other parcels.

Again, the trajectory calculations shown here reveal that the MM5 model was able to develop very complex 3-D mesoscale flow patterns that continually evolve over time. It would be extremely difficult to discern these details from the very sparse observations available in the data base. However, these circulations clearly can have important impacts on the fate of emissions and secondary chemical species as they are advected through the domain. Despite the absence of sufficient data to verify every aspect of these locally complex flows, the good agreement between the model fields and the manual mesoscale analyses, plus the results of the statistical evaluations, provide considerable confidence in the general accuracy of these flows. This conclusion applies equally to all three cases investigated in the present study.

For the evening of 22 August, the trajectories of parcels released at 0000 UTC are shown in Figure 133. In this 6-h segment all four parcels experience the shift to southwesterly winds over Cape Cod and southeastern MA mentioned above and shown in Figure 25. Notice that Parcel 1 from the Brayton Point plant descends toward the surface as it travels northeastward over land toward Boston. This indicates that there is substantial low-level divergence over the area, which is consistent with the development of a land breeze during the evening hours. By contrast, Parcel 2 (also heading northeastward) immediately leaves the coast and does not experience significant subsidence. Again this is consistent with a land breeze.

Next, Figure 134 shows the trajectories taken during the second half of the night, following the release of another set of parcels in Case 3 at 0600 UTC (0200 EDT), 22 August 2000. By this time, the winds have shifted back to the northwest (also see Figures 26, 29 and 51). Also, by this time, the land breeze was approaching its maximum intensity and both of the elevated plumes, represented by Parcels 1 and 2, appear to be subsiding toward the surface while still over land. Moreover, there is a distinct difference in the wind directions experienced by Parcel 1, compared to Parcels 2-4, which indicates that significant low-level divergence exists over Upper Cape Cod and southeastern MA. Thus, the trajectory calculations shown in Figure 134 corroborate the wind response expected with the development of a modest land breeze in the MM5 solutions for the night of 22 August 2000, even though it is somewhat masked by the northwesterly background winds.

The paths taken by parcels released shortly after sunrise on 22 August (1200 UTC) are shown in Figure 135. These 6-h trajectories reflect the weakening intensity of the synoptic-scale flow, which allows the sea breeze to develop more vigorously than on 21 August. All the parcels initially headed southward during the early morning. Parcel 1 (from the Brayton Point plant) encounters the initial stage of the sea breeze about 1430 UTC (1030 EDT) as the new circulation just begins to form ~3 km inland from the coast. However, it only rises to ~700-800 m because the vertical motions are still quite weak at this time. Parcel 2, representing the elevated plume from the Canal plant, passes the south shore of Upper Cape Cod by 1330 UTC (0930 EDT) before the sea breeze develops, so that it continues southward at fairly low altitude for another 2.5 h until it reaches Martha's Vineyard. At 1600 UTC (1200 EDT), Parcel 2 encounters the island-breeze front on the south shore of Martha's Vineyard, where it rises rapidly to ~1000-1100 m MSL. At that height, it is above the circulations and can continue southeastward over the Atlantic Ocean.

By contrast to Parcels 1 and 2, Figure 135 indicates that the trajectories taken by Parcels 3 and 4 on the morning and early afternoon of 22 August are quite different. The early-morning north-northwesterly surface winds over Upper Cape Cod carry these low-level parcels seaward before the sea breeze develops, but the slower wind speeds close to the surface prevents them from moving far offshore before the circulation takes hold around 1400 UTC (1000 EDT). Thus, by 1430 UTC (1030 EDT), both Parcels 3 and 4 reverse direction and head back north over Upper Cape Cod in the final 3 h of this time segment. Once onshore again, Parcel 3 encounters a convergence zone shortly after 1700 UTC (1300 EDT) and rises about 1000 m, while Parcel 4 (only a short distance to the west of the path taken by Parcel 3) apparently misses the convergence zone and remains in the surface layer.

Finally, the trajectories calculated during the late afternoon of 22 August, following their release at 1800 UTC, are shown in Figure 136. Since the sea breeze is well developed by that time, each of the parcels encounters one or another of the local convergence zones (not shown) and rises well above its release level. The only exception to this pattern is Parcel 2, which immediately travels over Massachusetts Bay, away from the convergence zones, so that it gradually sinks in the subsiding return branch of the eastern MA sea breeze. Note that Parcel 1 travels toward the east, rather than toward the north as seen for Parcels 2-4, because it is lifted considerably higher to almost 2000 m as it passes over southeastern MA and Upper Cape Cod.

4.5 Dispersion and Trajectory Results from CALPUFF and ISCST3

In this section we will make selected comparisons of the results of the CALPUFF/CALMET and ISCST3 modeling performed for the three meteorological case study periods.

4.5.1 Dispersion Results from CALMET /CALPUFF

As described earlier, the MM5 meteorological output data fields were used to establish input meteorological data for CALPUFF via the CALMET program. This section discusses the predicted air quality concentrations obtained using CALPUFF for the same sources. Rather than making detailed comparisons of the results for each case, we will focus more on comparing the capabilities of the models in illustrating the flow fields and concentration patterns. Reference should be made to the prior sections involving the descriptions of the meteorology encountered.

4.5.1.1 Case 1 CALPUFF Results

CALPUFF predictions for the Brayton Point plant emissions for July 1 at 7 am (0700 EDT, or 1100 UTC) are shown in Figure 137. The CalDESK graphics capability allows one to superimpose gridded land use and meteorological information as illustrated by the wind vectors in this figure. Time-wise, this figure shows the general flow situation modeled by SCIPUFF and shown in Figure 53 which corresponds to 5 am on the same day. Notice that the general direction of the plumes is similar.

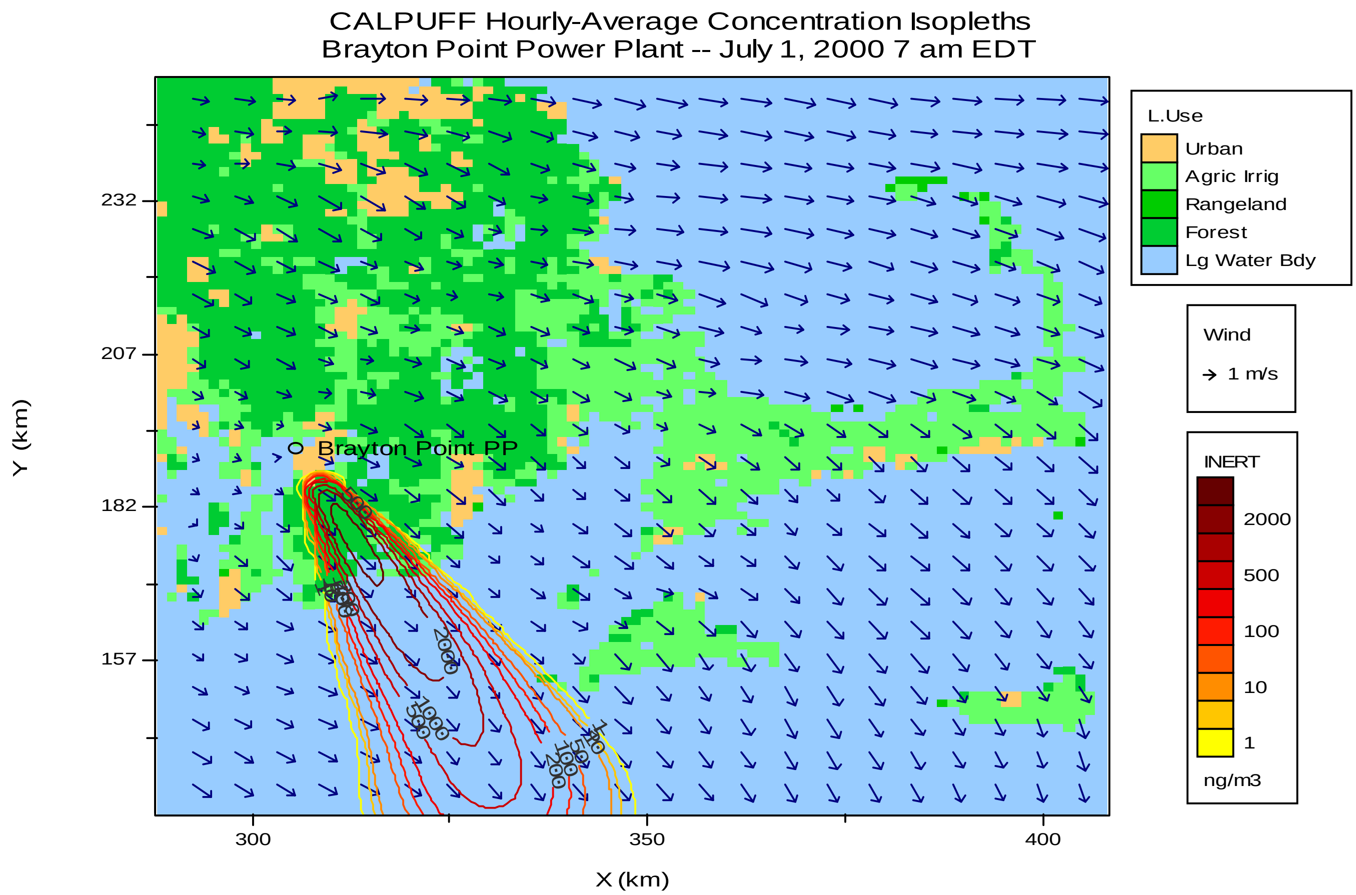

Figure 137. Hour-average concentration isopleths over the CALPUFF domain, arising from the Brayton Point Power Plant at an assumed emission rate of 100 g/s, for July 1 at 7 am EDT. Also shown are CALMET wind vectors for the surface layer.

Concentration units are in nanograms per cubic meter (ng/m3). The maximum contour shown is for 5000 ng/m3 corresponding to 5 ug/m3 or 5 X10 $^{-9}$ kg/m3. Thus for this particular comparison, CALPUFF predicts maximum concentrations closer in and about six times higher than SCIPUFF. We will see further cases where the predictions of the models differ. Figure 138 shows the CALPUFF predictions for 11 am on July 1. Here we see plume material, which was earlier advecting offshore, being brought back to the shore south of the plant. Notice that the wind vectors, which are hourly surface values, show the onshore flow occurring at 11 am and the converging flows over the upper Cape at this time. The maximum concentration predicted from the CALPUFF output is 37 ug/m3 and is more similar in magnitude to that predicted by SCIPUFF a few hours later: 9 ug/m3 at 2 pm. (See Figure 54). Figure 139 shows the concentrations and flow field for July 2 at 8 am. The flow pattern is similar to that depicted by the west southwest winds by SCIPUFF at 2 am EDT (see Figure 56). A feature of CalDESK which allows some isopleth contours to be filled rather than outlined is also illustrated.

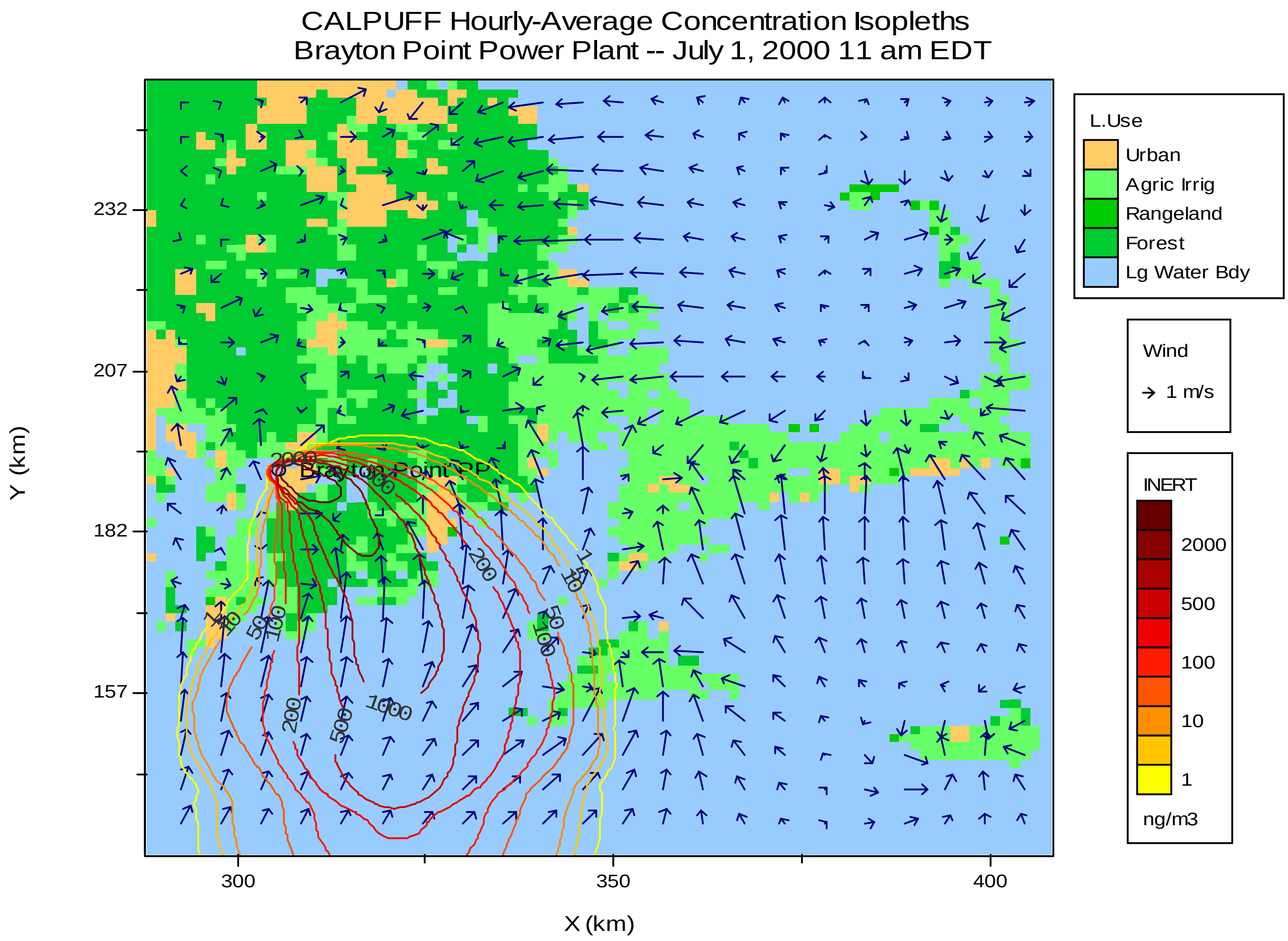

Figure 138. Hour-average concentration isopleths over the CALPUFF domain, arising from the Brayton Point Power Plant at an assumed emission rate of 100 g/s, for July 1 at 11 am EDT. Also shown are CALMET wind vectors for the surface layer.

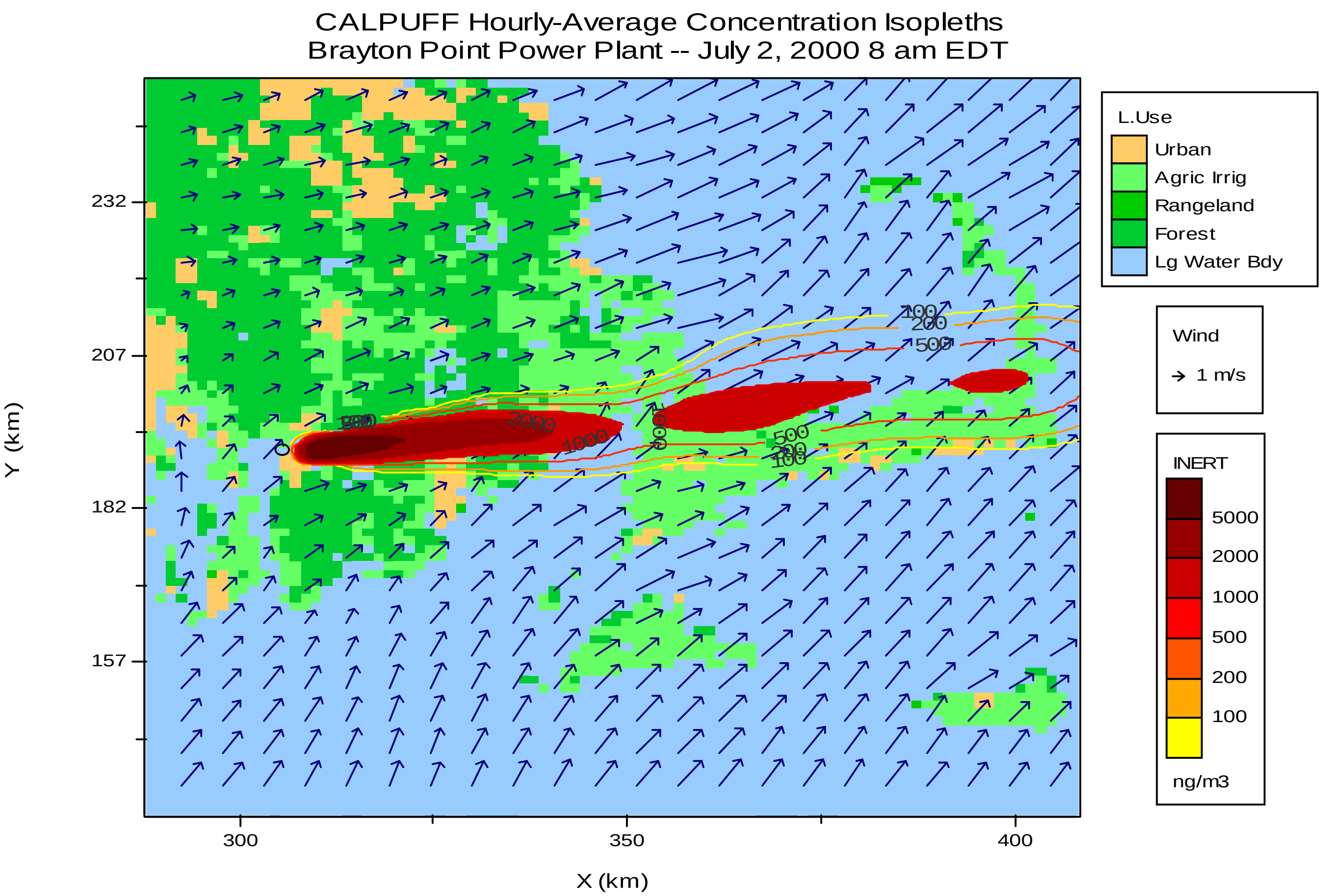

Figure 139. Hour-average concentration isopleths over the CALPUFF domain, arising from the Brayton Point Power Plant at an assumed emission rate of 100 g/s, for July 2 at 8 am EDT. Also shown are CALMET wind vectors for the surface layer.

The results for the Canal plant releases at 7am and at 11 am on July 1 are shown in Figures 140 and 141. The patterns are similar to those produced by CALPUFF for the Brayton Point plant for the same time period. Figure 142 shows the Canal plant plume caught in the early morning westerly flow of July 2. Figure 143 illustrates a capability which is not in the public version of SCIPUFF; the ability to calculate multi-hour average concentrations. The 24-hour average values for July 1 are shown. Because of the changing wind directions during the day, the pattern of concentrations are more diffuse and show lobes corresponding to the various wind directions that occurred during the day.

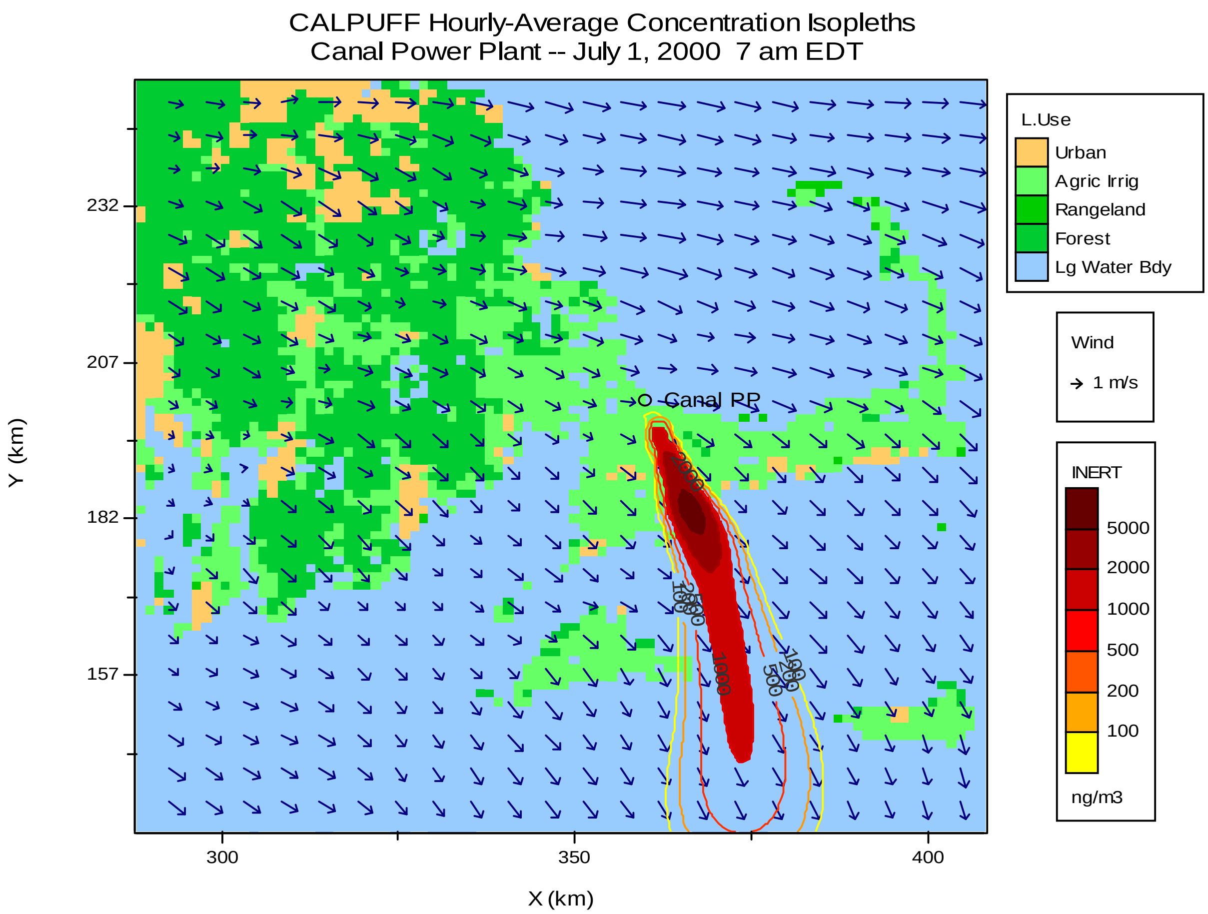

Figure 140. Hour-average concentration isopleths over the CALPUFF domain, arising from the Canal Power Plant at an assumed emission rate of 100 g/s, for July 1 at 7 am EDT. Also shown are CALMET wind vectors for the surface layer.

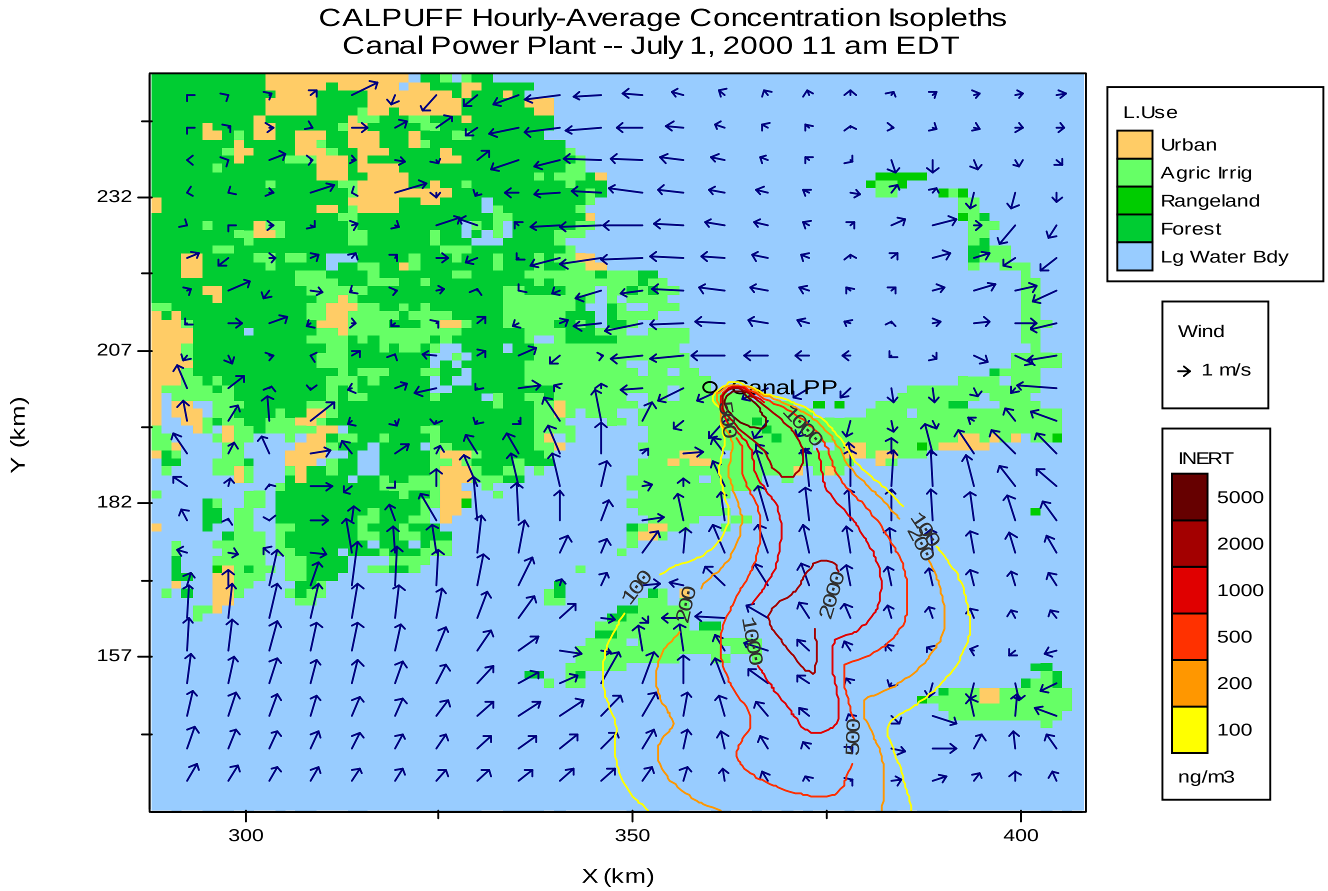

Figure 141. Hour-average concentration isopleths over the CALPUFF domain, arising from the Canal Power Plant at an assumed emission rate of 100 g/s, for July 1 at 11 am EDT. Also shown are CALMET wind vectors for the surface layer.

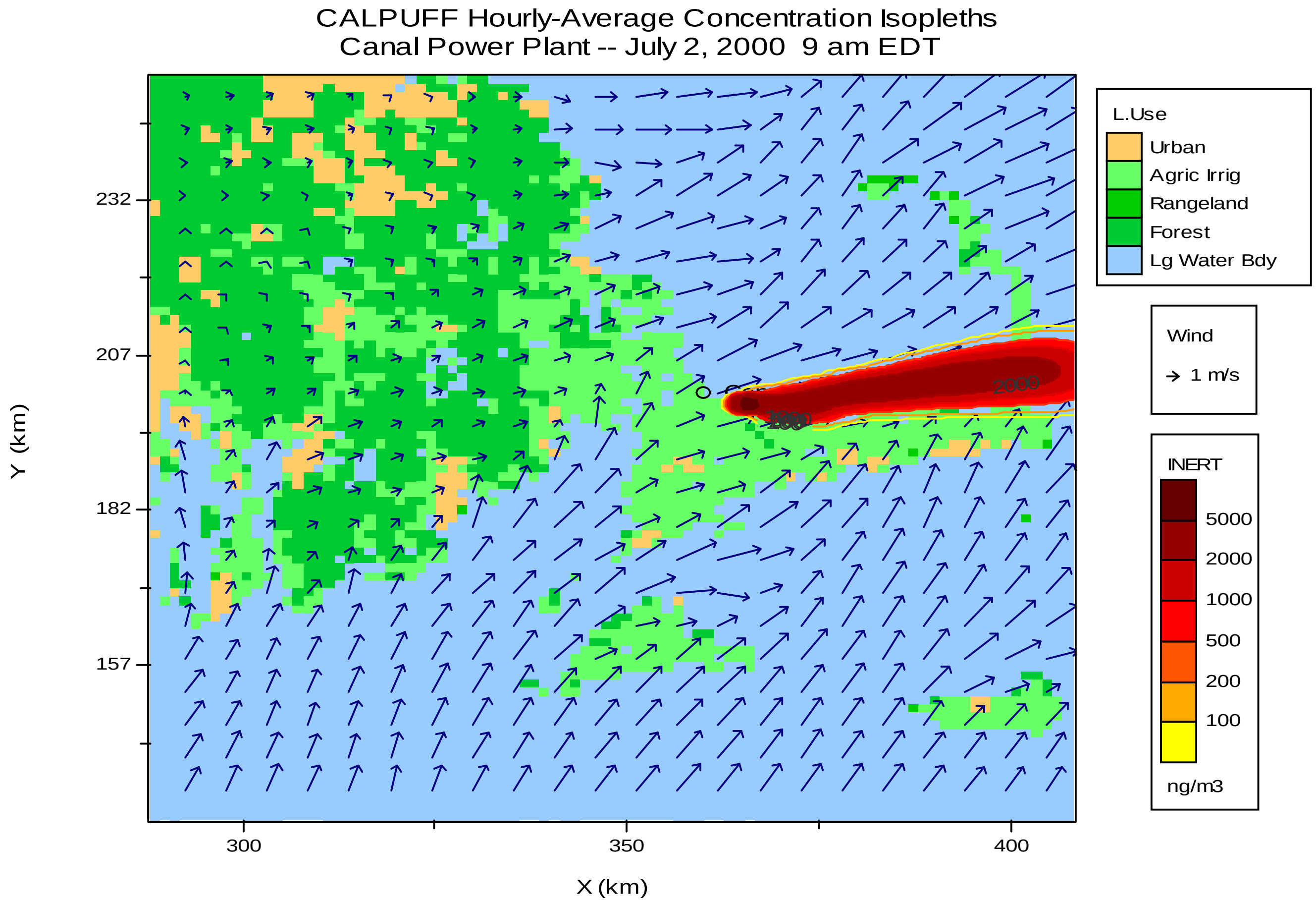

Figure 142. Hour-average concentration isopleths over the CALPUFF domain, arising from the Canal Power Plant at an assumed emission rate of 100 g/s, for July 2 at 9 am EDT. Also shown are CALMET wind vectors for the surface layer.

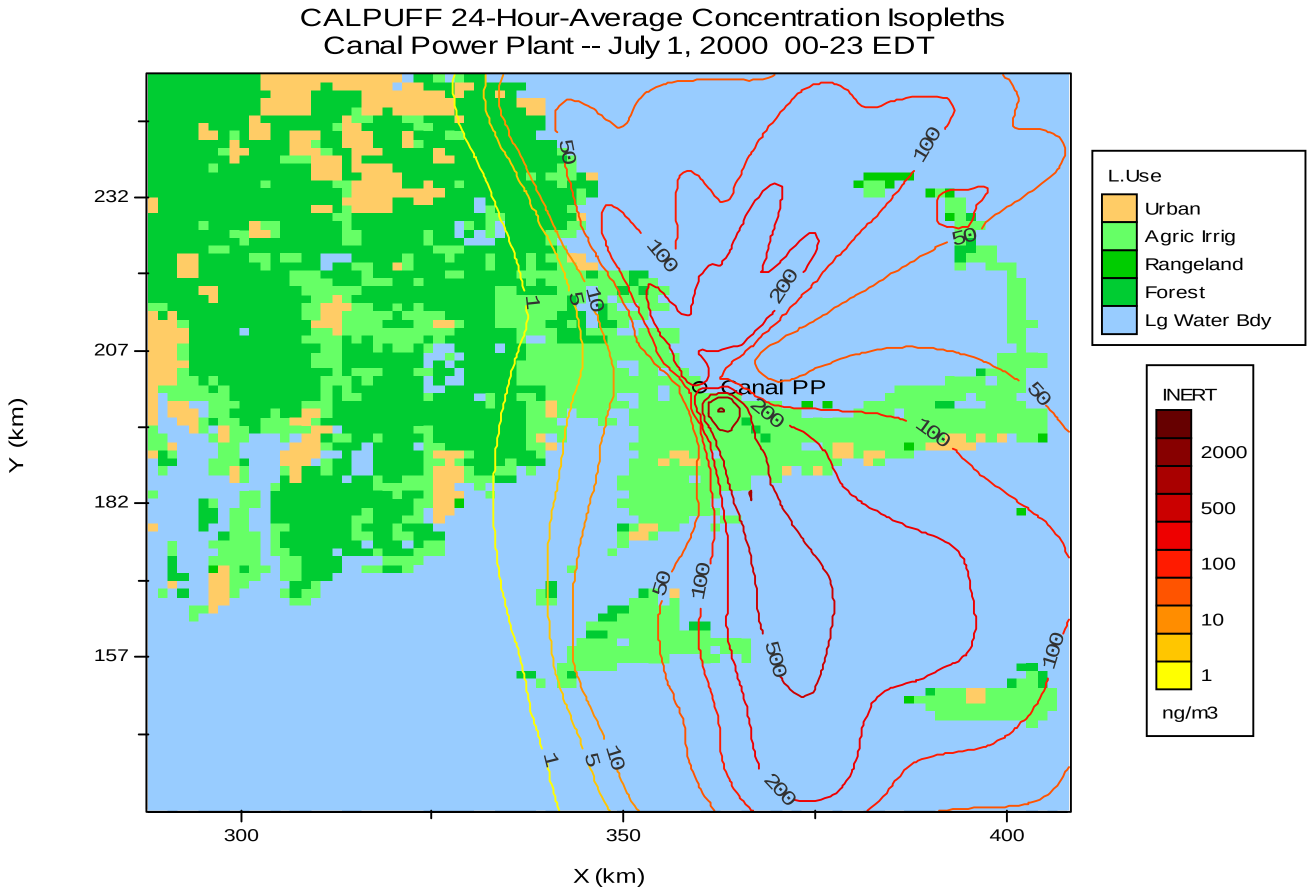

Figure 143. CALPUFF 24-hour-average concentration isopleths over the CALPUFF domain, arising from the Canal Power Plant at an assumed emission rate of 100 g/s, for July 1 from 00 to 23 EDT.

Figure 144 shows the isopleth and wind flow pattern for the simulation of the highway segments by CALPUFF for 4 am on July 1. The results illustrate a shortcoming of CALPUFF's ability to handle line sources. CALPUFF treats line segments as point sources, with a separate point assigned to each line segment entered. The plot shows circular ' hot spot' isopleths over each of the two segments modeled instead of the expected pattern of isopleths parallel to the lines except near the line ends. This deficiency could be overcome by breaking the straight lines into smaller segments or by modifying the code to automatically do that. The concentrations can be compared, with caution, to those predicted by SCIPUFF shown in Figure 62. The maximum concentrations predicted by CALPUFF exceed 500 ug/m3 or 5×10^{-7} kg/m3, a value substantially smaller than the maximum value of 1.2×10^{-5} kg/m3 from SCIPUFF. The caution is that with any low level source, because the maximum concentrations generally occur very near the sources, the spacing between the source area and a mathematical receptor location and the details of the dimensions of the source are critical. Some models (e.g. ISCST) establish a minimum separation distance between the source and receptors. Because the different models used in this study utilize different grid spacings, the maximum concentrations close to the highway may well depend more on the specific receptor locations than on the model used. A preferred comparison for our purposes is to look at the concentrations from SCIPUFF at larger distances from the roadway. For example, comparing the maximum concentrations predicted at the south coastline in Figures 144 and 62 indicates that the predictions are similar (3×10^{-8} for CALPUFF vs. 1 to 10×10^{-8} kg/m3 for SCIPUFF). Figure 145 shows the pattern for 11 am EDT with a snap shot depiction of the converging sea breeze wind directions..

Plots of the ground level concentration patterns resulting from potential emissions from the Otis AFB site for the same 11 am time period are shown in Figure 146. The 24-hour average concentrations for July 1 from the Otis source are shown in Figure 147. Comparing this with Figure 143 for the Canal Plant shows similar looking patterns but demonstrates that the local concentrations are higher on a per unit emission basis for releases from the Otis source.

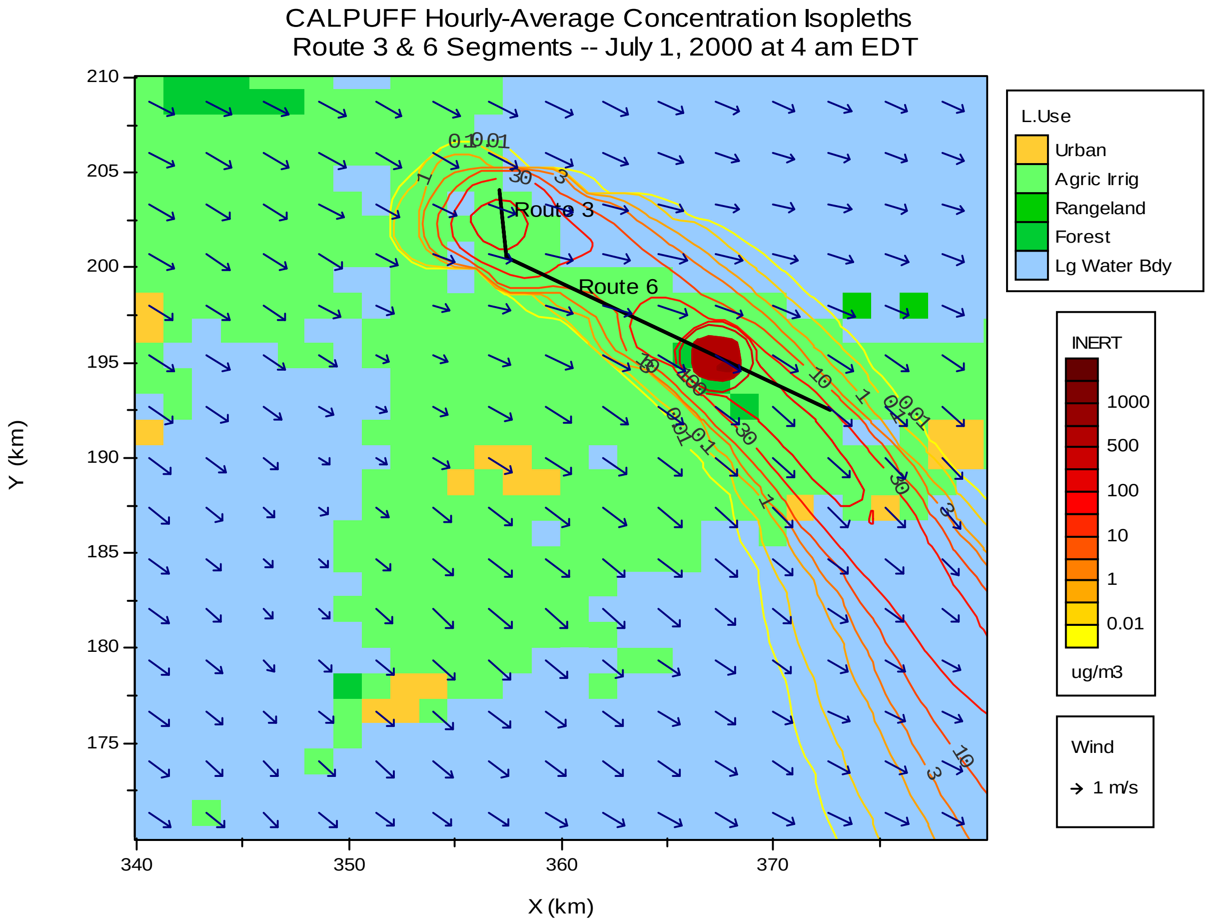

Figure 144. Hour-average concentration isopleths over UCC, arising from uniformly distributed emissions along segments of Routes 3 and 6 totaling 100 g/s, for July 1 at 4 am EDT. Also shown are CALMET wind vectors for the surface layer.

CALPUFF Hourly-Average Concentration Isopleths
Route 3 & 6 Segments -- July 1, 2000 at 11 am EDT

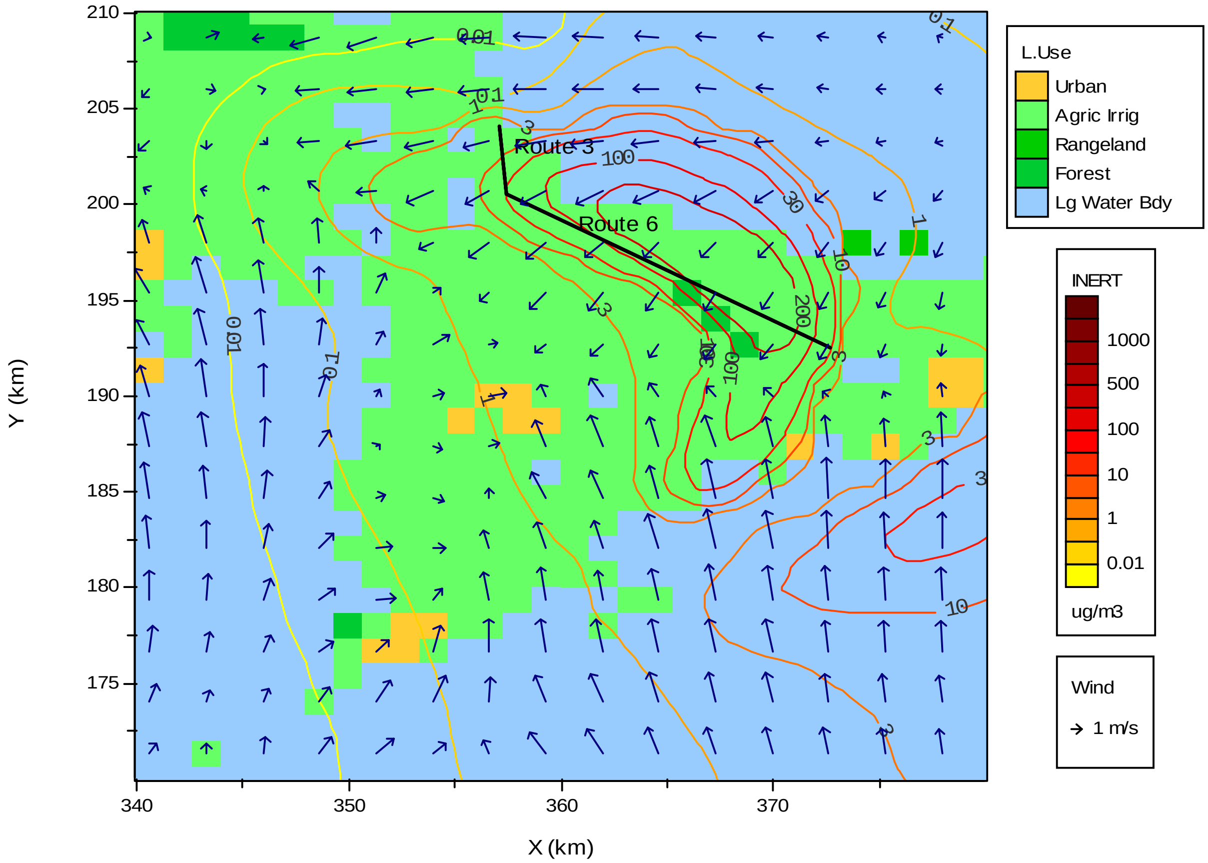

Figure 145. Hour-average concentration isopleths over UCC, arising from uniformly distributed emissions along segments of Routes 3 and 6 totaling 100 g/s, for July 1 at 11 am EDT. Also shown are CALMET wind vectors for the surface layer.

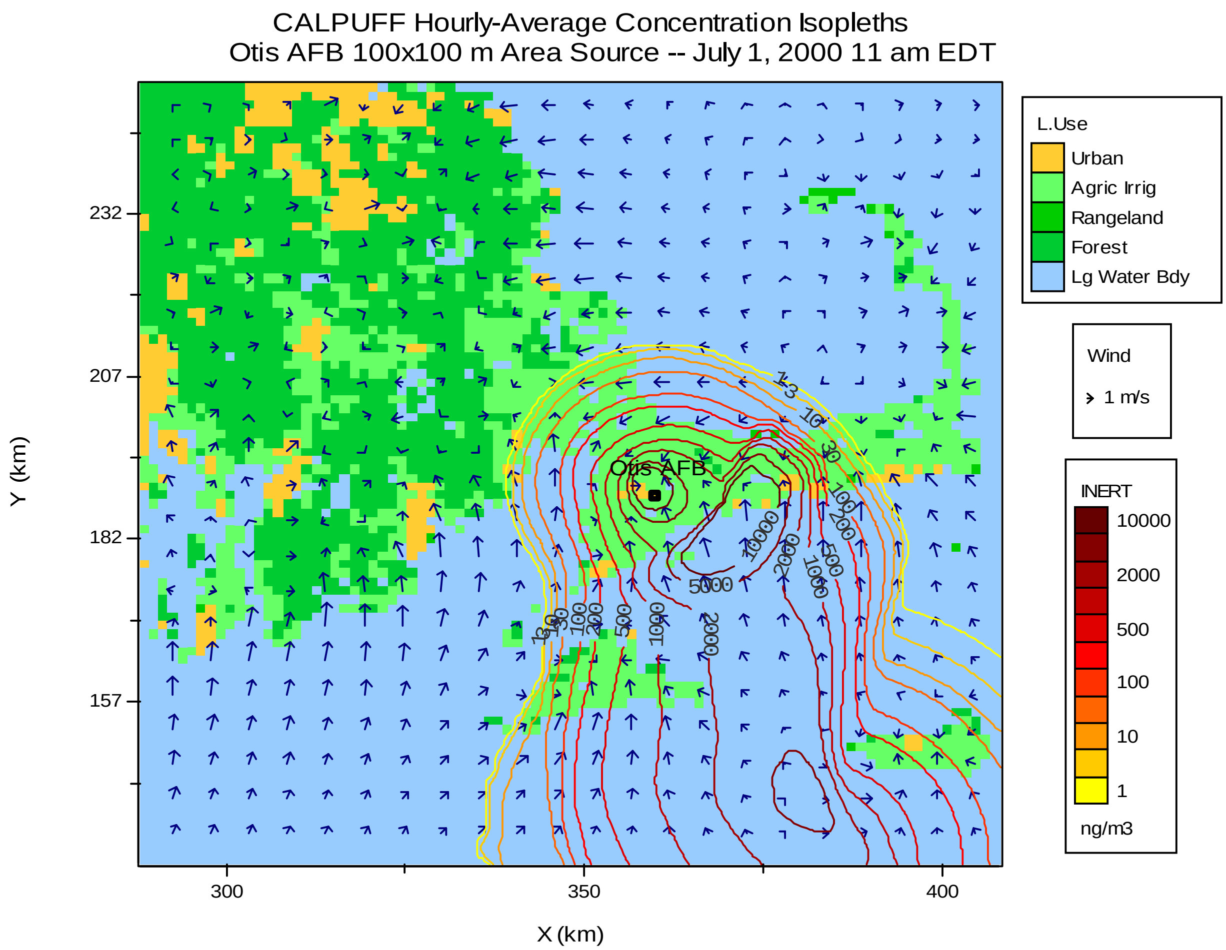

Figure 146. Hour-average concentration isopleths over the CALPUFF domain, arising from a uniform 10000 m^2 area source at Otis AFB with emissions totaling 100 g/s, for July 1 at 11 am EDT. Also shown are CALMET wind vectors for the surface layer.

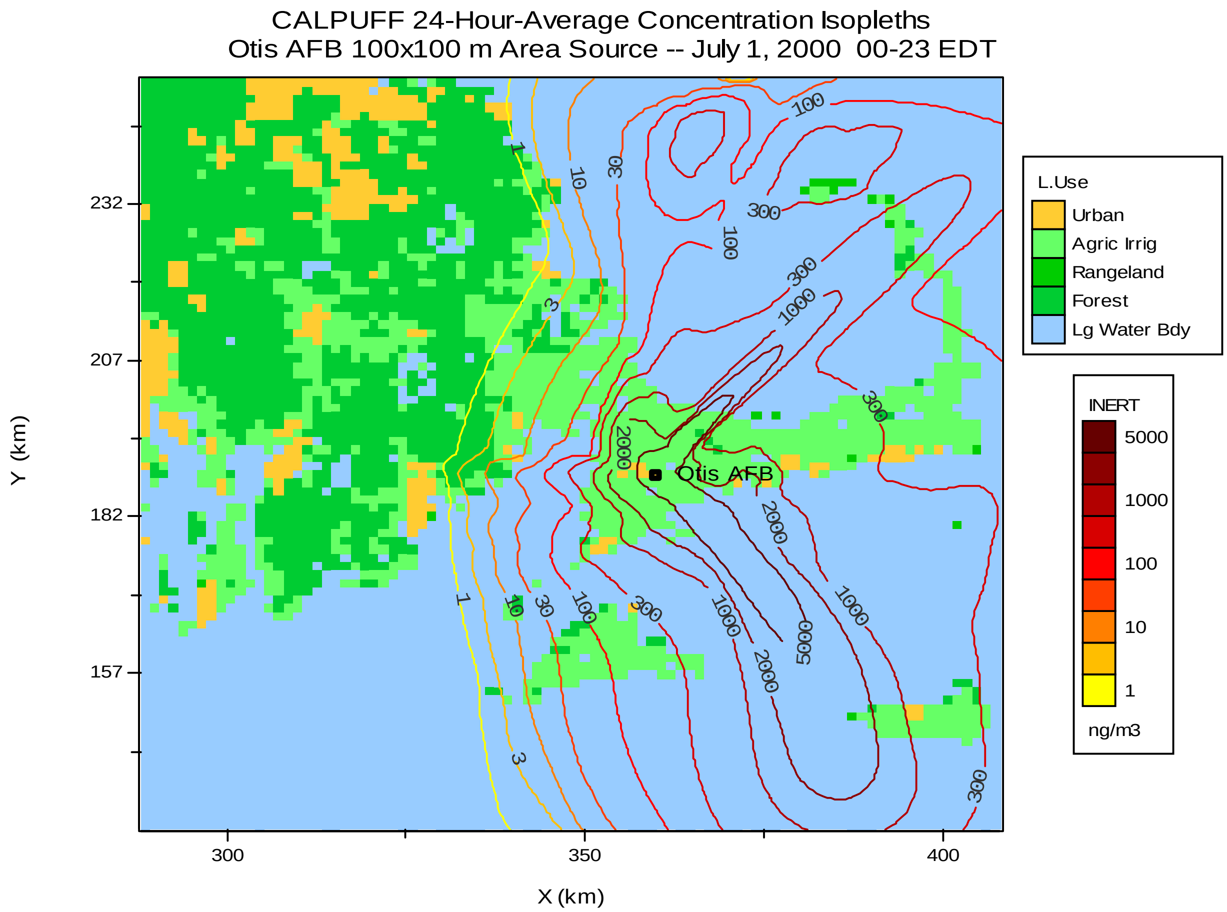

Figure 147. CALPUFF 24-hour-average concentration isopleths over the CALPUFF domain, arising from a uniform 10000 m^2 area source at Otis AFB with emissions totaling 100 g/s, for July 1, 2000 from 00 to 23 EDT.

4.5.1.2

Case 2 CALPUFF Results

Case 2 covers the time period of July 5 and 6, 2000. Figure 148 shows the wind fields from CALMET and the concentration pattern from the Brayton Point Power Plant at the time of the expected peak sea breeze intensity at 2 pm on July 6. The results can be compared directly with those in Figure 77 from SCIPUFF. Both the patterns and concentration values are similar although the higher values are shifted more to the south in the CALPUFF results. The maximum concentration predicted for this hour by CALPUFF is 35.8 ug/m3 comparing to the max value from SCIPUFF of 12.7 ug/m3. Figures 149 and 150 show the centerlines of the plume from Brayton Point at different times after a start time of 8 am (Figure 149) or 9am (Figure 150). The ability of CalDESK to use the CALMET results to show how the plume first moves out to sea to the south and then reverses direction in the sea breeze provides a good demonstration of the importance of the local circulations in understanding some of the air quality issues along coastlines. The release height in these cases was 875 meters, an approximate representative height of the plume after its initial rise. These particular plots also show the mixing depths as predicted by MM5 via CALMET. In Figure 149 the maximum mixing depth is 850 meters. This suggests that the simulated plume is above this height and traveling in a stable layer after its initial rise. In Figure 150, the mixing depth is at places as high as 1500 m, suggesting that the plume could be dispersing more vigorously within the well-mixed layer. It is interesting to note that just an hour delay in the start time results in very different subsequent trajectories, a result of both the sea breeze flow and the effect of mixing depth changes.

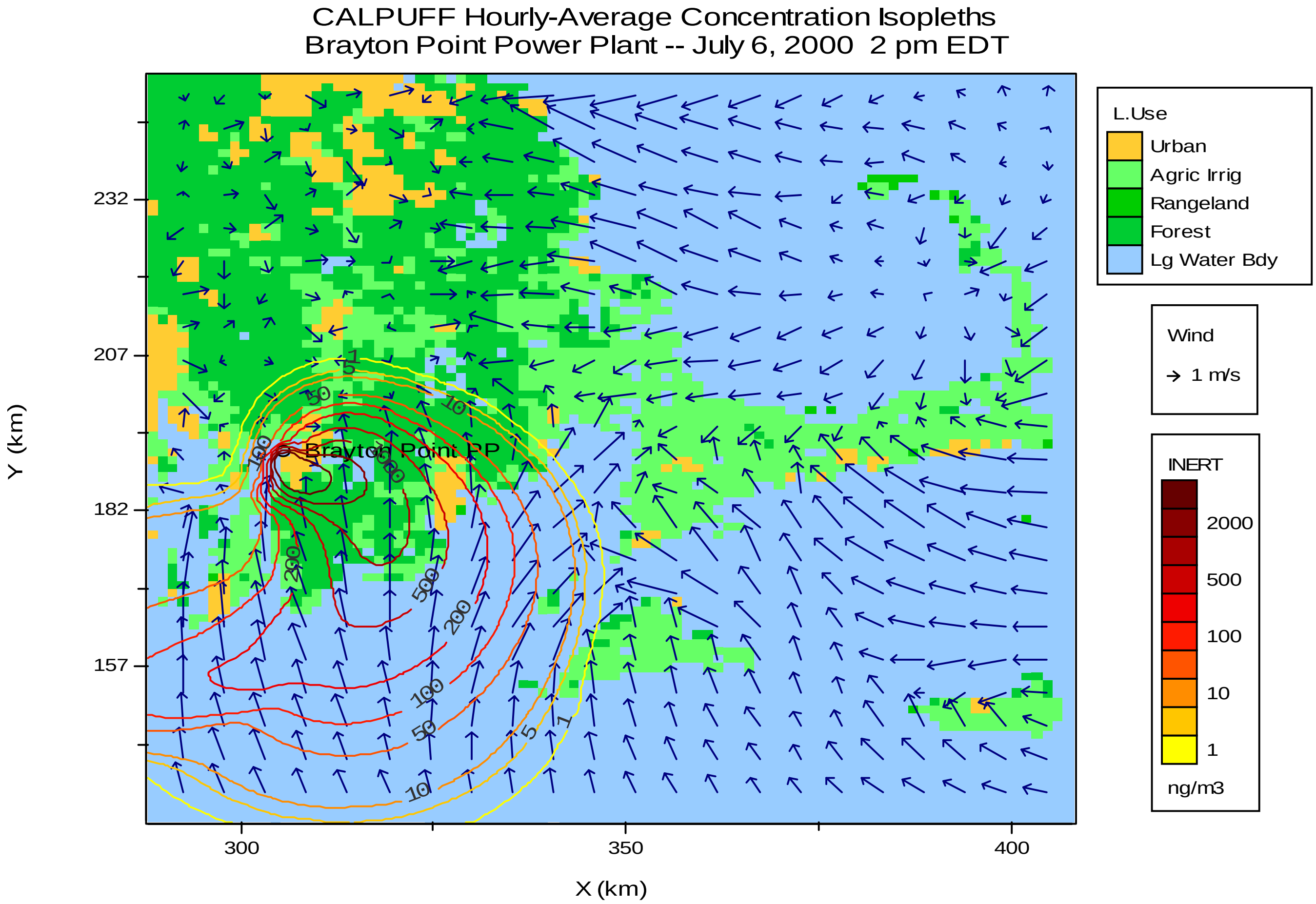

Figure 148. Hour-average concentration isopleths over the CALPUFF domain, arising from the Brayton Point Power Plant at an assumed emission rate of 100 g/s, for July 6 at 2 pm EDT. Also shown are CALMET wind vectors for the surface layer.

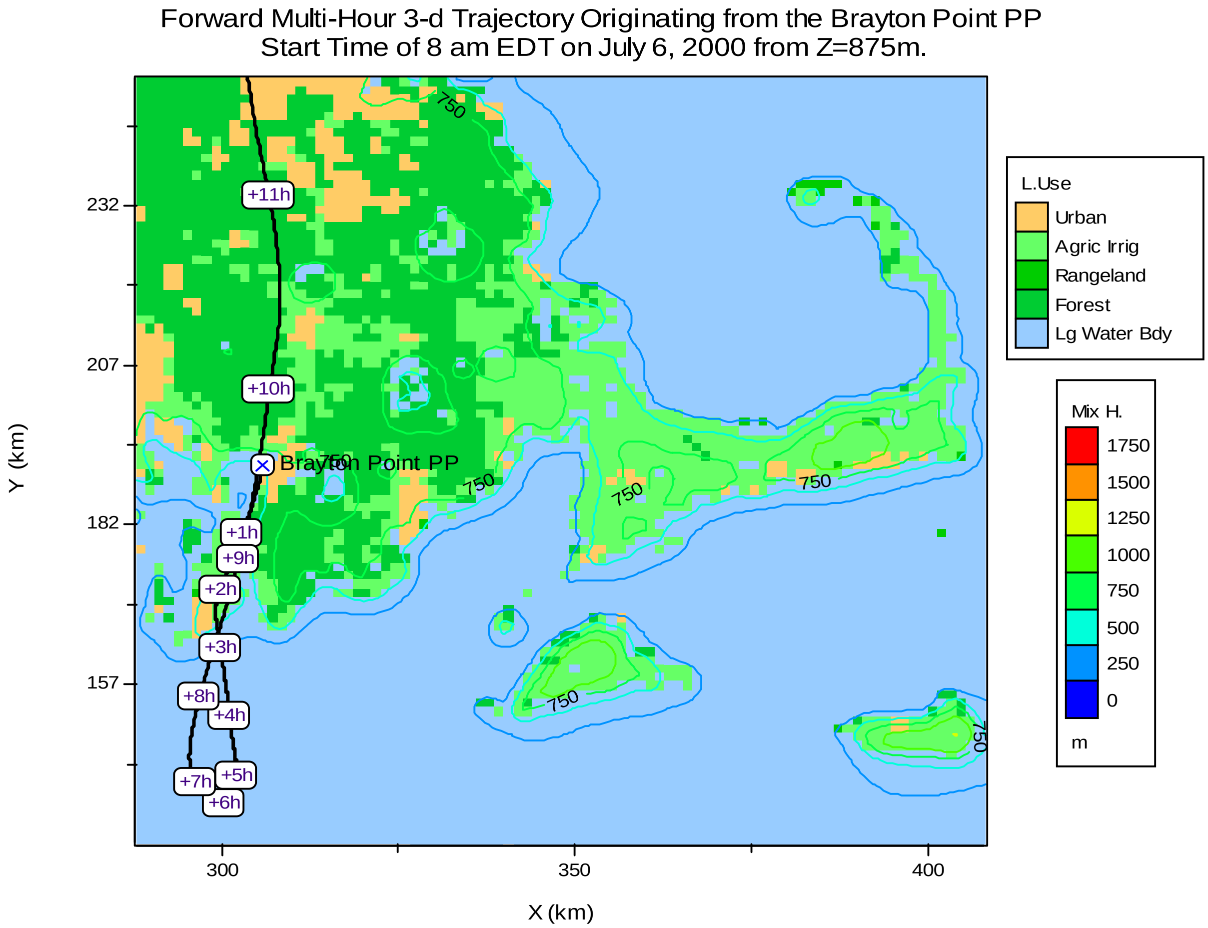

Figure 149. Forward-in-time, multi-hour, 3-d trajectory generated using CALMET winds and originating from a height of 875m directly above the Brayton Point PP at 8 am EDT on July 6, 2000. Numbers on the trajectory indicate hours of transport. Mixing depths are also shown and vary dramatically (from 200m to 850m) within several km of Brayton Point.

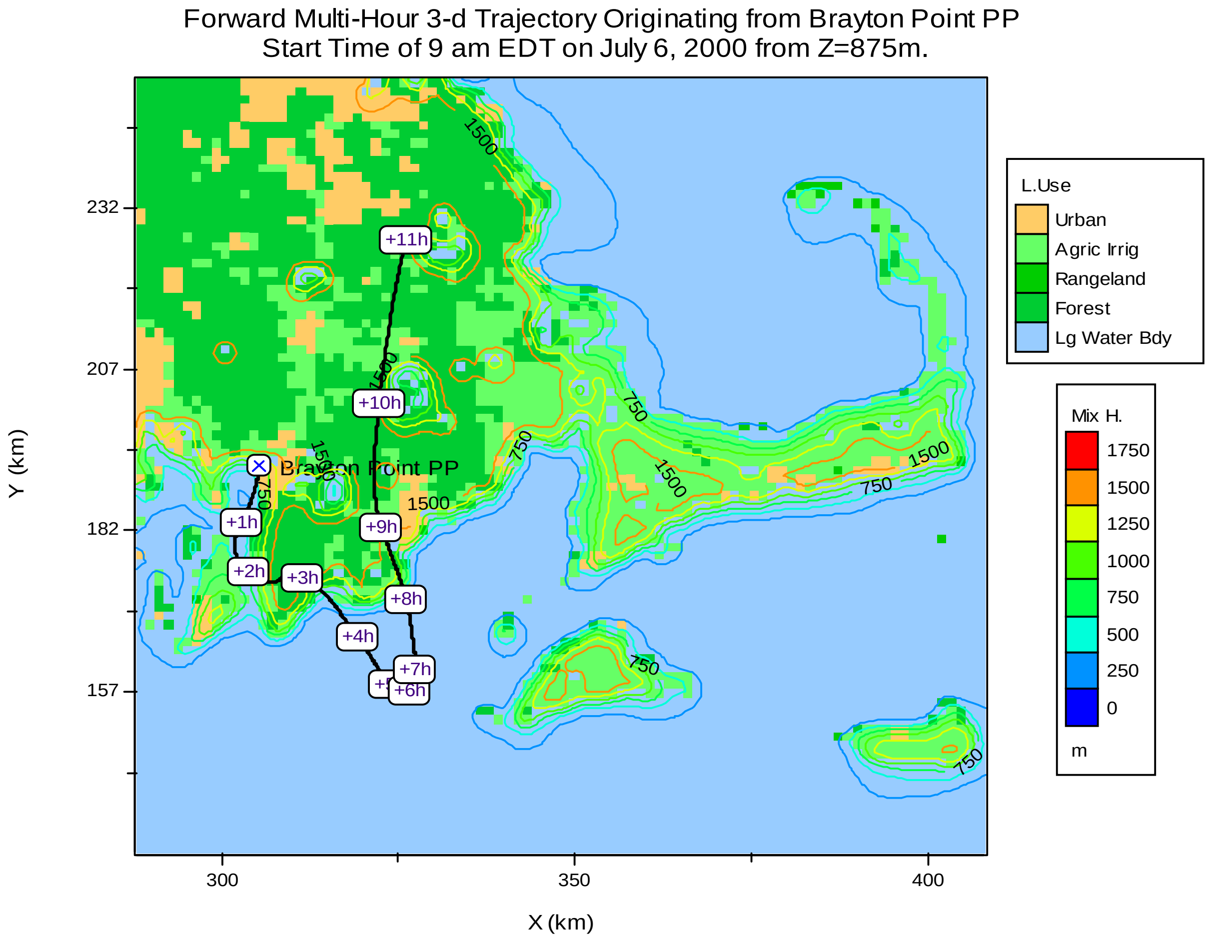

Figure 150. Forward-in-time, multi-hour, 3-d trajectory generated using CALMET winds and originating from a height of 875m directly above the Brayton Point PP at 9 am EDT on July 6, 2000. Numbers on the trajectory indicate hours of transport. Mixing depths are also shown and vary dramatically (from 300m to 1500m) within several km of Brayton Point.

Figure 151 shows a snapshot in time of the emissions from the Canal Plant at 2 pm on July 6. Converging sea breezes may be seen over the Upper Cape and also over the mainland about 50 km to the west. This figure may be compared directly with the pattern from SCIPUFF shown in Figure 82. The maximum value predicted by CALPUFF is 93.6ug/m3 compared to 12.9 ug/m3 predicted by SCIPUFF. Predicted trajectories of emissions from the Canal Plant are shown in Figures 152 and 153. These are for the same time period as the trajectories from Brayton Point shown in Figures 149 and 150.

The effects of circulations on near ground level releases can be seen in Figures 154 and 155 that show the releases from the highway segments at 2 pm and 5 pm respectively on July 6. Emissions which were taken offshore in the morning are carried back over Martha's Vineyard at 2 pm. By 5 pm this contaminated air is being drawn further back to the south coast of the Cape by the circulation.

The pattern is confirmed in Figures 156- 160 which show the contaminant flow of a release from Otis AFB. Figure 156 shows the offshore flow toward the southeast in the morning and Figures 157a and 157b show the converging sea breezes developing between 1 pm and 2 pm. Notice the pollutant material in the surface layer south of Martha's Vineyard in Figure 157a that is being advected northward at that time. The trajectories for this time period are shown in Figures 158-160. Whereas the release at 8am of Figure 158 first flows south and then turns northward, in Figure 159, the 9 am release trajectory continues to the southeast. This latter trajectory indicates that the plume parcels achieved an altitude above the sea breeze circulation. These observations were discussed earlier in the section describing the TRAJEC results.

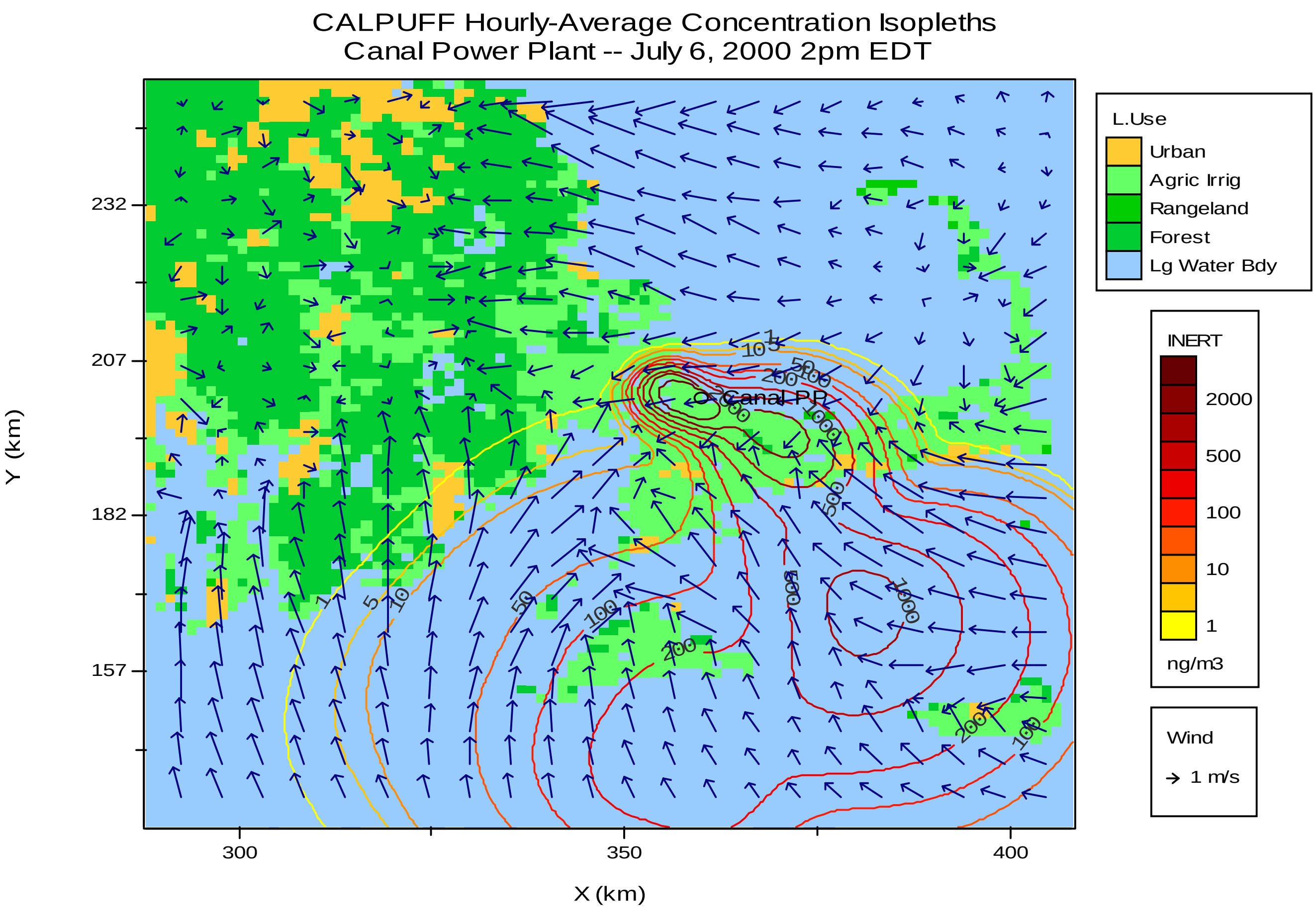

Figure 151. Hour-average concentration isopleths over the CALPUFF domain, arising from the Canal Power Plant at an assumed emission rate of 100 g/s, for July 6 at 2 pm EDT. Also shown are CALMET wind vectors for the surface layer.

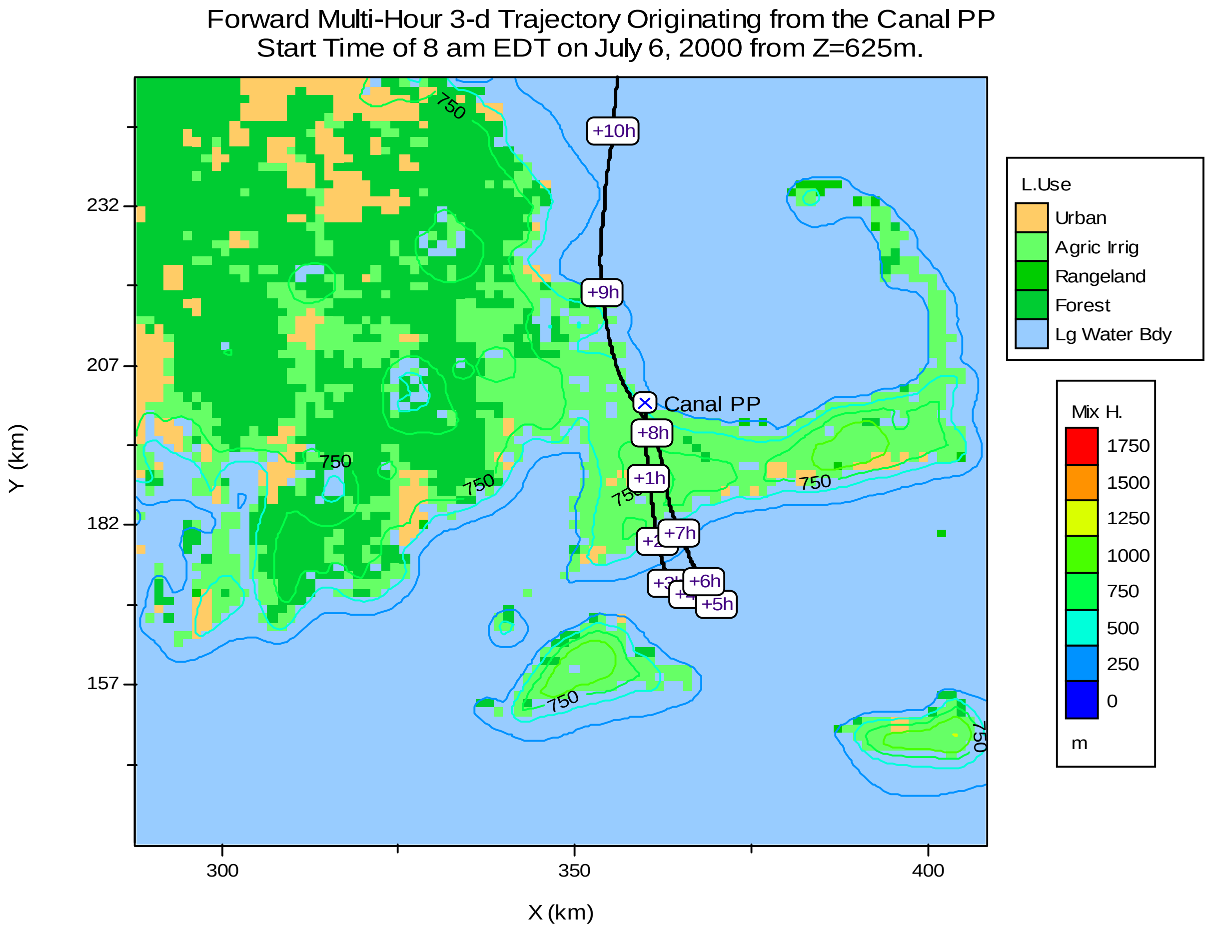

Figure 152. Forward-in-time, multi-hour, 3-d trajectory generated using CALMET winds and originating from a height of 625m directly above the Canal PP at 8 am EDT on July 6, 2000. Numbers on the trajectory indicate hours of transport. Mixing depths are also shown and vary dramatically (from 200m to 750m) within several km of the Canal plant.

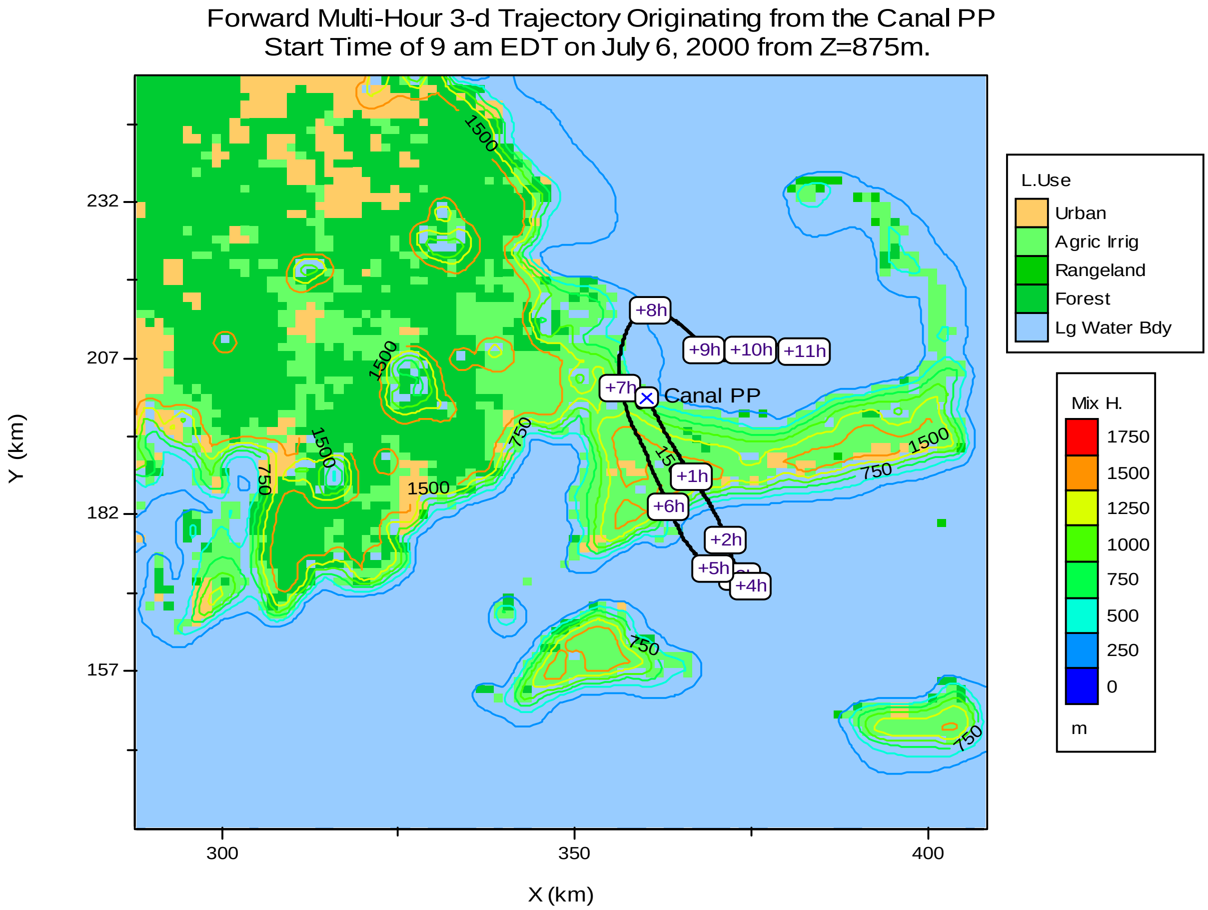

Figure 153. Forward-in-time, multi-hour, 3-d trajectory generated using CALMET winds and originating from a height of 875m directly above the Canal PP at 9 am EDT on July 6, 2000. Numbers on the trajectory indicate hours of transport. Mixing depths are also shown and vary dramatically (from 250m to 1200m) within several km of the Canal plant.

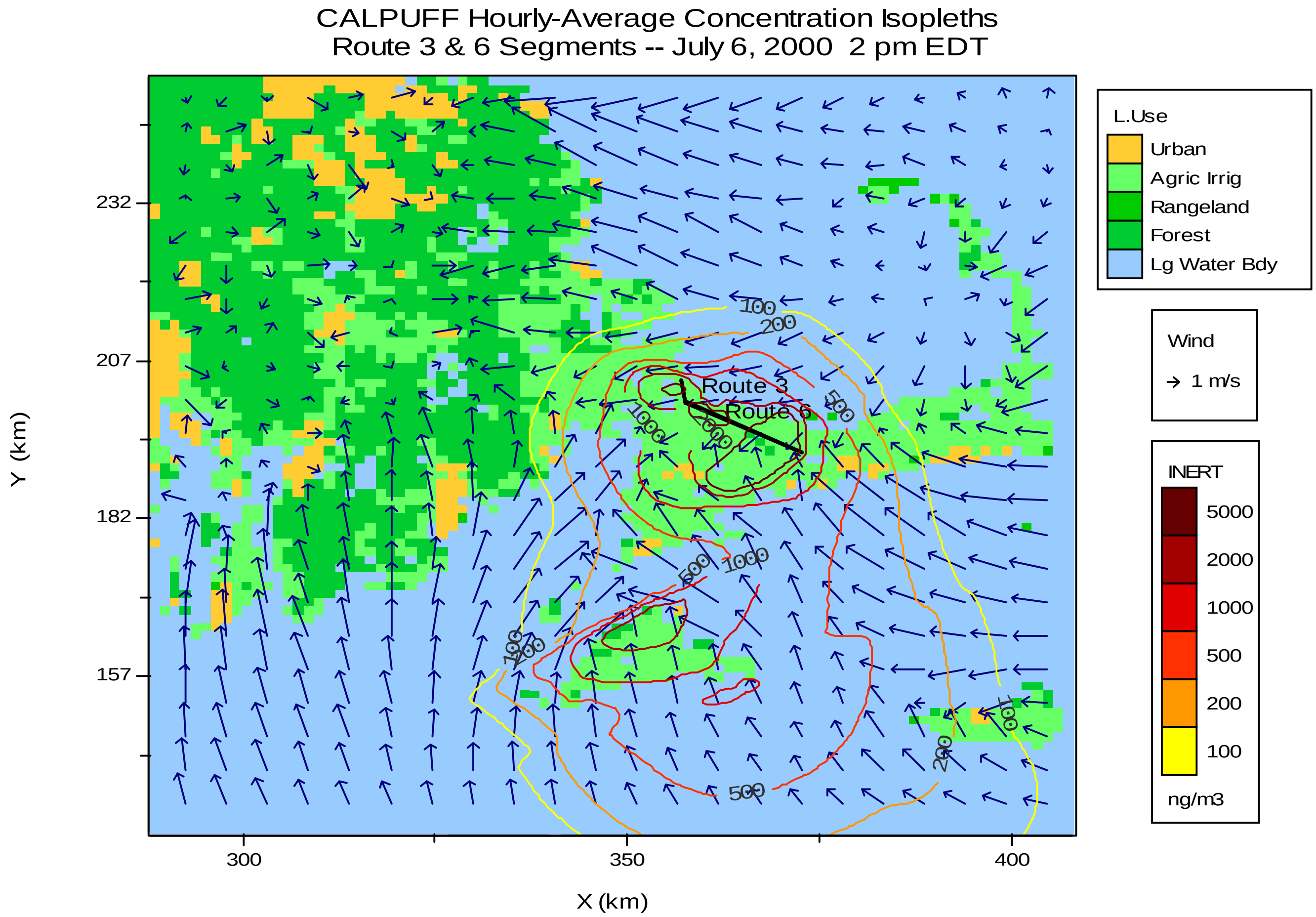

Figure 154. Hour-average concentration isopleths over the CALPUFF domain, arising from uniformly distributed emissions along segments of Routes 3 and 6 totaling 100 g/s, for July 6 at 2 pm EDT. Also shown are CALMET wind vectors for the surface layer.

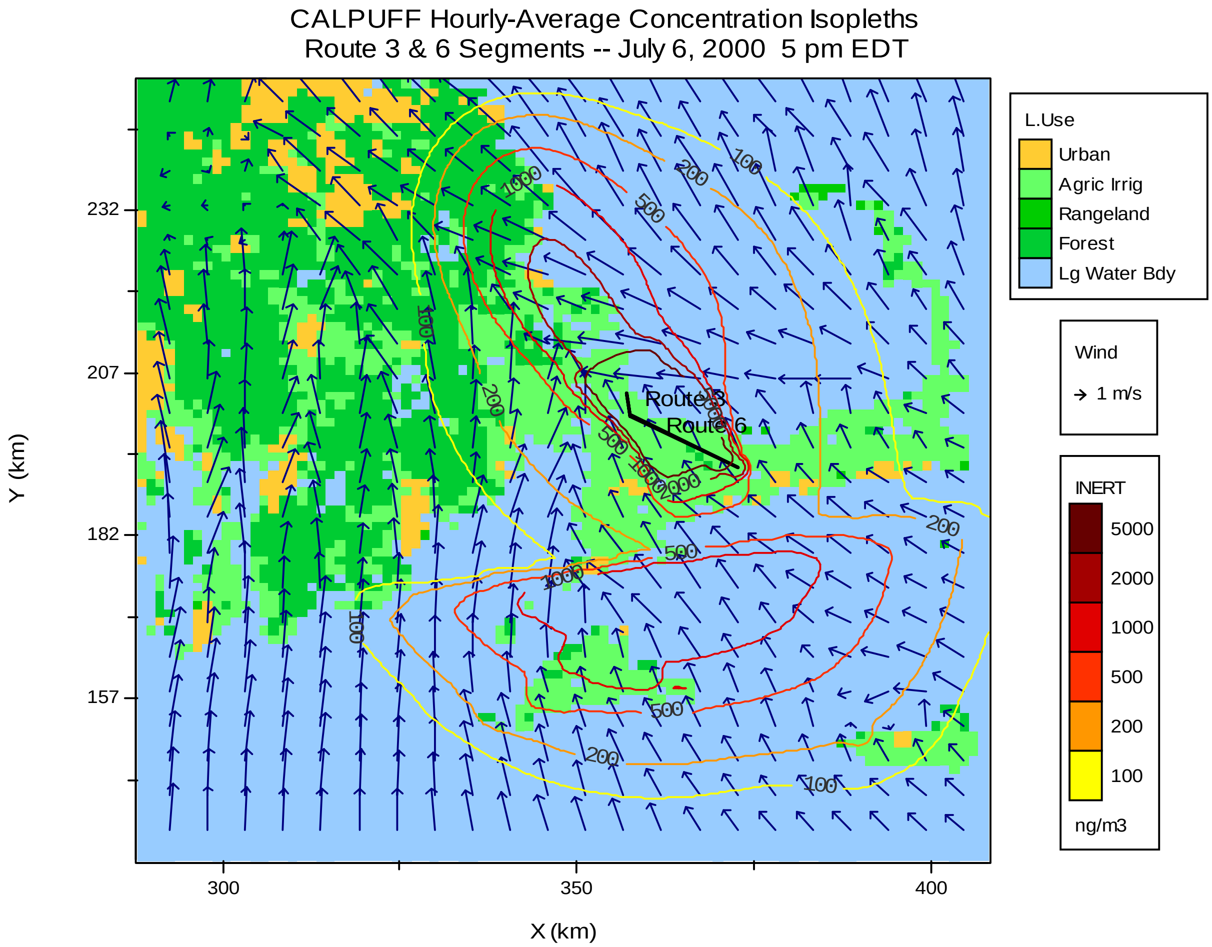

Figure 155. Hour-average concentration isopleths over the CALPUFF domain, arising from uniformly distributed emissions along segments of Routes 3 and 6 totaling 100 g/s, for July 6 at 5 pm EDT. Also shown are CALMET wind vectors for the surface layer.

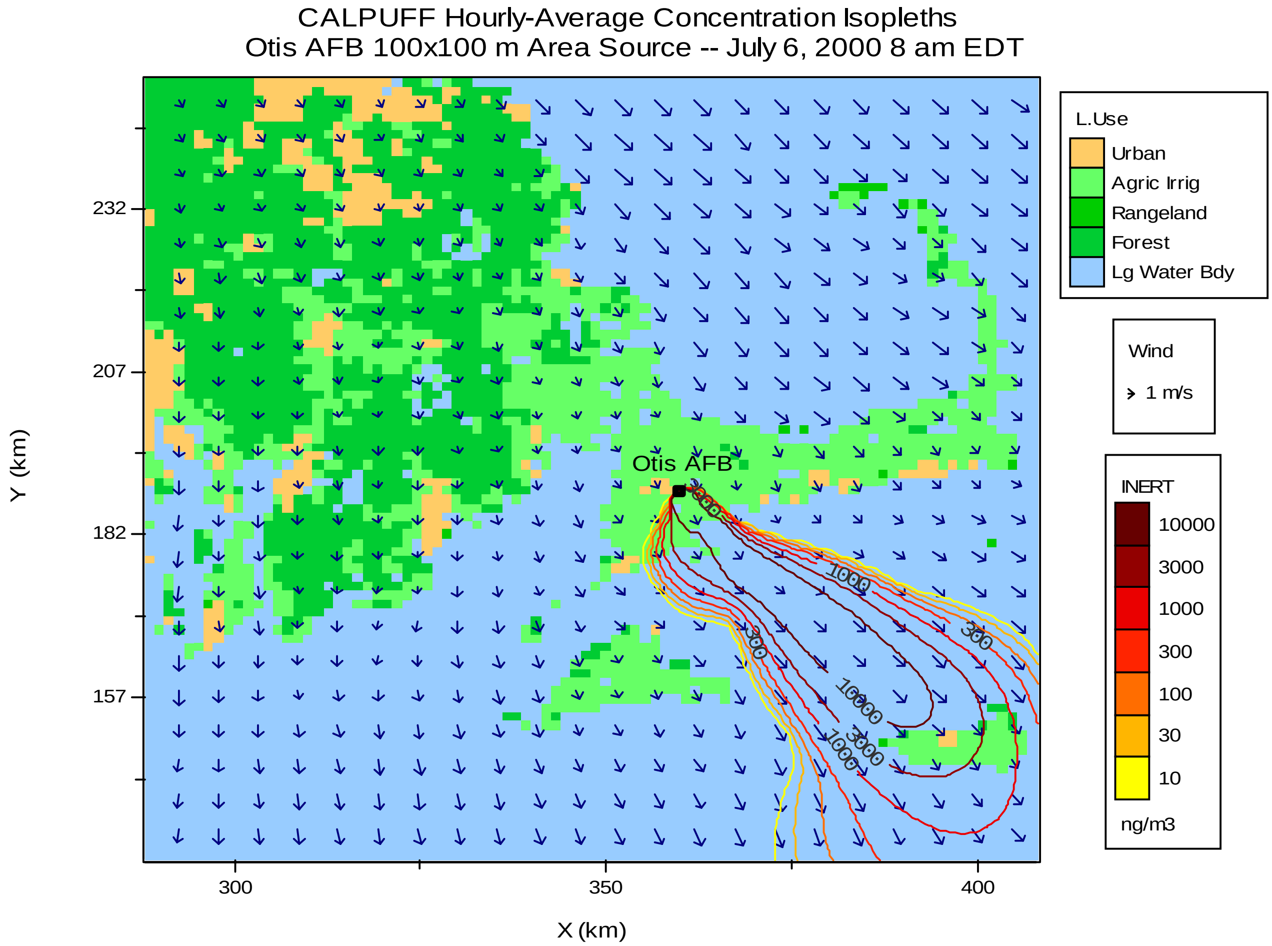

Figure 156. Hour-average concentration isopleths over the CALPUFF domain, arising from a uniform 10000 m^2 area source at Otis AFB with emissions totaling 100 g/s, for July 6 at 8 am EDT. Also shown are CALMET wind vectors for the surface layer.

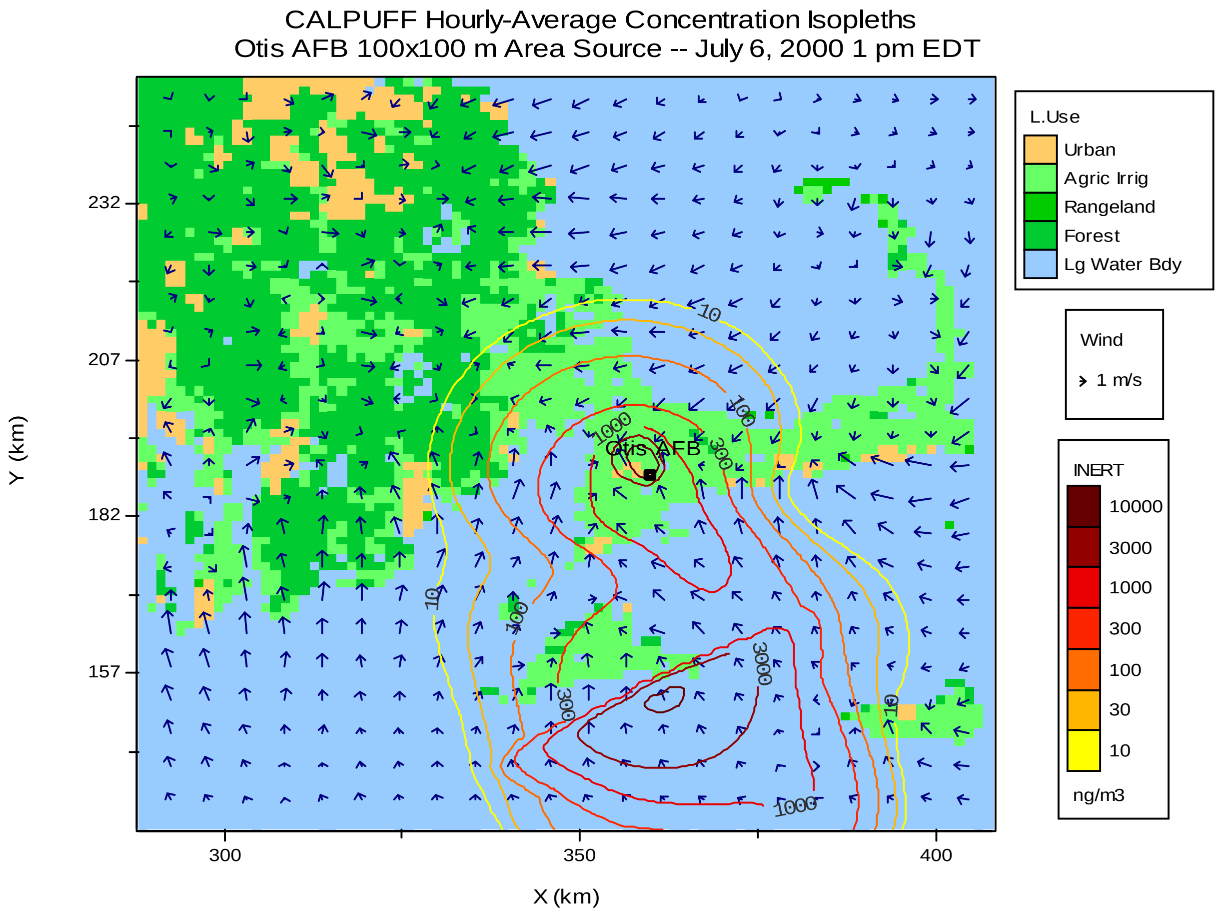

Figure 157a. Hour-average concentration isopleths over the CALPUFF domain, arising from a uniform 10000 m^2 area source at Otis AFB with emissions totaling 100 g/s, for July 6 at 1 pm EDT. Also shown are CALMET wind vectors for the surface layer.

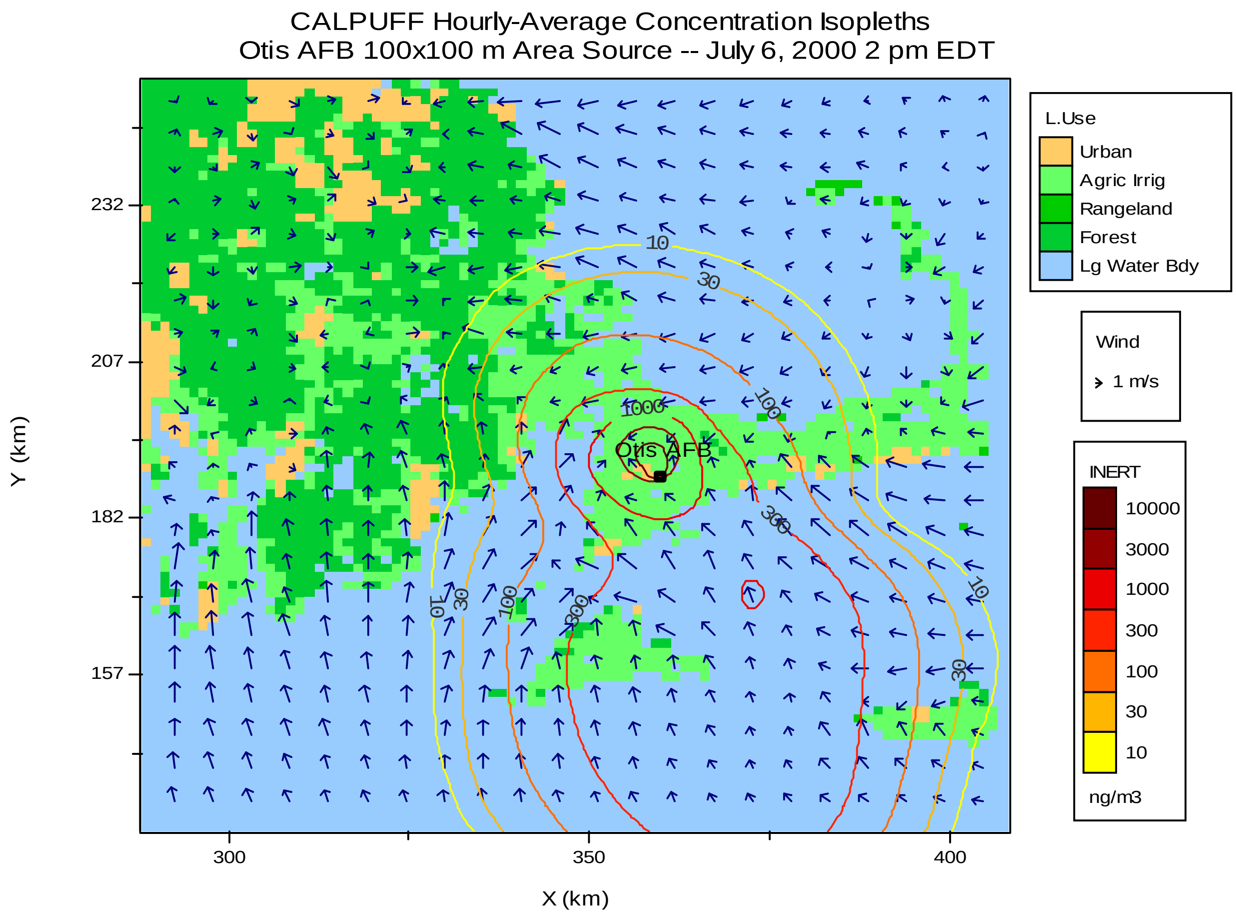

Figure 157b. Hour-average concentration isopleths over the CALPUFF domain, arising from a uniform 10000 km^2 area source at Otis AFB with emissions totaling 100 g/s, for July 6 at 2 pm EDT. Also shown are CALMET wind vectors for the surface layer.

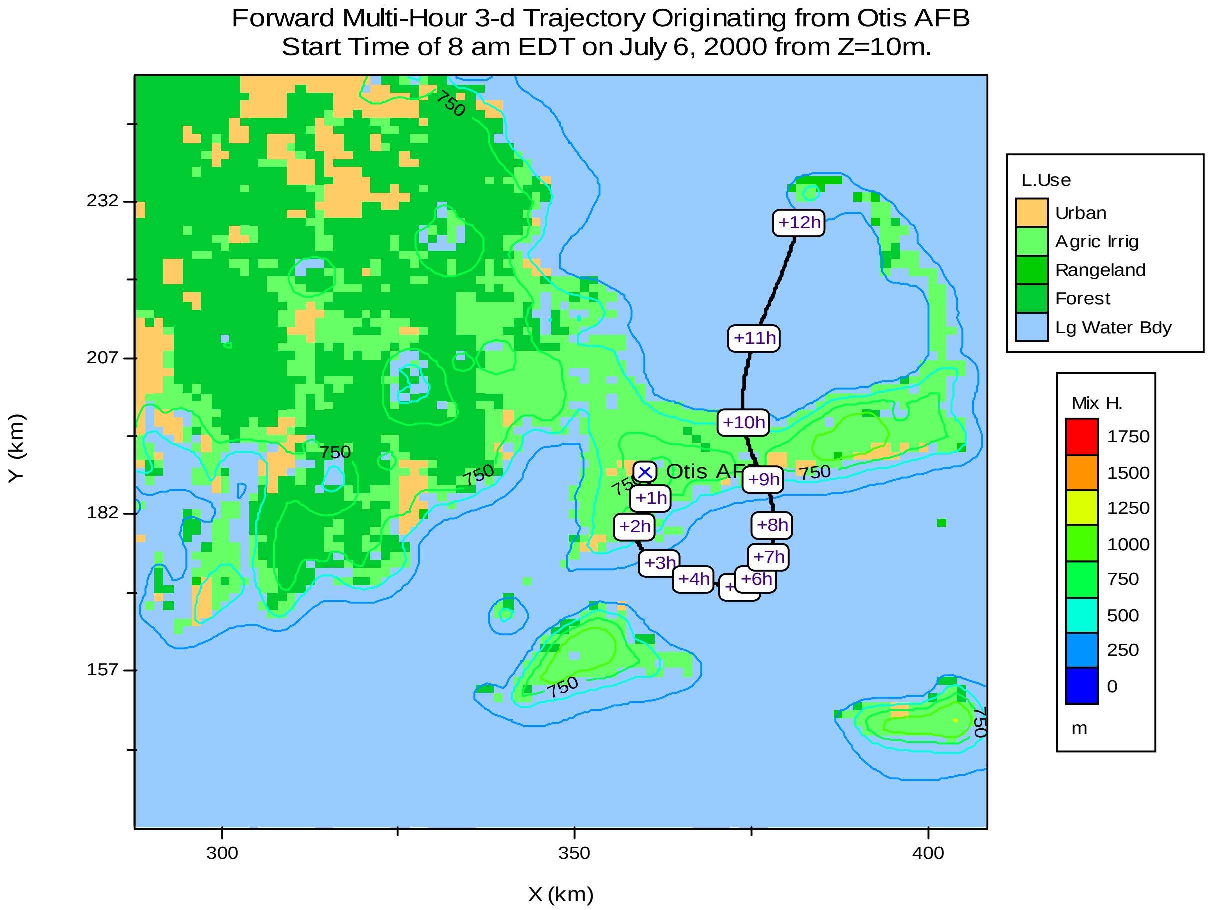

Figure 158. Forward-in-time, multi-hour, 3-d trajectory generated using CALMET winds and originating from a height of 10m from Otis AFB at 8 am EDT on July 6, 2000. Numbers on the trajectory indicate hours of transport. Mixing depths are also shown and are rather constant (about 700-800m) within several km of Otis AFB.

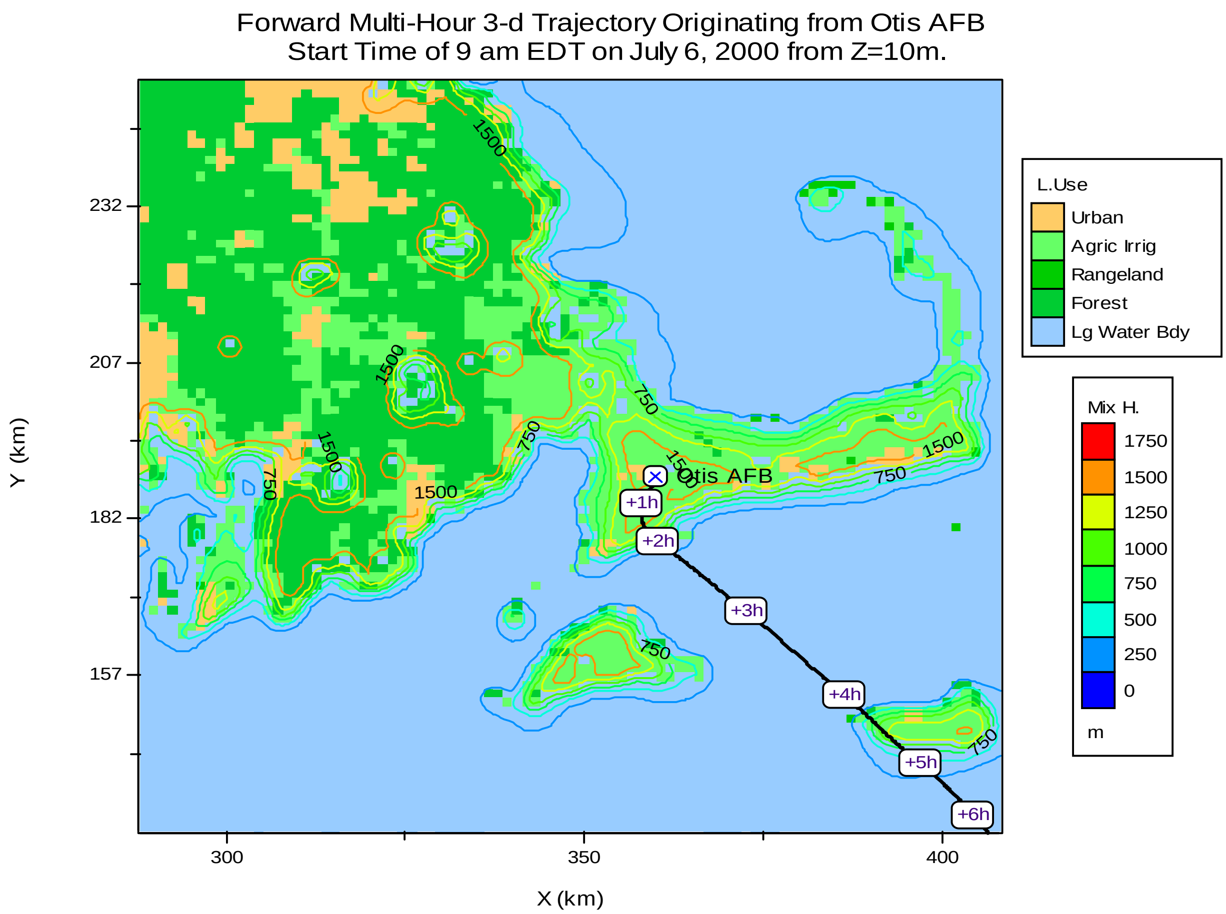

Figure 159. Forward-in-time, multi-hour, 3-d trajectory generated using CALMET winds and originating from a height of 10m from Otis AFB at 9 am EDT on July 6, 2000. Numbers on the trajectory indicate hours of transport. Mixing depths are also shown and are rather constant (about 1500m) within several km of Otis AFB.

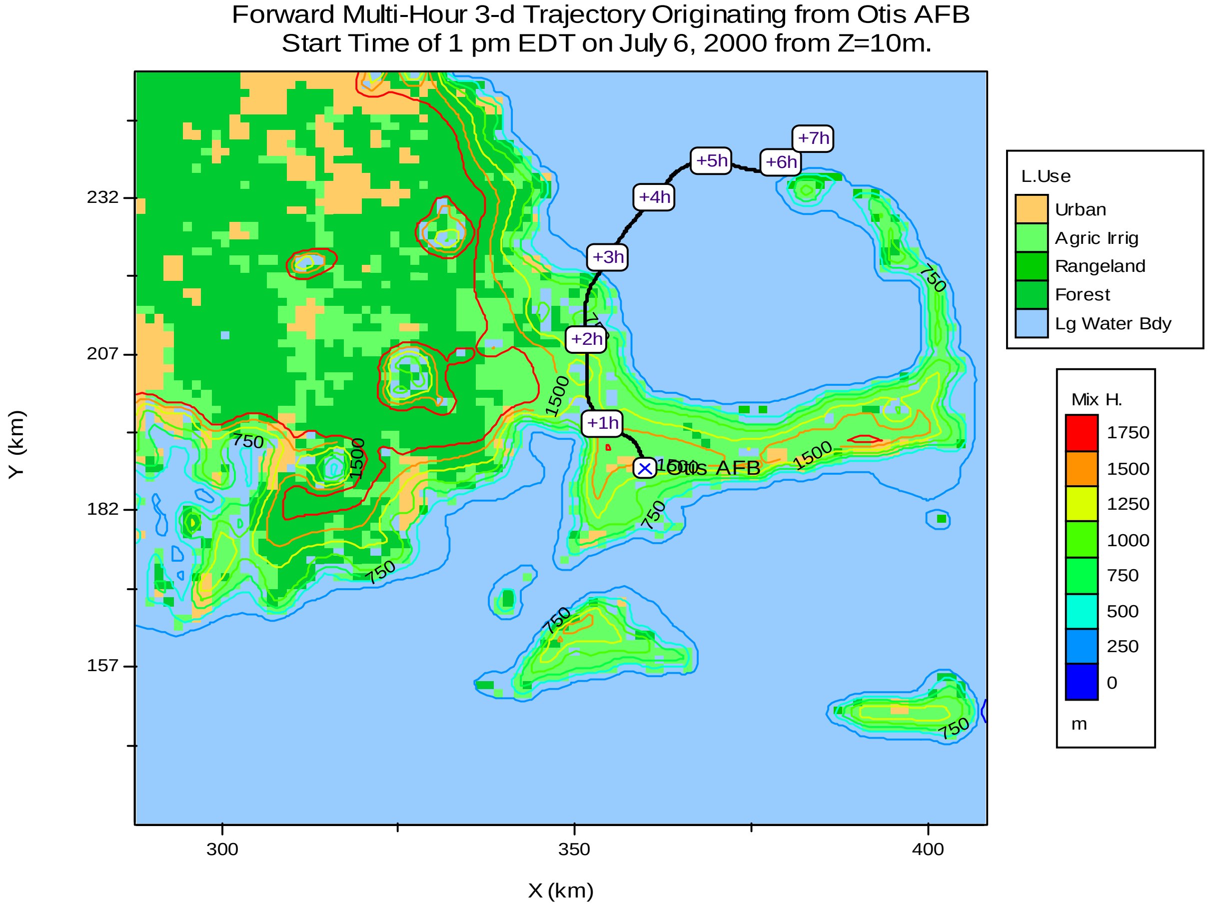

Figure 160. Forward-in-time, multi-hour, 3-d trajectory generated using CALMET winds and originating from a height of 10m from Otis AFB 4 hours later at 1 pm EDT on July 6, 2000. Numbers on the trajectory indicate hours of transport. Mixing depths are also shown and are rather constant (about 1500m) within several km of Otis AFB.

4.5.1.3

Case 3 CALPUFF Results.

Some results for the August 21-22 case are presented for the Brayton Point Plant in Figure 161. This figure is for a time period a few hours earlier than that depicted for SCIPUFF in Figure 95. The values of the predicted maximums, nevertheless, seem similar for the two models (4.2 ug/m3 for CALPUFF and 2.6 ug/m3 for SCIPUFF). Figure 162 shows the pattern for the Canal Plant releases at 8 am on August 22. The 2 am August 22 pattern for the Otis release is shown in Figure 163. The pattern may be compared to that produced by SCIPUFF in Figure 110. The winds are fairly uniform from the west over the region at this time and from the northwest for the later time of Figure 164. Figure 165 shows the complex wind field at 2 pm as a result of sea breeze flow circulations. Relatively high concentrations of released material are seen offshore to the south of the Cape at this time. The contaminants are on track to pass over Martha's Vineyard in the return sea breeze to the south side of Cape Cod. The pattern can be compared to that produced for the same hour by SCIPUFF for the highway source in Figure 107. Figure 111, also for the same hour and for the Otis AFB source, shows the concentration pattern from SCIPUFF only one hour after the release. For this reason it does not show the location of pollutant material that had been released in earlier hours. Figure 166 shows the 24 hour average concentration isopleths, indicating the wide spread of the contamination over a single day's time.

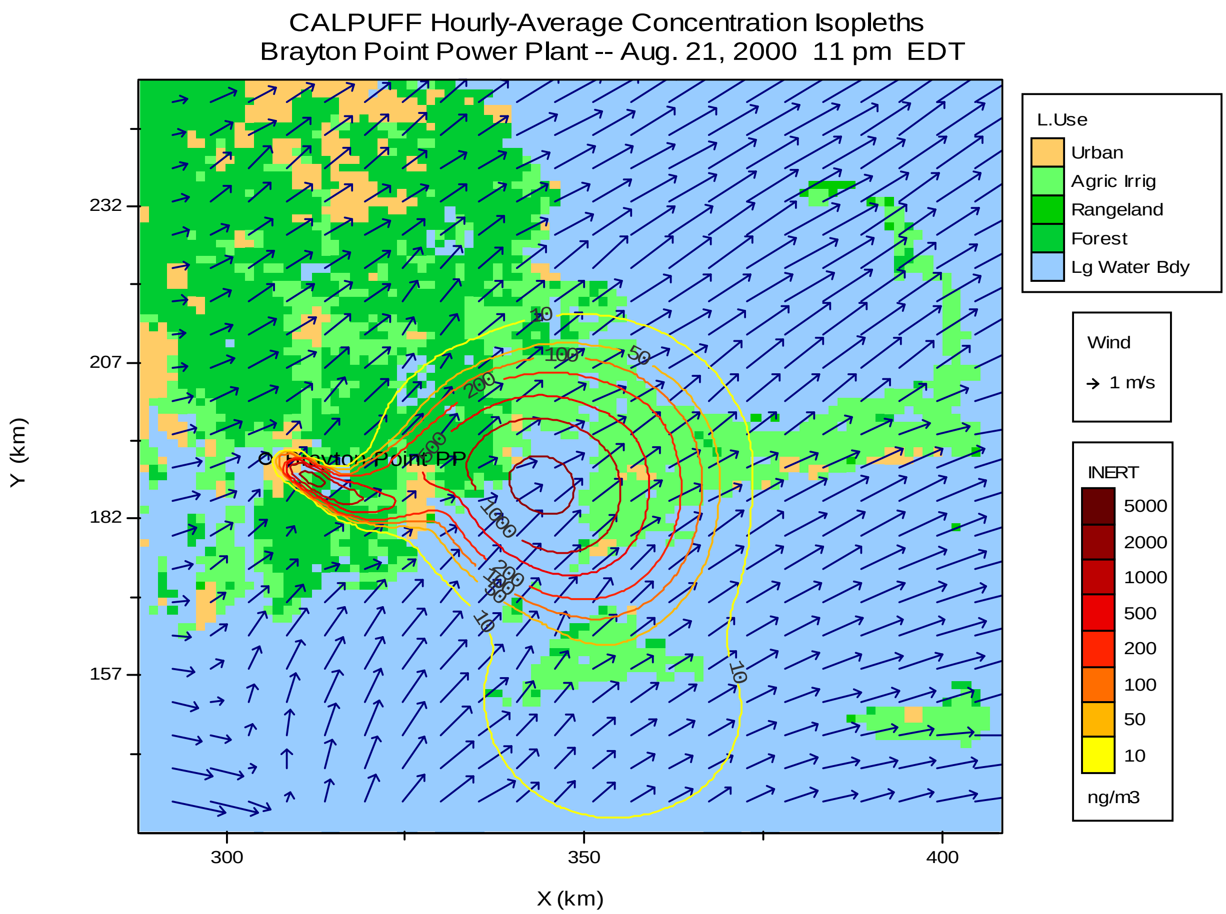

Figure 161. Hour-average concentration isopleths over the CALPUFF domain, arising from the Brayton Point Power Plant at an assumed emission rate of 100 g/s, for Aug. 21, 2000 at 11 pm EDT. Also shown are CALMET wind vectors for the surface layer.

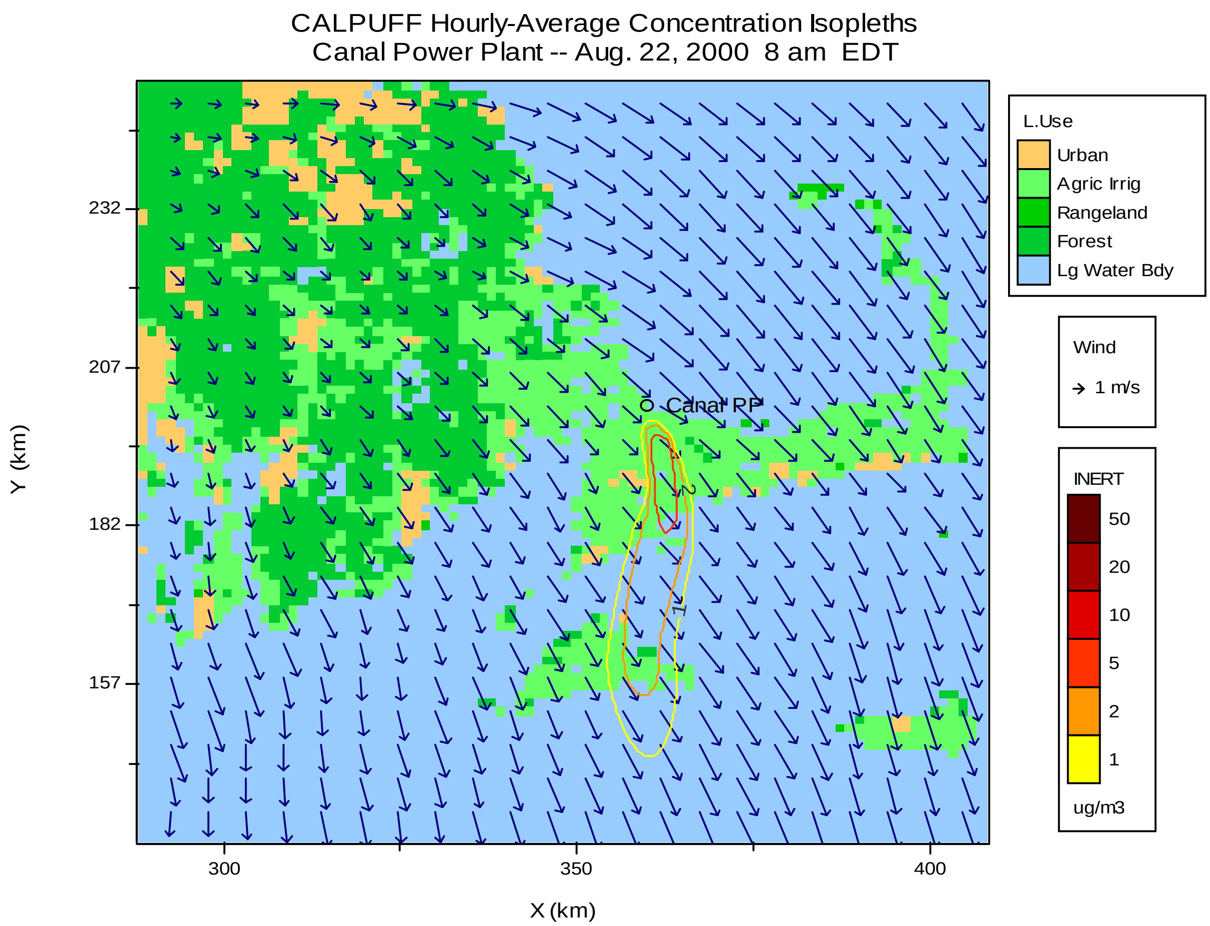

Figure 162. Hour-average concentration isopleths over the CALPUFF domain, arising from the Canal Power Plant at an assumed emission rate of 100 g/s, for Aug. 22 at 8 am EDT. Also shown are CALMET wind vectors for the surface layer.

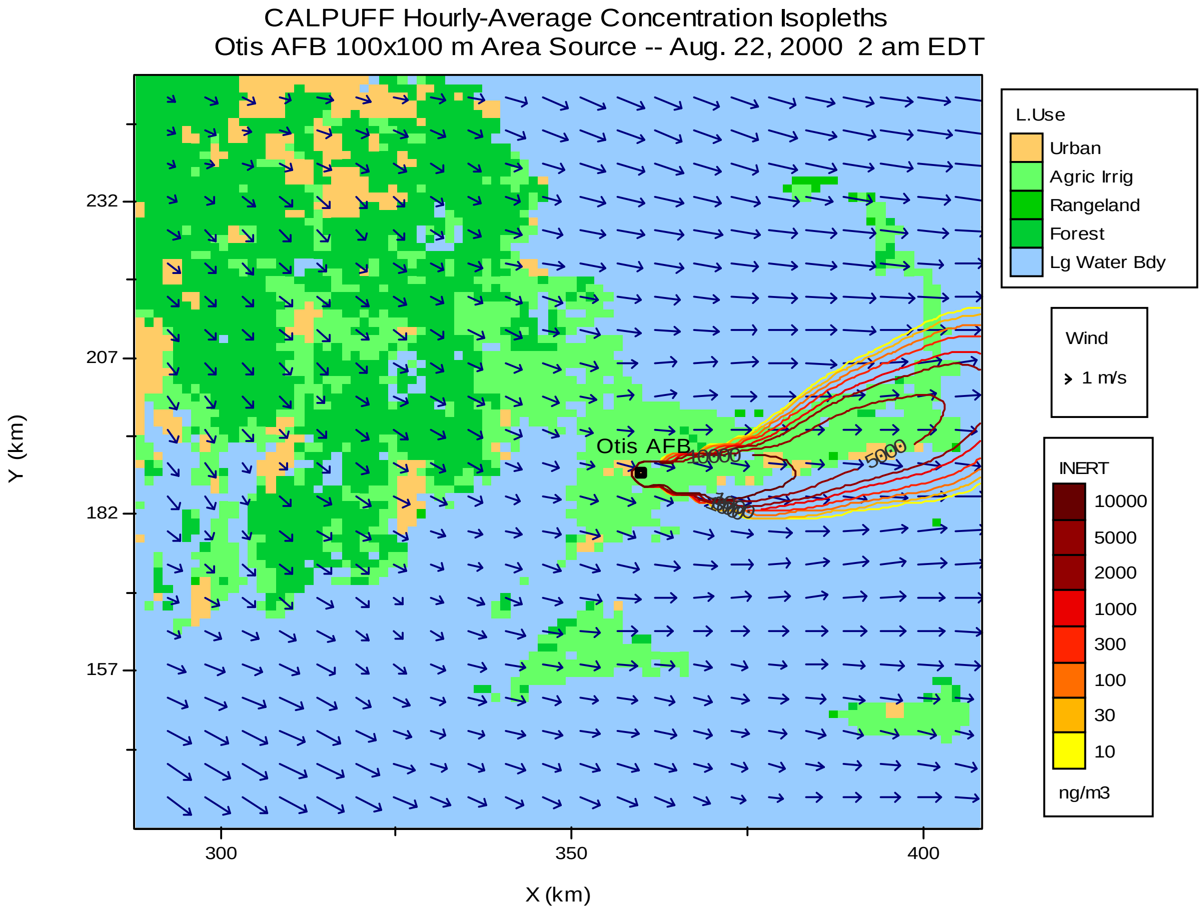

Figure 163. Hour-average concentration isopleths over the CALPUFF domain, arising from a uniform 10000 m^2 area source at Otis AFB with emissions totaling 100 g/s, for Aug. 22 at 2 am EDT. Also shown are CALMET wind vectors for the surface layer

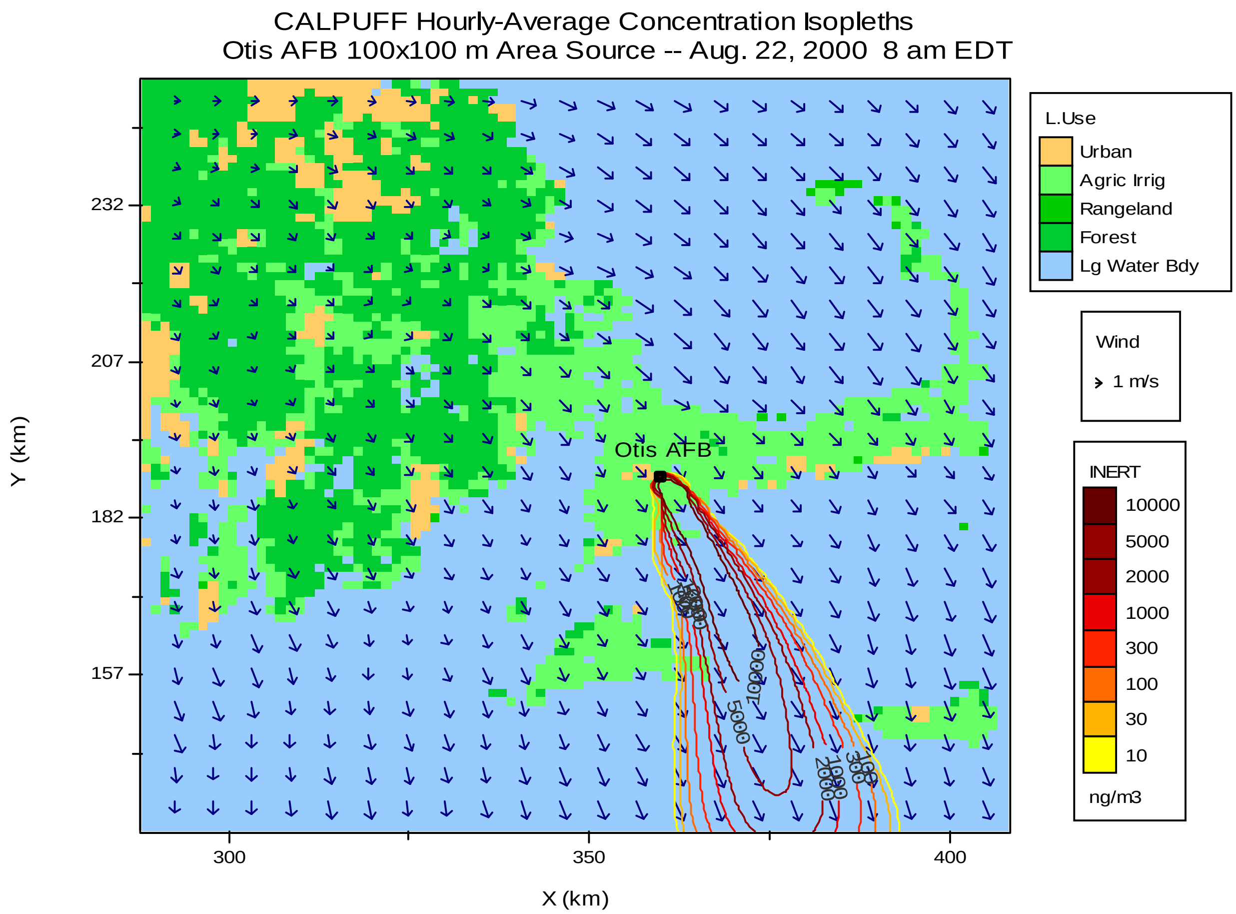

Figure 164. Hour-average concentration isopleths over the CALPUFF domain, arising from a uniform 10000 m^2 area source at Otis AFB with emissions totaling 100 g/s, for Aug. 22 at 8 am EDT. Also shown are CALMET wind vectors for the surface layer.

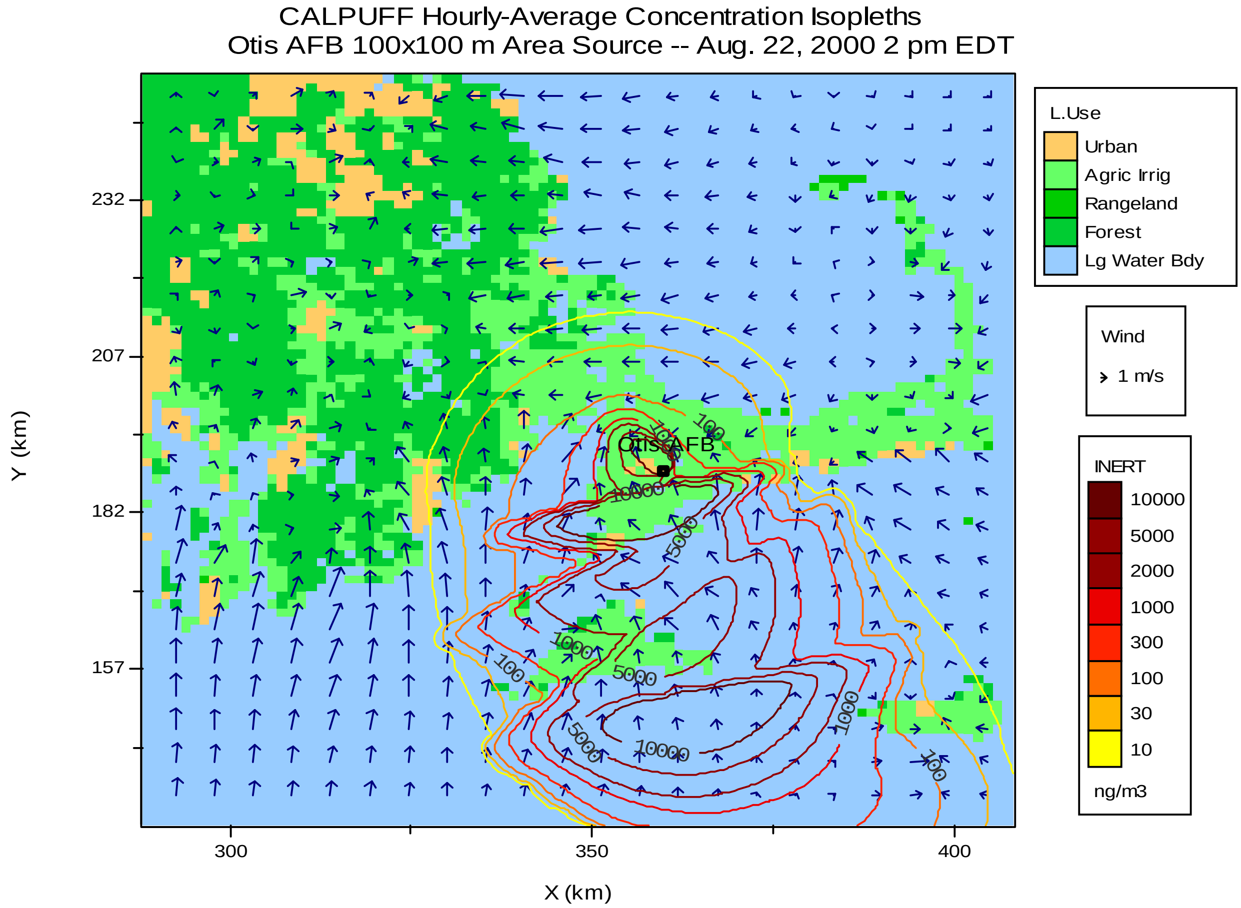

Figure 165. Hour-average concentration isopleths over the CALPUFF domain, arising from a uniform 10000 m^2 area source at Otis AFB with emissions totaling 100 g/s, for Aug. 22 at 2 pm EDT. Also shown are CALMET wind vectors for the surface layer.

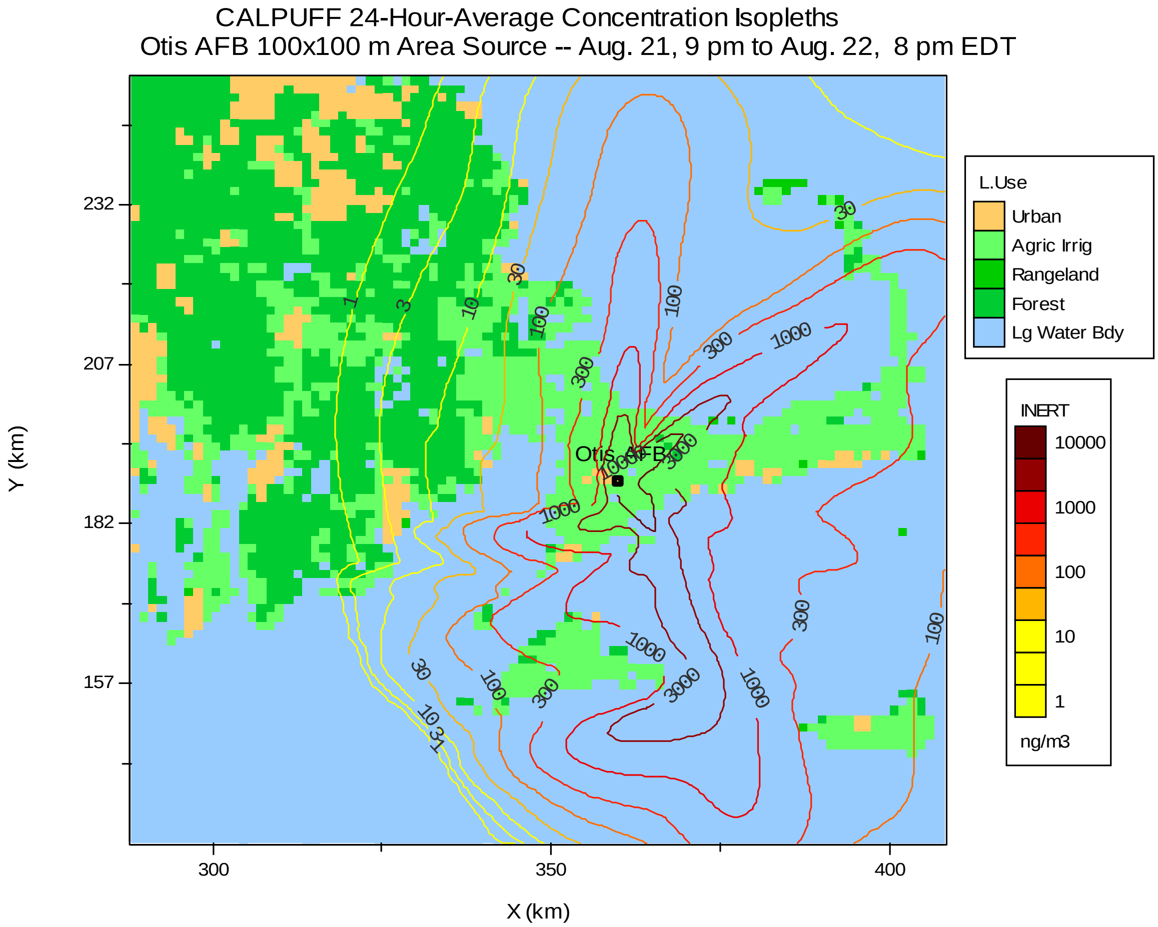

Figure 166. 24-Hour-average concentration isopleths over the CALPUFF domain, arising from a uniform 10000m^2 area source at Otis AFB with emissions totaling 100 g/s, from Aug. 21at 9 pm to Aug. 22, 2000 at 8pm EDT. Also shown are CALMET wind vectors for the surface layer.

4.5.2 Dispersion Results from ISCST3

ISCST3 is the model that the US EPA presently recommends for applications in non-mountainous terrain and for source configurations like those modeled in this effort. ISCST3 is typically run with representative local or on-site meteorological tower data or with data routinely collected at airports. The model can only accept and utilize a single value of wind speed and direction, atmospheric stability class and mixing depth for each hour. All sources being modeled are driven by the same meteorological inputs. Thus the model cannot simulate spatial variability of meteorological data in the horizontal. In the vertical, the model can accept changes of wind speed with height above ground but cannot include wind direction changes. Thus ISCST3 is incapable of utilizing the full meteorological inputs of MM5. To provide comparisons, we ran the model using data that might be used in current regulatory practice. Results are shown for the Canal Plant, the Routes 3 and 6 highway line sources and for Otis AFB. For these sources, we used the meteorology observed at Hyannis-Barnstable Municipal Airport for the case study hours.

4.5.2.1 Case 1 ISCST3 Results.

The concentration isopleths predicted by ISCST3 for 6 pm on July 1 are shown in Figure 167. Values shown are in ug/m3. In this Figure and in those that follow, the color coding of the isopleth lines is as listed below.

Table 23. Isopleth Coding Values for ISCST3 Runs

Color	Value (ug/m3)
Red	1000
Pink	500
Peach	250
Yellow	100
Green	50
Cyan	25
Blue	10
Magenta	5
Purple	2.5
40% BLACK	1
Black	0.5

The SURFER software employed allows the use of US Geodetic Survey maps as base maps. The concentration pattern shows the plume in a south southwesterly air flow and can be compared to that predicted by SCIPUFF in Figure 59 for 5 pm on that day. SCIPUFF shows a much more complex pattern with emissions being drawn in to impact the coast north of Duxbury.
Figure 168 shows the predicted 24-hour average concentrations. These 24-hour average concentrations can be compared to those predicted by CALPUFF in Figure 143. Whereas the

Figure167. Hour-average concentration isopleths from ISCST3, arising from the Canal Power Plant for July 1, 2000 at 6 pm EDT.

Figure 168. Twenty-four hour average concentration isopleths from ISCST3, arising from the Canal Power Plant for July 1, 2000, midnight-to-midnight EDT.

ISCST3 averages exceed 1ug/m3 only offshore over Cape Cod Bay, the CALPUFF model shows comparable values but over land areas to the immediate southeast of the plant. Figure 169 shows the impact of the two highway segments on July 1 at 11 am. ISCST3 handles line source geometries by numerical integration and the user has the option of specifying whether the line is depicted as a large number of virtual point sources or as an elongated area-type source. The results in Figure 169 can be compared to the CALPUFF predictions in Figure145. ISCST3 shows isopleths more or less aligned with the highway segment directions as would be expected from a uniform and steady wind field. Figure 170 shows the 24-hour average for July 1.

The ISCST3 isopleths for the Otis AFB simulated source for July 1 at 11 am are shown in Figure 171. These may be compared to those from the CALPUFF run shown in Figure 146. Very different results are apparent due to the differences in the way the two models treat the sea breeze influence. ISCST3 predicts higher maximum concentrations. Figure 172 shows the 24-hour average predicted by ISCST3 for July 1. The maximum isopleth value of 100 ug/m3 compares to the maximum from CALPUFF in Figure 147 of 5 ug/m3. This difference is perhaps associated with the fact that ISCST3 does not allow a non-buoyant surface release to be convected upward. The SCIPUFF and CALPUFF models, as discussed earlier, simulate the vertical rise resulting from converging flows. The predicted maximum ground level concentrations predicted by ISCST3 would therefore be an upper bound on the potential exposure in this situation.

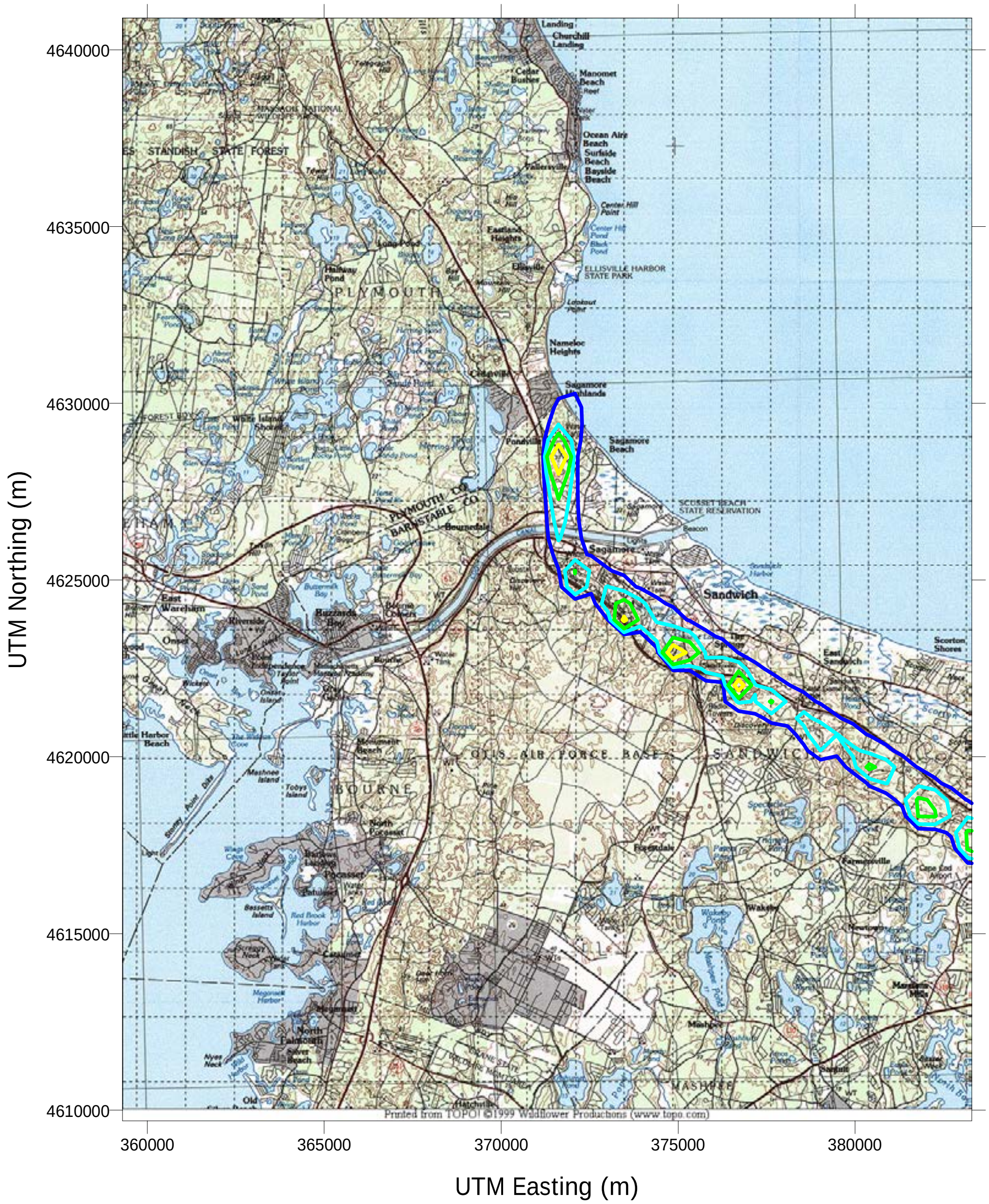

Figure 169. Hour-average concentration isopleths from ISCST3, arising from emissions from Routes 3 and 6 for July 1, 2000 at 11 am EDT.

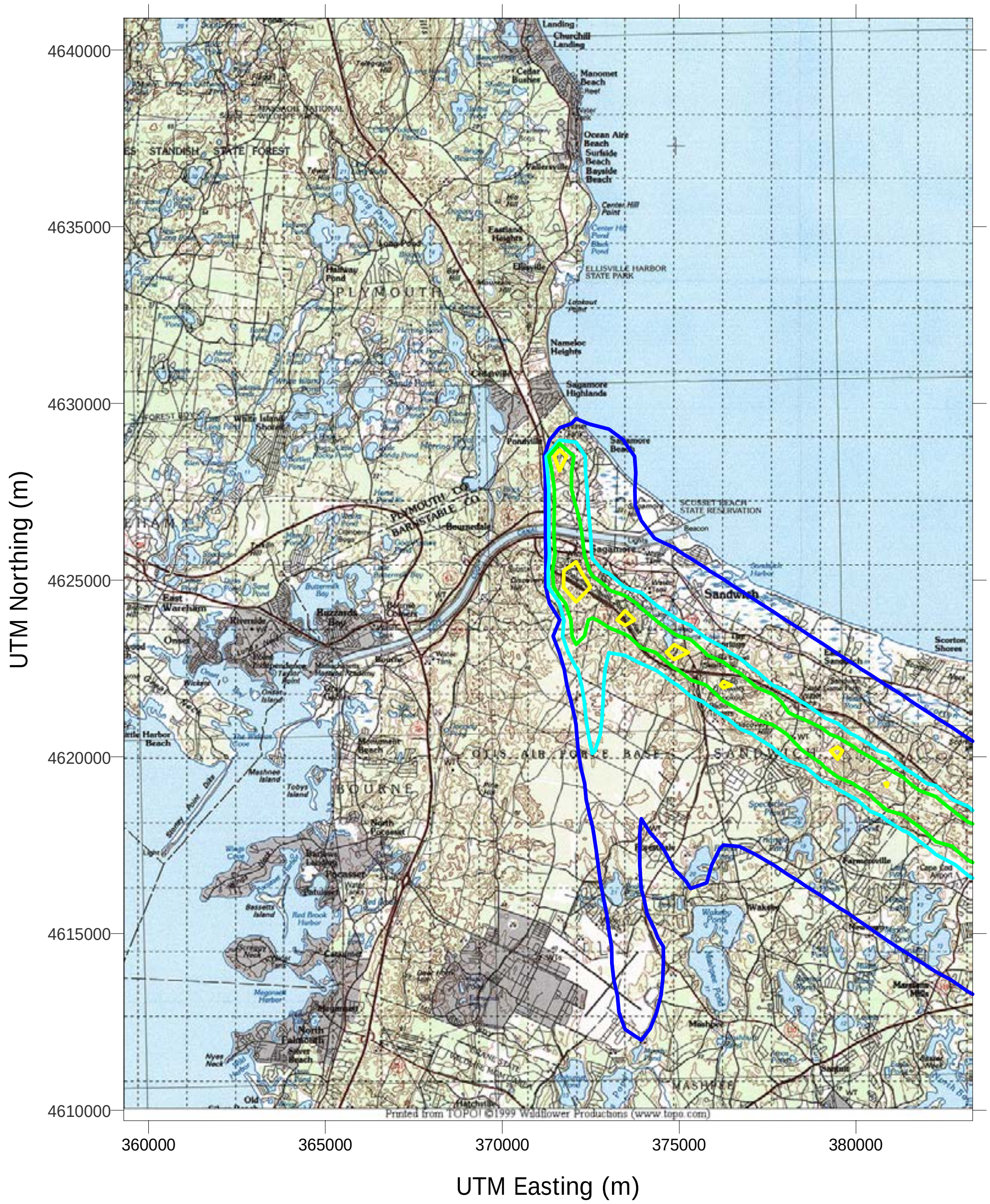

Figure 170. Twenty-four hour average concentration isopleths from ISCST3, arising from emissions from Routes 3 and 6 for July 1, 2000, midnight-to-midnight EDT.

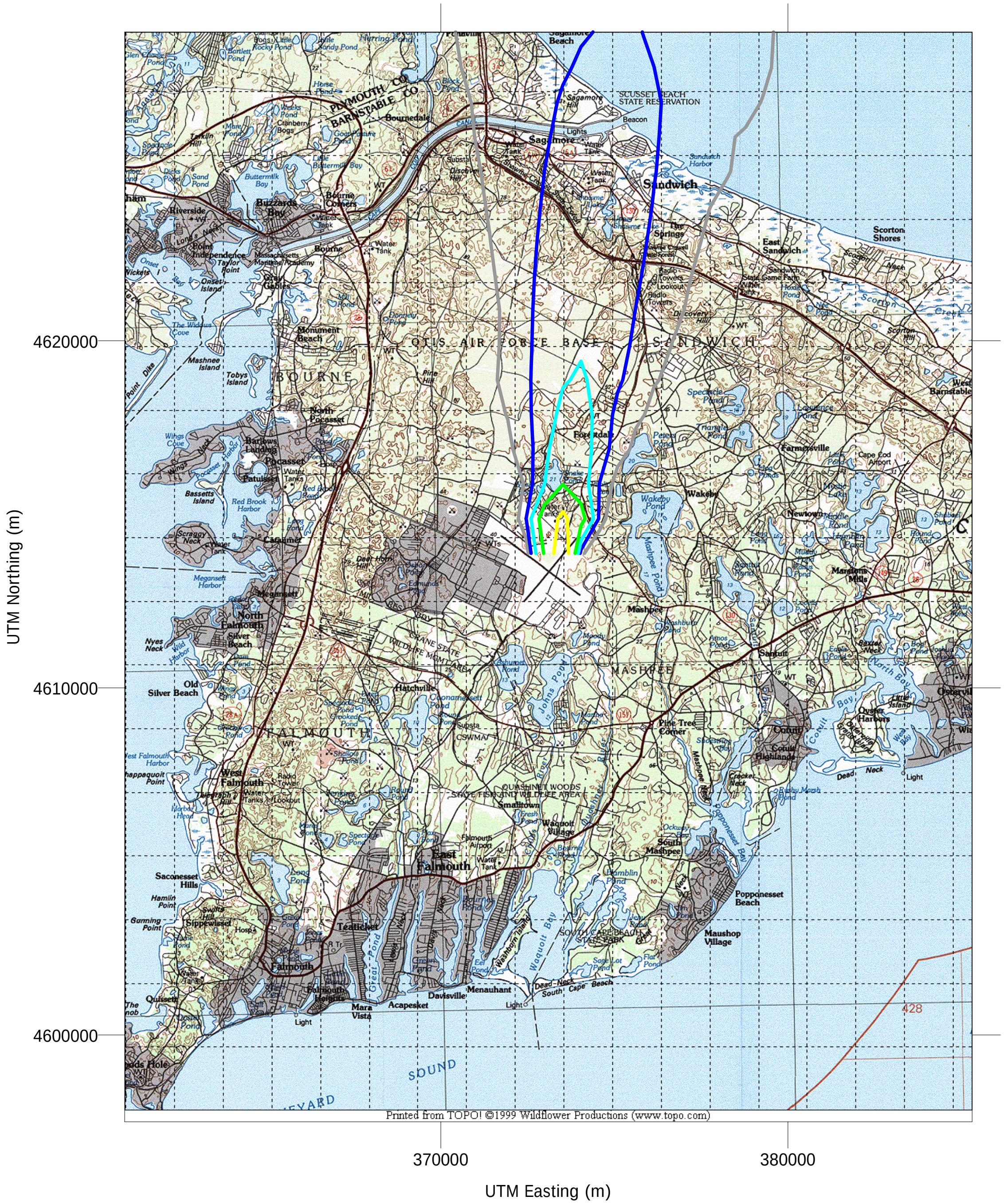

Figure 171. Hour-average concentration isopleths from ISCST3, arising from emissions from the Otis AFB source for July 1, 2000 at 11 am EDT.

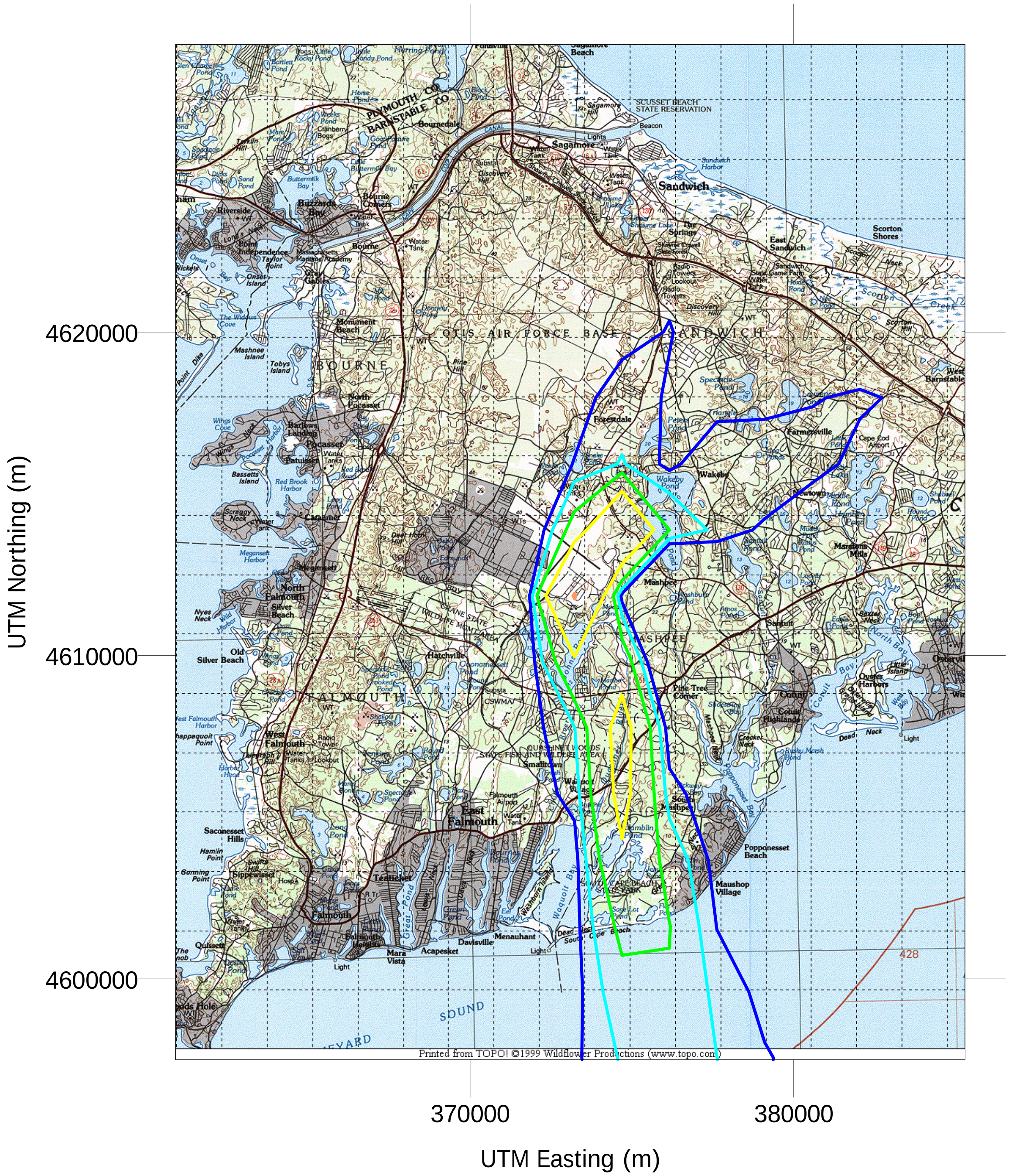

Figure 172. Twenty-four hour average concentration isopleths from ISCST3, arising from the Otis AFB source for July 1, 2000, midnight-to-midnight EDT.

4.5.2.2

Case 2 ISCST3 Results.

The Canal Plant results for July 6 at 2 pm are shown in Figure 173. The plot may be compared to the very different pattern in Figure 151 from the CALPUFF runs. The maximum concentration predicted by ISCST3 for this hour is 24.6 ug/m3; about twice that predicted by SCIPUFF (12.9 ug/m3), but about four times less than that predicted by CALPUFF (93.6 ug/m3). The concentrations predicted for the highway configuration at 5 pm on July 6 are shown in Figure 174. They may be compared to the CALPUFF results shown in Figure 155. ISCST3 again is found to generate higher values for the near surface releases.

The impact of the Otis AFB source is shown in Figure 175. Comparing these to those from CALPUFF in Figure 156, we see very similar concentration predictions; about 100 ug/m3 peak from both models. The similarities are associated with the fact that the wind field have been steady for the hours preceding the snapshot time period. Under these conditions, we expect similar results from ISCST3 and CALPUFF.

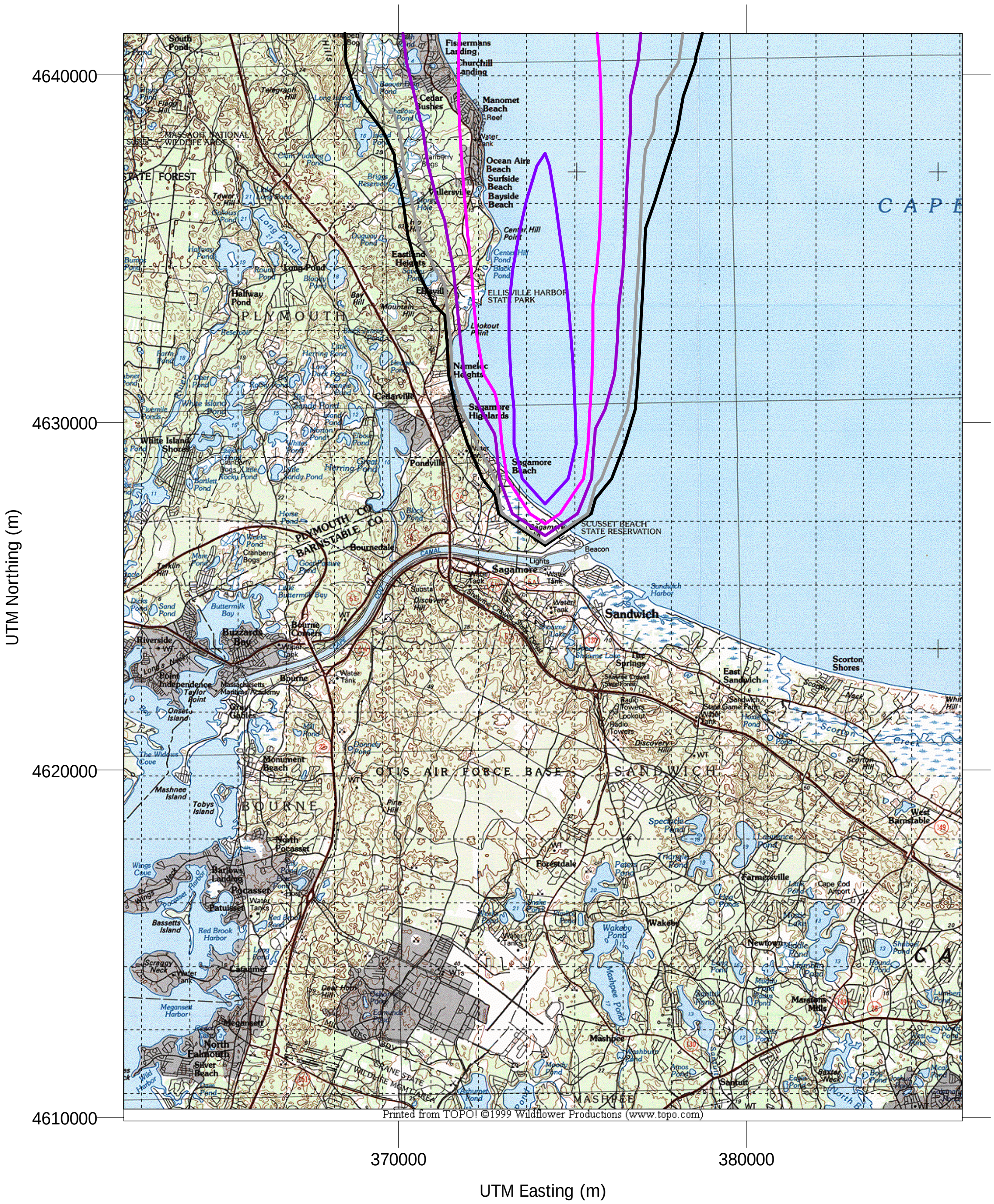

Figure 173. Hour-average concentration isopleths from ISCST3, arising from emissions from the Canal Power Plant for July 6, 2000 at 2 pm EDT.

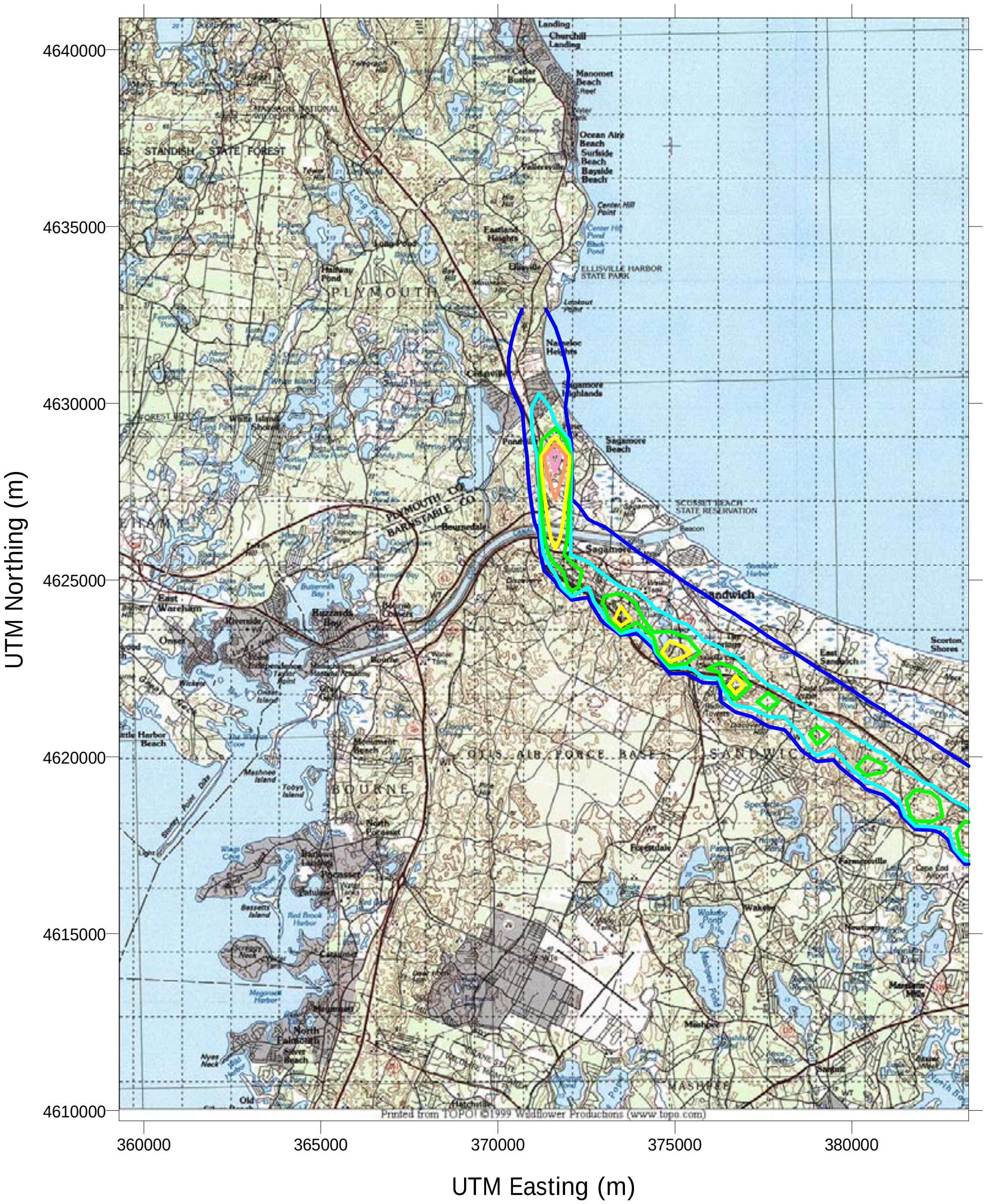

Figure 174. Hour-average concentration isopleths from ISCST3, arising from emissions from Routes 3 and 6 for July 6, 2000 at 5 pm EDT.

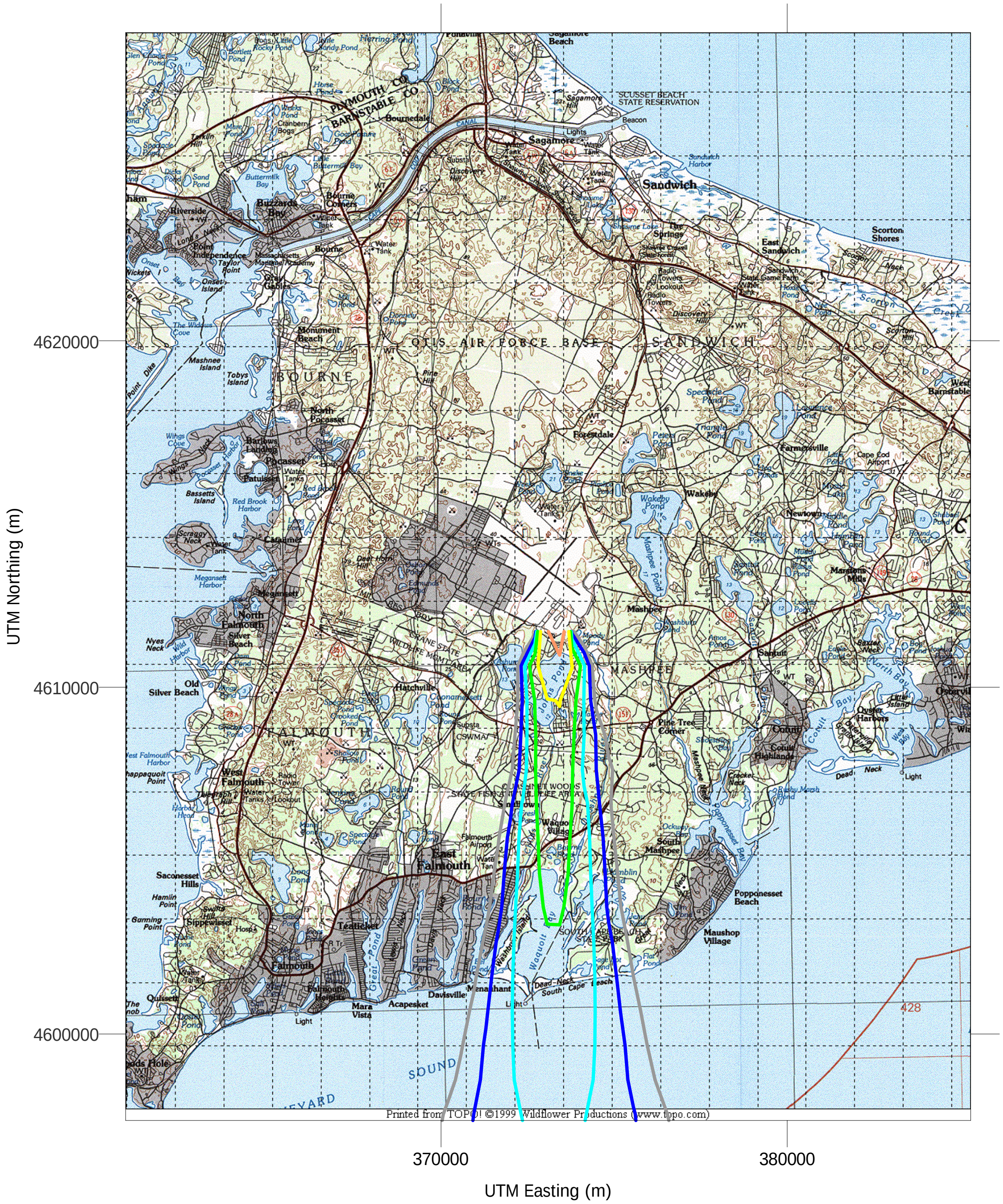

Figure 175. Hour-average concentration isopleths from ISCST3, arising from emissions from the Otis AFB source for July 6, 2000 at 8 am EDT.

4.5.2.3

Case 3 ISCST3Results.

ISCST3 results are shown for the highway configuration for 8 am on August 22 in Figure 176. Results for Otis AFB are in Figure 177. These may be compared to the CALPUFF results for the same hour in Figure 164. The wind directions differ, associated with the difference between the values for that hour at Hyannis Airport versus the MM5/CALMET values for the general area. However, the spreads of the plumes are similar, again reflecting the fact that CALPUFF is calculating concentrations for steady wind conditions.

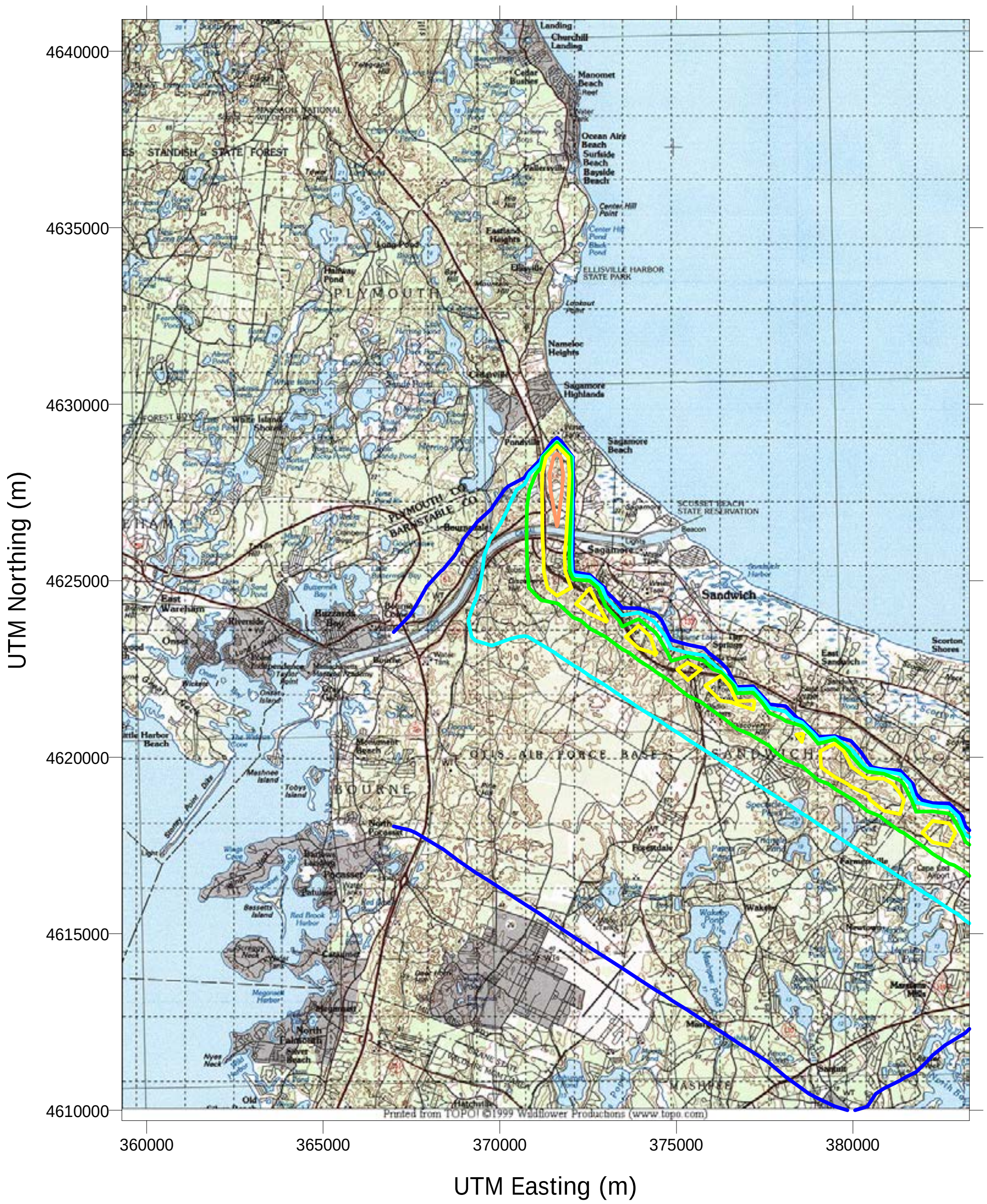

Figure 176. Hour-average concentration isopleths from ISCST3, arising from emissions from Routes 3 and 6 for August 22, 2000 at 8 am EDT.

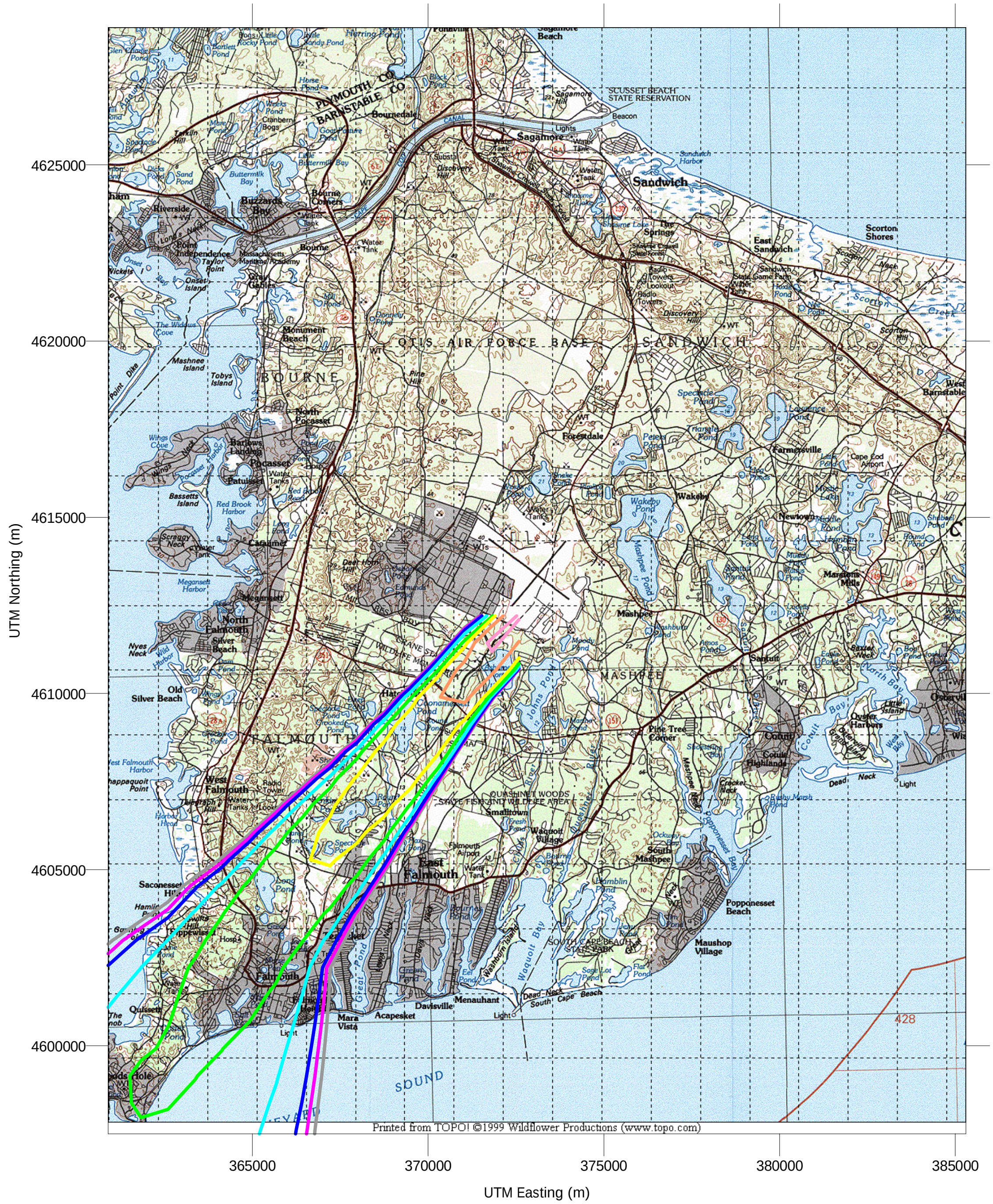

Figure 177. Hour-average concentration isopleths from ISCST3, arising from emissions from the Otis AFB source for August 22, 2000 at 8 am EDT.

4.5.3 Comparison of maximum predicted hourly concentrations.

The discussion in prior sections has focused on the different patterns of potential exposure to pollutants that have been transported by sea breeze related circulations. The spatial and temporal patterns are important to any epidemiological study of air pollution effects. For many air permitting or other regulatory applications, the focus is often on the maximum predicted concentrations as these values are compared to standards or allowable ambient air increases for compliance purposes. In Table 24, below, we have listed the maximum concentrations predicted for the three dispersion models used for the power plant releases for the hours for which SCIPUFF generated isopleths have been made. We note that this limited set of comparisons is too small a set on which to base firm conclusions. Also, in some cases the corresponding values from ISCST3 are not available due to missing meteorological data at Hyannis. Figure 178 compares the predicted concentrations for these hours for the three models. All plots show considerable scatter. SCIPUFF seems to predict values in the same range as ISCST3. CALPUFF, on the other hand tends to predict larger values than ISCST3. CALPUFF also seems to predict larger values than SCIPUFF. The results are not definitive but suggest that a model evaluation effort be undertaken that would compare the predictions of SCIPUFF and CALPUFF in sea breeze flow situations. Ideally, measurement data should be collected on Cape Cod.

Table 24. Maximum Hourly Average Concentrations for Selected Case Study Hours

			Brayton Point Power Plant				CANAL Power Plant		
Day	Hour (EDT)	SCIPUFF Figure Reference	SCIPUFF Conc. ug/m3	CALPUFF Conc. ug/m3	ISCST3 Conc. ug/m3	SCIPUFF Figure Reference	SCIPUFF Conc. ug/m3	CALPUFF Conc. ug/m3	ISCST3 Conc. ug/m3
1-Jul	5	53	0.86	5.34	2.48	58	0.08	1.2	
1-Jul	14	54	9.15	16.1				10.9	22.4
1-Jul	17	55	5.87	12.8	0.902	59	5.69	39	13.5
2-Jul	2	56	1.24	2.28	0.002	60	0.00	1.6	
2-Jul	14	57	23.70	15.6	1.01	61	4.19	1.36	9.9
5-Jul	2	73	2.06	10.1	0.006			5.9	0.99
5-Jul	8	74	20.30	16.4		79	34.90	12.1	
5-Jul	14	75	9.50	11.2	11	80	6.89	23.6	13.3
6-Jul	2	76	2.15	0.726		81	1.61	0.578	
6-Jul	14	77	12.70	8.54	0.398	82	12.90	93.6	24.6
6-Jul	17	78	6.22	21.1	1.08	83	17.70	11.3	14.6
21-Aug	2	92	1.42	3.56	0.016	99	1.73	5.9	0.026
21-Aug	14	93	14.20	16.2	10.3			2.56	22.3
21-Aug	20	94	1.99	27.8	0.017	100	5.44	18.4	
22-Aug	2	95	2.62	0.922	0.193	101	0.10	4.03	
22-Aug	5	96	2.08	0.884		102	0.65	2.81	0.36
22-Aug	14	97	8.25	61.1	9.63	103	8.53	26.5	13.3
22-Aug	17	98	18.20	68.7	1.87			12.6	15.1

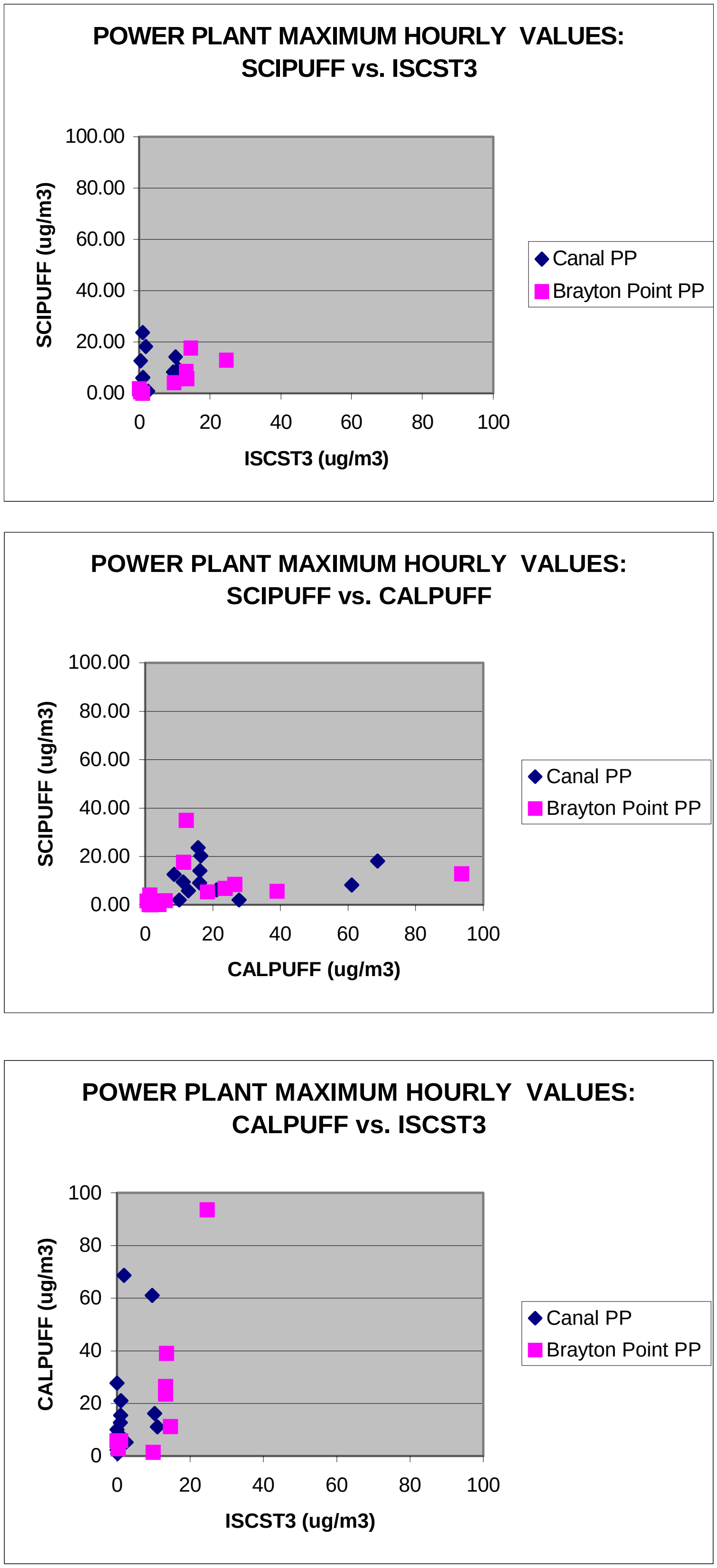

Figure 178. Comparisons of Maximum Hourly Concentrations for SCIPUFF, CALPUFF and ISCST3.

5 Conclusions

5.1 Accomplishments of this Effort

This project has developed a capability for numerically simulating the meteorology important to air pollution dispersion associated with sea breeze circulations and other mesoscale transient meteorological events that occur on Cape Cod. The MM5 mesoscale meteorological model was adapted and customized to the region using a multi-nested grid system. The MM5 model works by using available coarse grid information available from NOAA together with a dynamic simulation of local surface effects (e.g., radiational heating and cooling, surface roughness, albedo, etc) to numerically create local pressure differences and resulting wind and thermal fields on a fine grid scale of 1.33 kilometers for the entire Cape region and its surroundings. Three different two-day periods were chosen on the basis of limited National Weather Service data to be days where sea breeze circulations were expected. The meteorology of these days was then extensively manually analyzed to form a basis for comparing the observed meteorology to that predicted by MM5. The fine scale meteorological fields predicted by the MM5 model are shown to compare rather well to those from the manual analyses. The key features of sea breeze circulations that affect air pollution are also well simulated. In addition, the directions and speeds of the wind fields are predicted rather well on average. While the onset of the predicted sea breezes shows a tendency to occur earlier than suggested by the manual analyses for the cases studied, the depth of penetration of sea breeze fronts were well simulated for the days modeled, and the durations of the circulations seem to be about right. For all three case study periods, the predicted values of the wind speeds and directions, surface and upper level temperatures, sea level pressures, mixing ratios and relative humidity from MM5 were also compared to data collected at 10-15 local weather station reporting sites within the fine grid network and also to similar compilations on the larger, 4 kilometer resolution grid domain. CALMET predicted winds, nearly identical to MM5 winds, also compare favorably to wind data collected at several local beachfront stations by a wind surfing organization.

The success of the adaptation and customization of the MM5 model to the Upper Cape is evident in the comparisons of the computer generated flow fields with the manual analyses of weather data and with the specific meteorological variables measured during the case study hours

The MM5 model provides much more detailed information than is available to the manual analyst or that can be predicted by a purely diagnostic flow model such as CALMET. For example, the simulations provide far more detail on the horizontal wind patterns than is available from observations taken at widely scattered airport stations. Importantly, from an air pollution transport perspective, we see detailed information on the vertical motions associated with sea breeze and land breeze circulations. The simulations show how emissions from both near-ground-level sources, as well as from tall stack releases, can get into the return airflow of the sea breeze circulations. Thus, the application of the MM5 model as a means of developing 3-D depictions the detailed wind patterns that affect the dispersion of pollutants on the Cape represents a major improvement in the modeling technology available to researchers. Because MM5 is a meteorological driver program, its outputs can be used as inputs to alternative trajectory or atmospheric dispersion models other than those demonstrated in this study. Future uses of MM5 could obviously include dispersion models still in the development stage.

5.2 Implications of Modeling Results to the Selection of Models

Section 4 has provided considerable information on the modeling approaches through examples of the models' output data.

The MM5 model was coupled directly to the SCIPUFF model for each of the case study periods to predict air quality concentrations from the four different sources simulated. Snapshots of the plume patterns are shown in Section 4.3. SCIPUFF is a very capable model in that it is able to handle three-dimensional wind fields and fine grid scale meteorological data inputs. The combination of these models seems to work well in this application. The public domain SCIPUFF is available from EPA. Because most regulatory applications of dispersion models do not address the kind of detailed flow patterns studied here, the model has not yet been very widely used.   The coupling of the MM5 model to the TRAJEC model, as a parallel effort to running SCIPUFF, provides a great deal of insight into the three dimensional nature of the circulations encountered during the case study hours. Of particular interest is the ability of the model to show not only the horizontal, plan view, of the trajectory taken by a set of plume centerlines (each represented by a material parcel), but also to reveal whether the plume centerlines are ascending or descending during the period of the event. This will become an important feature in future analyses of the land breeze circulations, as well as for sea breeze flows.

CALPUFF has a more extensive history for regulatory use and has been advocated by EPA for several years for long-range transport modeling applications (specifically, if the distance between sources and receptors becomes greater than 50 km.). This is because the variations of wind direction and atmospheric stability, affecting even fairly uniform flow conditions over long distances can be incorporated in to the model. For applications involving more than single-station meteorology, the CALMET meteorological driver program is required to run CALPUFF. In this study we used the MM5 model outputs, supplemented by Hyannis-Barnstable Municipal Airport reported cloud cover, to drive CALMET. A comparison of the concentration patterns between SCIPUFF and CALPUFF show many similarities, as would be expected given the common MM5 origin for the wind fields. However, there are significant differences in both the magnitude and locations of some of the high concentrations predicted. These differences are presently thought to arise from two key factors: CALPUFF's reliance on the 2-D horizontal flow rather than the full 3-D flow utilized by SCIPUFF, and the often quite different mixing height fields produced by the MM5 model versus the CALMET model. As is discussed in the main body of the report, CALPUFF presently ignores vertical velocities (i.e., except for adjusting dispersion rates upward in convergence zones) and therefore is not fully responsive to all three-dimensional aspects of flows. While such 3-d responsiveness could easily be "switched-on" in the CALPUFF code, it would not be an EPA-approved change. The reason for this explicit insensitivity to vertical winds is based on the fact that most CALMET generated wind fields are produced using sparse observational data that result in poor determination of vertical velocities. Thus, it is prudent in many CALPUFF applications for it to ignore these vertical velocities, except in special situations (e.g., convergence zones). Chang (2001) has shown that this lack of responsiveness to vertical velocities can sometimes give the model predictions a certain robustness; however, in cases where the vertical velocities are well determined, as in this study's high-space-resolution application using MM5, use of the modeled velocities would likely lead to improved results. Just as the CalDESK model now has a switch to select three-dimensional vs. two-dimensional trajectories, so CALPUFF would benefit from a similar switch to incorporate vertical velocities into the mean transport of the puffs. Another factor that is involved in the differences between the predicted values from CALPUFF and SCIPUFF is associated with the fact that CALMET calculates mixing depths differently than MM5, and small differences in mixing height can often lead to significant changes in ground level concentrations, especially for elevated sources. This topic is expanded upon in Section 7. The dispersion rate algorithms in CALPUFF also differ from those in SCIPUFF; however, it is not possible from this study to determine which model is the more accurate. The ability of SCIPUFF to directly couple to the MM5 outputs without any intermediate processing is, however, a factor favoring SCIPUFF for this scale of meteorological flows. A similar direct coupling between MM4 and CALMET was tried several years ago, but subsequently disconnected because of mixing height discrepancy issues. Re-establishment of a direct MM5-CALMET connection, or even a somewhat more ambitious direct MM5-CALPUFF coupling, is something that deserves further consideration, given the greater accuracy of MM5 and the fact that it would greatly facilitate application of CALPUFF and would enable a CALPUFF/SCIPUFF intercomparison based solely on the features of the dispersion models themselves.

Another deliverable for this project is the CalDESK graphics capability. This proprietary software, purchased for this project, is not available in the public domain version of CALMET or CALPUFF. The software is especially useful in displaying both the meteorological and concentration fields simultaneously and should be a very useful tool to future research.

The ISCST3 model is an EPA recommended model and is commonly used for all the source types modeled in this study. The dispersion algorithms cannot handle spatially varying wind directions or horizontally varying meteorological variables such as winds or other parameters affecting atmospheric dispersion rates. For cases when such variability is important, such as for sea breezes circulations or for frontal passages, ISCST3 is clearly not an appropriate model. Because ISCST3 only uses a single value of wind speed and wind direction for the entire study region for a given hour, it cannot utilize the detailed information available from MM5. In this study ISCST3 was run with the Hyannis airport meteorological data in keeping with common practice.

There are, however, important circumstances when it would be appropriate to use ISCST3 or similar straight-line trajectory models. One situation is when building or structure downwash is important. This is often the case for industrial facilities that have stacks not much taller than nearby buildings. In such cases the maximum predicted concentrations occur just downwind of the buildings or structures and ISCST3, with its detailed downwash algorithms, is appropriate. The other circumstance is for time periods when the meteorology is spatially very uniform. This occurs when the winds are determined by synoptic scale meteorology with large pressure gradients and high wind speeds. For Cape Cod, this is more apt to occur during the winter or during regionally stormy periods. Therefore, for research studies involving long time periods when the frequency of occurrence of uniform, steady winds is high and the air flow not too complex, it would be efficient to use ISCST3 for those time periods. The modeling capabilities developed in this project would then be applied to the more limited time periods of anticipated complex flows.

6 Installation and Implementation of Programs on MADPH Computer

The project includes the delivery of the new modeling capability to the Bureau of Environmental Health Assessment of the Massachusetts Department of Public Health. Because of the special operating system requirements of the MM5 model and the need to interface with National Center for Environmental Predictions (NCEP) data sites, the software has been installed on a MADPH computer that is identically configured to the computer used by Meteorological Consultants of Pennsylvania for their development work. The hard drive of this computer has been configured to handle both the LINUX operating system used for MM5 and the Windows system used by CALMET/CALPUFF, CalDESK and ISCST3. Interface software has been set up to allow the MM5 model to run from archived and real time meteorological data available from the Eta Data Assimilation System (EDAS).

7 Research Needs

7.1 Needs for Meteorological modeling

As discussed in prior sections, the evaluations conducted as part of this study have demonstrated that the meteorological fields generated by the MM5 mesoscale model have considerable skill. That is not to say, however, that they are without error. Even though the observations are not dense enough to verify all aspects of the model circulations, the available data do indicate that there are some deficiencies that could affect the accuracy of the model's 3-D mesoscale flow. Two fairly important problems stand out. First, the results indicate that the model tends to underpredict the maximum daytime temperatures over land by 1-2 degrees C and overpredict the minimum nighttime temperatures by 1-3 degrees C. This means that the strength of the sea breeze and land breeze may be somewhat weakened. Second, the statistics suggest that the winds in the PBL above the surface layer may be consistently too strong by 0.5-2.0 ms^{-1}. This problem appears to be most severe over the Outer Cape (a strongly marine environment) and less severe over the land mass of New England and NY.

A preliminary analysis of these error tendencies suggests that two of the MM5 physics parameterizations could require some further improvements. These are (1) the longwave radiation scheme and (2) the planetary boundary layer parameterization. Results from this and other studies indicate that the radiation scheme underestimates outgoing longwave radiation in moist, but unsaturated atmospheres such as exist in marine environments. This would account for the inability to match observed minimum temperatures. Furthermore, results from this and other recent studies suggests that the downward momentum transport in the MM5's TKE turbulence scheme may be underestimated due to the method used to calculate a critical length scale. It should be possible to reduce these errors by introducing new research results to correct or replace the existing parameterizations.

Further work should also be directed toward a better understanding of the vertical motions associated with the sea and land breeze flows and specifically a more thorough analysis of the 3-D structure of the MM5 wind fields. For example, the study has identified a number of convergence zones that form along sea breeze fronts and that can become more potent when individual fronts collide. Moreover, these convergence zones are definitely NOT static, but continue to evolve and re-align themselves throughout the day. It would be useful to examine, on an hour-by-hour basis, how these features develop and change, and calculate the horizontal divergence, vertical motions, horizontal wind speed, stability, TKE, PBL height, etc. for these periods. The windsurfing wind data may provide a useful data set for evaluating the timing of the basic features of these motions.

Lastly, we believe that further development of the MM5's FDDA scheme would allow assimilation of surface temperature and humidity observations in such a way as to locally correct for inaccuracies in the soil moisture estimates and the surface fluxes for heat and water vapor.

At present the calculation of surface fluxes is hampered by the use of time-invariant soil moisture values that are specified from climatology on the basis of the local land-use type and the season. Introduction of time-variable soil moisture through an improved FDDA methodology would allow a more accurate predication of the surface temperature that is so critical to the development of sea breezes and land breezes.

7.2 Model Interface Research Issues

This high-resolution modeling study of the Upper Cape Cod region of Massachusetts highlights some long-standing deficiencies of meteorological and pollutant dispersion models. Many of these issues become more prominent because the UCC domain is a rather small landmass and one having a fine-structure coastline demanding high-resolution treatment. Nevertheless, the UCC is an area capable of giving rise to the observed multiple sea- and land- breezes that can be problematic to simulate accurately with a prognostic meteorological model. Further, even when these sea- and land- breeze phenomena are correctly simulated, most dispersion models are unable to utilize the significant vertical velocities and recirculation accompanying these thermally driven effects. These accompanying vertical velocities can have important impacts on a plume's centerline height and dispersion rate, and thus on ground-level concentrations and doses. In addition, the vertical displacement of a plume can place it in a very different horizontal flow regime -- a factor particularly important in the high wind shear flows associated with sea- and land- breezes.

One interesting example of this is seen in the generation of trajectories originating from the Canal power plant. Figure 179 shows a side-by-side comparison of a multi-hour trajectory that uses the horizontal winds only (left frame) and a similar trajectory derived from 3-D winds. The difference in these trajectories after three hours of transport (i.e., noon) is quite dramatic in that the 2-D trajectory stays over the water, while that utilizing 3-D winds returns to land. The return of this plume in the low-level sea-breeze flow will probably result in higher ground-level concentrations than would modeling that assumed that the originally emitted plume was well aloft.

Presently, the CALPUFF model would send its puffs along the 2-D trajectory, so that even though CALPUFF now treats enhanced plume dispersion in convergence zones (i.e., with updrafts), its puffs would not be in that convergence zone, but rather out over Nantucket Sound.

Thus, enhancements to the CALPUFF model would involve changes to both the transport and dispersion algorithms and must be done with care. For example, CalDESK was recently upgraded (at our request for this project) to be able to compute these 3-D trajectories to complement the existing 2-D trajectory option. The initial implementation had trajectories penetrating the ground, as forward marching of the trajectory based on the local U, V and W winds was done. This sort of forward-in-time marching is fine if there are no strong spatial gradients in the flow, but W always vanishes at the ground, and so the trajectory must curve away from the ground to avoid a collision, just as the flow streamlines do.

As mentioned in Section 3.2.2.4.1, CALPUFF's dispersion algorithm recognizes some added dilution due to updrafts, but does not presently treat downdrafts at all. This has important ramifications for the UCC environment, where broad areas of subsidence, involving downward W velocities of 5-10 cm/s or more can exist over much of the land for hours at a time, particularly during nighttime hours that coincide with land breeze situations. Such downward W velocities would cause elevated plumes to sink toward the ground and would cause ground level plumes to grow vertically at reduced or even "negative" rates, given stable nighttime vertical plume dispersion rates of only a few cm/s. In such contracting plume cases, the plume would spread out more rapidly in the horizontal, so that peak centerline concentrations would not rise in an unphysical manner, but could cause ground-level exposures from elevated and surface releases to rise markedly. Including such phenomena would significantly improve the modeling realism for the UCC domain.

Along with these improvements in the model physics, the UCC modeling process could be made much less cumbersome if CALMET accepted the MM5 binary outputs directly. Presently, one must convert from the MM5, Version 3 binary format to the older, less compact Version 2 binary form, and then convert these data to bulky ASCII files that are formatted to resemble radiosonde sounding data. These data are then input to CALMET along with presently necessary, but primarily redundant data from an upper air file, a surface file and a geophysical data file. While internal checks in CALMET prevent mismatches in data, all of the inputs needed could be extracted from the MM5 file. It would, of course, be desirable to retain the option to add in supplementary surface station observations to extract cloud cover, for example, but this desire should not prevent the CALMET model from running exclusively from MM5 data if desired.

This "MM5 only" option and the associated elimination of several tedious steps involving large intermediate files would definitely streamline the modeling process. Faced with a similar challenge in a recent European modeling effort using a variation of CALGRID (i.e., the grid model counterpart to CALPUFF), we bypassed CALMET entirely, and added the capability to read prognostic (or diagnostic) meteorological data directly into the dispersion model. This would render CALPUFF as easy to apply with MM5 simulated data as the SCIPUFF model.

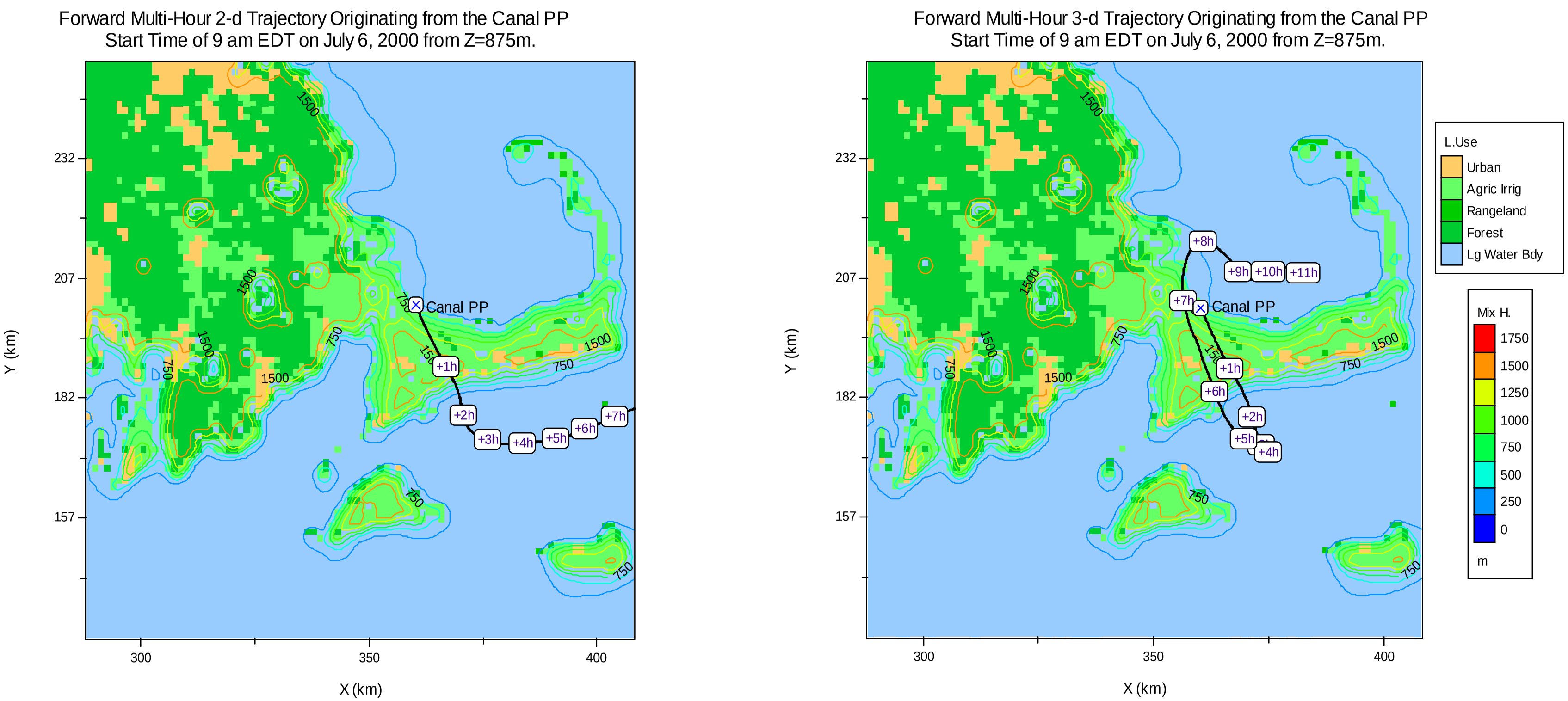

Figure 179. Forward-in-time, multi-hour, trajectories generated using CALMET winds and originating from a height of 875m directly above the Canal PP at 9 am EDT on July 6, 2000. Numbers on the trajectory indicate hours of transport. Mixing depths are also shown and vary dramatically (from 250m to 1200m) within several km of the Canal plant. The left frame shows the trajectory computed with 2-d horizontal winds only, whereas the trajectory in the right frame uses 3-d winds. The difference after hour 3 is quite dramatic in that the 2-d trajectory stays over the water while that utilizing 3-d winds returns to land with the sea breeze.

8 References

Arakawa, A. and V.R. Lamb, 1977: Computational design of the basic dynamical process of the UCLA general circulation mode. *Methods in computational Physics*, 17, 172-265.

Barnes, B. 2000: Cape sea breeze is no cocktail. The Upper Cape Codder, March 9, 2000. 1-2, 8

Chang, J. C., K. Chayantrakom, and S. R. Hanna, 2001: Evaluation of CALPUFF, HPAC, and VLSTRACK with the Over-Land Along wind Dispersion (OLAD) Field Data. George Mason University, School of Computational Sciences Report, 82 pp.

Chang, J. C. 2001: Uncertainty and Sensitivity of Dispersion Model Results to Meteorological Inputs, Two Case Studies. School of Computational Sciences, George Mason University. Fairfax VA.

Charlton, Randy, 2001: Personal communication with B.A. Egan. April 5, 2001

Dudhia, J., 1989: Numerical study of convection observed during the winter monsoon experiment using a mesoscale two-dimensional model. *J. Atmos. Sci*., 46, 3077-3107.

Dudhia, J., 1993: A nonhydrostatic version of the Penn State/NCAR mesoscale model: Validation tests and simulation of an Atlantic cyclone and cold front. *Mon. Wea. Rev.*, 121, 1493-1513.

EPA, 1995: User's Guide for the Industrial Source Complex (ISC) Dispersion Models. Volume II – Description of Model Algorithms. Document number EPA-454/B-95-003b

Gayno, G. A., 1994: Development of a higher-order, fog-producing boundary layer model suitable for use in numerical weather prediction. *M.S. thesis, Department of Meteorology, The Pennsylvania State University*, 104 pp.

Grell, G.A., J. Dudhia, and D.R. Stauffer, 1994: A description of the Fifth-Generation Penn State/NCAR Mesoscale Model (MM5). NCAR Tech. Note NCAR/TN-398+STR. 138 pp.

Kain, J. S., and J. M. Fritsch, 1990: A one-dimensional entraining/detraining plume model and its application in convective parameterization. *J. Atmos. Sci.*, 47, 2784-2802.

Lewellen, W.S. and R.I. Sykes (1986): Analysis of concentration fluctuations from lidar observations of atmospheric plumes. *J. Clim. & Appl. Met*., 25, 1145-1154.

Michelson, S.A. and N.L. Seaman, 2000: Assimilation of NEXRAD-VAD Winds in Meteorological Simulations over the Northeast U.S., *J. Appl. Meteor.*, 39, 367-383.

Moeng, C. -H. and J.C. Wyngaard, 1989: Evaluation of turbulent transport and dissipation closure in second-order modeling. *J. Atmos. Sci*., 46, 2311-2330.

Scire, J. S., F. R. Robe, M. E. Fernau, and R. J. Yamartino, 2000a: A User's Guide for the CALMET Meteorological Model (Version 5). EARTH TECH Inc. Report, 322 pp.

Scire, J. S., D. G. Strimaitis, and R. J. Yamartino, 2000b: A User's Guide for the CALPUFF Dispersion Model (Version 5). EARTH TECH Inc. Report, 521 pp.

Scire, J. S., F. R. Robe, M. E. Fernau, and R. J. Yamartino, 2000a: A User’s Guide for the CALMET Meteorological Model (Version 5). EARTH TECH Inc. Report, 322pp.

Seaman, N.L. and S.A. Michelson, 2000: Mesoscale meteorological structure of a high-zone episode during the 1995 NARSTO-Northeast study. *J. Appl. Meteor*., 39, 384-398.

Seaman, N.L., D.R. Stauffer and A.M. Lario-Gibbs, 1995: A multiscale four-dimensional data assimilation system applied in the San Joaquin Valley during SARMAP. Part I: Modeling design and basic performance characteristics. *J. Appl. Meteor*., 34, 1739-1761.

Shafran, P.C., N.L. Seaman, and G.A. Gayno, 2000: Evaluation of numerical predictions of boundary layer structure during the Lake Michigan Ozone Study. *J. Appl. Meteor*., 39, 412-426.

Stauffer, D. R. and N. L. Seaman, 1990: Use of four-dimensional data assimilation in a limited-area mesoscale model. Part I: Experiments with synoptic-scale data. *Mon. Wea. Rev*., *118*, 1250-1277.

Stauffer, D.R. and N.L. Seaman, 1994: Multiscale four-dimensional data assimilation. *J. Appl. Meteor*., 33, 416-434.

Stauffer, D.R. and N.L. Seaman, 1999: Intercomparison of turbulence parameterizations for simulating coastal-zone marine boundary layer structure. Preprints. *3rd AMS Conf. on Coastal Atmosphere and Ocean Predictions and Processes.* New Orleans, LA, 3-5 November, 7-12.

Stauffer, D.R., R.C. Munoz, and N.L. Seaman, 1999: In-cloud turbulence and explicit microphysics in the MM5. 9th PSU/NCAR Mesoscale Model Users' Workshop. Boulder, CO, 23-25 June, 177-180.

Sykes, R.I., D.S. Henn, S.F. Parker and R.S. Gabruck, 1996: SCIPUFF- A generalized hazard dispersion model. *9th AMS Joint Conf. on Applications of Air Poll. Meteor. with A&WMA*, Atlanta, GA, 28 Jan - 2 Feb., 184-188.

Sykes, R.I., W.S. Lewellen and S.F. Parker, 1984: A turbulent-transport model for concentration fluctuations and fluxes. *J. Fluid Mech.,* 139, 193-218.

Sykes, R.I., S.F. Parker, D.S. Henn, C.P. Cerasoli, and L.P. Santos, 1998: PC-SCIPUFF Version 1.2PD Technical Documentation. ARAP Report No. 718, Available for Titan Corp., Princeton, NJ, 170 pp.

USACHPPM, 1999: Human Health Risk Assessment: Open Burning of Propellant Bags. Massachusetts Military Reservation, MA. Project No. 39-EJ-6995-97. United States Army Center for Health Promotion Medicine and Preventive Medicine. Aberdeen Proving Ground, MD 21010-5422. January 1999

Weisman, L.M., W.C. Skamarock, and J.B. Klemp, 1997: The resolution dependence of explicitly modeled convective systems. *Mon. Wea. Rev.*, 125, 527-548.

Zanis, Paul. 2001: Personal communication with B.A. Egan. April 5, 2001.

9 Appendix A Beachfront Data Analysis

One of the supplementary meteorological data sources available on Cape Cod is a network of anemometers, established and operated by a meteorological group (Iwindsurf.com) and located at various Massachusetts beaches. As the Iwindsurf goal is to provide accurate, real-time measures of wind speed and direction to wind surfing enthusiasts via the Web, their monitors are sited directly on beaches or jetties to facilitate effective measurement of over-water winds at a height of about 10m. Their monitors are operated continuously, are maintained and calibrated by meteorologists, and have a data capture rate exceeding 98%. The monitors considered in this study are located at Chapin Memorial Beach (near Barnstable on the north shore and facing Cape Cod Bay), West Falmouth (facing west southwest on the east shore of Buzzards Bay), Kalmus Park (near Hyannis, facing Nantucket Sound to the south). West Dennis (also facing south) and Duxbury (facing east northeast). While north of the Cape, the Duxbury site is useful for identifying situations when land- and sea-breezes occur at a mainland site – where they are more likely to occur than over the smaller landmass of Upper Cape Cod (UCC) shown below in Figure A.1.

Figure A.1 Map of Upper Cape Cod Region.

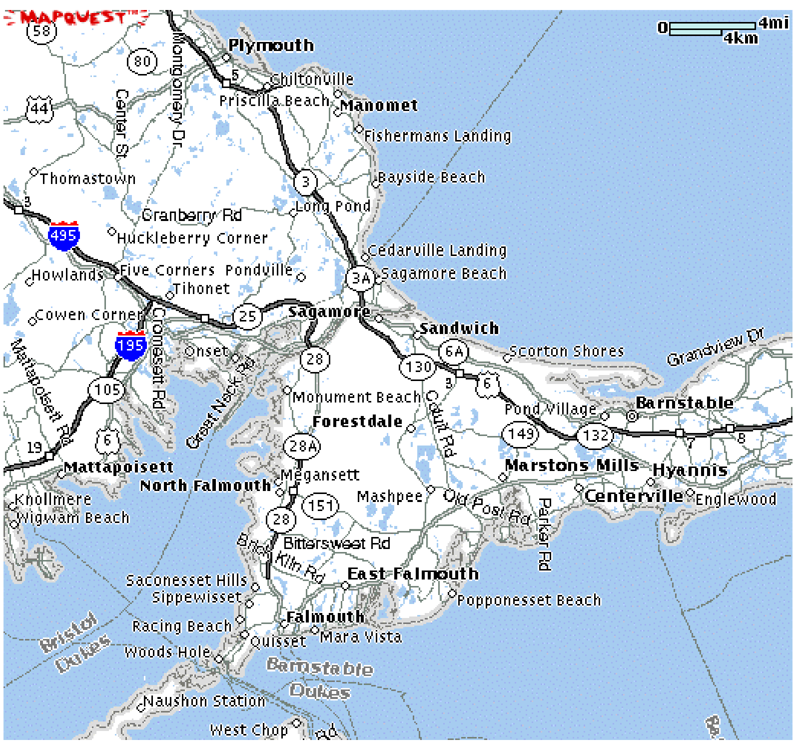

Data for the three month period July-September 2000 have been analyzed for the presence of on- or off-shore flows. One specific analysis involves considering the UCC region as approximately an equilateral triangle 25km on a side. Beach measured winds are assumed applicable to an entire side of this triangle and through a depth of about 240m. The net inward (or outward) flux into this triangular box is then converted to a compensatory vertical velocity, W, that would be required at the top face of the triangle box to conserve air mass in the absence of air density changes inside the box. A week-long (i.e., July 1-7) time-series of these W velocities is shown as an example in Figure A.2. These computed W values were then combined with additional data cuts[1] and data from the Northeast Regional Climate Center at Cornell University for Hyannis Barnstable Municipal Airport to compute instances of multiple (i.e., on 2 or 3 UCC shores simultaneously) land (L) or sea (S) breezes occurring on UCC. The so-identified cases found during the first three weeks of July 2000 are shown in Table A.1.

These analyses indicate that:

- negative W seen during land-breezes are about half to two-thirds the strength of corresponding positive W values in sea-breezes;
- computed positive W of 10-20 cm/s associated with multiple sea-breezes are somewhat smaller than typical, daytime, unstable plume dispersion rates of order 0.2*wind speed or in the range of 25-100 cm/s;
- computed negative W of 5-15 cm/s associated with multiple land-breezes are of the same magnitude as typical, nighttime, stable plume dispersion rates of order 0.05*wind speed or in the range of 5-20 cm/s.

This latter finding may have important consequences for subsequent dispersion model analyses, for as described previously, a downward W would cause elevated plumes to sink toward the ground and would cause ground level plumes to grow at reduced rates, or even contract, in the vertical.

Finally, these analyses of the Iwindsurf data, along with the synoptic-scale analyses of weather maps were used to identify appropriate periods to simulate with the Penn State University Mesoscale Model 5 (MM5).

---

[1] Supplemental data cuts include a requirement that the Coriolis rotated (+10 degrees) winds are within 55 degrees of normal to the beach orientation, that Hyannis Airport winds are less than 10 mph, that Hyannis cloud cover is less than 50%, and that flow speeds perpendicular to the beach are at least 0.5 mph. Also, the vertical velocity regime, $-5 < W < +10$ cm/s, was excluded as "ambiguous".

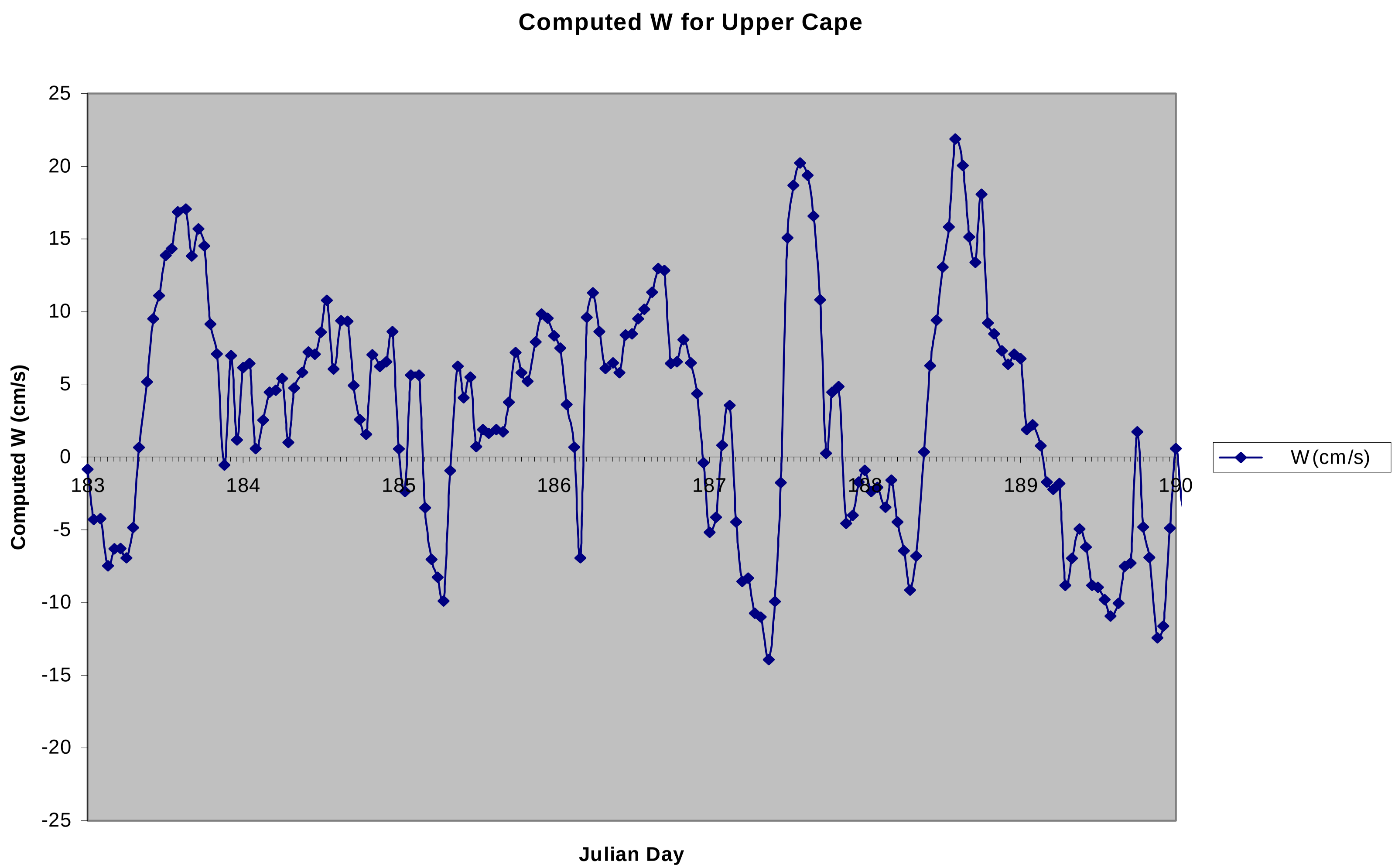

Figure A.2. Computed W velocities over Upper Cape Cod for the first week in July 2000 (i.e., Julian day 183 beginning at hour 00 through Julian day 190). These velocities were estimated using winds measured by Iwindsurf.com beach-sited monitors in Duxbury, Chapin, West Falmouth, and Kalmus. Days 183 (July 1) and 187-8 (July 5-6) show typical cycles of a nighttime land-breeze with over-land subsidence (i.e., W < 0) followed by an afternoon sea-breeze with accompanying over-land updrafts (i.e., W > 0).

Table A.1. Cases of Land (L) and Sea (S) Breezes Occurring Simultaneously on Two or Three of the Three Coasts of Upper Cape Cod During the First Three Weeks of July 2000.

Flow Type L/S	# of flows	MM	DD	HH	Sum V*n mph	W cm/s	Hyannis Airport data T degF	WD deg	WS mph	Pres in Hg	CC 0-1	Normal flow speed(mph) normal to beach) at: DUX	CHP	WFL	KAL	WDN	Observed Wind Dir. (in degrees) at: DUX	CHP	WFL	KAL	WDN
L	2	7	1	3	-7.	-7.5	57	0	0.0	29.90	0.0	-4.	-3.	0.	-4.	-3.	270	270	0	320	3
L	2	7	1	4	-6.	-6.3	54	0	0.0	29.90	0.0	-4.	-1.	0.	-5.	-4.	270	270	9	338	0
S	3	7	1	11	11.	11.1	76	190	8.1	29.97	0.0	3.	3.	3.	5.	6.	40	315	235	212	202
S	3	7	1	12	14.	13.9	76	170	8.1	29.97	0.0	4.	3.	4.	6.	2.	72	335	225	187	225
S	3	7	1	13	14.	14.3	77	190	9.2	29.97	0.2	3.	4.	4.	6.	2.	90	349	225	194	225
S	3	7	1	14	17.	16.9	76	180	8.1	29.96	0.0	3.	4.	6.	7.	1.	90	356	225	180	202
S	3	7	1	15	17.	17.1	76	210	8.1	29.96	0.0	4.	3.	5.	9.	4.	90	342	225	180	200
S	2	7	1	17	16.	15.7	74	210	8.1	29.94	0.0	7.	0.	5.	10.	8.	90	197	228	180	191
S	2	7	1	18	15.	14.5	72	200	8.1	29.94	0.0	5.	-2.	6.	11.	9.	121	173	225	183	186
L	2	7	5	5	-9.	-8.6	69	340	5.8	29.69	0.0	-5.	-4.	1.	-6.	-5.	270	270	0	315	338
L	2	7	5	7	-11.	-10.8	75	350	6.9	29.71	0.0	-7.	-5.	1.	-7.	-9.	273	270	0	319	0
S	2	7	5	12	15.	15.1	82	40	6.9	29.70	0.0	-3.	3.	5.	7.	1.	306	0	231	173	241
S	2	7	5	16	17.	16.6	80	40	8.1	29.70	0.2	3.	5.	9.	2.	10.	59	37	225	86	135
L	2	7	6	6	-6.	-6.4	63	330	4.6	29.83	0.0	-2.	0.	-3.	-4.	0.	315	315	45	315	0
S	2	7	6	13	16.	15.8	75	180	9.2	29.82	0.0	6.	6.	5.	5.	5.	86	0	225	216	225
S	3	7	6	14	22.	21.9	74	-1	6.9	29.83	0.0	6.	7.	6.	9.	9.	75	0	225	180	185
S	3	7	6	15	20.	20.0	74	180	9.2	29.83	0.0	6.	6.	6.	8.	9.	118	0	225	180	187
S	2	7	6	16	15.	15.1	72	200	8.1	29.82	0.0	4.	-1.	7.	9.	9.	135	158	225	168	173
S	2	7	6	17	13.	13.4	68	170	8.1	29.82	0.0	5.	-3.	8.	9.	11.	135	169	225	138	180
S	2	7	6	18	18.	18.1	67	170	8.1	29.82	0.0	5.	-1.	8.	11.	13.	135	138	225	177	180
L	2	7	7	15	-10.	-10.1	72	20	9.2	29.86	0.2	1.	4.	-5.	-8.	-8.	45	0	63	11	7
L	2	7	7	16	-8.	-7.5	71	10	6.9	29.87	0.0	1.	3.	-3.	-8.	-7.	45	0	57	0	2
L	2	7	7	17	-7.	-7.3	72	40	6.9	29.86	0.2	1.	2.	-4.	-6.	-6.	45	355	85	13	2
L	2	7	9	0	-7.	-7.2	60	290	4.6	29.95	0.0	-3.	-4.	2.	-5.	-3.	220	249	355	315	309
L	2	7	9	1	-9.	-8.8	60	300	4.6	29.95	0.0	-6.	-5.	3.	-6.	-5.	245	270	328	311	315
L	2	7	9	2	-11.	-10.7	57	320	3.5	29.95	0.0	-5.	-5.	0.	-6.	-5.	270	270	6	308	315
L	2	7	12	1	-6.	-5.9	65	20	6.9	29.82	0.0	-1.	6.	-4.	-8.	-5.	332	0	45	0	16
L	2	7	12	2	-6.	-6.0	65	30	6.9	29.83	0.0	-3.	5.	-2.	-9.	-5.	315	0	45	0	33
L	2	7	12	10	-9.	-9.0	76	330	5.8	29.89	0.0	-6.	-4.	2.	-6.	-7.	272	270	307	332	349
L	2	7	13	3	-8.	-7.9	64	360	5.8	29.92	0.0	-5.	-3.	1.	-6.	-6.	270	265	355	315	0
L	2	7	13	4	-10.	-10.1	64	350	4.6	29.93	0.2	-5.	-2.	-1.	-7.	-6.	270	225	28	315	0
L	3	7	13	5	-12.	-12.0	65	360	5.8	29.94	0.0	-4.	-2.	-2.	-8.	-6.	270	270	45	325	0
L	2	7	13	6	-10.	-10.4	69	360	4.6	29.95	0.0	-4.	-2.	-2.	-7.	-7.	270	308	48	356	0
S	2	7	13	15	18.	17.9	76	210	9.2	29.91	0.0	8.	-4.	9.	13.	6.	121	180	225	186	225
S	2	7	16	15	11.	10.5	75	100	5.8	29.78	0.0	5.	2.	4.	4.	7.	90	135	225	112	135
S	3	7	16	16	16.	16.0	77	-1	5.8	29.77	0.0	8.	6.	6.	4.	8.	90	17	256	118	135
S	3	7	16	17	16.	16.4	72	180	8.1	29.80	0.0	4.	5.	5.	7.	10.	85	57	239	135	143
L	2	7	19	9	-6.	-6.2	70	350	9.2	29.90	0.0	-10.	-6.	8.	-8.	-8.	270	270	315	314	32

Subsequent to running the three, two-day episodes of July 1-2, July 5-6, and August 21-22 with the MM5 model, the model's results were compared with the IWindsurf station data by extracting wind data from the nearest MM5 surface-level grid point.

Tables A.2 and A.3 summarize the comparison between IWindsurf measured winds and comparable MM5 surface, grid-point winds. The 143 hours of data span the three episodes modeled and consider four beach stations: Duxbury (N. of Cape) and the 3 UCC stations Chapin, Kalmus and W. Falmouth.

Table A.2 shows a comparison of the scalar wind speeds. Overall (i.e., all stations, all hours), we see that MM5 predicts speeds that are about 12% higher than observed; however, daytime speeds are reproduced significantly better than nighttime values. This fact is reflected in the superior match between daytime means and standard deviations as well as lower MSE, bias and dynamic variability percents. The correlation coefficient is also higher for the daytime speed data, and the daytime stochastic portion of MSE of 97.7% indicates that, during the daytime, the model is nearly free of bias and is able to reproduce the dynamic range of observations.

If one considers the individual station data, we see that MM5 average speeds span the 0.44 m/s range from 3.20 to 3.66 m/s, whereas the observations span the larger 1.10 m/s range from 2.55 to 3.65 m/s. Interestingly, Kalmus is observed to be the windiest of the four sites, whereas MM5 finds it to have the lowest average winds. This phenomena may be related in part to finer-coastline features than can resolved by the model, even with a 1.33 km grid mesh.

Table A.3 shows the same comparison for vector winds. Once again, one sees that daytime winds are predicted considerably better than nighttime winds. This fact is confirmed by the standard deviations, the MSE, the MSE components, and the correlation coefficient.

Considering individual station results, one sees the lowest MSE at Duxbury (i.e., on the MA mainland) and the highest MSE error at Kalmus, already mentioned as the site showing the greatest discrepancy between measured and modeled speeds.

Table A.2. Comparison of MM5 Predicted and IWindsurf Observed Surface Winds Speeds At Beach-Sited Monitors in Duxbury, Kalmus, West Falmouth, and Chapin.

Data Sample	No. Hours	Mean Speed (m/s)		Speed Std. Dev. (m/s)		MSE $(m/s)^2$	* MSE Parts (%)			RMSE (m/s)	Corr. Coef.
		MM5	Obs.	MM5	Obs.		Bias	Dyn.	Stoc.		
All Stations All Hours	572	3.41	3.04	3.63	3.49	2.49	5.5	9.3	85.2	1.58	0.50
Duxbury All Hours	143	3.43	2.57	3.59	2.79	2.01	37.0	0.1	62.9	1.42	0.44
Chapin All Hours	143	3.37	2.55	3.65	3.14	3.12	21.6	5.9	72.5	1.76	0.56
Kalmus All Hours	143	3.20	3.65	3.38	4.01	2.36	8.6	14.7	76.7	1.54	0.50
W. Falmouth All Hours	143	3.66	3.41	3.89	3.89	2.49	2.5	12.0	85.5	1.58	0.57
All Stations Day (08-16)	216	3.08	2.98	3.34	3.33	1.79	0.5	1.8	97.7	1.34	0.54
All Stations Night(20-04)	212	3.68	3.00	3.81	3.62	3.77	12.1	27,8	60.1	1.94	0.44

* Mean Square Error (MSE) is decomposed (H. Theil) as $MSE = (Xave - Yave)^2 + (\sigma_X - \sigma_Y)^2 + 2\cdot(1-R)\cdot\sigma_X\cdot\sigma_Y$
These three terms, normalized by MSE, are referred to as the bias, dynamic variability, and stochastic fractions.

Table A.3. Comparison of MM5 Predicted and IWindsurf Observed Surface Vector Winds At Beach-Sited Monitors in Duxbury, Kalmus, West Falmouth, and Chapin.

Data Sample	No. Hours	Speed Std. Dev. (m/s) MM5	Obs.	Slope Obs. / MM5	MSE $(m/s)^2$	MSE Parts (%) Bias	Dyn.	Stoc.	RMSE (m/s)	Corr. Coef.
All Stations All Hours	572	3.63	3.49	0.726	6.24	0.2	0.2	99.6	2.50	0.71
Duxbury All Hours	143	3.59	2.79	0.604	5.08	0.8	11.9	87.3	2.25	0.77
Chapin All Hours	143	3.65	3.14	0.623	6.57	3.4	2.4	94.2	2.56	0.71
Kalmus All Hours	143	3.37	4.01	0.913	6.69	1.5	4.6	93.9	2.59	0.71
W. Falmouth All Hours	143	3.89	3.89	0.780	6.64	0.2	0.1	99.7	2.58	0.66
All Stations Day (08-16)	216	3.34	3.33	0.734	5.86	7.5	0.1	92.4	2.42	0.75
All Stations Night(20-04)	212	3.81	3.62	0.702	7.22	8.3	1.8	89.9	2.68	0.61

10 Appendix B Hyannis–Barnstable AP Meteorological Data Sample

Table 3.4 Example set of data available at local airports.

Station: HYANNIS BARNSTABLE MUNI AP, MA

Date: yyyy=year mm=month dd=day
hh=hour, Local Standard Time
Temp=Temperature, degF
W Dir=Wind Direction, degree
W Speed=Wind Speed, miles/hour
W. Gust=Wind Gusts, miles/hour
Pk.W.Spd=Peak Wind Speed, miles/hour

Stat Pres=Station Pressure, inch_Hg
Sky Cov=Total Sky Cover, fraction
C.Ceiling=Ceiling Height, 100 feet
C.Hgt=Cloud Layer Heights, 100 feet
C.Cond=Cloud Layer Conditions, NRCC code
Weather=Weather Conditions, text
Separator: tab
Missing value: -999

yyyy	mm	dd	hh	Temp	W Dir	W Speed	W. Gust	Pk.W.Spd	Stat Pres	Sky Cov	C.Ceiling	C.Hgt1	C.Hgt2	C.Hgt3	C.Cond1	C.Cond2	C.Cond3	Weather
Hyannis																		
2000	6	30	20	67	270	5.8		-999	29.84	0	1000	0	-999	-999	7	-999	-999	
2000	6	30	21	66	270	5.8		-999	29.86	0	1000	0	-999	-999	7	-999	-999	
2000	6	30	22	64	0	0		-999	29.88	0	1000	0	-999	-999	7	-999	-999	
2000	6	30	23	62	0	0		-999	29.89	0	1000	0	-999	-999	7	-999	-999	
2000	7	1	0	58	0	0		-999	29.89	0	1000	0	-999	-999	7	-999	-999	
2000	7	1	1	57	0	0		-999	29.89	0	1000	0	-999	-999	7	-999	-999	
2000	7	1	2	61	350	4.6		-999	29.89	0	1000	0	-999	-999	7	-999	-999	
2000	7	1	3	57	0	0		-999	29.9	0	1000	0	-999	-999	7	-999	-999	
2000	7	1	4	54	0	0		-999	29.9	0	1000	0	-999	-999	7	-999	-999	
2000	7	1	5	55	0	0		-999	29.92	0	1000	0	-999	-999	7	-999	-999	
2000	7	1	6	65	350	3.5		-999	29.93	0	1000	0	-999	-999	7	-999	-999	
2000	7	1	7	69	340	3.5		-999	29.95	0	1000	0	-999	-999	7	-999	-999	
2000	7	1	8	71	0	0		-999	29.96	0	1000	0	-999	-999	7	-999	-999	
2000	7	1	9	73	10	3.5		-999	29.96	0	1000	0	-999	-999	7	-999	-999	
2000	7	1	10	75	180	5.8		-999	29.96	0	1000	0	-999	-999	7	-999	-999	
2000	7	1	11	76	190	8.1		-999	29.97	0	1000	0	-999	-999	7	-999	-999	
2000	7	1	12	76	170	8.1		-999	29.97	0	1000	0	-999	-999	7	-999	-999	
2000	7	1	13	77	190	9.2		-999	29.97	0.2	1000	30	-999	-999	25	-999	-999	
2000	7	1	14	76	180	8.1		-999	29.96	0	1000	0	-999	-999	7	-999	-999	
2000	7	1	15	76	210	8.1		-999	29.96	0	1000	0	-999	-999	7	-999	-999	
2000	7	1	16	75	210	5.8		-999	29.94	0	1000	0	-999	-999	7	-999	-999	
2000	7	1	17	74	210	8.1		-999	29.94	0	1000	0	-999	-999	7	-999	-999	
2000	7	1	18	72	200	8.1		-999	29.94	0	1000	0	-999	-999	7	-999	-999	
2000	7	1	19	69	230	6.9		-999	29.94	0	1000	0	-999	-999	7	-999	-999	
2000	7	1	20	67	250	6.9		-999	29.95	0	1000	0	-999	-999	7	-999	-999	
2000	7	1	21	65	240	5.8		-999	29.97	0	1000	0	-999	-999	7	-999	-999	
2000	7	1	22	65	0	0		-999	29.98	0	1000	0	-999	-999	7	-999	-999	
2000	7	1	23	63	0	0		-999	29.98	0	1000	0	-999	-999	7	-999	-999	
2000	7	2	0	62	0	0		-999	29.98	0	1000	0	-999	-999	7	-999	-999	
2000	7	2	1	58	0	0		-999	29.98	0	1000	0	-999	-999	7	-999	-999	
2000	7	2	2	57	0	0		-999	29.97	0	1000	0	-999	-999	7	-999	-999	
2000	7	2	3	56	0	0		-999	29.96	0	1000	0	-999	-999	7	-999	-999	
2000	7	2	4	55	0	0		-999	29.97	0	1000	0	-999	-999	7	-999	-999	
2000	7	2	5	58	0	0		-999	29.97	0	1000	0	-999	-999	7	-999	-999	
2000	7	2	6	68	0	0		-999	29.98	0	1000	0	-999	-999	7	-999	-999	
2000	7	2	7	72	260	3.5		-999	30	0	1000	0	-999	-999	7	-999	-999	
2000	7	2	8	74	200	3.5		-999	30	0	1000	0	-999	-999	7	-999	-999	
2000	7	2	9	74	180	5.8		-999	30	0	1000	0	-999	-999	7	-999	-999	
2000	7	2	10	76	-1	5.8		-999	30	0	1000	0	-999	-999	7	-999	-999	
2000	7	2	11	77	170	8.1		-999	29.99	0	1000	0	-999	-999	7	-999	-999	
2000	7	2	12	78	200	8.1		-999	30	0	1000	0	-999	-999	7	-999	-999	
2000	7	2	13	79	220	10.4		-999	29.99	0	1000	0	-999	-999	7	-999	-999	
2000	7	2	14	79	210	9.2		-999	29.97	0	1000	0	-999	-999	7	-999	-999	
2000	7	2	15	78	210	10.4		-999	29.97	0	1000	0	-999	-999	7	-999	-999	
2000	7	2	16	77	210	10.4		-999	29.96	0	1000	0	-999	-999	7	-999	-999	
2000	7	2	17	77	240	9.2		-999	29.96	0	1000	0	-999	-999	7	-999	-999	
2000	7	2	18	75	230	9.2		-999	29.96	0	1000	0	-999	-999	7	-999	-999	
2000	7	2	19	73	230	8.1		-999	29.96	0	1000	0	-999	-999	7	-999	-999	
2000	7	2	20	71	220	6.9		-999	29.96	0	1000	0	-999	-999	7	-999	-999	
2000	7	2	21	70	220	8.1		-999	29.98	0	1000	0	-999	-999	7	-999	-999	
2000	7	2	22	69	220	8.1		-999	29.98	0	1000	0	-999	-999	7	-999	-999	
2000	7	2	23	68	240	8.1		-999	29.99	0	1000	0	-999	-999	7	-999	-999	
2000	7	3	0	68	250	9.2		-999	29.98	0	1000	0	-999	-999	7	-999	-999	